VOLUME 49, NUMBER 12

December, 1961

published monthly by The Institute of Radio Engineers, Inc.

Proceedings of the IRE®

contents

COVER

The interaction of electromagnetic radiation with gases comprised of disassociated ions and electrons, as symbolized on the cover, represents one of several areas of plasma physics treated in this special issue which are becoming of great importance to communications and electronics engineers.

published monthly by The Institute of Radio Engineers, Inc.

Proceedings of the IRE®

DECEMBER

continued

PROCEEDINGS OF THE IRE, published monthly by The Institute of Radio Engineers, Inc., at 1 East 79 Street, New York, 21, N. Y. Manuscripts should be submitted in triplicate to the Editorial Department. Correspondence column items should not exceed four double-spaced pages (illustrations count as one-half page each). Responsibility for contents of papers published rests upon the authors, and not the IRE or its members. All republication rights, including translations, are reserved by the IRE and granted only on request. Abstracting is permitted with mention of source.

Thirty days advance notice is required for change of address. Price per copy: members of the Institute of Radio Engineers, one additional copy $1.25; non-members $3.00. Yearly subscription price: to members $9.00, one additional subscription $13.50; to non-members in United States, Canada, and U. S. Possessions $18.00; to non-members in foreign countries $19.00. Second-class postage paid at Menasha, Wisconsin, under the act of March 3, 1879. Acceptance for mailing at a special rate of postage is provided for in the act of February 28, 1925, embodied in Paragraph 4, Section 412, P. L. and R., authorized October 26, 1927. Printed in U.S.A.

December, 1961
Vol. 49 No. 12

Proceedings of the IRE

Poles and Zeros

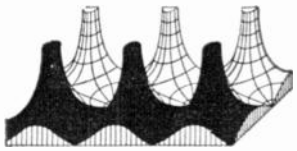

Plasma. On those occasions when a Special Issue of the PROCEEDINGS is assembled, the Editor uses this page to say a word about the issue. On this occasion, as usual, the Editor was preparing his "gaseous discharge" when he received a copy of the excellent introduction to this Special Issue. Messrs. Herold and Dow had produced such an all inclusive introduction that the Editor's "discharge" was thoroughly quenched. Your attention, therefore, is directed to the "Introduction to the Plasma Physics Issue," page 1747.

One cannot, however, fail to emphasize and acknowledge the outstanding effort of Guest Editor E. W. Herold and his Co-Guest Editor D. G. Dow. Their work, with the cooperation of the contributing authors, has produced this unusually well balanced treatment of an increasingly important subject. Not only did these editors solicit, review, and accept the eighteen papers that comprise the issue but also they suggested the cover design. As an addenda to this issue, for those with a special interest in the propagation aspects of the subject, watch for the January, 1962, issue of the TRANSACTIONS of the Professional Group on Antennas and Propagation.

Tutorial. The Board of Editors is aware of its primary responsibility to bring to IRE members the most up-to-date material of broad general interest and the most recent advances in all phases of the art. It discharges this responsibility through the pages of the PROCEEDINGS. The Board is equally aware of its obligation to provide IRE members with the opportunity to inform themselves of the essence of areas cognate to their own specialty. To satisfy this latter need and to meet its clear responsibility the Board of Editors has evolved an extensive plan for a series of review and tutorial papers.

To initiate this plan, suggestions were solicited from the Editors of the Professional Group Transactions. This solicitation, supplemented by ideas from the members of the Board, resulted in an initial list of over thirty topics and suggestions for authors for each. The Managing Editor then began the task of inviting selected authors to prepare contributions for publication in the PROCEEDINGS for this series of review and tutorial papers. Through the splendid cooperation of L. A. Zadeh, the series started in the October, 1961, issue. Professor Zadeh, a leading authority on the subject, presented Part I of a survey of time-varying network theory.

It is the hope of the Board of Editors that this new series of papers will enhance the value of the PROCEEDINGS to IRE members. It may not, however, meet the needs and desires of all members. To assure that all subjects of interest are ultimately covered, you are invited to send in your suggestions for topics and authors to the Managing Editor.

Dreams May Come True. For many years there has been an increasing tendency to ask why the profession of radio and electrical engineering should be represented by two professional technical societies. At the grass roots there has been an effort to compensate for this situation by a growing number of cooperative ventures, and this same tendency has been spreading to regional activities as well. Nevertheless, there has been a continuing trend toward the proliferation of meetings, redundancy of subject matter, and conflict of interest where there should be solidarity and a single minded approach to the same area of interest.

October, 1961, may well be a date never to be forgotten in the electrical and radio engineering profession. During that month, through arduous work on the part of members of both IRE and AIEE, through fortuitous circumstances, and through a sincere desire to move in a direction dictated by the clear necessity of the profession as a whole, the Boards of Directors of IRE and AIEE passed resolutions looking toward the possible amalgamation of the two organizations and the formation of a single organization for the entire profession. President Berkner's letter to Section Chairmen giving the background of this entire proposal will be found on page 1743. It deserves your thoughtful consideration.

Student Affairs. Student membership in IRE continues to grow. In recognition thereof and with full realization of the significance of its program for students in the further growth and development of IRE, a new and important post has been added to the headquarters staff. The Executive Committee authorized the organization of student affairs into a separate division of the IRE administration, and the appointment of an appropriate person to be designated as Student Affairs Secretary. It is a pleasure to announce the appointment of W. Reed Crone to this newly created position. The "IRE News and Notes" section of this issue of the PROCEEDINGS provides additional detail. We welcome Mr. Crone and wish him success in this new venture.

Section News. At its meeting in October, the Executive Committee approved the petition for the formation of an IRE Section in France. The section, to be known as the French Section, is Number 111; may it grow and prosper.

Texas claims another big first! The El Paso Section held a regular section meeting at Radio Station XELO in Juarez, Chihuahua, Mexico. They believe this to be the first regular meeting of a United States Section to be held in another country. IRE goes international again!—F. H., Jr.

B. R. Tupper

Director, 1961–1962

Bertram R. Tupper (A'36–SM'46–F'54) was born in Vancouver, British Columbia, on April 15, 1906. He received his B.Sc. degree from the University of British Columbia, Vancouver, in 1928.

After graduation he was employed by the British Columbia Telephone Company in the Transmission Engineering Department. The company was interested in the possibility of serving the Northern British Columbia coast by Radiotelephone, and the North-west Telephone Company, an associate company, was formed for this purpose. As Radio Engineer for the North-west Telephone Company, he took a leading part in building up a large medium frequency point-to-point and ship-to-shore network on the B.C. Coast.

In 1942 he was appointed Radio Consultant to the joint military services in the Pacific Coast area. The Telephone Company acted as prime contractors in providing defense communication in British Columbia and as a result of these defense requirements to the off-shore islands, FM VHF radio systems were built up which provided voice and teletype circuits between the radar sites and operational bases. Since 1958, he has been Chief Engineer of the British Columbia Telephone Company, which is an affiliate of General Telephone and Electronics Corporation, and which recently absorbed the North-west Telephone Company.

Mr. Tupper has served as a member of Sir Robert Watson Watts' Canadian Air Defence Communications Evaluation Committee in 1953–1954. For two years, he has been Chairman of the Electrical Board of Examiners for the Association of Professional Engineers of British Columbia and is a past Chairman of the Vancouver Section of the IRE.

He received the IRE Fellow Award in 1954 in recognition of his application of radio techniques to the extension of toll telephone services in Canada.

Open Letter from the President

The following letter from Lloyd V. Berkner, President of the IRE, is self-explanatory with reference to the actions of the two Boards concerning the possible consolidation of the IRE and AIEE. This letter is published to provide full information to the IRE members.—The Editor

October 20, 1961

Dear Mr. Section Chairman:

At its meeting on October 18, 1961, the IRE Board of Directors took action which makes possible future joint measures by IRE and AIEE aimed towards consolidation of their resources, membership and activities into a single new professional society dealing with the whole range of radio and electrical engineering and related professional interests. At its meeting on October 20, 1961, the Board of Directors of the AIEE took similar action. The action taken by the two Boards at this time is no more than a preliminary step toward the formulation of specific proposals on which each Board and the membership of each society must act subsequently in accordance with their statutes. Nevertheless, the proposal is now at a stage that the IRE Board desires the broadest possible discussion on the part of IRE membership. The Board has therefore instructed me to communicate with the Sections asking for their views after their careful consideration of the substantive effects of the proposal. The resolution of the Board is appended hereto.

Formation of a single professional radio and electrical engineering society through combination of IRE and AIEE is a matter of major international professional importance. I shall endeavor to outline the reasons that have led the IRE and AIEE Boards to join in discussions that open the potentiality of merger of the two societies into a single professional society in our field of technology. All related factors deserve the most mature consideration. But above all, the decision should be reached primarily on the judgment of that course of action that would lead the radio, electrical and electronic profession to develop in the most healthy and fruitful fashion.

The AIEE was founded as a New York corporation in 1884 to meet the professional needs represented in a growing power, telephone and telegraph industry. AIEE now has about 65,000 members, headquarters in the new Engineering Building in New York, and resources of about $1.5 million.

As you well know, the IRE was founded as a New York corporation in 1912 to meet the professional needs represented in radio communications. IRE now has about 92,000 members, its own headquarters in New York and resources of about $4.5 million.

Because of the basic evolution of each Institute toward the broad methods of electronics, on which both societies are founded, there has been an increasing overlap of interest in the two societies. This overlap has been in evidence in a number of ways.

1) Between 5000 and 6000 engineers are members of both AIEE and IRE.
2) Some technical standards committees of the two societies deal with similar standards problems that have produced conflicts. This has led to establishment of joint AIEE-IRE standards committees. Both societies deal with overlapping standards in the international field through ASA and IEC.
3) Standards for admission in the two societies are generally equivalent and by agreement members in a given grade of one society are admitted, upon application, to the corresponding grade in the other without further examination.
4) AIEE and IRE have formed joint student branches at many universities and technical institutes to avoid the obvious conflicts of common interest that arise from similar student interests in the same university departments.
5) Both IRE and AIEE are members of the Engineers' Council for Professional Development (ECPD), where their interests are very similar.

Moreover, the rapid evolution of training in radio, electrical and electronic engineering and in applied physics, in the universities and in industry is toward an identical curriculum for members of the two societies.

6) There is a broad overlap of much of the material published by the two societies.
7) A large number of local and U. S. national meetings are jointly sponsored by IRE and AIEE. The two societies have a major problem in avoiding the duplication and unnecessary proliferation of meetings on similar subjects.
8) AIEE is evolving toward formation of technical groups, very similar in purpose to the Professional Groups of IRE. This evolution promises a great increase in the area of conflict and duplication between the two societies.

The administration of these joint activities is complex and necessarily incomplete and consuming of major time and effort of the profession. Equivalent time on positive professional programs would greatly strengthen the profession.

Moreover, the areas of conflict are steadily enlarging as the advance of electronics brings both societies ever more into the same areas of interest. Typical examples of the problems that could be avoided by synthesis of the two societies are mentioned below:

1) Under one society and one Editorial Board, the publications of the two societies could be tailored for much better coverage of our professional field. Members would have a wider choice of the type of publications individually desired.
2) Meetings in the whole field could be simplified and duplication automatically avoided. Attendance would be improved.
3) The danger of increasing overlap and conflict of the IRE's professional groups and AIEE's technical groups could be avoided. The whole field of professional specialized technical societies could be more rationally covered by 35 to 40 professional groups of the new society.
4) The administration of student sections would be simplified, and one publication, such as the IRE STUDENT QUARTERLY, would serve the combined student needs.
5) Sectional activities would be simplified, the strengths of small sections enhanced, and activities in professional group chapters would become more rational.
6) Standards activities would be simplified, and dangers of conflict entirely removed, especially in view of IRE's vigorous participation in international standardization.
7) The new society would enjoy the international character of IRE with its attendant advantages. Likewise, it would carry the mantle of a "founder" society brought to it by AIEE.
8) The combined headquarters staffs could provide a much broadened service to our membership, our section organization, our professional group structure, our regional, national and international meetings, our technical committees, and our publication structure through reduction in duplication.

The synthesis of the new society would create an international professional institute with a membership of more than 150,000, an annual budget of about $6,000,000, and publications of great breadth and depth with wider opportunity for choice. The opportunities of its membership would be substantially increased within the new framework that is promised. The present office space controlled by IRE and AIEE appears sufficient to service the new institute, but with the elimination of obvious elements of duplication the service to the membership by the combined headquarters staffs would be substantially broadened.

Over the years there have been a number of joint committees charged with exploring possible areas of mutual interest, beginning with the attempt (1922) to merge the two societies in which Dr. Alfred N. Goldsmith (Founder IRE) and Professor A. E. Kennelly (then Past President of the IRE and President of the AIEE) were active. In spite of their efforts, the attempt failed because of the then preoccupation of AIEE in nonradio activities. The most recent committee was established in 1960, with Donald G. Fink as Chairman for the IRE, which seriously discussed the possibility of merger.

The emergence of electronics in the broad sense has, since that time, brought the two societies into more intimate juxtaposition. Typical is the growing preoccupation of both societies in the fields of surface and satellite communications, automatic control, computer techniques, magnetohydrodynamics and plasma physics (with its promise of nonrotating and more efficient power generation), solid-state physics, information theory, instrumentation, and a host of other new technical developments which are of common concern to both. Only merger of the two societies can avoid an ever larger scale duplication, overlap, and conflict since the membership of the two societies draw their strength in ever greater measure from the same basic scientific elements and the same educational backgrounds.

Therefore, the future of the radio, electrical and electronic professions would appear to be greatly benefited by synthesis of the two societies into a single institute.

For these reasons, the two Boards have felt that thorough exploration of a possible merger would be in the best interests of our members and of the profession.

The steps in this exploration have been as follows:

1) In January, 1961, Junior Past President Ronald L.

McFarlan, acting on my behalf, was invited to meet with the Board of AIEE in New York for discussion of mutual IRE-AIEE problems.

2) On March 20, 1961, the Board of IRE invited President Clarence Linder, AIEE, to join it at a luncheon where the mutual problems of IRE and AIEE and past history of attempts toward merger were discussed fully and frankly. At that meeting it became evident that while many mechanical problems of merger stood in the way, the professional interests of our membership should be the primary objective of closer cooperation.

3) At the Executive Committee meeting of April 27, 1961, I reported on a conversation which I had had with President-elect of AIEE Warren Chase, to explore IRE-AIEE cooperation. It was the consensus of the Executive Committee that I be authorized to appoint a suitable member of IRE to a committee, without limitations of scope, to discuss IRE-AIEE relations in conjunction with a suitably appointed delegate selected by AIEE. The Board of Directors of IRE, at their meeting the next day, April 28, concurred with the recommendation of the Executive Committee, whereupon, I appointed Dr. Patrick E. Haggerty as the IRE representative to that committee and the AIEE appointed Fellow Richard Teare.

4) Haggerty and Teare met in Pittsburgh, Pa., on May 21, 1961. During their discussion it became apparent that continued cooperation was becoming so complex to administer, and the danger of serious conflict was so rapidly increasing, that the possibilities of merger should be considered without delay. In the view of Haggerty and Teare the profession would be greatly strengthened by synthesis of AIEE and IRE into a single radio, electronic, and electrical engineering institute. They specifically recommended that Warren Chase and I appoint an *ad hoc* committee to explore this possibility more critically.

5) Upon this recommendation I acted to appoint P. E. Haggerty (now President-elect IRE) and Ron McFarlan (Junior Past President IRE) and Haraden Pratt (Secretary and Past President IRE), while President Warren Chase of AIEE appointed Clarence Linder (Junior Past President AIEE) and Richard Teare (Chairman AIEE Committee on Coordination). Chase and I served as *ex-officio* members.

6) This quasi-official Committee met in New York on September 13, 1961, to explore the problems of merger. The general recommendations were:

a) That in spite of mechanical problems, the professional advantages outweighed these problems, and that the two Institutes should move actively toward merger into a new professional society.

b) That the Committee should be voted authority by both Boards to draft statutes for a single society into which IRE and AIEE could be merged. These statutes could then be considered by the two Boards and, if satisfactory, referred to the membership of the two societies for adoption.

7) On October 18, 1961, and October 20, 1961, respectively, the IRE and AIEE Boards accepted the report. The Committee on formulation of plans for merger of AIEE and IRE into a single society has been activated with the membership shown in the resolution attached. Statutes and bylaws for eventual consideration by the Boards, publication and final action of the membership, will be drawn in the coming weeks.

As these plans have developed, I have consulted personally with many leaders and Section Chairmen of IRE. In the balance I have encountered a most favorable and enthusiastic response to the preliminary proposals. The feeling seems general that so much professional strength could be acquired by suitable action, that the mechanical problems should be appropriately solved in the interest of professional advantage.

I came away from the discussions of September 13, with the feeling that amalgamation could be accomplished without losing the vital aspects of IRE organization that have made it great. Both AIEE and IRE negotiators have approached the problem with a sense of statesmanship that would look to creation of a new institute having the best characteristics of both the IRE and the AIEE, at the same time dropping outmoded procedures. Both sides recognized that evolution of the profession requires changes from time to time that must be clearly foreseen, and undertaken promptly if the profession is to prosper.

I therefore ask you to discuss this whole matter in your next Section meeting, and advise me of your views before December 1, 1961, so that the drafting committee may have the benefit of your thinking.

Sincerely yours,

L. V. Berkner
President

RESOLUTION

WHEREAS, the Board of Directors of The Institute of Radio Engineers and the Board of Directors of the American Institute of Electrical Engineers have concluded that the advancement of the theory and practice of electrical and radio engineering, and the educational and scientific objectives of both Institutes, may be better served by a merger or consolidation of the two Institutes into one organization in which all present members would be included, and in which they would enjoy the same rights and privileges now conferred upon them

by their separate organizations, and it appearing that such consolidations would not affect the Institutes or their members, now therefore, be it

RESOLVED, that the Board of Directors of IRE deems it advisable, in accordance with the stated objectives of IRE, to move actively toward the consolidation of the activities and organization of IRE with those of the American Institute of Electrical Engineers (AIEE), by consolidation or otherwise, provided that the legal and operational problems incident to such consolidation can be satisfactorily resolved, and

FURTHER RESOLVED, that Lloyd V. Berkner, Patrick E. Haggerty, Ronald L. McFarlan, and Haraden Pratt, be and they hereby are appointed to join with Warren H. Chase, Clarence H. Linder, B. Richard Teare, Jr., and Elgin Robertson, when appointed by the Board of Directors of AIEE, as members of a committee, which shall be authorized and directed to undertake such studies as they shall deem necessary and appropriate to determine the feasibility, practicability and form of such consolidation, and to make a report thereon to the Boards of the two Institutes not later than February 15, 1962, with a view to submission to a vote of the memberships of the two Institutes, and consummation, if so approved, by January 1, 1963, and

FURTHER RESOLVED, that such committee shall be authorized to meet with the officers, directors and representatives of the two Institutes to consider the proposed amalgamation of the two groups and to make available to such persons such documents and information relating to IRE as such committee deems advisable under the circumstances, and

FURTHER RESOLVED, that this committee be directed to prepare, in consultation with representatives of IRE and AIEE, a proposed constitution and bylaws and such other documents as counsel may recommend, with a view to submission thereof to the Boards of Directors of the two Institutes on or before February 15, 1962, and

FURTHER RESOLVED, that the proper officers and directors of the Institute of Radio Engineers be and they hereby are authorized and directed to cause a copy of these resolutions to be delivered to the Board of Directors of the American Institute of Electrical Engineers, and

FURTHER RESOLVED, that these resolutions shall become effective as soon as the President of the Institute of Radio Engineers has been notified in form satisfactory to him and to counsel for the Institute of Radio Engineers that the Board of Directors of the American Institute of Electrical Engineers has adopted resolutions substantially to the effect of these presents.

Introduction to the Plasma Issue*

D. G. DOW†, MEMBER, IRE AND E. W. HEROLD‡, FELLOW, IRE
Guest Editors

THE study of the physics of ionized gases has had a long and complicated history. The word "plasma" was first coined by Langmuir and Tonks in 1929 to denote a gas in which an important fraction of the molecules are dissociated into ions and electrons, the gas as a whole remaining electrically neutral. The laboratory study of plasmas, of course, had been pursued long before that, many important discoveries in the realm of gas discharge phenomena having been made in the 1800's. These studies, continuing into the Twentieth Century as exemplified by the work of Langmuir, served as the foundation for many practical electronic devices used for the generation, rectification, and control of electrical energy. The plasmas used in these devices usually have a low-charge density, and the fractional ionization is ordinarily less than one per cent. This small percentage of ionization is sufficient to provide good electrical conductivity which can be controlled externally, but it is difficult to study theoretically because of the numerous competing processes involving neutral atoms, metastable atoms, ions, electrons, and collective oscillations of ions and electrons.

With the progress made in astronomy and theoretical physics in the early part of the Twentieth Century, it was realized that most of the matter in the Universe, that in the stars, exists in the fully ionized state. Thus, a new form of plasma physics evolved in which the study was largely theoretical, and was concerned with matter at immensely high temperatures and pressures, the latter being balanced by the gravitational forces of the stars. Much of the work currently of interest and many of the men of greatest stature in the field of plasma physics started in the field of astrophysics.

Recently the astrophysicists have tackled problems which are more earthbound, although hardly any less exotic. The advent of an understanding of thermonuclear fusion, and its possibilities for the generation of power, have created a great deal of activity concerned with high density, high temperature plasmas of terrestrial design. Since these cannot be confined by gravitational forces as they are in the stars, magnetic methods of confinement must be used, and a large amount of theoretical and experimental work has been conducted with an eye toward the generation and containment of hot dense plasmas by magnetic fields. In the U.S.A., this area of study began under the AEC-sponsored Sherwood project, which was originally highly classified, and thus developed a language and fraternity of its own before most of it was declassified in 1958.

A third group of investigators in the realm of plasma physics consists of those who were originally aerodynamicists. As airborne vehicles move faster and faster, their effect on the environment increases. One of the principle manifestations of this is the increasing temperature, eventually reaching a range in which appreciable ionization takes place, making the air conductive. The equations of gas dynamics are modified by this conductivity, and thus plasma physics is an important area of study for those in the missile and aircraft fields. In addition, the high temperatures which exist in rocket flames lead to appreciable ionization, and the conductivity of this material may be an important consideration. Recently, the desirability of extremely high velocity rocket exhaust has led to attempts to use electrically-accelerated particles for rocket propulsion.

Finally, we should discuss the field of radio propagation which has made important contributions to the understanding of plasmas and their interaction with electromagnetic radiation. It has long been recognized that portions of the earth's upper atmosphere are ionized enough to cause refraction and reflection of radio waves. The basis for much of the world's long range communication is the fact that the ionospheric layers will reflect radio signals with greater or lesser amounts of attenuation depending on the frequency, ion (and thus electron) density, and altitude (and thus the neutral density). In order to understand and make use of this phenomenon, many contributions had to be made to the understanding of the behavior of the ionosphere and the influence of a plasma on radio signals. Closely related to this has been a study of more recent origin which arises because of the high-speed aircraft and missile phenomena which concern the aerodynamicists. In spite of the plasma sheath surrounding these vehicles, we must communicate with them, and some interesting problems have been attacked, and system proposals have been evolved. The properties of this plasma sheath also result in some interesting radar return properties, with obvious military interest. (It should be noted that the word "sheath" in this context means the layer of plasma surrounding a a vehicle; much earlier, the word was used by Langmuir, and still is used by gas discharge physicists and engineers to denote the non-neutral layer which surrounds the plasma in a discharge. The reader should beware of this ambiguity.)

Plasma physics, then, might be divided up into four major disciplines, separated not so much by the concepts

* Received by the IRE, October 13, 1961.
† California Institute of Technology, Pasadena, Calif.
‡ Varian Associates, Palo Alto, Calif.

used as by their historical aims and the interests of those involved. These might be denoted by the following names: gas discharges, fusion plasma physics (including astrophysical applications), aerodynamical applications, and radio propagation plasma studies. As might be expected, this special issue of the PROCEEDINGS is aimed predominantly at the electronics engineer and emphasizes the fields most concerned with the communication and electronics arts, namely gas discharges and radio propagation. It has been our intention in laying out this issue to make it largely one in which the basic principles and known fundamentals of plasma physics are expounded as they apply to problems in these areas, without concentrating on specific devices and techniques. Wherever possible, the fundamentals are emphasized and detailed engineering concepts omitted. It is our hope that in this way an issue of reasonable size will communicate many of the basic ideas, and stimulate the reader's interest in some of the areas of plasma physics and its engineering applications.

With this background, let us scan this special issue on plasma physics.

Plasma Physics—An Elementary Review, (*Bachynski, p. 1751*). This paper summarizes most of the areas of current interest in plasma physics, and serves as a background article for almost all of the rest of the issue. The thermonuclear problem, astrophysics, propagation, noise, propulsion, and electronic devices are all treated in a form which allows the reader to grasp the basic concepts preparatory to reading the specialized articles.

Oscillations and Noise in Low-Pressure DC Discharges, (*Crawford and Kino, p. 1767*). All laboratory discharges seem to be plagued with an excess amount of low frequency noise, and in special cases, oscillation. In this paper the authors review the history of scientific investigation into this phenomenon, and present in a coherent package the bulk of present day knowledge about this noise as well as some tantalizing suggestions for controlling it. These phenomena take place in two different frequency ranges, the first generally below one megacycle and dominated in some manner by the ionic properties, and the second in the microwave range typically governed by the electron plasma frequency. The complete explanation of the source of either of these forms of noise is still lacking. However, much experimental data exists, and a qualitative picture has been presented which is consistent with the observations.

Ionic and Plasma Propulsion for Space Vehicles, (*Brewer, Currie, and Knechtli, p. 1789*). In their search for higher specific impulse (thrust per unit mass of propellant), rocket experts have turned to electrical acceleration of ions or plasmas as a potentially practical method for obtaining this objective. The engineering techniques required are an interesting mixture of electronics, power conversion, and astronautics. The authors of this paper present an outline of the basic principles underlying this line of approach, and follow with the basic system concepts appropriate to two somewhat different techniques, the ion engine in which ions are accelerated and then mixed with electrons to form a plasma, and the plasma rocket in which the neutral combination of ions and electrons is accelerated. A number of specific techniques are illustrated and the basic technological problems are presented. In this area, as with many space instrumentation problems, high efficiency, high-power electrical sources will be necessary for practical utilization of these techniques.

Transmission of Electromagnetic Waves Through an Ionized Layer in the Presence of a Strong Magnetic Field, (*Harley and Tyras, p. 1822*). This paper attacks the same problem, that is, the enhancement of propagation through a plasma by the use of a magnetic field. The plasma is approximated here by a succession of slabs so that the variations in density may be reasonably represented. A numerical calculation is given showing the transmission as a function of magnetic field for a specific model of density variation.

The Use of Magnetic Fields in the Elimination of the Re-Entry Radio Blackout, (*Hodara, p. 1825*). The effect of a plasma sheath on a re-entering space vehicle is to greatly reduce the high frequency propagation through this sheath. This paper discusses the technique of improving the communication with a space vehicle by imposing a magnetic field near the antenna which reduces the attenuation through the sheath.

RF Reflectance of Plasma Sheaths, (*Taylor, p. 1831*). As noted earlier, the plasma sheath about a re-entering space vehicle not only degrades the communication with it, but also changes markedly the radar return. This paper exhibits a calculation of the reflectance of a plane sheath which can be used as an approximation of the true sheath problem. The result is obtained in analytic form, in general as the ratio of two complex infinite series.

Mutual Coupling of Two Thin Infinitely-Long Slots Located on a Perfectly Conducting Plane in the Presence of a Uniform Plasma Layer, (*Yee, p. 1837*). The plasma sheath about a re-entering body is again considered, this time from a near-field point of view, in which the author considers the mutual coupling between two antennas located on the surface of the body. The result is expressed as a coupling coefficient between the two antennas. It is shown that the coupling is generally less than that which would exist in the absence of the plasma, provided the operating frequency is above the plasma frequency.

Antenna Noise Temperature in Plasma Environment, (*Bachynski, French, and Cloutier, p. 1846*). Again the reentry sheath is considered. In this paper, the authors are concerned with the degree to which the plasma itself contributes noise energy to the antenna. Since the sheath is at an extremely high temperature, even a small degree of coupling to the plasma may result in badly degraded noise performance. The analysis shows a peak in noise temperature in the vicinity of the plasma frequency, above which the noise is principally external, and below which it arises mostly in the vehicle. Because auxiliary

magnetic fields may also be used in these vehicles, the calculations have been extended to include the appropriate anisotropy. The noise then exhibits peaks at both plasma and cyclotron frequencies, but the structure is much more complicated, and general conclusions are harder to draw.

Generalized Appleton-Hartree Equation for any Degree of Ionization and Application to the Ionosphere, (*Shkarofsky, p. 1857*). This paper is motivated by the problems of ionospheric propagation, but may have much broader application. The author formulates the generalized equations for propagation of electromagnetic waves through a plasma, when the collisions result from both electron-neutral and electron-ion collisions in arbitrary mixtures. The analysis is compared with experimental results, and a proposal is made that ionospheric electron temperatures may be measured by correlating sufficient propagation data.

The Electrical Conductivity of a Partially Ionized Gas, (*Sengupta, p. 1872*). The problem of conductivity of a plasma is considered theoretically over the range where both electron-neutral, and electron ion collisions are important. Explicit expressions for both the real and imaginary parts of the conductivity are given in integral form. While these general forms are applicable to any degree of ionization, the author also presents expressions for the same quantities for the case that the plasma is fully ionized, in which case the conductivity may be expressed in terms of known transcendental functions.

Interaction of Microwaves in Gaseous Plasmas Immersed in Magnetic Fields, (*Rao, Verdeyen and Goldstein, p. 1887*). The 1930's saw the discovery of the Luxembourg effect, in which a strong radio transmitter passed its own modulating intelligence onto other signals whose propagation path passed over the region of the transmitter. Correctly explained as a nonlinear plasma effect (cross-modulation) in the ionosphere, the phenomenon has its modern counterpart and extension scaled down to laboratory size by use of microwaves. This paper covers basic studies of plasma characteristics in a strong 5 Gc/sec microwave field, using a weak sensing signal at 6 Gc/sec for the measurements. A magnetic field swept through cyclotron resonance is also used. The data are all taken in the inherently equilibrium state of the afterglow, using pulse techniques; thus, the rise in electron temperature due to absorption of power, and the changes in collision frequency, can be used for analytic comparison of the data with theory. Good qualitative agreement is found.

Frequency Conversion in a Microwave Plasma, (*Baird and Coleman, p. 1890*). Closely related to the above paper, is the present one in which plasma nonlinearity is used in a practical way to get microwave frequency multiplication and frequency mixing. The work indicates that the principal source of nonlinearity is modulation of the electron density at twice the drive frequency. Little or no magnetic field was used. In the experiments, a 9 Gc/sec high-level signal and 11 Gc/sec low-level signal produced a 20 Gc/sec output, about 25 to 30 db down; the same large conversion loss occurred for second harmonic generation. The values agree with those expected from this theory. Thus, the results are still rather far from useful, but it is expected that much higher power densities might improve matters.

A Plasma Microwave Detector, (*Taylor and Herskovitz, p. 1901*). In this paper, the authors describe a novel use of an activated plasma as a microwave detector. This is done in a most unusual way, by detecting the change in recombination radiation, as observed by a photomultiplier. It appears that the presence of microwaves changes the electron temperature slightly so as to reduce the recombination and to quench the light. Greatest sensitivity requires the low electron temperature of the afterglow equilibrium state. As little as a microwatt of input could be detected, which is rather remarkable even though it is considerably poorer than a video crystal. The authors point out that such a plasma detector is burn-out proof and has an extremely wide bandwidth. Several suggestions are proposed which might increase the sensitivity (with a reduction in bandwidth) but they have not yet been tried.

Interaction of a Modulated Electron Beam with a Plasma, (*Boyd, Gould, and Field, p. 1906*). There has been great interest in recent years in the use of electron-beams interacting with a gaseous plasma to produce microwave amplification. This paper describes the first successful experiments of a few years ago, in which the microwave modulation of an electron beam was increased by interaction with a "resonant" plasma. Later, traveling-wave amplification was achieved, by interaction with a slow propagating wave on the plasma column. These two different modes are compared and both theory and experiment are described. In the experiments, both helix coupling at 3 Gc/sec, and cavity coupling at 0.5 Gc/sec are employed. The observed gains of 7 db/cm in the plasma resonance case, though only half of the theoretical, are nevertheless significantly high. In the slow-wave case, about 0.8 db/cm is observed again well below theory. The discrepancies with theory are not unexpected because the theory assumes a uniform, loss-free plasma. Unfortunately, the present interactions are very noisy compared with conventional traveling-wave high-vacuum tubes.

A Method of Measurement of Flame Attenuation at 200 Mc, (*Biggs, p. 1917*). The first plasma ever produced by man on earth was the flame, *i.e.*, a gas ionized by its high temperature. Many years ago, the electrical conductivity of flame was studied, today it is once again of major importance in magnetohydrodynamic power generation or propulsion, and in missile trails. In the paper by Biggs, 200 Mc/sec measurements are described which can be used to obtain conductivity and dielectric constant of flames passing between a two-bar measuring line. Distilled water is used to calibrate, and theoretical curves are shown for electron densities ranging to 10^9 per cm^3.

Electrical Characteristics of a Penning Discharge, (*Helmer and Jepsen, p. 1920*). The Helmer and Jepsen paper concerns a most interesting type of magnetically-confined plasma known as the Penning discharge. Originally proposed as an ionization gauge, this discharge can take place at gas pressures as low as 10^{-12} mm of mercury, ordinarily considered an ultra-high vacuum. This type of discharge is the basis of the getter-ion vacuum pump. In this paper, it is shown that the trapping of electrons along the axis of symmetry is so effective that the axial potential is severely depressed. By a split anode structure, oscillations were obtained from the magnetron-like structure whose cathode is the space-charge cloud. With the normal anode, star-shaped sputtering patterns indicate that complex instabilities are present. Probably the most important result is the discovery that intense, nearly monochromatic, ion beams can be produced by such discharges.

Generation and Application of Highly Ionized Quiescent Cesium Plasma in Steady State, (*Wada and Knechtli, p. 1926*). This next paper covers work on the method of generating plasma which requires no electrical discharge. It has been known that highly ionized plasma can be generated by use of cesium vapor in the vicinity of a hot electron-emitting tantalum cathode. With two such plasma sources facing each other, and only a modest confining magnetic field, the authors show that plasma densities of 10^{12} per cm^3, and 90 per cent ionization, are obtained. This work is of importance in that such plasmas are basically quiescent, and need no applied electric field to maintain them. In practice, such plasmas are useful for physical measurements, in thermionic energy converters and in plasma sources for rocket propulsion.

A New Approach to Thermionic Energy Conversion, (*Bernstein and Knechtli, p. 1932*). The original work on high-efficiency thermionic energy converters used a self-generated cesium plasma resembling that described in the preceding paper. However, a low temperature electron emitter does not ordinarily release enough ionized cesium to make an efficient device. For a long time, workers have been trying to obtain an auxiliary source of ions which would not require too much energy to produce. In the Bernstein and Knechtli paper, such a source is described; while this work was going on, a similar concept was also explored independently in England. The structures devised appear to work well and to make a very important contribution to the low-temperature thermionic energy converter. In this paper, data on an argon plasma source are given; it is calculated that a 1500° K. cathode should be sufficient to provide an over-all efficiency of conversion of 25 per cent, if a sufficiently low work-function anode can be devised (*Editor's note:* a good low work-function anode is still a long way from realization). By modulating the plasma source, it should be possible to generate ac directly.

In concluding this Introduction, the *Editors* wish to thank the special group of reviewers who, although they must remain unnamed, are responsible for the selection of the papers, and much of the detailed editing of the papers.

Plasma Physics—An Elementary Review*

M. P. BACHYNSKI†, SENIOR MEMBER, IRE

Summary—**Although plasma phenomena have been observed in nature since the beginning of time, it is only in recent years that man has recognized the vast potential that plasmas hold for his future activities. One needs only to consider the scale of present day plasma physics experiments in order to realize the emphasis now being placed on the subject. At one extreme, there is the formation of artificial plasmas in nature such as in the Argus experiment and at the other is the study of microplasmas in tiny crystals of semiconducting material.**

This paper summarizes the role plasma physics is playing in present day scientific activities. A brief description is given of plasmas in nature, of the role of plasma physics in attempts at the ignition, control and diagnosis of thermonuclear fusion reactions, of the effect of plasmas on communication and telemetry from space and re-entry vehicles, of propulsion techniques (ionic, magneto-hydrodynamic, plasma) which utilize plasmas, and of the possibilities of incorporating plasmas in practical devices. In conclusion, the future prospects of plasma physics are outlined.

Introduction

LITTLE did prehistoric man realize, as he watched the sun, lightning discharges, the Aurora Borealis, or even his open fire, that he was observing plasma phenomena. Only in recent time has it become evident that the principal state of matter of the Universe is neither solid nor liquid nor gaseous, but plasma—a system including many free electrons and ionized atoms whose mutual interactions markedly affect its properties. This fourth state of matter probably comprises more than 99.9 per cent of the matter in our Universe.

Although an ideal plasma could readily be created in the laboratory many years ago in the form of a partially ionized gas, such investigations were not pursued very actively since the techniques for controlling a plasma were in a primitive state, and it appeared that they bore little relation to phenomena occurring on the earth. Consequently, the astrophysicists who realized the role played by ionized matter in Galactic processes were left unmolested in their ivory towers to make some of the earliest and most significant contributions to plasma physics. It remained for two very recent developments to give the necessary impetus to make plasma physics "fashionable." These were the successful creation of an uncontrolled thermonuclear fusion reaction in the form of the hydrogen bomb and the realization of large rocket thrusts which enabled vehicles to be propelled at hypersonic velocities and hence to open the door to the space age. The hydrogen bomb opened the search for techniques of controlling the thermonuclear fusion reaction for generation of electrical power on earth, while attempts to thrust further and further into space were confronted by communications and guidance problems involving plasma physics phenomena. Even the problem of propulsion in space itself has become a branch of the subject. As a result, plasma physics has become one of the most intensely investigated fields of science (see Fig. 1) with controlled experiments ranging in size from many earth diameters, such as the artificially formed plasmas in high-altitude nuclear explosions of the Argus experiment, to the minute microplasma of importance in tiny crystals of semiconducting material.

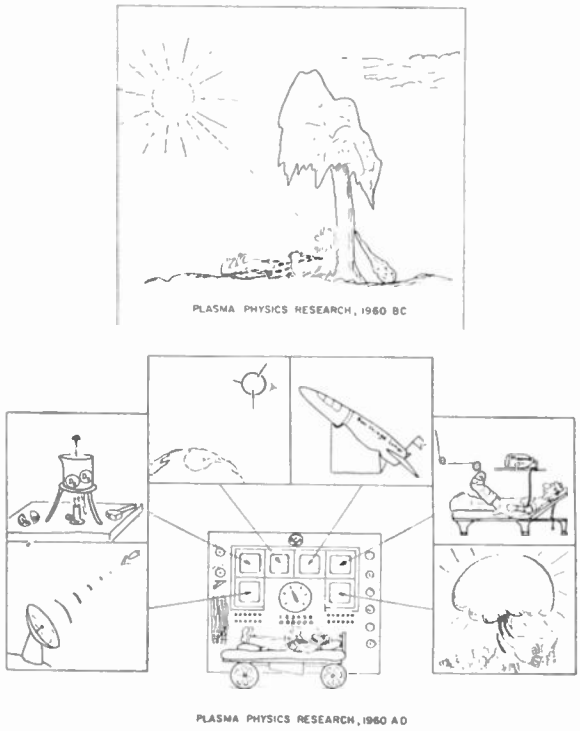

Fig. 1—(a) Plasma physics research, 1960 B.C.
(b) Plasma physics research, 1960 A.D.

This paper is intended as a short exposition of the role plasma physics is playing in present day scientific activities; of a number of the ideas presently being investigated and of some hopes for the future. A brief description is given of plasmas in nature, of plasma physics activities in attempts at control, ignition, and diagnosis of thermonuclear fusion reactions, of the interaction of electromagnetic waves with plasma and their effect on communications and on telemetry from space and re-entry vehicles, of plasma propulsion techniques, of the possible practical devices incorporating plasma properties, and of prospects for the future.

* Received by the IRE, August 14, 1961.
† Research Labs., RCA Victor Co., Ltd., Montreal, Can.

Plasmas in Nature

The Sun

The sun[1–3] and its activities, upon which the existence of life on earth fundamentally depends, is a plasma phenomenon. The visible part of the sun or the solar atmosphere can be considered to consist of three layers. The photosphere comprises the visible disk which is a few hundred kilometers thick. Present-day knowledge attributes an average particle density of $10^{16}/cm^3$ to this region with a free electron density of 10^{12} electrons/cm^3. The photosphere is thus a *plasma*. Surrounding the photosphere is a reddish ring approximately ten thousand kilometers thick above which flame-like prominences rise. This is the chromosphere, a very inhomogeneous region consisting principally of hydrogen, helium and calcium, which radiate energy due to electron-proton recombination and excitation of the light elements. Surrounding the chromosphere and extending millions of kilometers into space is a thin, hot atmosphere—the corona. The corona is very tenuous—stars are visible through it and comets traverse it unaltered. A steep temperature gradient extends from the chromosphere to the hotter corona where temperatures exceeding one million degrees exist (see Fig. 2). Although almost all

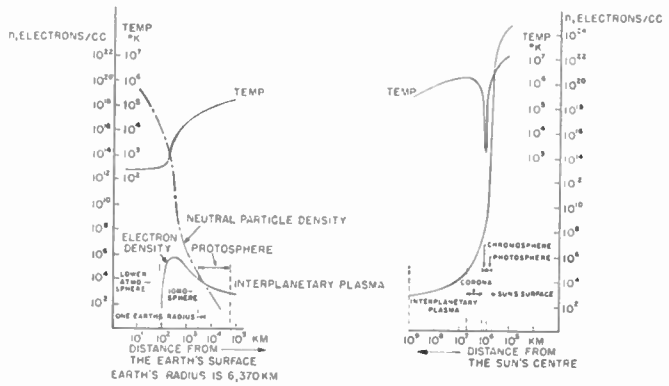

Fig. 2—Plasma between earth and sun.

known elements are seen in its spectrum, the presence of fully ionized hydrogen and helium ions is of prime significance.

It is now considered that the self-sustaining action of the sun is that of a huge thermonuclear device which releases energy by fusing together protons to form neutral helium atoms. The process can be written in short:

$$4p \rightarrow He^4 + 2e^+ + \text{energy (26.7 Mev)}.$$

This process proceeds at a slow rate establishing temperatures in the interior of the sun exceeding 20 million degrees. Due to the large mass of the sun, the force of gravity is sufficient to prevent the escape of all but the most energetic charged particles (plus radiation) from the hot plasma.

Plasma Phenomena Due to Sun's Radiation

As the ionizing radiation from the sun (principally ultraviolet and X-ray radiation) penetrates deeper and deeper into the atmosphere of the earth it encounters a larger and larger density of gas particles. As a result the radiation produces more and more electrons per unit volume. However, in this process the radiation is absorbed so that a position is reached where the rate of absorption of the radiation is greater than the rate of increase of the atmospheric density. Consequently, the rate of production of electrons decreases as one proceeds to lower altitudes. Hence there exists a height, which depends on the gas density gradient and the absorptivity of the radiation, where the rate of electron production is greatest. By this process, a great natural blanket of plasma, the ionosphere,[4–7] which envelopes the earth from an altitude of approximately 70 to over 300 kilometers, is produced. The various "layers" of the ionosphere (D, E, F in order of increasing altitude and also electron density) represent regions of ionization ranging from 10^1 to 10^6 electrons per cm^3, each merging into the next higher region without pronounced minima. An accurate, detailed explanation of the formation of the ionosphere is not yet available, although the gross features are readily accounted for.

In addition to the ionosphere, whose existence has been known for some time, recent satellite experiments have discovered other plasma effects due (at least in part) to radiation from the sun. These are the Van Allen radiation belts[8,9] (see Fig. 3) in which high-energy

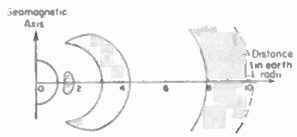

Fig. 3—Van Allen natural radiation zones.

charged particles (principally electrons and protons) are trapped in regions where they execute complicated trajectories which spiral to and fro along geomagnetic lines of force across the earth's equator and, at the same time, drift slowly around the earth. The net result is an

[1] G. P. Kuiper, Ed., "The Sun" ("The Solar System," vol. 1), University of Chicago Press, Chicago, Ill., and Cambridge University Press, Cambridge, Eng.; 1953.

[2] T. G. Cowling, "Nuclear reactions in stars," *Proc. Roy. Soc. (London) A*, vol. 260, pp. 170–174; Feb. 21, 1961.

[3] J. A. Ratcliffe, Ed., "Physics of the Upper Atmosphere," Academic Press, New York, N. Y.; 1960.

[4] "The Physics of the Ionosphere," The Physical Society, London, Eng.; 1955.

[5] Proc. IRE, Special Issue on the Ionosphere, vol. 47, pp. 131–323; February, 1959.

[6] "International Symposium on Fluid Mechanics in the Ionosphere," *J. Geophys. Res.*, vol. 62, pp. 2037–2238; December, 1959.

[7] "Symposium on the Exosphere and Upper F-Region," *J. Geophys. Res.*, vol. 65, pp. 2563–2636; September, 1960.

[8] J. A. Van Allen, "Radiation belts around the world," *Sci. Am.*, vol. 200, pp. 39–47; March, 1959.

[9] P. J. Kellogg, "Electrons of the Van Allen radiation," *J. Geophys. Res.*, vol. 65, pp. 2705–2713; September, 1960.

electric current associated with the belts which should slightly modify the magnetic field at the earth's surface. Particles can escape from the belts by collision with the atmosphere and recombination to form neutral particles. Due to this slow loss, the radiation regions are maintained only as a result of a continual replenishment of particles.

Completely different origins are attributed to the two radiation belts. (The data from U. S. satellite Pioneer V indicates a third radiation region[10] surrounding the earth at a distance of 8–10 earth radii.) The inner belt is ascribed to cosmic rays, which penetrate into the atmosphere forming proton-electron pairs which are "trapped" by the magnetic field of the earth and maintained in the belts. The outer belt is thought to be due to and maintained by streams of neutral plasma consisting mainly of protons and electrons which are ejected from time to time by the sun. This belt changes considerably in extent and intensity depending on the solar activity. These streams are considered to be ejected at very high velocities (1000 km/sec) so that the particles are confined by the magnetic fields associated with such intense electric currents.

Plasma Phenomena Resulting from Solar Disturbances

The emission of radiation and particles from the sun does not by any means proceed at a uniform rate. At times the chromosphere of the sun becomes turbulent and vortices (sunspots) appear. These sunspots reach a maximum (in number and size) about every 11 years. At the maximum the sunspots are found to be concentrated principally in one hemisphere of the sun, and, as the sunspot cycle proceeds, the spots decrease in number and intensity, move nearer the sun's equator and finally disappear at a time of sunspot minimum. These disturbances then proceed to break out again in the opposite solar hemisphere reaching a peak in another eleven-year period. The total sunspot cycle thus takes about 22 years to complete.

The result of the solar eruptions is an enhanced discharge of strongly electrified particles from the surface of the sun forming strong plasma whose fields and particles permeate interplanetary space. Simultaneously, intense ultraviolet and X-ray radiations are emitted which enhance the normal ionization of the earth's atmosphere. The streams of ejected particles travel into space and on occasion are intercepted by the earth. When this happens, about a day after the solar eruption, a *geomagnetic storm* resulting in sharp fluctuations in the strength and direction of the earth's magnetic field occurs. These streams of plasma are able to find their way into a circular zone around the geomagnetic poles (the auroral zone) where electric currents of millions of amperes are generated. This seriously distorts the normal magnetic fields around the polar regions, causing the incoming particles which produce auroras to spread further and further southward. Finally, the particles become trapped in the outer Van Allen radiation region forming a ring current about the equator which falls off slowly and in a few days attains its "normal" value.

At times of sunspot maxima, particularly violent solar eruptions with the projection of hot "fireballs" of material into space are also known. These explosions give rise to the arrival of energetic particles at the earth in about 1–4 hours after the event and long before the slower but more intense main stream of plasma. The density of particles is insufficient to distort the earth's magnetic field, but the particles enter into the polar cap following along the almost vertical magnetic field lines where they cause a prompt blackout of radio communications.

During the periods of sunspot maxima, observations of the solar-induced phenomena have been organized on an international scale. The International Geophysical Year (IGY) thus has been to a large extent devoted to a study of plasmas in nature.

Thermonuclear Plasma

The Thermonuclear Process

It is well known that the nucleus of any atom is composed of a number of protons and neutrons which are held together by strong binding forces and that, by modifying the atomic structure of certain nuclei, energy may be released. In one method, the energy arises from the splitting of *heavy* nuclei into lighter fragments. This process of fission creates a net energy yield due to the fact that the mass of the original nucleus is greater than the sum of the masses of the fragments after fission has occurred. An alternate method is the combination of certain *light* nuclei into heavier components whose mass is less than the sum of the masses of the original constituents. This is the fusion process.

Of the light elements, the two isotopes of hydrogen, deuterium (consisting of one proton and one neutron) and tritium (consisting of one proton and two neutrons) appear among the leading candidates as fuels for fusion reactions. (Hydrogen itself is not practical since its rate of fusion is much slower than either of its two isotopes under the same conditions.) Reactions of principal importance for these constituents are

$$D + D \begin{cases} \nearrow He^3 + n + 3.2 \text{ Mev} \\ \searrow T + p + 4.0 \text{ Mev} \end{cases},$$

$$D + T \rightarrow He^4 + n + 17.6 \text{ Mev}.$$

In each case, energy is released, and although this energy is appreciably less than that released in a fission reaction, the energy per unit mass of fuel is greater from fusion than from fission. Since deuterium occurs in na-

[10] L. V. Berkner, "Science in Space," Goldschmidt Memorial Lecture, XIIIth General Assembly of URSI, London, Eng.; September 6, 1960.

ture (about 1 part in 6000 of the most abundant element in our universe—hydrogen) and can be readily and inexpensively separated from hydrogen, it presents an almost inexhaustible supply of basic fuel for fusion.

The fundamental goal of thermonuclear research is the production of economic power from the controlled release of fusion energy.[11–14] In addition to the low cost and abundance of the fuel required, the fusion reaction holds the promise of being inherently safe in that there would be no possibility of "runaway" reactions. The fusion products are nonradioactive and hence present no disposal problems, and furthermore a controlled fusion device offers the possibility of direct generation of electric power by the elimination of the inefficient heat cycle.

For fusion to occur, the particles must approach sufficiently close to each other for long enough time that the short-range nuclear forces interact causing the nuclei to fuse. This is the so-called Thermonuclear reaction. Due to the positive charge on the nuclei, the particles tend to repel each other strongly. In order to overcome these Coulomb forces, the particles must be made to collide at high velocities corresponding to temperatures of the order of 10^8 °K (for a Maxwellian distribution of particle energies). At such temperatures, attainable only in gases, the gas is fully ionized consisting of ions and free electrons, *i.e.*, a *plasma*. Thermonuclear research is thus concerned with the confinement, heating, and diagnosis of very-high-temperature plasmas.

Confinement

One of the major requirements for thermonuclear fusion is a means to contain the hot plasma[15–18] in a given volume for a sufficient length of time such that an appreciable portion of the nuclei will fuse together. Solid material containers are of no value for this purpose due to the cooling effect on the plasma when it comes into contact with the walls and the consequent quenching of the reaction. It is thus necessary to use a force which acts at a distance, such as gravitational or electric or magnetic fields. For masses of the size encountered in laboratory experiments, gravitational forces are much too weak to be of practical use (although these are precisely the forces which are effective in confining the plasma particles in the sun and other large stellar masses). Static electric fields act in opposite directions on positive ions and electrons causing charge separation which creates opposing fields, making this method ineffective. The only plausible schemes are those involving magnetic fields (either static or slowly varying in time) and possibly combinations of RF electric fields and magnetic fields. Some of the suggested schemes of plasma confinement will now be discussed:

1) Pinch: This is one of the earliest schemes suggested for plasma confinement.[12,13,19,20] It is based on the principle that a current flowing in a conductor produces its own magnetic field which encircles the current [see Fig. 4(a)]. This magnetic field exerts an inwardly directed force which tends to constrict or "pinch" the conductor. A high-temperature plasma is a very good conductor (its resistance can be many times lower than that of copper), so that in the pinch confinement the current is made to flow in the plasma itself. As the current builds up, its associated magnetic field increases in strength and in turn pinches the plasma into a dense, hot region in the center of the container.

The pinch devices need not be linear in configuration. In fact, in order to eliminate end losses, one of the favorite configurations is the torus. ZETA, the British machine at Harwell, is an example of a toroidal pinch device.

Unfortunately, highly constricted columns of plasma are unstable against forces which distort its shape, and any initial disturbances tend to grow in amplitude so that the column rapidly disintegrates. It has been demonstrated that the presence of a longitudinal magnetic field within the plasma-current discharge has a stabilizing influence which inhibits the formation of small "kinks." In addition, theory predicts that external conducting shells may also assist in controlling the instabilities. A great deal of investigation still remains to be done on schemes of this type.

2) Magnetic Mirror: The use of a straight section of tube to contain a thermonuclear plasma requires some suitable technique for "stoppering" the ends of the container. One approach is to wind magnetic field coils about a straight section of tube so as to produce an axial magnetic field which is weak in the central region, but strong at the two ends [see Fig. 4(b)]. The strong fields at the ends tend to repel the charged particles of the plasma and hence tend to move them back towards the central region. These strong fields at the ends, which trap the particles[11–17] thus constitute the "magnetic mirrors."

The requirement for containment of plasma particles by a magnetic mirror is that the particle energy in the

[11] R. F. Post, "Controlled fusion research—an application of the physics of high temperature plasmas," PROC. IRE, vol. 45, pp. 134–160; February, 1957.

[12] "Controlled release of thermonuclear energy," *Nature*, vol. 20, pp. 217–223; January 25, 1958.

[13] Second U. N. Internatl. Conf. on the Peaceful Uses of Atomic Energy, vol. 31: "Theoretical and Experimental Aspects of Controlled Nuclear Fusion," vol. 32: "Controlled Fusion Devices," United Nations, Geneva, Switzerland; 1958.

[14] A. Simon, "An Introduction to Thermonuclear Research," Pergamon Press, New York, N. Y.; 1959.

[15] A. S. Bishop, "Project Sherwood—The U. S. Program in Controlled Fusion," Anchor Books, Doubleday & Co., Inc., New York, N. Y.; 1960.

[16] J. G. Linhart, "Plasma Physics," North-Holland Publishing Co., Amsterdam, The Netherlands; 1960.

[17] M. A. Leontovich, Ed., "Plasma Physics and the Problems of Controlled Thermonuclear Reactions," Pergamon Press, New York, N. Y., vols. 1–4; 1960.

[18] N. R. Nilsson, Ed., *Proc. 4th Internat. Conf. on Ionization Phenomena in Gases*, North-Holland Publishing Co., Amsterdam, The Netherlands, vols. 1, 2; 1960.

[19] R. Latham and J. A. Nation, "Report on linear pinch devices," *Nuclear Instr. and Methods*, vol. 4, pp. 261–272; June, 1959.

[20] R. J. Bickerton, "Brief review of the toroidal stabilized pinch," *Nuclear Instr. and Methods*, vol. 4, pp. 273–278; June, 1959.

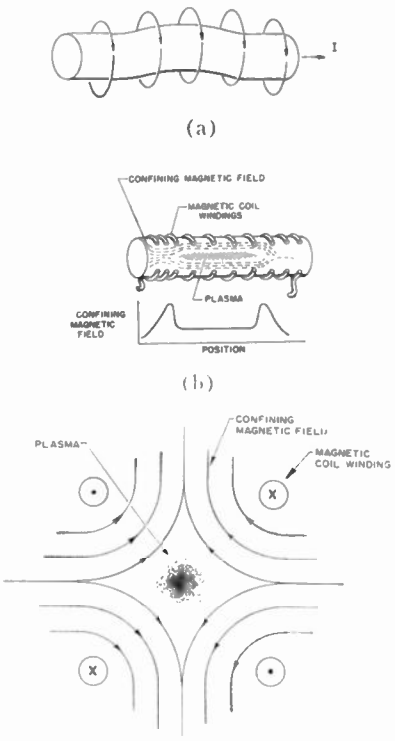

Fig. 4—(a) Pinch. A current in a column of plasma creates an encircling magnetic field which exerts an inward force on the charged plasma particles and hence "pinches" them to the center of the tube. The pinch effect unfortunately tends to be unstable. (b) Magnetic mirror. Current carrying coils are wound on a cylinder so as to produce strong magnetic fields at each end. The plasma can then be trapped between the two end "mirrors." (c) Cusp geometry. By suitable arrangement of magnetic field coils "cusp" configuration of confining magnetic fields is possible.

axial direction be small compared with its energy in the perpendicular direction. If the axial velocity of the particle is too great, the mirror fields will not turn the particle back, and hence it will escape. This creates the problem of how the particles should be injected so that trapping by the mirrors will occur. Suggested schemes include the injection of beams of low-energy ions which are given large perpendicular accelerations by RF electric fields as they pass slowly through the central mirror region, thus giving them sufficient transverse energy to be trapped. A second scheme is to inject a beam of high-energy neutral atoms as molecules and break these up as they pass through the confinement volume, thus providing a means for continuous re-injection of energetic particles.

A second problem is that the above-mentioned anisotropies in the velocity-space required for containment of the plasma in a mirror machine can give rise to instabilities. These instabilities are of two types; one is due to unstable electrostatic plasma oscillations which grow at the expense of the electron energy and the second to unstable hydromagnetic disturbances which cause the confining field to become "rippled" and to fluctuate rapidly, which in turn gives rise to enhanced diffusion of particles across the field.

The use of mirror machines is thus not without its problems, and considerable investigations are yet to be made.

3) Other Schemes: Other schemes for the containment of thermonuclear plasmas include the Stellarator,[21] which uses a magnetic field parallel to the axis of a toroidal tube and is produced by external currents flowing in solenoidal windings encircling the plasma. The confining fields are such that the magnetic lines of force generate not a single circle but an entire complex helical or toroidal surface suitable for the trapping of plasma particles. Some of the stability problems of the Stellarator are similar to those of the toroidal pinch, although the much smaller currents in the plasma interact less violently with the confining fields.

Another approach is based on the idea that, as a result of the gyroscopic action, a rotating plasma may be stable. In this "homopolar" device,[15] the application of radial electric and transverse magnetic fields causes the plasma particles to precess about a central axis, creating a centrifugal force which tends to keep the particles away from the axis and trap them in regions of magnetic field which have been caused to "bulge" by the rotating plasma.

Studies of magnetic confinement indicate that magnetic configurations with lines of force curving away from the plasma should be stable while those curving towards the plasma tend to be unstable. This suggests that configurations in which the magnetic lines of force curve everywhere away from the plasma might be stable. Such a scheme is the picket fence or cusp geometry shown in Fig. 4(c). There exists, of course, the problem of "stoppering" the regions of weak confinement. One idea is to use RF electric fields which are nonlinear in space and thus create a net force on the particles which inhibits their escape.[22–24] (Some consideration has been given to complete systems using RF gradient fields, however, the required power appears excessive compared to other techniques.)

A further idea has been to start from the high-energy side, that is, with a beam of particles having energies greater than those needed for thermonuclear reactions and by injecting and trapping them in a confined region to build up to densities which would sustain the thermonuclear reactions. To achieve this it is necessary to inject a high-energy beam of particles into a strong magnetic field and to dissociate the particles before they come out.

Many other schemes have been proposed and are under investigation.

[21] L. Spitzer, Jr., "The Stellarator Concept," *Phys. of Fluids*, vol. 1, pp. 253–264; July–August, 1958.
[22] H. A. H. Boot and R. B. R. S. Harvie, "Charged particles in a non-uniform radio-frequency field," *Nature*, vol. 180, p. 1187; November 3, 1957.
[23] H. A. H. Boot, *et al.*, "Containment of a fully ionized plasma by radio-frequency fields," *J. Electronics Control*, vol. 4, pp. 434–453; May, 1958.
[24] T. W. Johnston, "Time-averaged effects on charged particles in ac fields," *RCA Rev.*, vol. 21, pp. 570–610; December, 1960.

Heating

A crucial requirement for any thermonuclear machine is the means to heat the plasma to the required high temperatures[11-18] of one hundred million degrees or more. Of the several methods for heating the plasma, the simplest is the ohmic or Joule heating by the currents in the plasma which produce the confining fields. At high temperatures, the power input per unit volume becomes small due to the high conductivity of the plasma, so that interparticle collisions must occur to provide any Joule heating. The collisions, however, tend to diffuse the azimuthal confining fields and the axial stabilizing field into each other. Thus, the Joule heating requirements and those for stability are contradictory.

Another method of heating the plasma (used in mirror machines) is that of "adiabatic compression." In this technique the magnetic field strength of the entire mirror configuration is made to increase with time. Thus, particles (ions and electrons) injected into the machine at times of low field strength will increase their transverse energy as the magnetic field is increased, while their axial energy will remain the same. In fact, it turns out that the increase in transverse energy of the particles is directly proportional to the increase in magnetic field strength.

A plasma can also be heated by pulsing the axial confining field so as to produce an oscillating electric field which encircles the axis of the tube. This induced electric field can increase the energy of the gyrating charged particles. Such a method is aptly called "magnetic pumping." The magnetic pumping technique is particularly effective if the confining field is pulsed at the cyclotron frequency of the positive ions. This is due to the interaction between the oscillating electric field and the gyrating positive particles which move in the same direction and with the same velocity as the electric field so that resonance coupling is possible.

Of importance in the thermonuclear reaction is any process which might cause more energy to leave the reaction than is created and hence cool the plasma. Under the assumption of perfect containment, the basic energy loss is due to bremsstrahlung—radiation from the plasma itself due to deflection (through collision) of the rapidly moving charged particles. If the system is to be self-sustaining, the generated power within the plasma must exceed the radiated power. This occurs above a certain critical temperature, the so-called "ignition temperature." For the D-D reaction, this critical temperature is of the order of 4×10^{8}°K. A second form of radiation loss from the plasma which may be important is synchrotron radiation due to the radial acceleration of particles in a magnetic field.

In addition to the radiation losses from the plasma, particle losses will occur. There will always be a number of particles, particularly electrons, in the high-energy tail of the velocity distribution of particles in the plasma. These electrons are too energetic to be contained by the normal confining field strength and constitute "runaways."

Diagnostics

Since thermonuclear plasma research is in a highly exploratory state, a great number of techniques are necessary to diagnose[13,17] what is actually happening. These constitute such a variety of methods that most experimentalists in physics would be able to recognize at least some techniques with which they are familiar. No attempt will be made to give an exhaustive account of the possible approaches, but the number of different disciplines which can contribute to furthering the knowledge of thermonuclear plasmas will be indicated.

Visual diagnostics such as fluorescent screens and photographic methods are of value in obtaining qualitative information. Fluorescent screens have been used to determine the location of the plasma, ion orbit size and approximate density measurements. The same information can be obtained with fast-shutter photography, while streak photography enables a display of the time history of the position and light intensity of the plasma.

Spectrographic techniques have yielded much quantitative data, such as determination of the ion velocity distribution from Doppler and Stark broadening of the spectral lines, spectral line identification of the plasma species and impurities and determination of electron temperatures by measurement of the intensity ratio of the spectral lines of ionized and neutral species of the plasma. In addition, X-ray energy analysis has been applied to measurement of the radiation emitted from the hot plasma.

Direct current probe techniques have been used with moderate success (the major difficulty being that probes severely perturb the plasma) to obtain indications of electron temperature, ion and electron densities and distribution profiles. Current loops and probes are of value for plotting contours of magnetic field and current distributions. Considerable interest has been shown in solid-state probes based on the Hall effect for similar purposes.

RF techniques have proven extremely useful, since transmission of microwaves through the plasma yields information on the plasma electron density, while a measure of the intensity of RF energy emitted from a plasma yields the kinetic electron temperature. Furthermore, resonance absorption at certain RF frequencies can be used for ion identification since the gyrofrequency of a specific ion depends on its charge to mass ratio. The use of HF radio techniques in plasma diagnostics has in turn stimulated research on the generation of higher and higher frequency coherent EM energy.

Infrared measurements as thermonuclear diagnostics have been limited, due to the slow time response of most long-wavelength I-R detectors. As the time constant of these detectors continues to be improved with the advent of new semiconductor materials and techniques, their utility in such studies will gain prominence.

Many techniques first introduced in nuclear particle physics are of great value. Among these are the determination of temperature and velocity of runaway electrons by use of graded absorbers in front of scintillation counters and similar studies employing nuclear emulsion plates and the use of neutron counters for detecting neutrons, which should arise out of the thermonuclear process, but more usually are formed far too prematurely as a result of acceleration mechanisms, such as instabilities.

Of course, the true criterion of a thermonuclear reaction is to measure more energy being created by the plasma than is being put into the plasma. In the course of achieving this no doubt many byproducts will come to pass which may be of nearly as great importance as the final goal.

Of the numerous experimental approaches under investigation, none is in a position to achieve the "ignition" temperatures where the input energy begins to equal the energy generated. Before this is possible, a tremendous amount of basic knowledge of plasma properties is still required. These investigations point only to further clarification of the severe stability requirements, of the important energy loss mechanisms, of the necessary containment times, the techniques of heating and diagnosing plasma and many other problems. All the different approaches are studies of plasma physics necessary to build up the fundamental behavior of plasmas over the widest possible range of conditions. This is being achieved by the use of many relatively small-scale experiments devised to test crucial limitations and novel ideas in addition to the large machines, which create conditions approaching those in a genuine thermonuclear reaction.

Communications and Plasma Physics

Electromagnetic Wave Interaction with Plasmas

The interest in electromagnetic wave interaction with plasmas is many fold. First, there is the direct application to communication techniques. Secondly, there is the information which can be derived from a knowledge of such interaction. This is the basis for numerous fundamental studies in physics, diagnostic techniques, and in this same category can be included the effects on radar return. In addition, the effect of the plasma environment on the performance of a given system must be considered.

The interaction of an electromagnetic wave with a plasma can be described in terms of a number of "bulk" parameters of the plasma. These parameters in turn depend upon the basic particle interactions. The degree of ionization of the gas or mixture of gases comprising the plasma determines the "electron density" or number of electrons (the most important constituent) contained within the plasma. The interaction of these electrons with neutral atoms, ions, and with each other determines the "collision frequency" of the plasma constituents, *i.e.*, a measure of the average number of collisions an electron undergoes per unit time. Complicating factors are that the collisions can be elastic or inelastic, the electron can be interacting with several particles simultaneously and the nature of the interacting forces is different for electron-neutral particle interaction than for electron-ion or electron-electron collisions. The electron density, collision frequency and external forces determine the "conductivity" (and in turn the current density) of a plasma. For slightly ionized plasmas, the conductivity is almost exclusively due to the more mobile electrons. However, at high degrees of ionization, the ion conductivity becomes of importance. From a knowledge of the time and spatial variation of these quantities (electron density, collision frequency, conductivity), electromagnetic wave interaction with a plasma can, at least in principle, be deduced.

A fundamental quantity which enters into a discussion of the properties of a plasma, particularly when electromagnetic wave interaction is concerned, is the plasma frequency. The plasma frequency (ω_p) for electrons in a plasma, regarding the ions as stationary motionless points is defined as

$$\omega_p = (ne^2/\epsilon_0 m)^{1/2},$$

where

n = the electron number density per unit volume
e = the charge on the electron
m = the mass of the electron
ϵ_0 = the permittivity of free space.

Although the plasma frequency enters into most considerations as a convenient "lumped parameter" having the dimensions of frequency, it also is an inherent property of a plasma. If, in an infinite plasma, a small number of electrons are displaced from their equilibrium position, a restoring space charge field is created which, if the displacing force is suddenly removed, causes the electrons to oscillate about their equilibrium at a frequency proportional to the plasma frequency.

The electromagnetic properties of a plasma[25–28] change markedly depending upon whether the angular frequency of the electromagnetic wave is greater or less than the plasma frequency. For RF frequencies above the plasma frequency, a plasma behaves more or less like a dielectric, the lossiness of which is determined by the collision frequency. At frequencies well below the plasma frequency, the plasma acts like a very good conductor, while at frequencies around the plasma fre-

[25] J. A. Ratcliffe, "The Magneto-Ionic Theory and its Application to the Ionosphere," Cambridge University Press, Cambridge, Eng.; 1958.

[26] B. N. Gershmann, *et al.*, "Propagation of electromagnetic waves in a plasma (ionosphere)," *Upsekhi Fiz. Nauk*, vol. 61, pp. 561–612; 1957. (Translation: AEC-tr-3493.)

[27] L. Smullen, "Interaction between plasmas and electromagnetic fields," *J. Res. NBS*, vol. 64D, pp. 766–767; November/December, 1960.

[28] M. P. Bachynski, *et al.*, "Plasmas and the Electromagnetic Field," McGraw-Hill Book Co., New York, N. Y.; in press.

quency, cutoff or very high attenuation and reflection occurs so that the wave cannot penetrate to any great depth into the plasma.

A plot of the typical variation of the penetration depth of an incident electromagnetic wave into a given plasma with RF frequency is shown in Fig. 5. The effect of increasing electron density is to depress the entire variation, particularly in the dielectric region. Increasing the collision frequency has no effect in the cutoff region, but in the conducting region it increases the depth to which an EM wave can penetrate while it decreases the penetration depth in the dielectric region.

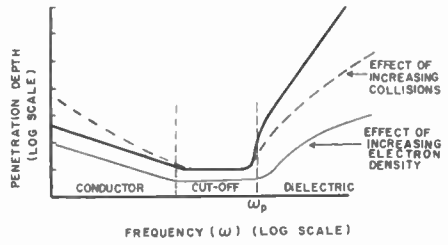

Fig. 5—Variation of depth of penetration of an electromagnetic wave into a plasma. At low frequencies the plasma acts as a conductor, while at high frequencies its behavior is similar to a dielectric. A cutoff region for the electromagnetic waves exists when $\omega \approx \omega_p$.

In the presence of a steady magnetic field, the electromagnetic properties of a plasma are drastically modified. In this case, the plasma behaves as a doubly refracting medium and exhibits band-pass characteristics. That is, for certain frequency ranges, depending upon the plasma properties and the strength and direction of the magnetic field relative to the incident wave, the plasma is transparent to radio waves, while in other frequency ranges it is opaque. This means that for specific conditions, radio energy at frequencies well below the plasma frequency can penetrate through the plasma.

Further electromagnetic wave-plasma phenomena of considerable interest occur when the effects of electron gradients are considered. These nonlinearities in the distribution of the electron density arise as a result of thermal currents in the plasma and give rise to longitudinal waves which travel at very low velocities (some as low as the sound velocity) in the plasma. Thus, the plasma can support a pressure wave in addition to the transverse electromagnetic wave. In most instances, the pressure and electromagnetic waves are coupled, and energy can be transferred from one type of wave motion into the other.

Communications and Natural Plasmas

The fact that an ionized region acts as a conductor and hence is a good reflector for incident radio waves of frequency below the plasma frequency has been utilized for communications for some time. Thus, the *ionosphere* is a naturally occurring plasma, and long-distance communication over the earth via reflection from the ionosphere is feasible for frequencies less than a critical frequency[5] (which depends on angle of incidence as well as the electron density). At these frequencies, the radio energy will be almost totally redirected (reflected) down towards the earth again. This is the basis of the so-called "sky-wave" in modern radio communications. Extensive exploration of the ionosphere has also been carried out by "radio soundings" in which a variable-frequency radio signal is directed at the ionosphere and the reflected wave observed until a frequency is found above which the signal penetrates into the ionosphere, and the reflected wave is appreciably reduced. If the electron density of the ionosphere changes, this critical frequency changes. In this manner, it has been possible to determine the stratification of the ionosphere by virtue of the differing electron densities of the various layers. Fortunately, the electron density is greater in the layers at higher altitudes so that frequencies can be found which penetrate the lower layers but are still reflected by the higher regions of the ionosphere.

The newer communication techniques which use meteor trails are based on the same principles.[29–31] A meteor re-entering the earth's atmosphere creates a column of ionization due to impact on the atmosphere and to ablation of the meteor material. When the electron density is sufficiently large, this cylinder of plasma reflects incident radio energy. The trails are transient phenomena since, due to diffusion, the electron density soon decreases below the critical value for reflection of the electromagnetic energy.

An electromagnetic wave traveling in an ionized region may, under certain circumstances, interact with a second wave in such a way that a modulation imposed on one of the waves becomes transferred to the other. To produce this crossmodulation or *Luxembourg effect*[32–37] (so-called because it was first observed from radio station Luxembourg), a nonlinear medium is required, and the absorption of energy from radio waves by an ionized region provides the necessary nonlinearity. If now another wave (the interacting wave) is absorbed in the same region, the energy from it will in-

[29] P. A. Forsyth and E. L. Vogan, "Forward scattering of radio waves by meteor trails," *Canad. J. Phys.*, vol. 33, pp. 176–188; May, 1955.

[30] P. A. Forsyth, *et al.*, "The principles of JANET—a meteor burst communication system," PROC. IRE, 45, vol. pp. 1642–1657; December, 1957.

[31] R. J. Carpenter, and G. R. Ochs, "The NBS meteor burst communication system," IRE TRANS. ON COMMUNICATIONS SYSTEMS, vol. CS-7, pp. 263–271; December, 1959.

[32] B. D. Tellegen, *Nature*, vol. 131, p. 840; 1933.

[33] G. W. O. Howe, "Accurate measurements of the Luxembourg effect," *Wireless Engr.*, vol. 15, p. 187; April, 1938.

[34] L. G. H. Huxley, "Ionospheric cross-modulation at oblique incidence," *Proc. Roy. Soc.*, vol. A200, p. 486; 1950.

[35] V. L. Ginsburg and A. V. Gurevich, "Non-linear phenomena in a plasma located in an alternating electromagnetic field," *Upsekhi Fiz. Nauk*, vol. 70, pp. 201–246; February, 1960, pp. 393–428; March, 1960.

[36] F. H. Hibberd, "Ionospheric self-interaction of radio waves," *J. Atmos. Terr. Phys.*, vol. 6, pp. 268–279; May, 1955.

[37] V. L. Ginzburg, "Non-linear interaction of radio waves propagating in a plasma," *Zh. Eksp. Teo. Fiz.*, vol. 35, pp. 1573–1575; December, 1958.

crease the velocity of the electrons and hence the frequency of their collisions with the net result that the wanted wave will be more strongly absorbed. Thus in the presence of the interacting wave, the wanted wave will become weaker. If the amplitude of the interacting wave is varied, the velocity of the electrons will follow, and the absorption of the wanted wave will also vary. In this way, the modulation of the interacting wave becomes superimposed on the wanted wave.

Due to the doubly refracting nature of the plasma in a magnetic field, a further effect occurs when radio waves are propagated in a plasma in the direction of the magnetic field lines. This is a rotation of the plane of polarization of the wave, namely *Faraday rotation*. Communication systems whose signals must pass through the ionosphere, for instance, suffer from this effect.

The band-pass behavior of the plasma in the presence of a dc magnetic field discussed earlier, explains "whistler" propagation.[38,39] These decreasing-frequency audio whistles observed by radio means are the result of LF electromagnetic energy being generated by natural lightning discharges and propagating from one earth hemisphere along the magnetic lines of force of the earth to the conjugate positions of their origin in the opposite hemisphere.

At low radio frequencies, the ions in the plasma profoundly affect the electromagnetic characteristics of the plasma.[40,41] As a result, the band-pass structure of the plasma is modified with electromagnetic wave propagation now being possible at very low frequencies. These LF EM waves are the classic *magnetohydrodynamic* or *Alfven* waves[42] that propagate at a velocity which is often nine orders of magnitude less than the velocity of light. Such magnetohydrodynamic waves have been detected both in the laboratory and during the high-altitude nuclear detonations of the Argus experiments[43–45] of 1958.

The Plasma Sheath

A space vehicle moving at hypersonic velocities within a planetary atmosphere will be surrounded by a shock-induced envelope of ionized gas (Fig. 6). This layer of

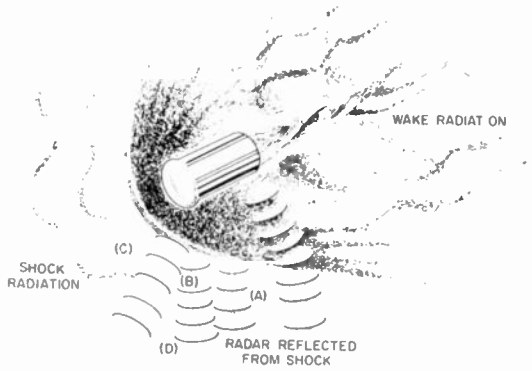

Fig. 6—A plasma sheath surrounds a hypersonic space vehicle as it re-enters the atmosphere.

ionized gas or "plasma sheath" can have a profound influence on communications and telemetry to and from the vehicle[46,47] and can also seriously alter the radar reflecting characteristics of the vehicle and hence its radar detectability.

The effect of the plasma sheath on communications is to attenuate the signal severely and markedly degrade the antenna performance.[48] At typical re-entry velocities for missiles and space vehicles, the signal attenuation is sufficient to cause "blackout," except at extremely high microwave frequencies. For a manned re-entry vehicle which descends slowly in altitude, the plasma sheath ionization can persist over a large part of its flight path. This makes it extremely difficult to guide and control such vehicles from the ground by means of telemetered signals. The same difficulties apply to information transmitted from space probes and other scientific data measurements. Consequently, it is very important to understand the plasma phenomena created on re-entry in order to select the optimum system requirements.

Of great importance for defense applications is knowledge of the behavior of the radar scattering cross sections of ballistic missiles at launch and during re-entry caused by the ionized sheaths and trails of the vehicles. In general, the plasma sheath enhances the scattering cross sections, but under specific conditions, the scattering properties can even be reduced.

Basically, the above phenomena involve the interaction of electromagnetic waves and plasmas. This is, however, only part of the story, since to specify the plasma properties and the plasma geometry at any time, a detailed knowledge of aerophysics for determining the shock front configuration and related aerodynamic flow fields and flow rates is required.[49] These factors, in turn,

[38] L. R. O. Storey, "An investigation of whistling atmospherics," *Phil. Trans. Roy. Soc. (London) A*, vol. 246, pp. 113–141; July, 1953.

[39] R. M. Gallet and R. A. Helliwell, "Origin of 'very-low-frequency' emissions," *J. Res. NBS*, vol. 63D, pp. 21–27; July/August, 1959.

[40] C. O. Hines, "Heavy-ion effects in audio frequency radio propagation," *J. Atmos. Terr. Phys.*, vol. 11, no. 1, pp. 36–42; 1958.

[41] R. E. Barrington and T. Nishizaki, "The hydrogen ion effect in whistler dispersion," *Canad. J. Phys.*, vol. 38, pp. 1642–1652; December, 1960.

[42] A. Alven, "Cosmical Electrodynamics," Oxford University Press, Oxford, Eng.; 1950.

[43] N. C. Christofilos, "The Argus experiment," *J. Geophys. Res.*, vol. 64, pp. 869–875; August, 1959.

[44] P. Newman, "Optical, electromagnetic and satellite observations of high-altitude nuclear detonations: part 1," *J. Geophys. Res.*, vol. 64, pp. 923–933; August, 1959.

[45] A. M. Peterson, "Optical, electromagnetic and satellite observations of high-altitude nuclear detonations: part 2," *J. Geophys. Res.*, vol. 64, pp. 933–938; August, 1959.

[46] M. P. Bachynski, *et al.*, "Electromagnetic properties of high-temperature air," PROC. IRE, vol. 48, pp. 347–356; March, 1960.

[47] A. V. Phelps, "Propagation constants for electromagnetic waves in weakly ionized, dry air," *J. Appl. Phys.*, vol. 31, pp. 1723–1729; October, 1960.

[48] J. W. Marini, "Radiation and admittance of an insulated slotted-sphere antenna surrounded by a strongly ionized plasma sheath," *J. Res. NBS*, vol. 64D, pp. 525–532; September/October, 1960.

[49] W. Rotman and G. Meltz, Eds., "Electromagnetic Effects of Re-Entry," Pergamon Press, New York, N. Y.; 1960.

depend upon the environment in which the body is moving and hence upon upper atmospheric physics as well as depending on the atomic processes of particle interaction in the plasma, dissociation, ionization rates and products, etc. This is, indeed, a formidable problem.

Plasma sheath phenomena have been reported associated with orbiting satellites.[50-56] It is speculated, with some experimental evidence, that due to space charge which may build up on the satellite, a cloud of ions could be projected in front of the satellite. This plasma cloud is thought to be sufficiently dense to reflect HF (megacycle) radio waves at times of intense solar activity. More quantitative measurements are neces ary before the existence of this effect can be proven.

Atmospheric Breakdown

Gas "breakdown" or gas "discharge" in a given region occurs when the number of electrons being created by ionization is equal to or exceeds the number of electrons which are lost through diffusion, recombination and attachment. In the breakdown process,[57-62] the residual electrons in the gas gain sufficient energy from the RF electric fields to cause primary ionization by collision with the neutral constituents. Initially, since there are few electrons, the ionizing collisions are infrequent, but as the number of electrons created increases, an avalanche process is initiated until breakdown occurs. At high pressures, the mean free time between collisions of the electrons is small compared to the RF period so that the electron does not have time to gain much energy before collision. At low pressures, the time between collisions is long so that in the interval the electron gains sufficient energy from the RF fields to cause an ionizing collision. At extremely low pressures, there are few particles for the electrons to collide with, so an optimum pressure exists at which a minimum voltage is required for breakdown.

Thus the electric field strength required to break down a gas at low pressure is, in general, less than that required at atmospheric pressure. As a consequence, even low-power antennas on a high-altitude vehicle may be susceptible to voltage breakdown.[59,62] The effect on the antenna performance when voltage breakdown occurs is to alter the radiation pattern of the antenna, lower the total power radiated, change the pulse shape of the radiated power and modify the input impedance of the device. When the number density of electrons in the discharge is such that the plasma frequency exceeds the RF frequency, little transmission and considerable mismatch will occur.

Direct application of breakdown theories to antenna-voltage breakdown characteristics are difficult due to the complex fields which exist near the antenna and which vary with the antenna configuration. The effect of pulse shape, pulse repetition rate (since electrons may be left in the gas in front of an antenna due to the previous pulse), and peak powers under varying conditions before breakdown occurs are yet not fully understood. The environmental conditions of a space vehicle complicate the problem due to the questionable validity of concepts such as diffusion length at high altitudes, the unknown effects on breakdown of air turbulence, plasma sheaths, etc., around the vehicle and the effects of preionized regions such as the ionosphere in which large initial electron densities exist through which the vehicle must pass.

Plasma Noise

As a result of the interaction between electrons, ions and neutral molecules in a plasma, electromagnetic energy is generated and emitted by the plasma.[63] This emission of "passive" radiation from the plasma can be due to a variety of physical processes such as: bremsstrahlung—the deceleration of particles due to an atomic encounter; the release of energy during recombination of an electron-ion pair; or Cerenkov radiation from the "bow wave" formed when particle velocities exceed the velocity of light in the medium or unstable plasma oscillations arising from gradients of electron density which exist in nonuniform plasmas. The radiated energy is in general noncoherent, varying over a wide continuous spectrum of frequencies and thus appears principally as a noise signal.

This noise can impose limitations on the sensitivity of an antenna receiving system by raising the noise level of the environment in which the transmitting and receiving system operates and hence defeating the advantages

[50] A. Flambard and M. Reysat, "Electromagnetic waves and satellites: echoes from ionized trails of satellies at high frequency," *Onde Elect.*, vol. 38, pp. 830–837; December, 1958.
[51] C. R. Roberts and P. H. Kirchner, "Radio reflections from satellite-produced ionization," PROC. IRE, vol. 47, pp. 1156–1157; June, 1959.
[52] D. B. Beard and F. S. Johnson, "Charge and magnetic field interaction with satellites," *J. Geophys. Res.*, vol. 65, pp. 1–7; January, 1960.
[53] S. Rand, "Wake of a satellite traversing the ionosphere," *Phys. of Fluids*, vol. 3, pp. 265–273; March/April, 1960.
[54] J. D. Krauss, *et al.*, "The satellite ionization phenomenon," PROC. IRE, vol. 48, pp. 672–678; April, 1960.
[55] J. D. Krauss, "Evidence of satellite-induced ionization effects between hemispheres," PROC. IRE, vol. 48, pp. 1913–1914; November, 1960.
[56] J. D. Krauss and R. C. Higgy, "The relation of the satellite ionization phenomena to the radiation belts," PROC. IRE, vol. 48, pp. 2027–2028; December, 1960.
[57] L. Gould and L. W. Roberts, "Breakdown of air at microwave frequencies," *J. Appl. Phys.*, vol. 27, pp. 1162–1170; October, 1956.
[58] A. D. MacDonald, "High-frequency breakdown in air at high altitudes," PROC. IRE, vol. 47, pp. 436–441; March, 1959.
[59] J. B. Chown, *et al.*, "Voltage breakdown characteristics of microwave antennas," PROC. IRE, vol. 47, pp. 1331–1337; August, 1959.
[60] P. M. Platzmann and E. H. Solt, "Microwave breakdown of air in non-uniform electric fields," *Phys. Rev.*, vol. 119, pp. 1143–1149; August 15, 1960.
[61] D. Kelly and H. Margenau, "High frequency breakdown of air," *J. Appl. Phys.*, vol. 31, pp. 1617–1620; September, 1960.
[62] W. E. Scharfman and T. Morita, "Voltage breakdown of antennas at high altitude," PROC. IRE, vol. 48, pp .1881–1887; November, 1960.
[63] G. Bekefi and J. L. Hershfield, "Incident microwave radiation from plasmas," *Phys. Rev.*, vol. 116, pp. 1051–1056; December 1, 1959.

gained in using masers, parametric amplifiers and other low noise receiving devices. The "noise" radiated from a plasma is not, in all cases, necessarily a detrimental effect such as it is in communications. Thus if the spectral distribution of the emitted energy is characteristic of the plasma properties, a measurement of the microwave radiation provides specific information on the plasma. As an example, knowledge of the radiated power gives a measure of the electron temperature in the plasma, and this has been used as a powerful diagnostic technique. Further investigations have been focused on the microwave radiation from plasmas produced by hypervelocity bodies in the hope of providing a means for detection and discrimination of such vehicles as they enter the atmosphere.

A major difficulty in the above-mentioned applications is an understanding of the fundamental processes. For a plasma in a steady state, macroscopic radiative transfer concepts without detailed knowledge of the atomic processes can be applied and the emission spectrum determined from the electromagnetic wave absorption, transmission and reflection properties of the plasma. These determinations are complicated by the nonuniformity and geometrical configuration of the emitting plasma. However, most practical plasmas of interest are not in equilibrium, and as yet a considerable amount of theoretical work remains to be done on nonequilibrium radiation. Furthermore, few reliable quantitative measurements are available to guide the theoretical work.

Plasma Propulsion

General Rocket Considerations

After a vehicle has been placed out of the reach of strong gravitational forces into a low satellite orbit by conventional means (*e.g.*, a chemical rocket), there no longer exists a need for a high-thrust device. One then can look towards more novel methods for reducing the cost of propelling large payloads in space. The use of electrical propulsion techniques for this purpose greatly increases the size of the payload that can be projected into larger orbits.

To show that this is the case, consider some fundamental system parameters of a rocket.[64] The basic parameters are the specific impulse (defined as thrust in weight units/propellant mass flow rate) whose units are seconds and the thrust (in weight units) per unit weight which is a dimensionless parameter. For a rocket to take off from a planet, the thrust per unit weight of the rocket must be greater than one. However, in regions where the forces of gravity are small, even small values of thrust/weight may be useful. In a chemical rocket, the thrust power is limited to the specific energy content within the chemical propellant so that the highest specific impulse possible is desired. In electrical propulsion however, the source of the power and the working fluid are completely separate, hence the optimum specific impulse is not necessarily the greatest one. Thus the source of power increases with increasing specific impulse, and the propellant or working fluid decreases with increasing specific impulse with an optimum specific impulse when the sum weight of the propellant and power plant (*i.e.*, vehicle) is minimized. For operations within the influence of the earth's gravitational field, such as a complete round trip of a lunar mission or the establishment of a communications satellite in a "stationary" 24-hour orbit at a height of 22,500 miles, the optimum specific impulse required ranges from 1500 to 5000 seconds. For interplanetary flights, a specific impulse of 7500 to 20,000 seconds is desirable.

These values of specific impulse are beyond the limit of the energy of conventional rocket propellents so that new methods are required. In Fig. 7 are illustrated the limit of thrust per unit weight and specific impulse of chemical rockets and the regions of operation of some of the devices to be discussed in the sequel.

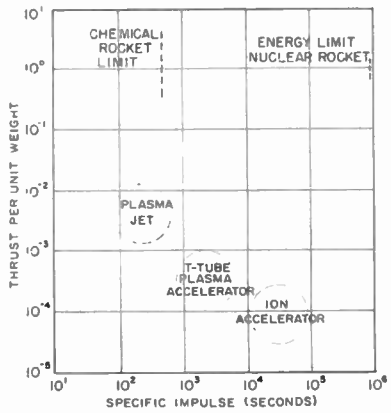

Fig. 7—General rocket characteristics of some plasma propulsion devices.

Electrostatic or Ion Propulsion

One technique for attaining a large specific impulse is to electrostatically accelerate a beam of charged particles and expel them at very high velocities.[65–68] In this manner, it may be possible to design a low-thrust system suitable for space flight. In its simplest form, an ionic rocket would consist of an ion source to supply the "fuel" and an electrostatic accelerator or gun to accelerate the ions, the ejection of the ions from the device corresponding to the mass flow from an ordinary rocket.

[64] H. S. Seifert, Ed., "Space Technology," John Wiley and Sons, Inc., New York, N. Y.; 1959.

[65] E. Stuhlinger and R. Seitz, "Some problems in ionic propulsion systems," IRE Trans. on Military Electronics, vol. MIL-3, pp. 27–33; April, 1959.

[66] F. Hecht, Ed., *Proc. 10th Internatl. Astronautical Congr.*, London, Eng., 1959, Springer-Verlag, Vienna, Austria, vols. 1 and 2; 1960.

[67] S. W. Kash, "A comparison of ion and plasma propulsion," Proc. IRE, vol. 48, pp. 458–465; April, 1960.

[68] F. I. Ordway, Ed., "Advances in Space Science," Academic Press, New York, N. Y., vol. 2; 1960.

Considerable thought has gone into a choice of fuel for an ionic rocket. The basic requirements are that the ion source yield an ion of sufficient mass (to give an appreciable thrust) and at the expense of a minimum amount of power. Most present experimentation has been with the contact-ionization type of ion source using vapors of alkali metals as the "fuel." In this technique, cesium or rubidium, which have very low ionization potentials, are passed through regions of incandescent tungsten (which has a higher work function than either cesium or rubidium). The alkali atoms readily lose their valence electrons to the tungsten and nearly 100 per cent ionization can be achieved.

A more serious problem in the development of ion rockets is the space charge limitation upon the maximum current densities which can be obtained for a particular accelerating voltage, electrode configuration and propellant. Practical current densities which have been achieved at accelerating voltages below 10 kv are of the order of 12 ma/cm^2 for cesium.

Since ion bombardment can cause serious electrode erosion, secondary-electron emission and impact heating, it is necessary to focus the ion beam to overcome the beam spread resulting from the space charge repulsion of the charged ions. To obtain collimated beams, cylindrical-beam and converging-beam Pierce Gun accelerating systems have been studied.

In order to preserve the electrical neutrality of the ion rocket and to prevent space charge from building up behind the ship and hence inhibiting the ejection of ions, it is necessary to neutralize the "exhaust" of the ion rocket. To achieve space charge neutrality, particles of the opposite charge must be introduced into the exhaust. The entire ensemble, consisting of negative and positive particles and hopefully neutrals due to recombination, is electrically neutral, so in effect, it is a *plasma*. One technique of neutralizing is to inject electrons into the positive-ion beam from electron emitters located around the perimeter of the beam. The electrons are attracted into the ion beam by the space charge fields in the unneutralized portion of the beam and oscillate through the beam, thus giving some degree of neutralization to the ion beam. Since the mass of the electron is a small fraction of the ion mass, an ejection of electrons would make a negligible contribution to the net thrust and is therefore useful solely in an attempt to attain charge neutrality. A further suggestion for an ion rocket which may overcome the charge neutralization problem is to have the rocket composed of ion diodes, each alternately accelerating positive and *negative* ions. The exhaust of such a system would be electrically neutral, and furthermore, if a suitable negative ion of comparable mass to the positive ion were known, then the over-all thrust of the system could be doubled. The difficulty is, of course, in obtaining a suitable negative ion source. Such a dual ion device is illustrated in Fig. 8.

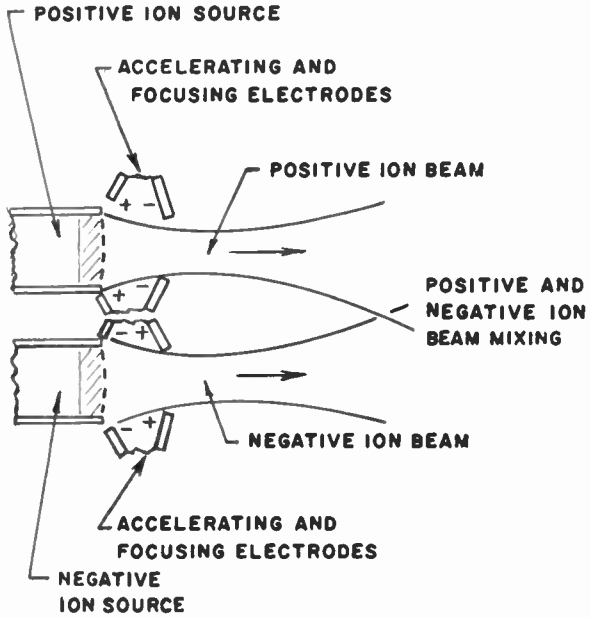

Fig. 8—Positive and negative ion accelerators to achieve space charge neutrality in exhaust of an ion rocket system.

Other charged masses such as colloidal suspensions, dust particles and heavy molecules have been suggested as possible fuel for an ionic propulsion system and are currently being investigated.

Neutral Plasma or Magnetohydrodynamic Propulsion

High specific impulse devices are possible using a partially or fully ionized gas (*i.e.*, a plasma) as the propellant[69–71] in which the ion and electron densities are essentially neutral. Such a device is not affected by the space charge limitations of the ion rocket. Since the plasma is an electrically conducting fluid, electromagnetic fields can be used to interact with it in order to heat the plasma to higher temperatures or to accelerate it to high velocities. Electromagnetic fields can transfer energy to a plasma by two basic methods, namely, Joule heating which increases the thermal energy of the plasma and by the interaction of the plasma current with the magnetic field which creates a force accelerating the plasma and hence increases the energy of motion of the plasma. The manner in which this force interacts with the plasma is strongly dependent on the geometry of the apparatus and on the plasma properties, and is the basis for a number of schemes for plasma propulsion devices.

The plasma arc jet is an example of a device in which a plasma is used to Joule heat a gas. In the plasma jet,

[69] M. Alperin and G. P. Sutton, Eds., *Proc. Symp. on Advanced Propulsion Systems*, Los Angeles, 1957, Pergamon Press, New York, N. Y.; 1959.

[70] M. Camrac, *et al.*, "Plasma propulsion devices for space flight," IRE TRANS. ON MILITARY ELECTRONICS, vol. MIL-3, pp. 34–41; April, 1959.

[71] W. Rayle, "Plasma propulsion possibilities," IRE TRANS. ON MILITARY ELECTRONICS, vol. MIL-3, pp. 42–45; April, 1959.

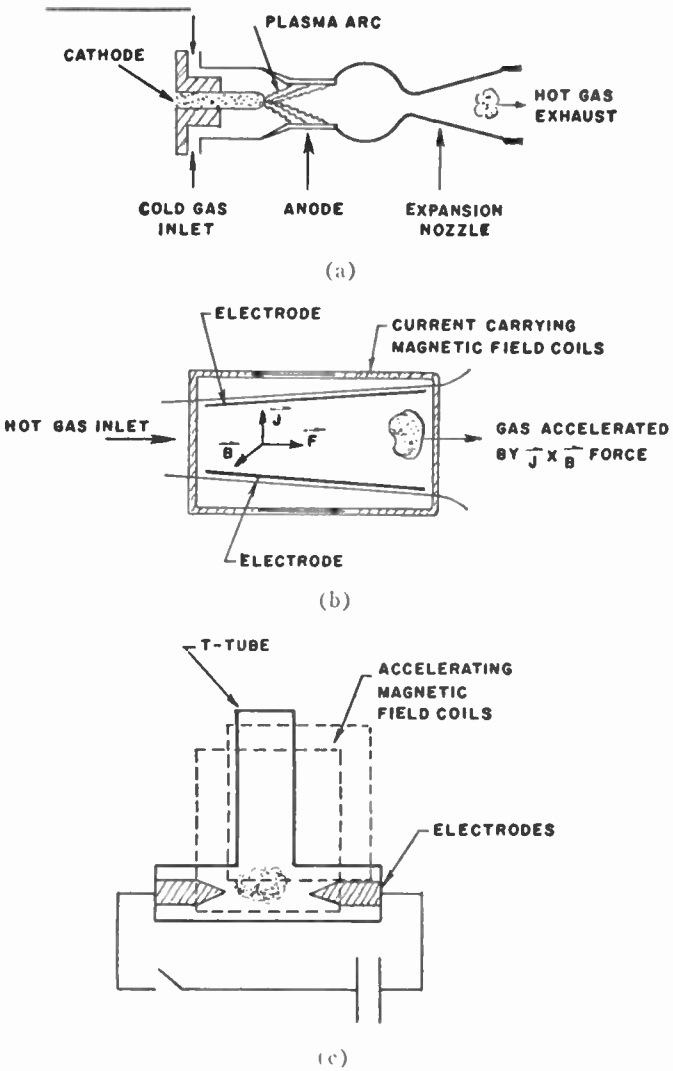

Fig. 9—(a) Plasma jet. A plasma arc is used to heat a gas to high temperatures. The gas is then passed through an expansion nozzle and forms a high velocity exhaust. (b) MHD accelerator. In the magnetohydrodynamic accelerator an ionized gas is passed through crossed electric and magnetic fields which accelerate this plasma. (c) T tube accelerator. In the T tube, the energy stored in a capacitor bank is discharged into a gas creating a plasma which is accelerated up the stem of the T using magnetic fields.

a dc voltage is applied between the operating electrodes [see Fig. 9(a)] causing a breakdown of the gas in the chamber. The propelled gas is then forced through this electric arc and is heated upon passing through the arc. After heating, the hot gas is expanded in a conventional nozzle. The limitation of specific impulse in the plasma jet is caused by the inability to recover the energy expended on dissociation and ionization of the gas as it passes through the arc. Unless recombination occurs before the gas is expelled from the nozzle, this energy will not appear as kinetic energy of the gas flow and hence is lost.

A device which minimizes the above losses can be made by accelerating a preheated gas using magnetic fields. In this scheme [Fig. 9(b)], a hot gas (~3000°K) is passed into the acceleration chamber where electric currents are caused to flow through the plasma in a given direction. A magnetic field permeates the plasma in a direction normal to the electric current. The action of the current and the magnetic field creates a $J \times B$ (where J is the current density, B the magnetic field) force which accelerates the plasma in a direction perpendicular to both the magnetic field and the electric current.

Considerable experimentation has been performed with the T tube [Fig. 9(c)] in which the gas is highly ionized by passing a large current through the head of the T and then accelerating the plasma up the stem of the tube using magnetic fields. Further sophistication of this device is to use additional magnetic fields orientated along the stem of the T which act as magnetic nozzles increasing the velocity of the plasma and furthermore keeping it away from the walls of the tube to prevent cooling and erosion. In this manner, specific impulses up to 5000 seconds are possible.

Techniques have been developed on a laboratory scale whereby donut-shaped "blobs" of plasma or plasmoids[72,73] can be projected by magnetic forces at speeds exceeding 10^7 cm/sec. Such a plasma gun constitutes another possible means of propulsion.

As the interaction between magnetic fields and plasmas becomes better understood, a greater and greater number of novel propulsion techniques[74,75] will be suggested, and some of these will inevitably prove to be practical.

Plasma Devices

Pre-Plasma-Era Devices

Many years before the full importance of plasmas in the field of science was realized, devices employing plasma were in operation. These devices, of course, did not require a detailed understanding of plasma properties and included the fluorescent lamp, noise sources for the calibration of radio receiving devices and as laboratory standards and transmit-receive tubes for radar applications. The fluorescent lamp, for example, is just a gaseous discharge plasma whose light emission is used to activate the fluorescent material coating of the light tube. Most noise sources for laboratory calibrations are also gaseous discharges operating well below the plasma frequency in the "opaque region." In radar systems, on the other hand, it is necessary to have a switch to disconnect the receiver from the transmission line during the transmitted pulse and to disconnect the transmitter the rest of the time. Such a switch can be obtained

[72] W. H. Bostick, "Experimental study of ionized matter projected across a magnetic field," *Phys. Rev.*, vol. 104, pp. 292–299; October, 15, 1956.

[73] W. H. Bostick, "Experimental study of plasmoids," *Phys. Rev.*, vol. 106, pp. 404–412; May 1, 1957.

[74] M. M. Klein and K. A. Brueckner, "Plasma propulsion by a rapidly varying magnetic field," *J. Appl. Phys.*, vol. 31, pp. 1437–1448; August, 1960.

[75] G. A. Askaryan, "Acceleration of charged particles in travelling or standing electromagnetic waves," *Zh. Eksp. Teor. Fiz.*, vol. 36, pp. 619–621; February, 1959.

using appropriately connected spark gaps which "break down" during transmission and act as a low-impedance device, while normally they are high-impedance open circuits. The T-R tube is merely a sophisticated spark gap which operates at lower voltages (since the gas in the tube is at low pressure) and whose properties are not affected by external environment conditions such as humidity and temperature.

In addition, many important vacuum tube devices of long standing used for rectification and regulation purposes have utilized plasma in their operation. Among these can be listed the ignition, the mercury vapor rectifier and even the common voltage regular tube.

Microwave Devices

Promising applications of the properties of plasmas appear in the field of guidance and generation of high RF energy. Since a column of plasma will support the propagation of various field configurations of electromagnetic waves,[76–80] a considerable effort is presently being devoted to an understanding of "plasma waveguides." The waveguide is the basic component of the microwave system, and its characteristics will determine and limit the other microwave devices which are possible. Since a plasma waveguide exhibits specific mode and band-pass characteristics (which can be controlled by external magnetic fields), waveguide filters are obvious applications. An electromagnetic wave traveling down a plasma column will have its phase and amplitude altered, depending on the plasma properties and configuration and prototype attenuators,[81] and phase shifters have been built in several laboratories. Plasma properties can also be used for waveguide switching.[82–85] In addition, since plasmas exhibit interesting properties such as the Faraday effect, polarization characteristics, double refraction and nonlinearity, they present a host of phenomena that can be utilized for circuit and microwave applications.

It has been demonstrated that slow electromagnetic waves can propagate in a plasma cylinder in the presence of a dc magnetic field. As a consequence, intense investigations are being made in attempts to utilize a plasma[86–92] as the slow-wave structure of traveling-wave tubes. In this manner, the characteristics of the slow-wave structure can be altered externally by changing the plasma properties. By using modulated electron beams[93,94] passing through a plasma, a growth of the modulation has been observed. This has stimulated interest in the possibility of obtaining microwave amplification by such techniques. A diagram of such an electron beam-plasma interaction amplifier is shown in Fig. 10. Suggestions have been put forth in which the nonlinear effects of a plasma at high power levels is utilized as the nonlinear propagating medium of a parametric amplifier. The generation of millimeter waves by plasma techniques, such as high-intensity arcs and harmonic generation where the plasma provides the nonlinearity, excitation of coherent plasma oscillations and their conversions to short wavelength radio waves, etc., is another field of great interest[95–100] and current importance.

In a gaseous discharge (plasma) system, it is possible for metastable states of a given atom to be used as car-

[76] L. D. Smullin and P. Chorney, "Propagation in ion-loaded waveguides," *Proc. Symp. on Electronic Waveguides*, pp. 229–248; April, 1958.

[77] A. W. Trivelpiece and R. W. Gould, "Space charge waves in cylindrical plasma columns," *J. Appl. Phys.*, vol. 30, pp. 1784–1793; November, 1959.

[78] V. B. Fainberg and M. F. Gorbatenko, "Electromagnetic waves in a plasma situated in a magnetic field," *J. Tech. Phys. (USSR)*, vol. 29, pp. 549–562; May, 1959.

[79] V. E. Golant and A. P. Zhilinski, "Propagation of electromagnetic waves through waveguides filled with plasma," *Soviet Tech. Phys.*, vol. 5, pp. 12–21; July, 1960.

[80] L. Goldstein, "Non-reciprocal E-M wave propagation in ionized gaseous media," IRE TRANS. ON MICROWAVE THEORY & TECHNIQUES, vol. MTT-6, pp. 19–29; January, 1958.

[81] P. D. Lomer and R. M. O'Brien, "A microwave pulsed attenuator using an RF excited discharge," *Proc. IEE*, vol. 105, pt. B, suppl. No. 10, pp. 500–504; 1958.

[82] S. J. Tetenbaum and R. M. Hill, "High power magnetic field controlled microwave gas discharge switches," IRE TRANS. ON MICROWAVE THEORY AND TECHNIQUES, vol. MTT-7, pp. 73–82; January, 1959.

[83] R. S. Braden, "A new concept in microwave gas switching elements," IRE TRANS. ON ELECTRON DEVICES, vol. ED-7, pp. 54–59; January, 1960

[84] D. W. Downton and P. D. Lomer, "A pre-TR tube for high mean power duplexing," IRE TRANS. ON MICROWAVE THEORY AND TECHNIQUES, vol. MTT-8, pp. 654–659; November, 1960.

[85] R. M. Hill and S. K. Ichiki, "Microwave switching with low-pressure arc discharge," IRE TRANS. ON MICROWAVE THEORY AND TECHNIQUES, vol. MTT-8, pp. 628–632; November, 1960.

[86] E. V. Bogdanov, *et al.*, "Interaction between an electron stream and plasma," *Proc. Symp. on Millimeter Waves*, Brooklyn Polytechnic Press, Brooklyn, N. Y., pp. 57–72; April, 1959.

[87] G. S. Kino, "A proposed millimetre-wave generator," *Proc. Symp. on Millimeter Waves*, Brooklyn Polytechnic Press, Brooklyn, N. Y., pp. 233–248; April, 1959.

J. R. Baird and P. D. Coleman, "High power gas discharge frequency multiplier," *Proc. Symp. on Millimeter Waves*, Brooklyn Polytechnic Press, Brooklyn, N. Y., pp. 289–300; April, 1959.

[88] Z. S. Tchernov, "Interaction of E-M waves and electron beams with centrifugal electrostatic focusing," *Proc. Symp. on Electronic Waveguides*, Brooklyn Polytechnic Press, Brooklyn, N. Y., pp. 339–344; April, 1959.

[89] A. Javan, "Possibility of production of negative temperature in a gas discharge," *Phys. Rev. Lett.*, vol. 3, pp. 87–89; July 15, 1959.

[90] W. O. Schumann, "The backward wave in a metal waveguide filled with longitudinally magnetized plasma," *Z. Angew. Phys.*, vol. 11, pp. 333–335; September, 1959.

[91] J. M. Anderson, "Possible low-noise electron beam plasma amplifier," *J. Appl. Phys.*, vol. 30, pp. 1624–1625; October, 1959.

[92] G. S. Kino, "Parametric amplifier theory for plasmas and electron beams," *J. Appl. Phys.*, vol. 31, pp. 1449–1458; August, 1960.

[93] G. D. Boyd and L. M. Field, "Excitation of plasma oscillations and growing plasma waves," *Phys. Rev.*, vol. 109, pp. 1393–1394; February 15, 1958.

[94] G. D. Boyd, *et al.*, "Interaction between an electron stream and an arc discharge plasma," *Proc. Symp. on Electronic Waveguides*, Brooklyn Polytechnic Press, Brooklyn, N. Y., pp. 367–378; April, 1958.

[95] K. D. Froome, "A new microwave harmonic generator," *Nature*, vol. 184, p. 808; September 12, 1959.

[96] R. M. Hill and S. J. Tetenbaum, "Harmonic generation in a cyclotron resonant plasma," *J. Appl. Phys.*, vol. 30, pp. 1610–1611; October, 1959.

[97] N. R. Bierrum and D. Walsh, "Harmonics from a microwave gas discharge," *J. Electronics Control*, vol. 8, pp. 81–90; February, 1960.

[98] N. R. Bierrum, *et al.*, "Coherence and bandwidth of a gas discharge harmonic generator," *Nature*, vol. 186, p. 626; May 21, 1960.

[99] K. D. Froome, "Millimetre waves from mercury arc harmonic generator," *Nature*, vol. 186, p. 959; June 18, 1960.

[100] J. M. Anderson, "Microwave detection and harmonic generation by Langmuir-type probes in plasmas," PROC. IRE, vol. 48, pp. 1662–1663; September, 1960.

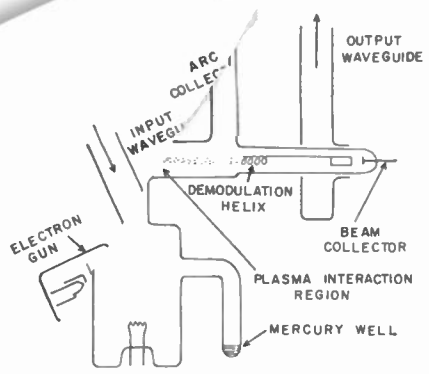

...lectron beam-plasma interaction amplifier. (From Boyd and Field.[93])

...ers of energy to excite specific quantum energy levels of another atom.[101] If the excitation cross section for this process is large, then a "population inversion" or excess of atoms in this excited state will occur. This is precisely the condition required for maser action, and the successful operation of such a quantum plasma device producing maser oscillations at optical frequencies has been achieved recently.[102]

Further schemes have been put forth whereby the ion sheaths surrounding hypersonic re-entry vehicles would be utilized as coherent radiative elements and hence as a plasma antenna. However, considerably more work is still required in this direction. Other novel applications of plasma are also in progress.[103–107]

Electric Power Generation

If a dc magnetic field is applied in a direction perpendicular to a moving conducting fluid, an electric field is generated in a direction normal to both the magnetic field and the fluid flow. If now electrodes connected to an external load are appropriately placed, the electric field will cause a current to flow in the external circuit (as well as in the plasma). Energy is transferred to the load at the expense of the kinetic energy of directed motion of the conducting fluid. This is the basis of the dc magnetohydrodynamic generator.[108,109] The advantages of such magnetohydrodynamic (MHD) devices are that no moving parts, only a moving fluid, is required. The difficulties include characteristics of the working fluid (ionization and dissociation potentials, heat transfer properties), the methods of achieving adequate flow velocities, geometry, contamination and corrosion problems. MHD generators have been proposed for ac power generation[110] as well. These devices can be either pulsed or steady-state.

A plasma device for the conversion of heat into electricity is the thermionic diode[111–124] in which some of the electrons liberated from the cathode have sufficient energy to overcome the internal work function of the cathode and proceed to the anode where they lose their kinetic and potential energy. If the resulting energy level of the electrons in the anode is more negative than the original energy level at the cathode, then the device is capable of driving a current through a load and hence do useful work by this conversion of heat into electricity. The most serious limitation of such a scheme is the space charge of electrons which builds up near the anode and which inhibits electrons emitted from the cathode from reaching the anode. One technique of overcoming the space charge problem is to introduce cesium vapor into the device, which, upon contact with the hot anode, becomes a positive cesium ion and hence tends to neutralize the negative electron space charge. Other suggested schemes for controlling the charge effects include the use of a grid as a third control element and the use of crossed electromagnetic fields. Considerably more study is required on anode work functions

[101] A. Javan, in "Quantum Electronics," C. H. Townes, Ed., Columbia University Press, New York, N. Y.; 1960.
[102] A. Javan, *et al.*, "Population inversion and continuous optical maser oscillation in a gas discharge containing a He-Ne mixture," *Phys. Rev. Lett.*, vol. 6, pp. 106–109; February 1, 1961.
[103] W. Schmidt, "The microwave plasma burner," *Electron. Rundschau*, vol. 13, pp. 404–406; November, 1959.
[104] J. M. Anderson and L. A. Harris, "Negative-glow plasma as a cathode for electron tubes," *J. Appl. Phys.*, vol. 31, pp. 1463–1468; August, 1960.
[105] H. W. Lewis and J. R. Reitz, "Efficiency of the plasma thermocouple," *J. Appl. Phys.*, vol. 31, pp. 723–727; April, 1960.
[106] H. W. Lewis and J. R. Reitz, "Open-circuit voltages in the plasma thermocouple," *J. Appl. Phys.*, vol. 30, pp. 1838–1839; November, 1959.
[107] R. W. Pidd, *et al.*, "Characteristics of a plasma thermocouple," *J. Appl. Phys.*, vol. 30, pp. 1861–1865; December, 1959.
[108] L. Steg and G. W. Sutton, "The prospects of MHD power generation," *Astronautics*, vol. 5, pp. 22–25; August, 1960.
[109] H. Hurwitz, *et al.*, "Influence of tensor conductivity on current distribution in a MHD generator," *J. Appl. Phys.*, vol. 32, pp. 205–216; February, 1961.
[110] I. B. Bernstein, *et al.*, "Magnetohydrodynamics ac power generator," *Proc. Natl. Aerospace Electronics Conf.*, pp. 205–214; May, 1961.
[111] H. Moss, "Thermionic diodes as energy converters," *J. Electronics*, vol. 2, pp. 305–322; January, 1957.
[112] G. R. Feaster, "Thermionic diodes as energy converters—an addendum," *J. Electronics Control*, vol. 5, pp. 142–145; August, 1958.
[113] K. G. Hernquist, *et al.*, "Thermionic energy converter," *RCA Rev.*, vol. 19, pp. 244–258; June, 1958.
[114] G. N. Hatsopoulos and J. Kaye, "Analysis and experimental results of a diode configuration of a novel thermoelectron engine," Proc. IRE, vol. 46, pp. 1574–1579; September, 1958.
[115] W. B. Nottingham, "Thermionic diode as a heat-to-electrical power transducer," *J. Appl. Phys.*, vol. 30, pp. 413–417; March, 1959.
[116] V. C. Wilson, "Conversion of heat to electricity by thermionic emission," *J. Appl. Phys.*, vol. 30, pp. 475–481; April, 1959.
[117] J. M. Houston, "Theoretical efficiency of the thermionic energy converter," *J. Appl. Phys.*, vol. 30, pp. 481–487; April, 1959.
[118] H. F. Webster, "Calculation of the performance of a high vacuum thermionic energy converter," *J. Appl. Phys.*, vol. 30, pp. 488–492; April, 1959.
[119] H. W. Lewis and J. R. Reitz, "Thermoelectric properties of the plasma diode," *J. Appl. Phys.*, vol. 30, pp. 1439–1445; September, 1959.
[120] F. E. Jablonski, *et al.*, "Space-charge neutralization by fission fragments in the direct conversion plasma diode," *J. Appl. Phys.*, vol. 30, pp. 2017–2018; December, 1959.
[121] N. S. Rasor, "Figure of merit for thermionic energy conversion," *J. Appl. Phys.*, vol. 31, pp. 163–167; January, 1960.
[122] P. A. Lindsay and F. W. Parker, "Potential distribution between two plane emitting electrodes: pt. 2—thermionic engines," *J. Electronics Control*, vol. 9, pp. 81–111; August, 1960.
[123] F. G. Block, *et al.*, "Construction of a thermionic energy converter," Proc. IRE, vol. 48, pp. 1846–1852; November, 1960.
[124] E. N. Carabateas, *et al.*, "Interpretation of experimental characteristics of cesium thermionic converters," *J. Appl. Phys.*, vol. 32, pp. 352–357; March, 1961.

under operating conditions and materials to withstand the high temperatures required at the cathodes as well as on the space charge problem.

Semiconductor Microplasmas

A good analogy exists between the process of electrical breakdown in a low-density gas and the "avalanche effect" which occurs in some reverse-biased semiconducting diodes.[125–130] In these devices, a slight increase in the reverse voltage above some critical value causes a very rapid increase in current and the junction is said to "break down." The breakdown occurs due to the multiplication and resulting avalanche of the charge carriers both positive (holes) and negative (electrons) in the depletion layer of the device in a manner analogous to the creation of ionization by electrons in a gaseous discharge. Observations indicate that the breakdown occurs in very minute highly ionized regions or *microplasmas* of about 500 A in diameter. Such devices are of great practical potential for applications which require switching times of milli-microseconds. In addition, a number of other effects[131–133] found in gaseous plasmas may also be observed in semiconductors.

The above are only a few of the devices and applications for which plasmas are suitable. The current intense investigations on the properties of plasmas will undoubtedly result in [illegible] cal uses.

THE F[illegible]"he[illegible] *December*

[illegible] of further practi-

Today plasma physics is a [illegible] search in which exist many proble[illegible] tory solutions. It encompasses many [illegible] ing particle physics, physical electronics, radiation physics, electromagnetic wave t[illegible] netohydrodynamics, thermodynamics, spec[illegible] physical chemistry, quantum mechanics and others. The interplay between these various fiel[illegible] study cannot help but further the frontiers of scienc[illegible]

As slowly and surely solutions are found to the many pressing problems of plasma physics, what can we hope to achieve? The promise of the future includes a better understanding of the creation of the Universe and the forces at work in it, an almost inexhaustible supply of electrical power using thermonuclear fusion reactions, reliable communications with space and re-entry vehicles, propulsion devices appropriate for interplanetary travel, devices for producing and amplifying HF radio energy, electrical generators with no mechanical parts, and numerous new semiconductor devices. These are the goals of plasma physics research.

The immediate future must be devoted to a better understanding of the behavior of plasmas and related phenomena under various conditions. The most significant progress is thus most likely to be made in fundamental studies under controlled conditions. Application of the basic knowledge gleaned in this manner will follow immediately.

It is difficult to predict what the long-term future will hold. Will the present hopes and dreams be realized, or will some now incidental and little understood by-product of the present effort prove to be an even greater achievement than our present goals? Only the future will tell. One can, however, safely predict that plasma physics will grow both in importance and in scope. The present problems are indeed formidable, but the richness of the rewards for their solution warrant the interest and effort which is and will be devoted to plasma physics.

---

[125] D. J. Rose, "Microplasma in silicon," *Phys. Rev.*, vol. 105, pp. 413–418; January 15, 1957.
[126] R. Yee, *et al.*, "Avalanche breakdown in *N-P* germanium diffused junctions," *J. Appl. Phys.*, vol. 30, pp. 596–597; April, 1959.
[127] K. S. Champlin, "Microplasma fluctuations in silicon," *J. Appl. Phys.*, vol. 30, pp. 1039–1050; July, 1959.
[128] A. G. Chynoweth and K. G. McKay, "Light emission and noise studies of individual microplasmas in silicon *P-N* junctions," *J. Appl. Phys.*, vol. 30, pp. 1811–1813; November, 1959.
[129] M. Kikuchi and T. Iizuka, "Observation of microplasma pulses and electroluminescence in gallium phosphide single crystal," *J. Phys. Soc. Japan*, vol. 15, p. 935; May, 1960.
[130] C. D. Root, *et al.*, "Avalanche breakdown voltages of diffused silicon and germanium diodes," IRE TRANS. ON ELECTRON DEVICES, vol. ED-7, pp. 257–261; October, 1960.
[131] L. M. Roth, *et al.*, "Theory of optical magneto-absorption effects in semiconductors," *Phys. Rev.*, vol. 114, pp. 90–104; April 1, 1959.
[132] M. Glicksman and M. C. Steele, "Plasma pinch effects in indium antimonide," *Phys. Rev. Lett.*, vol. 2, pp. 461–463; June 1, 1959.
[133] M. Date, "Magneto-plasma resonance in semi-conductors," *J. Phys. Soc. Japan*, vol. 15, pp. 1488–1492; August, 1960.

Oscillations and Noise in Low-Pressure DC Discharges*

F. W. CRAWFORD† AND G. S. KINO‡, ASSOCIATE MEMBER, IRE

Summary—**This is a review paper concerned mainly with oscillations and fluctuations which have been observed to occur either spontaneously or as a result of deliberate excitation in low-pressure, hot-cathode plasmas. Experimental observations on high- and low-frequency effects occurring spontaneously are discussed, and speculations are made about the possible generation mechanisms. In many cases, theories of these mechanisms have been treated in experiments involving deliberate excitation of oscillations, and comparisons are made where relevant.**

For device applications, and to relieve the difficulties which occur in quantitative experiments in plasma physics, it is important that the sources of spontaneous oscillations be understood and suppressed, if possible. The paper includes a discussion of work which has been carried out to reduce these effects, and concludes with some suggestions for further lines of attack on the problems.

I. Introduction

THE production of a plasma by means of a discharge in a gas at low pressure is of considerable interest today not only from the point of view of fundamental physics, but also for the possible device applications in fields as widely varied as nuclear fusion, generation of electromagnetic waves, and microwave amplification. The plasma medium is, however, complex. Its motion involves the many degrees of freedom associated not only with its internal space-charge properties and its several ionization processes, but also with the additional hydrodynamic properties analogous to those of a neutral conducting fluid, and the surface motion of a finite medium. It is not surprising then that an unfortunate feature of the plasma is its inclination towards instability, and most properties of a "steady-state" plasma, *e.g.*, number density, current, and maintaining voltage, are found on close examination to be fluctuating with amplitudes far above reasonable estimates for such phenomena as thermal noise. For example, voltage fluctuations at the anode of a discharge tube are typically in the range of hundreds of millivolts to volts. The presence of strong collective processes is indicated, and analysis of the frequency spectrum of the disturbances usually indicates strong components in two distinct ranges: zero to a few Mc, and the microwave band. In this paper we shall call these unwanted fluctuations "noise," regardless of whether they are coherent or incoherent.

* Received by the IRE, August 7, 1961. The research reported in this paper has been jointly sponsored by the Electronics Research Directorate, AF Cambridge Research Labs., Office of Aerospace Res., USAF and by the U. S. Atomic Energy Commission.

† Service de Physique Appliquee, Section d'Ionique Generale, Centre des Etudes Nucleaires de Saclay, Gif-sur-Yvette (Seine-et-Oise), France. Formerly at Microwave Lab., W. W. Hansen Labs. of Physics, Stanford University, Stanford, Calif.

‡ Microwave Lab., W. W. Hansen Labs. of Physics, Stanford University, Stanford, Calif.

For microwave applications such as amplification and frequency generation, it is clearly desirable to minimize the level of the high-frequency fluctuations, but it is also necessary to reduce the low-frequency components since they can cause substantial modulation of propagated or generated signals. Kino and Allen [1] have shown theoretically and experimentally that there is strong phase modulation of propagated signals, and that phase information is lost rapidly near cutoff, while the results of Boyd, Field, and Gould [2]–[5] on microwave amplification in plasmas have indicated amplitude modulation of the output in the tens of kilocycles range to a depth of as much as 30 per cent [3].

Before approaching the problem of suppressing the fluctuations, it is necessary to determine their generation mechanisms and to establish which of them, if any, are present as essential processes in the maintenance of the plasma. This last point is extremely important because it has been recognized for many years that some features of the dc discharge cannot be explained by a steady-state theory. The most notable is the phenomenon known as "Langmuir's paradox." This is the experimental observation that a Maxwellian distribution is maintained in circumstances where the effects of collisions could not offset the depletion of the high-energy tail by wall losses [6], [7]. Refined theoretical calculations showed that strong microscopic interaction processes would be required [8]–[10], but experiment showed that they were not present [11]. There is the possibility of macroscopic effects, and collective oscillations have been postulated as the means for making up the deficiency [12], though the site of origin and nature of their generation is still controversial [13], [14].

The purpose of this paper is to review the experimental and theoretical work which has been carried out on oscillations and noise in dc discharges at pressures where the mean free path for electron-neutral collisions is comparable to the dimensions of the discharge tube. We shall exclude much of the work carried out at higher pressures, the work on oscillations and noise occurring in magnetic fields, and the great volume of work on instabilities peculiar to fusion devices (mainly in the presence of a magnetic field), except where they serve to throw light on an effect of interest. References to noise and oscillation problems at higher pressures are to be found summarized in the work of Cobine and Gallagher [15], Fite [16], Sears [17], and Van der Ziel [18]. An excellent summary of the American work on the problem of instabilities and

TABLE I

Quantity	Symbol	Typical Value	Variation
Radius of column	a	1 cm	
Pressure	p	1.1 μ	Increases with temperature of coolest part of tube. Range 0.2–10μ.
Longitudinal field	E	0.8 v/cm	
Current density	J	0.1 amp/cm^2	
Average number density:			
Neutrals	N	3.9×10^{13}/cm^3	$N=9.7\times10^{15}p/T_N$
Electrons	n_e	10^{10}/cm^3	$n_e=n_i=n$ approximately proportional to current density; depends on pressure. Range 10^8–10^{13}.
Ions	n_i	10^{10}/cm^3	
Temperature:			
Neutrals	T_N	293°K	Range 273°K–320°K
Electrons	T_e	30,000°K	Decreases with increasing pressure or plasma volume; increases slightly with current. Range 10–50,000°K
Ions	T_i	~500°K	Probably increases with T_e
Average collision frequencies:			
Neutral-neutral (elastic)	ν_{NN}	5 kc	$\nu_{NN}=v_{tN}/L_{NN}$
Ion-neutral (elastic)	ν_{iN}	~5 kc	$\nu_{iN}\propto p\cdot\nu_{iN}\ll$collision frequency for charge exchange.
Electron-neutral (elastic)	ν	25 Mc	$\nu\doteq v_{te}/L_{eN}$
Electron-ion (elastic)	ν_{ei}	20 kc	$\nu_{ei}\doteq 2.6nT_e^{-3/2}$ ln Λ where ln Λ is a parameter of the order of 4, tabulated by Spitzer [68].
Electron-electron (elastic)	ν_{ee}	25 kc	$\nu_{ee}=3.1nT_e^{-3/2}$ ln Λ
Ion-wall (recombination)	ν_{iW}	~350 kc	$\nu_{iW}\doteq 2v_{ia}/a$
Electron-wall (recombination)	ν_{eW}	~350 kc	$\nu_{eW}=\nu_{iW}$
Electron-neutral (ionizing)	ν_{eN}^{I}	~350 kc	$\nu_{eN}^{I}=\nu_{iW}$
Mean free path:			
Neutral-neutral (elastic)	L_{NN}	4.4 cm	$L_{NN}=4.9/p$
Ion-neutral (elastic)	L_{iN}	5 cm	L_{iN} of same order as L_{NN}
Electron-neutral (elastic)	L_{eN}	5 cm	$L_{eN}\propto 1/p\cdot L_{eN}$ usually in range where it is a rapidly decreasing function of T_e.
Electron-ion (elastic)	L_{ei}	7×10^3 cm	$L_{ei}=v_{te}/\nu_{ei}$
Electron-electron (elastic)	L_{ee}	8.5×10^3 cm	$L_{ee}=v_{te}/\nu_{ee}$
Thermal speed:			
Electrons	v_{te}	1.3×10^8 cms	$v_{te}=6.74\times10^3T_e^{1/2}$
Ions	v_{ti}	$\sim2.5\times10^6$ cms	$v_{ti}=11.1T_i^{1/2}$
Neutrals	v_{tN}	2.0×10^4 cms	$v_{tN}=11.1T_N^{1/2}$
Drift velocities:			
Axial-electrons	v_{ez}	6.3×10^7 cms	$v_{ez}=6.25\times10^{18}J/n_e$
Radial-ions at edge of positive column	v_{ia}	1.7×10^5 cms	$v_{ia}\doteq 325T_e^{1/2}$
Plasma frequency:			
Electrons	f_{pe}	900 Mc	$f_{pe}=8980n_e^{1/2}$
Ions	f_{pi}	1.5 Mc	$f_{pi}=14.8n_i^{1/2}$
Debye length (electrons)	l_e	0.022 cm	$l_e\doteq v_{te}/\omega_{pe}$
Potential drop across sheath	V_s	18 volts	$V_s\doteq 6\times10^{-4}T_e$

oscillations in fusion devices may be found in the book by Glasstone and Lovberg [19].

Our range of interest includes one of the most common experimental discharges, mercury vapor at room temperature, which has a pressure of the order of 1 μ; unless stated, it may be assumed that the experimental data described were taken in this gas. In general, the gas used has little effect on the nature of the phenomena, though there may be variations in degree. Similarly, many mechanisms to be discussed are independent of the type of cathode used. The majority of the work has been carried out with hot cathodes, and except where stated, their use also may be assumed.

After sketching briefly the characteristics of a low-pressure discharge, we shall survey low-frequency and high-frequency phenomena separately, and conclude with some reference to relations between these two ranges and possible techniques for reducing the amplitude of plasma noise.

II. Characteristics of a Typical Low-Pressure Plasma

To give some idea of the ranges of values encountered experimentally, typical figures are quoted in Table I for a mercury-vapor discharge at a pressure of 1.1 μ (~20°C).

Further information on the experimental determination of electron temperatures and general properties of plasmas is to be found in the papers of Killian [20], Klarfeld [21], and Boyd [22], and in the pioneer work of Langmuir and Mott-Smith on the use of probes [23]–[27].

A. Regions of the Discharge

Probe measurements and visual observations of discharges have some measure of correlation, and Fig. 1 shows the appearance of a typical discharge.

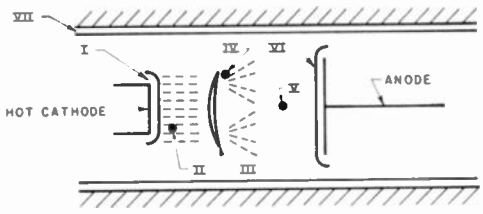

Fig. 1—Characteristic regions of a typical low-pressure discharge. I. Cathode sheath. II. Unscattered primaries and ultimates. III. Meniscus. IV. Slowed primaries, secondaries, and ultimates. V. Ultimates. VI. Anode fall. VII. Wall sheath.

Region I: The properties of this region, which are analogous to those of a simple diode in which electrons are emitted at the cathode and ions at the anode, have been treated analytically by Langmuir [28]. In this low potential region, which has a thickness of a millimeter or less [29], electrons are emitted at the cathode, yielding an excess of electron space charge, *i.e.*, an electron sheath, near the cathode. Ions stream toward

the cathode from the main plasma region, forming an ion sheath at the surface of the plasma facing the cathode. The potential drop across region I is of the order of the ionization potential of the gas; consequently very few electrons and ions are produced by collisional ionization in this region. As the number of elastic collisions of electrons with neutrals is also small in this region, the majority of the electrons emerge from region I with energy appropriate to the voltage drop across the sheath, and the electron stream has only a very small velocity spread.

Region II: It had been shown in the early experiments of Langmuir [6] and Dittmer [12], using flat probes to intercept the primary beam from a tungsten filament cathode, that at low anode currents two classes of electrons could be observed: the electrons emerging from region I ("primary" electrons) and a group of electrons with an isotropic Maxwellian velocity distribution ("ultimate" electrons). The ultimate electrons were approximately 1000 times more numerous than the primary ones. However, as current was increased a scattering phenomenon occurred introducing a small additional electron velocity group ("secondary" electrons) with an isotropic Maxwellian velocity distribution, and energies intermediate between the primary and the ultimate groups. Concurrent with this effect was a slowing down of the mean velocity of the primary electrons and a superimposition of an approximately Maxwellian distribution upon it. As a typical result, it was observed that a 50-v beam was slowed to a mean velocity corresponding to 36 v, but some electrons from it could reach potentials as high as 90 v. The anisotropy of the primary beam and the isotropy of the secondary and ultimate groups were established by turning the probe parallel to the primary stream [6]. The results for secondary and ultimate electrons were identical, but no primary electrons were observed.

Druyvesteyn and Warmoltz [30]–[32] were able to show that changes in velocity distribution, space potential, and electron concentration occurred in distinct narrow regions a few tenths of a millimeter thick. These were studied in greater detail by Merrill and Webb [33] using a probe movable with considerable precision. Further work by Emeleus and his co-workers [34]–[42] has shown that the first of these scattering regions lies to the cathode side of, or in, region III.

Region III: This is a bright meniscus-shaped region of the same diameter as the primary beam and with its convex side towards the cathode. It may be bounded on its anode side by a dark layer. Increasing pressure or current moves the meniscus toward the cathode. Continued increase into current saturation may produce a second meniscus near the anode [42].

Region IV: This is a region in which there is considerable "turbulence" [43], [44]. The primary electrons are deviated laterally into approximately conical converging and diverging beams. The converging beams do not appear to cross over, but there may be a bright spot at the focus. The diverging "wings" may have semi-vertical angles up to 30° or more. No definite explanation has yet been given for them. Sturrock [45]–[48] has suggested that they are the result of a wave-damping mechanism, while Emeleus has proposed a wave-diffraction explanation [37].

If anode-cathode spacing is reduced [36], [37], the wings bow in and attach themselves to the anode. Further decrease in spacing causes the wings to disappear and the meniscus to lose definition. Photographs showing these phenomena clearly are given in [35] and [41].

Region V: Further out in the discharge, only ultimate electrons can be detected. Their temperature depends on the factors indicated in Table I and also on the operating point on the current/voltage characteristic: for example, there is a sharp drop in temperature at the point of cathode current saturation [49].

In this region, known as the positive column of the discharge, the theoretical treatment of Tonks and Langmuir [50] assumes that the electrons have a Maxwellian distribution of velocities and that there are radial variations of electron charge density and potential over the cross section of the discharge column. The ions are assumed to move radially outward from their point of generation towards the wall, with a velocity corresponding to free motion over the potential drop through which they fall. The theoretical treatment, which has been confirmed by probe measurements [21], [50], [51], predicts that the density near the wall may be as much as 50 per cent below its value at the center of the column.

Region VI: At the anode of the discharge there is a sheath, the polarity of which is dependent on anode size and current [50]. Most commonly, the anode will be negative with respect to the potential of the positive column (the space potential) by a few volts.

Region VII: At the nonconducting walls of the tube, a thin dark sheath forms. Both the thickness of this sheath and the potential drop across it are dependent on the electron temperature in the positive column. Criteria for the formation of this sheath have been given by Bohm [52] and by Tonks and Langmuir [28], [50].

B. Scattering Effects

It is interesting to observe the effect of crossing two beams of primary electrons. This was explored by Langmuir [6] using identical probe-cathode assemblies mounted at right angles, and by Garscadden and Emeleus [41] using a movable low-voltage electron gun emitting a beam which passed across the main discharge column. Both sets of experiments indicated that the second beam became scattered only if it passed through a volume of plasma in which the primary beam was being, or had been, scattered. In the moving-gun ex-

periment the degree of energy spread of the secondary beam was found to be quite substantial: A 40-v secondary beam traversing a region containing a 22-v primary beam from the cathode obtained an energy spread along its direction of motion corresponding to an excess energy of approximately 8 v, while the cathode beam incurred a spread of 14 v. This implies that there are strong transverse fields, an observation supported by some experiments of Allen, Bailey, and Emeleus [35] in which the cathode beam was split into a number of flat strips by a grid close to the cathode. At the usual position of a meniscus, parallel flow was observed to break down. The beams spread and merged into each other.

The early experiments on scattering failed to explain several features, *e.g.*, the variation of distance to the scattering region with beam voltage and current, and the problem of why only the primary electrons were scattered in a region containing many times more ultimate electrons. The ultimate and secondary electrons could be explained as resulting from elastic and inelastic collisions with neutrals, but the mechanism of the scattering process proved elusive. Both Langmuir and Dittmer realized that high-frequency oscillations in the plasma could produce the effect, but neither succeeded immediately in observing their presence. The issue was, however, reopened by Penning [53], [54], whose experiments verified that such oscillations did exist. The nature of these oscillations, and the experimental data on them, will be taken up again in Section III.

III. High-Frequency Oscillations

A. *Waves in a Uniform Plasma*

1) *Zero Temperature Theory*

In order to understand what types of oscillations may occur in a plasma, it is necessary to consider the waves which can propagate through such a medium. When only the high-frequency oscillations are considered, it is usual to adopt a model in which the plasma is regarded as a neutral medium in which the relatively heavy positive ions do not move in response to the RF fields. The first derivation of this type was published as long ago as 1906 by Lord Rayleigh, who found an expression for the natural oscillation frequency of electrons embedded in positive charge [55]. Similar results were obtained by Mott-Smith and by Tonks, their work being quoted by Langmuir [8] in 1928 in a paper which apparently introduced the term "plasma" for the first time. Further extensions of the same principles were given by Thompson [56] and discussed fully in the classic paper by Tonks and Langmuir in 1929 [57], [58].

It is instructive to present here some of these early results, using the Eulerian derivation which is now common, and to consider some of the later implications of this work. We consider a zero-temperature plasma in which the ions are regarded as stationary. All ac quantities will be denoted by the subscript 1. The motion of the electrons within the plasma is given by the Eulerian equation of motion,

$$\frac{\partial v_1}{\partial t} + (v_1 \cdot \nabla) v_1 = -\frac{e}{m_e} E_1, \tag{1}$$

where $-e$ is the electron charge, m_e is the electron mass, v_1 is the velocity, and E_1 is the electric field strength. For small perturbations we may neglect the second term in this equation and assume that all quantities vary as $\exp(j\omega t)$. Eq. (1) then takes the form

$$j\omega v_1 = -\frac{e}{m_e} E_1. \tag{2}$$

For small perturbations, the current density J_1 is

$$J_1 = -en_e v_1, \tag{3}$$

it follows that the current density is related to the field by

$$J_1 = \frac{e^2 n_e}{j\omega m_e} E_1. \tag{4}$$

We may now find the ac charge density $\rho_1 (= -en_1)$ by using the equation of continuity:

$$\nabla \cdot J_1 + j\omega \rho_1 = 0. \tag{5}$$

The divergence equation for the electric field is

$$\nabla \cdot E_1 = \frac{\rho_1}{\epsilon_0}, \tag{6}$$

where ϵ_0 is the permittivity of free space. In order to satisfy (4)–(6) simultaneously, we find that

$$\left(1 - \frac{\omega_{pe}^2}{\omega^2}\right) \nabla \cdot E_1 = 0, \tag{7}$$

where

$$\omega_{pe}^2 = \frac{n_e e^2}{\epsilon_0 m_e}. \tag{8}$$

$f_{pe} (= \omega_{pe}/2\pi)$ is usually called the electron plasma frequency. It follows from (7) that either $\nabla \cdot E_1 = 0$, and there is no ac space charge within the volume of the plasma, or $\omega = \omega_{pe}$. Let us consider the first alternative: it will be seen from (4) that Maxwell's equations imply that

$$\nabla \times H_1 = j\omega\epsilon_0 E_1 + J_1 = j\omega\epsilon_0 (1 - \omega_{pe}^2/\omega^2) E_1, \tag{9}$$

where H_1 is the magnetic field intensity. We can regard the plasma as behaving like a medium with dielectric constant $\epsilon = \epsilon_0 (1 - \omega_{pe}^2/\omega^2)$. This dielectric constant is negative below the plasma frequency, but positive and smaller in magnitude than the dielectric constant of free space at frequencies above the plasma frequency. When $\omega \neq \omega_{pe}$ there is no space charge within the volume

of the plasma. Consequently, in an infinite plasma, plane electromagnetic waves can propagate at frequencies above the cutoff at the plasma frequency. In a plasma bounded by metal conductors, waves somewhat similar to the usual waveguide modes can propagate above the plasma frequency. With insulating boundaries, it has been shown by Gould and Trivelpiece [59], [60], Smullin and Chorney [61], Fainberg and Gorbatenko [62], and Schumann [63], [64] that waves with a phase velocity slower than the velocity of light in free space can propagate along the plasma column at frequencies below the plasma frequency. These waves have fields which have a maximum amplitude at the plasma surface. The addition of magnetic fields changes this picture radically, as it causes the plasma to behave like a medium with a tensor dielectric constant. Of particular importance is the possibility of a slow backward wave propagating at frequencies above the plasma frequency. This behavior has been demonstrated theoretically and experimentally by Gould and Trivelpiece [59], [60], and discussed theoretically by the authors already mentioned [61], [62], [64].

The alternative solution of (7), $\omega=\omega_{pe}$, implies that there is a possibility of natural oscillations at the plasma frequency. These oscillations, by virtue of (9), have no ac magnetic fields associated with them, and hence are usually referred to as electrostatic oscillations. Because their frequency does not depend on the spatial variation of the fields, they have zero group velocity and are entirely local in character. The behavior is such that the electrons, when disturbed, oscillate about their equilibrium position at the plasma frequency.

2) *Finite Temperature Theory*

In practice, the nonpropagating disturbance at the plasma frequency is not localized because the electrons are not at zero temperature. The Thomsons [65]–[67] took account of the electron temperature and derived a dispersion relation for one-dimensional waves of the form

$$\omega^2 = \omega_{pe}^2 + \frac{\gamma k T_e}{m_e}\beta^2, \tag{10}$$

where k is Boltzmann's constant and β is the propagation constant of the wave. This dispersion relation was based incorrectly on isothermal expansion of the plasma medium, with the result that the constant γ was found to be unity. Subsequent treatments of the type given by Spitzer [68] indicated different values of γ lying between 1 and 3.

Thermal velocities of the electrons in a plasma may also be taken into account by making the alternative assumption of no collisions and working directly with Boltzmann's equation, or by regarding the plasma as a number of electron streams of number density n_r with individual dc velocity v_r, as was done by Pierce and Morrison [69] and Walker [70]. Then for a one-dimensional system, assuming a wave with field components that vary as $\exp[j(\omega t-\beta z)]$, it follows from (1) that the ac velocity of the rth electron stream is

$$v_{1r} = -\frac{eE_1}{jm_e(\omega-\beta v_r)}. \tag{11}$$

By using the familiar relations between current and charge, and the equation of continuity, it is found that the ac charge density associated with this stream is

$$\rho_{1r} = -\frac{je^2 n_r \beta E_1}{m_e(\omega-\beta v_r)^2}. \tag{12}$$

Finally by using the divergence equation for the field, (6), and summing up the total contribution to the charge of all the individual electron streams, we find that

$$\beta E_1 = \sum_{r=1}^{r=s} \frac{e^2 n_r \beta E_1}{m_e \epsilon_0(\omega-\beta v_r)^2} \tag{13}$$

or

$$1 = \sum_{r=1}^{r=s} \frac{e^2 n_r}{m_e \epsilon_0(\omega-\beta v_r)^2}. \tag{14}$$

This is the dispersion relation for a system of s streams of electrons.

If we now regard a plasma as consisting of an infinity of electron streams, so that the number density of electrons contained within the velocity range $v\rightarrow(v+dv)$ is $n_e f(v)dv$, where

$$n_e = \sum_{r=1}^{r=\infty} n_r$$

and $f(v)$ is the velocity distribution, we have in the limit

$$\frac{n_r}{n_e} \rightarrow f(v)dv, \tag{15}$$

and (14) takes the form

$$1 = \omega_{pe}^2 \int_{-\infty}^{\infty} \frac{f(v)dv}{(\omega-\beta v)^2}. \tag{16}$$

An often-quoted form of (16) may be deduced by partial integration:

$$1 = -\frac{\omega_{pe}^2}{\beta}\int_{-\infty}^{\infty} \frac{(\partial f/\partial v)dv}{(\omega-\beta v)}. \tag{17}$$

The integral relation of (17) was first deduced by Vlasov [71], [72] by using Boltzmann's equation. Vlasov integrated this expression by expressing the denominator in terms of an expansion in powers of $\beta v/\omega$ and retaining only terms up to second order in $\beta v/\omega$. He obtained the dispersion relation of (10) with $\gamma=3$. It was pointed out by Landau [73] that such a

procedure is not valid because there is a pole in the integrand at $v=\omega/\beta$, and Vlasov had only considered the principal integral. Using a Laplace transform method, Landau integrated (17), his integral being taken to the right-hand side of the pole at $v=\omega/\beta$. The contribution of the pole in the integrand then yielded the modified dispersion relation

$$\omega^2 = \omega_{pe}^2\left[\left(1+\frac{3kT_e}{m_e}\beta^2\right) - j\pi\left(\frac{\omega}{\beta}\right)^2\left(\frac{\partial f}{\partial v}\right)_{v=\omega/\beta}\right]. \quad (18)$$

For a Maxwellian distribution of electron velocities,

$$f(v) = \left(\frac{m_e}{2\pi kT_e}\right)^{1/2}\exp\left(-m_e v^2/2kT_e\right), \quad (19)$$

we have

$$\omega^2 = \omega_{pe}^2\left[1+\frac{3kT_e}{m_e}\beta^2 + j\left(\frac{\omega}{\beta}\right)^3\left(\frac{m_e}{kT_e}\right)^{3/2}\cdot\sqrt{\frac{\pi}{2}}\exp\left(-m_e\omega^2/2\beta^2kT_e\right)\right]. \quad (20)$$

The additional term in this dispersion relation implied that any wave set up in the plasma would be damped, the damping being most severe for a wave with a phase velocity comparable to the mean velocity of the electrons, a phenomenon now known as Landau damping.

Van Kampen [74], [75], Bohm and Gross [76]–[78], and Berz [79] derived (17) directly from Boltzmann's equation, carefully considering the region near $v=\omega/\beta$. Berz showed that Landau damping becomes appreciable for wavelengths shorter than 20 Debye lengths. Van Kampen, and Bohm and Gross found the following form for the ac perturbation in charge density, $f_1(v)$:

$$f_1(v) = -\frac{\omega_{pe}^2\dfrac{\partial f}{\partial v}}{\beta(\omega-\beta v)} + g_1(v)\delta(\omega-\beta v), \quad (21)$$

where $g_1(v)$ is an arbitrary function of v, and $\delta(\omega-\beta v)$ is Dirac's delta function. This result gives rise to an extra term, $g_1(\omega/\beta)$, on the right-hand side of (17) which represents a periodic motion transported by all electrons at their own velocity. There is, therefore, no unique dispersion relation between ω and β. This feature was considered in great detail in a series of papers by Bohm and Gross [76]–[78], who gave a physical meaning to the damping in terms of trapped electrons. They demonstrated theoretically that a wave of finite amplitude propagating in a plasma medium would interact strongly with electrons traveling at a velocity near to its phase velocity. Electrons moving slightly slower than the phase velocity of the wave would tend to be accelerated and thus absorb energy from the wave; the converse would be true for electrons traveling slightly faster than the wave. For a velocity distribution function which decreases monotonically with velocity, there are more slow electrons than fast ones, so that there is a damping of the wave.

It has been remarked by Allis [80] that in a steady state, $(\partial f/\partial v)_{v=\omega/\beta}=0$, so that there is then no Landau damping and Vlasov's dispersion equation is correct. A class of solutions can be obtained for which $(\partial f/\partial v)_{v=\omega/\beta}=0$, representing undamped disturbances. These can be of large amplitude. They have been examined in detail by Bernstein, Greene, and Kruskal [81], but it is difficult to see under what physical conditions they could be set up. In practice, all waves are damped by collisions which tend to re-Maxwellianize the trapped electrons taking part in such a steady-state wave motion.

Further discussions of plasma wave solutions have been given by Allis [80], Gross and his co-workers [82]–[84], Berz [79], Bohm and Pines [85]–[87], Twiss [88]–[90], Bailey [91], and Piddington [92], [93]. Clear summaries of the issues are given by Van Kampen [74], [75] and Ecker [94]–[96]. The work has been extended to take account of the effect of magnetic field on the propagation of waves in a hot plasma by, among others, Drummond [97], [98], Mower [99], Gordeyev [100], and Bernstein [101]. An alternative physical picture of Landau damping in terms of "phase mixing" has been given by Case [102] and Van Kampen [74], [75].

Recent reviews of the theory of plasma oscillations have been made by Oster [103], Jackson [104], Bernstein and Trehan [105], and Drummond [106]. The last two contain very comprehensive bibliographies.

Another type of damping due to nonlinear effects in a plasma has been discussed by Dawson [107] and Sturrock [45]–[48], who show that a single electrostatic wave may remain undamped. Sturrock shows also that two electrostatic waves of frequencies ω_1 and ω_2, propagating at an angle to each other, can interact to transfer energy into a plane electromagnetic wave of frequency $(\omega_1+\omega_2)$. This model also yields a possible mechanism to explain the strong radiation at $2\omega_{pe}$ observed from the sun.

3) *Experimental Observations*

From the foregoing discussion we might expect to find that there would be oscillations occurring naturally in the discharge near the plasma frequency. Such oscillations would have low group and phase velocities, and would be difficult to detect from outside the chamber. This last point follows from (7), where it may be seen that for a zero temperature plasma the total current is zero at the plasma frequency. When the temperature is finite, the total current is extremely small as compared with either the displacement or conduction current within the plasma, so that the fields outside the plasma due to this type of oscillation should be small.

The first observation of high-frequency oscillations appears to have been made by Penning [53], [54] in 1926. Using a Lecher wire system connected to the elec-

trodes, he observed oscillations around 500 Mc in both argon and mercury under conditions when the scattering phenomenon described in Section II was taking place. Langmuir [8] and Tonks confirmed these observations measuring frequencies up to 1200 Mc in regions of the plasma not traversed by the primary beam, and an additional component of about 100 Mc in the beam region, which appears to have been due to oscillations of the beam alone. Later measurements [57] by these workers showed the relation for the oscillation frequency $f \propto n_e^{1/2}$ to be true within the limits of experimental error. Some additional frequencies observed appear to be related to the effects of heater current and its direction of flow. This effect has been examined in more detail by Armstrong and Emeleus [108] using a tungsten filament at the axis of a cylindrical anode in mercury vapor, argon, and other gases. They discovered that the oscillation intensity diminished considerably during the off-periods when the filament current was interrupted at 2 kc, and that such factors as length and inclination of the filament were important. Further influences on the amplitude and frequency of oscillations were exerted by the choice of operating point on the V/I characteristics (filament current and pressure) of the discharge. Increases in filament current and pressure both caused increases in frequency. Oscillations could be observed even in the Townsend discharge region before a plasma was formed. No essential changes in these results could be observed when the anode voltage was swept at 50 cps. The highest frequency observed was 6 kMc, and up to 1 per cent conversion efficiency could occasionally be obtained. Later experiments by Emeleus and Bailey [109] were directed towards increasing the plasma frequency by increasing the pressure, and 10 kMc was achieved at 70 μ, though the power withdrawable was only 1 μw.

So far we have considered only experiments involving observation of oscillations near the plasma frequency. Early experiments involving simultaneous measurements of electron density and plasma frequency indicated agreement with the theoretical value to within 10 per cent [110]: that there were specific regions of generation, and that there were relations between frequency and tube geometry. These results are discussed in the following Subsections.

B. Beam-Plasma Interactions without Sheaths

1) Basic Mechanisms

The theories that we have discussed described propagation through a plasma which was either at zero temperature or in which the velocity distribution of the electrons was a monotonically decreasing function of velocity. In the latter case, the waves were in some theories undamped and in others damped. Bohm and Gross [76]–[78] discussed the interpretation of the wave solutions when the velocity distribution was not a monotonic function of velocity and showed that under certain conditions growing waves could exist. Physically, the phenomenon is best understood by considering the interaction between two interpenetrating charged beams of different velocity. This was first done almost simultaneously by Haeff [111], [112], Nergaard [113], Pierce [114], [115], and Hebenstreit [116]. They showed that when two beams of velocities v_a and v_b and plasma frequencies $\omega_{pa}/2\pi$ and $\omega_{pb}/2\pi$ interact, the following dispersion equation, which may be derived directly from (14), is valid:

$$\frac{\omega_{pa}^2}{(\omega - \beta v_a)^2} + \frac{\omega_{pb}^2}{(\omega - \beta v_b)^2} = 1. \tag{22}$$

This dispersion equation predicts that when the two beams travel in the same direction with approximately, but not exactly, the same velocities, growing waves can propagate along the system in the direction of motion of the beams. These authors also demonstrated the phenomenon experimentally, using two electron beams.

The same theory describes the interaction of an electron beam with a stationary plasma through which it passes, and was also used by Pierce [117] to explain the ion oscillations which occur when an electron beam in a gassy system passes through the ion cloud generated by its collisions with gas molecules. The dispersion equation becomes

$$\frac{\omega_p^2}{\omega^2} + \frac{\omega_{pb}^2}{(\omega - \beta v_b)^2} = 1 \tag{23}$$

where ω_p is the electron plasma frequency of the plasma through which the beam passes, or the ion plasma frequency of the stationary ion cloud, and ω_{pb} is the plasma frequency of the electron beam. This equation may be written in the form

$$\beta = \frac{\omega}{v_b} \pm \frac{\omega_{pb}}{v_b(1 - \omega_p^2/\omega^2)^{1/2}}. \tag{24}$$

It will be seen that the propagation constant for waves traveling along the beam becomes complex for frequencies below ω_p. There will be the possibility of strong amplification effects at frequencies in the neighborhood of the plasma frequency, the gain becoming infinite when $\omega = \omega_p$. Physically, this effect takes place because, below ω_p, the plasma behaves like a medium of negative dielectric constant in which the space-charge forces due to bunching of the electron beam are reversed in sign from their values in free space.

These results and their interpretations have been discussed at length by Piddington [93], Twiss [118], Sturrock [119], [120], Buneman [121], and Drummond [106]. These authors pointed out that knowing the dispersion relation of a system is not sufficient. For instance, (23) yields complex β, *i.e.*, a growing wave with real ω. But it also implies that with real β, ω can be complex, *i.e.*, the waves will grow in time. However, because this latter instability is "convective," as Sturrock describes it, such a result can only be obtained in

an infinite system, or in one where there is feedback.

Physically, this is because the waves that are present propagate and grow in the direction of motion of the electron beam. The solution with ω complex, *i.e.*, oscillations, cannot apply unless energy can be returned from the output end of the system to the input. This will only occur if there is some additional feedback mechanism not included in the theory.

The results have been generalized by Budker [122], Sturrock [123], Tchernov and his co-workers [124], [125], Trivelpiece [126], Boyd, Field and Gould [2]–[5], and Allen and Kino [127], [128], to take into account the effects of finite diameter of the beam, finite diameter of the plasma, and the presence of a magnetic field in the direction of motion of the beam. Fig. 2 indicates the basic conclusions reached by these authors, *i.e.*, that the gain does not become infinite, and that there can be gain above the plasma frequency. In a finite magnetic field, the gain reaches its maximum above the plasma frequency and can remain finite up to a frequency given by

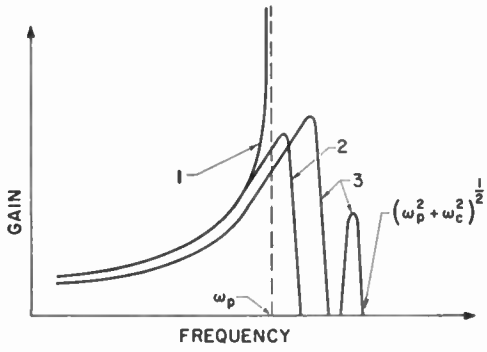

Fig. 2—Gain/frequency characteristics for beam-plasma interactions in an infinite plasma.

$$\omega = (\omega_{pr}^2 + \omega_{cr}^2)^{1/2}, \tag{25}$$

where $\omega_{cr} = (eB/m_r)$ is the cyclotron frequency of an electron in the magnetic field B.

The original Bohm and Gross [76]–[78] treatment took account of the thermal velocity distribution of the plasma electrons by a simple extension of (23), and resulted in the dispersion relation

$$\frac{\omega_{pr}^2}{\omega^2 - 3(kT_r/m_r)\beta^2} + \frac{\omega_{pb}^2}{(\omega - \beta v_b)^2} = 1. \tag{26}$$

The regions of amplification given by this formula have been studied by Akhiezer and Fainberg [129], Feinstein and Sen [130], Twiss [118], [131], Lampert [132], Sumi [133], [134], Boyd, Field and Gould [3]–[5], Sturrock [119], Filiminov [135], Buneman [136], and Tchernov and Bernashevski [125], who considered the effects of thermal motions in both the beam and the plasma, collisions of electrons with neutrals and ions, and in the case of Sumi, the effect of an electron beam density comparable to that of the plasma. As might be expected, both collisions and finite temperature reduce the gain to a finite value. However, these effects on the gain are not likely to be as great as that of finite beam diameter. In addition, the gain is found to reach its maximum above the plasma frequency, when the electron temperature of the plasma is finite, although it decreases to zero rapidly with further increase in frequency.

2) *Experimental Verifications*

Before considering whether beam-plasma interactions might occur naturally in plasmas, we shall discuss the experimental verification of the contentions made above concerning amplification. The first published confirmation of the effect was presented by Boyd, Field, and Gould [2]–[5] in 1958, and extended subsequently by Tchernov and his co-workers [124], [125], Demirkhanov, Gevorkov and Popov [137], and by Allen and Kino [127], [128].

The type of experimental tube used by Boyd, Field, and Gould [2]–[5] is shown schematically in Fig. 3.

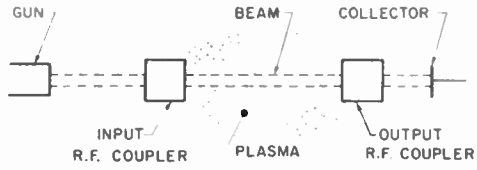

Fig. 3—Typical apparatus for beam-plasma interaction experiments of the type performed by Boyd, Field, and Gould.

Using helices coupled to external waveguides to modulate and demodulate the electron beam, gain was observed over the frequency range 500–4000 Mc. Gain of a few db/cm was observed reaching a maximum at the plasma frequency, as calculated from additional measurements. Allen and Kino [127], [128], using helix coupling to a beam traversing a magnetically-confined synthetic cesium plasma, obtained good agreement with their theoretical analysis of the gain parameter, taking magnetic field and the finite dimensions of the plasma and the beam into account. Typical gain figures were approximately 5–10 db/cm at 1 kMc and approximately 10–15 db/cm at 3 kMc. Tchernov, *et al.* [124], [125], used an experimental arrangement similar to that of Boyd, but with the plasma density increased by immersing the tube in an axial magnetic field. They were able to obtain amplification between 20 and 40 db over the range of plasma frequencies 1–10 kMc. It also appeared that the gain parameter reached a saturation value with increasing current. A possible explanation for this phenomenon, due to the finite diameter of the beam, has been given by Sturrock [123]. The influence of increasing the mercury vapor pressure was studied and it was shown that a smaller discharge current is required to obtain maximum gain with increasing pressure. It is worth noting that, with a Philips-type (PIG) discharge, sufficiently high plasma densities

were obtained for amplification of 8-mm waves with a gain of 10 db/cm [125].

Some attempts were made by Tchernov and Bernaskevski [125] to determine the noise levels in operation. It was found that noise figures as low as 40 db were obtained at pressures of a few microns. However, it appears that in the noise measurements no account was taken of any narrow-band low-frequency modulation present on the output signal, such as might be caused by low-frequency plasma oscillations. They also tested between 2 and 28 kMc a similarity law showing that the gain was fixed, at 10 db/cm in their case, if the beam diameter, measured in wavelengths of the slow wave propagating along it, was kept constant.

Although these experiments showed gain on a modulated beam, we would expect that noise modulation on an otherwise unmodulated beam could also grow, perhaps even to the extent of ultimately breaking up the beam itself. An explanation along these lines was proposed by Haeff [138] for the generation mechanism of solar radio noise, and showed good agreement with observed noise spectra. After unsuccessful attempts by Looney and Brown [139], Kojima, *et al.* [140], and Gordon [141], the first successful laboratory experiments of this nature were performed by Demirkhanov, Gevorkov, and Popov [137], and Kharchenko, *et al.* [142]. Demirkhanov, *et al.*, used an unmodulated beam passing along the axis of a discharge tube. With one tube, oscillations were picked up on a probe within the discharge; with another, on a probe outside. The amplitude of the oscillations was always strongest in the beam region. A cavity perturbation technique was used to measure the electron density in the discharge, and the comparison of the frequency of the highest output amplitude and calculated plasma frequency was always very close. Moving the probe along the direction of motion of the beam electrons showed increasing signal amplitude at first, then a slow decrease. This was probably a result of slowing and scattering of the beam by collisions or by the RF signal itself. Similar results were obtained over a pressure range 1–10 μ in argon, nitrogen, and hydrogen.

Kharchenko and his co-workers [142] investigated this phenomenon at higher pressures (30–100 μ) with an 80-kv electron beam. They observed strong high-frequency signals with a maximum amplitude at the plasma frequency, provided a long enough interaction distance was allowed (10–20 cm).

3) *Natural Oscillations*

We may now speculate as to whether interaction of the type established above can occur naturally in a discharge. The necessary ingredients are there since we have a homogeneous stream of primaries leaving the cathode sheath and entering the plasma. It is, therefore, worth examining some of the experiments in which high-frequency oscillations were investigated spatially in the plasma. The first of these was the scattering experiment of Merrill and Webb [33] mentioned in Section II. They found a remarkable correlation between the scattering regions and the points of maximum oscillation amplitude. There was in each case an equal number of these (usually 2 or 3) with the high-frequency amplitude reaching its maximum approximately midway between the scattering regions (see Fig. 4). The oscillation frequency was close to the

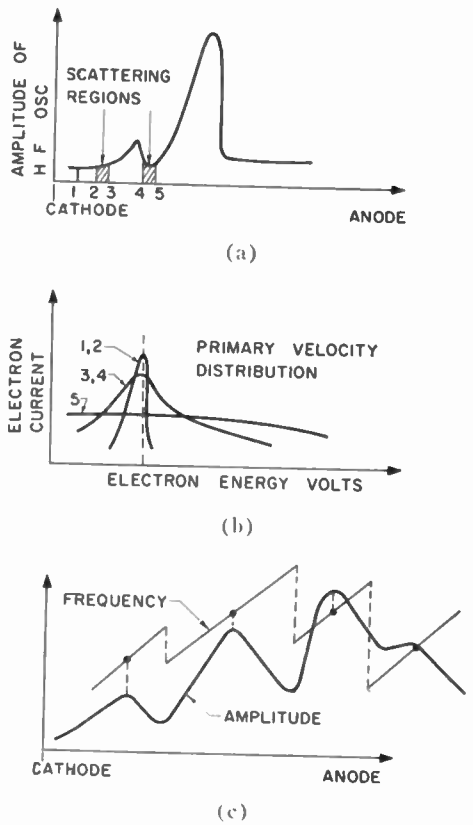

Fig. 4—Typical results of scattering experiments of the type performed by Merrill and Webb. (a) Regions of scattering and positions of RF maxima. (b) Velocity distributions at points 1–5 in (a). (c) The frequency-pulling effect of a probe.

plasma frequency as calculated from probe measurements. Increases in pressure or current moved the scattering regions towards the cathode. The authors explained their results in terms of the phenomenon of velocity modulation, a process novel then, but familiar today in tubes such as the klystron. Assuming that plasma oscillations occurred strongly in the scattering regions, bunching of the primary beam would occur somewhat further towards the anode, impressing an RF current on the probe. Very little variation in maximum RF amplitude could be observed as the probe potential was varied. Twiss [131] analyzed this experiment in terms of growth of noise from the cathode caused by the interaction of primary electrons with the plasma ultimate electrons. He showed that gains as high as 170 db/cm could be expected at the plasma frequency. This gain would yield perturbations in elec-

tron velocity of sufficient amplitude to explain the results observed.

Neill and Emeleus [143], using a filamentary cathode, observed a variation in oscillation amplitude increasing slowly with distance from the cathode to a maximum, then falling away, both increase and fall being complicated by a number of minor peaks. This experiment and that of Merrill and Webb were repeated and extended by Bailey and Emeleus [42], [144]. By ascertaining that similar results were obtained with a back-bombarded flat tantalum cathode, they showed that the more sudden build-up of oscillation amplitude in the case of flat cathodes was associated with geometry rather than cathode material. They also noted the powerful disturbing influence of a probe, which could produce frequency pulling. This, they attributed to reflection of primaries providing a feedback action analogous to that in a reflex klystron. Evidence for this was supplied by the fact that the minor peaks corresponded to the center frequencies of the modes (see Fig. 4). The effect was similar if the wire probe was replaced by a quartz fiber of the same size and was most pronounced when a small flat probe at right angles to the cathode was used.

It is clear that the results obtained for scattering and oscillation amplitude profiles must be considered with caution, particularly in view of the pronounced instability of the meniscus as it is approached by a probe. Bailey and Emeleus [42] found that a magnetic field of the order of 100 gauss exerted a stabilizing influence on the discharge; it yielded purer RF oscillations, and tended to eliminate the pulling effect of the probe. At the same time the magnetic field tended to eliminate the low-frequency oscillations present, a phenomenon discussed in Section VI below. We might associate this result with the elimination of the modulation of the HF signals by LF oscillations. Mahaffey [37] continued the work, using plane oxide-coated cathodes, and made simultaneous measurements of charge density, electron temperature, oscillation intensity, and frequency. A strong tendency was found for oscillations to grow in intensity in the direction of decreasing charge density, and to die out when the beam moved up a density gradient. This result is in agreement with the suggestions of Allis [145], who pointed out that as the primary beam became lost by scattering, an oscillation at the plasma frequency would be cut off as it traveled into a region of higher plasma density, but would be enhanced as it traveled into a region of lower plasma density. In Mahaffey's work, close correlation between the frequency of oscillation and the measured plasma frequency was always observed.

As would be expected from the theoretical work of Sturrock [119]–[120], and Bunemann [121] discussed earlier, there is no clear experimental evidence that natural oscillations can occur without some feedback mechanism present. Either there seems to be growth from noise, or in the experiments in which standing waves along a beam passing through a plasma have been observed, feedback mechanisms have been present which could cause the standing waves. For example, an experiment by Kofoid [146], carried out in argon at 11-μ pressure, involved identical oppositely-directed beams entering through parallel plane electrodes held at space potential. Strong standing waves near the plasma frequency were indicated only when both beams were present. If, however, the electrode potentials were changed to provide sheaths, thereby introducing a feedback mechanism, standing waves were observed with a single beam. This type of oscillation is discussed more fully below.

C. Beam-Plasma Interactions Dependent on Sheaths

The deliberately excited oscillations discussed so far could occur independently of the presence of sheaths. In the case of spontaneous oscillations, the cathode sheath is necessary to form the beam of primaries, but the growth mechanism is, of course, independent of the origin of the beam. In a bounded plasma of dimensions sufficiently small for a primary beam not to break up completely in transit, it is possible that sheaths can provide a feedback mechanism analogous to that in a reflex klystron, the plasma representing a drift space between the sheaths. Standing waves can be set up with wavelengths dependent on factors such as beam velocity and tube geometry.

An observation of standing waves was made by Looney and Brown [139] in an unsuccessful experiment to observe spatially-growing waves on a high-density beam. The reason for their lack of success has been dealt with by Sturrock [123], who develops the appropriate dispersion relation for a thin beam and shows that the interaction distance was too small for a noise signal to grow to a measurable amplitude, the maximum gain being only about 20 db. A schematic of their experiment is shown in Fig. 5. By varying the potentials

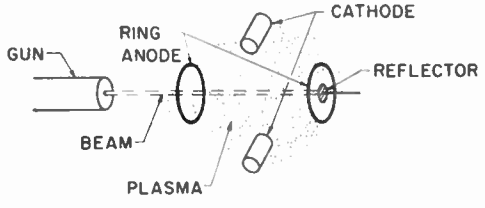

Fig. 5—Experimental arrangement used by Looney and Brown.

of the gun and its anode relative to the plasma, ion sheaths could be produced on these electrodes. A movable probe coupled to a receiver could be moved axially along the beam to measure oscillation intensity and frequency. It was found by varying gun current and sheath thickness that standing wave patterns were set up with nodes at the two sheath edges. The number of loops adjusted itself to keep the frequency as close as possible to the beam plasma frequency.

Although Looney and Brown showed that a transit

time mechanism fitted their experimental results, a clearer picture of the mechanism was offered by Demirkhanov, Gevorkov, and Popov [137], who repeated the experiment and showed that the feedback mechanism required to maintain the oscillations is provided by secondary electrons ejected from the anode by the impinging beam. These are trapped in the interelectrode space, where they oscillate. Several frequencies are possible, but we might expect the maximum oscillation amplitude near the plasma frequency.

A similar explanation of these experiments has been given in the unpublished work of Gordon [141]. Using an improved version of the Looney-Brown experimental tube, he was able to show that oscillations only occurred when there was a returning beam of secondary electron. Gordon suggested a theory for the oscillation modes based on a klystron-type mechanism in which the primary beam took no part. It assumed that secondaries were emitted from the reflector, traveled to the gun end of the tube, and were reflected at the sheath there. In his experiment, the oscillation frequency f and transit time τ of the secondaries were related to within a few per cent by the usual expression for reflex klystrons $f\tau = n + \frac{3}{4}$. Gordon also obtained oscillations in another tube when the primary beam was itself reflected by the sheath at the reflector. However, these oscillations were weak. Gordon added further evidence of the disturbing influence of probes in experiments of this nature. He found that the oscillations, and the standing wave pattern associated with them, became erratic when the probe was in the beam. They could be detected from outside, though the field strength decreased rapidly with distance of the probe from the beam edge. Detection became difficult more than a centimeter from the beam.

An even clearer illustration of the klystron-type mechanism had been given earlier by Wehner [147], [148], using a discharge tube of the type shown in Fig. 6 and described by Fetz [149], [150], Schumann [151], and Wehner [152]. This material is reviewed by Gabor [153]. The Wehner oscillator is worthy of interest as one of the few practical devices to emerge as a result of plasma research. It is capable of producing several watts of microwave power up to a few kMc. The primary electron beam emerges from the low-temperature, nonluminous plasma in the gridded cathode container and is reflected by the repeller electrode. Sheaths with potentials up to 1 kv across them can easily be formed on the grid and the repeller. Wehner detected oscillations using a Lecher wire system connected between the repeller and the anode of the device. He was able to observe meniscus-shaped oscillation layers close to the sheaths, and the existence of 5 separate modes over a range of beam voltage and frequency. Good agreement was obtained between these experimental results and a theoretical analysis based on a klystron-type transit-time mechanism.

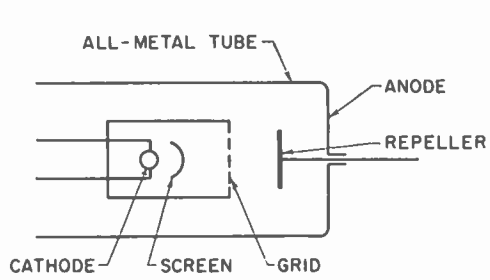

Fig. 6—The Wehner oscillator.

Although we have shown that this type of oscillation can be induced deliberately, there seem to be no definitive experiments in which such oscillations have been observed to occur naturally.

D. Beam-Surface Wave Interactions

The observation that propagation with phase velocity very much less than that of light occurs below the plasma frequency in finite plasmas has been put on a firm theoretical basis and checked experimentally by Gould and Trivelpiece [59], [60], [126]. As already discussed, they have shown that two basic modes of propagation can occur: surface waves involving only a perturbation of charge at the surface of the plasma, and body waves involving charge density variation within the plasma, which occur only in the presence of a magnetic field. The former effect is unrelated to sheaths since it can occur in a zero temperature plasma which has no sheath. In his experiments, Boyd [2] was able to observe interaction of an electron beam with the surface wave at frequencies below the plasma frequency, producing growth rates of about 1 db/cm. It is possible that such an interaction may be observed with the beam emerging from the cathode region of a discharge, but so far there has been no definite experimental evidence of this effect occurring.

E. Sheath Oscillations

From vacuum tube theory, we are familiar with the concept of negative beam-loading due to the transit time of electrons passing through a gap. It was pointed out by Emeleus [109], [143] that there is the possibility that, if the sheath is regarded as a gap, nonreturning beams traversing sheaths in plasma may maintain oscillations in these regions through such a mechanism.

It may be shown theoretically [141] that the characteristics of such oscillations are

$$\lambda I^{1/2} = \text{a constant} \tag{27}$$

and

$$\lambda V^{1/2} = \text{a constant} \tag{28}$$

for temperature-limited and space-charge-limited emission conditions, respectively, where λ is the free-space wavelength, V is the cathode sheath voltage, and I is the saturated emission current. Gordon [141] suggests that (27) is a direct result of the assumption that the

width of the oscillating region is very small compared with the mean free path for collisions. The presence of such oscillations in cylindrical plasma diodes has been observed by Armstrong and Emeleus [108], and Sluzkin and Maydanov in the USSR, who are quoted by Gordon as having obtained results in good agreement with the theoretical relations given above.

Allis [145] has shown that, through the mechanism of oscillations, a beam of electrons entering a plasma can deliver energy to a region about ten times the cathode sheath thickness, a result corroborated by the experimental observations of Emeleus [154] and Merrill and Webb [33]. It is possible that the oscillations observed in the cathode sheath do not grow from noise alone, but that nonuniformity, or transit time effects in the sheath, may provide a direct feedback mechanism to produce them.

It was pointed out by Langmuir that there is an apparent contradiction associated with the Maxwellian distribution of electron velocities normally observed in low-pressure discharges at points far from the cathode. High-velocity electrons should escape through the sheath to recombine with ions at the wall of the discharge. As the electron mean free paths for collisions are very large, there is no obvious dc mechanism for Maxwellianization, and there should be a lack of high-velocity electrons near the sheath. Gabor [10] called this phenomenon "Langmuir's paradox." It was suggested by both Langmuir [8] and Gabor [10] that strong collective oscillations must be taking place. Gabor, Ash, and Dracott [13] pointed out in a later paper that this type of collective interaction could occur in the sheath, and proposed a mechanism analogous to that of the reflex klystron in which electrons entered the sheath and returned to the plasma, the sheath behaving as a klystron gap. In an elegant set of experiments using a finely collimated high-energy low-current electron beam traveling parallel to a plane plasma-sheath interface, they determined not only the dc field strength in the sheath, but also that of the superposed ac field which was found to be present. Both fields were found to have an approximately linear increase with distance from the plasma. The frequency of the oscillations was about $\frac{1}{5}$ of the plasma frequency.

It is interesting to note that a linear field distribution is isochronous for incoming electrons, *i.e.*, that the transit time is independent of velocity, and that the reciprocal of the transit time for the field distribution, determined experimentally, corresponded to about half the frequency of the sheath oscillations. Physically this means that, depending on its time of arrival, a slow electron may be able to reach the wall, while a fast one arriving a half-cycle later will not. The authors put this forward as a Maxwellianizing mechanism which would offset the loss of high-velocity electrons to the wall that would have to be assumed on a steady-state theory.

Gordon [141] has shown, using an approximate theory, that the wall sheath can absorb energy from an almost Maxwellian distribution of electrons entering and being reflected from it. He has also obtained reasonable numerical agreement with the frequency of oscillations observed in the sheath by Gabor, Ash, and Dracott [13].

The problem of the Langmuir paradox and the oscillation mechanisms that have been demonstrated experimentally lead to serious doubt as to whether a plasma could exist in a low-pressure gas without the presence of oscillations. Certainly it is difficult to understand how a plasma would maintain its essential nature near the wall of a discharge without oscillations, for these high-velocity electrons provide the necessary ionizing collisions. One alternative to the sheath oscillation hypothesis has been advanced by Martin and Emeleus [14], who suggested that high velocity electrons to maintain the tail of the velocity distribution are also generated in the scattering region near the cathode. It is not certain, however, that this mechanism could supply sufficient high-velocity electrons in a long discharge tube.

IV. Low-Frequency Oscillations

A. Ion Waves

Studies of low-pressure discharges in the late 1920's revealed not only the high-frequency oscillations discussed already, but also low-frequency fluctuations in a frequency band from zero to a few megacycles per second. Among the earliest papers dealing with this topic were two contributions by Pardue and Webb published in 1928 [155], [156]. Using a straight uniform tube with an oxide-coated filament at one end and an anode at the other, they explored a pressure range of 15–90 μ in air. They found that the most prominent frequency peaked at about 20 μ, and that several frequencies related to this component were usually present. By analogy to the electron plasma oscillations, they suggested that these might be ion plasma oscillations. The properties of such oscillations were quoted by Langmuir in 1928 [8], and the derivations were published by Tonks and Langmuir in 1929 [57], [58].

1) Theoretical Approaches

Following Tonks and Langmuir, we assume that the unperturbed ions are at rest, so that we can use (2) to represent the ion motion and write for the one-dimensional case

$$j\omega v_{i1} = j\frac{eB}{m_i}\phi, \tag{29}$$

where the subscript i denotes ion parameters. All quantities are taken to vary as $\exp j(\omega t - \beta z)$, and the electric field has been derived from a potential ϕ by writing

$$E = -\nabla\phi = j\beta\phi. \tag{30}$$

By using the relation between current density and velocity, (3), and the equation of continuity, (5), it is

found that the ac charge density of the ions, $\rho_{i1}(=en_{i1})$, is

$$\rho_{i1} = \frac{\rho_i e\beta^2}{m_i\omega^2}\phi. \tag{31}$$

Tonks and Langmuir assumed that the ion oscillations are so slow that the electrons remain in a Maxwell-Boltzmann distribution. With this assumption, we can write

$$\rho_{e1} = -\rho_e\left[\exp\left(\frac{e\phi}{kT_e}\right) - 1\right]. \tag{32}$$

If we assume that $e\phi/kT_e \ll 1$, it follows that

$$\rho_{e1} = -\frac{e\rho_e\phi}{kT_e}. \tag{33}$$

Finally, the application of Poisson's equation yields the relation

$$\beta^2\phi = \frac{\rho_{e1}+\rho_{i1}}{\epsilon_0} = \phi\left(-\frac{e\rho_e}{kT_e\epsilon_0} + \frac{\beta^2 e\rho_i}{\omega^2 m_i\epsilon_0}\right). \tag{34}$$

Assuming $\rho_e = \rho_i$, the phase velocity $v_p(=\omega/\beta)$ of the wave is given by

$$v_p = \left(\frac{kT_e}{m_i}\right)^{1/2}\left(1 - \frac{\omega^2}{\omega_{pi}^2}\right)^{1/2}, \tag{35}$$

where the ion plasma frequency $f_{pi}(=\omega_{pi}/2\pi)$ is defined by

$$\omega_{pi}^2 = \frac{n_i e^2}{\epsilon_0 m_i}. \tag{36}$$

It follows from the dispersion relation of (35) that an electrostatic wave can exist between zero frequency and the ion plasma frequency. For $\omega \ll \omega_{pi}$, $v_p \rightarrow (kT_e/m_i)^{1/2}$. The wave then has the characteristics of a sound wave in which the atoms of the gas have the mass of the ions, but the temperature of the electrons and the velocity is independent of the density. Consequently, this type of wave is called an "electrostatic sound wave" [57].

The Tonks and Langmuir theory assumes, essentially, an isothermal expansion of the plasma. A better description has been used by Spitzer [68], introducing a pressure term into the equation of motion of the average electron, or ion. He assumed that the pressure p is a scalar, defined in terms of the mean square velocity fluctuation $p = \overline{m(v-\bar{v})^2}$. If the plasma expands adiabatically, it may be assumed that $p \propto n^\gamma$. By using these assumptions, the following dispersion equation may be derived [157], [158]:

$$1 = \frac{\omega_{pe}^2}{\omega^2 - \beta^2 w_e^2} + \frac{\omega_{pi}^2}{\omega^2 - \beta^2 w_i^2}. \tag{37}$$

where $w_e = (\gamma_e kT_e/m_e)^{1/2}$ is the electron acoustic velocity and w_i is defined similarly for the ions. When $T_i = 0$, the expression reduces to that of (35), if it is assumed that $m_i \gg m_e$, and if T_e in (35) is replaced by $\gamma_e T_e$.

This theory may be easily generalized to take account of the finite dimensions of a plasma and of collisions between electrons and neutrals, ions and neutrals, and electrons and ions [157]–[160]. As for ordinary sound waves, a low-frequency cutoff for the propagation is predicted, dependent on the dimensions of the plasma column. If it is assumed that the potential is zero at the edge of a uniform cylindrical column of radius a, the low-frequency cutoff ω_c of a wave with components that vary as $\exp j(\omega t - \beta z)\cos n\theta$ will be determined by the relation $J_n(\omega_c a/w_e) = 0$, where J_n is the nth-order Bessel function of the first kind, $T_i = 0$, and $\omega_c \ll \omega_{pi}$. The collision frequency ν between electrons and ions or neutrals is taken into account by replacing the ω^2 in the denominator of the first term of (37) by $\omega(\omega - j\nu)$. In practice, such collisions exert a negligible effect. For instance, when $T_i = 0$ the damping term in the propagation constant is of the order $-(j\nu/2\omega)(m_e/m_i)\beta$.

We might expect, then, to observe ion oscillations in a plasma in the two frequency ranges corresponding to cutoff of the ion modes: (1) at the ion plasma frequency, the high-frequency cutoff, and (2) at the low-frequency resonances of a finite plasma.

The type of theory described so far postulates a high electron-electron collision frequency and zero temperature for the ions. The properties of ion waves have been attacked using the collision-free Boltzmann equation by Newcomb [161], Fried and Gould [157], [158], and Bernstein, *et al.* [162], [163]. They showed that if the ions were at zero temperature, waves very similar to those obtained in the early theories were derived. However, if the ions have a finite temperature, there is strong Landau damping, the damping being strongest in the region $T_e \doteq T_i$. This effect is explained physically by Fried and Gould as being due to the majority of the ions traveling at about the same phase velocity as the wave. On the other hand, if there is a relative drift velocity between the ions and electrons, the authors cited above and Bunemann [136], [164], [165] all show that a two-stream instability develops and the ion waves become unstable: for $T_i = 0$, only negligible drift velocity is needed for instability. For $T_e = T_i$, the minimum drift velocity for very long wavelength instabilities is

$$v_D = 0.925\left[1 + \left(\frac{m_e}{m_i}\right)^{1/2}\right]\left(\frac{2kT_e}{m_e}\right)^{1/2}. \tag{38}$$

Fried and Gould [157] suggested that this type of instability should take place in a mercury vapor discharge, due to the relative longitudinal drift motion of ions and electrons along the positive column. However, as the radial motion of the ions and electrons, the ionizing collisions, and the rate of collisions of ions with the wall in such a discharge were not taken into account in their theory, it is not clear whether the effects predicted should occur in practice.

Bunemann [165], who had previously obtained some of the same results as Fried and Gould, also carried out

computations of the large amplitude oscillations. On the basis of this work, he suggested that such collective interactions could provide a rapid mechanism for restoring grossly non-Maxwellian distributions to near Maxwellian, and thus give rise to an extremely high effective collision frequency between electrons and ions.

2) Oscillations in Beams

The problem of ion oscillations was approached from a different point of view by Pierce [166], who gave a theoretical treatment of the oscillations which occur when an electron beam passes through the ion cloud formed by its collisions with gas molecules. This theory predicted that wave amplification should occur at frequencies below the ion plasma frequency, with maximum gain at the ion plasma frequency. It has been proposed that the feedback mechanism necessary to cause oscillations is supplied by slow secondaries moving in the backward direction. In this case the oscillations would be expected to occur near the ion plasma frequency. Such oscillations were observed unequivocally by Hernqvist [167], [168].

Low-frequency oscillations of other kinds are also observed in electron beams. Some of these oscillations are due to low-velocity secondaries alone, but most are due to ions. Hernqvist [167], [168], Cutler [169], Moreno [170], and Ettenberg and Targ [171] have described these effects. Relaxation oscillations often occur, usually of a modified sawtooth shape, and are probably connected with the ionization and deionization processes occurring in the beam. There is also a class of oscillations connected with interaction of the electron beam with a backward wave propagating along the ion cloud in the presence of a magnetic field. The theory of this effect has been dealt with by Pierce [166] and by Smullin and Chorney [61], [172]. Another class seems to occur in short beams where, as has been pointed out by Jepsen [173], it is extremely unlikely that the beam length is long enough to allow sufficient phase delay around the oscillation loop to yield the two-stream oscillations described by Pierce [166]. A theory of ion oscillations in a gridded drift tube in which the electric field in the drift tube is postulated to undergo one or more space reversals has been given by Jepsen [173], and Smullin and Chorney [61], [172]. They show that when a beam of fast electrons traverses such a region, the beam loading can be negative, and oscillations can occur.

3) Experimental Observations of Ion Oscillations

Tonks and Langmuir [57] searched for evidence of ionic oscillations in a gas discharge plasma with little success, except for an isolated observation of a naturally-occurring frequency component near to the predicted value of plasma frequency. Later, Revans [174], Druyvesteyn and Warmoltz [30], Funk and Seeliger [175], and others have reported naturally-occurring low-frequency oscillations without establishing their exact origin. Direct attempts to set them up and study their characteristics failed for reasons described by Armstrong, Emeleus, and Neill [159], whose experiments involved pulsing between the anode and an electrode immersed in a plasma, and observing the transient at other points along the tube. In view of the low velocity of propagation of ion waves ($\sim 10^5$ cm), phase shift should have been easily measured. Instead, an apparently instantaneous response was observed at all observation points. This result has been confirmed by Kino and Woods [176] using a wide variety of techniques to attempt ion wave excitation.

The presence of a high level of low-frequency noise would mask low-level ion wave amplitudes, and it should be remembered that the dispersion relation was derived using a small-signal approximation. It is possible, of course, that the noise itself propagates as an ion wave, and experiments have been carried out by Thong Saw Pak [177], and Crawford and Lawson [178] to measure propagation velocities of noise in tubes. The former concluded that propagation velocities must exceed 10^7 cm and that the entire positive column was fluctuating coherently. The latter used hot-cathode discharge tubes of the type illustrated in Fig. 7, having a positive column of smaller diameter than the cathode region. By observing potential and number density fluctuations along the tube, these workers were able to show that the noise was generated close to the cathode and that the propagation velocity was $>10^9$ cm over most of the column. This high-velocity mode of propagation can be regarded as a low-frequency version of the surface wave propagation described by Gould and Trivelpiece [59], [60], [126] or, at even lower frequencies, as due to conduction along the column.

Crawford and Lawson also noted that in the first 20 cm or so of the column, after the constriction, there was a smearing of phase, and that the main component of the noise appeared to have a phase velocity of the order of 10^7 cm. The frequency spectrum of the noise, which was typically as shown in Fig. 7, contained two or three low-frequency peaks which varied little in frequency or amplitude with current. This phenomenon was suggestive of sound wave modes, and the experiments were extended by Crawford [160], [179] using different discharge tubes, with a wide range of column diameters, to see whether the frequency peaks were related to each other, and to the column diameter. It was found that the frequency peaks f_0, f_1, and f_2 in any given tube had approximately the same ratio to each other as the three lowest zeros of $J_n(x)$, *i.e.*, the lowest two roots of $J_0(x)=0$ and the first root of $J_1(x)=0$. The measured frequency was also inversely proportional to the column diameter of the tube involved. In accordance with the theory for a finite column already described, there was a strong suggestion of the presence of radial sound wave modes, *i.e.*, oscillations at the low-frequency cutoff for

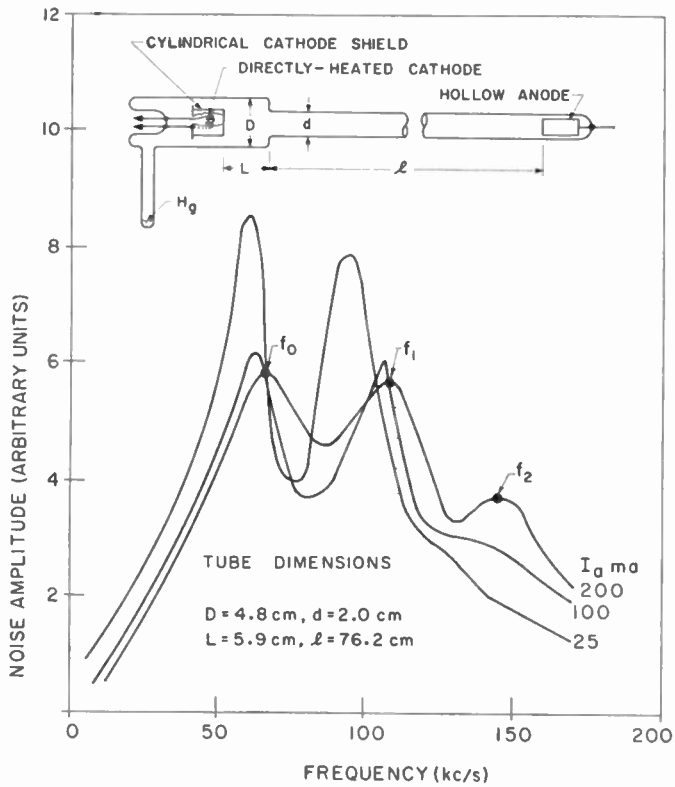

Fig. 7—Discharge tube used in the experiments of Crawford and Lawson with typical low-frequency noise spectra.

sound wave modes. By carrying out temperature measurements on two of the tubes, Crawford was able to arrive at a value of γ_e of the order of 2. Thus the measured frequencies were also in the correct range for ion sound wave modes. However, an objection to this hypothesis is that one of the strongest modes observed corresponds to an azimuthal variation of field. This seems unlikely, since detection of such modes should be difficult on a symmetrically-placed anode, or pickup ring outside the tube.

Some observations of low-frequency resonances reported by Gabovitch, *et al.* [180], who applied a low-frequency signal to a probe whose dc potential was varied, may also have been associated with ion wave oscillations.

Careful examination of noise frequency spectra under widely varying discharge conditions should give further clues as to whether ion waves constitute the basic components. The first comprehensive measurements of this kind were made by Cobine and Gallagher [15] using argon at pressures from 10 μ to 2 mm Hg. Unfortunately, commercial tubes with relatively complicated noise spectra containing a number of peaks were employed. One feature which emerged was that above a certain critical frequency, varying inversely as the atomic weight of the gas, there was a falling-off in high-frequency noise. This effect does not seem to have been observed in work at lower pressures. Cobine and Gallagher also ascertained that fluctuations in light output corresponded in waveform to the voltage fluctuations observed.

Results obtained by Martin and Woods [181] using a tungsten filament and hemicylindrical anode showed spectra containing many peaks whose frequency increased with current, but which were difficult to analyze. However, using tubes with simpler geometries, Crawford [179], [182] has been able to show that frequency components at both extremes of the ion wave spectrum can exist. With uniform tubes having plane cathodes, a high-frequency oscillation near the ion plasma frequency, varying as the square root of the anode current, is observed. Occasionally, fixed peaks suggestive of the sound wave modes are also present in a broader spectrum of oscillations. Complicating the tube or electrode geometry enhances the fixed-frequency effects, probably by introducing more turbulent conditions in the discharge.

Impedance measurements made by Crawford and Lawson [178], [183] have been interpreted theoretically to derive equivalent circuits for a plasma, the parameters of which can be related to diffusion and collision processes occurring in the positive column [183]. The various time-constants and resonances seem to be associated closely with the frequencies at which strong noise components were observed in their experiments.

4) *Oscillations at the Cathode Sheath*

It was pointed out by Cobine and Gallagher [15] that a small movement of the ion sheath at the column side of the double sheath in front of the cathode would be sufficient to give rise to the oscillation potentials observed. Such a movement could be excited by a two-stream instability due to the primary electrons passing through this sheath. Another possibility closely connected to this one is negative loading of the primary beam by the ion sheath, in the manner described for electron beams by Jepsen [173] and Smullin and Chorney [61], [172]. Neither type of theory has, however, been fully worked out for this case. We would expect, though, that there would be oscillations near the ion plasma frequency of the plasma in front of the cathode. The current-dependent oscillations measured by Crawford, and described in the last paragraph, are probably evidence of the existence of this effect. As confirmation, it is worth noting that the actual values of frequency obtained from several tubes of different diameters, containing various different cathodes, normalized closely with respect to cathode current density in the case of current-dependent frequency variation. This implies that these oscillations were generated close to the cathode. Using tubes with movable anodes, further support has been added to this view by the fact that the frequencies remain unchanged until the anode is brought to a few millimeters from the cathode and begins to disturb such fundamental features of the discharge as the meniscus.

B. Potential Minimum Oscillations

Under space-charge-limited emission conditions, there will always be a retarding potential at the cathode in either a hard tube or a gas discharge tube. This results in the formation of a potential minimum close to the cathode. It was suggested as long ago as 1929 by Kingdon [184] that positive ions could get trapped in this minimum and oscillate there, and that this could occur even at discharge currents in the Townsend region preceding plasma formation. Such oscillations in the pre-plasma state have been reported by Ballantine [185] and others [15], [181], [186], [187].

A theory of potential minimum oscillations has been given recently by Waymouth [188], who has derived a modified form of the Tonks-Langmuir dispersion relation quoted in (35).

In the experiments of Crawford [179], [182] in which an ion plasma frequency proportional to $I_a^{1/2}$ was observed, there was in some tubes a second peak in the spectrum at a frequency approximately 1/10 of this, which moved with increasing anode current according to a power law between $\frac{1}{3}$ and $\frac{1}{2}$. This has not been explained but may well be a potential minimum oscillation. Experiments with several tubes indicated that the frequency depended on cathode current density rather than on column current density, and was unaffected by the movement of the anode, as in the case of the first type of current-varying oscillation.

In experiments with fluorescent tubes van Boort and Klerk [189] and Waymouth [188] also observed oscillations, which they postulated were potential minimum oscillations. It may be seen from Waymouth's data that the frequency of these oscillations was proportional to $I_a^{1/3}$. These workers noted that the oscillations measured at the anode of the discharge or on a probe disappeared when the cathode was temperature-limited. Waymouth suggested that this result was evidence that the oscillations took place in the potential minimum and used the vanishing point as a measure of the saturation current of the cathode. However, Crawford and Lawson [178] showed that, as the impedance of the discharge becomes very large when it is temperature limited, any oscillations generated internally would not be observed easily outside the discharge. In one experiment, using a microwave resonant cavity perturbation technique, they were able to show that there were still substantially unchanged fluctuations of charge density in the plasma column, even when the cathode was temperature limited, and no oscillations could be measured on the anode of the discharge.

C. Striations

It has been mentioned earlier that the study of oscillations by use of probes within the discharge is complicated by the disturbing effects of the probe itself, particularly in the vicinity of sheaths. These matters and the feasibility of using external probes are discussed by Emeleus [190], [191], who points out that much valuable information can be obtained by observing the light output from the discharge. The results of such studies by Cobine and Gallagher [15] and Landecker and Robinson [192] indicate close correlation between the frequency spectra of anode voltage and light output fluctuations.

A familiar feature of discharges at pressures of the order of 1 mm is the presence of either fixed or moving striations. Their mechanisms and theory are still not fully understood, but it is indicated by Pupp [193] that they are associated with potential fluctuations of several volts and large changes in electron temperature and concentration. The early experiments of Appleton and West [194] suggest that the striations are accompanied by a high level of low-frequency noise. Druyvesteyn and Penning [29] summarized much of the early work, but did not indicate the existence of striations at pressures below 100 μ. Loeb [195] suggests they may exist down to pressures of about 10 μ, and that they are more likely to occur in impure gases or gas mixtures. Much of the more recent experimental work has been carried out by Dieke and his co-workers [196], [197], and Pekarek [198], [199], and a theoretical discussion has been given by Robertson [200].

There seem to have been no published observations of striations occurring in mercury vapor discharges at a few microns until a paper by Foulds [201] in 1956. In a cold cathode tube, using photocell techniques and a rotating mirror camera, Foulds was able to observe almost regular striations moving toward the cathode and some evidence for irregular striations moving toward the anode. Frequencies and velocities of the order of 10 kc and 2.10^5 cm were involved. This conflicts with some earlier results of McCurdy, *et al.* [202]–[204], who found that pure mercury vapor gave no standing striations. There could possibly have been unobserved moving striations in their experiments, however. The present state of the theory does not allow us to predict the occurrence and characteristics of striations, but the velocities involved agree reasonably well with the results of an experiment of Armstrong, Emeleus, and Neill [159], in which a region of heavy ionization was forced to pulsate under the influence of abrupt changes in electrode potentials.

D. Anode Spots

Armstrong, Emeleus, and Neill [159] have pointed out that instabilities can occur near to the anode of a low-pressure discharge in certain regions of the voltage/current characteristic. Small spots may form, generating low-frequency oscillations which have considerable energy associated with them [205]. The authors describe experiments in which the tube became a source of audible noise.

The exact mechanism of this anode glow instability is still obscure, but it seems to be more pronounced when the anode fall is positive than when it is negative. It is further intensified when there is large curvature of the

glow (for example, when the discharge anode is small or when impurities are present). Pupp's experiments suggest a connection with the existence of striations [206].

Armstrong, *et al.* [159], suggest that pressure instabilities may be responsible. Langmuir [207] showed as long ago as 1923 that steady currents produce differences of gas pressure in a tube, but the subject of instability under these conditions does not seem to have received attention. It may have relevance to the production mechanism of striations.

E. Miscellaneous

Several other mechanisms not included in the foregoing sections have been suggested as being important in noise generation [154]. The majority of these effects are associated with the cathode. It is felt that, although they might occur under special conditions, they are not the major sources of noise in most tubes; neither are they inherent in the maintaining mechanism of the discharge. When the gross components described above have been eliminated, these mechanisms may become important.

Emeleus [154] has suggested that noise could be caused by irregular movements of the boundary between parts of the cathode emitting space-charge-limited and temperature-limited current. Clarke [208] has advanced the hypothesis that a type of flicker effect may occur, enhanced by the presence of positive ions and possibly associated with mode-jumping of standing space-charge waves in the gas very close to the cathode.

Many observations on noise frequency components have shown the presence of harmonics [155], [182]. These might be generated from sinusoidal oscillations by nonlinearities in the plasma or may be evidence of the existence of relaxation oscillations with more complicated waveforms. For example, the discharge might have two stable modes and jump from one to the other [57]. Few details of such mechanisms are available but a possible means by which they might be excited is discussed in Section V.

Two further mechanisms, the levels of which are extremely low relative to the noise actually observed, are shot and thermal effects analogous to the phenomena observed in hard tubes.

V. Interdependence of Low- and High-Frequency Oscillations

Since low- and high-frequency fluctuations have often been observed in the same tubes, we may question whether there is a causal relation between oscillations in these two ranges. Mahaffey [37] has suggested, as a result of experiments in which anode-cathode spacing could be varied, that there may be an association between the occurrence of strong positive ion oscillations and the appearance of a fully-formed meniscus. Allen, Bailey, and Emeleus [35] have also found close association of high- and low-frequency oscillations using a modified form of beam discharge similar to that of Looney and Brown [139], but relying on the cathode for formation of the beam. A flat probe which was placed perpendicular to the beam caused a diffuse glow to appear midway between probe and cathode. High- and low-frequency oscillations were observed to occur together. The glow was unstable and disappeared together with the oscillations, when a fine wire probe was used in an attempt to explore it. This last effect was observed by Bailey and Emeleus [42] who also noted that as current increased and the meniscus became blurred, there was an increase in amplitude of the low-frequency oscillations.

A suggestion advanced by Allen, Bailey, and Emeleus [35] is that the high-frequency interaction between the beam and the plasma electrons builds up so rapidly near the meniscus that the resulting violent disturbance of the discharge might lead to low-frequency ionic or relaxation oscillations. It is further suggested by Emeleus and Mahaffey [209] that transverse ion oscillations might be responsible for the transverse scattering of the cathodic beam described in Section II.

VI. Reduction of Noise in Discharges

The feasibility of reducing noise depends on whether or not the generation mechanism is an inherent process in maintenance of the plasma. Those fluctuations that are caused by the presence of the cathodic electron beam might well be eliminated if the beam could be spread or broken up without loss of energy, and it is possible that if the charge concentration could be made to increase from the cathode outwards, there would be no forward propagation of disturbances. The low-frequency noise involving cathode sheath oscillations might be reduced if the potential of the column edge were clamped firmly, while those disturbances which are of geometrical origin (for example, the effects of a constriction in the discharge) might be reduced by some sort of focusing of the streams passing through.

Some experiments along these lines have already been carried out. Cobine and his associates [15], [210], [211] investigated the effects of a magnetic field transverse to current flow on oscillations in discharges at pressures around 100 μ, and established that the low-frequency effects observed at the anode were reduced when the primaries were deflected to miss the anode. They also discovered that as the magnetic field strength was increased, the over-all noise passed through a minimum and increased again. Similar effects to those in hot cathode tubes were also observed by Ruthberg [212], using cold cathodes. Cobine and Gallagher's results for a transverse field were confirmed by Armstrong, Emeleus, and Neill [159], while the case of an axial magnetic field was examined by Bailey and Emeleus [42]. They found that field strengths of the order of tens of gauss would reduce the low-frequency noise and stabilize the meniscus. They made no comment about the effect of the high-frequency noise component on the amplitude.

These results have been extended by Crawford [179],

who has shown that axial magnetic fields less than 50 gauss can reduce the level of the relatively fixed frequency noise components occurring in long discharge tubes by as much as 20–30 db. Beyond the minimum the noise increases again. This effect may be related to the well-known anomalous diffusion mechanism [52], [213]. The strongly current-dependent mechanisms located in or near the cathode sheath are not affected materially by an axial magnetic field.

The use of an auxiliary electrode to reduce low-frequency fluctuations was investigated by Thong Saw Pak [214]. He describes a tube in which a wire filament was placed at the focus of a parabolic wire gauze electrode, the open side of which faced the anode. Noise figures of the order of 50 db lower than those usually obtained without such an electrode were observed for currents up to about 80 ma, when noise again appeared. Even then, a positive bias on the auxiliary electrode could reduce the noise somewhat.

Further experiments involving fine-mesh grids between cathode and anode of a plasma have confirmed these results, and Johnson, Olmstead, and Webster [215] have coined the apt (but etymologically questionable!) term "Tacitron" for a low-noise device of this type operating in the anode glow mode, and have described its characteristics.

Crawford [179] has carried out experiments with a gridded tube in which the grid-cathode spacing was of the order of a Debye length. The grid potential assumed a value approximately equal to the ionization potential of mercury ($\sim$10 volts) and variation of grid and anode current divided the noise characteristics into two regions: for $I_a/I_u > K$ there was a very low noise level, and for $I_a/I_u < K$ the noise increased sharply. For the tube tested K was approximately constant, and was about 3.

VII. Discussion

Recent years have seen the growth of a complex structure of plasma theory on the foundations laid by Langmuir and his co-workers 30 years ago. The study of wave propagation at microwave frequencies has been carried to a highly sophisticated level, though the models with which this study have been conducted have not always represented accurately the behavior of actual experimental plasmas. Certain of the oscillations which occur naturally in most dc discharges may provide a check on the theories. If these oscillation mechanisms can be elucidated and effectively suppressed, it should be possible to carry out more detailed quantitative experiments to check the theoretical studies of propagation. Such work would be useful not only to the fusion field and to the general study of instabilities, but should also suggest new possibilities in the field of microwave generation [216] and amplification: already, Wehner [147], [148] has demonstrated that reflex klystron-type oscillations involving sheaths can be utilized in wide-band electronically tunable oscillators of reasonable efficiency, while electron beam-plasma interactions offer the intriguing prospect of high-gain microwave amplification. The permeable, structureless nature of this type of amplifier is an attractive possibility for millimeter wave amplification. In addition, there may be entirely new methods for coupling in and out of the system, based on the unusual radial propagation effects in the presence of a magnetic field, on the high rate of amplification, as discussed by Feinstein [217], or on the nonlinear interaction with an electromagnetic wave of the type described by Sturrock [45]–[48]. These coupling mechanisms, which are not necessarily subject to the usual limitations of slow-wave devices, have been discussed by Kino [218]. A major drawback to such devices at the present time is the presence of high- and low-frequency oscillations in the discharge. Broad-banding the device, for example, by using a nonuniform plasma may help to discriminate against low-frequency fluctuations in charge density, but effort is required to reduce spontaneous oscillations which may be generated in the working range.

It is still not clear whether a plasma can exist without self-generated oscillations, but it seems reasonable to assume that all but those required for Maxwellianization of the electron velocity distribution might be eliminated if sufficient care were taken. The presence of the sheath oscillations detected by Gabor, Ash, and Dracott [13] would seem to be necessary for this process. However, because they are at a relatively low frequency compared to the plasma frequency and because their fields are normal to the plasma edge, they may well have only weak fields within the plasma itself. By deliberately increasing the charge density in the direction of the cathodic electron beam, we might cause the effect of the RF oscillations generated in the vicinity of the meniscus to be very weak in the amplifying region also.

Two alternatives would be: 1) to use other types of discharges such as the highly ionized, synthetic cesium plasmas based on the resonance ionization phenomenon first investigated by Langmuir and Kingdon [219] and studied in more detail recently by Allen and Kino [128], D'Angelo and Rynn [220], and Knetchtli and Wada [221], or 2) to use the negative-glow mode which occurs at rather higher pressures and has electron temperatures which can be only a few hundred degrees. These properties and possible applications have been described by Anderson [222], [224] and Harris [223].

Although there is now fairly good qualitative understanding of the mechanisms giving rise to spontaneous RF oscillations, considerably more work is required for a detailed understanding of scattering and Maxwellianization through sheath oscillations. Although Landau damping is now well established theoretically, there does not appear to be any direct experimental confirmation of the phenomenon available. It is understood, however, that several projects are currently in progress to study this effect in electron beams.

Although a wide variety of mechanisms has been suggested for the generation of low-frequency oscillations and noise, there are few convincing demonstrations of the existence of such fundamental phenomena as ion waves and potential minimum oscillations. On the other hand, theoretical explanations of many effects that have

been observed (for example, striations) still have no firm basis. Ion wave phenomena deserve attention because of the part they may play in causing instability and enhanced diffusion across magnetic fields, an effect particularly important in work on thermonuclear fusion. Longitudinal ion waves in the presence of a magnetic field have been reported by Alexeff and Neidigh [225], [226]. There are also possible applications of such longitudinal waves to generation and amplification in the millimeter range [227].

Work on the suppression of low-frequency fluctuations looks promising, and as there seems to be no reason why their existence should be essential to maintenance of a steady-state discharge, it may well be possible to eliminate them by careful design of the apparatus.

List of Symbols

B magnetic field strength
E electric field strength
H magnetizing intensity
J current density
N neutral density
T temperature
a positive column radius
$-e$ electronic charge
f_p plasma frequency
k Boltzmann's constant
m particle mass
n number density
p pressure
t time
v velocity
w acoustic velocity
β propagation constant
ϵ permittivity
θ azimuthal angle
λ wavelength
ν collision frequency
ρ charge density
τ transit time
ϕ potential
ω radian frequency

Subscripts:

e quantity associated with electrons
i quantity associated with ions
N quantity associated with neutrals
1 ac component

References

[1] G. S. Kino and M. A. Allen, "The Effects of Fluctuations on Propagation through a Plasma Medium," Stanford University, Stanford, Calif., Microwave Lab. Rept. No. 802, April, 1961; *Proc. 5th Internatl. Conf. on Ionization Phenomena in Gases*, Munich, Germany, August, 1961.

[2] G. D. Boyd, "Experiments on the Interaction of a Modulated Electron Beam with a Plasma," Electron Tube and Microwave Lab., Calif. Inst. Tech., Pasadena, Calif., Tech. Rept. No. 11; May, 1959.

[3] G. D. Boyd, L. M. Field, and R. W. Gould, "Excitation of plasma oscillations and growing plasma waves," *Phys. Rev.*, vol. 109, pp. 1393–1394; February, 1958.

[4] ——, "Interaction between an electron stream and an arc discharge plasma," *Proc. Symp. on Electronic Waveguides*, Brooklyn Polytechnic Inst., Brooklyn, N. Y., April 8–10, 1958, Interscience Publishers, Inc., New York, N. Y., pp. 367–375; 1958.

[5] F. H. Clauser, "The dynamics of electron beams," *Symp. of Plasma Dynamics*, Woods Hole, Mass., June 9–13, 1958, R. W. Gould, Ed., Addison-Wesley Publishing Co., Reading, Mass., pp. 78–118; 1960.

[6] I. Langmuir, "Scattering of electrons in ionized gases," *Phys. Rev.*, pp. 585–613; November, 1925.

[7] —— Über elektrische Entladungen in Gasen bei niedrigen Drüken," *Z. Phys.*, vol. 46, pp. 271–299; November, 1927.

[8] ——, "Oscillations in ionized gases," *Proc. Natl. Acad. Sci. U. S.*, vol. 14, pp. 627–637; August, 1928.

[9] J. H. Cahn, "Elektronic interaction in electrical discharges in gases," *Phys. Rev.*, vol. 75, pp. 293–300; January, 1949.

[10] D. Gabor, "Wave theory of plasmas," *Proc. Roy. Soc. (London)*, vol. A 213, pp. 73–86; June, 1952.

[11] E. A. Ash and D. Gabor, "Experimental investigations on electron interaction," *Proc. Roy. Soc. (London)*, vol. A 228, pp. 477–490; March, 1955.

[12] A. F. Dittmer, "Experiments on the scattering of electrons by ionized mercury vapor," *Phys. Rev.*, vol. 28, pp. 507–520; September, 1926.

[13] D. Gabor, E. A. Ash and D. Dracott, "Langmuir's paradox," *Nature*, vol. 176, pp. 916–919; November, 1955.

[14] H. Martin and K. G. Emeleus, "The Langmuir paradox in discharge plasma," *Nature*, vol. 177, pp. 943–944; May, 1956.

[15] J. D. Cobine and C. J. Gallagher, "Noise and oscillations in hot cathode arcs," *J. Franklin Inst.*, vol. 243, pp. 41–54; January, 1947.

[16] W. L. Fite, "Final Report on Contract AF 18(600)-487," University of Pennsylvania, Philadelphia, Pa.; August, 1954.

[17] R. D. Sears, "Investigation of Plasma Noise," Armour Research Found., Illinois Inst. Tech., Chicago, Rept. 1982-12; 1960.

[18] A. van der Ziel, "A Study of Noise in Gas Discharge Lamps," ASTIA Document No. AD 204803; November, 1958.

[19] S. Glasstone and R. H. Lovberg, "Controlled Thermonuclear Reactions," D. Van Nostrand Co., Inc., New York, N. Y.; 1960.

[20] T. J. Killian, "The uniform positive column of an electric discharge in mercury vapor," *Phys. Rev.*, vol. 35, pp. 1238–1252; May, 1930.

[21] B. Klarfeld, "The positive column of a gaseous discharge," *J. Phys. Acad. Sci. (U.S.S.R.)*, vol. 5, pp. 913–929; 1941.

[22] R. L. F. Boyd, "The collection of positive ions by a probe in an electrical discharge," *Proc. Roy. Soc. (London)*, vol. A 201, pp. 329–347; April, 1959.

[23] I. Langmuir and H. Mott-Smith, "Studies of electric discharges in gases at low pressure, part I," *Gen. Elec. Rev.*, vol. 27, pp. 449–455; July, 1924.

[24] ——, "Studies of electric discharges in gases at low pressure, part II—typical experimental data illustrating the use of plane collectors," *Gen. Elec. Rev.*, vol. 27, pp. 538–548; August, 1924.

[25] ——, "Studies of electric discharges in gases at low pressure, part III—typical experimental data illustrating the use of cylindrical collectors," *Gen. Elec. Rev.*, vol. 27, pp. 616–624; September, 1924.

[26] ——, "Studies of electric discharges in gases at low pressure, part IV—data on discharges in mercury vapor obtained with cylindrical electrodes," *Gen. Elec. Rev.*, vol. 27, pp. 762–771; November, 1924.

[27] ——, "Studies of electric discharges in gases at low pressure, part V—the use of spherical collectors and the effects of magnetic fields," *Gen. Elec. Rev.*, vol. 27, pp. 810–820; December, 1924.

[28] I. Langmuir, "The interaction of electron and positive ion space charges in cathode sheaths," *Phys. Rev.*, vol. 33, pp. 954–990; July, 1929.

[29] M. J. Druyvesteyn and F. M. Penning, "The mechanism of electrical discharges in gases of low pressure," *Rev. Mod. Phys.*, vol. 12, pp. 87–174; April, 1940.

[30] M. J. Druyvesteyn and N. Warmoltz, "Ein neuer Dunkelraum in der Nähe einer Glühkathode in einer Bogenentladung," *Physica*, vol. 4, pp. 51–68; January, 1937.

[31] ——, "Electron emission of an oxide cathode in an arc discharge," *Physica*, vol. 4, pp. 41–50; January, 1937.

[32] N. Warmoltz, "A second sheath near the cathode of an arc discharge," *Nature*, vol. 138, p. 36; July, 1936.

[33] H. J. Merrill and H. W. Webb, "Electron scattering and plasma oscillations," *Phys. Rev.*, vol. 55, pp. 1191–1198; June, 1939.

[34] T. K. Allen, "A spectroscopic study of plasma-electron oscillations," *Proc. Phys. Soc. (London)*, vol. A 68, pp. 696–700; July, 1955.

[35] T. K. Allen, R. A. Bailey and K. G. Emeleus, "The appearance of some oscillating discharges," *Brit. J. Appl. Phys.*, vol. 6, pp. 320–322; September, 1955.

[36] D. W. Mahaffey and K. G. Emeleus, "Suppression of plasma oscillations," *J. Electronics and Control*, vol. 4, pp. 301–304; April, 1958.
[37] D. W. Mahaffey, "New experimental results for plasma electron oscillations," *J. Electronics and Control*, vol. 6, pp. 193–203; March, 1959.
[38] D. W. Mahaffey, G. C. McCullagh and K. G. Emeleus, "Beam-plasma interaction," *Phys. Rev.*, vol. 112, p. 1052; November, 1958.
[39] E. B. Armstrong, "Plasma-electron oscillations," *Nature*, vol. 160, p. 713; November, 1947.
[40] T. R. Neill, "Plasma electron oscillations," *Nature*, vol. 163, pp. 59–60; January, 1949.
[41] A. Garscadden and K. G. Emeleus, "Exploration of oscillating beam-plasma fields with a transverse electron beam," *J. Electronics and Control*, vol. 9, pp. 473–476; December, 1960.
[42] R. A. Bailey and K. G. Emeleus, "Plasma-electron oscillations," *Proc. Roy. Irish Acad.*, vol. 57A, pp. 53–62; May, 1955.
[43] M. Rosenbluth, "Plasma physics 'quantum' and 'classical,'" *Phys. Today*, vol. 13, pp. 27–30; August, 1960.
[44] K. G. Emeleus, "Turbulence in gaseous conductors," *Proc. Phys. Soc. (London)*, vol. B 64, pp. 166–169; February, 1951.
[45] P. A. Sturrock, "Nonlinear effects in electron plasmas," *Proc. Roy. Soc. (London)*, vol. A 242, pp. 277–299; November, 1957.
[46] ——, "A variation principle on an energy theorem for small-amplitude disturbances of electron beams and electron-ion plasmas," *Ann. Phys.*, vol. 4, pp. 306–324; March, 1958.
[47] ——, "Action-transfer and frequency-shift relations in the nonlinear theory of waves and oscillations," *Ann. Phys.*, vol. 9, pp. 422–434; October, 1960.
[48] ——, "Nonlinear effects in electron plasmas," *J. Nuclear Energy*, pt. C, vol. 2, pp. 158–163; January, 1961.
[49] Thong Saw Pak and H. Martin, "Electron temperature and noise in hot cathode discharges," *J. Electronics and Control*, vol. 2, pp. 128–130; September, 1956.
[50] L. Tonks and I. Langmuir, "A general theory of the plasma of an arc," *Phys. Rev.*, vol. 34, pp. 876–922; September, 1929.
[51] M. Hoyaux and P. Gans, "Some properties of the mercury vapor arc at low pressures," *Proc. 4th Internatl. Conf. on Ionization Phenomena in Gases*, Uppsala, Sweden; August 17–21, 1959, North Holland Publishing Co., Amsterdam, Neth., pp. 364–368; 1960.
[52] A. Guthrie and R. K. Wakerling, "Characteristics of Electrical Discharges in Magnetic Fields," McGraw-Hill Book Co., Inc., New York, N. Y.; 1949.
[53] F. M. Penning, "Scattering of electrons in ionized gases," *Nature*, vol. 118, p. 301; August, 1926.
[54] ——, "Abnormale electronensnelheden en Trilligen van Zeer Hooge Frequentie in Ontladingsbuizen," *Physica*, vol. 6, pp. 241–248; 1926. (In Dutch, with English summary.)
[55] Lord Rayleigh, "On electrical vibrations and the constitution of the atom," *Phil. Mag.*, vol. 11, pp. 117–123; January, 1906.
[56] J. J. Thomson, "The electrodeless discharge through gases," *Proc. Phys. Soc. (London)*, vol. 40, pp. 79–89; March, 1928.
[57] L. Tonks and I. Langmuir, "Oscillations in ionized gases," *Phys. Rev.*, vol. 33, pp. 195–210; February, 1929.
[58] ——, "Note on 'oscillations in ionized gases,'" *Phys. Rev.*, vol. 33, p. 990; June, 1929.
[59] R. W. Gould and A. W. Trivelpiece, "Electro-mechanical modes in plasma waveguides," *Proc. IEE*, vol. 105 B, Suppl. 10, pp. 516–519; May, 1958.
[60] R. W. Gould and A. W. Trivelpiece, "Space charge waves in cylindrical plasma columns," *J. Appl. Phys.*, vol. 30, pp. 1784–1792; November, 1959.
[61] L. J. Smullin and P. Chorney, "Wave propagation in ion-plasma loaded waveguides," *Symp. on Electronic Waveguides*, Brooklyn Polytechnic Inst., Brooklyn, N. Y., Interscience Publishers, Inc., New York, N. Y., pp. 229–247; September, 1958.
[62] Y. B. Fainberg and M. F. Gorbatenko, "Electromagnetic waves in a plasma situated in a magnetic field," *J. Tech. Phys. U.S.S.R.*, vol. 29, pp. 487–500; May, 1959. (Translation in: *Soviet Phys.—Tech. Phys.*, vol. 4, pp. 487–500; May, 1959.)
[63] W. O. Schumann, "On the propagation of electric waves along a dielectrically confined plasma layer," *Z. angew. Phys.*, vol. 10, pp. 26–31; 1958.
[64] ——, "On wave propagation in a plasma between two perfectly conducting planes in an externally impressed magnetic field," *Z. angew. Phys.*, vol. 8, pp. 482–485; 1956.
[65] J. J. Thomson and G. P. Thomson, "Conduction of Electricity through Gases," Cambridge University Press, England, vol. 2, pp. 353–358; 1933.
[66] J. J. Thomson, "Oscillations in discharge tubes and allied phenomena," *Phil. Mag.*, vol. 2, pp. 697–735; March, 1931.
[67] ——, "Electronic waves and the electron," *Phil. Mag.*, vol. 6, pp. 1254–1281; December, 1928.
[68] L. Spitzer, "Physics of Fully Ionized Gases," Interscience Publishers, Inc., New York, N. Y.; 1956.
[69] J. R. Pierce and J. A. Morrison, "Disturbances in a multi-velocity plasma," IRE Trans. on Electron Devices, vol. ED-6, pp. 231–236; April, 1959.
[70] L. R. Walker, "The dispersion formula for plasma waves," *J. Appl. Phys.*, vol. 25, pp. 131–132; January, 1954.
[71] A. A. Vlasov, M.S. thesis, *J. Exp. Theoret. Phys. (U.S.S.R.)*, vol. 8, p. 291; 1938.
[72] ——, "On the kinetic theory of an assembly of particles with collective interaction," *J. Phys. U.S.S.R.*, vol. 9, pp. 25–40; 1945.
[73] L. Landau, "On the vibration of the electronic plasma," *J. Phys. U.S.S.R.*, vol. 10, pp. 25–34; 1946.
[74] N. G. Van Kampen, "On the theory of stationary waves in plasmas," *Physica*, vol. 21, pp. 949–963; 1955.
[75] ——, "The dispersion equation for plasma waves," *Physica*, vol. 23, pp. 641–650; July, 1957.
[76] D. Bohm and E. P. Gross, "Theory of plasma oscillations A: origin of medium-like behavior," *Phys. Rev.*, vol. 75, pp. 1851–1864; June, 1949.
[77] ——, "Theory of plasma oscillations B: excitation and damping of oscillations," *Phys. Rev.*, vol. 75, pp. 1864–1876; June, 1949.
[78] ——, "Effects of plasma boundaries in plasma," *Phys. Rev.*, vol. 79, pp. 992–1001; September, 1950.
[79] F. Berz, "On the theory of plasma waves," *Proc. Phys. Soc. (London)*, vol. B 69, pp. 939–952; September, 1952.
[80] W. P. Allis, "Electron plasma oscillations," *Proc. Symp. on Electronic Waveguides*, Brooklyn Polytechnic Inst., Brooklyn, N. Y., April 8–10, 1958, Interscience Publishers, Inc., New York, N. Y., pp. 149–159; 1958.
[81] I. B. Bernstein, J. M. Greene and M. D. Kruskal, "Exact nonlinear plasma oscillations," *Phys. Rev.*, vol. 108, pp. 546–550; November, 1957.
[82] E. P. Gross, "Plasma oscillations in a static magnetic field," *Phys. Rev.*, vol. 82, pp. 232–242; April, 1951.
[83] P. L. Bhatnagar, E. P. Gross and M. Krook, "A model for collision processes in gases. I. Small amplitude processes in charged and neutral one-component systems," *Phys. Rev.*, vol. 94, pp. 511–525; May, 1954.
[84] E. P. Gross and M. Krook, "Model for collision processes in gases: II. Small amplitude oscillations of charged two-component systems," *Phys. Rev.*, vol. 102, pp. 593–604; May, 1956.
[85] D. Bohm and D. Pines, "A collective description of electron interactions. I. Magnetic interactions," *Phys. Rev.*, vol. 82, pp. 625–634; June, 1951.
[86] ——, "A collective description of electron interactions: II. Collective vs individual particle aspects of the interactions," *Phys. Rev.*, vol. 85, pp. 338–353; January, 1952.
[87] ——, "A collective description of electron interactions: III. Coulomb interactions in a degenerate electron gas," *Phys. Rev.*, vol. 92, pp. 609–625; November, 1953.
[88] R. Q. Twiss, "On Bailey's theory of growing circularly polarized waves in a sunspot," *Phys. Rev.*, vol. 80, pp. 767–768; November, 1950.
[89] ——, "On Bailey's theory of amplified circularly polarized waves in an ionized medium," *Phys. Rev.*, vol. 84, pp. 448–457; November, 1951.
[90] ——, "Propagation in electron-ion streams," *Phys. Rev.*, vol. 88, pp. 1392–1407; December, 1952.
[91] V. A. Bailey, "Plane waves in an ionized gas with static electric and magnetic fields present," *Australian J. Sci. Research Ser. A*, vol. 1, pp. 351–359; December, 1948.
[92] J. H. Piddington, "Growth electric space-charge waves," *Australian J. Phys.*, vol. 9, pp. 31–43; March, 1956.
[93] ——, "Growing electric space-charge waves and Haeff's electron-wave tube," *Phys. Rev.*, vol. 101, pp. 14–16; January, 1956.
[94] G. Ecker, "Zur Statistischen Beschreibung von Gesamtheiten mit Kollektiver Wechselwirkung. I. Grundlagen und Grenzen Kollektiver Beschreibung," *Z. Phys.*, vol. 140, pp. 274–292; March, 1955.
[95] ——, "Zur Statistischen Beschreibung von Gesamtheiten mit Kollektiver Wechselwirkung. II. Die Bedeutung der Beschränkungen des D-Modelles für die Begriffsbildung und Ergebnisse Kollektiver Beschreibung," *Z. Phys.*, vol. 140, pp. 293–307; March, 1955.
[96] ——, "Zur Statistischen Beschreibung von Gesamtheiten mit Kollektiver Wechselwirkung. III. Die Verschiedenen Formulierungen der Trägerkinetik," *Z. Phys.*, vol. 141, pp. 294–306; July, 1956.
[97] J. E. Drummond, "Basic microwave properties of hot magneto-plasmas," *Phys. Rev.*, vol. 110, pp. 293–306; April, 1958.
[98] ——, paper presented at the Lockheed Symposium on Waves in a Plasma, December 1–2, 1960, to be published.
[99] L. Mower, "Conductivity of a warm plasma," *Phys. Rev.*, vol. 116, pp. 16–18; May, 1959.

[100] G. V. Gordeyev, "Plasma oscillations in magnetic field," *J. Exp. Theoret. Phys. (U.S.S.R.)*, vol. 23, pp. 660–669; 1952. In Russian.
[101] I. B. Bernstein, "Waves in a plasma in a magnetic field," *Phys. Rev.*, vol. 109, vol. 10–21; January, 1958.
[102] K. M. Case, "Plasma oscillations," *Ann. Phys.*, vol. 7, pp. 349–364; July, 1959.
[103] L. Oster, "Linearized theory of plasma oscillations," *Rev. Mod. Phys.*, vol. 32, pp. 141–168; January, 1960.
[104] J. D. Jackson, "Plasma oscillations," *J. Nuclear Energy*, Pt. C, vol. 1, pp. 171–189; July, 1960.
[105] I. B. Bernstein and S. K. Trehan, "Plasma oscillations, I," *Nuclear Fusion*, vol. 1, pp. 3–41; 1960.
[106] J. E. Drummond, "Oscillations in plasma," in "Plasma Physics," McGraw-Hill Book Co., Inc., New York, N. Y., pp. 1–32; 1961.
[107] J. M. Dawson, "Nonlinear oscillations in a cold plasma," *Phys. Rev.*, vol. 113, pp. 383–387; September, 1959.
[108] E. B. Armstrong and K. G. Emeleus, "The generation of high-frequency oscillations by hot-cathode discharge tubes containing gas at low pressure," *Proc. IEE*, vol. 96, pp. 390–394; January, 1949.
[109] K. G. Emeleus and R. A. Bailey, "High-frequency plasma-electron oscillations," *Brit. J. Appl. Phys.*, vol. 6, pp. 127–128; January, 1955.
[110] R. Rompe and M. Steenbeck, "Der Plasmazustand der Gase," *Ergeb. exakt. Naturw.*, vol. 18, pp. 257–376; 1939.
[111] A. V. Haeff, "Space-charge wave amplification effects," *Phys. Rev.*, vol. 74, pp. 1532–1533; November, 1948.
[112] ——, "The electron-wave tube—a novel method of generation and amplification of microwave energy," PROC. IRE, vol. 37, pp. 4–10; January, 1949.
[113] L. S. Nergaard, "Analysis of a simple model of a two beam growing-wave tube," *RCA Rev.*, vol. 9, pp. 585–601; December, 1948.
[114] J. R. Pierce, "Increasing space-charge waves," *J. Appl. Phys.*, vol. 20, pp. 1060–1066; November, 1949.
[115] ——, "Note on stability of electron flow in the presence of positive ions," *J. Appl. Phys.*, vol. 21, p. 1063; October, 1950.
[116] —— and W. B. Hebenstreit, "A new type of high-frequency amplifier," *Bell Sys. Tech. J.*, vol. 28, pp. 33–51; January, 1949.
[117] ——, "Possible fluctuations in electron streams due to ions," *J. Appl. Phys.*, vol. 19, pp. 231–241; March, 1948.
[118] R. Q. Twiss, "On oscillations in electron streams," *Proc. Phys. Soc. (London)*, vol. B 64, pp. 654–665; August, 1951.
[119] P. A. Sturrock, "Kinematics of growing waves," *Phys. Rev.*, vol. 112, pp. 1488–1503; December, 1958.
[120] ——, "Amplifying and evanescent waves, convective and non-convective instabilities," in "Plasma Physics," J. E. Drummond, Ed., McGraw-Hill Book Co., Inc., New York, N. Y., pp. 124–142; 1961.
[121] O. Buneman, "How to distinguish between attenuating and amplifying waves," in "Plasma Physics," J. E. Drummond, Ed., McGraw-Hill Book Co., Inc., New York, N. Y., pp. 143–164; 1961.
[122] G. J. Budker, "Relativistic stabilized electron beam," *Proc. CERN Symp. on High Energy Accelerators and Pion Physics*, Geneva, Switz., June 11–23, 1956, CERN Service d'Information, pp. 68–75; 1956.
[123] P. A. Sturrock, "Excitation of plasma oscillations," *Phys. Rev.*, vol. 117, pp. 1426–1429; March, 1960.
[124] E. V. Bogdanov, V. J. Kislov and Z. S. Tchernov, "Interaction between an electron stream and a plasma," *Symp. on Millimeter Wave Generation*, Brooklyn Polytechnic Inst., Brooklyn, N. Y., April 1–2, 1959, Interscience Publishers, Inc., New York, N. Y., pp. 57–72; 1959.
[125] Z. S. Tchernov and G. A. Bernashevski, "Amplification of Microwaves by Means of Plasma," presented at the Symp. on Electromagnetics and Fluid Dynamics, Brooklyn Polytechnic Inst., Brooklyn, N. Y., to be published in 1961.
[126] A. W. Trivelpiece, "Slow Wave Propagation in Plasma Waveguides," Electron Tube and Microwave Lab., California Inst. of Tech., Pasadena, Calif., Tech. Rept. No. 7; May, 1958.
[127] M. A. Allen and G. S. Kino, "Interaction of an electron beam with a fully ionized plasma," *Phys. Rev. Lett.*, vol. 6, pp. 163–165; February, 1961.
[128] ——, "Experiments with a Fully Ionized Cesium Plasma," presented at Lockheed Symp. on Waves in a Plasma, Palo Alto, Calif., December 1–2, 1960. To be published.
[129] A. I. Akhiezer and Y. B. Fainberg, "High-frequency oscillations of an electron plasma," *J. Exsptl. Theoret. Phys. U.S.S.R.*, vol. 21, pp. 1262–1269; 1951.
[130] J. Feinstein and H. K. Sen, "Radio wave generation by multi-stream charge interaction," *Phys. Rev.*, vol. 83, pp. 405–412; July, 1951.
[131] R. Q. Twiss, "Discussion on the generation of plasma oscillations," presented at the Conf. on Ionized Media, University College, London; April 7, 1951.
[132] M. A. Lampert, "Plasma oscillations at extremely high frequencies," *J. Appl. Phys.*, vol. 27, pp. 5–11; January, 1956.
[133] M. Sumi, "Theory of excited plasma waves," *J. Phys. Soc. (Japan)*, vol. 13, pp. 1476–1485; December, 1958.
[134] ——, "Excitation of oscillations in a plasma layer," *Phys. Rev. Lett.*, vol. 2, pp. 37–38; January, 1959.
[135] G. F. Filiminov, "Growing wave propagation in a plasma," *Radiotechnics and Electronics*, vol. 4, pp. 75–87; January, 1959. (In Russian.)
[136] O. Buneman, "Dissipation of currents in ionized media," *Phys. Rev.*, vol. 115, pp. 503–517; August, 1959.
[137] R. A. Demirkhanov, A. K. Gevorkov and A. P. Popov, "The interaction of a beam of charged particles with a plasma," *Proc. 4th Internatl. Conf. on Ionization Phenomena in Gases*, Uppsala, Sweden, 1959, North-Holland Publishing Co., Amsterdam, Neth., vol. 2, pp. 665–669; 1960.
[138] A. V. Haeff, "On the origin of solar radio noise," *Phys. Rev.*, vol. 75, pp. 1546–1551; May, 1949.
[139] D. H. Looney and S. C. Brown, "The excitation of plasma oscillations," *Phys. Rev.*, vol. 93, pp. 965–969; March, 1954.
[140] S. Kojima, K. Kato, and S. Hagiwara, "Oscillations in plasma I," *J. Phys. Soc. (Japan)*, vol. 12, pp. 1276–1281; November, 1957.
[141] E. I. Gordon, "'Plasma Oscillations,' the Interaction of Electron Beams with Gas Discharge Plasmas," Ph.D. dissertation, Phys. Dept., Mass. Inst. Tech., Cambridge; January, 1957.
[142] I. F. Kharchenko, *et al.*, "Experimental and theoretical investigation of the interaction of an electron beam with a plasma," *Proc. 4th Internatl. Conf. on Ionization Phenomena in Gases*, Uppsala, Sweden, 1959, North-Holland Publishing Co., Amsterdam, Neth., vol. 2, pp. 671–680; 1960.
[143] T. R. Neill and K. G. Emeleus, "Plasma electron oscillations," *Proc. Roy. Irish Acad.*, vol. 53, pp. 197–222; January, 1951.
[144] K. G. Emeleus, "Plasma electron oscillations," *Appl. Sci. Research*, vol. B 5, pp. 66–68; 1955.
[145] W. P. Allis, "Electron Oscillations in Gas Discharges," presented at URSI Meeting, Commission 7, Boulder, Colo.; 1957.
[146] M. J. Kofoid, "Experimental two-beam excitation of electron oscillations in a plasma without sheaths," *Phys. Rev. Lett.*, vol. 4, pp. 556–557; June, 1960.
[147] G. Wehner, "Plasma oscillator," *J. Appl. Phys.*, vol. 21, pp. 62–63; January, 1950.
[148] ——, "Electron plasma oscillations," *J. Appl. Phys.*, vol. 22, pp. 761–765; June, 1951.
[149] H. Fetz, "On the control of a mercury arc by means of a grid in the plasma," *Ann. Phys. (Lpz.)*, vol. 37, pp. 1–40; January, 1940.
[150] ——, "Stability of the controlled mercury arc," *Arch. Elektrotech.*, vol. 36, pp. 378–381; June, 1942.
[151] W. O. Schumann, "The stabilization of the controlled vacuum arc and the arc constants," *Arch. Elektrotech.*, vol. 36, pp. 362–377; June, 1942.
[152] G. Wehner, "Sondenuntersuchungen am stabilisierten Quecksilberdampfbogen," *Ann. Phys. (Lpz.)*, vol. 4, pp. 501–519; July, 1942.
[153] D. Gabor, "Plasma oscillations," *Brit. J. Appl. Phys.*, vol. 2, pp. 209–218; 1951.
[154] K. G. Emeleus, "Oscillations and fluctuations in gas discharges," *Nuovo cimento (Suppl. 10)*, vol. 3, pp. 490–495; March, 1956.
[155] L. A. Pardue and J. S. Webb, "Ionic oscillations in the glow discharge," *Phys. Rev.*, vol. 32, pp. 946–949; December, 1928.
[156] ——, "Ionic oscillations in the glow discharge," *Phys. Rev.*, vol. 31, p. 1122; June, 1928.
[157] B. D. Fried and R. W. Gould, "On the Detection of Ion Oscillations in a Mercury Discharge," Space Tech. Labs., Los Angeles, Calif., Rept. STL/TR 60-0000 GR 413; December, 1960.
[158] ——, "Longitudinal ion oscillations in a hot plasma," *Phys. Fluids*, vol. 4, pp. 139–147; January, 1961.
[159] E. B. Armstrong, K. G. Emeleus, and T. R. Neill, "Low-frequency disturbances in gaseous conductors," *Proc. Roy. Irish Acad.*, vol. A 54, pp. 291–310; December, 1951.
[160] F. W. Crawford, "Electrostatic sound wave modes in a plasma," *Phys. Rev. Lett.*, vol. 6, pp. 663–665; June, 1961.
[161] W. Newcomb, USAEC Repts. 239 and 326; Washington, D. C.; June, 1955.
[162] I. B. Bernstein, *et al.*, "Ion wave instabilities," *Phys. Fluids*, vol. 3, pp. 136–137; 1960.
[163] I. B. Bernstein and R. M. Kulsrud, "Ion wave instabilities," *Phys. Fluids*, vol. 3, pp. 937–945; November, 1960.
[164] O. Buneman, "Instability, turbulence, and conductivity in current-carrying plasma," *Phys. Rev. Lett.*, vol. 1, pp. 8–9; July, 1958.

[165] ——, "Maintenance of equilibrium by instabilities," *J. Nuclear Energy*, pt. C, vol. 2, pp. 119–134; January, 1961.
[166] J. R. Pierce, "Possible fluctuations in electron streams due to ions," *J. Appl. Phys.*, vol. 19, pp. 231–236; March, 1948.
[167] K. G. Hernqvist, "Plasma ion oscillations in electron beams," *J. Appl. Phys.*, vol. 26, pp. 544–548; May, 1955.
[168] ——, "Plasma oscillations in electron beams," *J. Appl. Phys.*, vol. 26, pp. 1029–1030; August, 1955.
[169] C. C. Cutler, "Spurious modulation of electron beams," PROC. IRE, vol. 44, pp. 61–64; January, 1956.
[170] T. Moreno, "Spurious modulation of electron beams," PROC. IRE, vol. 44, p. 693; May, 1956.
[171] M. Ettenberg and R. Targ, "Observations of plasma and cyclotron oscillations," *Proc. Symp. on Electronic Waveguides*, Brooklyn Polytechnic Inst., Brooklyn, N. Y., April 8–10, 1958, Interscience Publishers, Inc., New York, N. Y.; 1958.
[172] P. Chorney, "Electron-Stimulated Ion Oscillations," Res. Lab. of Electronics, M.I.T., Cambridge, Mass., Tech. Rept. 277; May, 1958.
[173] R. L. Jepson, "Ion oscillations in electron beam tubes: ion motion and energy transfer," PROC. IRE, vol. 45, pp. 1069–1080; August, 1957.
[174] R. W. Revans, "The transmission of waves through an ionized gas," *Phys. Rev.*, vol. 44, pp. 798–802; November, 1933.
[175] W. Funk and R. Seeliger, "Untersuchungen über die inneren Schwingungen von Niedervoltbogen," *Z. Phys.*, vol. 113, pp. 203–217; July, 1939.
[176] G. S. Kino and H. A. Woods, unpublished work.
[177] Thong Saw Pak, "Noise from hot cathode discharges," *Proc. Phys. Soc. (London)*, vol. B 68, pp. 292–296; May, 1955.
[178] F. W. Crawford and J. D. Lawson, "Some Measurements of Fluctuations in a Plasma," Microwave Lab., Stanford University, Stanford, Calif., M.L. No. 753, October, 1960; *J. Nuclear Energy*, Pt. C; July, 1961.
[179] ——, "Low-Frequency Fluctuations in a Plasma," Internatl. Conf. of Ionization Phenomenon in Gases, Munich, Germany, August 26–30, 1961, to be published.
[180] M. D. Gabovitch, L. L. Pasechik, and V. G. Yazevo, "Observation of ion oscillations in a plasma," *Soviet Phys. JETP*, vol. 11, pp. 1033–1035; November, 1960.
[181] H. Martin and H. A. Woods, "Low-frequency noise spectra of hot-filament, low-pressure discharge tubes," *Proc. Phys. Soc. (London)*, vol. B 65, pp. 281–286; April, 1952.
[182] F. W. Crawford, "Frequency Spectra of Low-Frequency Fluctuations in a Plasma," Stanford University, Stanford, Calif., Microwave Lab. Rept. No. 762; November, 1960.
[183] ——, "Impedance Characteristics of a Low-Pressure Mercury-Vapor Plasma," Stanford University, Stanford, Calif., Microwave Lab. Rept. No. 761; November, 1960.
[184] K. H. Kingdon, "Rectification by oscillation of positive ions about the potential minimum of a thermionic triode," *Phys. Rev.*, vol. 33, p. 1075; June, 1929.
[185] S. Ballantine, "Fluctuation noise due to collision ionization in electronic amplifier tubes," *Physics*, vol. 4, pp. 294–306; September, 1933.
[186] K. G. Emeleus and N. R. Daly, "Ion oscillations in a cathode potential minimum," *Proc. Phys. Soc. (London)*, vol. 69 B, pp. 114–115; January, 1959.
[187] ——, "Initiation of hot cathode discharges," *Brit. J. Appl. Phys.*, vol. 6, pp. 370–372; July, 1955.
[188] J. F. Waymouth, "The measurement of thermionic emission in discharge tubes," *Sylvania Technologist*, vol. 13, pp. 2–10; January, 1960.
[189] H. J. J. Van Boort and M. Klerk, "High-frequency oscillations in low-pressure mercury arcs," *Appl. Sci. Research*, vol. B 5, pp. 69–74; 1955.
[190] K. G. Emeleus, "Plasma studies survey of experiments, I. Mainly optical studies," *J. Nuclear Energy*, Pt C, vol. 2, pp. 65–68; January, 1961.
[191] ——, "Plasma studies survey of experiments, II. Mainly Probe studies," *J. Nuclear Energy*, Pt. C, vol. 2, pp. 69–72; January, 1961.
[192] K. Landecker and B. J. Robinson, "Study of high-frequency fluctuations from light sources using phototubes and tuned RF amplifiers," *Proc. Phys. Soc.*, vol. B 66, pp. 737–742; September, 1953.
[193] W. Pupp, "Oszillographische Sondenmessungen an laufenden Schichten der positiven Saüle von Edelgasen," *Z. Phys.*, vol. 36, pp. 61–66; January, 1935.
[194] E. V. Appleton and A. G. D. West, "Ionic oscillations in the striated glow discharge," *Phil. Mag.*, vol. 45, pp. 879–881; May, 1923.
[195] L. B. Loeb, "Fundamental Processes of Electrical Discharge in Gases," John Wiley and Sons, Inc., New York, N. Y., pp. 563–574; 1939.
[196] H. Y. Loh and G. H. Dieke, "Fluctuations in gas discharges," *J. Opt. Soc. Am.* vol. 37, pp. 837–848; October, 1947.
[197] T. Donahue and G. H. Dieke, "Oscillatory phenomena in direct current glow discharges," *Phys. Rev.*, vol. 81, pp. 248–261; January, 1951.
[198] L. Pekarek, "Factors affecting the self-excitation of low-frequency oscillations in an electric discharge," *Czech. J. Phys.*, vol. 8, pp. 32–45; 1958.
[199] ——, "New method of measurement of relaxation times in glow discharge plasma," *Proc. 4th Internatl. Conf. on Ionization Phenomena in Gases*, Uppsala, Sweden, 1959, North-Holland Publishing Co., Amsterdam, Neth., vol. 2, pp. 306–308; 1960.
[200] H. S. Robertson, "Moving striations in direct current glow discharges," *Phys. Rev.*, vol. 105, pp. 368–377; January, 1957.
[201] K. W. H. Foulds, "Moving striations in low-pressure mercury vapor," *J. Electronic and Control*, vol. 1, pp. 270–278; November, 1956.
[202] W. H. McCurdy, "The striated discharge in mercury vapour," *Phil. Mag.*, vol. 48, pp. 898–917; November, 1924.
[203] K. T. Compton, L. A. Turner, and W. H. McCurdy, "Theory and experiments relating to the striated glow discharge in mercury vapor," *Phys. Rev.*, vol. 24, p. 597; 1924.
[204] W. H. McCurdy and P. Dalton, "Low voltage discharges in He," *Phys. Rev.*, vol. 27, p. 163; 1920.
[205] K. G. Emeleus and A. H. Gregg, "The association of ionic oscillations with negative glow and anode glow," *Phil. Mag.*, vol. 16, pp. 1079–1082; December, 1933.
[206] W. Pupp, "Influence of the anode on the stability of discharges in argon," *Z. Phys.*, vol. 34, pp. 756–761; October, 1933.
[207] I. Langmuir, "The pressure effect and other phenomena in gaseous discharges," *J. Franklin Inst.*, vol. 196, pp. 751–762; December, 1923.
[208] W. W. H. Clarke, "The influence of cathode standing waves on valve stability," *Brit. J. Appl. Phys.*, vol. 6, pp. 433–441; July, 1955.
[209] K. G. Emeleus and D. W. Mahaffey, "Plasma oscillations," *J. Nuclear Energy*, pt. C, vol. 2, pp. 117–118; January, 1961.
[210] J. D. Cobine and C. J. Gallagher, "Effect of magnetic field on oscillations and noise in hot-cathode arcs," *J. Appl. Phys.*, vol. 18, pp. 110–116; January, 1947.
[211] J. D. Cobine and J. R. Curry, "Electrical noise generators," PROC. IRE, vol. 35, pp. 875–879; September, 1947.
[212] S. Ruthberg, "Cold cathode gas tubes as noise generators," *Phys. Rev.*, vol. 70, p. 112; July, 1946.
[213] K. F. C. Hoh and B. Lehnert, "Diffusion processes in a plasma column in a longitudinal magnetic field," *Phys. Fluids*, vol. 3, pp. 600–607; July, 1960.
[214] Thong Saw Pak, "New effects of an auxiliary cathode on a discharge at low pressure," *J. Electronics and Control*, vol. 3, pp. 471–480; November, 1957.
[215] E. O. Johnson, J. Olmstead, and W. M. Webster, "The tacitron, a low noise thyratron capable of current interruption by grid action," PROC. IRE, vol. 42, pp. 1350–1362; September, 1954.
[216] G. C. McCullagh, "A simple plasma oscillator," *J. Sci. Inst.*, vol. 38, p. 164; April, 1961.
[217] J. Feinstein, "Condition for radiation from a solar plasma," *Phys. Rev.*, vol. 85, pp. 145–146; January, 1952.
[218] M. A. Allen and G. S. Kino, "Beam Plasma Amplifiers," presented at IRE WESCON, San Francisco, Calif., August 22–25, 1961.
[219] I. Langmuir and K. H. Kingdon, "Thermionic effects caused by vapors of alkali metals," *Proc. Roy. Soc. (London)*, vol. A 107, pp. 61–79; 1925.
[220] N. D'Angelo and N. Rynn, "Diffusion of a cold cesium plasma across a magnetic field," *Phys. Fluids*, vol. 4, pp. 275–276; February, 1961.
[221] R. C. Knechtli and J. Y. Wada, "Generation and measurement of highly-ionized quiescent plasmas in steady state," *Phys. Rev. Lett.*, vol. 6, pp. 215–217; March, 1961.
[222] J. M. Anderson, "Ultimate and secondary energies in the negative glow of a cold-cathode discharge in helium," *J. Appl. Phys.*, vol. 31, pp. 511–515; March, 1960.
[223] J. M. Anderson and L. A. Harris, "Negative glow plasma as a cathode for electron tubes," *J. Appl. Phys.*, vol. 31, pp. 1463–1468; August, 1960.
[224] J. M. Anderson, "Possible low noise beam-plasma amplifier," *J. Appl. Phys.*, vol. 30, pp. 1624–1625; October, 1959.
[225] I. Alexeff and R. Neidigh, "Apparent Observation of Ionic Sound Waves in a Plasma," Oak Ridge Natl. Lab., Tenn., Rept. No. 61-2-57; February, 1961.
[226] ——, "Apparent observation of ionic sound waves in a plasma," *Bull. Am. Phys. Soc.*, vol. 6, pp. 309–311; April, 1961.
[227] G. S. Kino, "A proposed millimeter wave generator," *Proc. Symp. on Millimeter Waves*, Brooklyn Polytechnic Inst., Brooklyn, N. Y., March 31, April 1–2, Interscience Publishers, Inc., New York, N. Y., pp. 233–248; 1959.

Ionic and Plasma Propulsion for Space Vehicles*

G. R. BREWER†, M. R. CURRIE†, SENIOR MEMBER, IRE, AND
R. C. KNECHTLI†, MEMBER, IRE

Summary—**The propulsion of future space vehicles by means of electrical engines appears to be the most practical and effective method for long interplanetary missions. The basic principles of the major class of such electrical engines, *viz.*, those utilizing ionic or plasma acceleration, involve technologies familiar to and largely stemming from the work of electronics engineers and plasma physicists. This paper describes the various methods under investigation today for the acceleration and neutralization of charged particles for use in propulsion. The several topics discussed include the problem of beam neutralization, cesium ion engines, electron-bombardment engines, and magnetic plasma acceleration.**

Introduction

THE SUBJECT of electrical propulsion represents an exciting new area of applied science and technology which is rapidly growing in interest and importance and which has, literally, an unlimited future. Electrically propelled spacecraft provide the only feasible means for exploring the further reaches of our solar system, for economically transporting large manned expeditions and heavy payloads to our neighboring planets and for probing the solar system away from the ecliptic plane.

It is inevitable that such vast new concepts as this build on fundamental knowledge and experience in a variety of fields and, in turn, provide strong motivation for vigorous new work and progress in these areas. This is certainly the case here. From an over-all viewpoint a nuclear-electric propulsion system consists of three major components: a lightweight nuclear reactor, an efficient method for converting thermal energy to electrical energy, and the thrust unit itself. The first two of these are giving strong impetus to fundamental and applied work in the areas of new types of high-temperature reactors and methods of direct energy conversion such as thermionic and MHD devices.

The third major component, the electrical thrust unit, is the subject of this paper. As will be shown, it builds directly on the broad field of electronics concerned with plasma physics and devices, beam and particle dynamics, electron optics and electron tube technology. The purpose of this paper is to discuss electrical propulsion devices from this point of view. Rather than present a detailed picture of the increasing number of specific engineering developments in this field, we intend that the discussion shall relate the general directions of current efforts to basic problems in plasma physics, ion beam generation and control, and particle dynamics. We take the point of view that the rapid development and future success of electrical propulsion will depend upon continued fundamental research in these areas and that, conversely, progress in electrical propulsion will have a significant impact on these basic areas in terms of new understandings and new tools for attacking problems of fundamental importance. In short, electrical propulsion is a field which is fertile for invention, research, innovation, and cross-fertilization with other major areas of applied physics and electronics.

The concept of the ion rocket engine has existed for many years. In 1906 R. H. Goddard mentioned it in his notebook [1], and in 1929 H. Oberth devoted a chapter of his book, *Wege zur Raumschiffahrt* [2], to the concept. However, active research and development effort has only taken place during the last few years; some of the earliest articles on electrical propulsion in the U. S. literature were written in 1954 by Dr. Ernst Stuhlinger, now of NASA, who has continued to provide much of the stimulus and leadership for this program. Although a large and growing body of literature on the subject exists, no attempt is made here to give a complete list of references.

The importance of electrical propulsion can be seen from the following basic relations. Thrust is equal to the rate of change of momentum imparted by the exhaust of a rocket engine. For simplicity, let it be assumed that all particles in the exhaust have the same velocity v_{ex}. Then the thrust T is simply

$$T \equiv \dot{m}_p v_{ex}, \tag{1}$$

where $\dot{m}_p$ is the propellant mass flow rate. If this thrust lasts for a time τ, the total impulse imparted to the vehicle is equal to $T\tau$.

The *specific impulse*, defined as the impulse per unit weight of propellant exhausted, is

$$I_{sp} \equiv \frac{T\tau}{w_p} = \frac{T}{\dot{w}_p}, \tag{2}$$

where $w_p = m_p g$ is the propellant weight exhausted in time τ. This gives the specific impulse as thrust per unit of propellant weight flow rate. Combining (1) and (2), we obtain

$$I_{sp} = \frac{v_{ex}}{g} \text{ seconds}, \qquad (g = 9.8 \text{ m/second}^2) \tag{3}$$

which identifies specific impulse as a measure of the exhaust velocity.

Consider, now, the equation of motion in free space for a vehicle whose mass M and velocity v are functions of time:

$$Mdv = -v_{ex}dM. \tag{4}$$

* Received by the IRE, October 3, 1961.
† Hughes Research Laboratories, Malibu, Calif.

For an initial mass M_i starting from rest, (4) gives

$$v = I_{sp} g \ln\left(\frac{M_i}{M}\right). \tag{5}$$

Thus, the effectiveness of mass expenditure to gain velocity is a function of specific impulse, *i.e.*, from a mass point of view, a given velocity increment is achieved more efficiently with a system having high specific impulse.

With low specific impulse chemical rockets, the mass loss is very high. These systems, of course, have high thrust and are needed for overcoming gravitational forces and injecting payloads into orbit. However, for many projected space missions starting from an earth orbit, the tremendous mass of a chemical or even nuclear rocket, which is necessary to deliver a heavy payload, is completely unfeasible. The specific impulse of a chemical rocket is limited to values below about 400 seconds; the primary limitation is imposed by the maximum reaction temperature and minimum molecular weight of the fuel. By choosing hydrogen for the propellant, the direct nuclear heat transfer rocket (*e.g.*, Rover) is expected to increase the specific impulse to 800 and perhaps even 1000 seconds; here the temperature limitations of the material establish an upper limit. Because of their high thrust, chemical and nuclear rockets will be important for near-earth missions. However, many interplanetary and deep-space scientific missions requiring heavy payloads are impossible to accomplish with foreseeable chemical or nuclear vehicles. Low thrust propulsion systems operating over long periods of time and having very high specific impulse values are mandatory in such cases.

It is clear that the acceleration of ions to any desired velocity by electrostatic or electromagnetic fields is unrelated to thermal heating; *i.e.*, in the former process, the specific impulse can be adjusted to any desired value. The power required to accelerate the particles is proportional to the product of thrust and velocity. The weight of the nuclear-electric power supply increases roughly in proportion to power. Therefore, depending upon the mission, there exists an optimum exhaust velocity or specific impulse which results in minimum over-all weight (*i.e.*, compromise between power system weight and propellant weight). This optimum specific impulse is larger for longer missions and heavier payloads but is invariably above several thousand seconds, varying from roughly 5000 seconds for a 5000-pound payload in a Mars orbit using the Atlas-Centaur booster and a 60-kw power supply, to more than 10,000 seconds for a 15-ton terminal mass in a Jupiter orbit using Saturn and a 1-Mw power supply. Thus, nuclear-electric propulsion systems constitute an ideal solution for the types of missions discussed above.

Many detailed calculations have shown that for a given over-all initial weight and, for example, for a round-trip mission to and from a Mars parking orbit, payloads of up to four or more times those possible with direct nuclear rockets or, conversely, much shorter mission durations with the same payload weight will result. For more ambitious space experiments (*e.g.*, to Jupiter) the figures are even more impressive. Often a factor of ten increase in payload or a considerable reduction in initial vehicle weight can be attained. It should be noted that these calculations include the nuclear-electric power supply as part of the propulsion system. However the use of the power supply for wideband data transmission and for primary power for other purposes at the destination makes the effective payload weight ratios between electric and nuclear systems even higher.

There are several varying approaches to the electrical generation of thrust. These are usually classified as electrothermal, electrostatic, and electromagnetic. All have in common the requirements for very long life, high power efficiency, and high propellant utilization efficiency.

Of the above types of electrical propulsion, this paper will be concerned only with the latter two approaches. The thermal arc jet is not a true electric thrust unit in the sense of overcoming material temperature limitations and thus permitting very high specific impulse. In it, a high-current arc is used to resistively heat a propellant gas (*e.g.*, hydrogen) to high temperatures. The gas is then expanded through a nozzle where the thermal energy is converted to directed kinetic energy. It is limited to specific impulses in the neighborhood of 1000 seconds, the efficiency decreasing very rapidly beyond that point.

The electrostatic engine appears to offer the possibility of efficiently achieving higher specific impulses than the other types, *i.e.*, in the range of several thousand seconds and higher. Ion propulsion is very simple in concept since it involves the imparting of energy to ions by electrostatic acceleration. To serve as a reference, Fig. 1 shows specific impulse as a function of net accelerating voltage for some of the common propellants. However, in transforming this essentially simple idea to practical fruition, there are a number of problems involving fundamental considerations in plasma physics and electronics. First, an efficient ion source is required. A number of such sources are possible: contact ionization, Penning discharges, magnetically stabilized arcs, and various combinations of these. All are the subject of intensive research efforts, the results of which will add significantly to the technology of this and related fields in physics and electronics. Second, sophisticated high-perveance ion-optical acceleration and focusing systems are mandatory with a perfection exceeding even that required by electron guns and beams for use in high-power microwave tubes. Third, space-charge-neutralization mechanisms are required which introduce intriguing new concepts such as synthetic nonthermal plasmas and the basic questions relating to them.

The other major class of electrical propulsion engines involves the direct acceleration of plasmas by magnetic

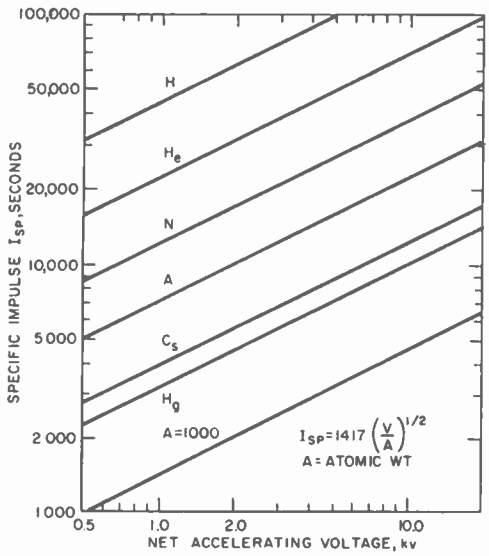

Fig. 1—Curves showing specific impulse as a function of net accelerating voltage for various propellant gases (singly ionized) in electrostatic rocket engine.

fields. This class is usually limited to the range of specific impulses between roughly 2000–5000 seconds. Here the problem of achieving space-charge neutrality is not present. Again, a number of mechanisms for acceleration are possible, including the use of dc crossed electric and magnetic fields (MHD types), traveling-wave systems, and quasi-stationary RF systems. These involve problems which are fundamental to other fields (*e.g.*, energy conversion and high-temperature plasma generation and containment) as well as to the attainment of high-efficiency thrust devices.

In this review paper it is hoped that discussion of some of the basic problems in achieving practical electric propulsion systems and of the broad current approaches to their solution will stimulate increased interest and imaginative effort in this field on the part of investigators in applied physics and electronics, on whose technology this new art is directly based.

I. Basic Problems

In the process of developing electric propulsion systems, there are several technical objectives and problems which are common to the various types of systems outlined above. Obviously, the primary objective involves the devising of field configurations (electric and/or magnetic) capable of accelerating charged particles in a controlled manner to the desired exhaust velocity.

One of the primary considerations in the invention of propulsion systems is efficiency—efficiency both in use of the electrical power and of the propellant. In the elementary equations presented above, it was shown that the performance of the space vehicle is critically dependent on the weight of both the electric power generating system and the propellant that must be carried. It is therefore essential to devise propulsion systems which will convert as much as possible of the electrical power available in the vehicle into useful thrust, and power efficiencies larger than about 80 or 90 per cent are desirable. Fortunately, work to date, which will be reported in more detail below, indicates that such efficiency values are attainable. The propellant-utilization efficiency should be high (greater than 90 per cent) for the simple reason that we do not wish to carry excess propellant which would decrease the performance of the space craft. As we shall see later, in the electrostatic rocket even higher ionization or propellant-utilization efficiency is essential, in order to reduce the effects of charge-exchange reactions.

The second serious consideration is neutralization of the charges associated with the particles of the exhaust beam. As mentioned earlier, the class of electric engines in which the acceleration of the charged particles results from magnetic fields will presumably exhaust a neutral beam, *i.e.*, the accelerated and exhausted medium will be very close to a true plasma. In the case of electrostatic rockets, on the other hand, the acceleration of the charged particles is accomplished by means of electric fields; therefore only one species can be accelerated in a given region. In this case, the charges must be separated. In order to prevent buildup of space-charge forces at the engine exhaust, the accelerated charges must be neutralized by the injection of particles of the opposite sign. (We do not mean that the positive and negative particles must recombine, but merely that in any given region of the exhaust beam, there must be an equal number of positive and negative charges.)

Since the electrostatic rocket imparts acceleration to the positive and negative charges separately, some mechanism must be provided to ionize the neutral propellant particles. As we shall see, the ionization mechanisms used in the engines to be considered are contact ionization of cesium on tungsten and ionization by electron impact. This ionization must be accomplished with the minimum possible loss of energy, in order to maintain high over-all efficiency. Not only must the ionization process be efficient in terms of the energy required to create the ions, but the mechanism must be capable of supplying a relatively high density of ion current to the accelerator system. Typical ion current densities of the two mechanisms mentioned above are 10 to 20 ma/cm^2. These values are sufficiently high to allow the development of electric engines suitable for space missions; however, higher-density sources are definitely needed for future engines, and this consideration does form a fundamental limitation on the performance of electric propulsion engines.

Another fundamental limitation is the erosion of electrodes involved in the acceleration of the charged particles due to impingement of the charged particles on these electrodes. The electric propulsion engines that we are describing here will be used for space vehicles in in-

terplanetary travel, and the mission times involved are measured in years. Therefore, a serious constraint on the design of the engines is that the total erosion of the electrodes must be small enough that it does not interfere with engine operation over lifetimes of tens of thousands of hours. This imposes, for example, the condition of very careful control over the ion optical characteristics of the accelerator structure so that the impingement of the accelerated ions on any of the surrounding electrodes may be avoided. In the electrostatic rocket, a maximum of about one ion can be allowed to strike the accelerating electrode for each 100,000 ions emitted from the ionizer, *i.e.*, an interception ratio of about 10^{-5}.

In the rest of this paper, we shall discuss the several types of electric propulsion engines from the point of view of these basic objectives, and attempt to show how these fundamental problems are being approached. In other words, we shall try to understand the physics involved rather than the details of the engineering of these engines. The reader must bear in mind, however, that there are many engineering and technological problems which must be solved, and, in many cases, the development of electric engines will depend as much on a solution of these engineering problems as on the invention of solutions to the more fundamental ones.

II. Electrostatic Acceleration

Electrostatic acceleration is characterized by the *separate* acceleration by electrostatic fields of the positive and negative charges; *i.e.*, ions are created by some ionization process prior to acceleration. In the cesium-type engine this ionization occurs at a hot tungsten surface; in the Penning or Kaufman engine the ionization mechanism is electron impact. This class of engines also has the common requirement for neutralization of the exhaust ion beam by the injection of charged particles of the opposite polarity. We shall describe first this common problem of neutralization, followed by discussions of several of the electrostatic engines being investigated today.

A. Neutralization

As mentioned earlier, in the electrostatic rocket the ionized propellant particles are accelerated separately from the negative particles, after which electrons are injected to neutralize the positively charged beam. The successful neutralization of the space-charge fields of this ejected ion beam is one of the most difficult and controversial problems in the ion engine today. Progress in this technical area could spell the difference between success and failure of an ion engine in producing useful thrust in space (we can easily be misled by successful tests in a ground-based laboratory, where electrical conditions can be quite different from those in space). The real test of the requirement for and the effectiveness of neutralization must await a space flight; in the meantime, some demonstrations of neutralization in practical engines have been made in laboratory tests. We shall try to present here a brief but fairly complete picture of the neutralization problem, indicating insofar as possible all sides of this controversial subject; it will be clear, however, that many important questions remain unanswered. In addition to its obvious application to electrical propulsion, a neutralized and directed beam of ions represents a new and novel form of plasma with many interesting properties and with potential uses so far almost completely unexplored.

There are two types of neutralization which must be clearly differentiated:

1) Current Neutralization: A positive ion beam which is ejected from an electrically isolated space vehicle will produce on this vehicle a net negative charge. This charge will build up very quickly to such a magnitude that all of the ions will be pulled back. It is necessary, therefore, to eject an equal current of negative charges along with the positive ions. This step is essential in order to maintain the entire space vehicle electrically neutral. In principle, we could accomplish this current neutralization merely by ejecting negative particles (*e.g.*, electrons) from any part of the vehicle [see Fig. 2(a)], and they would ultimately be attracted toward the cloud of positive ions [see Fig. 2(b)].

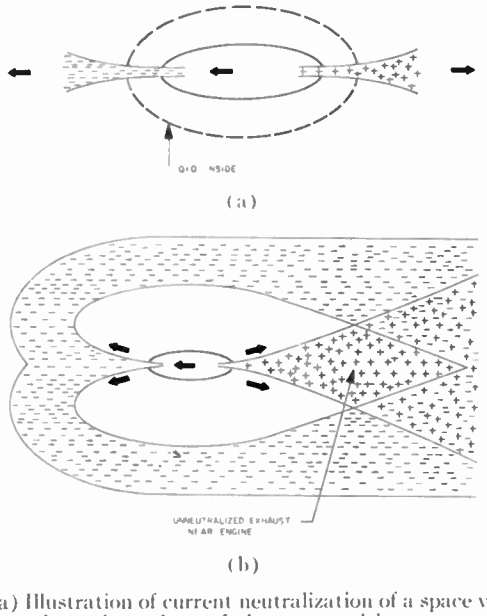

Fig. 2—(a) Illustration of current neutralization of a space vehicle by ejection of equal numbers of electrons and ions per second, but from opposite ends of the vehicle. The charge inside a surface surrounding the vehicle can be made equal to zero. (b) The fields of the charges ejected as shown in (a) will attract the more mobile electrons toward the ions, leaving an uncompensated region of positive charge near the vehicle.

2) Charge Neutralization: The question of the need for detailed neutralization of the *charge* in the ejected ion beam is currently the controversial aspect of this problem. The following discussion will be limited to the need for charge neutralization, since this is the aspect of the neutralization problem requiring more discussion and study at present; it is tacitly assumed here that the requirement of current neutralization is met exactly.

TABLE I

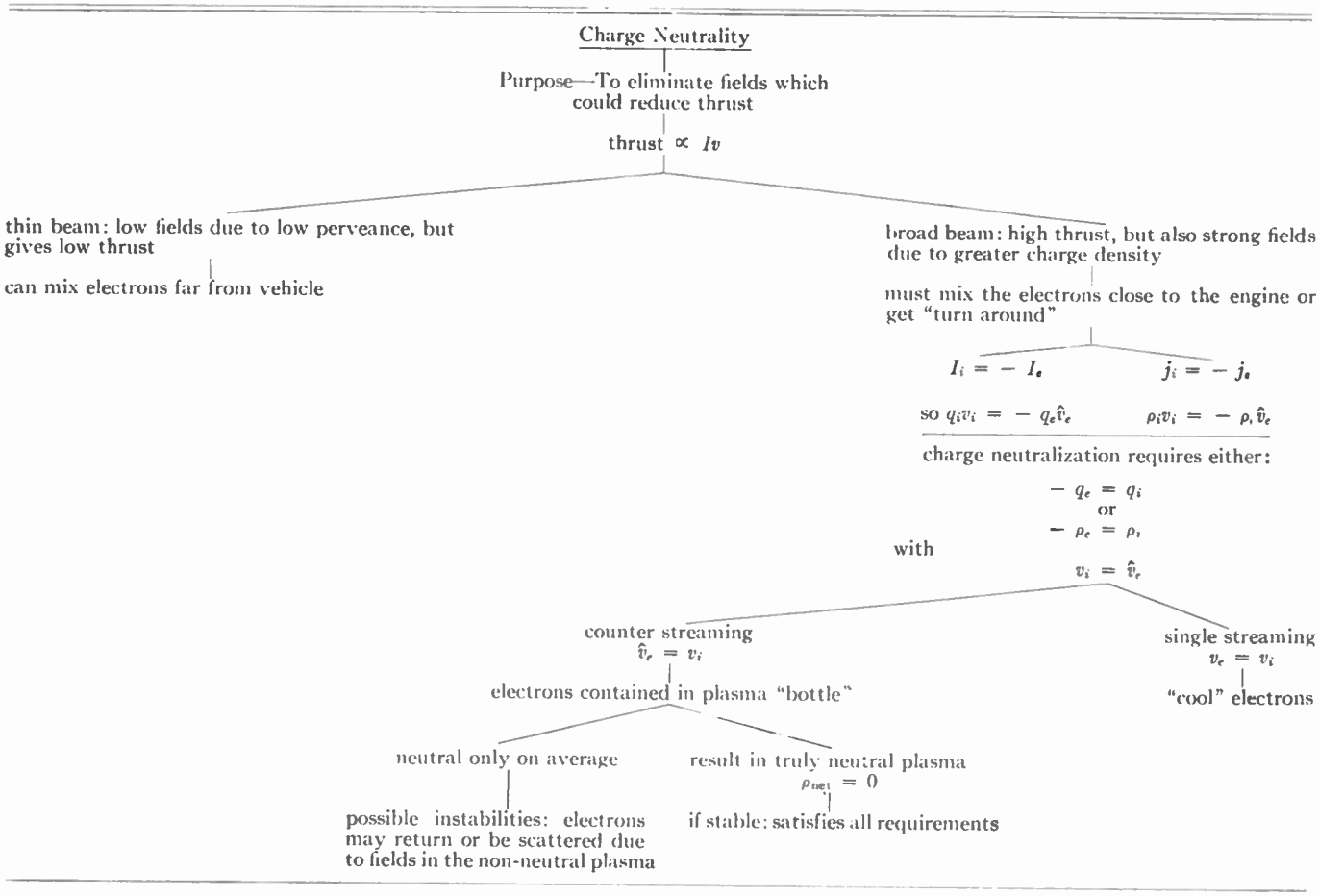

Since this neutralized ion beam can be thought of as possessing many of the properties of a very energetic non-thermalized synthetic plasma, with interesting possible applications other than propulsion, we shall treat this subject in a fair amount of detail, and include some of the experiments which have been performed. We can perhaps see this problem in broad perspective by examining Table I, which will be referred to during the subsequent discussion.

In order to obtain charge neutrality of the ion beam, negative particles must be injected either into or close to the ion beam. A heavy particle such as a negative ion offers certain advantages as the neutralization particle; however, the far more copious supply of electrons available makes the electron the more attractive negative particle to use for neutralization. Therefore, we shall confine our discussion to the use of electrons as the neutralizing particles.

The fundamental purpose of neutralizing an ion beam, of course, is to eliminate, or to reduce to the point of ineffectiveness, any electric fields in the vicinity of this beam which can diminish the thrust obtainable from the ion engine. Since the thrust is proportional to the product of the beam current and the ejected velocity of the propellant, any fields which act to reduce either the beam current or the ejected velocity will adversely affect the thrust; mere transverse expansion of the beam after leaving the engine will not produce such a counter thrust.

At this point we can distinguish two broad classes of ion beams, giving rise to different neutralization problems:

1) The Broad Beam: This class of beam corresponds to an aspect ratio [3] considerably greater than unity; *i.e.*, the area of the beam is considerably greater than the square of the spacing between the ionizer and the accelerating electrode. This beam in idealized form can be thought of as originating in a large accelerator structure with a grid over the accelerator electrode aperture. Because of the shape of this beam, the electric flux lines will be predominantly axial, *i.e.*, from the positive charges in the beam to negative charges on the outer surface of the accelerator electrode [see Fig. 3(a)]. These axial field lines will act to reduce the velocity of the ejected particles and therefore to diminish the thrust obtainable. In fact, *if* the proper boundary conditions are forced along the outer edge of the beam (to ensure that all of the flux lines will be truly axial in direction), the ions will be stopped and will form a "virtual cathode" at a distance from the accelerator electrode equal to the accelerator-ionizer spacing [4]. A close analogy can be drawn between this "one-dimensional" flow of ions and

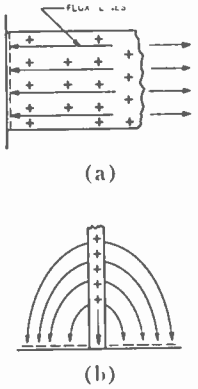

Fig. 3—The effect of the shape factor of the ion beam on the axial electric field, which, if unneutralized, will accelerate the electrons axially. (a) Schematic configuration—broad beam. (b) Shape of the flux lines in the case of a thin strip or pencil beam.

the flow of charged particles between planar grid surfaces, as treated by Fay, Samuel, and Shockley [5].

This "broad" type of ion beam obviously exhibits attractive advantages, in that it provides relatively high values of thrust density (thrust per unit of ion source area); however, if unneutralized, the strong axial fields can reduce the exhaust velocity of the propellant and/or, in the extreme case, produce "turn around" [6] so that particles are returned to the accelerator, thus reducing the exhaust current.

2) The "Thin" Beam: A "thin" beam is one for which the transverse dimension at a point near the engine is small compared with the acceleration distance (*i.e.*, $R \ll 1$). The electric flux lines associated with the charges of this beam will be predominantly transverse to the beam boundary [see Fig. 3(b)] so that the space charge will result in a transverse beam spread rather than in a decrease in axial velocity of the particles, as in the "broad" beam. A thin beam can travel long distances from the engine unneutralized. This beam has the severe disadvantage, however, of very low thrust density and is therefore impractical for space propulsion.

3) The "Intermediate" Beam: From the above arguments, it appears that practical ion engines will be designed in an "intermediate" range (which turns out to be an aspect ratio roughly equal to unity measured for each individual beam) but in some type of cluster so that the desired thrust density can be achieved. The problem, then, is to design the individual beams to behave somewhat as a thin beam and arranged just close enough together to give an efficient engine design without danger of the system degenerating into a broad beam with subsequent problems of "turn around" and return current.

The broad or intermediate ($R \approx 1$) types of beams, in which neutralization appears to be a definite requirement, will be discussed below. But first let us try to provide a more quantitative justification for the need for charge neutralization in an ejected ion beam by means of the following examples:

1) One serious consequence of the lack of neutralization will be the transverse spreading of the beam due to space-charge forces. A typical cesium ion beam of current density 10 ma/cm² at an exhaust potential of 10 kv and an initial diameter of 9 cm will double in diameter in a distance of less than 2 cm. This spreading is so rapid as to invalidate the simple beam-spread theory used, but the example does serve to illustrate the seriousness of the spreading problem. While such spreading may not reduce the engine thrust, it must be considered in the engine design in order to avoid any interception, etc.

2) If the same beam is considered as in one-dimensional flow, with entirely axial electric fields, the velocity of the ions will be reduced to zero due to the space-charge fields, in a distance of only 0.7 cm! This "turn around" will return particles to the engine and will obviously reduce or even eliminate the thrust.

We shall assume now that neutralizing electrons are injected either into or in close proximity to the ion beam. The next question is: How intimately should the electrons and ions be mixed? Since the currents in the electron and ion beams must be equal and opposite, we can write

$$I_i = q_i v_i = -I_e = -q_e \hat{v}_e,$$

where q denotes the charge per unit length of electrons or ions and v the velocity ($\hat{v}$ represents the average velocity). If the electrons are mixed intimately so that the current *density* j in the ion and electron beams is equal, then

$$j_i = \rho_i v_i = -j_e = -\rho_e \hat{v}_e$$

(ρ denotes the charge per unit volume).

We really do not know as yet whether the neutralization must be effected on a microscopic scale, with equal values of ion and electron charge per unit volume, or merely equal charge per unit length. The choice will depend on the seriousness of possible instabilities which may be excited by less than perfect neutralization.

In any event, these equalities require in turn that the ion velocity be equal to the electron velocity. The next question to be resolved, then, is whether equality of velocity must be true on an absolute basis, with essentially all of the electrons moving with the velocity of, and in the same direction as, the ions, or whether it is sufficient to require that the average velocity of the electrons be equal to, and in the direction of, the ion motion. The latter possibility would allow the existence of double-streaming electrons, *i.e.*, electrons moving both away from and toward the engine with a net average drift velocity away from the engine. One can understand how this situation might arise by thinking of the neutralized ion beam as a "plasma bottle" [7] (see Fig. 4) with the electrons moving around inside and being reflected at the edges and at the end by an electron sheath, thus giving rise to both transverse and axial components

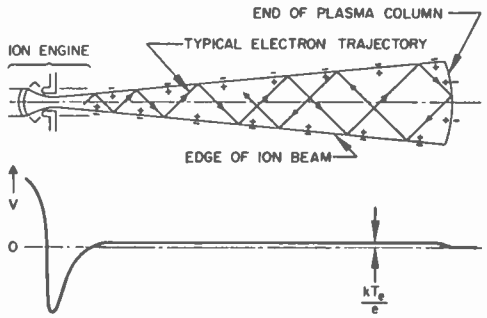

Fig. 4—Schematic representation of the "plasma bottle" concept of a neutralized ion beam. The plasma sheath at the end and edges and the potential "hill" at the engine end will confine the electrons to the interior of this "bottle." These reflections can give rise to a counter-streaming effect as shown. The potential in the plasma column will be uniform at a value roughly kT_e/e above the space potential.

of electron velocity. If the electrons cannot be returned from the end of the plasma column, *i.e.*, if they are forever lost from the system, then the neutralization requirement means that the electron and ion velocities must be equal on an instantaneous basis. For most reasonable values of specific impulse, the ejection velocity of the ions is considerably less than the mean thermal velocity of the electrons emitted from the thermionic emitter. Therefore, if the electron and ion velocities must be equal on an instantaneous basis, some kind of interaction mechanism must be used to reduce the mean velocity of the electrons to that of the ions. The term "mean velocity" denotes here the average over the velocity distribution of the electrons, but the electrons all have the same direction: away from the engine.

In the counter-streaming case, where the electrons are contained within a plasma bottle, we see that there are two possibilities. First, this mixture could result in a truly neutral plasma with the net volume charge density equal to zero throughout the volume of the bottle. This condition obviously satisfies all the requirements of neutralization and, if stable, forms the most ideal situation. The second possibility is that the beam is neutral on the average only, *i.e.*, there can be small volumes throughout the bottle in which the net charge is not zero, though by integrating over the entire bottle the total net charge will be equal to zero. The local fields resulting from the localized regions of nonzero charge density can give rise to instabilities and may cause the electrons either to return to the engine or to scatter transversely. In general, it is believed that this type of plasma will probably be satisfactory if the instabilities are of such a nature that they do not grow in amplitude with either time or distance.

Let us discuss the plasma bottle concept in a little more detail, with the object of showing that in this model charge neutralization can occur in either a laboratory or a space situation and under conditions where the injected axial electron velocity exceeds the ion velocity. Consider that the ejected "plasma" consists of three particle streams: 1) the outgoing ion stream of current density j_i, velocity v_i, and an electron gas with a velocity distribution which may be considered to be made up of two counter-streaming components; 2) the outgoing electron stream of current density j_e' and average stream velocity v_e'; and 3) a returning electron stream of current density j_e'' and average stream velocity v_e''. The outgoing electrons are reflected by the sheath at the end of the plasma bottle (considered, for the moment, to be of finite extent) so that the reflected electron velocity is given (under the assumption of ion mass much larger than electron mass) by

$$v_e'' = - v_e' + 2v_i, \tag{6}$$

which can be seen easily by transforming to a coordinate system moving with the end of the plasma sheath, *i.e.*, at velocity v_i.

We have assumed that the total electron and ion currents are equal. There is no loss of generality in assuming that the current densities are also equal; which must certainly be true on the average over the beam cross section. Then

$$j_i = \rho_i v_i = - (j_e' - j_e'') = - (\rho_e' v_e' - \rho_e'' v_e''). \tag{7}$$

We can define an *average* electron velocity $\hat{v}_e$ as

$$j_e' - j_e'' \equiv j_{et} = \hat{v}_e(\rho_e' + \rho_e''), \tag{8}$$

where j_{et} is the total net electron current density, which has been assumed equal to the ion current density. By combining (7) and (8), we find that

$$\hat{v}_e = - \frac{\rho_i v_i}{\rho_e' + \rho_e''} . \tag{9}$$

The condition for the ion beam to be charge neutralized is that

$$\rho_i = \rho_e' + \rho_e'', \tag{10}$$

i.e., that the net charge density be zero. Therefore, under the neutralized condition we see from (7) and (10) that

$$\hat{v}_e = v_i, \tag{11}$$

and this condition applies *independent of the velocity of the incident electrons*, v_e'. The importance of this conclusion lies in the fact that in general the ion velocity is less than the mean thermal velocity of emission of an electron from a hot cathode. Therefore, if the above conclusion were not valid, some mechanism for slowing down the injected electrons below their mean thermal velocity would be required in order to ensure that $v_e = v_i$.

In the above analysis it was not necessary to use (6); therefore, the conclusion applies not only to the steady-state space situation, where the end of the ion beam is moving away from the engine, and to the transient situation in a ground-based laboratory test during the time of transit of the ions from engine to the beam collector electrode, but also to the steady-state laboratory test, where the collector electrode is electrically

"floating" in potential so that an electron reflecting sheath exists at the collector surface. From (7), (10), and (11), we can show by using (6) that $\rho_e' = \rho_e''$, *i.e.*, that the densities of incident and reflected streams are equal in the space situation. In the laboratory floating collector case, (6) becomes $v_e' = -v_i$, and $\rho_e' = \frac{1}{2}\rho_i(1+v_i/v_e')$, $\rho_e'' = \frac{1}{2}\rho_i(1-v_i/v_e')$ [*i.e.*, the densities of incident and reflected electron streams are not equal]; the reflected density is lower because electrons are collected by the collector electrode.

As mentioned earlier, a second possible model of the neutralized ion beam (in addition to the plasma bottle with counter-streaming electrons discussed above) involves the neutralization by equality of the ion velocity and the average electron velocity with the electrons moving randomly away from the engine. This condition requires, however, that the electrons move very slowly. (In fact, if the ions and electrons have the same average directed velocity, this would correspond to the average directed velocity of electrons emitted from a cathode at a temperature of the order of 100°K, for a cesium ion beam at 2500 volts.) Even in this case, however, processes like those described for the plasma bottle model appear inescapable at the beam front and edges.

We shall now discuss briefly some of the experimental techniques which have been used to inject electrons into an ion beam and to measure the degree of neutrality of that beam. Perhaps the most sophisticated system which has been used involves the injection of electrons from both sides of an ion beam into a region constituting a potential trap for electrons [8]. This trap can be created by an arrangement of electrodes similar to that shown in Fig. 7, which creates a potential distribution as shown in Fig. 5. It is seen that this potential distribution represents the accelerator-decelerator mode of operation, in which the neutralizing system is maintained at a potential higher than that of the accelerator electrode to provide a potential "hill" that prevents electron flow into the accelerator region. In addition, the potentials on the several neutralizing electrodes are adjusted to provide a region free of axial fields, into which the electrons are injected, followed by a small

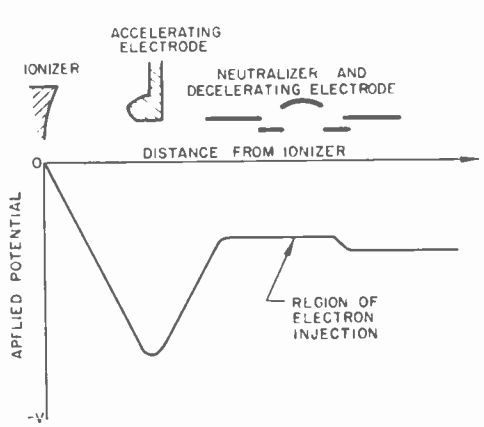

Fig. 5—Potential distribution along the axis of a cesium ion engine shown in Fig. 7; the neutralizing electrodes shown there produce the potential trap for electrons drawn here.

potential "hill" that the electrons must pass over in order to leave the trap. Electrons injected from each side of this trap region execute both transverse and longitudinal oscillatory motion and can interact with the ions. The average residence time of the electrons in the trap is quite long compared with any oscillation or collision period, and there are several mechanisms which could make the electrons random and mix them intimately with the ion beam. It is, however, rather unlikely that this interaction could lead to a truncation of the electron velocity distribution (so that it is not Maxwellian), or to some other process which would allow the electrons to emerge from the trap with an average velocity equal to the ion velocity. At any rate, the intimate mixing in the trap region results in a more uniform distribution of electrons over the cross section of the ion beam upon emergence from the engine and, in particular, results in lower transverse oscillatory energy. If this process takes place, the electrons will not execute violent lateral excursions, but will progress in an orderly one-dimensional pattern along the ion beam.

The effectiveness of the system shown in Figs. 5 and 7 in neutralizing both solid cylindrical beams and large, thin, hollow ion beams has been demonstrated by measuring the transverse spread of the beam due to space-charge forces [9]. When electrons are injected under the correct potential conditions, this transverse spread can be made zero indicating essentially no space-charge forces in the ion beam. Under these neutralized conditions, it has also been found possible to isolate the ion beam collector from the rest of the system electrically, and still to maintain the neutralized state of the beam (that is, to have the beam remain collapsed).

Somewhat simpler means of injecting electrons into an ion beam have also been used; *e.g.*, wrapping an electron-emitting filament around the outer edge of the beam, or arranging such a filament through the center of the beam. In these experiments the electron-emitting cathode was located outside the engine, *i.e.*, downstream from the point of emergence of the beam from the engine.

In a very careful series of experiments, Sellen, *et al.* [10], have applied pulse techniques to studies of the neutralization problem for beams of high aspect ratio ($R \approx 10$ to 30). By means of the pulse method which they use they have been able to study the behavior of the ion beam in the transient state before and after injection of neutralizing electrons from symmetrically arranged impregnated cathodes close to the edge of the ion beam. They found, for example, that with careful adjustment of these neutralizing emitters, in both potential and position, it is possible to neutralize a broad beam in such a way as to eliminate the turn-around effect which occurs without the electron injection (*i.e.*, without electron injection the space-charge forces cause this broad beam to turn around and return to the engine after moving only a short distance, while with neutralizing electrons the beam will move all the way to the

collector). It is possible that these experiments also involved the creation of a potential trap in the ion beam by the potential and placement of the electron emitters.

In addition to the pulsed-beam neutralization experiments described above, Eilenberg, *et al.* [11] have measured the degree of neutralization of a hollow-ring cesium ion beam by pulsing the beam and measuring the current induced in a surrounding loop by the pulse of charge passing through it. The oscilloscope traces in Fig. 6 show these induced currents. This figure shows the collector, grid, and loop (top to bottom) currents for the unneutralized beam (*i.e.*, without injection of neutralizing electrons in the engine); it is seen that current is induced in the loop as the pulse of charge approaches and departs from the loop. The grid and collector currents are very low in this unneutralized case because the space-charge spread of the beam between the engine and collector is so large that only a small part of the beam actually strikes the collector. When the beam is neutralized by injection of electrons (in a trap system of the type shown in Fig. 7) the loop current vanishes, as shown in Fig. 6 (no net charge in the beam), but the grid and collector exhibit displacement and conduction currents, respectively, as expected. Quantitative analysis of these data reveal that the beam was at least 99 per cent neutralized (*i.e.*, the imbalance in charge per unit length was less than 1 per cent) in the neutralized state. The beam could be altered from the neutralized to the unneutralized state by slight adjustments of the potential in the electron trap region.

These experiments certainly show that with proper injection of electrons in both a broad and an intermediate beam, charge neutralization is obtainable in a laboratory experiment. However, these experiments do not yet allow us to distinguish between the counterstream and the single-stream models discussed above.

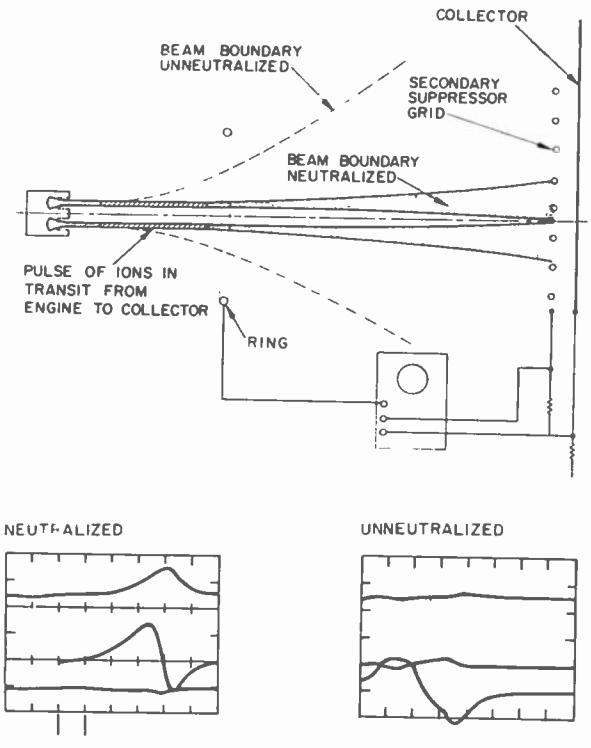

Fig. 6—Schematic diagram of the pulsed beam experiment. The currents induced in the collector, grid, and ring electrode (top to bottom) are reproduced from oscilloscope traces in the insets.

It is evident from the foregoing discussion that the neutralized exhaust beam from an ion engine possesses some of the characteristics of the usual plasma. The greatest similarity results from the neutrality condition, *i.e.*, equal electron and ion densities. Also, the formation of sheaths reflecting the electrons at the edges of the plasma bottle has an analogy in the ambipolar diffusion of conventional plasmas. On the other hand, the ion beam possesses directed motion of high velocity (ion velocities typically 7×10^6 cm/second); the ions will have a longitudinal "temperature" corresponding to that of the emitter (typically 1400°K) and a transverse temperature several times this value (because of the beam compression in the accelerator). Measurement of the electron velocity distribution [12] has shown it to be approximately Maxwellian with a temperature in excess of 10,000°K, and electrons have been detected moving in the "reverse" direction, *i.e.*, from collector to engine. Thus, the ion engine system has provided us with a rather novel form of plasma, a highly energetic or directed nonthermalized plasma, which should find application in other areas of electronics and physics.

B. Cesium Ion Engine

A simplified schematic diagram of a typical cesium ion engine is shown in Fig. 7. At the left we see the propellant heating and storage system, where cesium, the propellant, is converted into a vapor and caused to flow up to and through the ionizer. At the surface of the ionizer, the cesium atoms are converted into cesium ions. These positive ions are accelerated by means of an electric field in the accelerator region and then ejected through the neutralizer region as shown. The space-charge fields of the ejected ions must be neutralized; otherwise these fields give rise to image charges on the vehicle which retard the ions, thereby diminishing or possibly eliminating completely the thrust of the engine. In order to neutralize this ion beam space charge, we must inject negative particles, *e.g.*, electrons, into the beam. A practical system for accomplishing this electron injection is also shown in Fig. 7. In this system, electrons are injected from a cathode surrounding the ion beam and are mixed with the ions in the electron trap created by the electrodes shown.

The electrode system marked "neutralizer region" in Fig. 7 serves two functions: 1) The shapes and potential differences of the electrodes have been designed so as to achieve most efficiently the injection of electrons for neutralization. 2) The electrodes are held at an average potential well above the accelerator in order to decelerate the ion beam. Essentially all modern cesium ion engines operate in this so-called accel-decel mode. In this mode, the final exhaust of the propellant takes

place at or near the potential V_f corresponding to the final or decelerator electrode, but between this electrode and the ionizer the accelerator electrode is arranged at potential V_a. The fraction V_a/V_f is called the accel-decel ratio; typical values are approximately 2 to 10. This system will produce a potential distribution along the beam similar to that illustrated in Fig. 5. The principal reason for operation in this mode is that the potential hill between the decelerator and accelerator electrodes prevents electrons in the ion beam from being attracted into the accelerator region and thereby bombarding the ionizer, which would result in subsequent power loss and possible overheating.

Let us discuss now some of the considerations entering into the design of the accelerator system of such a cesium ion engine, starting from the basic requirement that the engine produce a certain value of thrust with a specified value of specific impulse. These two parameters, thrust and specific impulse, are usually chosen as criteria in specifying the performance of the rocket, for the reason that mission analyses show that the flight time for a given mission is dependent almost entirely on the thrust level, whereas the mass which can be carried, *i.e.*, the payload, is dependent almost entirely on the specific impulse. Let us accept thrust level and specific impulse as the fundamental parameters and work out the "paper" design of an accelerator system. The total ion current I_i needed to produce the desired thrust can be expressed in terms of this thrust level and the specific impulse value from (1) and (3), as follows:

$$I_i = \dot{n}_p e = \frac{\dot{m}_p}{m_i} e = \frac{T}{I_s} \frac{e}{m_i g}$$

$$= 32.8 \times 10^4 \frac{T(\text{lb})}{I_s(\text{sec})} \text{ amperes (for cesium)}, \quad (12)$$

where $\dot{n}_p$ represents the number of ions of mass m_i ejected per second.

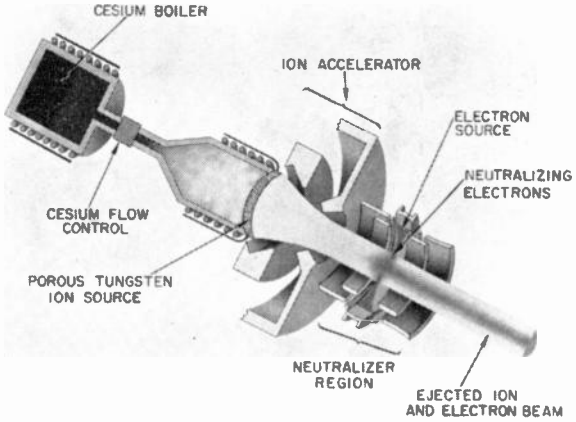

Fig. 7—Schematic diagram showing the various components of an ion engine. The complex shape of the accelerator electrodes provides close control of the ion trajectories to avoid electrode impingement and erosion. The electrode system in the neutralizer region provides the potential distribution necessary to allow the neutralizing electrons to enter the ion beam and to leave the engine along with the ions.

It is convenient to express the geometrical structure of the accelerator of the engine in terms of a parameter called the perveance, which is defined as the total ion beam current divided by the three-halves power of the accelerator voltage:

$$P_i = I_i / V_a^{3/2}.$$

The expressions for the perveance of structures possessing planar, cylindrical, or spherical symmetry can be easily derived from the corresponding Child-Langmuir equations [13] for space-charge-limited emission in these geometrical forms. From these equations, the emitter current density J_i is given by

$$J_i = \frac{4}{9} \epsilon_0 \sqrt{\frac{2e}{m}} V_a^{3/2} \delta$$

$$= 2.335 \times 10^{-6} \sqrt{\frac{m_e}{m_i}} V_a^{3/2} \delta, \quad (13)$$

where m_i/m_e represents the ratio of mass of the appropriate ion to the electron; for example, for cesium $m_i/m_e = 1837 \times 134 = 246{,}000$. Thus, the current density of cesium ions is about 500 times less (for a given accelerator electrode potential V_a and given geometrical structure) than that for the electrons. δ is a geometrical factor and can be written.

$$\delta = \frac{1}{d^2} \quad \text{for planar structures,} \quad (14a)$$

$$\delta = \frac{1}{r_a r_e \beta^2} \quad \text{for concentric cylinders,} \quad (14b)$$

$$\delta = \frac{1}{4\pi \bar{r}_e^2 \alpha^2} \quad \text{for concentric spheres,} \quad (14c)$$

where d is the distance between emitter and accelerating electrode, r_a and r_e are the radii (cylindrical) of the accelerator electrode and emitter, respectively, and $\bar{r}_e$ is the radius (measured from the center of curvature of the sphere) of the emitter. α and β are functions of the radius ratio tabulated by Langmuir [14].

It is sometimes convenient to refer the ion perveance P_i to an equivalent electron perveance P_e. This latter value is obtained by multiplying the ion perveance by the square root of the ratio of ion mass to electron mass, as follows:

$$P_e = P_i \sqrt{\frac{m_i}{m_e}} = 493 P_i \text{ (for cesium)}. \quad (15)$$

The cesium-type electrostatic ion engine is very similar in concept and design to electron guns used in microwave tubes, and the considerable body of knowledge which has been accumulated in past years on this subject can be applied directly to these engines. The perveance parameter P is useful because it is a function of only the geometrical configuration of the accelerator

structure, *i.e.*, it is related to the total area divided by some function of the distance from the accelerating electrode to the emitter.

The total ionizer area needed to supply the beam current I_b is then given [from (12)] by

$$A_i = \frac{I_b}{J_i} = 32.8 \times 10^4 \frac{T}{I_s J_i} \text{ cm}^2 \text{ (for cesium)}, \quad (16)$$

where J_i represents the ionizer current density (in amp/cm² of ionizer) which is assumed in the design. The final or decelerator potential V_f, which will produce the propellant exhaust velocity corresponding to the specified specific impulse, is

$$V_f = \frac{1}{2}\frac{m_i}{e} v_p^2 = \frac{1}{2}\frac{m_i}{e}(I_s g)^2$$
$$= 6.65 \times 10^{-5} I_s^2 \text{ volts}. \quad (17)$$

Let us discuss for a moment a simple planar engine consisting of the accelerator region only (no decelerator). With the above equations we can show, perhaps a little more clearly, the source of the thrust obtainable from an electrostatic propulsion engine. The thrust obtainable from an ion engine per unit of ionizer area may be considered in terms of a unit called the specific thrust T_s. From (1) and (12), for this simple engine,

$$T_s \equiv \frac{T}{A_i} = \frac{m_i v_p I_b}{e A_i} = \frac{m_i}{e}\sqrt{2\frac{e}{m_i} V_a}\, J_e. \quad (18)$$

The current density J_e can be obtained from (13) and (14a), from which (18) becomes

$$T_s = \frac{8}{9}\epsilon_0 \left(\frac{V_a}{d}\right)^2. \quad (19)$$

The electric field at the anode of a space-charge-limited planar diode can be shown to be $E_a = (4/3)(V_a/d)$. Thus, we can write (19) as

$$T_s = \tfrac{1}{2}\epsilon_0 E_a^2. \quad (20)$$

The reader will recognize that this equation represents the stress transmitted across a unit area of surface at which the electric field has the value E_a. In this simple idealized example, we are considering a plane-parallel electrode system of unit area in which a space-charge-limited current flows. This current flows through the anode plane, which is permeable to the charged particles. The electric field at this anode plane produces a stress or force which accelerates the particles outward from the engine; this force (or thrust) may be thought of as "pushing" the engine in the opposite direction to the motion of the propellant particles. The purpose of the neutralization system is to prevent the existence of any longitudinal components of electric field *outside* the engine, since these would act in the opposite direction, pulling the ions back to the engine and so reducing the thrust.

In the design of an ion propulsion engine, we have seen that analysis of the intended mission provides information on the desired values of specific impulse and thrust. We have seen also that these numbers are sufficient to determine the total current, the mass flow rate, and the potential difference between the emitter and the final or decelerator electrode, and therefore to determine also the total power which must be used to accelerate the ion beam. A knowledge of ionizer characteristics allows us to choose an acceptable value of emitter current density, from which the total emitter area can be determined. There are several geometrical forms in which the ionizer, and therefore the entire engine, can be arranged to produce this required area: 1) a planar structure with grids across the accelerator aperture, 2) an array of small solid-beam accelerators with an open accelerator aperture (Fig. 8), 3) an accelerator to produce a long narrow strip beam, and 4) a structure producing a thin hollow-ring beam (Fig. 9). The gridded design, form 1), is very susceptible to electrode erosion, since in this design it is difficult to control the optical characteristics in such a way as to prevent interception in the accelerating electrodes, which, in addition, are relatively weak structurally. The linear strip system, form 2), is difficult to maintain in accurate

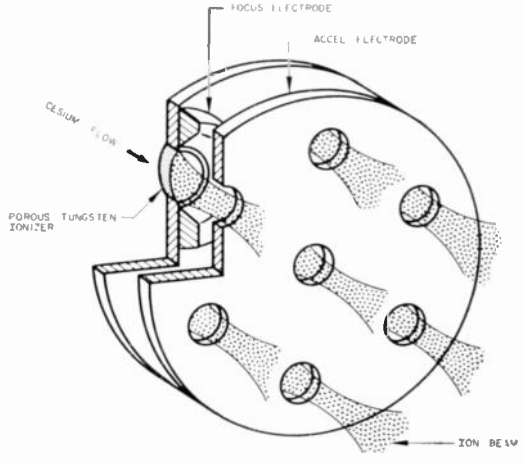

Fig. 8—Schematic drawing of a multiple-solid-beam ion engine.

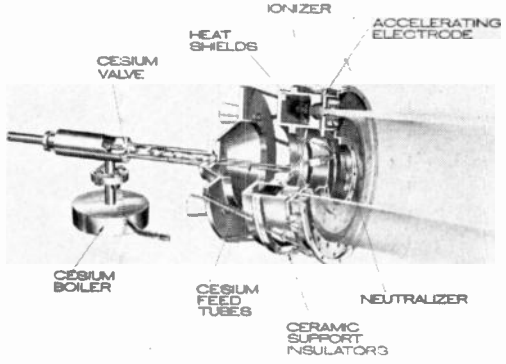

Fig. 9—Artist's cutaway sketch of a cylindrical hollow-ring ion engine with neutralizer system similar to that shown in Fig. 7 and with a laboratory-type axial feed system (Hughes Aircraft Company).

alignment. Therefore, the hollow-ring system and the multiplicity of solid-beams system, each of which possess certain advantages and disadvantages, are the two in most common use today. The hollow-ring geometry is simply the strip beam bent around into a circle, but this arrangement allows the electrode alignment to be maintained accurately, and the beam can be neutralized in detail by the electron injection and trapping system shown in Fig. 9 (which is similar to that in Fig. 7).

Let us now turn to two of the more detailed but important problem areas in the cesium ion engine: the ionizer and the ion trajectory problem.

The process of converting the cesium atoms to ions is one of the interesting physics problems associated with the ion engine. For purposes of this discussion we can show one practical way of accomplishing this ionization process (see Fig. 10). The cesium atoms are fed from behind a porous tungsten pellet; they migrate along the walls of the very thin capillary tubes between the grains of tungsten and emerge on the top surface, from which they are emitted predominantly as ions. This process of contact ionization of alkali metals on hot tungsten has been studied in great detail by Taylor and Langmuir [15]; the valence electrons of the low-ionization-potential alkali metals remain with the higher-work-function tungsten surface as the particle is evaporated from this surface. Thus, the current-voltage characteristics appear as in Fig. 11 [16], where they are seen to be similar to the saturation characteristics of an electron emitter. Below the level of maximum space-charge-limited emission, the cesium supply is excessive and many particles evaporate as neutrals; above this level all of the ions which the surface is capable of supplying can be drawn off so that the neutral efflux is low. For proper control of the optical properties of the accelerator, the source should be operated space-charge limited; thus the optimum point of operation is at the "knee" of the curves in this figure.

Although cesium has many undesirable properties, it is usually chosen as the propellant chiefly because it is the most easily and effectively ionized on those atoms with a mass that ensures an optimum specific impulse or propellant velocity at reasonable values of voltage. Other propellant materials are being investigated and may eventually replace cesium, but cesium will be used in almost all of the first-generation ion engines.

Another very serious problem in ion engines is the erosion of the accelerating electrode that can result from bombardment by high-velocity cesium ions. Sputtering studies have shown that as many as ten atoms of the engine electrodes can be eroded away by the impact of one cesium ion. This electrode erosion may ruin the operation of the engine over the long periods (*e.g.*, one year to Mars) for which an ion engine must be operated. For satisfactory long-time operation, therefore, it appears that a maximum of about one ion can be allowed to strike the accelerating electrode for each 100,000 ions which leave the ionizer. The ions which do impinge on the electrodes can arise from any of several defects and phenomena in the ion engine; the principal cause is incorrect design of the ion-optical characteristics of the accelerator structure. It is therefore extremely important to be able to control very accurately the trajectories of the accelerated ions so that they flow in a uniform and "laminar" manner through the accelerator and neutralizer regions of the "gun." This process is somewhat analogous to the problem of designing optical lenses that will produce images free of aberrations. Such close control of the ion-optical design of the accelerator structure makes use of techniques which were found essential in the design of high-current-density electron guns for beam-type microwave tubes.

Perhaps the most significant advance in the design of electron guns, including the effects of space charge, was

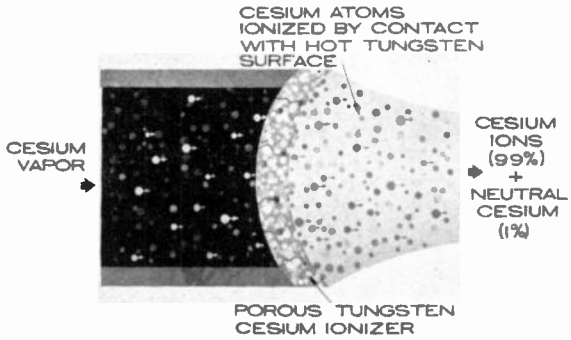

Fig. 10—A simplified diagram of a porous tungsten contact ionizer for cesium. The cesium atoms diffuse through the hot (1150°C) tungsten and migrate onto the surface. Under proper conditions, the evaporation from this surface consists predominantly of ions with a few neutral cesium atoms.

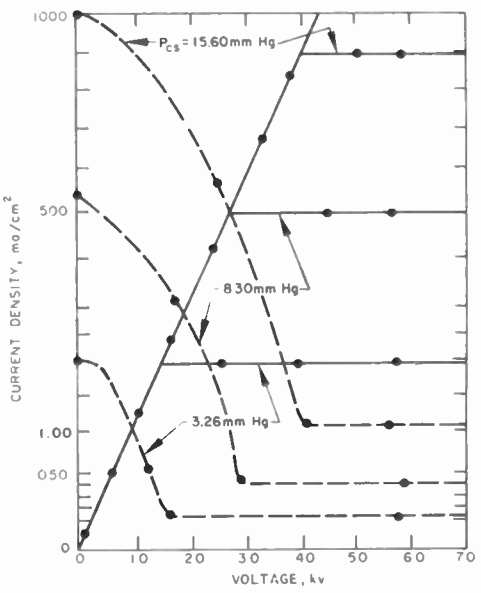

Fig. 11—Porous-tungsten cesium ion emitter characteristics as a function of accelerating voltage. The solid lines show the ion current for several values of cesium flow rates (or cesium vapor pressure), and the dashed lines show the evaporation rate of neutral cesium particles. (Data courtesy of Dr. Otto Husmann.)

made by Pierce [17]. Although the Pierce design technique has proved extremely useful and has formed the basis for the design of many guns over the past ten years or so, it suffers from a fundamental limitation when applied to the design of those high-perveance guns which do not have a grid across the accelerator electrode aperture. That is, the ideal Pierce gun can be divided into two regions: 1) the region of rectilinear electron flow, in which the potential is given by the Langmuir relations for space-charge-limited flow for the geometry used, and a unipotential electrode is designed to effect the proper electrical boundary conditions at the beam edge, and 2) a thin electric aperture lens in the vicinity of the anode. When this method of analysis and design is used, it is assumed that trajectories in the two regions can be joined smoothly and that no appreciable distortion of the ideally shaped electric fields exists away from the immediate vicinity of the anode aperture. Since higher perveance guns do exhibit a considerable distortion of electric field due to the aperture in the accelerating electrode, this simple design criterion must be modified somewhat. Modified techniques of design of high perveance electron guns [18], including the use of an automatic ion trajectory tracer with space-charge simulation, have been found to be similarly successful in the design of ion accelerators. For example, by the use of these proven design techniques, ion guns have been built which exhibit laminar beam flow and electrode interception values of 10^{-4}–10^{-5} or less of the emitted current, values which are lower by orders of magnitude than those observed in engines designed by less careful techniques, and which are good enough now for a long mission. These excellent optical characteristics must of course be obtained consistent with uniform emitter current density.

A second cause of ion interception on the engine electrodes can arise from ions which deviate from their laminar or design trajectories as a result of emission from the ionizer with a transverse component of velocity. This transverse thermal spreading is a rapidly decreasing function of accelerator potential, and with correct design of the accelerator electrode aperture, it can be made negligible at usual operating voltages.

A third cause of ion interception results from ions created in the flow region of the accelerator and decelerator by charge-exchange reaction between the cesium atoms in this region and the moving ions. Since the accelerator structure is usually designed so as to control the trajectories of ions originating at the ionizer, those charge-exchange ions created elsewhere in the flow region can be accelerated so that they impinge on the engine structure, thus producing erosion. There are at least two ways of controlling this process: 1) reducing the atom density in the flow region by decreasing the neutral efflux from the ionizer, and 2) performing additional design studies (*e.g.*, on a trajectory tracer) on the engine so as to deflect the charge-exchange ions from the electrodes.

The process of cesium ionization by contact with hot tungsten provides one of the principal advantages of the cesium ion type of electrostatic propulsion engine, in that the ionization is effected at a well-defined and carefully shaped equipotential surface. This emitter surface can form the basis for accurate design of the ion-optical characteristics of the accelerator in much the same way as a space-charge-limited electron cathode forms the basis for design of Pierce-type electron guns.

The cesium ion engine is seen to be amenable to accurate design, based on both analytical and carefully controlled experimental techniques, which yields very predicatable engine performance. These engines are capable of supplying ion beams of attractive densities (particle densities of the order of 10^{11} ions/cm^3 and current densities of 20 to 80 ma/cm^2 in the exhaust beam). These ion beams have been successfully neutralized (at least as far as laboratory tests can determine).

As shown in Fig. 12, the cesium ion engine can be made to be quite efficient. The principal energy loss is in the form of power required to heat the ionizer to the necessary emitting temperature. Some additional power is required to heat the neutralizer filament and the cesium boiler, but, for reasons mentioned before, no power dissipation due to current interception on the electrodes is tolerable. Fig. 12 shows the efficiency (power into the beam to produce thrust divided by the total input power) as a function of specific impulse of the exhaust beam. This curve is derived from calculations based on experimental data on operating engines and other sources. It is seen that efficiency values in excess of 80 per cent are possible for specific impulses of interest for space missions.

Cesium ion engines of the type shown in Figs. 8 and 9 have been built and are undergoing extensive laboratory development and evaluations [19], [20]. Progress in cesium ion engines has been very rapid in the past year: feasibility has been demonstrated, neutralization has been successfully accomplished in a laboratory environment, erosion has been reduced to the point where lifetime appears long enough for space missions, etc. The cesium ion engine therefore appears to be an ef-

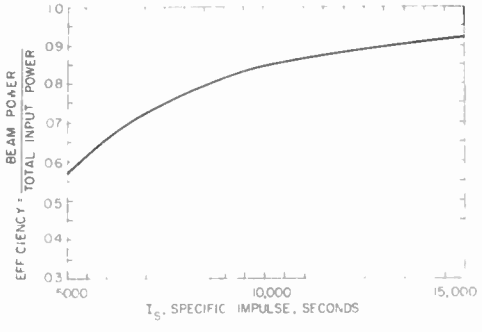

Fig. 12—Power efficiency of a cesium ion engine vs specific impulse for a value of ionizer current density equal to 20 ma/cm^2. These data were calculated from measured data of current density vs ionizer temperature and of ionizer heating power requirements. The power input includes that required to heat the neutralizer emitter.

ficient, practical, and effective device for the propulsion of space vehicles, an engine around which plans can now be made for future space exploration. These engines have been built so far to produce thrust levels of several millipounds, but larger thrust unit engines appear quite feasible, and such engines can be clustered for even higher thrust levels, *e.g.*, 1.5-pound thrust for a 300-kw system or even 10-pound thrust for a 2-Mw system. These engines can also be built efficiently at the micropound thrust level for propulsion of lightweight scientific packages out of the plane of the ecliptic. Engines such as those shown in Figs. 9 and 14 are currently being developed [21] for use in the first space test of an electrical propulsion engine in late 1962.

C. Penning Discharge Ion Engines

A second important class of ion engines employs a fundamentally different type of ion source in which the propellant gas is ionized by electron bombardment. Since for any reasonable geometries and particle densities the mean free path for ionization (of the order of meters) is much larger than the dimensions of the ionization chamber, it is evident that the efficiency of such a source depends upon increasing the mean lifetime of the primary electrons. Such an increase can be accomplished by the use of Penning-type discharges in which magnetic and electric fields are arranged so as to trap the electrons and thus increase the ionization probability. Such sources have been found to have good power efficiency (in terms of energy expended per ion produced) and relatively high propellant utilization efficiency, together with the other obvious advantages of mechanical simplicity and ability to use a number of different types of propellant gases. The major problem concerns the design of high-quality ion optical systems for low electrode interception, and hence for long life.

The most advanced engine of this type utilizes a configuration proposed by Kaufman [22]; it is shown schematically in Fig. 13. The ionization chamber is composed of a cylinder with the neutral propellant gas introduced at one end and the ions extracted at the other. The center portion of the cylinder (*i.e.*, the anode for the discharge) is maintained at a positive potential with respect to the ends of the cylinder, thus providing electron trapping in the longitudinal direction. Electrons are emitted from a filament located on the axis. The longitudinal magnetic field prevents the electrons from reaching the anode directly; in the crossed electric and magnetic fields, they tend to spiral around the axis, thus increasing their mean lifetime and the probability of making an ionizing collision. A plasma is formed which fills the discharge chamber out to the screen; ions are extracted from this plasma boundary by an array of accelerating electrodes.

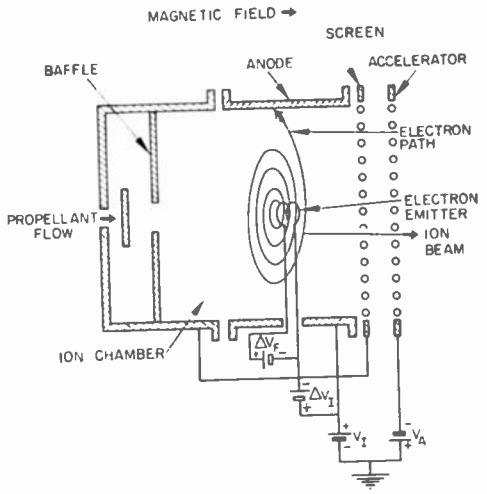

Fig. 13—Schematic illustration of the type of Penning-discharge ion engine proposed by Kaufman [22].

The energy range of interest for the primary electrons is dependent upon the ionization potentials of the propellant gas. To date, only mercury vapor has been utilized extensively in this type of ion engine. The ionization cross sections for single and double ionization of mercury have broad maxima at roughly 50 and 100 volts, respectively. Consequently, the energy range of interest for production of singly-charged ions is from about 30 to 70 ev. It should be noted, however, that the threshold potential for removal of a second electron from a singly-ionized mercury atom is 29.4 volts [23]. Although no data seem to be available on the cross section for this process, it might be expected that it would have a maximum somewhat below 100 ev; therefore, caution must, in general, be exercised in interpreting performance data and in adjusting conditions so that the ratio of doubly- to singly-charged ions is kept very small.

The low-velocity electrons in the plasma have been estimated [22] to have a temperature corresponding to about 5 ev for the case of mercury with an axial plasma resistivity of less than 0.01 ohm-cm.

Optimum magnetic field strength is dictated by a compromise between ionization efficiency and plasma resistivity in the radial direction. A strong magnetic field is evidently necessary in order to obtain high ionization efficiency. On the other hand, if the magnetic field is too high, the plasma resistivity in the radial direction is increased, thus resulting in heating losses, increased diffusion losses of low-velocity electrons, and a radial inflow of ions. A radial inflow of ions leads to nonuniform ion current density through the accelerator system and results in deteriorated optics and increased electrode erosion. Optimum magnetic fields of the order of a few tens of gauss have been found in the experimental engine configurations studied thus far.

When the electron mean free path $\bar{l}$ is much greater than the cyclotron radius r_c the plasma resistivity in the radial direction is increased by a factor proportional to $(\bar{l}/r_c)^2$. From this, the functional dependence of the radial potential difference can be simply calculated [22] to be

$$\Delta V_{\text{rad}} \sim \frac{j\sqrt{T_e}}{L r_c^2 n_-^2 \sigma_{\text{eff}}}, \tag{21}$$

where L is the length of the ionization chamber, j is the discharge current, T_e the effective electron temperature, n_- the electron density and σ_{eff} the total effective collision cross section. This relationship has been used to guide scaling studies on this type of source. However, it is evident that much more work is required before an adequate theoretical understanding of this type of ion source is attained; this may constitute a fruitful field for further research.

Fig. 14 pictures a typical engine configuration based on these concepts. Such units have been investigated and developed by the NASA Lewis Research Center. Typical performance of a 10-cm source operating at a specific impulse of 5500 seconds with mercury as the propellant has been given as follows [24]: An ion beam of 130 ma was obtained with a magnetic field of the order of 20 gauss; a discharge in the ionization chamber of 1.7 amperes at 50 volts, and a net acceleration voltage of 3000 volts. This corresponds to an average beam current density over the beam cross section of about 1.6 ma/cm², or of the order of several ma/cm² in the screen apertures. Current densities in this range appear to be typical for this type of source. The over-all power efficiency under these conditions was about 70 per cent, including filament power, magnet power, and power lost due to electrode interception. A measure of ionization efficiency is the cost in energy of producing one ion, which in this case was about 700 ev/ion. Propellant-utilization efficiency was about 80 per cent. The thrust corresponding to these numbers would be of the order of 3 millipounds.

Various studies of geometry and effects of magnetic field have been made. For example, ionization efficiency depends upon the manner in which the propellant gas is introduced; best results have been obtained when it is injected through the distributor on the axis where the density of high-velocity ionizing electrons is highest. It has been observed that grid erosion near the axis is greater than that near the periphery indicating a similar variation of ion beam current density due, at least in part, to the radial potential difference previously discussed.

A scaling study was carried out [25] with beam sources 5, 10, and 20 cm in diameter, designed for constant current densities in the extracted beams and otherwise identical in proportions. Some typical data are indicated in Fig. 15, where energy per ion is plotted as a function of magnetic field for the three sources. Here the ion-chamber potential difference was 50 volts, which was approximately optimum in the three cases; the specific impulse was held constant at 7000 seconds (4900 volts) as well as beam current density. It is seen that roughly the same performance is achieved for the larger sources. This similarity is more striking if plotted as a function of the product of magnetic field and diameter (*e.g.*, curves reach a minimum at 16 and 32 gauss for the 20- and 10-cm sources, respectively). The efficiency of the smaller source was, however, quite poor. Note from (21) that for a cyclotron radius proportional to diameter D (in this case at 64 gauss), with $L \sim D$, T_e and σ_{eff} constant, and $j \sim j_0 D^2$, where j_0 is the beam current density and $n_- \sim j_0$, we find that

$$\Delta V_{rad} \sim (D j_0)^{-1}. \tag{22}$$

Thus, at small diameters, the radial potential difference increases, reaching a point where much of the power goes into heating of the plasma. It has also been verified that with increased current density j_0 the ionization efficiency goes up.

Fig. 16 shows a curve of expected power efficiency as a function of specific impulse for this type of engine.

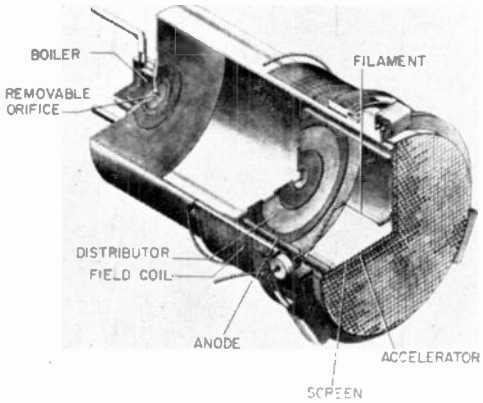

Fig. 14—Artist's cutaway drawing of the electron-bombardment engine being investigated at the NASA Lewis Research Center.

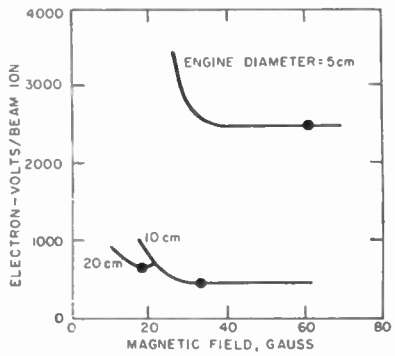

Fig. 15—Results of scaling experiments [25] showing the ionization efficiency (energy per beam ion) as a function of magnetic field, for Penning-discharge engines of three different diameters.

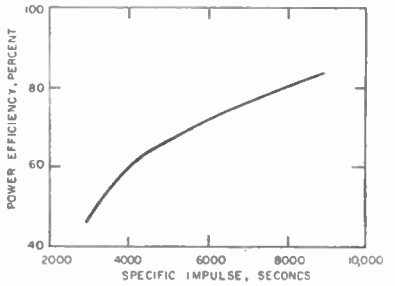

Fig. 16—Power efficiency as a function of specific impulse for Penning-discharge engines of the type being studied at NASA Lewis Research Center. Performance close to that shown has been demonstrated in several laboratory tests.

Some of these relatively high efficiencies have already been obtained on experimental engines, indicating the promise of this approach.

An area for intensive investigation in the development of the Penning-discharge source for long life is the ion optics system. In fact, it poses a challenging problem: the study of the boundary condition for injection of ion trajectories into the electrode system. It is evident that the shape of the plasma boundary or sheath can be varied over a wide range (indicated in Fig. 17) by the potential and shape of the extraction electrode. Thus, geometry and potential configuration must be adjusted to achieve high-perveance laminar optics and, at the same time, to maintain optimum plasma boundary shape. Interception on the acceleration electrode of the engines discussed above has been of the order of 1 per cent, which can no doubt be improved considerably by systematic study of this interesting optics problem.

No special neutralization mechanisms have been developed for the Penning engine. This opens, therefore, an area for further study, as was carried out in the case of the cesium engine. Neutralization has been accomplished in the laboratory testing of these engines simply by electrons from a hot filament stretched across the beam, as well as by trapping secondary electrons from the electrodes and beam collector over the length of the beam. Because of heavy sputtering, an array of filaments stretched across the ion beam is not attractive for practical space applications.

As previously mentioned, all the results to date have been obtained with mercury as the propellant. The study of other types of gases seems to offer possible further gains in efficiency, current density, etc. We direct particular attention to the use of cesium. Although it is not generally true that higher ionization efficiencies can be obtained for lower ionization potentials, data [23] show that the ionization efficiency (in terms of ion pairs per cm mm Hg at 1 mm Hg) is the same, within a factor of two, as that for mercury, with the peak occurring at less than 20 ev for primary electrons as compared with about 50 to 70 ev for mercury. In addition, the ionization potential leading to doubly-ionized cesium is 36.9 volts with a first ionization potential of 3.9 volts, compared with the respective figures of 29.4 volts and 10.4 volts for mercury [23]. Thus, it would appear that there might be a much greater and more favorable range of discharge voltage over which conditions could be adjusted for higher efficiency without establishing production of doubly-ionized cesium. Besides higher efficiency, we might hope that a denser, lower-temperature plasma would result, thus leading to higher ion current density and improved optics. Also, the lower discharge voltage with cesium could reduce or suppress the problem of sputtering of the hot electron-emitting filament.

Another kind of ion source which utilizes a Penning- or PIG-type discharge is the so-called grid-type ion source used at the Oak Ridge National Laboratory in separating stable isotopes and in controlled fusion research. This type of source is shown schematically in Fig. 18. Here the ion beam is extracted normal to the direction of the magnetic field which constricts the discharge. Although high ($\sim$100 ma/cm^2) current densities are obtained at typical acceleration potentials of the order of 25 kv, this configuration has not been applied to the range of parameters of interest for propulsion purposes. Luce [26], however, has conducted some electrode erosion studies using this source and has discussed its application to ion engines.

D. The Duoplasmatron-Type Ion Engine

A third major class of sources which is being extensively investigated and developed for the electrostatic acceleration of dense ion beams is based on the so-called Duoplasmatron concept of Von Ardenne [27]. As in the Penning-type source, ionization is achieved by electron bombardment and the ion beam is extracted from a plasma. Of all such bombardment sources, the Duoplasmatron is capable of producing the highest ion current densities. Densities two or three orders of magnitude greater than those attained by means of contact ionization *i.e.*, of the order of amperes or even tens of amperes per cm^2, are possible (although they have not

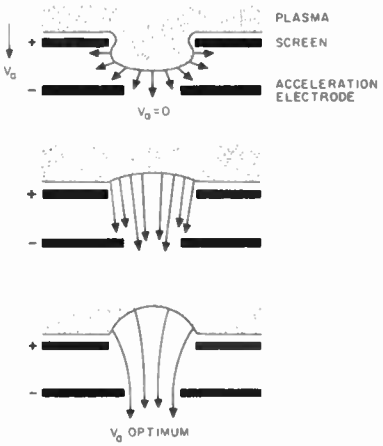

Fig. 17—Illustration showing how the shape of the plasma boundary or sheath can vary as the field configuration in the accelerating region changes. The interesting problem is posed of suitably shaping the plasma meniscus so as to "match" the plasma system optimally to an ion optical system.

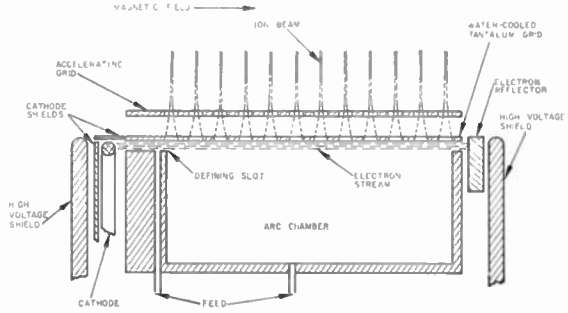

Fig. 18—Schematic drawing of the grid-type Penning-discharge source developed at the Oak Ridge National Laboratory [26].

yet been achieved in well-focused beams). This characteristic, together with an inherently high ionization efficiency and the prospects for eventually reaching high power efficiencies, makes this class of sources of considerable interest for development as part of an ion thrust system for propulsion. Although major problems exist in reducing electrode erosion, increasing emission area, and controlling and focusing the output beam, it is believed that these may not constitute fundamental limitations and that, with intensive and imaginative effort, the inherent promise of the Duoplasmatron-type ion engine may eventually be realized. It should be noted that such development may also have great importance to other areas of plasma research and application (*e.g.*, injection sources for controlled fusion experiments, or linear accelerators).

Fig. 19 illustrates the basic Duoplasmatron configuration. A low-pressure arc is produced between a filament (or thermionic cathode) and the anode, which typically operates in a potential range from somewhat above the ionization potential of the working gas to about 100 volts. An "intermediate electrode," conical in shape and held either at an intermediate potential or sometimes floating, serves to constrict the discharge and increase the plasma density. This is the form originally suggested by Von Ardenne in 1946 for use as an ion source for experiments in isotope separation. The addition of a high (essentially axial) magnetic field between the tip of the baffle and the anode (Von Ardenne [27]) acts to constrain the discharge further. These dual constraints—mechanical and magnetic—produce a very dense plasma in the extraction orifice. Since neutral particles have to pass through this cloud of hot dense plasma to escape from the source, the propellant-utilization efficiency can be high. A very dense ion beam is obtained from the plasma by means of large negative potential (typically 10 to 60 kv) applied to the extractor electrode.

The complex geometry of the Duoplasmatron makes exact analysis of its operation impossible. However, the basic mechanisms which determine its characteristics can be discussed qualitatively, and can serve as a guide in its development. The arc inside the source has the typical characteristics of a low-pressure discharge in which the electron mean free path is of the same order as the discharge length. A positive sheath close to the cathode supports a potential difference approximately equal to the ionization potential of the working gas. Following this cathode drop there exists a region of small potential gradient which contains an essentially neutral plasma; here, ionization as well as randomizing elastic collisions occur. The pressure in the arc region is typically of the order of ten to several hundred microns.

In such a discharge *per se* the plasma density would not normally be sufficiently great to permit extraction of large ion currents. As mentioned previously, this is accomplished through the use of magnetic and mechanical constraints. The magnetic field has two functions: first, it gives rise to electron reflection (Penning-discharge effect), and second, it exerts a magnetic confining effect on the arc which serves to constrict it and to reduce radial diffusion losses. Both effects increase the plasma density.

Fig. 20 indicates schematically a typical magnetic field configuration in the neighborhood of the baffle canal and the anode [28]. The magnetic field, usually of the order of several kilogauss, is highly convergent in this region. In fact, it can be regarded as a magnetic mirror configuration [29] in which electrons entering with an initial transverse velocity component can be reflected. It should be noted that because of the geometry there must exist a region of crossed E and B fields which gives rise to transverse velocities and thus cycloidal motions which emphasize this effect. Total reflection can occur for a large part of the incident electron current.

The electrons that are trapped by the magnetic field and reflected along their original path can be reflected again by the original electric field existing in the arc discharge, thus giving rise to electron trapping similar to that present in the Penning discharge. Such trapping may last until collisions or field inhomogenieties allow

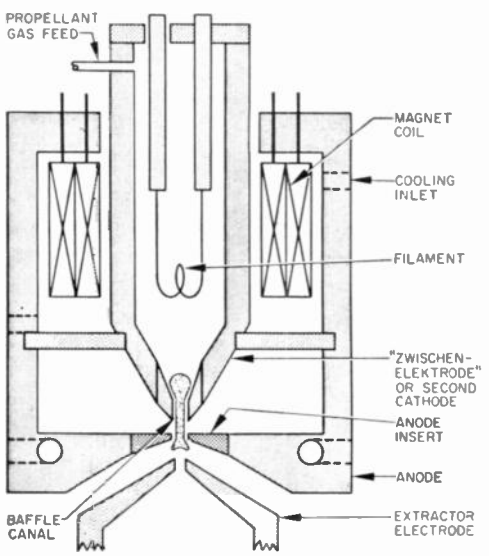

Fig. 19—Basic Duoplasmatron configuration.

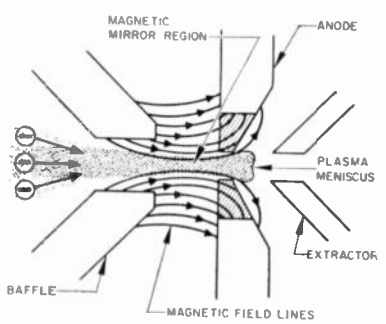

Fig. 20—Magnetic field configuration in the neighborhood of the baffle canal and anode of a Duoplasmatron ion source. The converging magnetic field constitutes a magnetic "mirror" for reflection of electrons. It also constricts the discharge and reduces radial diffusion losses.

the electrons to reach the anode. The probability of ionization by the primary electrons is increased by increasing their effective lifetime, which, combined with a decreased rate of radial electron diffusion, leads to higher ionization density and power efficiency. High-energy axial electrons which penetrate the mirror region can be reflected back into the plasma by the negative extractor potential.

It is evident that the magnetic field can also exert a confining effect on the plasma which guides it through the baffle and extraction orifice and reduces the effective plasma boundary surface area and diffusion losses. The current density in the baffle canal is greater than that on either side of the baffle; most of the current passing through the baffle consists of electrons. The potential gradient which supports this current is sustained by a positive space charge in the anode side of the canal and a corresponding negative space charge on the cathode side [30]. As the canal length is increased, the tendency toward neutrality in this region becomes larger. Various estimates place the electron temperature in the baffle region of the order of 10^5°K, with somewhat lower temperatures ($\sim 10^4$°K) in the extraction region. The ion temperature was estimated by Von Ardenne [27] at several times 10^3°K.

The discussion thus far has considered the Duoplasmatron only as a high-density ion source per se, with the potential of high propellant utilization and power efficiency. Its ultimate success as an ion engine configuration will depend in large measure on the development of high-quality ion optical systems which are compatible with practical ranges of specific impulse (5000 to 15,000 seconds) and with very low electrode erosion rates, which is also true of other types of sources. There are, in addition, a number of practical engineering problems relating to cooling, efficient magnetic circuits, and weight reduction. Most of the research effort to date has been concerned with understanding the basic mechanisms in order to improve the efficiency of the Duoplasmatron as an ion source. A great deal of additional effort must be directed toward solving these other problems before its full potentiality as an ion engine can be realized.

Although the ion-beam extraction process is space-charge limited, measurements often show significant deviations from a 3/2 power dependence of current on extraction voltage. In addition to the possibility of partial neutralization of the positive space charge by trapped electrons in the extraction region, it is evident that the shape of the plasma boundary from which positive ions are extracted is a sensitive function of the potential distribution, geometry, and magnetic field configuration in the region of the extraction orifice. Indeed, the plasma meniscus can be given almost any desired shape by appropriate adjustment of these conditions [31]; it can be made either convex or concave, and can have widely differing surface areas.

A very interesting problem in the Duoplasmatron, as in the Penning-type engine, is that of suitably shaping the plasma meniscus so that the plasma system can be "matched" to an ion optical system. Not only does the meniscus shape constitute the initial boundary condition for the analytical design of optimum optics, but also it influences the over-all operation in a more subtle way. For example, the exact shape of the plasma bubble which is formed at the extraction orifice by the combination of electric and magnetic fields and geometry has a pronounced effect on propellant efficiency. High propellant efficiency is, of course, important in itself; but it is also critical in reducing erosion. Neutrals which leak out of the plasma complicate seriously the problem of beam formation and electrode erosion because of charge exchange with energetic ions.

In the specific impulse range of interest, the cross section for charge exchange of the positive ion is at least two orders of magnitude larger than that for other reactions with neutrals present in the acceleration region. In the high-density beams produced by this type of source, this constitutes a major prblem. Even with refined optics, ions generated by charge exchange with the neutral efflux will bombard the extractor electrodes and release new neutrals due to sputtering. The resulting erosion of material can be serious. More fundamental data on sputtering as a function of electrode material, ion energy, and atomic weight of the ions are required in reaching practical solutions to the problem of long engine life.

Only the axially symmetric pinhole-type source has been considered here. It is evident that these ideas can be extended to rectangular and annular slit configurations so that total current can be increased, and several laboratories are pursuing these approaches. Also, some major modifications of Von Ardenne's original work hold considerable promise; these involve extending the magnetic field into the cathode region itself and varying the cathode, anode, and extraction orifice locations and geometries.

In short, the promise of this general kind of source for ion propulsion, as well as other applications, makes it a fruitful area for research, invention, and development. Energy expenditures as low as 450 ev/ion and propellant efficiencies of the order of 90 per cent have been demonstrated. Although the high-current-density capabilities have not been realized simultaneously with reasonably good optics, the practical current densities achieved to date are still higher than those obtained with other sources. It is expected that the space-charge-neutralization techniques developed in connection with the cesium ion engines may also be applied in this case.

E. Oscillating Electron Engines

1) Basic Principle: All the engines of the class which we shall call "oscillating electron engines" have in common the presence of high-energy axially oscillating electrons. A number of them have in common other features which in many respects may be regarded as dual to

those of the ion engines described above. It seems appropriate to begin the discussion of this class of engine with an idealized model, in order to emphasize their common features. After analysis of this model, a detailed description of actual engines from a more unified view will be possible.

The principle of the oscillating electron engine in its idealized form is shown in Fig. 21. Electrons emitted from a cathode are accelerated electrostatically and focused into a beam in region I. They are slightly decelerated in region II, and are made to pass through region III in an axial stream. Ions which neutralize the electron space charge are then injected into region III. The potential maximum to the left of region III prevents the flow of ions from region III to the cathode. In region IV a potential gradient is caused in the plasma; it reflects those electrons which do not have a sufficient energy to pass the potential barrier, and accelerates the ions. Most of the reflected electrons will then be reflected again by the cathode and oscillate back and forth between the cathode and region IV until they are ultimately collected in region II or III by one of the positive electrodes. The accelerated ions are ejected axially to the right of region IV with an energy approximately corresponding to the potential difference between the cathode and region III. Also, those electrons which are energetic enough to pass the potential ΔV will escape, together with the ions; in fact, the potential ΔV must be adjusted to just such a value that the number of electrons escaping from region IV will be equal to the number required for neutralization of the ejected ion beam. From there on, the processes of neutralization of the energetic plasma beam ejected from region IV are the same as those described for the ion engine.

The possible existence of a potential gradient of finite axial extent in a plasma beam was first pointed out by Rose [32] and Saltz, *et al.* [33]. Qualitatively, if an electron-velocity distribution of finite width exists, the existence of a potential gradient in a neutral or near-neutral plasma can be understood as follows: As the potential decreases in axial direction, part of the electrons are reflected; this diminishes the electron density. This same potential decrease accelerates the ions, and hence the ion density decreases. By maintaining the proper balance between the two mechanisms, it is possible to keep electron and ion density equal or nearly equal; the difference between both densities is then just sufficient to make up the space-charge contribution to the gradient of electrostatic potential, when such a contribution is required for a self-consistent solution of the equations of motion of the particles and of Poisson's equation.

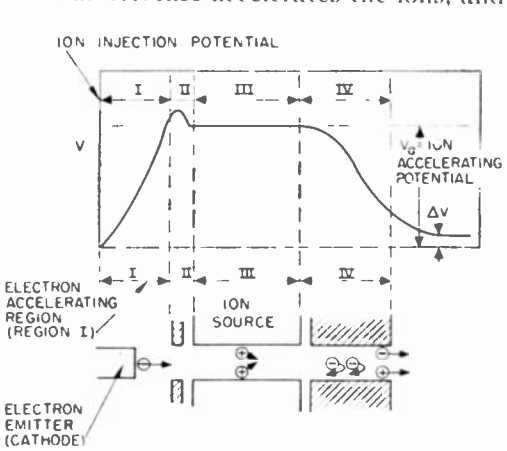

Fig. 21—Principle of accelerated electron engine.

It is important to observe that the potential gradient in a region such as IV can exist in a plasma as a consequence of two separate causes. In one case, the presence of an electrode close to cathode potential around the plasma beam in region IV and penetration of the vacuum field into the plasma are essential. Electrostatic forces between this electrode and the ions cannot be ignored; they directly cause the acceleration of the ions. Momentum is imparted to the vehicle via this electrode and via the electrostatic fields accelerating the ions. In the other case, penetration of external electrostatic fields into the plasma is negligible; electrostatic forces between plasma and electrodes in region IV are insignificant, and most of the potential gradient in region IV results from space-charge fields. Momentum is then imparted to the ions in region IV through these space-charge fields. In other words, it is transferred in region IV from the energetic electrons entering region IV to the accelerated ions leaving region IV via the space-charge field existing in region IV. The momentum of the high-energy electrons entering region IV from region III has been imparted to them by electrostatic forces in region I. The momentum imparted to the vehicle therefore corresponds in this idealized case to the vehicle's reaction to these forces in region I.

A quantitative analysis of the conditions for momentum transfer by space-charge forces in region IV (momentum transfer from energetic electrons to the ions) is given in the Appendix. This analysis is based upon the observation that, in the absence of electrostatic forces between plasma and electrodes in region IV, all the momentum gained by the accelerated ions leaving region IV comes from the energetic electrons entering region IV from region III. This leads, as shown in the Appendix, to the following interesting relation between the density of oscillating electron current j_{e3}' flowing toward region IV (from the left) and the ion current density j_i accelerated through region IV:

$$j_{e3}' \simeq \frac{1}{2}\sqrt{\frac{\overline{m_i}}{m_e}}\sqrt[4]{\frac{\overline{W_{i4}}}{W_{i3}}}\cdot j_i \tag{23}$$

where

m_i = ion mass,

m_e = electron mass,

W_{i3} = average energy of ions entering region IV from region III,

W_{i4} = average energy of ions ejected to the right after acceleration through region IV.

Eq. (23) shows that the electron current density j_{e3}', most of which is reflected by the potential gradient in region IV, is much larger than the ion current density accelerated through this region. This is in agreement with what one intuitively expects when considering the transfer of momentum between light electrons and heavy ions as described above. The net electron current density emerging to the right of region III, together with the ion current density j_i, is given by

$$|j_e| = |j_{e3}'| - |j_{e3}''| = j_i. \tag{24}$$

This relation results from the condition that the total current density j_i+j_e emerging from the plasma accelerator be zero, a condition enforced by the processes outlined in the earlier discussion of ion beam neutralization.

It may be of some interest to observe that for desirable ion current densities j_i, the electron current density j_{e3}' becomes quite large; *e.g.*, for $j_i=1$ ampere/cm², $\sqrt{m_i/m_e}=500$, and $W_{i1}/W_{i3}=10^4$, $j_{e3}'\simeq 2500$ amperes/cm². This result, however, is of no particular concern, as j_{e3}' consists of currents due to multiple reflections between the cathode and region IV. The net current density which must be emitted by the cathode in this example equals only $|j_e|=|j_e'|-|j_e''|=j_i=1$ ampere/cm², plus the contribution corresponding to the current ultimately collected on the positive electrode.

Although some emphasis has been given above to the direct transfer of momentum from electrons to ions in region IV by space-charge forces, it is not yet clear which conditions prevail in actual oscillating electron engines. It may be plausible, in fact, that part of the momentum transfer to the ions occurs directly through electrostatic forces between electrodes and ions, another part of the momentum being transferred from the energetic electrons through space-charge forces. In either case, however, oscillating electrons exist in region III and are ultimately collected by a positive electrode. It is clear that this collected (or "intercepted") electron current must, in any event, be kept as small as possible for reasons of efficiency; it represents a power loss which is basically unnecessary. For this reason, good focusing of the beam of oscillating electrons in regions II and III is essential. In the engines considered so far, this is done by means of a dc magnetic field, as in a Penning discharge. If the cathode is itself immersed in the focusing dc magnetic field, it is of interest to ask how the plasma beam can escape from the diverging magnetic field at the end of the engine without being itself caused to diverge intolerably. Although a theoretical answer to this question does not seem to exist yet, Meyerand's experiments [33], [34] (described below) on oscillating electron ion engines seem to indicate that, in fact, such a plasma beam divergence can be avoided.

A further quantity to be evaluated is the plasma density $n_i=n_e$ required in region III for a given ion current density j_i in the plasma beam escaping to the right of region IV. If the rate of ion generation in region IV can be neglected as compared with the rate of ion injection or generation in region III, it is seen that

$$n_i = \frac{j_i}{e\bar{v}_{i3}}, \tag{25}$$

where $\bar{v}_{i3}$ is the average axial velocity of ions leaving region III toward region IV. For $j_i=1$ ampere/cm² (which is a respectable ion current density) and $v_{i3}=2\cdot 10^6$ cm/second (which corresponds to argon ions at an energy of the order of 1 ev),

$$n_e = n_i \cong 3\cdot 10^{13} \text{ particles/cm}^3.$$

Although this plasma density is relatively high, it does not appear excessive for an intense hot-cathode Penning-type discharge; this shows, therefore, the potential capability of this type of engine for achieving quite high thrust densities at a high specific impulse.

A few additional observations can be made about the rate of ion generation in region IV. In the above calculations, this rate was assumed to be zero. In some engines (*e.g.*, Meyerand's oscillating electron ion engine), however, this rate is finite. The consequences of having a finite rather than vanishing rate of ion generation in region IV are:

1) Requirement for a lower plasma density in region III than predicted by (25). This lowering of the plasma density, however, will not be larger, typically, than one order of magnitude.
2) Introduction of an undesirable velocity spread for the accelerated ions.

It is now possible to see the following striking analogies between the oscillating electron engines and accelerated ion engines:

1) Electrostatic acceleration of electrons, which is dual to electrostatic acceleration of ions.
2) Minimization of electron collection by the accelerating electrode through electron focusing (electrostatic and magnetic); is dual to suppression of ion interception by careful electrostatic ion focusing in the ion engine (even though electron interception here is very much higher than ion interception in ion engines).
3) Ion injection for space-charge neutralization, which is dual to electron injection in the ion engine.
4) Prevention of ion flow to the cathode by an ion deceleration potential maximum (region II), which is dual to the prevention of electron flow to the ion emitter by a potential minimum in the ion engine.

The major basic difference between the oscillating electron engine and the ion engine is possibly the process of momentum transfer from electrons to ions, which was discussed above.

The actual oscillating electron engines to which the above considerations pertain differ from one another primarily in their methods of ion generation or ion

injection (in region III of Fig. 21). Three types of ion source have been considered so far:

1) Ion generation through the oscillating electrons themselves (Penning discharge).
2) Ion generation by an arc.
3) Ion generation by contact ionization of cesium.

Type 1) was investigated by Meyerand, *et al.* [33], [34] in the oscillating electron engine; type 2) was first proposed and investigated by J. S. Luce [35]; type 3) is being investigated by W. Eckhardt. This list, of course, does not exhaust the types of ion source which can be considered or which may be in a preliminary state of investigation.

2) The Oscillating Electron Ion Engine: The oscillating electron ion engine as invented and investigated by Meyerand, *et al.*, is sketched in principle in Fig. 22; a typical axial potential distribution is also shown qualitatively in Fig. 22. It is seen that this potential distribution is closely similar to that in Fig. 21, with the difference that the well-defined potential maximum of region II in Fig. 21 does not exist; it is replaced by a moderate potential gradient in region III. The ions are generated by collisions between the fast electrons and neutral gas molecules or atoms admitted into region III. This device is therefore seen to be a modification of a hot-cathode Penning discharge.

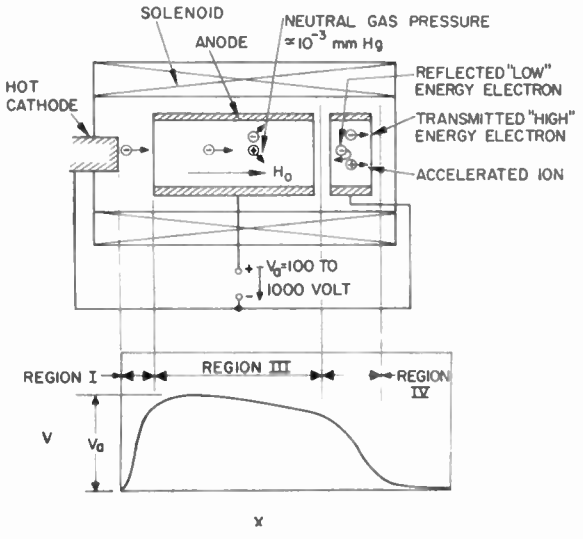

Fig. 22—Oscillating electron ion engine (modified Penning discharge).

Typical performance obtained to date by an engine of this type is, according to Meyerand:

Specific impulse—up to 3000 seconds with argon.
Beam power efficiency—25 per cent.
Ion current density in escaping plasma beam—of the order of several amperes/cm².

Sputtering of the cathode (lanthanum hexaboride) was visible after several hundred hours of operation, but did not interfere with normal operation of the device. Appreciably less than 50 per cent of the total ion current went to the cathode. No data on fuel-utilization efficiency seem available yet.

The most important result from Meyerand's experiments appears to be attaining ion current densities above 1 ampere/cm² in the plasma beam, an achievement which appears rather outstanding at the present state of the art.

3) The Arc-Type Engine: In the arc-type engine, ions are generated in what corresponds to region III of Fig. 21 by means of a high-intensity vacuum arc. The type of arc developed by Luce [35] at Oak Ridge has been proposed for this purpose. Because of the high ion density (up to about 10^{14} ions/cm³) and the high degree of ionization (resulting in good fuel utilization efficiency), this type of arc has definite merits as an ion source for an accelerated electron engine. The arc will be established between a hollow cathode and a cylindrical anode, the accelerated electron beam being injected through the cathode hole. Two possible disadvantages of this type of arc are the relatively fast rate of erosion (sputtering) of the cathode of the arc, and the requirement for a relatively strong axial dc magnetic field in the arc region. The latter, of course, is also a requirement for Meyerand's Penning-type oscillating-electron ion engine.

4) Accelerated-Electron Cesium Ion Engine: It is conceivable that the ions in region III of Fig. 21 could be provided by means of a cylindrical cesium ion emitter, producing ions by contact ionization. In principle, such an ion emitter could be made by a method similar to that described for the cesium ion engine. Possible advantages of the accelerated-electron cesium ion engine then appear to be: 1) the ability to draw the maximum ion current density available from the ionizer, without limitations imposed by the perveance of the accelerating ion gun electrodes, and 2) better thermal efficiency, because the thermally radiating area (approximately equal to the area of the plasma beam cross section) can be made much smaller than the ion emitting area. A reduction of one order of magnitude in radiative heat loss does not seem impossible.

Further apparent advantages of the accelerated-electron cesium ion engine over other types of oscillating electron engines are: 1) better fuel utilization efficiency; and 2) better control of the potentials in regions I and II to minimize the back-flow of ions onto the cathode, minimize the power loss, and suppress the cathode sputtering associated with this ion back-flow.

Questions still to be resolved about this type of engine are the details of potential distribution in the vicinity of the ion-injecting cylinder through which the electron beam passes in region III, the optimization of the electron beam focusing in region III (it is possible that an appreciable dc magnetic field may be required), and a detailed understanding of the plasma potential gradient needed in region IV. No experiments have been performed as yet on the accelerated-electron cesium ion engine.

III. Magnetic Plasma Acceleration

The dual to electrostatic acceleration of charged particles is magnetic acceleration; Coulomb forces are used in the former, Lorentz forces in the latter.

In magnetic plasma acceleration, the accelerating force is given by $F = qv \times B$, where q is the charge of the accelerated particle, v its velocity, and B the magnetic induction. Because the average value of F can be finite even when both v and B are time varying and quasi-periodic, the possibility exists, in principle, of accelerating a plasma with either dc or ac magnetic fields. Both methods are being investigated and will be discussed below.

A. DC Magnetic Plasma Acceleration

1) Theory: A schematic of a dc magnetic plasma accelerator is shown in Fig. 23. An electron current I is emitted from a cathode, passed through the plasma which is to be accelerated, and collected by an anode; a dc magnetic field perpendicular to both the direction of plasma flow and of electron current flow is provided. As a result, a volume force

$$f = j \times B$$

is exerted on the plasma by the flowing electron current and is available to accelerate the plasma.

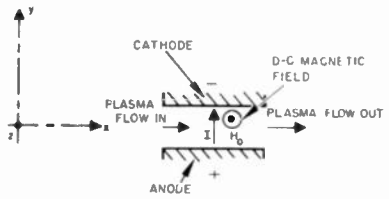

Fig. 23—Principle of dc magnetic plasma acceleration.

Both the current flow perpendicular to a dc magnetic field and the momentum transfer from the electron current I to the ions and neutrals of the gas imply collision processes. Because these collisions are necessary, it also follows that a finite ohmic plasma resistivity ρ is unavoidable. Therefore, joule heating of the plasma must necessarily accompany its acceleration by continuous Lorentz forces. It is therefore of interest: 1) to evaluate the importance of this joule heating, 2) to compare it with the transfer of ordered kinetic energy by Lorentz forces, and 3) to determine what basic limits are imposed on this type of plasma accelerator as a consequence of joule heating [36].

The kinetic power u_k transferred to the plasma is given by

$$u_k = T(v_2 - v_1) = IhB(v_2 - v_1), \tag{26}$$

where

T = total thrust,
v_2 = exit gas velocity,
v_1 = input gas velocity,
I = total current flowing across magnetic field H between cathode and anode,
$B = \mu_0 H$ = magnetic induction,
h = distance between cathode and anode.

The power lost by joule heating of the plasma is given by

$$u_j = R_p I^2, \tag{27}$$

where R_p is the total plasma resistance between the cathode and anode.

From (26) and (27) the efficiency η of a dc magnetic plasma accelerator is seen to be

$$\eta \cong \frac{u_k}{u_k + u_j} = \frac{1}{1 + \dfrac{R_p}{hB(v_2 - v_1)} \cdot I}. \tag{28}$$

From (26) I can be expressed as a function of the thrust T; substituting $I = T/hB$ into (28) yields

$$\eta = \frac{1}{1 + R_p \cdot \dfrac{T}{h^2 B^2 (v_2 - v_1)}}. \tag{29}$$

These expressions are only rather crude approximations. End effects, Hall currents, boundary layer effects, power to maintain the magnetic field are all neglected; a constant channel cross section (which may not be optimum) is assumed. Nevertheless, these expressions are helpful in gaining an insight into the nature and importance of the fundamental limitations of this acceleration mechanism. To this end, it is useful to express the total plasma resistance R_p in terms of the plasma resistivity ρ_p, which is a more fundamental and more readily evaluated quantity. Under the assumption of constant plasma resistivity ρ_p throughout the region of current flow, this leads from (29) to

$$\eta \cong \frac{1}{1 + \dfrac{\rho_p}{B^2} \cdot \dfrac{T}{V(v_2 - v_1)}}. \tag{30}$$

where V is the volume of interaction space. Eq. (30), although approximate, is important because it shows which parameters should be optimized. For a given mission, the total thrust T will be prescribed; the specific impulse, and therefore the exhaust velocity v_2, will also be prescribed. For an effective plasma accelerator, $v_2 \gg v_1$; hence, $v_2 - v_1 \simeq v_2$. The parameters remaining available for optimization are, therefore:

1) The plasma resistivity ρ_p,
2) The magnetic induction B,
3) The volume of the interaction space V.

According to (30), it is desirable: 1) to minimize ρ_p, and 2) to maximize $B^2 V$.

In order to evaluate the plasma resistivity ρ_p and de-

termine how far it can be reduced, it is necessary to consider how the plasma can be injected into a Lorentz accelerator. In the devices considered and tested to date [37], the plasma is generated by a plasma jet [38]. This implies gas temperatures of the order of 1 ev. At such temperatures, a fractional ionization of the order of a few per cent can be achieved by seeding the gas with an alkali metal of low ionization potential (*e.g.*, Cs, Na, or K). This degree of ionization is high enough to make electron-neutral collisions negligible as compared with Coulomb (electron-ion) collisions. The resistivity of such a plasma can therefore be made about as low as that of a fully ionized gas of corresponding temperature. The resistivity of a fully ionized plasma is given by [39]

$$\rho_p = 6.53 \cdot 10^3 \frac{\log \Lambda}{T_e^{3/2}} \text{ ohm cm}, \tag{31}$$

where $\log \Lambda$ is a slowly varying function of density and temperature whose value is between 6 and 9 in the range of parameters of interest here and T_e (this should not be confused with those equations where T is used for thrust) is the electron temperature in °K. For a temperature between 5000°K and 10,000°K, this leads to a plasma resistivity of the order of $\rho_p \simeq 0.1$ ohm-cm. To reduce ρ_p below this value would require a higher electron temperature. With a plasma jet, this is not practical because of materials and life problems. An alternative process providing additional heat to the electrons is the joule heating itself, which results from the current flow through the interaction space of the plasma accelerator. An upper limit to the electron temperature, however, is probably set by the heat transfer from the plasma to the electrodes with which it is in contact, and by the subsequent electrode cooling and erosion problem. The existence of sheaths at the electrodes and of temperature gradients through the plasma cross section makes difficult a more accurate evaluation of the maximum tolerable electron temperature and of the minimum corresponding plasma resistivity in the present state of the art.

The maximum tolerable value of B^2V in (30) is determined by the following considerations:

1) Since engine weight tends to increase with volume, it will usually be desirable to keep V reasonably small. Hence, to maximize B^2V, it is more desirable to make B large than to make V large. (Note that B^2V is proportional to the total stored magnetic energy W_m. Since the solenoid power or the weight of permanent magnet material needed for the required magnetic field is approximately proportional to W_m, it does not matter, from the standpoint of cost of the field, whether B^2 or V is increased.)

2) The upper limit to B is determined by the condition that the required current flow in the direction of the applied electric field and perpendicular to the magnetic field can take place and that the momentum transfer from the electrons to the ions and neutrals be effective. In order to determine this upper limit to B, it is necessary to investigate in more detail the flow of electron current perpendicular to a dc magnetic field in an ionized gas. To this end, it is convenient to proceed from the following equation, which relates electron current density j, electric field E, and magnetic field B in a partially ionized gas [40]:

$$j \cong \frac{1}{\rho_p}\left[E + (v \times B) - \frac{1}{n_e e} \cdot j \times B\right] + \frac{2}{B^2} \cdot \left[\frac{R_{ce} \cdot R_{ci}}{\lambda_{ei} \cdot \lambda_{ia}}\right]^{-1} \cdot [j \times B] \times B, \tag{32}$$

where

R_c = cyclotron radius of particle considered,
e = charge of electron (absolute value),
m = mass of particle considered,
λ = mean free path,
e = electron,
i = ion,
index a = neutral,
v = velocity of mass motion of whole gas,
$1/\rho_p = n_e e^2 \tau_{ei}/m_e$ = plasma conductivity with $1/\tau_{ei}$ = electron-ion collision frequency,
n_e = electron density.

Eq. (32) was obtained using the following simplifying assumptions, which are valid in the plasmas under consideration:

1) gravity forces on the plasma are negligible,
2) $\lambda_{ia}/\lambda_{ea} \ll m_i/m_e$,
3) $\lambda_{ei} < \lambda_{ea}$,
4) $n_e/n_a < 10^{-1}$,
5) the gradient of electron pressure is small compared with other forces per unit volume.

Eq. (32) is needed to find the components of the current density j and of the thrust density $f = j \times B$. The y direction is chosen parallel to the applied dc electric field; the z direction is parallel to the applied dc magnetic field. A further simplifying assumption is made as follows:

$$2\left(\frac{\lambda_{ia}}{R_{ci}}\right)\left(\frac{\lambda_{ei}}{R_{ce}}\right) \gg 1. \tag{33}$$

This inequality is satisfied for magnetic inductions $B \geq 0.1$ weber/m^2 at plasma densities $n_i = n_e < 10^{15}$ cm^{-3} and electron temperatures $T_e \geq 1$ ev. Eq. (32) then yields

$$j_x \simeq -\frac{1}{\alpha B} j_y, \tag{34}$$

$$j_y \simeq \frac{1}{1 + \alpha^2 B^2} \cdot \frac{E_y'}{\rho_i}. \tag{35}$$

where

$$\alpha = \frac{2}{B}\cdot\frac{\lambda_{ia}}{R_{ei}} = \frac{2e}{\nu_{ia}m_i},$$

$\nu_{ia} \equiv$ ion-neutral collision frequency,

$$E_y' = E_y - v_x B,$$

$$\rho_i = \frac{m_i}{2n_e e^2 \tau_{ia}} \equiv \text{plasma resistivity to ion flow.}$$

From (34) and (35), the components of the thrust density $f = j \times B$ (thrust per unit volume) are found to be

$$f_x \cong \frac{j_0 hB}{1 + \alpha^2 B^2}, \tag{36}$$

$$f_y \cong \frac{1}{\alpha B}\cdot f_x, \tag{37}$$

$$f \cong \sqrt{f_x^2 + f_y^2} = \frac{j_0 h}{\alpha}\cdot\frac{1}{\sqrt{1 + \alpha^2 B^2}}, \tag{38}$$

where

$$j_0 = \frac{E_y'}{\rho_i}.$$

Because of the assumption of (33), the results of (34) to (38) do not hold for $\alpha B \to 0$ or $\alpha B \ll 1$, even though they are still approximately valid when αB is somewhat smaller than 1. They are, of course, quite good approximations for $\alpha B \geq 1$. Further, for reasons of efficiency [see (30)], very small values of αB are of no interest for the purpose of propulsion. Therefore, (34)–(38) are valid within the range of values of magnetic field of practical interest.

Considering at the same time the efficiency given by (30) and the thrust density given by (38), it becomes apparent that an approximate optimum value for the magnetic field is given by the condition

$$\alpha^2 B^2 \simeq 1, \tag{39}$$

which may be rewritten, by definition of α, as

$$R_{ei} \simeq 2\lambda_{in}. \tag{40}$$

This result [41] shows for the optimum magnetic field a value such that the ion cyclotron radius is about twice the ion-neutral mean free path. This follows from the predominant importance of the last term of (32), when $R_{ei} < \lambda_{ei}$. This result differs markedly from that which would be obtained in a fully ionized gas, where the last term of (32) would not exist; in that case the optimum magnetic field would correspond to the condition $R_{ei} \simeq \lambda_{ei}$ and would be much smaller.

2) Experiments: Experimental results in apparent agreement with the theory outlined above have been obtained in a dc magnetic plasma accelerator by Demetriades [42]. They are summarized below as an indication of the present state of the art. A schematic representation of the plasma accelerator is shown in Fig. 24; a diagram of the complete experimental apparatus is given in Fig. 25. Of most interest is a series of measurements of thrust as a function of dc magnetic field. These measurements, shown in Fig. 26, provide an experimental verification of (38) and condition (40) for the optimum magnetic field. For the conditions of the experiment shown in Fig. 26, B_{opt} can be

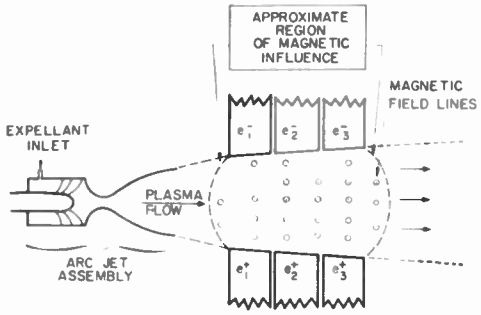

Fig. 24—Schematic diagram of arc jet plasma source and dc magnetic plasma accelerator.

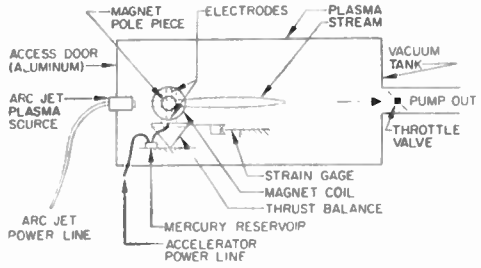

Fig. 25—Schematic diagram of experimental apparatus showing dc magnetic plasma accelerator mounted on thrust stand within vacuum tank. Arc jet is mounted in vacuum tank door.

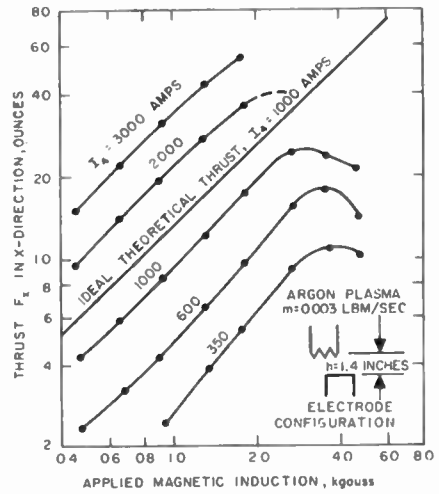

Fig. 26—Experimental data showing accelerator thrust as a function of applied magnetic induction.

evaluated from the following values of the parameters estimated by Demetriades for this experiment:

Ion-neutral mean free path—$\lambda_{ia} = 1/n_a\sigma_{ia}$,
Neutral density—$n_a = 10^{16}$ atoms/cm^3,
Gas—argon,
Ion-neutral collision cross section [43]—$\sigma_{ia} = 4 \cdot 10^{-16}$ cm^{-2},
Relative ion-neutral velocity—$v = 2.3 \cdot 10^2 \sqrt{T_i} \simeq 1.85 \cdot 10^5$ cm/second,
Electron density—$n_e = 10^{14}$ cm^{-3},
Electron temperature—$T_e \cong 10{,}000°$K,
Ion temperature—$T_i = 6400°$K.

The theoretical magnetic field for maximum thrust in the x direction, then, is given with $R_{ei} = 2\lambda_{ia}$ by

$$B_{\text{opt}} = \frac{\nu_{ia} m_i}{e} \simeq 0.15 \text{ weber}/m^2.$$

The experimental value, according to Fig. 26, is $B \simeq 0.3$ to 0.4 weber/m^2. Considering the uncertainty in the evaluation of σ_{ia} and ν_{ia}, agreement between theory and experiment appears reasonably good. It is clear, in particular, that the criterion $R_{ce} \simeq \lambda_{ei}$, which would prevail in a fully ionized plasma, does *not* apply to those experiments. Indeed, the condition $R_{ce} \simeq \lambda_{ei}$ would lead to an optimum magnetic induction of about $2.5 \cdot 10^{-2}$ weber/m^2, for the values of electron density (about 10^{14} cm^{-3}) and electron temperature (about 10,000°K) estimated for these experiments.

Further results of interest from the Demetriades experiments are:

Maximum specific impulse achieved—2400 seconds,
Maximum acceleration efficiency—44 per cent.

While the above theoretical considerations and experimental results show that Lorentz force plasma accelerators hold basically good promise for the achievement of high specific impulse with good efficiency and high thrust density, a number of problems still remain to be investigated. The limitations imposed by overheating of the electrodes by the hot plasma stream [45], boundary layer effects, and end effects still remain to be investigated in more detail, particularly at higher specific impulse. While, from the results obtained to date, specific impulses up to about 5000 seconds with efficiencies above 60 per cent can probably be expected, it is not clear how much more will ultimately be achieved.

B. AC Magnetic Plasma Acceleration

In dc magnetic plasma acceleration, important limitations seem to be imposed by the presence of electrodes in direct contact with the hot plasma. A possibility of avoiding these difficulties while still applying the concept of magnetic plasma acceleration by $j \times B$ Lorentz forces is to produce induced currents in the plasma by time-varying (ac) fields, thus obviating in principle the need for physical contact between plasma and electrodes. A further advantage of currents induced by ac fields is the possibility of exerting accelerating forces on the plasma without the need for any particle collisions. For this reason, the use of plasmas with very low resistivity is, in principle, possible. This contrasts with dc magnetic plasma acceleration, where a finite plasma resistivity has been shown to be basically unavoidable. (Because, however, the effect of plasma resistivity in the dc case was found in itself to be tolerable, the latter advantage is probably of more academic than practical significance.)

1) Traveling-Wave Magnetic Plasma Acceleration: One class of ac magnetic fields available for plasma acceleration is traveling fields, or magnetic "traveling waves"; the other, of course, is stationary fields.

Traveling-wave devices may be subdivided [46] for convenience into the following categories: 1) magnetic piston plasma accelerators, 2) traveling-wave plasma bunch accelerators, and 3) traveling-wave plasma ring accelerators.

a) Magnetic piston plasma accelerators: A schematic illustration of a magnetic piston device is shown in Fig. 27. The pressure p exerted by the magnetic field on the plasma, if the penetration of the magnetic field into the plasma is limited to a surface region, is given by

$$p = \frac{\mu_0 H^2}{2}. \tag{41}$$

A simple derivation of this relation will be given for a one-dimensional case because it provides some insight into the physical significance of (41). Consider a slab of plasma as illustrated in Fig. 28. Let a field H be established in the z direction at the left of the plane x_1. As this field tends to penetrate into the plasma, it induces a current density j_y. Then, from Maxwell's equa-

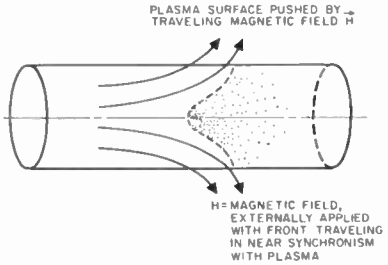

Fig. 27—Magnetic piston.

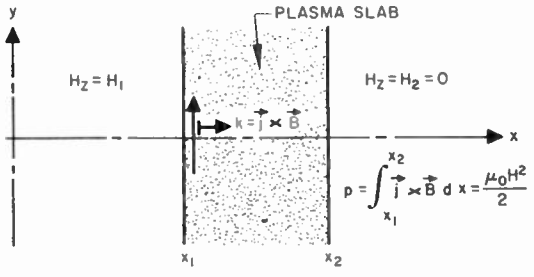

Fig. 28—Magnetic pressure on plasma slab.

tion $\nabla \times H = j$, it follows that, for this one-dimensional case,

$$j_y = -\frac{\partial H_z}{\partial x}. \tag{42}$$

The force per unit volume exerted on the plasma in the surface region is given by $f = j \times B$:

$$f_x = j_y B_z = \mu_0 j_y H_z. \tag{43}$$

From (42) and (43),

$$f_x = \mu_0 H_z \frac{\partial H_z}{\partial x} = -\frac{\mu_0}{2}\frac{\partial}{\partial x}(H_z^2).$$

Integrating f_x between $x = x_1$ and $x = x_2$ to obtain the force per unit area yields the pressure p exerted by the magnetic field on the plasma:

$$p = -\frac{\mu_0}{2}\int_{x_1}^{x_2}\frac{\partial}{\partial x}(H_z^2) = \frac{\mu_0(H_1^2 - H_2^2)}{2} = \frac{\mu_0 H^2}{2}$$

if $H_1 = H$ and $H_2 = 0$.

This elementary derivation illustrates the fact that the pressure exerted by a traveling magnetic field acting as a piston on a plasma does result from the Lorentz force $j \times B$. A further consequence evident from this derivation is that the full magnetic pressure is exerted on the plasma only if the magnetic field is prevented from penetrating through it (otherwise, the above derivation leads to $p = (\mu_0/2)(H_1^2 - H_2^2)$, with $p = 0$ when $H_2 = H_1$!). This means that the diffusion of the magnetic field into the plasma must be slow compared with the time available for plasma acceleration. In order to determine, in principle, the feasibility of magnetic piston acceleration of a plasma, it is necessary to consider the process of diffusion of a magnetic field into a plasma. This process is expressed by the following diffusion equation [47]:

$$\frac{\partial H}{\partial t} = D \cdot \nabla^2 H, \tag{44}$$

where

$D = \rho/\mu_0$ = diffusion coefficient of the magnetic field in a plasma of resistivity ρ, (45)

μ_0 = permitivity of vacuum $= 4\pi \times 10^{-7}$ henry/m.

Let τ be the time available for acceleration of the plasma, l the depth to which the magnetic field is allowed to diffuse into the plasma during this time τ, and v_d the mean velocity of diffusion of the magnetic field during this time τ. The condition determining the maximum tolerable rate of diffusion of the magnetic field into the plasma is then

$$v_d \tau < l.$$

Further, by definition of v_d and D,

$$v_d \simeq \frac{D}{l}.$$

Hence,

$$D < \frac{l^2}{\tau}. \tag{46}$$

The time τ available for acceleration is related to the available acceleration length L and to the final plasma velocity v_p by

$$\tau = \frac{2L}{v_p}, \tag{47}$$

which is valid under the assumption that $v_p \gg v_1$, if v_1 is the initial plasma velocity (before acceleration) and if the accelerating force is constant during the time interval τ. The following condition results from (45)–(47), for the plasma resistivity ρ:

$$\rho \leq \mu_0 \cdot \frac{l^2 v_p}{2L}.$$

For a representative numerical application, let

$l = 10^{-2}$ m,
$2L = 0.5$ meter,
$v_p = 10^5$ m/second,
$\mu_0 = 4\pi \cdot 10^{-7}$ henry/m.

Then

$$\rho \leq 2.5 \cdot 10^{-5} \text{ ohm-meter}$$

or

$$\rho \leq 2.5 \cdot 10^{-3} \text{ ohm-cm}.$$

Assuming the degree of ionization of the plasma to be high enough that Coulomb collisions will predominate over electron-neutral collisions leads, with (31), to the following limit for the electron temperature T_e of the plasma:

$$T_e > 6 \text{ ev (about } 70{,}000°\text{K}).$$

This calculation is, of course, only approximate, and it aims only at determining orders of magnitude. As such, it shows that the requirement imposed on plasma resistivity and temperature, while not trivial, is not unrealistic. By proper preionization, or plasma injection, such plasma temperatures should, in principle, be attainable. For this reason also, plasma acceleration by a traveling magnetic piston as illustrated in Fig. 27 appears, in principle, possible.

Two modifications [48] of the device in Fig. 27 are shown in Figs. 29 and 30. In the device in Fig. 29 a "biasing" magnetic field is applied before the (traveling) field of the magnetic piston is applied. The purpose of this biasing field is to provide a magnetic insulation between the plasma and the walls. Special care has to be taken to avoid excessive trapping of this field in the accelerated plasma. In the device of Fig. 30 the traveling magnetic field is made sinusoidal; plasma bunches can be trapped every half wavelength in the vicinity of the axis, in the region where the magnetic field is minimum.

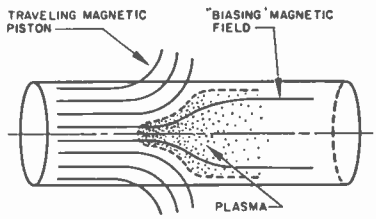

Fig. 29—Magnetic piston with "biasing" magnetic field.

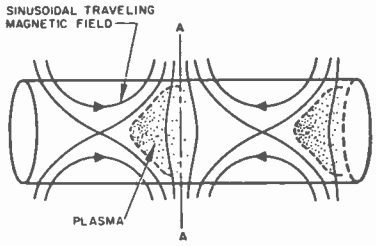

Fig. 30—Sinusoidal magnetic traveling-wave plasma accelerator.

Plasma will tend to accumulate in the dotted regions, and to be carried with the magnetic field. For a high enough plasma conductivity (small rate of diffusion of magnetic field into plasma), conditions similar to those described above will prevail, with the advantage that the shape of the lines of force of the magnetic field will tend to reduce the plasma diffusion to the walls. In the plane AA one has, with a circular cylindrical symmetry, a "cusped" field which, while it leads to a finite rate of plasma leakage, keeps this leakage below that which would exist in the absence of a magnetic field.

b) Traveling-wave plasma bunch accelerator: An alternative possibility exists for operating a device of the type shown in Fig. 30: if the plasma conductivity does not satisfy the condition of (33), the plasma will "leak" through the saddle points of the magnetic field, from one minimum to the preceding one, and so on. In this process, however, as a consequence of the relative motion between plasma and magnetic field, transverse azimuthal currents perpendicular to the magnetic field are induced in the plasma, and the resulting $j \times B$ force will still tend to accelerate the plasma, even though the force is more evenly distributed throughout the plasma volume than in the case of the magnetic piston. The advantage of this mode of operation is that it conceivably permits quasi-continuous operation, where the plasma is fed continuously into one end of the device, and is dragged and accelerated by the traveling magnetic field to the other end of the accelerator. One penalty for this mode of operation, as compared with the magnetic piston, is the requirement for a higher ac magnetic field for a given average thrust density.

c) Traveling-wave plasma ring accelerator: The principle of a traveling-wave plasma ring accelerator is illustrated in Fig. 31. It does not differ basically from that of a magnetic piston device of the type in Fig. 30. Although the concept of magnetic pressure $p_m = \frac{1}{2}\mu_0 H^2$ could also be applied to the plasma ring device, it is

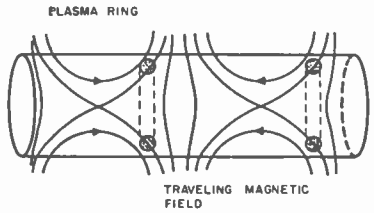

Fig. 31—Traveling-wave plasma ring accelerator.

preferable to consider directly the interaction between the magnetic field and the azimuthal current induced in the plasma ring by the change of magnetic flux enclosed by the plasma ring as a consequence of slippage between traveling magnetic field and plasma ring. For this process of plasma acceleration to be effective, the total slippage has to be kept smaller than one-fourth the wavelength of the traveling magnetic field. This condition is equivalent to the condition of (46) derived for the magnetic piston devices and leads to similar requirements for the plasma conductivity. More detailed calculations [49] show that the $j \times B$ forces exerted on the plasma ring not only accelerate the plasma axially, but also tend to make the ring collapse radially inward. It appears possible, however, to prevent the rate of inward radial acceleration from being excessive in relation to the rate of axial acceleration.

d) Limitations and experimental results: One important feature of all traveling-wave devices is that the energy stored in the accelerating magnetic field is at least of the same order of magnitude as the kinetic energy of the plasma being accelerated. Hence if the traveling-wave circuit were simply terminated in a matched load, this flux of magnetic energy would be lost; because it is at least equal to the flux of kinetic energy of the plasma, quite poor efficiencies would result. One way to avoid this waste is to recuperate the magnetic energy at the output of the accelerating circuit by feeding it back through an appropriate feedback circuit to the input of the accelerating circuit; the accelerating circuit is then part of a race-track circuit.

While loss of magnetic energy at the end of the traveling-wave circuit could, in principle, be avoided, ohmic losses in the conductors of the circuit causing the magnetic field cannot be suppressed. Because of the relatively low frequencies involved (typically of the order of 1 Mc or less), these losses can be kept relatively small, at least in those cases (magnetic piston, plasma rings) where the penetration of the magnetic field into the plasma or the slippage are kept small. Indeed, in those cases, the magnetic pressure on the plasma is of the same order of magnitude as the magnetic pressure on the conductor. If the magnetic field at the conductor leads to a pressure p, it can be shown [50] that the power dissipated per unit area of conductor is, for copper at room temperature,

$$P_1 = 4.15\sqrt{f_{\text{Mc}}} \times p_{at} \text{ kw/cm}^2,$$

where

$f_{Mc} \equiv$ frequency of ac field in Mc/sec,
$p_{at} \equiv$ magnetic pressure in atmospheres.

The pressures involved in plasma acceleration being substantially smaller than one atmosphere, one can expect

$$P_1 \ll 1 \text{ kw/cm}^2.$$

In comparison to this, the kinetic power transferred per unit area of accelerated plasma is

$$P_{k1} \cong p \cdot v_p \cong 10^{-2} p_{at} v_p \text{ kw/cm}^2,$$

where

$p =$ magnetic pressure in Newton/m^2,
$p_{at} =$ magnetic pressure in atmospheres,
$v_p =$ plasma velocity in m/second.

It is interesting to evaluate P_1/P_{k1} from the above relations, assuming p to be about the same on plasma and conductors

$$P_1/P_{k1} \simeq \frac{415 \cdot \sqrt{f_{Mc}}}{v_p} \ll 1.$$

With $v_p = 10^4$ to 10^5 m/second, it is seen that the ohmic circuit losses can be kept relatively unimportant, even if the conductor surfaces would much exceed the surface over which the magnetic pressure is exerted upon the plasma.

An additional feature common to these traveling-wave devices, where near synchronism is required between traveling magnetic field and plasma, is the necessity of increasing progressively with distance the phase velocity of the accelerating magnetic field wave; *i.e.*, a "tapered" traveling-wave circuit is required. This applies to the magnetic piston devices; it also applies to the traveling-wave plasma ring accelerator described above.

A further requirement common to all traveling-wave accelerators is low plasma resistivity. In all the above cases, plasma resistivity has been shown to lead to unwanted effects (diffusion of the field into the plasma, slippage of plasma rings). In other words, electron collisions with ions or neutrals are to be minimized. It could be asked at this point how momentum is transferred to the ions in the absence of electron-ion collisions. In all traveling-wave devices, the current flow is indeed carried by the electrons; the Lorentz force $j \times B$ acts, therefore, on the electrons, and the electrons alone will first be accelerated. However, as the electrons are accelerated and leave the ions behind, a charge separation occurs and leads to a space-charge field; this space-charge field then accelerates the ions and decelerates the electrons until they all have the same average velocity. This process is analogous to ambipolar diffusion and is effective as long as the Debye length is small compared with the dimensions of the plasma. One exception occurs when the electron current flow is closed on itself, as in a plasma ring; in this case, an azimuthal electron current can flow without dragging ions with itself and without charge separation. This exception is important because it makes the flow of a net electric current transverse to the magnetic field possible. However, the axial motion of electrons, under the accelerating $j \times B$ force, does not lead to a closed path of electron current. For this reason, momentum is transferred by space-charge fields from electrons to ions in the axial direction without need for collisions. Returning to the requirement for minimizing electron-ion and electron-neutral collisions leads to the need for highly ionized plasmas of relatively high temperature (typically above 5×10^4 °K, as shown above). For this reason, it does not seem practical to ionize the gas and accelerate it by means of the same electromagnetic field. Separate ionization and injection seems necessary for traveling-wave devices. (It is indicated below that similar requirements on low plasma resistivity and separate plasma generation are also apparent in stationary ac field plasma accelerators.)

This list of requirements is rather severe; even so it is not exhaustive. In experiments performed by Penfold [51] the basic principle of this acceleration mechanism has been demonstrated. Plasma rings with velocities of about 1.2×10^7 cm/second ($I_{sp} \simeq 10^4$ seconds) have been obtained; evidence has been found for plasma ring currents of at least several hundred amperes.

2) Stationary AC Magnetic-Field Plasma Acceleration: It is also conceivable that currents can be induced into a plasma by means of a stationary ac magnetic field and that accelerating forces can be obtained by the interactions between these currents and the inducing magnetic field. One model of a device based upon this principle is shown in Fig. 32. The ac magnetic field is produced by a single-turn coil which is made part of a tank circuit by connection to an appropriate capacitor. A plasma ring is produced by preionization of the gas in the vicinity of the "exit" of the coil, as shown ideally in Fig. 32. The ac magnetic field induces an azimuthal current in the plasma ring; this results in a force $j \times B$ as shown in Fig. 32. For optimum conditions the current density j should be in phase with the ac magnetic field H; hence, it should be in quadrature with the induced electric field, except for the phase shift of the electrons produced by the acceleration itself. This means that the plasma ring should have only negligible ohmic resistance; in this case, as well as in that of traveling-wave acceleration, electron-ion and electron-neutral collisions are, if anything, detrimental. In the extreme, if the plasma ring were purely resistive (instead of inductive) as a consequence of high ohmic resistivity, j and B would be in quadrature and the average force would be zero.

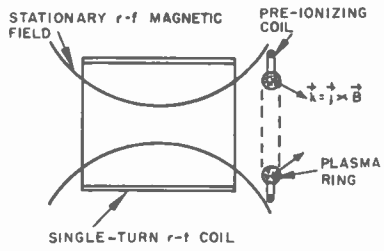

Fig. 32—Stationary ac magnetic field plasma accelerator.

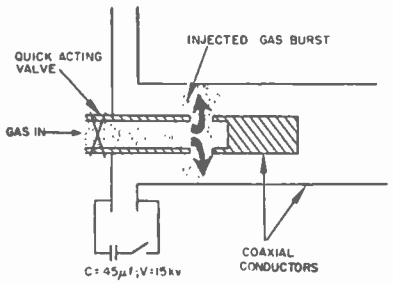

Fig. 33—Hydromagnetic plasma gun.

The requirement for minimizing collisions and plasma resistivity appears to be in contradiction with the need of collisions for ionizing the gas. For this reason, preionization of the gas or separate injection of the plasma seems necessary. This can be done on a pulse basis (where plasma rings are formed or injected periodically while the accelerating ac field is off). This procedure has been used by Miller [52] in the experiments in which he provided a preionizing coil in the vicinity of the region where the plasma ring was wanted. In Miller's experiment, the frequency (55.5 Kc/sec) and strength (up to 1 weber/m^2) of the ac magnetic field were chosen of such magnitude that the plasma ring was accelerated away from the coil within about $\frac{1}{4}$ cycle. Acceleration efficiencies of the order of 5 per cent have been measured, with axial exit velocities up to 10^5 m/second; energies up to 25 joules per pulse were transferred from the circuit to the axial motion of the gas.

An alternative mode of operation, still pulsed, would consist in using higher ac frequencies and lower field strengths, with the result that the plasma ring would remain several ac periods in the ac field. Because little analytical work and no experimental work seem to be available on this mode of operation, a more extensive treatment does not seem indicated at this time.

Finally, it is possible to consider cw operation. This implies continuous gas feeding and ionization in the accelerating region. Because of the apparent conflict between ionization and acceleration pointed out earlier, no satisfactory solution to the problem of CW stationary ac magnetic plasma acceleration has yet been reported.

In conclusion, although the idea of plasma acceleration by stationary ac magnetic fields seems interesting, both the problems of proper plasma or gas injection and the problem of optimization of the circuit geometry for optimum utilization of the ac magnetic field still remain to be solved.

C. *Pulsed Magnetic Plasma Acceleration*

An example of a pulsed magnetic field plasma accelerator is shown in Fig. 33. This "hydromagnetic plasma gun," in the form invented by Marshall [53], consists of two coaxial conductors with provision for pulsed admission of gas bursts through openings in the center conductor. Shortly after a burst of gas is admitted between the two coaxial conductors, the power from a high-voltage capacitor bank is suddenly applied. The gas is ionized, a large radial current flows through it, and an azimuthal magnetic field is established by the flow of the current through the central conductor. This azimuthal magnetic field interacts with the radial plasma current to produce axial $j \times B$ forces which result in a magnetic pressure of the order of $\mu_0 H^2/2$. In this respect, this device is analogous to the magnetic piston type of accelerators described above. The essential differences are that, in the hydromagnetic plasma gun: 1) current flow through the plasma results from direct contact to the electrodes instead of being induced, and 2) the magnetic field is not supported by a slow-wave circuit, but by a simple coaxial line.

Basic limitations to this type of plasma accelerator may result from

1) Difficulty of efficient energy transfer from the capacitor bank or pulsing circuit to the coaxial line,
2) Loss of magnetic energy tending to escape or be reflected from the end of the plasma gun,
3) Power loss due to physical contact between the plasma and electrodes,
4) Disadvantage of requiring a pulsed power supply.

Typical characteristics quoted for the performance of such a plasma accelerator are [53]:

Output gas (H_2) velocity—1.5×10^5 m/second.
Total kinetic energy of gas, per pulse—1200 joules.
Total efficiency of energy transfer from capacitor bank to directed kinetic energy—23.5 per cent.
No evidence of electrode erosion was observed under proper timing of the electrical pulse with respect to the gas burst.

These results so far appear encouraging. Because of the limitations suggested above, much still remains to be done before it will be possible to state how much performance can be improved. Further investigations of modifications of the Marshall gun [54] have led so far to results very similar to those quoted above, the major difference being that lower specific impulses (about 6000 seconds) have been obtained with heavier gases, with about the same efficiency.

IV. Electromagnetic Plasma Acceleration

In a nonuniform ac electromagnetic field, a charged particle of charge e experiences an average force given by [55]

$$F = \frac{-e^2}{\epsilon_0 m \omega^2} \cdot \nabla E^2. \tag{48}$$

Although it does not appear explicitly, the effect of the ac magnetic field is also included in (48). [The magnetic field has been eliminated by the use of Maxwell's equation $\nabla \times E = -\mu_0(\partial H/\partial t)$, to arrive at (48).]

In a plasma, the force of (48) will be acting mainly on the electrons and will produce a force f per unit volume given by

$$f = -\left(\frac{\omega_p}{\omega}\right)^2 \nabla \left(\frac{\epsilon_0 E^2}{2}\right), \tag{49}$$

where $\omega_p \equiv$ electron plasma frequency. (Momentum transfer from electrons to ions is caused by space-charge forces in the same process as described above.)

In electromagnetic plasma acceleration, forces of the type given by (49) are produced by nonuniform RF fields and are being used to accelerate plasmas. It may be observed that when the RF field penetration inside the plasma is negligible (which it will tend to be at high plasma densities), (49) can be integrated to lead to a puressure $p = \epsilon_0 E^2/2$ from the RF field on the plasma surface. A more rigorous derivation would lead to

$$p = (1/2)(\mu_0 H^2 + \epsilon_0 E^2),$$

which may also be interpreted as radiation pressure.

A general feature of (48) and (49) is that they indicate that the RF fields will tend to push the plasma toward regions of minimum RF electric field. When the RF electric field is parallel to the plasma surface, the plasma can actually be pushed toward these regions where the RF vacuum field would be minimum. When the RF electric field is parallel to the gradient of the plasma density, this conclusion is no longer always true; it applies only when the frequency of the RF fields is higher than the electron plasma frequency. If the RF frequency is lower, a "peeling" effect takes place at the plasma surface and tends to draw the plasmas toward the region of maximum RF electric fields [50].

The only attempt at electromagnetic plasma acceleration reported to date is that of Swartz, *et al.* [56]. In these experiments, fields substantially parallel to the plasma density gradient were used, as shown in Fig. 34. For this reason, plasma acceleration could only be obtained for the relatively low plasma densities corresponding to a plasma frequency below that (140 Mc) of the applied RF fields ($n \lesssim 3 \times 10^8$ electrons/cm^3). Under these conditions, plasma acceleration up to velocities of the order of 2.5×10^4 m/second (specific impulse of 2500 seconds) has been observed. Because of the low plasma density, however, resulting thrusts would be too low to be of practical interest, even if higher microwave frequencies were used.

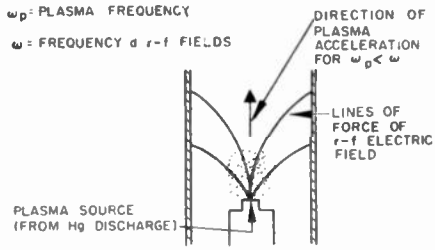

Fig. 34—Electromagnetic plasma accelerator.

In conclusion, the basic principle of electromagnetic plasma acceleration has been demonstrated. To make it useful for propulsion purposes, however, it will be necessary to devise means of applying the electromagnetic RF fields perpendicular to the density gradient of the plasma, avoiding RF electric fields normal to the plasma surface and thus being able to operate with relatively high plasma densities where the plasma frequency exceeds the frequency of the accelerating RF fields.

V. Space Simulation

We shall discuss here fairly briefly some of the problems associated with the testing and evaluation of performance of electrical propulsion engines. As we shall see, the simulation of space environment for an electrical propulsion engine is somewhat more complex than the usual space-simulation problem; however, adequate and detailed ground testing of these engines is an essential step in their development. There are a number of reasons for the importance of this ground testing, including the relatively high cost of conducting space tests, the much greater detail with which the physical phenomena can be studied on the ground, the ease of making changes and adjustments in the experiment, etc. All point toward very comprehensive ground tests prior to the real test in space.

Since electrical propulsion engines are to operate in the excellent vacuum of space, it is obvious that they must be tested under conditions where the background gas pressure will not influence the operation. The tolerable level of background pressure depends, of course, on the mean free path of the ions in this residual gas but will in general be of the order of 10^{-7} mm Hg. Additional features of the physical environment simulation which may be desirable are: 1) cold surfaces to simulate the regions of infinite space as far as radiation from the engine is concerned, 2) artificial solar radiation to simulate the power received from the sun, and 3) possibly other types of radiation such as gamma rays, cosmic rays, etc. All these physical environment factors have been successfully simulated in various test chambers. The most difficult aspects of space simulation, as far as electrical engines are concerned, are the electrical conditions. It is apparent that the walls and col-

lector of the test chamber must not act as sources of electrons; *i.e.*, suitable grids or other barriers must be arranged so that the bombardment by ions or other particles does not cause emission of electrons which can get into the beam and influence its behavior. A second and equally important aspect of the electrical simulation problem arises because in the space environment the ion beam is sent into essentially an infinite region with no boundary condition beyond the edges of the space vehicle. In the ground-based test chamber, walls must be imposed around the engine and beam in order to provide the vaccum and a collector must be provided to collect the ion beam; both of these arrangements impose artificial boundary conditions at the edges and the end of the ion beam. Programs are under way to develop improved techniques of simulating electrically the conditions of space in a finite-size ground-based chamber; we hope that by the time of the first electrical engine flight test we shall have improved facilities for more reliable testing of these engines on the ground.

Conclusions

This paper has dealt with some of the fundamental concepts and problems which lie at the heart of a rapidly growing scientific and engineering effort in the field of electrical propulsion. No attempt has been made to include complete references to the many important contributions to this field, nor to some of the interesting approaches based on modification of the basic types of ion sources and acceleration mechanisms presented here. It is hoped, however, that the discussion has served to emphasize both the strong dependence of progress in this field on broad areas of plasma physics and electronic technology, and the fact that it remains a fertile field for basic investigation and invention.

Electrostatic engines have received more attention to date than those based on direct acceleration of plasmas and are consequently somewhat nearer the stage of practical usefulness. Of these, the cesium ion engine is the most refined in terms of progress toward meeting all of the difficult requirements of practical thrust units, *i.e.*, high efficiency, excellent optics (low electrode erosion for long life), and techniques for controlled neutralization of the exhaust beam. This may be because the cesium ion engine is amenable to analytical treatment and is better understood than plasma devices. At any rate, this type of engine may well provide the ultimate optimum answer for systems requiring a specific impulse of 8000 seconds and higher. Although the thrust density is low, units of 20- to 30-millipound thrust can be clustered to provide total thrusts of the order of pounds for megawatt-level systems. However, each of the basic types of engines discussed here has its particular attractive features (*e.g.*, high thrust density in the case of the Duoplasmatron and oscillating-electron engines) and will, no doubt, find its own area of application.

The fact that the electrical propulsion concept is fast becoming an engineering reality is borne out by the plans of NASA to begin the flight testing of small prototype ion engines (at the several-millipound-thrust level) in late 1962. These tests will be carried out on ballistic trajectories using the Scout launch vehicle as the booster. The principal purpose of these tests will be to demonstrate thrust, with the additional objectives of studying the neutralization problem in an actual space environment and correlating the performance in detail with data obtained under laboratory conditions. Orbital testing of electrical propulsion system is projected at a future date.

It is evident that progress in electrical propulsion will be very closely related to the development of lightweight nuclear-electric power systems, and an intensive effort is required in this direction. The performance of an electrically propelled vehicle depends strongly on achieving high power levels at low weight-to-power ratios (in most mission analyses a ratio of around 10 pounds/kw is assumed). The SNAP-8 program, which is sponsored jointly by the NASA and AEC, is aimed at developing 30 kw at a weight-to-power ratio of around 50 pounds/kw. This power system (or a 60-kw version) will probably be used in the first orbital testing of electrical thrust units. Detailed design studies (*e.g.*, SPUR) indicate the feasibility of using high-temperature operation to attain thrust levels from 300 kw to the megawatt level at thrust-to-weight ratios of 8 to 10 pounds/kw. It is probable that, by using direct conversion concepts currently under study, ratios as low as 3 pounds/kw may be achieved early in the next decade, *i.e.*, by the time ionic and plasma propulsion comes into large-scale use for the exploration of the solar system.

Appendix

Momentum Transfer Between Electrons and Ions in Accelerated Electron Engines

This calculation is intended to determine the rate of momentum transfer from energetic electrons to ions in a region in which a plasma potential gradient exists in the absence of electrostatic forces between plasma and electrodes. Such a region would be the equivalent of region IV of Fig. 21 and will be referred to simply as region IV. It should, however, be observed that, in the absence of electrode fields, it does not appear possible in a one-dimensional situation to maintain such a region at a fixed region in space; it appears that it should move in space (*e.g.*, at the beam front) with the mean velocity of the accelerated ions [57]. Assuming now that the axial electrostatic forces between plasma and electrodes in region IV are negligible, the flux of momentum flowing into the plasma from the left of region IV must be equal to the flow of momentum carried by the plasma out to the right of region IV:

$$\frac{du_{\text{in}}}{dt} = \frac{du_{\text{out}}}{dt}, \tag{50}$$

where

$\frac{du_{in}}{dt}$ = flux of momentum into region IV (from left),

$\frac{du_{out}}{dt}$ = flux of momentum out of region IV (with plasma beam to right).

Assuming most electrons to be reflected in region IV and assuming the ion energy in region III to be much smaller than the electron energy leads to the following expression, for the flow of momentum du_{in}/dt into region IV:

$$\frac{du_{in}}{dt} = n_{e3} m_e \bar{v}_{e3}^2, \tag{51}$$

where

n_{e3} = electron density in region III,
m_e = mass of the electron,
v_{e3} = axial electron velocity in region III,
$\bar{v}_{e3}^2$ = mean square axial electron velocity in region III.

(Note that because of the assumption of near total reflection, $(n_{e3}/2)$ electrons/cm^3 will have a velocity directed toward region III and experience a change of momentum equal to $2m_e v_{e3}$ upon reflection; also, the velocity distribution of electrons flowing in $+x$ and $-x$ direction will be nearly identical.)

Assuming, at the exit of region IV, the electron energy to be much smaller than the energy of the accelerated ions leads, for the flux of momentum leaving region IV, to

$$\frac{du_{out}}{dt} = n_{i3} m_i \overline{v_{i3} v_{i4}}, \tag{52}$$

where

n_{i3} = ion density in region III,
m_i = ion mass,
v_{i3} = axial velocity of ions flowing toward region IV,
v_{i4} = axial velocity of ions leaving region IV.

Eqs. (51) and (52) express that the momentum flux into region IV is essentially carried by the electrons, while the momentum flux out of region IV is essentially carried by the accelerated ions [in effect, the latter assumption means that $(m_i + m_e)v_{i4} \simeq m_i v_{i4}$].

Using (50)–(52), it is possible to relate the oscillating electron current density in region III to the ion current density emerging in the plasma beam to the right of region IV. To this effect, the following quantities are defined:

j_{e3}' = density of electron current flowing in $+x$ direction (away from cathode) in region III.
j_{e3}'' = density of electron current flowing in $-x$ direction in region III.
$j_{e3} = j_{e3}' + j_{e3}'' = |j_{e3}'| - |j_{e3}''|$.
j_i = density of ion current flowing in $+x$ direction (no ions reflected toward $-x$ direction exist with the potential distribution shown in Fig. 21).

Using (50)–(52) the following relation is found between j_{e3}' and j_i:

$$\frac{j_{e3}'}{j_i} = \frac{1}{2}\sqrt{\frac{m_i}{m_e}} \cdot \sqrt{\frac{\bar{v}_{i4}}{\bar{v}_{i3}}},$$

with the simplifying assumptions, in (52) and (51), that $\overline{v_{i3}v_{i4}} \cong \bar{v}_{i3} \cdot \bar{v}_{i4}$, and $v_{e3}^2/\overline{v_{e3}} \cong \bar{v}_{e3}$.

Under these conditions,

$$\bar{v}_{i4}/\bar{v}_{i3} \cong \sqrt{W_{i\,out}/W_{i\,in}},$$

where W_{out} is the average energy of ions leaving region IV (to the right) and W_{in} is the average energy of ions in region III (at the entrance to region IV). Hence,

$$j_{e3}' \simeq \left[\frac{1}{2}\sqrt{\frac{m_i}{m_e}} \cdot \sqrt[4]{\frac{W_{i\,out}}{W_{i\,in}}}\right] \cdot j_i. \tag{53}$$

Q.E.D.

Acknowledgment

In an attempt to present in this review paper as broad a discussion as possible of the ion and plasma propulsion field, we have made use of material from many sources. We would particularly like to acknowledge valuable discussions with R. N. Seitz, NASA Marshall Space Flight Center; Harold Kaufman, NASA Lewis Research Center; Dr. Sam Nablo, Goodrich-High-Voltage Astronautics; Dr. R. G. Meyerand, United Aircraft Corporation; Dr. S. T. Demetriades, Northrop; and S. L. Eilenberg, Dr. W. Eckhardt, and Dr. O. Husmann of Hughes Research Laboratories.

References

[1] R. H. Goddard, Notebook (dated September 6, 1906), *Astronautics*, vol. 4, pp. 24–27; April, 1959.
[2] H. Oberth, "Wege zur Raumschiffahrt," R. Oldenbourg, Munchen-Berlin, Germany; 1929.
[3] It is well known that the perveance of an electron or ion gun structure is dependent only on a dimensionless factor relating to the geometrical form of this structure. Specifically, it is the area of the emitter A_i divided by the square of the emitter-anode spacing d (for a plane-parallel system); the "aspect ratio" R is defined as $R \equiv \sqrt{(4A_i/d^2)}$.
[4] D. B. Langmuir, "Space Technology," John Wiley and Sons, Inc., New York, N. Y., pp. 9–18; 1959.
[5] C. E. Fay, A. L. Samuel, and W. Shockley, "On the theory of space charge between parallel plane electrodes," *Bell Sys. Tech. J.*, vol. 17, pp. 49–79; January, 1938.
[6] Ramo-Wooldridge Research Laboratory Staff, "Electrostatic propulsion," PROC. IRE, vol. 48, pp. 477–491; April, 1960.
[7] W. H. Wells, Jet Propulsion Laboratory, Pasadena, Calif., Tech. Release No. 34-118; 1960.
Also, W. Eckhardt, private communication.
[8] J. E. Etter, *et al.*, "Neutralization of ion beams," in "Electrostatic Propulsion," Academic Press, Inc., New York, N. Y., pp. 357–372; 1961.
[9] G. R. Brewer, J. E. Etter, and J. R. Anderson, "Design and Performance of Small Model Ion Engines," presented at American Rocket Society Meeting, Los Angeles, Calif.; May, 9 1960.
See also, [8].
[10] J. M. Sellen, *et al.*, "Beam diagnostic techniques," in "Electrostatic Propulsion," Academic Press, Inc., New York, N. Y., p. 451; 1961.
See also, J. M. Sellen and R. F. Kemp, "Cesium Ion Beam Neutralization in Vehicular Simulation," presented at American Rocket Society Meeting, Los Angeles, Calif., Paper No. 61-84-1778; June 13–16, 1961.
[11] S. L. Eilenberg, R. A. Hubach, and J. W. Ward, Hughes Research Labs., Malibu, Calif., private communication.

[12] S. L. Eilenberg, Hughes Research Labs., Malibu, Calif., private communication.
[13] See, for example, K. Spangenberg, "Vacuum Tubes," McGraw-Hill Book Co., Inc., New York, N. Y., p. 170; 1948.
[14] I. Langmuir and K. Blodgett, "Currents limited by space charge between coaxial cylinders," *Phys. Rev.*, vol. 22, pp. 347–356; 1923.
——, "Currents limited by space charge between concentric spheres," *Phys. Rev.*, vol. 24, pp. 49–59; 1924.
[15] J. B. Taylor and I. Langmuir, "The evaporation of atoms, ions and electrons from cesium film on tungsten," *Phys. Rev.*, vol. 44, pp. 423–458; September, 1933.
[16] These data were obtained from a comprehensive study of surface ionization being carried out by Dr. O. Husmann, Hughes Research Labs., Malibu, Calif.
[17] J. R. Pierce, "Rectilinear electron flow in beams," *J. Appl. Phys.*, vol. 11, pp. 548–554; March, 1940.
[18] G. R. Brewer, "Note on the determination of electrode shapes for a Pierce-type electron gun," *J. Appl. Phys.*, vol. 28, p. 634; May, 1957.
[19] M. P. Ernstene, *et al.*, "Development of High Efficiency Cesium Ion Engines," presented at National IAS-ARS Joint Meeting, Los Angeles, Calif., Paper No. 61-83-1777; June 13–16, 1961.
[20] J. E. Etter, *et al.*, "The Development of a Flight Test Ion Engine," presented at American Rocket Society Meeting, Los Angeles, Calif., Paper No. 61-81-1775; June 13, 1961.
[21] J. R. Anderson, *et al.*, "Evaluation of Ion Engine Performance," Am. Roc. Soc., Paper No. 2185-61; October 9–13, 1961.
[22] H. R. Kaufman, "An Ion Rocket with an Electron Bombardment Source," Lewis Research Center, Cleveland, Ohio, NASA Technical Note D-585; 1960.
[23] A. von Engel, "Ionized Gases," Oxford Clarendon Press, New York, N. Y., ch. 3; 1955.
[24] H. R. Kaufman and P. D. Reader, "Experimental Performance of Ion Rockets Employing Electron-Bombardment Ion Sources," presented at Am. Rocket Soc. Electrostatic Propulsion Conf., Monterey, Calif., Paper No. 1374-60; November 3, 1960.
[25] P. D. Reader, "Experimental Effects of Scaling on the Performance of Ion Rockets Employing Electron Bombardment Ion Sources," presented at National IAS-ARS Joint Meeting Los Angeles, Calif.; June 13, 1961.
[26] J. S. Luce, "Ion Erosion of Accelerating Electrodes in Space Vehicles," presented at Am. Rocket Soc. Meeting, Los Angeles, Calif., Paper No. 1159-60; May 9, 1960.
[27] M. Von Ardenne, "Electronenphysik, Ionenphysik und Übermikroskopie," VEB Deutscher Verlag der Wissenschaften, Berlin, Germany, p. 554; 1956.
[28] R. J. Hayes, C. A. Heubner, and J. M. Glassmeyer, "The
[28] X. X. Hayes, X. X. Heubner, and X. X. Glassmeyer, "The Duo-Plasmatron Ion Rocket," MIT, Cambridge, Mass., M.S. Thesis; 1960.
[29] L. Spitzer, "Physics of Fully Ionized Gases," Interscience Publishers, Inc., New York, N. Y., 1955.
[30] B. S. Burton, "The Duoplasmatron; Theoretical and Experimental Studies," presented at Electrostatic Propulsion Conf., Monterey, Calif.; November, 1960.
[31] Dr. S. Nablo, Goodrich-High-Voltage Astronautics, Burlington, Mass., private communication.
[32] D. Rose, "Acceleration of a neutralized ion beam," Research Labs. on Electronics, M.I.T., Cambridge, Mass., RLE Quarterly Rept. No. 53, p. 3; April 15, 1959.
[33] F. Salz, R. G. Meyerand, *et al.*, "Electrostatic potential gradients in a Penning discharge," *Phys. Rev. Lett.*, vol. 6, pp. 523–525; November 10, 1961.
[34] J. W. Davis, *et al.*, "Theoretical and Experimental Descriptions of the Oscillating Electron Ion Engine," presented at National IAS-ARS Joint Meeting, Los Angeles, Calif.; June 13–16, 1961.
[35] J. S. Luce, "Intense gaseous discharges," *Proc. 2nd U. N. Internatl. Conf. on Peaceful Uses of Atomic Energy*, Geneva, Switzerland, vol. 31, pp. 305–314; 1958.
[36] The assumption in the present considerations is that plasma heat is considered nonrecuperable and is therefore equivalent energy loss.
[37] S. T. Demetriades and R. W. Ziemer, "Direct Thrust and Efficiency Measurements of a Continuous Plasma Accelerator," *Am. Rocket Soc. J.*, to be published.
[38] G. M. Giannini, "The Arc Jet," presented at 2nd Symp. on Advanced Propulsion Concepts, Boston, Mass.; October 7–8, 1959.
[39] L. Spitzer, "Physics of Fully Ionized Gases," Interscience Publishers, New York, N. Y., p. 84; 1956.
[40] S. Chandrasekchar, "Plasma Physics," University of Chicago Press, Chicago, Ill., p. 211, Eq. (134); 1960.
[41] The importance of the last term of (32) in a non-fully-ionized gas and the subsequent condition (40) for the optimum magnetic field have been brought to the authors' attention by Dr. S. T. Demetriades. Because of its apparent agreement with experimental results of Demetriades, the above theory has been outlined in spite of its possibly controversial character.
[42] S. T. Demetriades, "Operating Characteristics of Continuous MGD Engines," Norair Div., Northrup Co., Hawthorne, Calif., Rept. ASG-TM-61-6; 1961.
[43] Because of the lack of data on μ_{in}, it is assumed that the ion-neutral collision cross section equals the neutral-neutral collision cross section. This, of course, may be a poor approximation.
[44] The acceleration efficiency is the efficiency of transfer of ordered kinetic energy from the electric power supply to the plasma beam injected into the plasma accelerator.
[45] It is possible that overheating of the electrodes could be limited to some extent by the existence of a temperature gradient across the plasma streams. Preliminary experimental evidence to this effect has been obtained by S. T. Demetriades (private communication).
[46] This subdivision is somewhat superficial, of course, as in all three cases the force exerted on the plasma does result from the interaction between a traveling magnetic field and the currents which it induces in the plasma.
[47] T. G. Cowling, "Magnetohydrodynamics," Interscience Publishers, Inc., New York, N. Y., p. 4; 1957.
[48] Devices of the type shown in Figs. 27 and 29 have been proposed by M. U. Clauser, "The magnetic induction plasma engine," Space Technology Lab., Los Angeles, Calif., Rept. No. STL/TR-60-0000-00263; August 19, 1960.
Devices of the type shown in Fig. 30 have been proposed by R. X. Meyer, ("Magnetic Plasma Propulsion by means of a Traveling Sinusoidal Field," in "Plasma Acceleration," S. W. Kash, Ed., Stanford University Press, Stanford, Calif., p. 37; 1960) and are presently being investigated at the Space Technology Labs., Los Angeles, Calif.
[49] W. Eckhardt, private communication.
[50] D. Dow and R. C. Knechtli, "Plasma containment by r.f. and d.c. field combinations," *J. Electronics and Control*, vol. 7, pp. 316–343; November, 1959.
[51] A. S. Penfold, "Experimental Results Concerning the Electromagnetic Acceleration of Plasma Toroids," presented at 4th AFOSR Contractor's Meeting on Ion and Plasma Acceleration, Beverly Hills, Calif.; April 20–21, 1961.
[52] D. B. Miller, "Acceleration of Plasmas by Inductively Generated Electro-Magnetic Fields," University of Michigan Research Institute, Ann Arbor; April, 1961.
[53] J. Marshall, "Hydromagnetic plasma gun," in "Plasma Acceleration," S. W. Kash, Ed., Stanford University Press, Stanford, Calif., pp. 60–72; 1960.
[54] B. Garovity and P. Gloersen, "Experimental Performance of a Pulsed Gas Entry Coaxial Plasma Accelerator and Applications to Space Missions," presented at Am. Rocket Soc., New York, N. Y., Paper No. 1535-60; December, 1960.
[55] H. A. H. Boot, *et al.*, "Containment of a fully ionized plasma by r.f. fields," *J. Electronics and Control*, vol. 4, pp. 434–453; April, 1958.
[56] T. T. Reboul, C. D. Gordon, and G. A. Swartz, "Plasma Acceleration by a Quasistatic RF Electric Field Gradient," presented at ARS Meeting, Washington, D. C., Paper No. 1532-60; December 5–8, 1960.
[57] W. Eckhardt, private communication. This remark applies in particular to the model proposed by D. Rose for a plasma potential gradient due to the electron velocity distribution.

Transmission of Electromagnetic Waves Through an Ionized Layer in the Presence of a Strong Magnetic Field*

T. P. HARLEY†, MEMBER, IRE, AND G. TYRAS†, MEMBER, IRE

Summary—It is well known that the dielectric property of an ionized gas in the presence of a steady magnetic field is of tensorial character. Two of the three distinct components of this tensor are functions of the steady magnetic field. Generally, these two components decrease in magnitude with an increase of the steady magnetic field, thereby improving transmission of an RF wave.

The effect of a strong steady magnetic field on the transmission of an RF wave through a homogeneous and a stratified layer of ionized gas is illustrated by means of graphs. The graphs are based on certain fixed values of electron densities and collision frequencies and on certain fixed values of a steady magnetic field oriented parallel or normal to the interface, while the normally incident plane wave is either linearly or circularly polarized.

It was found that the best improvement in transmission is obtained when the steady magnetic field is normal to the interface and the oncoming plane wave is circularly polarized.

Introduction

A HYPERSONIC vehicle reentering the earth's atmosphere produces a strongly ionized, highly inhomogeneous plasma sheath about itself. This plasma sheath may degrade the transmission of RF energy for communication, guidance, and so forth, to a point below discernment. A steady magnetic field of sufficient strength produces the macroscopic effect of reducing the magnitudes of certain components of the permittivity tensor and thus tends to improve the transmission through the sheath.

The phenomena associated with the propagation of electromagnetic waves through homogeneous anisotropic plasma are well understood at present mainly due to work done in connection with ionospheric propagation.[1,2] The effect of a strong magnetic field (stronger than the earth's magnetic field which is about 0.4 gauss) on propagation was also investigated by Poeverlein,[3] who analyzed the effect of a strong steady magnetic field on the components of the permittivity tensor and predicted improvement of transmission for sufficiently strong, steady magnetic fields. This paper utilizes the results obtained by Tyras and Held[4] for analysis of transmission through inhomogeneous anisotropic plasma. The formula for the power transmission coefficient was programmed for the type 704 IBM digital computer to obtain the results in this paper.

The Transmission Formula

The theory of propagation through anisotropic layers may be found elsewhere.[4] Here we review only briefly the pertinent formulas leading to the results presented in this paper.

Consider the geometry of a stratified plasma in Fig. 1.

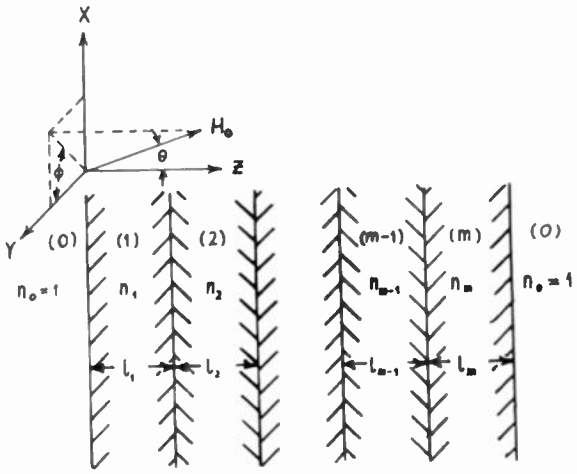

Fig. 1—Stratified plasma model.

The power transmission coefficient or the ratio of the transmitted power intensity to the incident power intensity for normal incidence of a plane wave linearly polarized along the x axis propagating in the positive z direction, is given by

$$\frac{P^t}{P^i} = |A^o|^2 \cos^2\phi + |A^e|^2 \sin^2\phi, \tag{1}$$

where $\theta = \pi/2$ (steady magnetic field in the plane of the interfaces) and

$$\frac{P^t}{P^i} = \tfrac{1}{2}\{|A^o|^2 + |A^e|^2\}, \tag{2}$$

* Received by the IRE, August 24, 1960; revised manuscript received, July 13, 1961. This paper was presented at the 4th Natl. Convention on Military Electronics, Washington, D. C., June 27–29, 1960.

† The Boeing Co., Aero-Space Div., Seattle, Wash.

[1] J. A. Ratcliffe, "The Magneto-Ionic Theory and Its Applications to the Ionosphere," Cambridge University Press, Cambridge, Eng., pp. 15–20; 1959.

[2] K. G. Budden, "Radio Waves in the Ionosphere," Cambridge University Press, Cambridge, Eng., pp. 47–57; 1961.

[3] H. Poeverlein, "Peculiar wave propagation characteristics of a plasma with constant magnetic field," paper delivered at AFCRC Plasma Sheath Symp., Boston, Mass.; December 7–9, 1959.

[4] G. Tyras and G. Held, "On the propagation of electromagnetic waves through anisotropic layers," IRE Trans. on Antennas and Propagation, vol. AP-7, Special Supplement, pp. S296–S300; 1959.

when $\theta=0$ (steady magnetic field normal to the interfaces). If the incident plane wave is circularly polarized, that is $E_{oy}{}^{i}=\pm jE_{ox}{}^{i}$ and $\theta=\pi/2$, one gets

$$\frac{P^t}{P^i}=\tfrac{1}{2}\{|A^o|^2+|A^e|^2\}. \tag{3}$$

When $\theta=0$

$$\frac{P^t}{P^i}=\begin{cases}|A^e|^2 & \text{when} \quad E_{oy}{}^{i}=+jE_{ox}{}^{i}\\ |A^o|^2 & \text{when} \quad E_{oy}{}^{i}=-jE_{ox}{}^{i}.\end{cases} \tag{4}$$

The A's are given by

$$A^{o,e}=(1+\tanh\gamma_o{}^{o,e})\exp\left(-j\sum_{k=1}^{m}\psi_k{}^{o,e}\right)\cdot\prod_{k=1}^{m}\frac{1+\tanh\gamma_k{}^{o,e}}{1+\tanh\gamma_{k-1}{}^{o,e}\tanh\beta_k{}^{o,e}}, \tag{5}$$

where for both superscripts o and e

$$\tanh\gamma_i=\frac{n_i-n_{i+1}}{n_i+n_{i+1}}$$

$$\tanh\beta_i=\tanh(\gamma_i+\beta_{i+1})\exp(-j2\psi_i)$$

$$\psi_i=\frac{2\pi}{\lambda}n_id_i. \tag{6}$$

Note that $n_0=n_{m+1}=1$ and $\beta_{m+1}=0$. The n's are the indices of refraction given by the Appleton-Hartree formula

$$\begin{matrix}n^o\\ n^e\end{matrix}\Big\}=\sqrt{\epsilon\mp\eta}, \tag{7}$$

when the steady magnetic field is in the z direction and

$$n^o=\sqrt{\zeta}$$

$$n^e=\sqrt{\frac{\epsilon^2-\eta^2}{\epsilon}} \tag{8}$$

when the steady magnetic field is in the x-y plane. The parameters ϵ, ζ, and η are complex if the plasma is lossy and are given by

$$\epsilon=1-\frac{p^2(1-\sigma^2+q^2)}{\Delta}-j\frac{qp^2(1+\sigma^2+q^2)}{\Delta}$$

$$\zeta=1-\frac{p^2}{1+q^2}-j\frac{qp^2}{1+q^2}$$

$$\eta=\frac{\sigma p^2(\sigma^2-1+q^2)}{\Delta}-j\frac{2\sigma qp^2}{\Delta}$$

$$\Delta=[(\sigma+1)^2+q^2][(\sigma-1)^2+q^2], \tag{9}$$

where the p's, q's, and σ's are the ratios of plasma, collision, and the cyclotron frequency, respectively, to the carrier frequency.

Analysis of Results

The graphs of Fig. 2 show the power transmission coefficient for a single homogeneous layer of plasma with an electron density of 10^9 electrons per cubic centimeter, a collision frequency of 10^8 collisions per second, and a layer thickness of 0.6 m. Several values of the steady magnetic field strengths are considered when the latter is oriented either normal or parallel to the interface and when the normally incident plane wave is either linearly or circularly polarized.

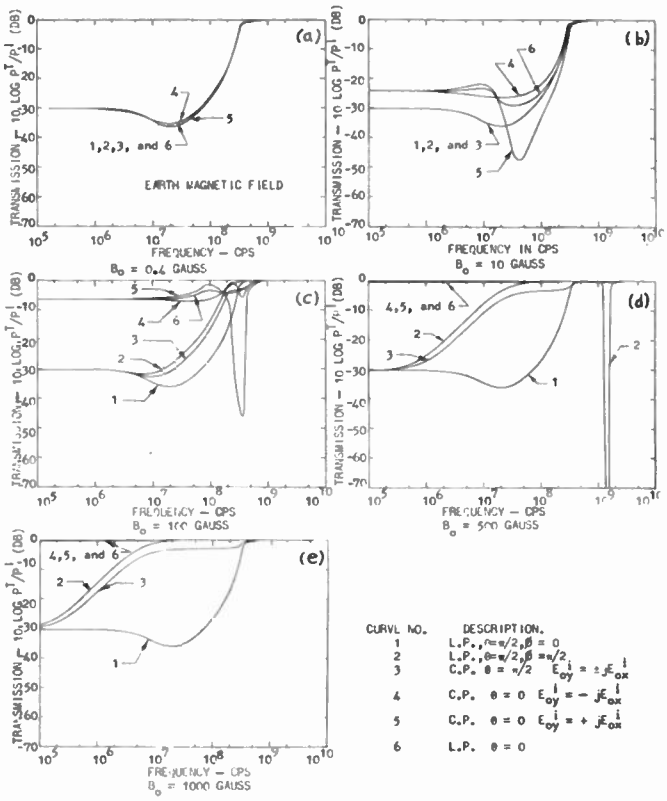

Fig. 2—Transmission through a one-layer plasma subjected to different values of steady magnetic-field strengths. $l=60$ cm; $N=10^9$ electrons per cubic centimeter; and $V=10^8$ collisions per second.

The graph of Fig. 3 depicts the situation of a stratified plasma under conditions similar to those above. The description of the stratifications is listed in Table I, and the total layer thickness is approximately 0.6 m as before. The plasmas in Table I are approximations of representative models for what may be considered as reentry-type inhomogeneous plasma.

It may be seen from the graphs of Figs. 2 and 3 that, in general, the magnitude of the transmitted power is a function of the wave polarization and the orientation and the magnitude of the steady magnetic field. The earth's magnetic field, which for the purpose of this paper was assumed to be 0.4 gauss, has no apparent effect on these changes in transmission.

It is interesting to examine the phenomena in transmission produced by a steady magnetic field stronger than that of the earth. Consider first the case of the steady magnetic field in the plane of interface ($\theta=\pi/2$), which is represented by curves 1, 2, and 3 of Figs. 2 and 3. We note that curve No. 1 is not affected by the steady magnetic field. This is not surprising, since in this case

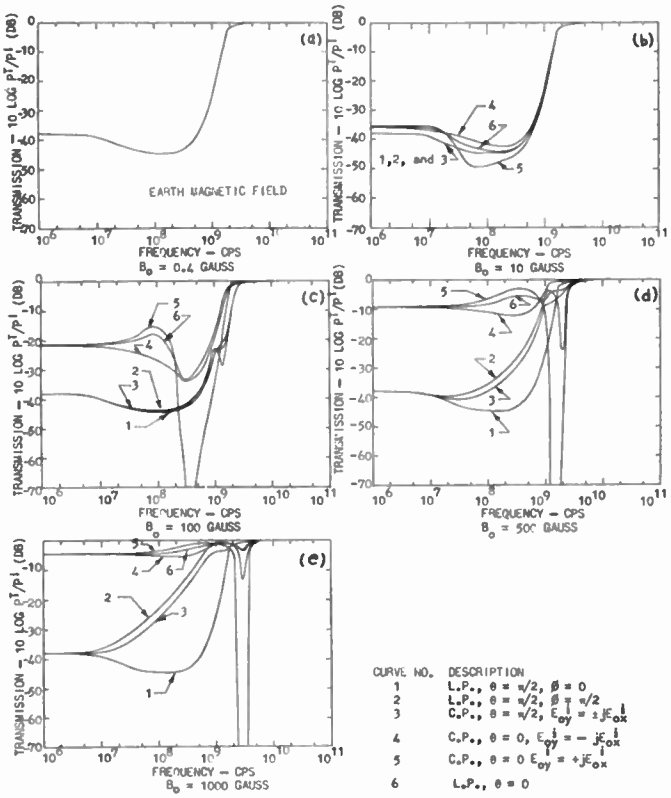

Fig. 3—Transmission through an eight-layer plasma subjected to different values of steady magnetic-field strengths.

TABLE I

Stratification Number	Thickness (meters)	Electron Density (electrons per cubic centimeter)	Collision Frequency (collisions per second)
1	0.05	2.1×10^{6}	2.1×10^{8}
2	0.08	1.2×10^{6}	3.4×10^{8}
3	0.08	1.1×10^{7}	6.3×10^{8}
4	0.08	1.0×10^{8}	1.2×10^{9}
5	0.07	9.0×10^{8}	2.3×10^{9}
6	0.10	4.1×10^{9}	3.6×10^{9}
7	0.06	1.8×10^{10}	1.3×10^{9}
8	0.05	3.1×10^{10}	2.1×10^{8}

the alternating component of the electric field is along the steady magnetic field and thus there is no interaction. When the alternating electric field is perpendicular to the steady magnetic field, some interaction is expected to occur, and this can be noted by examination of the graphs.

The most pronounced effects of the steady magnetic field on transmission should, of course, be expected in the case where the magnetic field is normal to the interface so that the alternating electric field is always normal to it. Here we observe that the left-hand and right-hand circularly polarized waves are affected differently by the steady magnetic field. Moreover, the transmission curve of the linearly polarized signal always lies between transmission curves for left-hand and right-hand circularly polarized waves.

At lower frequencies, when the indices of refraction n' and n'' are much larger than unity, examination of the graphs of Figs. 2 and 3 will reveal that the transmission of the signal is independent of frequency. This comes about from the asymptotic behavior of (5). In the case of a homogeneous layer when the steady magnetic field is normal to the interface ($\theta=0$), it can be shown that

$$|A^{o,e}|^2 \xrightarrow[\omega\to 0]{} \frac{16c^2(\omega_o^2+\nu^2)}{l^2\omega_p^4}, \tag{10}$$

where $\omega_o=eB_o/m$, $\omega_p=e\sqrt{N/m\epsilon_o}$, and ν are the cyclotron, plasma, and collision frequency, respectively. A similar asymptotic limit can be derived for the case of the steady magnetic field in the plane of the interface.

Conclusions

It has been shown that a steady magnetic field of sufficient strength will enhance the transmission of radio waves through an ionized layer. The following further remarks are appropriate:

1) Transmission is generally better when the steady magnetic field is normal to the interface than when it is in the plane of the interface.
2) Improvement in the transmission due to a steady magnetic field is more pronounced at lower frequencies.
3) At frequencies low enough, the transmission is frequency independent and is proportional to the square of the steady magnetic field.

Acknowledgment

Thanks are extended to T. G. Dalby of The Boeing Company for his encouragement throughout the course of this investigation.

The Use of Magnetic Fields in the Elimination of the Re-Entry Radio Blackout*

H. HODARA†

Summary—**This paper reviews first the most significant results concerning wave propagation through the plasma sheath surrounding a re-entering missle; second, it presents a new evidence showing that the re-entry radio blackout can be eliminated when a static magnetic field of the order of 500 Gauss is applied through the sheath. The evidence is based on the results of an analysis of transmission and reflection losses taking place at a plasma-air interface. The analysis also shows that in the special case of the absence of collisions, ($\nu=0$) maximum transmission occurs when the signal frequency (ω) is half the gyrofrequency (ω_b); the ratio of transmitted to incident power, in this case, equals approximately the ratio of gyro to plasma frequency. This result is also shown to hold when collisions are present, provided that $\nu^2 \ll (\omega_b-\omega)^2$.**

Introduction

HYPERSONIC space vehicles re-entering the atmosphere are surrounded by a sheath of ions and free electrons known as a "plasma sheath." The mechanism by which the sheath is formed is described elsewhere and need not be repeated here.[1] The presence of the sheath reflects and attenuates propagating electromagnetic waves so severely that radio communications with re-entering space vehicles are temporarily interrupted. This interruption or "radio blackout" is a problem of concern, in particular with future manned flights when continuous radio contact with the ground is necessary.

Extensive work is being done on the radio-blackout problem. Several solutions have been proposed, such as recombination,[2] transpiration cooling,[3] and shaping of the re-entering vehicle;[4] all three methods attempt to reduce the electron concentration in the plasma sheath. Another method currently in use is to transmit above the plasma resonant frequency, as the attenuation is much less severe.[5] Finally, a method advocated by the author[6–8] and others[9] consists of altering the electromagnetic properties of the plasma by superposing a static magnetic field. Several comparative analyses of the above methods have been published;[10,11] the present paper discusses only the magnetic-field approach and presents new evidence showing that the re-entry radio blackout can be eliminated with relatively low magnetic fields of a few hundred Gauss.

Electromagnetic Properties of Plasma—Physical Justification of the Static Magnetic-Field Approach

The electromagnetic properties of plasmas have been discussed extensively in the literature and more recently in connection with microwave tubes[12] and the re-entry problem.[13] Electromagnetic plasma properties are best expressed in terms of three basic parameters: 1) electron-plasma resonant frequency ω_p, 2) electron collision frequency ν, and 3) electron gyrofrequency ω_b.

The plasma resonant frequency varies directly with the square root of the electron density N and plays a role which is analogous to that of the cutoff frequency of a waveguide; a lossless plasma cannot support wave propagation at frequencies below ω_p. The plasma resonant frequency is

$$\omega_p = \sqrt{\frac{Q^2}{M}\frac{N}{\epsilon_v}}. \tag{1}$$

(Q, M, and ϵ_v are, respectively, charge and mass of the electron and dielectric constant of free space in mks units.)

The collision frequency is a measure of the attenuation of electromagnetic waves in the plasma. When the collision frequency is zero, the attenuation is zero; as shown in another section of this paper, the attenuation is also zero when $\nu=\infty$.

* Received by the IRE, August 28, 1961. Portions of this paper are abstracted from the author's Ph.D. dissertation at the Illinois Institute of Technology, Chicago, Ill.

† The Hallicrafters Co., Chicago, Ill.

[1] W. B. Sisco and J. M. Fiskin, "Electromagnetic Wave Propagation in Shock Ionized Media," Douglas Aircraft Co., Long Beach, Calif., Engineering Paper No. 633; October, 1958.

[2] J. S. Butz, Jr., "Hypersonic aircraft," *Aviation Week*, vol. 70, pp. 156–169; June 22, 1959.

[3] K. R. Stehling, "Re-entry cooling," *Space/Aeronautics*, vol. 32, pp. 43–45; September, 1959.

[4] "Telemetry Blackout and Re-entry Radar Cross-Section for Different Re-entry Vehicles," Aeronutronic Div. of Ford Motor Co., Newport Beach, Calif., Tech. Rept. No. U-1029; October 20, 1960.

[5] K. M. Baldwin, O. E. Bassett, and E. I. Hawthorne, "Telecommunication during Re-entry," Avco Research: Symp. on the Plasma Sheath, Boston Mass.; December 7–9, 1959.

[6] H. Hodara, H. R. Raemer, and G. I. Cohn, "Space Communications during Re-entry," presented at the meeting of the IRE Professional Group on Space Electronics and Telemetry, Chicago, Ill.; February 12, 1960.

[7] H. Hodara, H. R. Raemer, and G. I. Cohn, "A new approach to space communications," *Proc. XIth Internatl. Astronautical Conf.*, Stockholm, Sweden; August 16–20, 1960.

[8] H. Hodara, "A New Approach to Space Communications during Re-entry," presented at 15th Annual Meeting, American Rocket Society, Washington, D. C., Paper No. 1529–60; December 5–8, 1960.

[9] G. T. Flesher, "On the Elimination of Communications Dropout during Space Vehicle Re-entry," *NAECON Proc.*, Dayton, Ohio; May 2–4, 1960.

[10] E. F. Dirsa, "The telemetry and communication problem of re-entrant space vehicles," PROC. IRE, vol. 48, pp. 703–713; April, 1960.

[11] I. L. Carbine, H. G. Adam, and W. C. Bunyea, "The Problem of Miss-Distance Measurement for Intercept of a Re-entry Body," New Mexico State University, Physical Science Lab., University Park, N. M., BTL P. O. No. D-232136; December 29, 1960.

[12] R. F. Whitmer, "Principles of microwave interactions with ionized media," *Microwave J.*, pt. II, Electron-Cyclotron Resonance, vol. 2, pp. 47–50, Sylvania Products Co., Microwave Physics Lab.; March, 1959.

[13] M. P. Bachynski, I. W. Johnston, and I. P. Shkarotsky, "Electromagnetic properties of high temperature air," PROC. IRE, vol. 48, pp. 347–356; March, 1960.

In the presence of a static magnetic field B_0, a free electron describes a circular motion in a plane normal to the field lines. It revolves at the gyrofrequency ω_b. The gyrofrequency increases directly with the strength of the magnetic field; it is a vector quantity defined by

$$\omega_b = -\frac{Q}{M} B_0. \tag{2}$$

(For an electron, $Q<0$ and ω_b has the same sense as B_0.)

The presence of a static magnetic field alters the electrons' motion in the plane transverse to B_0, thus introducing new propagation modes. Consider, for instance, an electromagnetic wave at a frequency $\omega<\omega_p$ in a collisionless plasma ($\nu=0$). When $B_0=0$, no propagation is possible. As B_0 increases, the radius of the electron's orbit decreases. When B_0 is infinite, the orbit's radius is zero and the electrons' motion in the transverse plane is frozen; no interaction takes place between electrons and an electromagnetic plane wave whose wave front is normal to B_0. Under these conditions, the medium is no longer dispersive; a "spectral window" is opened through which a plane wave travels as if in vacuum.

The preceding reasoning suggests the possibility that windows exist in the plasma over a finite frequency band for finite values of B_0. In particular, attention is directed to the existence of windows in the band of frequencies below plasma resonance. The spectral characteristics of a collisionless plasma in the presence of a static magnetic field are illustrated in Fig. 1; their derivation is given elsewhere.[8] The results are not new, as they stem from the classical Appleton-Hartree formula; they are presented graphically in terms of normalized frequencies

$$\Omega = \frac{\omega}{\omega_p} = \frac{f}{f_p} \tag{3a}$$

$$m = \frac{\omega_b}{\omega_p} = \frac{f_b}{f_p}. \tag{3b}$$

Similar spectral characteristics have been published previously in unnormalized form.[12] Fig. 1 reveals the existence of a window below the gyrofrequency when a right-handed (RH) circularly polarized wave propagates in the direction of B_0 (longitudinal field). This mode of propagation is of interest since the location of the window is not dependent on the plasma resonant frequency. The window's location is determined solely by the strength of the static magnetic field independent of the electron density, provided that the plasma is collisionless. For instance, an unbounded collisionless plasma with 10^{12} electrons/cm^3 sustains wave propagation with no attenuation up to about 1 kMc when a static magnetic field of 357 Gauss is applied. On the other hand, Fig. 1 shows that, under the same conditions, a left-handed (LH) circularly polarized wave is transmitted free of attenuation down to about 1.2 kMc, provided the applied field is at least 2000 Gauss. It does pay to select the "RIGHT" mode in order to eliminate radio blackout during re-entry.

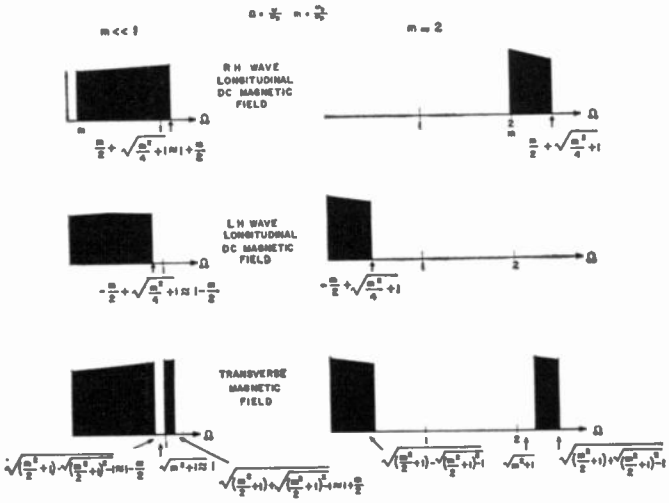

Fig. 1—Spectral characteristics of collisionless plasma with dc magnetic field. Shaded areas are regions of no propagation.

Plane-Wave Analysis

The re-entry radio blackout is caused by the plasma cutoff characteristics, the attenuation losses due to collisions, the reflections taking place at interfaces or in regions of rapidly varying electron density, and the changes in the antenna-radiation pattern. The results on which the elimination of radio blackout is predicated in this paper are based entirely on a plane-wave analysis. Associated with a plane-wave analysis are several sources of errors. To mention a few: first, the signal wavelength is often long with respect to the thickness of the sheath, and second, the near fields from the antenna cannot be neglected. Considerable work, both experimental[14] and theoretical,[15–18] is being carried on in connection with the effects of the plasma sheath on the radiation pattern of antennas. Results from this work seem to confirm the validity of the plane-wave analysis.[18] Measurements of signal-attenuation loss at about 200 Mc for a dipole transmitting antenna immersed in a plasma stream 3 inches in diameter shows favorable comparison between experimental results and the results of a plane-wave analysis.[19] This last investigation supports the static magnetic-field approach based on such an analysis.

[14] R. L. Chuan, H. H. Kuehl, and Z. Kaprielian, "A Study of the Transmission of Radio Signals from a Hypersonic Vehicle," University of Southern California, Los Angeles, Calif., USCEC Rept. 70-101; June 30, 1960.

[15] J. R. Wait, "The Electromagnetic Fields of a Dipole in the Presence of a Thin Plasma Sheath," Natl. Bureau of Standards, Boulder, Colo., NBS Rept. 6083; April 4, 1960.

[16] H. H. Kuehl, "Radiation from a Gap-Excited Cylinder Surrounded by a Uniform Plasma Sheath," University of Southern California, Los Angeles, Calif., USCEC Rept. 71-202; June 30, 1960.

[17] C. M. Knop, "The radiation fields from a circumferential slot on a metallic cylinder coated with a lossy dielectric," IRE Trans. on Antennas and Propagation, vol. AP-9; November, 1961.

[18] H. Hodara and G. I. Cohn, "Radiation characteristics of slot antennas in the presence of a lossy anisotropic plasma sheath," *Proc. NEC*, Chicago, Ill.; October, 1961.

[19] P. W. Huber and P. G. Gooderun, "Experiments with Plasmas Produced by Potassium-Seeded Cyanogen Oxygen Flames for Study of Radio Transmission at Simulated Re-entry Vehicle Plasma Conditions," NASA, Washington, D. C., Tech. Note D-627; Washington, D. C.; January, 1961.

Effect of a Static Magnetic Field on Signal Transmission through Plasma

Attenuation and Phase Shift

The plane-wave theory yields the value of attenuation α and phase shift β when collisions are present in the plasma.[8] The results are presented graphically in Figs. 2–6 for an RH wave; the collision-frequency parameter ν is normalized with respect to ω_p as follows:

$$q = \frac{\nu}{\omega_p} = \frac{\nu/2\pi}{f_p} . \tag{4}$$

The curves in the figures display the well-known fact that collisions remove the discontinuities in the spectrum and make propagation possible at all frequencies with varying degrees of attenuation. Furthermore, the range over which the phase function β is linear increases with the collision frequency. The peaks and valleys of the β-curves (Figs. 5 and 6) are typical of the rapid phase variations exhibited by lossy media near resonance or cutoff.

Of major interest is the reduction in attenuation brought about when a static magnetic field is applied.

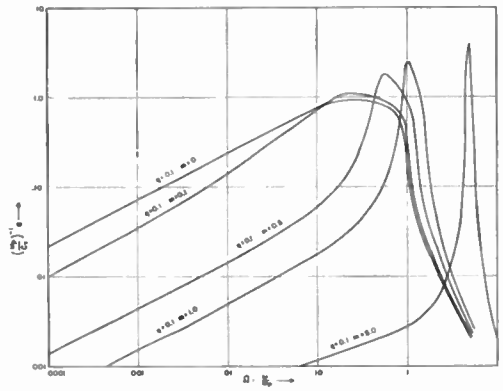

Fig. 2—Normalized attenuation vs normalized frequency, RH wave. Variable static longitudinal magnetic field m; fixed collision frequency $q=0.1$.

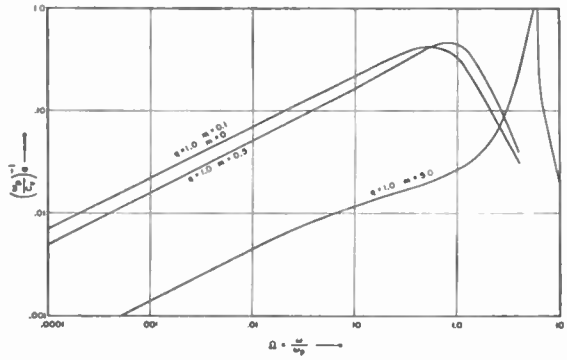

Fig. 3—Normalized attenuation vs normalized frequency, RH wave. Variable static longitudinal magnetic field m; fixed collision frequency $q=1.0$.

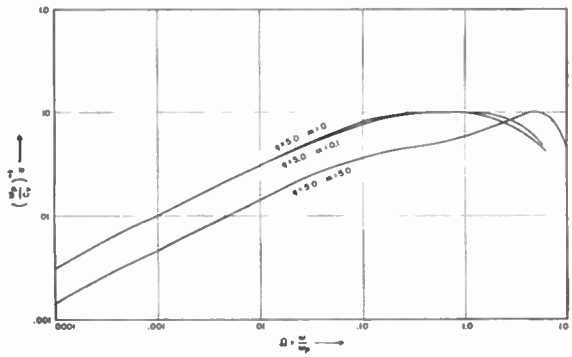

(a)

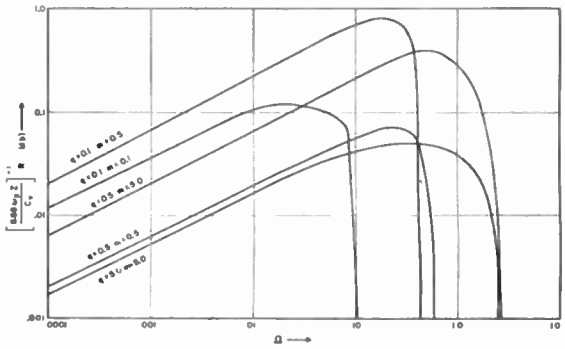

(b)

Fig. 4—(a) Normalized attenuation vs normalized frequency, RH wave. Variable static longitudinal magnetic field m; fixed collision frequency $q=5.0$. (b) Normalized loss reduction vs normalized frequency.

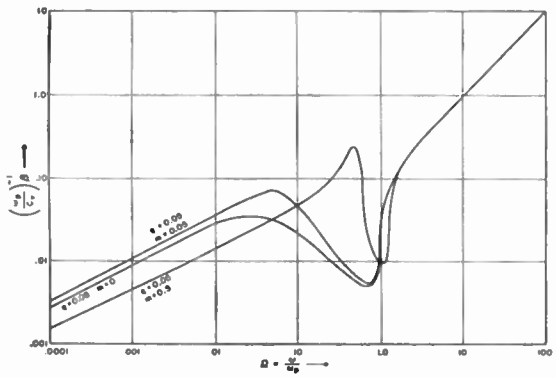

Fig. 5—Normalized phase shift vs normalized frequency, RH wave. Variable static longitudinal magnetic field m; fixed collision frequency $q=0.05$.

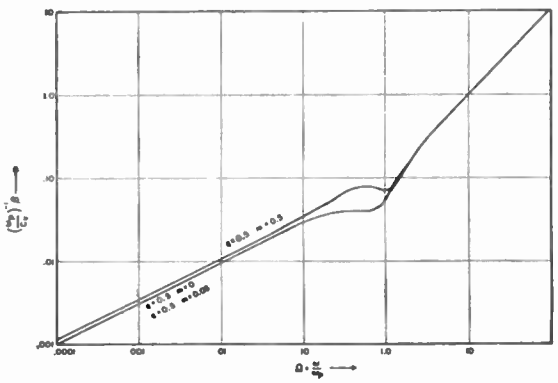

Fig. 6—Normalized phase shift vs normalized frequency, RH wave. Variable static longitudinal magnetic field m; fixed collision frequency $q=0.5$.

The reduction caused by the magnetic field is more significant at low ($q<1$) collision frequencies. From the data of Figs. 2–4, a loss reduction factor R in decibels is plotted vs Ω. The factor R gives the loss reduction with several values of applied static magnetic field at various collision frequencies. R is given by:

$$R(\text{db}) = 20 \log_{10} \frac{E_{q,m}}{E_{q,0}} = (20 \log_{10} e)(\alpha_{q,0} - \alpha_{q,m})z. \quad (5)$$

$E_{q,m}$ is the reduction in the electric-field amplitude over a distance of z-meters in the plasma for a given normalized collision frequency q and gyrofrequency m. $E_{q,0}$ is the reduction under the same conditions when the static magnetic field is absent ($m=0$). $\alpha_{q,m}$ and $\alpha_{q,0}$ are the attenuation factors in nepers per meter at some collision frequency q for gyrofrequencies m and zero, respectively. The abscissa R in Fig. 4(b) is normalized with respect to z and ω_p ($c_v = 3\times10^8$ m/sec, $8.68 = 20 \log_{10} e$); the relative decibel reduction in attenuation attained with a magnetic field increases directly with the operating frequency, the plasma resonant frequency and the thickness of the sheath.

On the other hand, there is little improvement in loss reduction at high collision frequencies ($q=5$) when moderate magnetic fields are used ($m=0.5$). For instance, assume a plasma resonant frequency of 10 kMc, a collision frequency of 6 kMc ($q=0.1$), a sheath thickness of 4 cm, a magnetic field of 357 Gauss ($m=0.1$), and an operating frequency of 500 Mc. Under these conditions, the loss reduction is 7 db; if the magnetic field is increased fivefold, the reduction in attenuation is 35 db. When collisions increase to 50 kMc ($q=5$), the absolute attenuation is considerably lessened while the relative loss reduction caused by a static magnetic field is minor; thus, 2000 Gauss are required to further reduce the attenuation by 2 db. The benefits to be derived from the application of a static magnetic field are significant at collision frequencies below plasma resonance; for a given magnetic field, the loss reduction factor R increases considerably as ν decreases. When the re-entry blackout occurs, ν is believed to be of the order of 0.1 f_p;[11] under such conditions, an extrapolation of the curves of Fig. 4(b) shows a 70-db reduction in attenuation when the applied static magnetic field is 350 Gauss, if $f=500$ Mc and $f_p=10$ kMc.

Reflection Losses

The presence of a plasma-air interface creates additional losses in the signal transmitted through the sheath. In the present paper, an expression is derived for the power transmitted into a semi-infinite plasma slab. The slab has constant electron density and constant collision frequency; it is threaded by a static magnetic field normal to the interface and parallel to the direction of propagation. Work is in process to extend the analysis to a plasma sheath of finite thickness; however, the results obtained from the present analysis are of considerable interest. When a linearly polarized TEM wave impinges on the interface, both RH and LH waves are generated. Straightforward application of Maxwell's equations and boundary conditions yields the following expressions for the reflected fields in terms of the incident fields E_{x1}^+ and H_{y1}^+:

$$E_{x1}^- = \frac{1 - y_R y_L}{(1 + y_R)(1 + y_L)} E_{x1}^+, \quad (6)$$

$$E_{y1}^- = j \frac{y_R - y_L}{(1 + y_R)(1 + y_L)} E_{x1}^+, \quad (7)$$

$$H_{x1}^- = - j \frac{y_R - y_L}{(1 + y_R)(1 + y_L)} H_{y1}^+, \quad (8)$$

$$H_{y1}^- = - \frac{1 - y_R y_L}{(1 + y_R)(1 + y_L)} H_{y1}^+. \quad (9)$$

The subscript 1 refers to free space, the superscripts + and − refer respectively to incident and reflected waves. The symbols R and L indicate RH and LH waves, and the subscript 2 in the expressions which follow refers to the plasma medium.

$$E_{x2}^{R,L} = \frac{1}{1 + y_{R,L}} E_{x1}^+ \quad (10)$$

$$H_{y2}^{R,L} = \frac{y_{R,L}}{1 + y_{R,L}} H_{y1}^+. \quad (11)$$

The other components are related by

$$E_{x2}^R = jE_{y2}^R, \quad (12)$$

$$E_{x2}^L = - jE_{y2}^L, \quad (13)$$

$$H_{x2}^R = jH_{y2}^R, \quad (14)$$

$$H_{x2}^L = - jH_{y2}^L. \quad (15)$$

y_R and y_L are the wave admittances of the plasma normalized with respect to the characteristic admittance of free space. y_R and y_L are identical to the complex index of refraction of the plasma for the RH and LH mode; they are given by the following:

$$y_R = \sqrt{1 + \frac{1}{\Omega[(m - \Omega) + jq]}} \quad (16)$$

$$y_L = \sqrt{1 - \frac{1}{\Omega[(m + \Omega) - jq]}}. \quad (17)$$

In the absence of collisions, (16) and (17) reduce to the familiar expressions for the index of refraction in terms of the denormalized parameters ω_b and ω_p:

$$y_R = \sqrt{1 + \frac{\omega_p^2}{(\omega_b - \omega)\omega}} \quad (18)$$

$$y_L = \sqrt{1 - \frac{\omega_p^2}{(\omega_b + \omega)\omega}}. \quad (19)$$

The power transmitted into the plasma is calculated as follows:

$$P_+ = \tfrac{1}{2}\Re(\boldsymbol{E} \times \boldsymbol{H}^*). \tag{20}$$

$\Re$ means "real part of," and the asterisk indicates conjugate values. Substitution of (6) to (15) into (20) gives the transmitted to incident power ratio p:

$$p = \frac{P_r}{P_{in}} = \frac{P_r}{\frac{1}{2}E_x{}^+H_y{}^+} \tag{21}$$

$$p = \frac{2\Re y_R{}^*}{|1 + y_R|^2} + \frac{2\Re y_L{}^*}{|1 + y_L|^2}. \tag{22}$$

The power ratio for the *RH* wave is

$$p_R = \frac{2\Re y_R{}^*}{|1 + y_R|^2} = \frac{y_R + y_R{}^*}{|1 + y_R|^2}. \tag{23}$$

Similarly for the *LH* wave,

$$p_L = \frac{2\Re y_L{}^*}{|1 + y_L|^2} = \frac{y_L + y_L{}^*}{|1 + y_L|^2}. \tag{24}$$

and the total transmitted to incident power ratio p is given by

$$p = p_R + p_L. \tag{25}$$

The ratio is plotted in Fig. 7 for the collisionless case ($q=0$). It reaches a peak at $\omega=\omega_b/2$. When $\omega_b<0.10\ \omega_p$, the maximum ratio is approximately $m=\omega_b/\omega_p$. For instance, let $f_p=10$ kMc; if a static magnetic field of 350 Gauss corresponding to a gyrofrequency of 1 kMc is applied, the maximum amount of power transferred into the plasma is 10 per cent of the incident power at 0.5 kMc. Increasing the static field fivefold only gives a 3-db improvement in power transfer. If the incident wave is right-handed polarized, no LH is generated in the medium and 3-db additional power penetrates the plasma, but no propagation takes place above gyrofrequency. When collisions are present, several important results stem from Figs. 8–10. For a given collision frequency, reflection losses at the interface are reduced when a static magnetic field is applied. The reduction is more significant at lower collision frequencies. For instance, if $\nu=200$ Mc, $f_p=2$ kMc and $B_0=350$ Gauss, reflection losses are reduced approximately by 5 db below 200 Mc. Under the same condition, except for $\nu=10$ kMc, a static field of 3500 Gauss reduces reflection losses by only 1.8 db. Another important result is the fact that when large magnetic fields are applied ($m=5$), the collisions have little influence on reflection losses. In this case, reflection losses are determined mostly by the operating frequency. For low static fields the mismatch at the interface is lessened as the collision frequency increases. High collision frequencies not only decrease attenuation losses through the plasma but also decrease the reflection losses at the plasma-air interface. The reason for the reduction in reflection losses as collisions

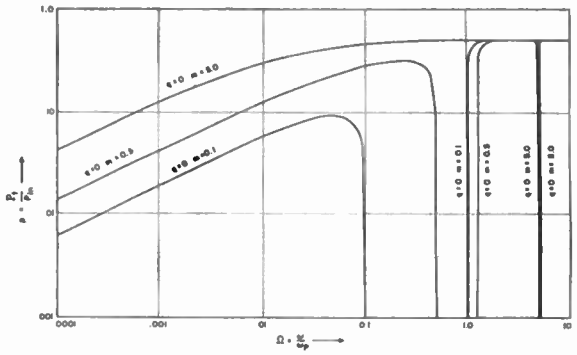

Fig. 7—Transmitted to incident power ratio vs normalized frequency, RH wave. Variable static longitudinal magnetic field m; fixed collision frequency $q=0$.

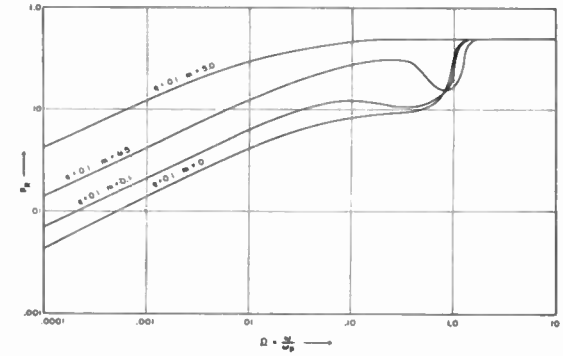

Fig. 8—Transmitted to incident power ratio vs normalized frequency, RH wave. Variable static longitudinal magnetic field m; fixed collision frequency $q=0.1$.

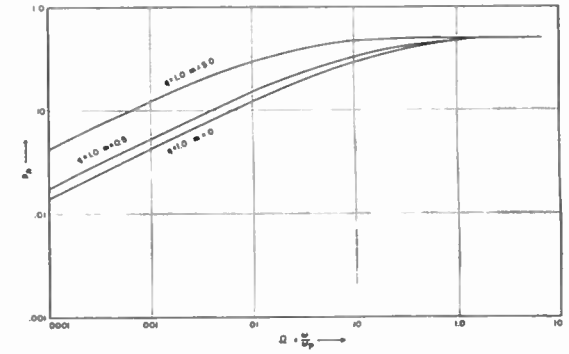

Fig. 9—Transmitted to incident power ratio vs normalized frequency, RH wave. Variable static longitudinal magnetic field m; fixed collision frequency $q=1.0$.

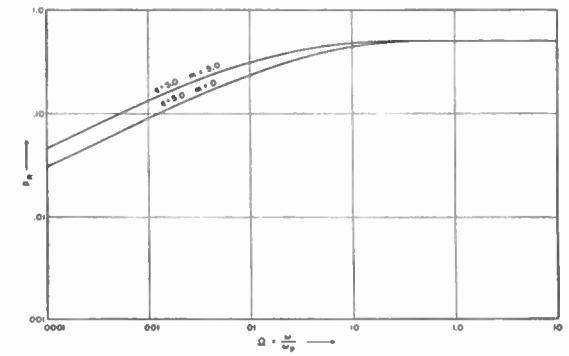

Fig. 10—Transmitted to incident power ratio vs normalized frequency, RH wave. Variable static longitudinal magnetic field m; fixed collision frequency $q=5.0$.

increase is easily seen from Maxwell's second equation when $\omega_b = 0$:

$$\nabla \times H = j\omega\epsilon_r \check{\epsilon}_r E. \tag{26}$$

$\check{\epsilon}_r$ is the complex relative dielectric constant given by[8]

$$\check{\epsilon}_r = \epsilon_r + \frac{\sigma}{j\omega\epsilon_r} = 1 + \frac{\omega_p^2}{j\omega(\nu + j\omega)}. \tag{27}$$

Substitution of (27) into (26) gives

$$\nabla \times H = \omega_p^2\epsilon_r \frac{\nu}{\nu^2 + \omega^2} E + j\omega\epsilon_r\left(1 - \frac{\omega_p^2}{\nu^2 + \omega^2}\right)E. \tag{28}$$

The first term on the RHS of (28) is the conductance current in phase with E. The second term is the displacement current. Rewriting (28),

$$\nabla \times H = \sigma E + j\omega\epsilon_r\epsilon_r E, \tag{29}$$

σ is the effective conductivity of the medium and ϵ_r the effective relative dielectric constant; they are given by the following:

$$\sigma = \omega_p^2\epsilon_r \frac{\nu}{\nu^2 + \omega^2} \tag{30}$$

$$\epsilon_r = 1 - \frac{\omega_p^2}{\nu^2 + \omega^2}. \tag{31}$$

σ becomes zero at $\nu = 0$ as well as $\nu = \infty$; it follows that signals through the plasma suffer little attenuation at low collision frequencies:

$$\nu^2 \ll \omega^2 \tag{32a}$$

if

$$\omega_p^2 \ll \omega^2. \tag{32b}$$

Similarly, they suffer little attenuation at high collision frequencies:

$$\nu^2 \gg \omega^2 \tag{33a}$$

if

$$\frac{\nu}{\omega} \gg \frac{\omega_p^2}{\omega^2}. \tag{33b}$$

The low attenuation at high collision frequencies occurs because the electrons, having a mean free path of small duration, do not have enough time to abstract energy from the incoming wave and convert it into incoherent radiation.

The conductivity is maximum at $\nu = \omega$; maximum attenuation, however, does not occur at this frequency since it depends on the power factor of the medium, that is, on σ as well as $\omega\epsilon$.

From (16) and (17) it is seen that the curves for power transfer in the collisionless slab (Fig. 7) apply to the lossy plasma provided that

$$q^2 \ll (m - \Omega)^2 \tag{34a}$$

or

$$\nu^2 \ll (\omega_b - \omega)^2. \tag{34b}$$

Conclusion as to the Practical Feasibility of the Static Magnetic-Field Approach

The preceding discussion shows that magnetic fields of a few hundred Gauss are sufficient to reduce appreciably the attenuation loss through the plasma sheath and the reflection loss at the plasma-air interface during re-entry, thus possibly allowing uninterrupted communications. Justification of the plane-wave analysis is borne out by recent experimental work at NASA[19] and theoretical work by the author.[18]

A feasible antenna system is described by Carbine, *et al.*, in a recent report.[11] The antenna is circularly polarized, of the spiral type, 12 in in diameter, and designed to operate at 250 Mc. The magnetic field is generated by means of a 1000-turn coil and no. 10 aluminum wire. The coil weighs about 35 lbs and dissipates 150 watts; a standard 28-v dc source is used. The magnetic-field intensity is expected to reach about 500 Gauss at the boundary layer, where the plasma sheath reaches its highest electron concentration. To save power consumption, the system would be programmed to be turned on shortly prior to re-entry.

RF Reflectance of Plasma Sheaths*

LEONARD S. TAYLOR†, MEMBER, IRE

Summary—**The wave equation for the propagation of a TE wave in a plane stratified plasma sheath is solved by the method of series, and an expression for the reflection coefficient is abstracted. In special cases the series may be identified with certain known functions, and simple formulas for the reflectance are obtained. In general, however, the reflection coefficient appears as the ratio of complex infinite series.**

I. Introduction

THE presence of ionized layers about reentry and other high speed vehicles in the atmosphere has created interest in the propagation of electromagnetic radiation in stratified plasmas. In these layers, ionization levels of the order of a per cent at temperatures of several thousand degrees Kelvin are achieved. In view of the physical dimensions of the objects and the wavelengths involved, it is often a legitimate approximation to consider the interaction of the field and the plasma in terms of a plane wave propagating into a plane stratified medium.[1] This approximation is also valid when the application of the results to ionospheric soundings are required. The present study, which is largely a review, shall be restricted to the TE wave geometry (Fig. 1). It is assumed that the plasma is bounded to the right by a plane infinite metal wall.

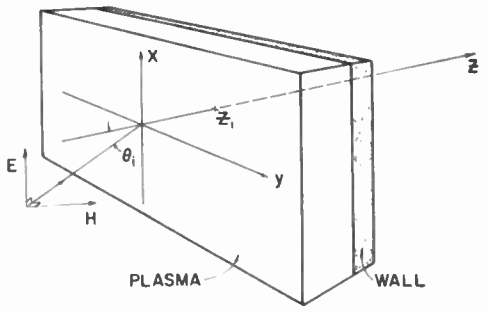

Fig. 1—TE wave geometry.

This latter assumption offers no real restriction since, in most cases, we are assured on physical grounds that the radiation does not effectively penetrate deeply into the plasma, particularly when high ionization densities exist in the plasma. Thus the insertion of a wall at these depths will not affect the situation, and offers mathematical advantages. We shall also assume that the variation of ionization density may be adequately represented as a parabolic function of the depth. Thus the results will encompass certain special solutions previously obtained[2,3] but not those cases[4,5] of density variations with z^{-2} or e^z, which have been considered at length elsewhere. Although the results are sufficient to determine the fields in the plasma, primary interest will be centered in the (voltage) reflection coefficient R of the sheath.

II. The Wave Equation

To begin, we review the theoretical background of the wave equation for the field component. In a medium stratified the in z-direction, Maxwell's equation for the propagation of a TE wave ($E_y = E_z = 0$) reduce to the scalar set,[6]

$$\begin{aligned}
&\frac{\partial H_z}{\partial y} - \frac{\partial H_y}{\partial z} - \frac{i\epsilon\omega}{c} E_x = 0 \\
&\frac{\partial H_x}{\partial z} - \frac{\partial H_z}{\partial x} = 0 \\
&\frac{\partial H_y}{\partial x} - \frac{\partial H_x}{\partial y} = 0 \\
&\frac{\partial E_x}{\partial z} + \frac{i\omega\mu}{c} H_y = 0 \\
&\frac{\partial E_x}{\partial y} - \frac{i\omega\mu}{c} H_z = 0 \\
&H_x = 0,
\end{aligned} \tag{1}$$

where we use Gaussian units and assume that the fields vary as $e^{i\omega t}$. Eq. (1) shows that H_y, H_z, E_x are functions of y and z only. When we eliminate the magnetic field components, and assume $\mu = 1$, these equations reduce to the scalar wave equation

$$\nabla^2 E_x(y, z) + n^2 k_0^2 E_x(y, z) = 0, \tag{2}$$

where $n^2 = \epsilon$ and $k_0 = \omega/c = 2\pi/\lambda_0$. A separation of variables in conjunction with the boundary conditions is sufficient to show that

$$E_x(y, z) = u(z) e^{ik_0(\sin\theta_i)y} \tag{3}$$

* Received by the IRE, September 5, 1961. This work was supported by Air Force Contract 30(602)-1968.

† General Electric Space Sciences Lab., Valley Forge, Pa.

[1] The reader is referred to L. M. Brekhovskikh, "Waves in Layered Media," Academic Press, Inc., New York, N. Y., 1960, as a general reference.

[2] F. A. Albini and R. G. Jahn, "Reflection and transmission of electromagnetic waves at electron density gradients," *J. Appl. Phys.*, vol. 32, pp. 75–82; January, 1961.

[3] L. S. Taylor, "Microwave reflection and absorption by a nonuniform plasma sheath," *Proc. 2nd Symp. on Engineering Aspects of Magnetohydrodynamics*, Philadelphia, Pa., March, 1961; Columbia University Press, New York, N. Y.

[4] L. S. Taylor, "Electromagnetic propagation in an exponential ionization density," IRE Trans. on Antennas and Propagation, vol. AP-9, pp. 483–487; September, 1961.

[5] L. S. Taylor, "Reflection of a TE wave from an inverse parabolic ionization density," IRE Trans. on Antennas and Propagation, vol. AP-9, p. 582; November, 1961.

[6] M. Born and E. Wolf, "The Principles of Optics," Pergamon Press, Inc., New York, N. Y., pp. 50–54; 1959.

where θ_i is the angle of incidence and $u(z)$ satisfies

$$\frac{d^2u(z)}{dz^2} + k_0^2(n^2 - \sin^2\theta_i)u(z) = 0. \tag{4}$$

The form of (3) is an expression of the generalized Snell's Law, $k \sin\theta = \text{constant}$.

The dielectric constant which appears in (1) is, in general, complex. It is related to the complex conductivity by the usual formula

$$\epsilon = \epsilon_0 + 4\pi\sigma/i\omega, \tag{5}$$

where we take $\epsilon_0 = 1$ in the plasma and $\sigma = J/E$; σ may be derived[7] by considering the motion of electrons in the plasma (neglecting the ion current) as the sum of the individual electron velocities. The individual electron velocities may be represented as a sum of the isotropic thermal velocity $\dot{r}(t)$ plus a field-induced drift velocity $\dot{r}'(t)$. The equation of motion of an individual electron (charge $-e$, mass m) can therefore be written as

$$\begin{aligned}\ddot{r}_{tot}(t) &= \ddot{r}(t) + \ddot{r}'(t)\\ &= F(t)/m + r'(t)\cdot[\text{grad}_r F(t)]/m\\ &\quad + \dot{r}'(t)\cdot[\text{grad}_{\dot{r}} F(t)]/m - eDe^{i\omega t}/m\\ &\quad + 8\pi ePe^{i\omega t}/3m,\end{aligned} \tag{6}$$

where $F(t)$ represents the stochastic force due to collisions between the electron and the other particles and D is produced by the sources of the external field, which may be regarded as the true charges on a parallel plate capacitor. Eq. (6) is derived by considering that the radiation-induced motion is a small perturbation of the thermal motion. The terms $\text{grad}_r F(t)$ and $\text{grad}_{\dot{r}} F(t)$ represent the small change of the collisional forces due to the radiation-induced displacement and velocity. The terms in $\ddot{r}(t)$ and $F(t)/m$ refer to the thermal motion only and may be cancelled. Thus

$$\begin{aligned}\ddot{r}'(t) &= r'(t)\cdot[\text{grad}_r F(t)]/m + \dot{r}'(t)\cdot[\text{grad}_{\dot{r}} F(t)]/m\\ &\quad - eDe^{i\omega t}/m + 8\pi ePe^{i\omega t}/3m.\end{aligned} \tag{7}$$

The average of the first term on the right of (7) is zero for collisions with neutral particles. For collisions with ions, this term has been shown by Darwin[8] to cancel the polarization field created by the displacement of the other electrons in the plasma so we may write

$$\ddot{r}'(t) = \dot{r}'(t)\cdot[\text{grad}_{\dot{r}} F(t)]/m - eEe^{i\omega t}/m. \tag{8}$$

After averaging over the orbits of the individual electrons, (8) yields the celebrated Lorentz phenomenological equation,

$$\overline{m\ddot{r}'(t)} = -m\nu_c\overline{\dot{r}'(t)} - eEe^{i\omega t}, \tag{9}$$

for the motion of electrons in a plasma. The parameter ν_c is best described as a coefficient of dynamical friction. In the case of a slightly ionized gas, with isotropic scattering of the electrons by heavy neutral particles, ν_c may indeed be shown to be the electron collision frequency.[9] In other cases, it is customary to refer to ν_c as the effective collision frequency in the medium. Integrating (9) and comparing the current density so obtained with the driving field, yields the complex conductivity

$$\sigma(z) = -iN(z)e^2/m(\omega - i\nu_c), \tag{10}$$

where $N(z)$ is the electron number density.

Combining (10) with (4) and (5), we find

$$\frac{d^2u(z)}{dz^2} + k_0^2\left[\cos^2\theta_i - \frac{4\pi e^2N(z)}{m\omega^2(1 - i\nu_c/\omega)}\right]u(z) = 0. \tag{11}$$

It shall be assumed that ν_c may be treated as a constant independent of z. This assumption requires justification in individual cases, but following an argument similar to one introduced previously,[2] the comparative sensitivity of the dielectric constant to variations of ν_c and N may be estimated from

$$\frac{\left(\frac{\partial\epsilon}{\partial z}\right)_{\nu_c}}{\left(\frac{\partial\epsilon}{\partial z}\right)_{N}} = \frac{\left(\frac{\partial\epsilon}{\partial N}\right)_{\nu_c}\frac{dN}{dz}}{\left(\frac{\partial\epsilon}{\partial\nu_c}\right)_{N}\frac{d\nu_c}{dz}} = (1 - i\omega/\nu_c)\frac{d[\ln N]}{d[\ln\nu_c]}. \tag{12}$$

Thus the effect of collision frequency variations is small when the variation in the electron concentration is large compared to the variation in the collision frequency (especially in the case $\omega \gg \nu_c$, which is of particular interest). In Fig. 2, we display the results of aerodynamic calculations for a typical case of interest.[10] The magni-

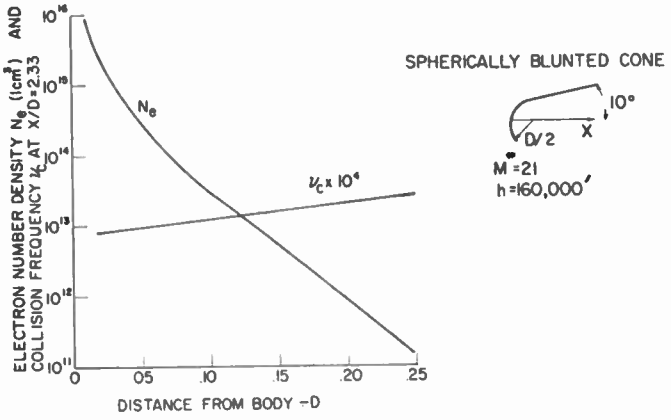

Fig. 2—Aerodynamic electron densities and collision frequencies about a spherically blunted cone at Mach 21 and 160,000-foot altitude.

[7] O. Theimer and L. S. Taylor, "The dependence of the plasma conductivity on frequency and collision time," *Ann. Phys.*, vol. 11, pp. 377–392; November, 1960.

[8] C. G. Darwin, "The refractive index of an ionized medium. II," *Proc. Roy. Soc. A*, vol. 182, pp. 152–166; April, 1943.

[9] L. S. Taylor, "The conductivity of slightly ionized gases," *The Physics of Fluids* (to be published).

[10] H. G. Lew and V. A. Angelo, "Plasma Sheath Characteristics about Hypersonic Vehicles," GE Space Science Lab., Philadelphia, Pa., Tech. Information Ser. No. R60SD356; 1960.

tude of the quantity $d[\ln N]/d[\ln \nu_c]$ is of the order of 10 in this case. Finally, we write (12) in the form

$$\frac{d^2u(z)}{dz^2} + [\beta^2 - \gamma N(z)]u(z) = 0 \tag{13}$$

where

$$\beta = k_0 \cos\theta_i$$
$$\gamma = 4\pi e^2/mc^2(1 - i\nu_c/\omega) = \gamma_0/(1 - i\nu_c/\omega). \tag{14}$$

III. The Series Solution for the Reflection Coefficient

Under the assumption

$$N(z) = \sum_{r=0}^{M} q_r z^r \tag{15}$$

(M finite), the coefficients of the wave equation are everywhere holomorphic, it is possible to solve the wave equation by the method of series, and the series converge for finite z.[11] Thus,

$$u(z) = \sum_{s=0}^{\infty} c_s z^s. \tag{16}$$

This solution contains two arbitrary constants, c_0 and c_1. We rewrite the above in the form

$$u(z) = c_0 \sum_{s=0}^{\infty} a_s z^s + c_1 \sum_{s=0}^{\infty} b_s z^s, \tag{17}$$

where

$$a_1 = b_0 = 0, \qquad a_0 = b_1 = 1. \tag{18}$$

Therefore

$$u(0) = c_0, \qquad \left.\frac{du(z)}{dz}\right|_{z=0} = c_1. \tag{19}$$

In the left-hand plane, the wave consists of an incident wave of unit amplitude plus a reflected wave. Remembering that we have taken the positive exponential for the time dependence

$$u(z) = e^{+i\beta z} + Re^{-i\beta z}, \tag{20}$$

for $z \leq 0$ where R is the (complex) voltage reflection coefficient. The continuity of the field and its first derivative at $z = 0$ now requires that

$$c_0 = 1 + R$$
$$c_1 = i\beta(1 - R). \tag{21}$$

It is most convenient to work in terms of the normalized impedance

$$Z = \frac{1 + R}{1 - R} = i\beta c_0/c_1. \tag{22}$$

[11] E. G. C. Poole, "Introduction to the Theory of Linear Differential Equations," Dover Publications, Inc., New York, N. Y., pp. 4–6; 1960.

Finally, we apply the boundary condition $u(z_1) = 0$. Thus

$$c_0 \sum_{s=0}^{\infty} a_s z_1^s + c_1 \sum_{s=0}^{\infty} b_s z_1^s = 0. \tag{23}$$

As a result,

$$Z = -i\beta \sum_{s=0}^{\infty} b_s z_1^s \Big/ \sum_{s=0}^{\infty} a_s z_1^s, \tag{24}$$

completing the formal solution.

It is evident on physical grounds that at large z_1, the impedance becomes independent of z_1. This occurs when, because of the processes of refraction and absorption, the field does not penetrate effectively to the wall. We shall refer to this circumstance as the "infinite depth" case, and denote it by the subscript ∞.

Example: $N(z) = Constant$

As a first example, we consider the trivial case $N(z) = N$. Writing

$$\beta^2 - \gamma N = \alpha^2, \tag{25}$$

we have immediately

$$u(z) = c_0 \sum_{s=0,\ even}^{\infty} \frac{(-1)^{s/2}\alpha^s z^s}{s!} + \frac{c_1}{\alpha} \sum_{s=0,\ odd}^{\infty} \frac{(-1)^{(s-1)/2}\alpha^s z^s}{s!}. \tag{26}$$

Thus

$$Z = -\frac{i\beta}{\alpha} \sum_{s=0,\ odd}^{\infty} \frac{(-1)^{(s-1)/2}\alpha^s z_1^s}{s!} \Big/ \sum_{s=0,\ even}^{\infty} \frac{(-1)^{s/2}\alpha^s z_1^s}{s!}. \tag{27}$$

Of course, we recognize the series, with the result

$$Z = -\frac{i\beta}{\alpha} \tan \alpha z_1 = -\frac{\beta}{\alpha} \frac{e^{2i\alpha z_1} - 1}{e^{2i\alpha z_1} + 1}. \tag{28}$$

Taking the principal value (arg $\alpha < \pi$), we have in the case of infinite plasma depth

$$Z_\infty = \beta/\alpha. \tag{29}$$

Thus

$$R_\infty = \frac{\beta - \alpha}{\beta + \alpha}. \tag{30}$$

(Recalling that

$$\alpha^2 = k_0^2[n_p^2 - \sin^2\theta_i], \tag{31}$$

where n_p is the complex index of refraction of the plasma, we find

$$R_\infty = \frac{\cos\theta_i - \sqrt{n_p^2 - \sin^2\theta_i}}{\cos\theta_i + \sqrt{n_p^2 - \sin^2\theta_i}} \tag{32}$$

correctly.[12]) It may be noted that no rearrangement of the series solution was necessary to separate (26) into terms proportional to c_0 and c_1. This will occur whenever $N(z)$ is expressed in even powers of z only.

IV. Thin Sheath Case

Considering only plasmas which zero electron density at $z=0$, (13) may be written as

$$\frac{d^2u(z)}{dz^2} + [\beta^2 - \gamma(q_1z + q_2z^2 + \cdots)]u(z) = 0. \quad (33)$$

Thus the recursion relation for the coefficients of the series solution is

$$(n+2)(n+1)c_{n+2} + \beta^2c_n - \gamma q_1c_{n-1} - \gamma q_2c_{n-2} - \cdots = 0. \quad (34)$$

The first few coefficients are c_0, c_1,

$$c_2 = -\frac{\beta^2}{2}c_0,$$

$$c_3 = \frac{1}{6}(\gamma q_1c_0 - \beta^2c_1). \quad (35)$$

For sheaths that are thin compared to a wavelength, with a low electron density gradient, it is appropriate to retain only these first terms, with the result

$$u(z) \approx c_0\left[1 - \frac{\beta^2}{2}z^2 + \frac{1}{6}\gamma q_1z^3\right] + c_1\left[z - \frac{\beta^2z^3}{6}\right]. \quad (36)$$

$$Z \approx -i\frac{\beta z_1 - \beta^3z_1^3/6}{1 - \beta^2z_1^2/2 + \gamma q_1z_1^3/6}. \quad (37)$$

Thus

$$R = \frac{Z-1}{Z+1}$$

$$\approx -\frac{1 + i(\beta z_1) - (\beta z_1)^2/2 + (\gamma q_1/\beta^3 - i)(\beta z_1)^3/6}{1 - i(\beta z_1) - (\beta z_1)^2/2 + (\gamma q_1/\beta^3 + i)(\beta z_1)^3/6}. \quad (38)$$

(Thus, if the terms in $(\beta z_1)^3$ may be ignored also, we find $|R| = 1$.)

In general, the series are poorly convergent and best suited to machine computation, even for sheaths only a few wavelengths thick. If the variations in electron density are small over distances comparable to a wavelength, however, perturbation solutions of the wave equation may be employed.[13]

[12] N. K. H. Panofsky and M. Phillips, "Classical Electricity and Magnetism," Addison-Wesley Publishing Co., Reading Mass., p. 180; 1955.

[13] M. Klein, H. D. Greyber, J. I. F. King, and K. A. Brueckner, "Interaction of a Non-Uniform Plasma with Microwave Radiation," General Electric Co., Philadelphia, Pa., Tech. Information Ser. No. R59SD467; 1960.

V. Parabolic Density Profile

For many applications, a density variation

$$N(z) = q_1z + q_2z^2 \quad (39)$$

adequately represents the profile. We first consider two special cases of this formula.

Case 1: $q_2 = 0$

In the case of a linear ramp in electron density $q_2=0$, and the wave equation is

$$\frac{d^2u(z)}{dz^2} + [\beta^2 - \gamma q_1z]u(z) = 0. \quad (40)$$

It is indeed possible to carry out the series solution by the method discussed. The series thus obtained could then be identified with the Airy functions. In the present case, this is quite artificial and it is preferable to transform directly, writing

$$\zeta = -(\beta^2 - \gamma q_1z)/(\gamma q_1)^{2/3}. \quad (41)$$

We have Airy's equation:

$$\frac{d^2u}{d\zeta^2} - \zeta u = 0. \quad (42)$$

Thus

$$u = A\mathfrak{A}i(\zeta) + B\mathfrak{B}i(\zeta). \quad (43)$$

Extensive numerical results, based on calculations with somewhat different boundary conditions have been given previously.[2] In the present case, writing

$$\zeta_0 = \zeta(z=0) = -\beta^2/(\gamma q_1)^{2/3}$$
$$\zeta_1 = \zeta(z=z_1) = (-\beta^2 + \gamma q_1z_1)/(\gamma q_1)^{2/3} \quad (44)$$

and noting that

$$c_0 = u(z=0) = A\mathfrak{A}i(\zeta_0) + B\mathfrak{B}i(\zeta_0)$$
$$c_1 = \left(\frac{du}{dz}\right)_{z=0} = (\gamma q_1)^{1/3}[A\mathfrak{A}i'(\zeta_0) + B\mathfrak{B}i'(\zeta_0)]$$
$$u(z_1) = 0 = A\mathfrak{A}i(\zeta_1) + B\mathfrak{B}i(\zeta_1) \quad (45)$$

where the prime indicates differentiation with respect to ζ, we find

$$Z = \frac{i\beta}{(\gamma q_1)^{1/3}}\cdot\frac{\mathfrak{A}i(\zeta_0)\mathfrak{B}i(\zeta_1) - \mathfrak{A}i(\zeta_1)\mathfrak{B}i(\zeta_0)}{\mathfrak{A}i'(\zeta_0)\mathfrak{B}i(\zeta_1) - \mathfrak{A}i(\zeta_1)\mathfrak{B}i'(\zeta_0)}. \quad (46)$$

In the limiting case of infinite depth,

$$0 < \arg\zeta_1 = \tfrac{1}{3}\arg\gamma < \pi/3, \quad (47)$$

and we may employ the asymptotic forms[14]

$$\mathfrak{A}i(\zeta_1) \sim \frac{1}{2\sqrt{\pi}}\zeta_1^{-1/4}\exp(-\tfrac{2}{3}\zeta_1^{3/2})$$
$$\mathfrak{B}i(\zeta_1) \sim \frac{1}{\sqrt{\pi}}\zeta_1^{-1/4}\exp(\tfrac{2}{3}\zeta_1^{3/2}). \quad (48)$$

[14] A. Erdelyi, "Asymptotic Expansions," Dover Publications, Inc., New York, N. Y., p. 95; 1956.

Whence

$$Z_\infty = \frac{i\beta}{(\gamma q_1)^{1/3}} \mathfrak{A}i(\zeta_0)/\mathfrak{A}i'(\zeta_0). \tag{49}$$

As described previously, the wall has disappeared back into the plasma. The condition $|\zeta_1| \gg 1$ is a rough estimate of the depth to which the field penetrates.

For steep density gradients, $|\zeta_0| \ll 1$, and the relation between the Airy function and the modified Bessel functions

$$\begin{aligned}\mathfrak{A}i(\zeta_0) &= \tfrac{1}{3}\zeta_0^{1/2}[I_{-1/3}(\tfrac{2}{3}\zeta_0^{3/2}) - I_{1/3}(\tfrac{2}{3}\zeta_0^{3/2})] \\ &\approx [3^{2/3}\Gamma(2/3)]^{-1} - [3^{4/3}\Gamma(4/3)]^{-1}\zeta_0 \end{aligned} \tag{50}$$

yields

$$Z_\infty = -i\beta[3^{2/3}\Gamma(4/3)/\Gamma(2/3)](q_1\gamma)^{-1/3}. \tag{51}$$

Case 2: $q_1 = 0$

In the event of a purely parabolic density variation[15] the wave equation

$$\frac{d^2u(z)}{dz^2} + [\beta^2 - \gamma q_2 z^2]u(z) = 0 \tag{52}$$

may be transformed by the substitutions

$$\begin{aligned}\xi &= (4\gamma q_2)^{1/4} z \\ \rho &= \tfrac{1}{2}[\beta^2(\gamma q_2)^{-1/2} - 1]\end{aligned} \tag{53}$$

into the Weber equation

$$\frac{d^2u}{d\xi^2} + [\rho + \tfrac{1}{2} - \tfrac{1}{4}\xi^2]u = 0. \tag{54}$$

In the present instance, it is useful to treat this equation in the following way: The usual transformation

$$u = e^{-\xi^2/4}v \tag{55}$$

is even in ξ (or z) and will not affect the identification of the appropriate coefficients. Upon substitution we find

$$\frac{d^2v}{d\xi^2} - \xi\frac{dv}{d\xi} + \rho v = 0. \tag{56}$$

The series solution leads to the recursion relation

$$a_{r+2} = \frac{r - \rho}{(r+1)(r+2)} a_r. \tag{57}$$

Thus

$$\begin{aligned} v_1 &= 1 - \frac{\rho}{2!}\xi^2 + \frac{\rho(\rho-2)}{4!}\xi^4 \\ &\quad - \frac{\rho(\rho-2)(\rho-4)}{6!}\xi^6 + \cdots \\ v_2 &= \xi - \frac{\rho-1}{3!}\xi^3 + \frac{(\rho-1)(\rho-3)}{5!}\xi^5 \\ &\quad - \frac{(\rho-1)(\rho-3)(\rho-5)}{7!}\xi^7 + \cdots . \end{aligned} \tag{58}$$

From (24) the impedance is

$$Z = -i\beta\frac{v_2(\xi_1)}{v_1(\xi_1)}\left(\frac{dz}{d\xi}\right). \tag{59}$$

In general, it is at this point that numerical work is required. In the present instance, however, these series may be identified with the Kummer series, which is derived from the confluent hypergeometric function[16]

$$\Phi(a, c; x) = 1 + \frac{a}{c}x + \frac{a(a+1)}{c(c+1)}\frac{x^2}{2!} + \cdots . \tag{60}$$

Thus

$$\begin{aligned} v_1 &= \Phi(-\tfrac{1}{2}\rho, \tfrac{1}{2}; \tfrac{1}{2}\xi^2) \\ v_2 &= \xi\Phi(\tfrac{1}{2} - \tfrac{1}{2}\rho, \tfrac{3}{2}; \tfrac{1}{2}\xi^2). \end{aligned} \tag{61}$$

Whence

$$Z = -i\beta\xi_1(4\gamma q_2)^{-1/4}\frac{\Phi(\frac{1}{2} - \frac{1}{2}\rho, \frac{3}{2}; \frac{1}{2}\xi^2)}{\Phi(-\frac{1}{2}\rho, \frac{1}{2}; \frac{1}{2}\xi^2)}. \tag{62}$$

But for $\mathrm{Re}\{x\} \to \infty$

$$\Phi(a, c; x) \sim [\Gamma(c)/\Gamma(a)]e^x x^{a-c}. \tag{63}$$

Whence, in the case of infinite depth,

$$Z_\infty = -i\beta(\gamma q_2)^{-1/4}\Gamma(-\tfrac{1}{2}\rho)/2\Gamma(\tfrac{1}{2} - \tfrac{1}{2}\rho). \tag{64}$$

The gamma functions of complex argument have been tabulated.[17] Using this table, we find for example at $\lambda_0 = 3$ cm, $\nu_c/\omega = 0.1$ and $q_2 = 10^{12}$, $Z_\infty = 0.29 - 0.27i$, $|R_\infty| = 0.58$.

The result obtained in the foregoing paragraph now reduces the solution of the more general problem ($q_1 \neq 0 \neq q_2$) to a simple transformation. Writing the wave equation as

$$\frac{d^2u}{d\xi^2} + (\rho + \tfrac{1}{2} + \tau\xi - \tfrac{1}{4}\xi^2)u = 0, \tag{65}$$

[15] Since the writing of this article, an extensive treatment of this problem apropos to the ionosphere has been given by K. G. Budden, "Radio Waves in the Ionosphere," Cambridge University Press, England; 1961. (The formula for the reflection coefficient in this case was first given by O. E. H. Rydbeck, *Chalmers tek. Högskol. Handl.*, No. 34; 1944.) Many of the results obtained in this paper have also been independently obtained by D. J. BenDaniel and H. Hurwitz, Jr., "WKB Matching Conditions at Gradual Interfaces," GE Res. Lab., Internal Rept., Schenectady, N. Y. (to be published).

[16] Bateman Manuscript Project, "Higher Transcendental Functions," McGraw-Hill Book Co., Inc., New York, N. Y., vol. 1, ch. 6; vol. 2, ch. 8; 1955.

[17] U. S. Natl. Bur. Standards, Washington, D. C., "Tables of the Gamma Function for Complex Arguments," Applied Mathematics Series 34; 1954.

where $\tau = -\gamma^{1/4} q_1 (4q_2)^{-3/4}$, and completing the square with the substitutions

$$\xi = \xi' + 2\tau, \qquad \rho = \rho' - \tau^2, \tag{66}$$

reduces (65) to the Weber equation (54). Thus we recognize the series solution in the primed variables as

$$u = e^{-\xi^2/4} \left[A\Phi(-\tfrac{1}{2}\rho', \tfrac{1}{2}; \tfrac{1}{2}\xi'^2) + B\xi'\Phi(\tfrac{1}{2} - \tfrac{1}{2}\rho', \tfrac{3}{2}; \tfrac{1}{2}\xi'^2) \right]. \tag{67}$$

The coefficients c_0 and c_1 and the ratio A/B are obtained in (45). The relation[16]

$$\frac{d}{dx}\Phi(a, c; x) = \frac{a}{c}\Phi(a + 1, c + 1; x) \tag{68}$$

which may be derived by term-by-term differentiation of (60) has been used to arrive at the following expression for the impedance:

$$Z = + i\beta(4\gamma q_2)^{-1/4} \times \left[2\tau\Phi(\tfrac{1}{2} - \tfrac{1}{2}\rho', \tfrac{3}{2}; 2\tau^2) - \frac{A}{B}\Phi(-\tfrac{1}{2}\rho', \tfrac{1}{2}; 2\tau^2) \right] \times \Big[(1 - 2\tau^2)\Phi(\tfrac{1}{2} - \tfrac{1}{2}\rho', \tfrac{3}{2}; 2\tau^2) + \tfrac{4}{3}\tau^2(1 - \rho')\Phi(\tfrac{3}{2} - \tfrac{1}{2}\rho', \tfrac{5}{2}; 2\tau^2) + \frac{A}{B}\tau\{\Phi(-\tfrac{1}{2}\rho', \tfrac{1}{2}; 2\tau^2) + 2\rho'\Phi(1 - \tfrac{1}{2}\rho', \tfrac{3}{2}; 2\tau^2)\} \Big]^{-1}, \tag{69}$$

where $\xi_1' = \xi'(z = z_1)$,

$$\frac{A}{B} = -\xi_1'\Phi(\tfrac{1}{2} - \tfrac{1}{2}\rho', \tfrac{3}{2}; \tfrac{1}{2}\xi_1'^2)/\Phi(-\tfrac{1}{2}\rho', \tfrac{1}{2}; \tfrac{1}{2}\xi_1'^2). \tag{70}$$

In the case of an infinite effective depth, (70) reduces to

$$\frac{A}{B} = -\frac{\Gamma(-\frac{1}{2}\rho')}{\sqrt{2}\,\Gamma(\frac{1}{2} - \frac{1}{2}\rho')}. \tag{71}$$

VI. Conclusion

The methods outlined in the present work may be extended to electron density distributions containing cubic and higher order terms, either as outlined in Section IV, or by development of the wave function in functional series. In the latter case, it is possible to employ limiting forms to determine the solution in the infinite depth case. The utility of such formulas is limited, however, by the difficulty in abstracting numerical results from such formal solutions.

Correction

W. W. Siekanowicz, author of "A Small-RF-Signal Theory for an Electrostatically Focussed Traveling-Wave Tube," which appeared on pp. 1888–1901 of the November, 1960, issue of Proceedings, has called the following to the attention of the *Editor*.

On page 1891, (17) and (18), the denominator of the third term within the parentheses should be

$$2u_0^2 \text{ instead of } u_0^2.$$

On page 1892 (36), the upper term in the parentheses to the left of the equal sign should be

$$^{n+1}Q_{3a}.$$

The right-hand side of (45) should read as follows:

$$-2\left|\hat{K}\right|^2 \left\{ \frac{\omega_a}{u_a}(rg + d) + j2\omega_a\tau_i\left[e^{(\phi - j\theta_c)} - 1\right] \right\} \sin\theta.$$

On page 1893 (55), the term to the left of the equal sign should be

$$^{n}Q_{1a\,s}.$$

Mutual Coupling of Two Thin Infinitely-Long Slots on a Perfectly Conducting Plane in the Presence of a Uniform Plasma Layer*

JAMES S. YEE†, MEMBER, IRE

The investigation of antenna coupling was motivated by communication with a hypersonic vehicle which upon reentry produces a plasma sheath over the antennas. The model chosen for analysis consists of two infinitely-long thin slots on a ground plane covered by a uniform plasma layer which is assumed to be a lossless gaseous dielectric slab having a dielectric constant less than unity but greater than zero. The coupling effects are described in terms of a mutual admittance parameter in an equivalent π network from which other admittance parameters are derivable. The problem is formulated by spatial Fourier transforms which, upon inversion, would yield the desired results. The transform integral for the case of a thick plasma layer is evaluated approximately by the method of steepest descent. The results are explained in terms of multiple reflections of rays by the sharply defined plasma-air interface. When the quantities are plotted as functions of slot separation, the perturbations show up in the form of ripples about the curve for the unbounded plasma. In a realistic situation, there is no well-defined boundary and the rippling may show up in a statistical manner. The coupling effect is found to be less serious in the presence of a plasma than in its absence. When the operating frequency is appreciably higher than the plasma frequency, the change in driving point admittance is small. Also, inside a thick plasma layer, no unattenuating pole waves are excited.

I. Introduction

WHEN two identical antennas are located near one another, mutual coupling effects exist. Various authors have studied the mutual coupling problem with regard to certain antenna geometry and antenna operating characteristics. For example, Lucke [1] studied the mutual admittance between slots located on the surface of a large-radius cylinder and compared the results with those in an infinite ground plane. Nishida [2], [3] investigated the effect of mutual coupling between two parallel slits located on a ground plane and on a cylinder on leaky-wave propagation. Edelberg and Oliner [4] considered mutual coupling effects in large slot antenna arrays.

The problem considered in this paper was motivated by a study of communication with a hypersonic reentry vehicle such as the Dyna-Soar which introduces an additional interface into the antenna geometry. This interface is due to the plasma sheath that is created about the vehicle upon re-entry. When antennas are located within this sheath, it is important to investigate the effects which the sheath may have on the antenna operating characteristics. When the sheath is treated in its most elementary form as a gaseous dielectric slab [5], [6], the sheath problem in many respects resembles the solid dielectric interface problem of surface waves which has been studied quite extensively [7]—[10]. The techniques of analysis employed by these people are quite applicable to the present problem.

In this paper an attempt is made to study the effects of the plasma sheath on the antenna admittance parameters. The sheath is assumed to have a real dielectric constant less than unity but greater than zero. This assumption implies that the operating frequency is greater than the plasma frequency and that the electron-neutral particle collision frequency is negligible in comparison with the operating frequency. Because of the way the admittance parameters are defined, the problem is essentially one of finding the surface current due to the slot on the ground plane which is covered by a uniform plasma sheath.

II. Field Formulation

Consider a two-dimensional, double-layer problem as shown in Fig. 1. In this figure two parallel, infinitely-long thin slots (S_1 and S_2) separated by a distance z_0 are located on the surface of a perfectly conducting plane. Above this ground plane is a uniform plasma layer (Region II). It has a thickness a and equivalent electromagnetic parameters σ_2, μ_2, and ϵ_2, which are the conductivity, permeability, and permittivity of the region. On top of the plasma layer is free space (Region I) with equivalent electromagnetic parameters σ_1, μ_1, and ϵ_1. Let S_1 be the origin of a rectangular coordinate system. If $e^{j\omega t}$ time dependence is assumed, ω being the operating angular frequency, the fields are completely determined in each region by solving the differential equation for Hy^{I} and Hy^{II}:

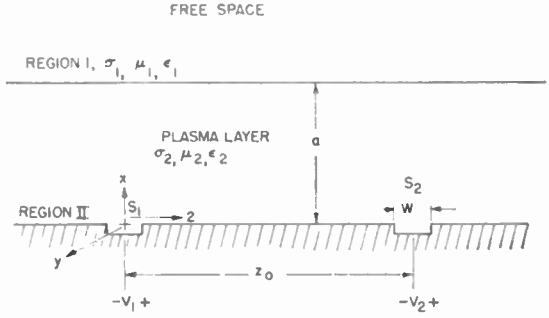

Fig. 1—Uniform plasma layer on two thin, infinitely-long slots in a perfectly conducting plane.

* Received by the IRE, September 27, 1961.
† Antennas and Radomes Unit, Boeing Co., Seattle, Wash.

$$\frac{\partial^2 H_y^{\,I}}{\partial x^2} + \frac{\partial^2 H_y^{\,I}}{\partial z^2} + k^2 H_y^{\,I} = 0 \qquad a \le x < \infty \tag{1}$$

$$\frac{\partial^2 H_y^{\,II}}{\partial x^2} + \frac{\partial^2 H_y^{\,II}}{\partial z^2} + n^2 k^2 H_y^{\,II} = 0 \qquad 0 \le x \le a \tag{2}$$

where

$$k^2 = \omega^2 \mu_1 \epsilon_1 \quad \text{and} \quad n^2 = \frac{\mu_2 \epsilon_2}{\mu_1 \epsilon_1} \qquad 0 < n \le 1.$$

Other field components can be derived in terms of Hy^{I} and Hy^{II} from Maxwell's equations:

$$E_x^{\,I,II} = -\frac{1}{i\omega\epsilon_{1,2}} \frac{\partial H_y^{\,I,II}}{\partial z} \tag{3}$$

$$E_z^{\,I,II} = \frac{1}{i\omega\epsilon_{1,2}} \frac{\partial H_y^{\,I,II}}{\partial x} \tag{4}$$

$$E_y^{\,I,II} = 0 \tag{5}$$

$$H_x^{\,I,II} = H_z^{\,I,II} = 0. \tag{6}$$

Let ϕ_1 and ϕ_2 be the spatial Fourier transforms of Hy^{I} and Hy^{II} respectively; then the transform pair associated with the magnetic field in each region is:

Region I

$$a \le x < \infty$$

$$\phi_1(x, h) = \int_{-\infty}^{\infty} H_y^{\,I}(x, z) e^{-ihz} dz \tag{7}$$

$$H_y^{\,I}(x, z) = \frac{1}{2\pi} \int_{-\infty}^{\infty} \phi_1(x, h) e^{+ihz} dh \tag{8}$$

Region II

$$0 \le x \le a$$

$$\phi_2(x, h) = \int_{-\infty}^{\infty} H_y^{\,II}(x, z) e^{-ihz} dz \tag{9}$$

$$H_y^{\,II}(x, z) = \frac{1}{2\pi} \int_{-\infty}^{\infty} \phi_2(x, h) e^{+ihz} dh. \tag{10}$$

In terms of the Fourier transforms ϕ_1 and ϕ_2, the differential equations (1) and (2) reduce to one variable:

$$\frac{d^2\phi_1}{dx^2} - \lambda^2 \phi_1 = 0 \tag{11}$$

$$\frac{d^2\phi_2}{dx^2} - \mu^2 \phi_2 = 0 \tag{12}$$

where

$$\lambda^2 = h^2 - k^2 \tag{13}$$

$$\mu^2 = h^2 - n^2 k^2 \tag{14}$$

and the solutions of which can be written:

$$\phi_1 = A_1 e^{-\lambda x} \tag{15}$$

$$\phi_2 = A_2 e^{-\mu x} + A_3 e^{+\mu x} \tag{16}$$

where the real part of λ is equal to $+i\sqrt{k^2 - h^2}$ for outgoing

The appropriate boundary conditions when $|h| > k$ and continuity of tangential fields along the vanishing of Ez^{II} everywhere a plane except the slots which are assumed sources with voltages V_1 and V_2, respectively. transforms ϕ_1 and ϕ_2 must necessarily satisfy conditions which are:

$$\phi_1\Big|_{x=a} = \phi_2\Big|_{x=a} \tag{17}$$

$$\frac{1}{\epsilon_1} \frac{d\phi_1}{dx}\Big|_{x=a} = \frac{1}{\epsilon_2} \frac{d\phi_2}{dx}\Big|_{x=a} \tag{18}$$

$$\frac{d\phi_2}{dx}\Big|_{x=0} = i\omega\epsilon_2 \left[\int_{S_1} E_{z_1}^{\,II} e^{-ihz} dz + \int_{S_2} E_{z_2}^{\,II} e^{-ihz} dz \right]. \tag{19}$$

Since the electric fields across the slots are constant, they are given by:

$$E_{z_1}^{\,II} = V_1 \delta(z) \qquad \text{Slot 1 } (z = 0) \tag{20}$$

$$E_{z_2}^{\,II} = V_2 \delta(z - z_0) \qquad \text{Slot 2 } (z = z_0) \tag{21}$$

where $\delta(z)$ and $\delta(z - z_0)$ are Dirac-Delta functions.

Incorporating the boundary conditions in (17), (18), and (19) leads to a set of three simultaneous equations for the coefficients A_1, A_2, and A_3:

$$e^{-\lambda a} A_1 - e^{-\mu a} A_2 - e^{+\mu a} A_3 = 0 \tag{22}$$

$$\frac{\lambda}{\epsilon_1} e^{-\lambda a} A_1 - \frac{\mu}{\epsilon_2} e^{-\mu a} A_2 + \frac{\mu}{\epsilon_2} e^{+\mu a} A_3 = 0 \tag{23}$$

$$\mu A_2 - \mu A_3 = -g(h) \tag{24}$$

where

$$g(h) = i\omega\epsilon_2 (V_1 + V_2 e^{-ihz_0}).$$

The solutions for the coefficients are:

$$A_1 = \frac{-2\, g(h)\epsilon_1}{e^{-\lambda a}(e^{+\mu a} + e^{-\mu a})(\mu\epsilon_1 \tanh \mu a + \lambda\epsilon_2)} \tag{25}$$

$$A_2 = \frac{-g(h)(\mu\epsilon_1 + \lambda\epsilon_2) e^{+\mu a}}{\mu(e^{+\mu a} + e^{-\mu a})(\mu\epsilon_1 \tanh \mu a + \lambda\epsilon_2)} \tag{26}$$

$$A_3 = \frac{-g(h)(\mu\epsilon_1 - \lambda\epsilon_2) e^{-\mu a}}{\mu(e^{+\mu a} + e^{-\mu a})(\mu\epsilon_1 \tanh \mu a + \lambda\epsilon_2)}. \tag{27}$$

In terms of the transforms, the magnetic field in each region is:

Region I

$$a \le x < \infty$$

$$H_y^{\,I}(x, z) = -\frac{1}{2\pi} \int_{-\infty}^{\infty} \frac{2g(h)\epsilon_1 e^{-\lambda(x-a)} e^{+ihz} dh}{(e^{+\mu a} + e^{-\mu a})(\mu\epsilon_1 \tanh \mu a + \lambda\epsilon_2)} \tag{28}$$

Region II

$$0 \leq x \leq a$$

$$H_y^{II}(x, z) = -\frac{1}{2\pi}\int_{-\infty}^{\infty} \frac{g(h)(\mu\epsilon_1 + \lambda\epsilon_2)e^{+ihz}}{\mu(1 + e^{-2\mu a})(\mu\epsilon_1 \tanh \mu a + \lambda\epsilon_2)} \cdot \left[e^{-\mu x} + \frac{\mu\epsilon_1 - \lambda\epsilon_2}{\mu\epsilon_1 + \lambda\epsilon_2} e^{-2\mu a}e^{+\mu x}\right]dh. \quad (29)$$

III. Admittance Parameters

In discussing the admittance characteristics of one slot in the vicinity of another it is convenient to represent the fields by a four-terminal π network as shown in Fig. 2. The circuit elements (Y_{11}) and (Y_{22}) are self-admittances of the respective slots. The mutual admittance (Y_{12}) is a measure of the coupling of one slot into the other. The circuit equations are:

$$I_1 = Y_{11}V_1 + Y_{12}V_2 \quad (30)$$

$$I_2 = Y_{21}V_1 + Y_{22}V_2. \quad (31)$$

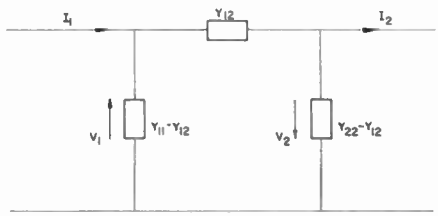

Fig. 2—Equivalent circuit representation.

Define

$$Y_{12} = \frac{I_{21}}{V_1} \quad (32)$$

where I_{21} is the short-circuited current ($V_2 = 0$) induced in slot S_2 due to the voltage excitation of V_1 in S_1. Similarly, the driving point admittance (Y_1' and Y_2') for each slot in the presence of the other is:

$$Y_1' = \frac{I_1}{V_1} \quad \text{when} \quad I_2 = 0$$

$$= Y_{11} - \frac{Y_{12}^2}{Y_{22}} \quad (33)$$

$$Y_2' = \frac{I_2}{V_2} \quad \text{when} \quad I_1 = 0$$

$$= Y_{22} - \frac{Y_{12}^2}{Y_{11}}. \quad (34)$$

The next step is to relate the circuit quantities to the appropriate fields. The surface current, I_{21}, per unit length in y is given by the magnetic field evaluated on the ground plane $x = 0$. It is defined as

$$\mathbf{a}_z I_{21} = \mathbf{a}_x \times \mathbf{a}_y H_{y_{21}}^{II}(0, z). \quad (35)$$

The voltage excitations of slot S_1 and S_2 are given by the line integrals of the tangential electric fields over the apertures. These are

$$V_1 = \int_{S_1} E_{z_1}^{II} dz = \int_{S_1} V_1\delta(z)dz \quad (36)$$

$$V_2 = \int_{S_2} E_{z_2}^{II} dz = \int_{S_2} V_2\delta(z - z_0)dz. \quad (37)$$

The assumption of delta slot sources reduces the mathematical complexities of the problem by avoiding a complicated integration of the field distribution over the apertures as shown in (36) and (37). In view of (35), the mutual admittance Y_{12} per unit length in y as defined in (32) is simply:

$$Y_{12} = -\frac{H_{y_{21}}^{II}(0, z_0)}{V_1}. \quad (38)$$

IV. Evaluation of Hy_{21}^{II}

To determine Y_{12} as shown in Section III, it is necessary to evaluate the integral for the magnetic field Hy^{II} at S_2 due to S_1 when $V_2 = 0$. This integral can be shown to exist for all physical situations. Of special interest is the case for an electrically thick plasma layer which most likely resembles the situation during re-entry. Fortunately, the integral for this case can be evaluated approximately by the method of steepest descent. Another case which is worth considering but is not discussed in this paper is that of an electrically thin plasma layer. The expression for Hy^{II} in this case is left in the integral form.

A. *In the Presence of a Thick Plasma Layer*

From (29) and when $x = 0$, $z = z_0$, and $V_2 = 0$, Hy_{21}^{II} becomes:

$$H_{y_{21}}^{II}(0, z_0) = -\frac{i\omega\epsilon_2 V_1}{2\pi} \cdot \int_{-\infty}^{\infty} \frac{(\mu\epsilon_1 + \lambda\epsilon_2)\left(1 + \frac{\mu\epsilon_1 - \lambda\epsilon_2}{\mu\epsilon_1 + \lambda\epsilon_2} e^{-2\mu a}\right)e^{+ihz_0}}{\mu(1 + e^{-2\mu a})(\mu\epsilon_1 \tanh \mu a + \lambda\epsilon_2)} dh. \quad (39)$$

Let

$$\Gamma(h) = \frac{\mu\epsilon_1 - \lambda\epsilon_2}{\mu\epsilon_1 + \lambda\epsilon_2}. \quad (40)$$

As shown in Appendix I, $\Gamma(h)$ can be interpreted as the reflection coefficient of the magnetic field due to the interface in the h domain. Hy_{21}^{II} can now be expressed as:

$$H_{y_{21}}^{II}(0, z_0) = -\frac{i\omega\epsilon_2 V_1}{2\pi}\int_{-\infty}^{\infty} \frac{1 + \Gamma e^{-2\mu a}}{1 - \Gamma e^{-2\mu a}} \frac{e^{+ihz_0}}{\mu} dh. \quad (41)$$

In the complex h plane, because of the multiple-valued behavior of λ and μ the integrand of (41) possesses two branch point singularities when $\lambda = 0$ and $\mu = 0$, and possible simple poles when $1 - \Gamma e^{-2\mu a} = 0$. These poles, if they exist, give rise to characteristic propagating modes

that can be excited inside the plasma layer. However, because the index of refraction is greater than zero and less than unity, $0<n\leq 1$ (medium II is less dense than medium I), it is shown in Appendix III that there are no simple poles on the negative real axis in the h plane. Therefore, along the path of integration of the integral in (41), $1-\Gamma e^{-2\mu a}\neq 0$.

Because $\Gamma\leq 1$ and Reμ is positive as shown in Appendix II, it is clear that $\Gamma e^{-2\mu a}$ is always less than unity. Hence, it is permissible to expand:

$$[1-\Gamma e^{-2\mu a}]^{-1}=\sum_{m=0}^{\infty}(\Gamma e^{-2\mu a})^m. \tag{42}$$

From (42) the integral in (41) becomes a series of integrals:

$$H_{y_{21}}^{11}(0,z_0)=-\frac{i\omega\epsilon_2 V_1}{2\pi}\left[\int_{-\infty}^{\infty}\frac{e^{+ihz_0}}{\mu}dh+2\int_{-\infty}^{\infty}\frac{\Gamma e^{-2\mu a}e^{+ihz_0}}{\mu}\sum_{m=0}^{\infty}(\Gamma e^{-2\mu a})^m dh\right]. \tag{43}$$

Let

$$I_0=\int_{-\infty}^{\infty}\frac{e^{+ihz_0}}{\mu}dh$$

$$I_1=2\int_{-\infty}^{\infty}\frac{\Gamma e^{-2\mu a}e^{+ihz_0}}{\mu}dh$$

$$I_2=2\int_{-\infty}^{\infty}\frac{\Gamma^2 e^{-4\mu a}e^{+ihz_0}}{\mu}dh$$

$$\vdots$$

$$I_m=2\int_{-\infty}^{\infty}\frac{\Gamma^m e^{-2m\mu a}e^{+ihz_0}}{\mu}dh. \tag{44}$$

As shown in Appendix II, Re μ is always positive along the integration contours. It is apparent that as $a\rightarrow\infty$, a situation in which the slots are immersed in an unbounded plasma medium, all the terms except I_0 vanish. In terms of the reflection coefficient (Γ), I_0 represents contribution when there are no reflections ($\Gamma=0$), and I_1 represents the contribution due to rays emanating from S_1 toward the interface, which partially reflects them toward S_2. These reflected rays may be interpreted as coming from image sources located at $X=\pm 2a$. The strength of these rays is weighed by the appropriate reflection coefficient. Similarly, I_2 can be interpreted as a contribution from rays that have gone through two bounces of reflection by the interface. Alternately, these reflected rays come from image sources located at $X=\pm 4a$, the strength of which is weighed by Γ^2. Fig. 3 presents a physical picture of the reflection of rays that have gone through one bounce and two bounces to reach Slot S_2. It is clear that I_3 and I_4 through I_m represent contributions due to three, four, and m reflection bounces from the interface. The significance of these multiple reflection terms becomes less and less as the number of reflection bounces increases. For a relatively thick plasma, the first few terms should be sufficient.

The integral I_0 is evaluated in the complex h plane.

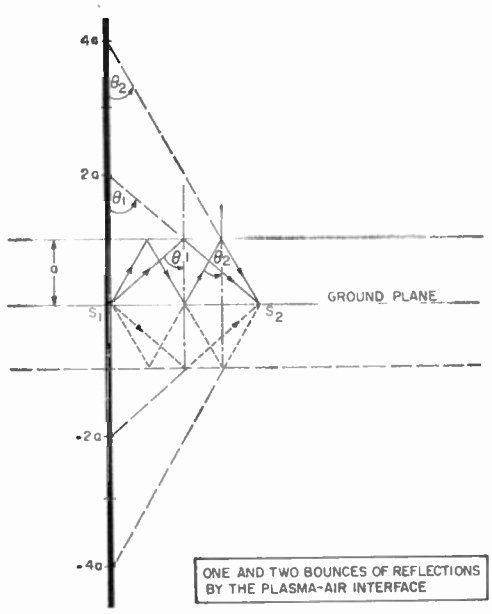

Fig. 3—Arrival of rays from slot S_1 to slot S_2.

The integrand has a branch point singularity when $\mu=0$. It has no poles; hence, it can be concluded that there are no waveguide-type modes excited in an unbounded plasma. By Cauchy's theorem on contour integration, the integral along the real axis is equivalent to the branch-cut integration as shown in Fig. 4. Hence:

$$I_0=\int_{-\infty}^{\infty}\frac{e^{+ihz_0}}{\mu}dh=\int_{\text{Branch Cut}}\frac{e^{+ihz_0}}{\mu}dh. \tag{45}$$

Let

$$h=-nk\sin\tau \quad \text{where} \quad \tau=\xi+i\eta. \tag{46}$$

The new contour in the complex τ plane is shown in Fig. 5. To be consistent with the convergence requirements along the contour, it is necessary that

$$\mu=\sqrt{h^2-n^2k^2}=-ink\cos\tau. \tag{47}$$

In terms of τ, the integral I_0 becomes [11]:

$$I_0=\frac{1}{i}\int_p e^{-inkz_0\sin\tau}d\tau=\frac{\pi}{i}H_0^{(2)}(nkz_0). \tag{48}$$

The perturbation terms I_1 and I_2 through I_m which involve the powers of Γ are more difficult to evaluate. The integrand has two branch points which arise when $\lambda=0$ and $\mu=0$. However, for a thick plasma when $a>z_0$ and $nka\gg 1$, the contribution from the μ branch may be approximated by the method of steepest descent and the contribution from the λ branch will be negligible.

Consider the general term I_m which is:

$$I_m=2\int_{-\infty}^{\infty}\frac{\Gamma^m e^{-2m\mu a}e^{+ihz_0}}{\mu}dh. \tag{49}$$

It was stipulated that μ has a positive real part. Because $a>z_0$, the integral will converge along the contour of integration.

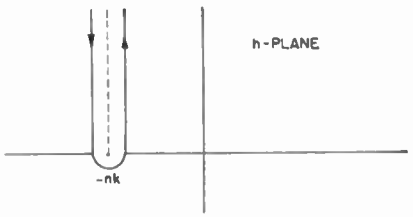

Fig. 4—Contour of branch-cut integration of I_0 in the h plane.

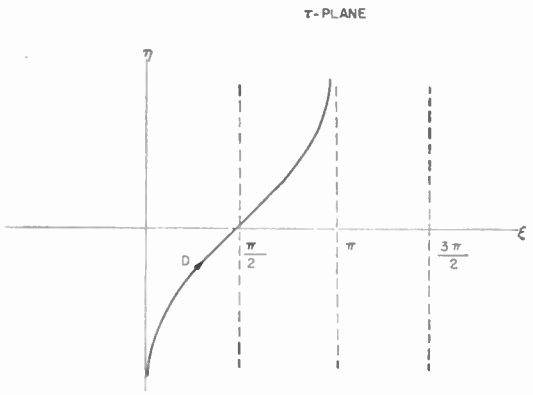

Fig. 5—Contour of branch-cut integration of I_0 in the τ plane.

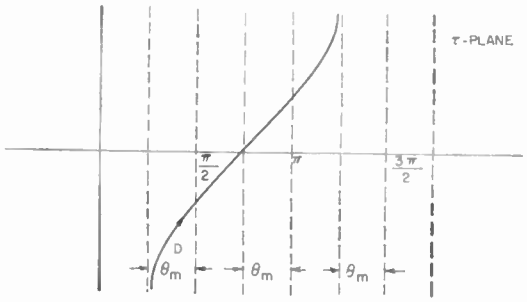

Fig. 6—Contour of the μ branch-cut integration of I_m in the τ plane.

Let

$$z_0 = r_m \sin \theta_m \tag{50}$$

$$2ma = r_m \cos \theta_m. \tag{51}$$

Hence:

$$\theta_m = \tan^{-1}\left(\frac{z_0}{2ma}\right) \tag{52}$$

$$r_m^2 = (2ma)^2 + z_0^2. \tag{53}$$

In terms of τ, (49) becomes:

$$I_m = \frac{2}{i}\int_D \Gamma^m e^{+ikr_m \cos(\tau+\theta_m)} d\tau. \tag{54}$$

The contour of integration is shown in Fig. 6.

The integrand is stationary when:

$$\frac{\partial}{\partial \tau}\cos(\tau + \theta_m) = -\sin(\tau + \theta_m) = 0$$

$$\tau_m = \pi - \theta_m \tag{55}$$

where θ_m is the angle of incidence of a ray from S_1 that has gone through m bounces of reflection to reach S_2.

By using the method of steepest descent and when $nkr_m \gg 1$, (54) becomes [12]:

$$I_m = \frac{2}{i}\Gamma^m(\tau_m)\int_D e^{ikr_m \cos(\tau+\theta_m)} d\tau$$

$$= \frac{2\pi}{i}\Gamma^m(\pi - \theta_m) H_0^{(2)}(nkr_m)$$

$$= \frac{2\pi}{i}\Gamma^m(\theta_m) H_0^{(2)}(nkr_m). \tag{56}$$

The above development brings out the phenomenon of multiple reflections by the plasma-air interface. The λ branch-cut integration contributes because of the refracted rays. However, inside the plasma region it is reasonable to expect such contributions to be negligible in the case of a thick plasma layer. In the neighborhood of the branch point when $\lambda = 0$; $h = -k$:

$$\mu^2 \sim k^2(1 - n^2)$$

$$\Gamma \sim 1. \tag{57}$$

In view of the approximation in (57), the general term I_m becomes:

$$I_m \sim 2\int_{\lambda \text{ branch}} \frac{e^{-2mak(1-n^2)^{1/2}} e^{+ihz_0}}{k\sqrt{1 - n^2}} dh. \tag{58}$$

The expression of (58) is analytic near the branch point $h = -k$ in the h plane; hence, the net contribution along both sides of the λ branch cut is zero.

If the branch-cut integration is carried out asymptotically, each term is attenuated by an exponential factor of $e^{-2mka(1-n^2)^{1/2}}$; where $m = 1, 2 \cdots$.

In summary of the preceding development, the magnetic field $Hy_{21}^{II}(0, z_0)$ in Region II in the presence of a thick plasma is:

$$H_{y_{21}}^{II}(0, z_0) = -\frac{\omega\epsilon_2 V_1}{2}\left[H_0^{(2)}(nkz_0) + 2\sum_{m=1}^{\infty}\Gamma^m(\theta_m) H_0^{(2)}(nkr_m)\right] \tag{59}$$

where θ_m and r_m are defined by (52) and (53).

B. In the Presence of a Thin Plasma Layer

When Hy_{21}^{II} is in the presence of a thin plasma layer, the image sources are located close together, and the incident angles for all rays from S_1 are almost at grazing with the interface ($\theta_0 \cong 90°$). This gives a reflection coefficient magnitude of almost unity. The series obtained in (59), when applied to the present case, converges too slowly to be of use. Therefore, the integral must be evaluated in another way.

It is convenient to write the $Hy_{21}^{II}(0, z_0)$ integral as:

$$H_{y_{21}}{}^{II}(0, z_0) = -\frac{i\omega\epsilon_2 V_1}{2\pi}\int_{-\infty}^{\infty}\frac{e^{+ihz_0}}{\mu}\cdot\left[\frac{\mu\epsilon_1 + \lambda\epsilon_2\tanh\mu a}{\lambda\epsilon_2 + \mu\epsilon_1\tanh\mu a}\right]dh. \quad (60)$$

When $ka \ll 1$ and $\tanh \mu a \cong \mu a$ (60) becomes:

$$H_{y_{21}}{}^{II}(0, z_0) = -\frac{i\omega\epsilon_2 V_1}{2\pi}\int_{-\infty}^{\infty}\frac{e^{+ihz_0}(\epsilon_1 + \epsilon_2\lambda a)}{(\lambda\epsilon_2 + \mu^2\epsilon_1 a)}\,dh. \quad (61)$$

The expression for $Hy^{II}(0, z_0)$ in (61) needs to be evaluated, either analytically or numerically. It is possible by employing Watson's lemma to arrive at an asymptotic series which is valid for large slot separation and finite plasma thickness. However, an expression which is valid for small z_0 has yet to be found. Because the plasma is physically thin, it is reasonable to look for major contributions to come from the situation when there is no layer and perturbations because of the layer.

In terms of a typical operating frequency employed in a hypersonic re-entry vehicle, a frequency in the X-band region (10 kMc), the thin plasma case is not too applicable. Under almost every flight environment, the plasma sheath created about the vehicle is many wavelengths thick.

V. Examination of Theoretical Results

In Section IV, the magnetic field or the surface current on the ground plane at $z = z_0$, the location of the second slot S_2 has been evaluated for three different situations: 1) unbounded plasma medium, 2) thick plasma layer, and 3) no plasma (free space).

When the surface current is known, it is possible to determine the various admittance parameters defined in Section III.

A. Mutual Admittance

The mutual admittance parameter Y_{12} is related to the surface current by (32). The results for Y_{12} under various situations can be readily tabulated as follows:

1) unbounded plasma medium:

$$Y_{12}{}^{p} = \frac{\omega\epsilon_2}{2}H_0{}^{(2)}(nkz_0); \quad (62)$$

2) thick plasma layer:

$$Y_{12}{}^{p} = \frac{\omega\epsilon_2}{2}\left[H_0{}^{(2)}(nkz_0) + 2\sum_{m=1}^{\infty}\Gamma^m(\theta_m)H_0{}^{(2)}(nkr_m)\right]; \quad (63)$$

3) no plasma (free space):

$$Y_{12}{}^{a} = \frac{\omega\epsilon_1}{2}H_0{}^{(2)}(kz_0). \quad (64)$$

To illustrate the effect of the plasma layer on Y_{12}, the ratio of the absolute value of $Y_{12}{}^{p}$, and $Y_{12}{}^{a}$, $|Y_{12}{}^{p}/Y_{12}{}^{a}|$ is plotted as a function of the slot separation kz_0 for two different plasma-layer thicknesses: 1) $ka \to \infty$, and 2) $ka = 10$. Fig. 7 presents the results for $n = 0.9$ ($\omega_p/\omega = 0.436$), for $n = 0.7$ ($\omega_p/\omega = 0.714$), and for $n = 0.5$ ($\omega_p/\omega = 0.865$).

In the thick plasma-layer case, the reflections from the plasma-air interface cause the curve to ripple about the dominant term. The perturbations become greater as the index of refraction departs further from unity. This is reasonable because as the two media become more different, the interface causes larger reflections. The effect is demonstrated for the cases of $n = 0.9$, $n = 0.7$, and $n = 0.5$. Fig. 8 shows three reflection-coefficient Γ curves as a function of the index of refraction n. Another point of interest is that mutual admittance in the presence of a plasma layer, whether it is thick or unbounded, is less than when there is no plasma. In the unbounded case, the ratio approaches the asymptotic ratio of $n^{3/2}$ for fairly small kz_0 (*e.g.*, $kz_0 = 1$).

B. Self-Admittance

The results in Section V-A for the mutual admittance can easily be extended to the present situation for self-admittance (Y_{11}) by letting z_0 approach the half width of the slot, which is assumed to be thin. If W is the slot width, then Y_{11} for the three different situations is as follows:

1) unbounded plasma medium:

$$Y_{11}{}^{p} = \frac{\omega\epsilon_2}{2}H_0{}^{(2)}\left(nk\frac{W}{2}\right); \quad (65)$$

2) thick plasma layer:

$$Y_{11}{}^{p} = \frac{\omega\epsilon_2}{2}\left[H_0{}^{(2)}\left(nk\frac{W}{2}\right) + 2\sum_{m=1}^{\infty}\Gamma^m(\theta_m \sim 0)H_0{}^{(2)}(2nkma)\right]; \quad (66)$$

3) no plasma (free space):

$$Y_{11}{}^{a} = \frac{\omega\epsilon_1}{2}H_0{}^{(2)}\left(k\frac{W}{2}\right). \quad (67)$$

C. Driving Point Admittance

The driving point admittance (Y_1') for each slot in the presence of the other as defined in Section III in terms of the other admittance parameters, is given by either (33) or (34). Since slot S_1 and slot S_2 are identical, the self-admittance Y_{11} of slot one and Y_{22} of slot two are equal. Values for Y_{12} and Y_{11} under various conditions may be obtained from expressions given in this section. With these known parameters, the driving point admittance (Y_1') may be readily evaluated. In the absence of mutual effects, Y_1' reduces to the self admittance Y_{11} of the slot. Fig. 9 is a plot of the ratio of the absolute values of $Y_1'{}^{p}$ and $Y_1'{}^{a}$ as a function of the slot separation kz_0. The quantity $Y_1'{}^{p}$ is the driving point

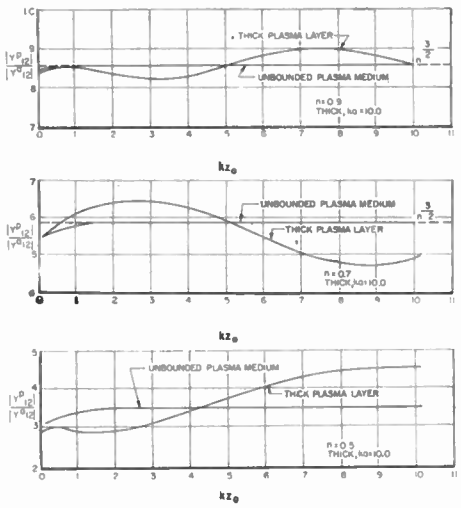

Fig. 7—Mutual admittance ratio vs slot separation.

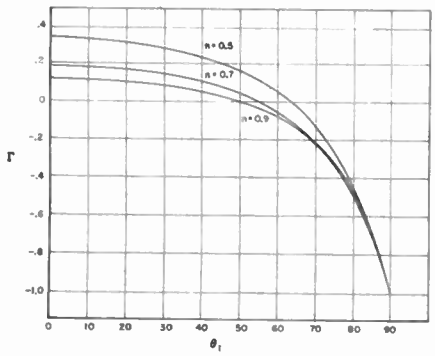

Fig. 8—Reflection coefficient vs angle of incidence.

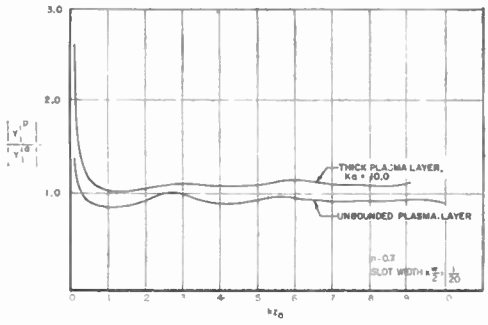

Fig. 9—Driving point admittance ratio vs slot separation.

admittance of slot S_1 in the presence of a plasma medium, and $Y_1'^a$ is the same parameter in free space. Two cases are shown in Fig. 9, unbounded plasma and a thick plasma layer. For the particular parameters shown, the curves for both cases indicated that the perturbations introduced by the plasma medium were not too serious. Of course, these variations in Y_1' affect the input VSWR of the antenna to a certain extent. Fortunately, the effect may not be too appreciable.

VI. Conclusions

The plasma model of an equivalent lossless, gaseous dielectric slab may have been too elementary to be realistic for re-entry conditions. The least realistic is perhaps the sharply defined plasma-air interface. However, such a model was employed to minimize the mathematical complexities of the problem. The situation when the equivalent dielectric constant of the plasma layer is negative has not been considered in detail because the region of interest is the operating frequency above the plasma frequency. In view of the foregoing investigation, several interesting points concerning the effects of a plasma layer on the antenna admittance characteristics have been uncovered.

1) There are no unattenuating pole waves excited inside the plasma layer whose equivalent dielectric constant is less than unity but greater than zero. However, the statement may not be true when the operating frequency is below the plasma frequency. Under this situation, the equivalent dielectric constant is negative.
2) Mutual coupling is less serious in the presence of a thick or unbounded plasma layer than in free space. In an unbounded plasma layer, the reduction approaches the asymptotic value of $n^{3/2}$ for small slot separations. When the plasma is thick, because of reflections from the interface, the mutual admittance parameter ripples about the value for the unbounded case. However, in an actual re-entry situation, the plasma-air boundary will not be sharply defined and these variations will probably appear in a statistical manner centering on the value for the unbounded case.[1]
3) The driving point admittance is not seriously affected by the presence of a thick layer of weakly ionized plasma whose index of refraction for the operating frequency is close to unity. When the slot is matched initially to free space, it will remain fairly well matched in the presence of the plasma layer.

Appendix I

It is possible to show that $\Gamma = (\mu\epsilon_1 - \lambda\epsilon_2)/(\mu\epsilon_1 + \lambda\epsilon_2)$ is equivalent to the reflection coefficient of the magnetic field when a plane wave is incident on the plasma-air interface. When the magnetic-field vector is normal to

[1] The reason for the decrease in coupling as shown in Fig. 7 is that the slots in the presence of a plasma medium are less heavily excited. The equivalent voltage of excitation for slot S_1 is $V_{eq} = \epsilon_2 V_1$. This means that an aperture antenna which is initially matched to free space will be a less efficient radiator in the presence of a thick or unbounded plasma layer. A part of incident power at the aperture will be reflected and the amount is proportional to

$$\left| \frac{1 - \epsilon_2/\epsilon_1}{1 + \epsilon_2/\epsilon_1} \right|^2.$$

However, if some automatic tuning device is incorporated in the feeding network of the antenna such that a match to the intrinsic admittance of the plasma medium is maintained, then the amount of power appearing at the aperture will be the same. Under this condition, the mutual coupling for the two slots actually increases. The plasma medium in essence brings the two slots closer together. The ordinate for the curves shown in Figs. 7 and 9 should be multiplied by the factor $1/n^2$.

the plane of incidence and parallel to the plasma-air interface, the ratio of the reflected magnetic field (H_{y_2}) and the incident magnetic field (H_{y_0}) is given by (19) in Stratton [13]. This equation is:

$$\Gamma = \frac{H_{y_2}}{H_{y_0}} = \frac{\mu_2 k_1 \cos\theta_0 - \mu_1 k_2 \cos\theta_1}{\mu_2 k_1 \cos\theta_0 + \mu_1 k_2 \cos\theta_1} \tag{68}$$

where θ_0 is the angle of incidence and θ_1 is the angle of refraction. Since $\mu_1 = \mu_2$ (68) can be written:

$$\Gamma = \frac{\epsilon_1 k_2 \cos\theta_0 - \epsilon_2 k_1 \cos\theta_1}{\epsilon_1 k_2 \cos\theta_0 + \epsilon_2 k_1 \cos\theta_1} . \tag{69}$$

Let

$$h = -k_2 \sin\theta_0 = -k_1 \sin\theta_1. \tag{70}$$

The relationship in (70) is merely a statement of Snell's Law of Refraction across the interface. In view of (70) and to be consistent with the convergence requirements of the context of the paper, the parameters λ and μ must necessarily be:

$$\lambda = -ik_1 \cos\theta_1 \tag{71}$$

$$\mu = -ik_2 \cos\theta_0. \tag{72}$$

In terms of λ and μ, the reflection coefficient from (69) becomes:

$$\Gamma = \frac{\mu\epsilon_1 - \lambda\epsilon_2}{\mu\epsilon_1 + \lambda\epsilon_2} . \tag{73}$$

Appendix II

It is also possible to show that μ always has a positive real part along the real axis in the h plane. For the time dependence of $e^{i\omega t}$, assume:

$$k = k_1 - ik_2 \tag{74}$$

where

$$k_2 \ll k_1.$$

In the h plane, the integration along the real axis from $-\infty$ to $+\infty$ lies in the strip-$ink_2 < \beta < +ink_2$, as shown in Fig. 10. Inside the strip, let ϕ_1 be the phase of $h+nk$ and ϕ_2 be the phase of $h-nk$.

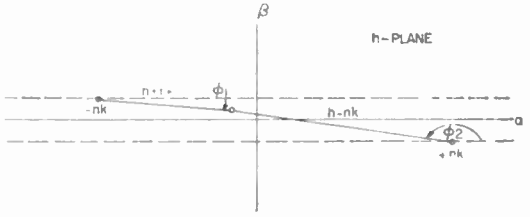

Fig. 10—Phase of μ in the h plane.

Because

$$\mu = \sqrt{(h - nk)(h + nk)} \tag{75}$$

the phase of μ is one half the sum of ϕ_1 and ϕ_2.

$$-\pi \leq \phi_1 \leq 0 \quad \text{and} \quad 0 \leq \phi_2 \leq \pi. \tag{76}$$

Hence:

$$|\text{phase } \mu| = \tfrac{1}{2}|\phi_1 + \phi_2| < \frac{\pi}{2} . \tag{77}$$

Eq. (77) proves that the real part of μ is always positive. Because of this requirement, when transforming into the τ plane, μ must take on the negative sign.

$$\mu = -ink \cos\tau. \tag{78}$$

The above proof is similar to problem 3 in Noble [12].

Appendix III

Existence of Unattenuating Pole Waves

Starting with the integral for Hy_{21}^{II} as in (41):

$$H_{y_{21}}^{II}(0, z_0) = -\frac{i\omega\epsilon_2\Gamma_1}{2\pi} \int_{-\infty}^{\infty} \frac{1 + \Gamma e^{-2\mu a}}{1 - \Gamma e^{-2\mu a}} \frac{e^{+ihz_0}}{\mu} dh. \tag{79}$$

It is necessary to examine the situation when $1 - \Gamma e^{-2\mu a} = 0$. Solutions to this characteristic equation give rise to pole singularities of the integrand. Their contributions can be evaluated by residue technique. Physically, these singularities represent characteristic wave modes which can be excited inside the plasma layer. These modes are similar to waveguide modes. Because of the multiple-valued behavior of the parameters λ and μ, the solutions must be examined rather critically to make sure that they are consistent with the stipulations of the problem. Mathematically, the poles must be located on the proper Riemann sheet in which the integration is carried out. A more general and thorough investigation of the existence of pole waves has been conducted by Karbowiak [10]. The results shown here are consistent with Karbowiak's findings. Consider the characteristic equation:

$$1 - \Gamma e^{-2\mu a} = 0 \tag{80}$$

where

$$\Gamma = \frac{\mu\epsilon_1 - \lambda\epsilon_2}{\mu\epsilon_1 + \lambda\epsilon_2}$$

$$\lambda^2 = h^2 - k^2$$

$$\mu^2 = h^2 - n^2k^2.$$

After some algebraic manipulation, this equation can be written:

$$\mu\epsilon_1 \tanh \mu a + \lambda\epsilon_2 = 0$$

$$\tanh \mu a = -\frac{\lambda}{\mu}\frac{\epsilon_2}{\epsilon_1} . \tag{81}$$

Eq. (81) is exactly the same equation that Karbowiak [10] studied in his paper.

To analyze the outgoing waves in the $+z$ direction, it is necessary to concentrate on possible poles on the negative real axis in the h plane. Medium II is less dense than medium I.

Hence:

$$n^2 = \frac{\epsilon_2}{\epsilon_1} \leq 1. \tag{82}$$

Eq. (82) implies operation above the plasma frequency. For discussion, divide the negative real axis into three ranges as shown in Fig. 11.

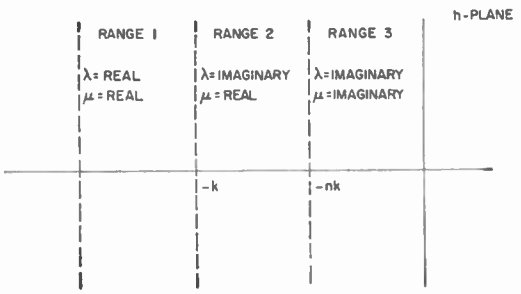

Fig. 11—Range of values of λ and μ in the h plane.

For k and n real, depending on the range of h, the parameters λ and μ may be real or imaginary along the real axis.

Range 1, $-k \leq -h \leq -\infty$
λ = real
μ = real
Range 2, $-nk \leq -h \leq -k$
λ = imaginary
μ = real
Range 3, $0 \leq -h \leq -nk$
λ = imaginary
μ = imaginary.

An investigation of (81) reveals that if λ is negative real, solutions are possible in Range 1. However, this stipulation of λ negative real violates the radiation condition of the fields in Region I. Therefore, the solutions are not admissible. Similarly, there are no solutions in Ranges 2 and 3. Hence, it is concluded that there are no unattenuating pole waves when medium II is less dense than medium I.

The above argument, however, does not rule out the possible existence of leaky waves. The poles that give rise to these waves are complex roots of the characteristic (81). They lie on the improper sheet of the Riemann surface on which the integration is carried out. In evaluating the transform integral by approximate techniques, it is customary to deform the contour into the one of steepest descent. A part of this deformed contour may lie in the improper sheet enclosing the leaky-wave poles which will contribute to the expansion of the integral. A leaky wave, unlike a surface wave, is characterized by a complex propagation constant along the interface, both in the longitudinal and in the transverse directions. It attenuates or leaks longitudinally but grows transversely. This report has not investigated the leaky-wave question thoroughly enough to ascertain its existence. Hence, its contribution to coupling cannot be evaluated. Intuitively, its contribution to coupling will probably be negligible because of its existence along the plasma-air interface which is quite remote from the slots in the thick plasma case.

The situation is different when medium II is more dense than medium I. In this case the index of refraction, $n = \sqrt{\epsilon_2/\epsilon_1}$, is greater than unity, and it can be demonstrated by similar argument that there are admissible solutions to the characteristic equation when $-k \leq -h \leq -nk$. Moreover, these poles waves can be shown to be slow waves (surface waves). It is possible to visualize three configurations that may give rise to pole waves:

1) medium I—free space
   medium II—solid dielectric
2) medium I—uniform unbounded plasma
   medium II—free space
3) medium I—free space
   medium II—plasma layer whose index of refraction is negative.

The first configuration corresponds to a dielectric slab on the ground plane and has been studied by Tai, Whitmer, Attwood [7], [8], [9], and others. The second situation may correspond to an elementary model of the ionosphere and conducting Earth. Also, it may represent a simplified model of a hypersonic vehicle upon reentry; Region I is then the plasma region and Region II is the region behind the shock and the surface of the vehicle. Finally, the third case corresponds to a situation when the operating frequency is below the plasma frequency of the layer.

Acknowledgment

The author wishes to express his appreciation to C. W. Armstrong, Chief of the Antennas and Radomes Unit, for the encouragements and support in the course of this investigation.

References

[1] W. S. Lucke, "Mutual Admittance of Slots in Cylinders," Stanford Res. Inst., Menlo Park, Calif., Tech. Rept. No. 36; February, 1953.
[2] S. Nishida, "Coupled leaky waveguides I: Two parallel slits in a plane," IRE Trans. on Antennas and Propagation, vol. AP-8, pp. 323–330; May, 1960.
[3] S. Nishida, "Coupled leaky waveguides II: Two parallel slits in a cylinder," IRE Trans. on Antennas and Propagation, vol. AP-8, pp. 354–360; July, 1960.
[4] S. Edelberg and A. A. Oliner, "Mutual coupling effects in large antenna arrays: Part I—Slot array," IRE Trans. on Antennas and Propagation, vol. AP-8, pp. 286–297; May, 1960.
[5] R. F. Whitmer, "Principles of microwave interactions with ionized media, part, I," *Microwave J.*, vol. 2, pp. 17–19; February, 1959.
[6] R. F. Whitmer, "Principles of microwave interactions with ionized media, part II," *Microwave J.*, vol. 2, pp. 47–50; March, 1959.
[7] C. T. Tai, "The effect of a grounded slab on the radiation from a line source," *J. Appl. Phys.*, vol. 22, pp. 405–414; April, 1951.
[8] R. M. Whitmer, "Fields in nonmetallic waveguides," Proc. IRE, vol. 36, pp. 1105–1109; September, 1948.
[9] S. S. Attwood, "Surface wave propagation over a coated plane conductor," *J. Appl. Phys.*, vol. 22, pp. 504–509; April, 1951.
[10] A. E. Karbowiak, "Radiation and guided waves," IRE Trans. on Antennas and Propagation (special suppl.), vol. AP-7, pp. s191–s200; December, 1959.
[11] A. Sommerfeld, "Partial Differential Equations," Academic Press Inc., New York, N. Y., p. 89; 1949.
[12] B. Noble, "The Wiener-Hopf Technique," Pergamon Press, Inc., New York, N. Y., pp. 34–35; 1958.
[13] A. Stratton, "Electromagnetic Theory," McGraw-Hill Book Co., Inc., New York, N. Y., ch. IX; 1941.
[14] E. C. Jordan, "Electromagnetic Waves and Radiating Systems," Prentice-Hall, Inc., chs. 11 and 15; 1950.
[15] N. W. McLachlan, "Complex Variable Theory and Transform Calculus," Cambridge University Press, Cambridge, Eng.; 1953.

Antenna Noise Temperature in Plasma Environment*

M. P. BACHYNSKI†, SENIOR MEMBER, IRE, I. P. FRENCH†, AND G. G. CLOUTIER†

Summary—**The total noise power available at a receiving antenna on a hypervelocity space vehicle is determined by considering the engulfing plasma sheath as a uniform slab of plasma. The noise emission from the plasma is treated as a boundary-value problem which for this simple model can be completely solved. The effect of the hot vehicle surface and other external sources is included.**

The general conclusions are that for an isotropic plasma the main noise contributions result from the vehicle surface for RF frequencies well below the plasma frequency, from external sources for RF frequencies well above the plasma frequency, and from direct emission by the plasma for RF frequencies about the plasma frequency. The noise power from the plasma is the most significant and exhibits a pronounced peak at an RF frequency just above the plasma frequency.

The effect of an anisotropic plasma sheath (due to an auxiliary magnetic field carried by the vehicle) has been investigated for magnetic field orientations normal to and parallel to the plasma. The anisotropy completely alters the spectral characteristics of the available noise power resulting in several frequency regions of weak and intense noise emission.

I. Introduction

THE advent of space exploration and missile technology has posed many communication and diagnostic problems. Among these is the behavior of antennas in an ionized environment such as the plasma sheath which forms about a hypersonic vehicle in a planetary atmosphere. Such information is essential in order to optimize systems parameters for communications and telemetry and for possible investigations of the engulfing shock front and plasma environment.

One topic of current interest is the noise power available to a receiving antenna located on board a hypervelocity vehicle. In this paper, the plasma sheath is approximated by a uniform plasma slab and the noise emission spectrum from the plasma determined from the absorptivity using a generalized form of Kirchhoff's law. In addition, the effect of the hot vehicle surface and external sources can be included by utilizing the reflectivity and transmissivity of the plasma. A numerical example illustrates the analytical considerations. Optimum frequencies for either maximum or minimum noise signals and for rapid transition regions can be ascertained from the analysis. Finally, the effect of anisotropy in the plasma (due to an auxiliary magnetic field on the space vehicle) is investigated and the spectral characteristics determined.

* Received by the IRE, August 14, 1961. Some of the computations of the electromagnetic parameters were performed under Contract No. AF19(604)-7334 with the AF Cambridge Res. Labs., and under Contract No. GX9-998054-0001-70-Q82 with RCA Moorestown, Missile and Surface Radar Div.

† Res. Labs., RCA Victor Co. Ltd., Montreal, Canada.

II. Antenna Noise Power

A receiving system under normal operating conditions will be subjected to two sources of noise—the noise signals originating from external sources which are received by the receiving antenna and the noise generated in the receiver components. In this treatise, the receiver noise will be omitted entirely, and only the effect of external sources on the receiving antenna considered.

The noise power P available to a receiving antenna (assumed to be matched to its surrounding environment) in a frequency interval between f and $f+\Delta f$ is given by:

$$P = \gamma A \Phi \Delta f,$$

where

γ = polarization coefficient (for instance, if the noise signal is randomly polarized, $\gamma = \frac{1}{2}$),

A = effective antenna area,

Φ = energy or power flux density at the receiving antenna,

Δf = frequency interval under consideration.

Let a radiating body with emissive power P_ω (where P_ω is the radiated power in a direction normal to the surface of the radiating body per unit frequency interval, per unit solid angle and per unit surface area for a given polarization) subtend a solid angle Ω_s at the receiving antenna (Fig. 1). The solid angle $\Omega_s = a_0/r^2$, where a_0

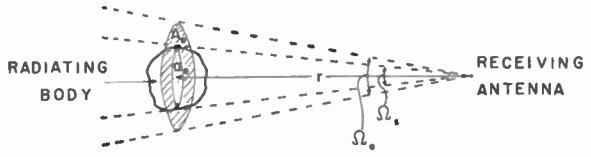

Fig. 1—Geometry for determining noise power available at receiving antenna.

is the projected area normal to and a distance r from the receiving antenna. Let the beam of the receiving antenna power pattern subtend a solid angle Ω_a where in the plane of the emitting body, $\Omega_a = A_0/r^2$. The power emitted per unit area of the radiating body is $4\pi P_\omega$, so that the power emitted by the area a_0 "seen" by the receiving antenna is $4\pi P_\omega a_0$. Hence, the flux density of power at the receiving antenna is

$$\Phi = 4\pi P_\omega a_0 / r^2.$$

Note that if the projected area of the emitting surface just fills the antenna beam or is larger than the projected area intercepted by the antenna beam, then the receiving antenna sees an area $a_0 = A_0$. In this case $a_0/r^2 = A_0/r^2 = \Omega_a$, the solid angle of the power pattern beam of the receiving antenna. If the emitting area a_0 is less than the area A_0 intercepted by the receiving antenna power pattern at the source, then the antenna "sees" only the area a_0. In this case we can write

$$\frac{a_0}{r^2} = \Omega_a \cdot \frac{\Omega_s}{\Omega_a}.$$

Thus, in summary, the total power flux density at the receiving antenna is

$$\Phi = 4\pi P_\omega \Omega_a \qquad \Omega_a \leq \Omega_s, \tag{2a}$$

$$\Phi = 4\pi P_\omega \Omega_a \left(\frac{\Omega_s}{\Omega_a}\right) \qquad \Omega_a \geq \Omega_s. \tag{2b}$$

The effective area of an antenna is[1]

$$A = \frac{\lambda^2}{4\pi} G_{\max}, \tag{3a}$$

and the solid angle of the power pattern of a receiving antenna is

$$\Omega_a = 4\pi/G_{\max}, \tag{3b}$$

where the antenna power gain $G(\theta, \phi)$ is defined in the usual manner, as:

$$G(\theta, \phi) = \frac{P(\theta, \phi)/\text{unit solid angle}}{P_{\text{total}}/4\pi} = \frac{4\pi P(\theta, \phi)}{\iint_{4\pi} P(\theta, \phi) d\Omega},$$

and $G_{\max}$ is the maximum value of $G(\theta, \phi)$; θ, ϕ are the elevation and azimuth spherical coordinates.

Utilizing (2) and (3) in (1), the total noise power is

$$P = \gamma 4\pi\lambda^2 P_\omega \Delta f \left(\frac{\Omega_s}{\Omega_a}\right), \tag{4}$$

where we take $\Omega_s/\Omega_a = 1$ when the solid angle of the source at the antenna exceeds the antenna beam angle, *i.e.*, $\Omega_s \geq \Omega_a$.

The available noise power attains a particularly simple form when appropriate forms for the emissive power P_ω are chosen. Thus, for equilibrium radiation:

1) Rayleigh-Jeans Approximation—in the Rayleigh-Jeans limit[2] (appropriate for long wavelengths such as those corresponding to microwave frequencies),

$$P_\omega = \frac{\kappa T_{\text{eff}}}{2\pi\lambda^2}$$

where κ is Boltzmann's constant and T_{eff} is the effective temperature of the emitting body. (For a black body, T_{eff} is the actual body temperature). Consequently, the available noise power is

$$P = 2\gamma\kappa T_{\text{eff}} \Delta f \left(\frac{\Omega_s}{\Omega_a}\right). \tag{5}$$

2) Kirchhoff's Law—a general formulation[3,4] of Kirchhoff's law for the energy radiated by a body, which enables the effective temperature to be evaluated from the electromagnetic properties of the body, gives

$$P_\omega = \frac{\kappa T}{2\pi\lambda^2} A_\omega$$

where A_ω is the power absorptivity of the body (an absorptivity of unity corresponds to a black body) and T is the temperature of the body. Thus the available noise power is

$$P = 2\gamma\kappa T A_\omega \Delta f \left(\frac{\Omega_s}{\Omega_a}\right), \tag{6}$$

so that

$$T_{\text{eff}} = T A_\omega.$$

The noise power at the receiving antenna can thus be calculated provided the absorptivity A_ω of the emitting body is known.

If more than one source of noise power lies in the beam of the receiving antenna, the contribution of each source must be evaluated as indicated above, and the sum of the individual contributions will give the total available noise power at the receiving antenna.

III. Noise Power Emission from an Isotropic Plasma Slab

In order to calculate the noise emission from a body, it is sufficient to know the absorptivity of the body. The absorptivity A_ω is defined as the fraction of energy absorbed by a body when a plane-polarized electromagnetic wave is incident upon it. Thus,[3,4]

$$A_\omega = \frac{\int_V \frac{1}{2} \operatorname{Re}(J \cdot E^*) dV}{\int_S \frac{1}{2} \operatorname{Re}(E_i \times H_i^*) dS}, \tag{7}$$

[1] J. C. Slater, "Microwave Transmission," Dover Publications, Inc., New York, N. Y., ch. 6, p. 264; 1959.
[2] F. K. Richtmeyer and E. H. Kennard, "Introduction to Modern Physics," McGraw-Hill Book Co., Inc., New York, N. Y., ch. 5; 1942.
[3] S. M. Rytov, "Theory of Electrical Fluctuations and Thermal Radiation," Academy of Sciences Press, Moscow, USSR; 1953.
[4] M. L. Levin, "The electrodynamic theory of thermal radiation," *Dokl. Akad. Nauk, USSR*, vol. 102, p. 53; 1955. Also see *Soviet Phys. JETP*, vol. 4, p. 225; 1957.

where J and E are the current density and the electric field in the body due to an incident electromagnetic field (E_i, H_i) on the body. The numerator represents the energy absorbed due to Joule losses by the body and can in principle be obtained from the electromagnetic properties of the body. The denominator represents the energy incident on the body.

The evaluation of the absorptivity is a boundary-value problem which has only been solved for very simple geometries.

Consider a uniform, infinite plasma slab of thickness d. Assume that the plasma is in thermal equilibrium, that the electron density is uniform and isotropic throughout the plasma and that the boundaries are infinitely sharp. This simple model neglects diffraction effects (since the slab is infinite), but does include interference phenomena (due to multiple internal reflections). These interference effects markedly affect the noise power emitted by the slab (as will be shown). An approximation to a more realistic plasma model which has gradual boundaries and nonlinear electron distributions can be made by applying this approach to a layer of uniform plasma slabs, each with different electrical properties.

Considering a plane electromagnetic wave to be normally incident on the plasma slab, applying Maxwell's equations and matching wave solutions at the boundaries, it is easy to obtain the fraction of incident electromagnetic energy which is transmitted through and reflected from the plasma slab. The power absorptivity can then be obtained from

$$A_\omega = 1 - R_\omega - T_\omega, \tag{8a}$$

where R_ω, T_ω are the power reflectivity and power transmissivity, respectively, of a plane wave incident normally on the slab surface. The corresponding expressions for the transmissivity and reflectivity in terms of the electromagnetic properties and thickness of the plasma slab are[5]

$$T_\omega = \left|(P^2+Q^2)(\sinh^2 \alpha d+\sin^2 \beta d)+2P \cosh \alpha d \sinh \alpha d + \sinh^2 \alpha d+\cos^2 \beta d-2Q \sin \beta d \cos \beta d\right|^{-1}, \tag{8b}$$

$$R_\omega = (L^2+M^2)(\sinh^2 \alpha d+\sin^2 \beta d)T_\omega, \tag{8c}$$

where

$$P = \frac{\beta}{2k}\frac{(k^2+\alpha^2+\beta^2)}{\alpha^2+\beta^2}, \qquad Q = \frac{\alpha}{2k}\frac{(k^2-\alpha^2-\beta^2)}{\alpha^2+\beta^2},$$

$$L = \frac{\beta}{2k}\frac{(k^2-\alpha^2-\beta^2)}{\alpha^2+\beta^2}, \qquad M = \frac{\alpha}{2k}\frac{(k^2+\alpha^2+\beta^2)}{\alpha^2+\beta^2}.$$

[5] I. P. French, G. G. Cloutier, and M. P. Bachynski, "Electromagnetic Wave Propagation and Radiation Characteristics of Anisotropic Plasmas," RCA, Montreal, Canada, Res. Rept. 7-801, 8, November, 1960.

$k = 2\pi/\lambda$ = wave number,

$\alpha/k = [\frac{1}{2}(|K| - K_r)]^{1/2}$ = normalized attenuation coefficient of the plasma,

$\beta/k = [\frac{1}{2}(|K| + K_r)]^{1/2}$ = normalized phase coefficient of the plasma,

$K = K_r - jK_i$ = dielectric coefficient of the plasma with real part K_r and imaginary part K_i, and

$|K| = [K_r^2 + K_i^2]^{1/2}$.

The dielectric coefficient of a plasma depends on the electron density, collision frequency, RF frequency, magnetic field strength and orientation should a magnetic field be present.

For a uniform plasma in the absence of magnetic fields and neglecting ion effects, the dielectric coefficient of the plasma is[6]

$$K = K_r - jK_i = \left(1 - \frac{\omega_p^2}{\omega^2}\frac{1}{1+\nu^2/\omega^2}\right) - j\left(\frac{\omega_p^2}{\omega^2}\frac{\nu/\omega}{1+\nu^2/\omega^2}\right),$$

where

ω_p = the plasma frequency $= (ne^2/m\epsilon_0)^{1/2}$, and ν the electron collision frequency considered to be independent of electron velocity. A discussion of the validity of this assumption and extensive numerical results have been presented by Shkarofsky, *et al.*[7]

n = the electron density

e, m = the electronic charge and mass, respectively, and

ϵ_0 = the permittivity of free space.

Choosing a fixed slab thickness ($d/\lambda_p = 2.5$, where λ_p is the wavelength corresponding to the plasma frequency and hence is a measure of electron density), typical variations of the transmissivity, reflectivity and absorptivity for a plasma slab as a function of ν/ω_p are shown in Fig. 2(a)–(c). These results will be utilized in Section IV.

Note the sharp transitions which occur around the region where the plasma frequency equals the RF angular frequency. At low collision frequencies, the reflectivity is very large for frequencies below the plasma frequency and small for RF frequencies above the plasma frequencies. The reverse is true for the transmissivity. The absorptivity, however, has a peak around the plasma frequency. This is due to the fact that for $\omega < \omega_p$ the reflections are so large that very little energy penetrates into the plasma, while for $\omega > \omega_p$ the plasma is

[6] M. P. Bachynski, I. P. Shkarofsky, and T. W. Johnston, "Plasmas and the Electromagnetic Field," McGraw-Hill Book Co., Inc., New York, N. Y. (in press).

[7] I. P. Shkarofsky, M. P. Bachynski, and T. W. Johnston, "Collision frequency associated with high temperature air and scattering cross-sections of the constituents," in "Electromagnetic Effects of Re-Entry," Pergamon Press, New York, N. Y.; 1961.

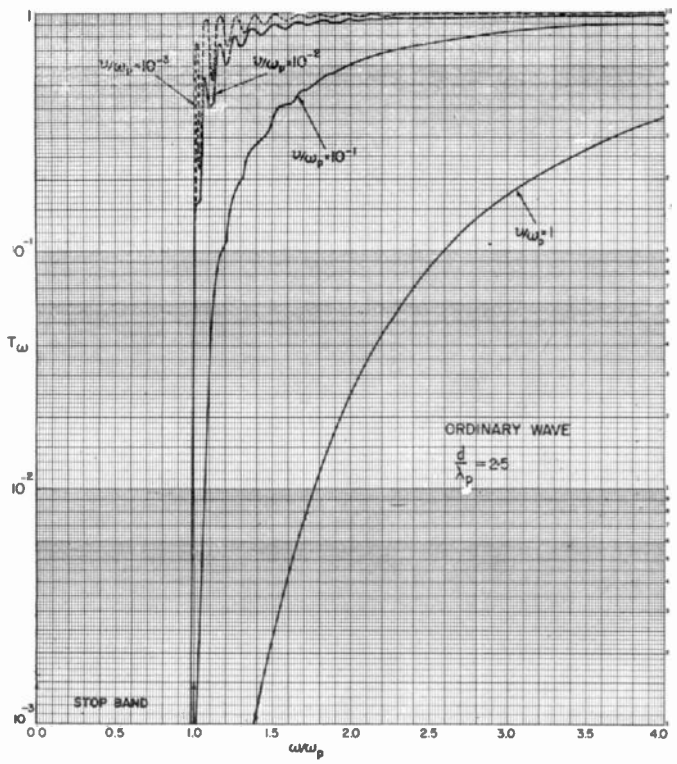

(a)

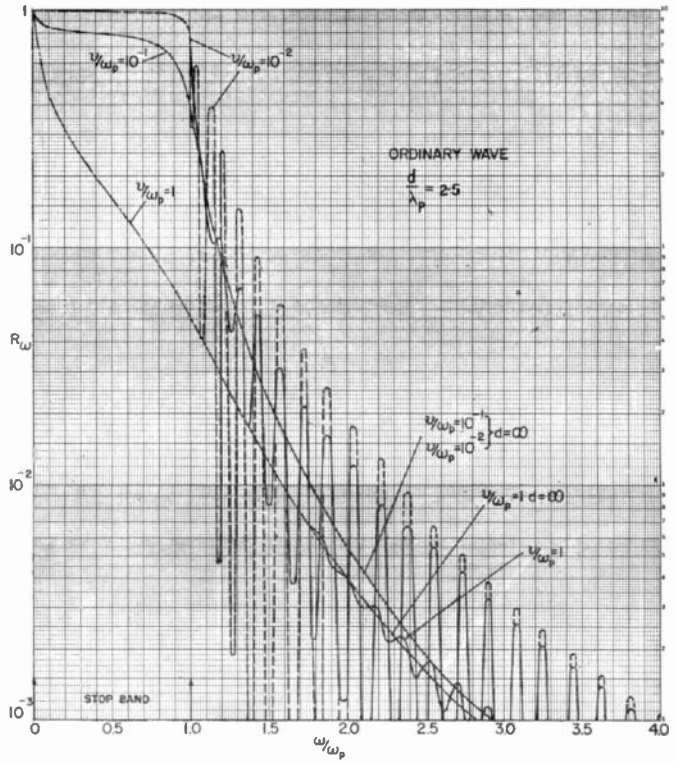

(b)

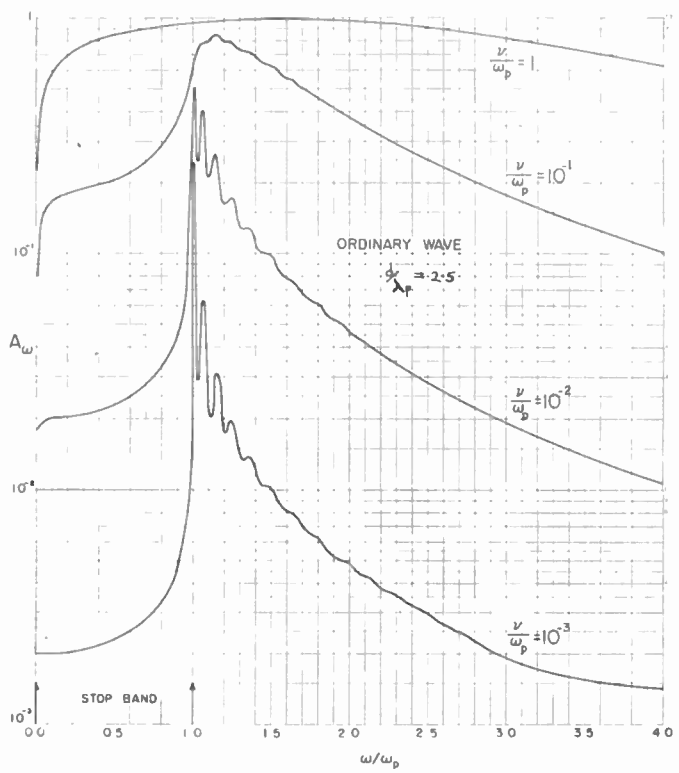

(c)

Fig. 2—(a) Transmissivity (T_ω) of an isotropic plasma slab as a function of RF frequency for various electron collision frequencies for a thickness $d/\lambda_p = 2.5$. (b) Reflectivity (R_ω) of an isotropic plasma slab as a function of RF frequency for various electron collision frequencies for a thickness $d/\lambda_p = 2.5$. (c) Absorptivity (A_ω) of an isotropic plasma slab as a function of RF frequency for various electron collision frequencies for a thickness $d/\lambda_p = 2.5$.

very nearly transparent and hence very little energy is absorbed. The peak absorption thus occurs in the region $\omega \approx \omega_p$, where the attenuation coefficient is high and a considerable amount of the incident energy penetrates the first boundary. As the collision frequency is increased, the reflectivity decreases and the absorptivity increases. In addition, the characteristic variations are much less abrupt. Another feature characteristic is the presence of undulations in the spectrum of the reflectivity, transmissivity and absorptivity. These undulations are due to the interference effects resulting from internal reflections from the slab boundaries. The undulations can be quite marked for low collision frequencies and are smoothed out at high collision frequencies. This type of behavior is characteristic for a large range of slab thicknesses[5] $(0.5 < d/\lambda_p)$.

IV. Antenna Noise Temperature in Plasma Environment

Of vital significance is the noise power received by an antenna located in a hypervelocity space vehicle. An understanding of the noise power spectrum is essential in order to determine the systems performance of the communications equipment and possibly guidance apparatus of the vehicle. In addition, the noise power spectrum may be utilized as a diagnostic tool and yield information regarding the environment through which the vehicle traverses.

A receiving antenna located in a space vehicle will be subjected to three main sources of external noise, namely RF emission from the engulfing plasma sheath, noise emission from the hot surface of the vehicle itself which finds its way into the receiving antenna, and noise sources external to both the vehicle and the plasma sheath. The latter sources may, for instance, be due to noise emission from the earth or from the sun or as a result of atmospheric absorption, depending upon antenna orientation.

As a model upon which to base an illustrative example, consider a hypersonic vehicle surrounded by a plasma sheath as shown in Fig. 3. The region of the plasma

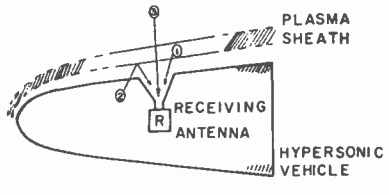

Fig. 3—Receiving antenna in hypersonic space vehicle. External sources of noise power are 1) the plasma sheath, 2) the hot vehicle itself, and 3) sources external to both the vehicle and the plasma such as the earth or the sun.

sheath facing the antenna is assumed to be a plane, parallel slab with sharp boundaries and uniform, isotropic electrical properties. The portion of the plasma "seen" by the antenna will have a large radius of curvature so that, to a very good approximation, the plasma can be considered as a planar slab. Hence, the analysis of the previous section applies. In addition to the noise power emitted by the plasma, noise emission from the hot surface of the vehicle which is *reflected* from the plasma sheath into the receiving antenna and noise radiation from other external sources which is *transmitted* through the plasma sheath must be considered in order to obtain the total noise power at the receiving antenna. The mismatch introduced by the plasma to the receiving antenna is not considered in this analysis. (A similar model has been assumed by Di Felice and Ward[8] who, in their analysis, neglect the important interference effects due to internal multiple reflections within the plasma sheath.)

For purposes of computation, assume that the solid angle of each of the radiating sources subtended at the antenna at least fills the receiving antenna beam so that it is permissible, to set $\Omega_s/\Omega_a = 1$. Further, consider the emitted noise power to be randomly polarized so that the polarization coefficient γ can be set equal to one-half. The total noise power received is then proportional to the sum of:

1) The plasma temperature times the absorptivity of the plasma.
2) The effective vehicle temperature times the reflectivity of the plasma (neglecting multiple reflections which may occur in the region between the vehicle and the plasma sheath and considering the reflection coefficient to be the same as the normal incidence reflectivity. Both of these conditions are very nearly true. Multiple reflections between the surface of the vehicle and the inner surface of the plasma are effective only in the region $1 \leq \omega/\omega_p \leq 1.3$. In this region, the contribution from the plasma is dominant since, in general, the temperature of the plasma is much greater than the temperature of the vehicle).
3) The effective temperature of outside external sources times the transmissivity of the plasma sheath.

The total noise power at the receiving antenna is thus

$$P = \kappa[.1_\omega T_p + R_\omega T_v + T_\omega T_{ex}] = \kappa T_n \qquad (9)$$

where

T_p = the temperature of the plasma
T_v = the temperature of the vehicle
T_{ex} = the temperature of any source external to both the vehicle and the plasma sheath
T_n = the total effective noise temperature.

As an illustrative example, choose for the plasma parameters $d/\lambda_p = 2.5$, $\nu/\omega_p = 10^{-2}$. This could, for example, correspond to a plasma of electron density n 4×10^{12} electrons/cc, collision frequency (ν) 1.12×10^9 $\sec^{-1}$ and of thickness (d) equal to 4.18 cm. All are typi-

[8] B. L. Di Felice and T. J. Ward, "An Experimental Method to Determine the Optimum Frequency for Hypersonic Vehicle Communications and Radar," RCA Airborne Systems Div. (DEP), Camden, N. J., TR60-597-15; 1960.

cal values for a hypersonic re-entry vehicle.[9] Let the temperature of the plasma be 5000°K, the temperature of the space vehicle 500°K and the temperature of an outside source 300°K (the receiving antenna looking at the earth, for instance). The noise temperature contributions from each of these sources and the total effective noise temperature as function of the normalized parameter ω/ω_p (effectively, frequency for a given plasma) are shown in Fig. 4. The main feature of the spectral behavior is the rapid increase in noise power as the RF frequency passes through the plasma frequency and the peak of noise emission at a RF frequency just higher than the plasma frequency. The general characteristic of the noise emission spectrum resembles the absorptivity spectrum with both the high and low frequency (relative to plasma frequency) regions pushed up. A general conclusion is that for RF frequencies much lower than the plasma frequency, the main noise source is the hot surface of the vehicle itself; for RF frequencies much greater than the plasma frequency, the greatest noise contribution arises from sources outside both the vehicle and the plasma, while in the frequency region about the plasma frequency the noise signal originates principally in the plasma sheath.

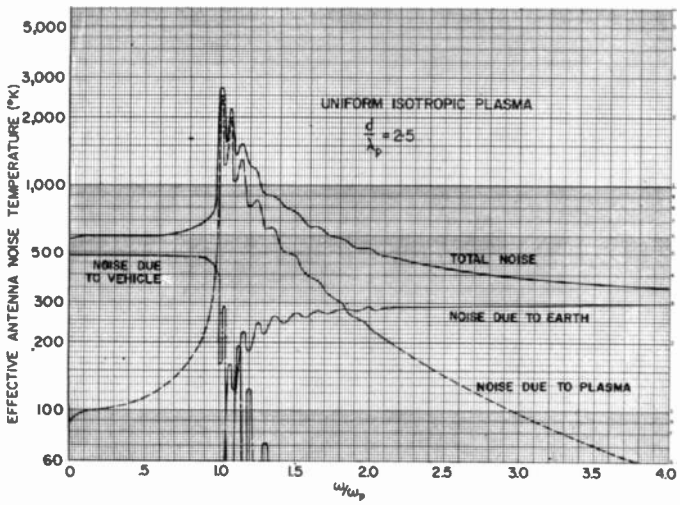

Fig. 4—Effective noise temperature for a hypersonic space vehicle (isotropic plasma with $\nu/\omega_p = 10^{-2}$ and $d/\lambda_p = 2.5$).

V. Effect of Magnetic Fields on Antenna Noise Temperature

Considerable speculation has been made on the possibilities of utilizing an auxiliary static magnetic field inside a space vehicle in order to alter the characteristics of the surrounding plasma sheath and hence permit modes of transmission in which RF frequencies well below the plasma frequency will readily penetrate through the plasma and hence establish reliable communications between the vehicle and an outside station. It is the purpose of this section to investigate the effect of an auxiliary dc magnetic field on the available noise temperatures at a receiving antenna in a space vehicle.

As is well known, in the presence of a static magnetic field, a plasma becomes anisotropic and can support two different waves for any direction of propagation (*i.e.*, the plasma is doubly refracting). Considering a uniform, anisotropic slab of plasma with a plane electromagnetic wave incident normally on the plasma boundaries, the transmissivity, reflectivity and absorptivity of the slab can be obtained from (8) provided the appropriate value of the dielectric coefficient for the plasma is used. For a uniform anisotropic plasma, the dielectric coefficient (neglecting the effects of ions) is[6]

$$K = \frac{B \pm \sqrt{B^2 - 4AC}}{2A}, \tag{10}$$

where

$$A = [\epsilon_{11} \sin^2\theta + \epsilon_{33}\cos^2\theta]$$
$$B = [(\epsilon_{11}^2 - \epsilon_{12}^2)\sin^2\theta + \epsilon_{11}\epsilon_{33}(1+\cos^2\theta)]$$
$$C = [\epsilon_{33}(\epsilon_{11}^2 - \epsilon_{12}^2)]$$

θ = the angle between the magnetic field direction field direction and the incident electromagnetic wave,

and

$$\epsilon_{11} = 1 + \frac{\omega_p^2(1 - j\nu/\omega)}{[\nu + j(\omega - \omega_b)][\nu + j(\omega + \omega_b)]} \tag{11a}$$

$$\epsilon_{12} = \frac{\omega_p^2}{\omega^2}\frac{\omega\omega_b}{[\nu + j(\omega - \omega_b)][\nu + j(\omega + \omega_b)]} \tag{11b}$$

$$\epsilon_{33} = 1 - \frac{\omega_p^2}{\omega^2}\frac{j\omega}{\nu + j\omega} \tag{11c}$$

$$\omega_b = \left|\frac{e}{m}B_0\right| = \text{the electron gyrofrequency corresponding to a static magnetic field of strength } B_0.$$

The above expressions simplify considerably when the direction of propagation is either parallel to the magnetic field ($\theta = 0°$) or perpendicular to the magnetic field ($\theta = 90°$). For these two cases, the dual valued dielectric coefficient is:[6]

1) Longitudinal propagation ($\theta = 0°$)

$$K_- = \left(1 - \frac{\omega_p^2}{\omega}\frac{(\omega - \omega_b)}{\nu^2 + (\omega - \omega_b)^2}\right) - j\left(\frac{\omega_p^2}{\omega}\frac{\nu}{\nu^2 + (\omega - \omega_b)^2}\right) \tag{12a}$$

$$K_+ = \left(1 - \frac{\omega_p^2}{\omega}\frac{\omega + \omega_b}{\nu^2 + (\omega + \omega_b)^2}\right) - j\left(\frac{\omega_p^2}{\omega}\frac{\nu}{\nu^2 + (\omega + \omega_b)^2}\right) \tag{12b}$$

[9] M. P. Bachynski, T. W. Johnston, and I. P. Shkarofsky, "Electromagnetic properties of high temperature air," Proc. IRE, vol. 48, pp. 347–356; March, 1960.

where K_- corresponds to the circularly polarized wave rotating in the same sense as negative particles (electrons) gyrate in the magnetic field (electron cyclotron wave), and K_+ corresponds to the circularly polarized wave rotating in the same sense as positive particles gyrate in the magnetic field (ion cyclotron wave).

2) Transverse propagation ($\theta = 90°$)

$$K_0 = \left(1 - \frac{\omega_p^2}{\omega^2}\,\frac{1}{1+\nu^2/\omega^2}\right) - j\left(\frac{\omega_p^2}{\omega^2}\,\frac{\nu/\omega}{1+\nu^2/\omega^2}\right) \tag{13a}$$

$$K_x = \left(1 - \frac{\omega_p^2}{\omega^2}\,\frac{(\omega^2-\omega_p^2)(\omega^2-\omega_h^2-\omega_p^2)+\nu^2\omega^2}{\left[\nu^2-(\omega^2-\omega_h^2-\omega_p^2)\right]^2+\nu^2\left[2\omega-\omega_p^2/\omega\right]^2}\right)$$
$$-j\left(\frac{\omega_p^2}{\omega^2}\,\nu\omega\,\frac{\left[\nu^2+\omega^2+\omega_h^2-\omega_p^2\right]+(\omega_p^2/\omega^2)(\omega_p^2-\omega^2)}{\left[\nu^2-(\omega^2-\omega_h^2-\omega_p^2)\right]^2+\nu^2\left[2\omega-\omega_p^2/\omega\right]^2}\right) \tag{13b}$$

where K_0 corresponds to the ordinary wave (E vector of EM wave parallel to B_0) and is the same as in the absence of a dc magnetic field, and K_x corresponds to the extraordinary wave (H vector of EM wave parallel to B_0).

The absorptivity, reflectivity and transmissivity have been computed for a plasma slab corresponding to longitudinal propagation (electron and ion cyclotron waves) and transverse propagation (extraordinary and ordinary wave) and are shown in Figs. 5–7 (pp. 1853–1855). (The ordinary wave is not shown since it is the same as given in Section III, Fig. 2, for an isotropic plasma.) The same parameters ($d/\lambda_p = 2.5$, $\nu/\omega_p = 10^0$, 10^{-1}, 10^{-2}, 10^{-3}) as in Section III have been chosen for the plasma. The main features of these variations are the high reflectivity in the "stop-regions"[5,6] of the magneto-ionic modes, the high transmissivity outside the stop-regions and the enhanced absorptivity in the transparent regions immediately adjacent to the stop-regions. Noteworthy are the several possible enhanced frequencies of absorption (and hence of noise emission) corresponding to these different modes. The effect of increased collision frequency is to increase the absorptivity and to broaden the resonances. (Inhomogeneities of the plasma properties would be expected to have the same result.) Again, undulations due to internal reflections within the plasma slab are apparent.

Considering a randomly polarized noise signal, the total reflectivity, transmissivity or absorptivity of an anisotropic plasma slab in a direction normal to its boundaries is a combination of the reflectivities, transmissivities or absorptivities of the two possible waves in that direction. Thus, for longitudinal (relative to the dc magnetic field) propagation,

$$\theta = 0° \qquad \begin{aligned} R_\omega &= \tfrac{1}{2}(R_- + R_+) \\ T_\omega &= \tfrac{1}{2}(T_- + T_+) \\ A_\omega &= \tfrac{1}{2}(A_- + A_+) \end{aligned} \tag{14}$$

where the $-$, $+$ subscripts refer to the electron cyclotron and ion cyclotron waves, respectively. Similarly, for the magnetic field along the plasma slab, normal to the incident electromagnetic wave (transverse propagation),

$$\theta = 90° \qquad \begin{aligned} R_\omega &= \tfrac{1}{2}(R_o + R_x) \\ T_\omega &= \tfrac{1}{2}(T_o + T_x), \\ A_\omega &= \tfrac{1}{2}(A_o + A_x), \end{aligned} \tag{15}$$

where the o, x subscripts refer to the ordinary and extraordinary waves, respectively.

The total noise power available at the receiving antenna for an anisotropic plasma sheath surrounding a hypervelocity space vehicle has been evaluated for the case of the magnetic field normal to the plasma slab and parallel to the emitted noise signal (longitudinal propagation) and for the case of the magnetic field parallel to the plasma slab and perpendicular to the normally incident electromagnetic wave (transverse propagation). The same model and parameters have been assumed as in Section III; *i.e.*, the plasma sheath can be approximated by a uniform but now *anisotropic* plasma slab with sharp boundaries, the plasma is assumed to be at a temperature of 5000°K, the space vehicle at 500°K, and an external source at 300°K. The plasma parameters were taken to be $d/\lambda_p = 2.5$ and $\nu/\omega_p = 10^{-2}$. In addition, an electron gyrofrequency to plasma frequency ratio of two was assumed ($\omega_h/\omega_p = 2$). For an electron density of 4×10^{12} electrons/cm^3, this corresponds to a magnetic field of 10,000 gauss. This is an unrealistic value for practical space applications, although it could be realized in laboratory tests. It is used here to demonstrate how drastically the spectral characteristics can be altered by a magnetic field. The results [utilizing Figs. 2, 5, 6 and 7 and (14) and (15) in (9)] are shown in Fig. 8(a) and (b), (p. 1856).

The effect of the magnetic field has been to alter completely the available noise power at the receiving antenna relative to that for an isotropic plasma sheath. The noise emission for the auxiliary magnetic field along the direction of propagation is characterized by two maxima, both due to the electron cyclotron wave (the main lobe occurring at a frequency just below the electron gyrofrequency), and is followed by a pronounced minima. The effect of lower magnetic fields would be to move this maxima to lower frequencies. The ion cyclotron wave for these low collision frequencies does not make a very substantial contribution to the total noise power. There is no significance to the plasma frequency in this case. The available noise power for the auxiliary magnetic field transverse to the direction of propagation exhibits four pronounced maxima, including one at the plasma frequency (as in the isotropic case). In general, the peak emitted power is greatest for this case and occurs at a frequency just above the electron gyrofrequency.

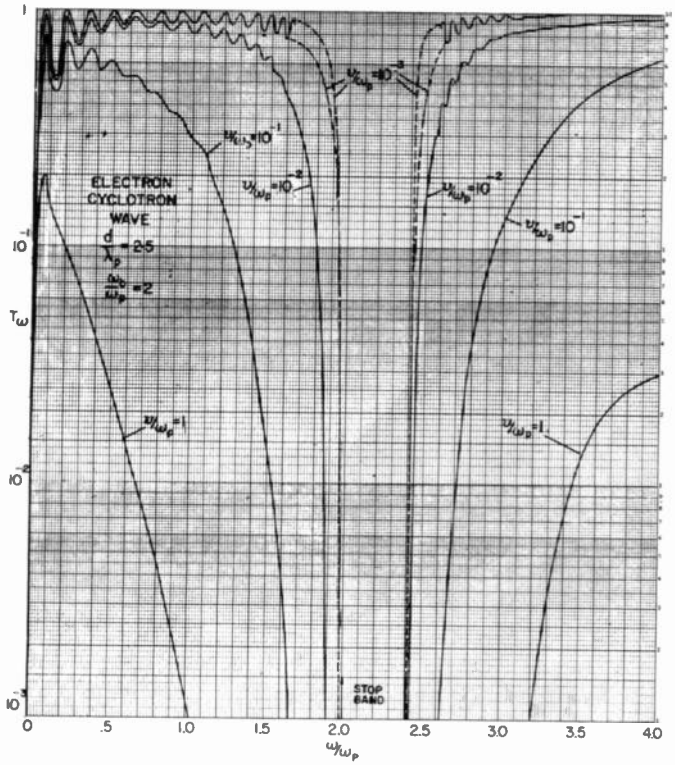

(a)

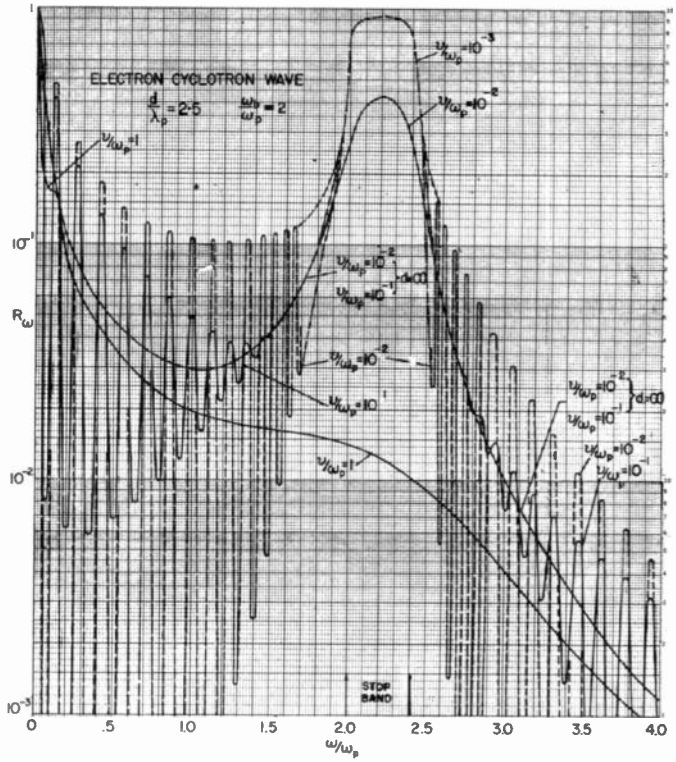

(b)

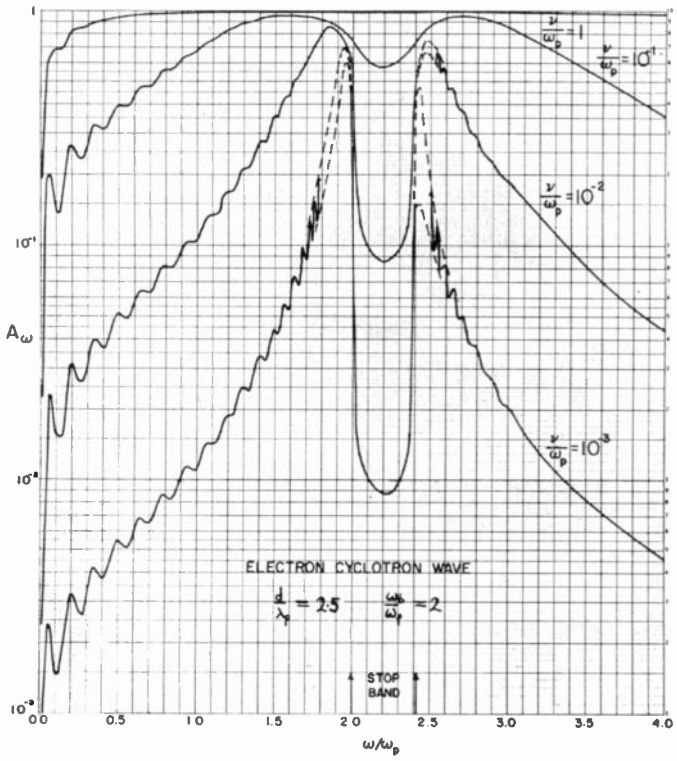

(c)

Fig. 5—(a) Transmissivity (T_ω) of an anisotropic plasma slab as a function of RF frequency for the electron cyclotron wave ($d/\lambda_p=2.5$, $\omega_h/\omega_p=2$) for various electron collision frequencies. (b) Reflectivity (R_ω) of an anisotropic plasma slab as a function of RF frequency for the electron cyclotron wave ($d/\lambda_p=2.5$, $\omega_h/\omega_p=2$) for various electron collision frequencies. (c) Absorptivity (A_ω) of an anisotropic plasma slab as a function of RF frequency for the electron cyclotron wave ($d/\lambda_p=2.5$, $\omega_h/\omega_p=2$) for various electron collision frequencies.

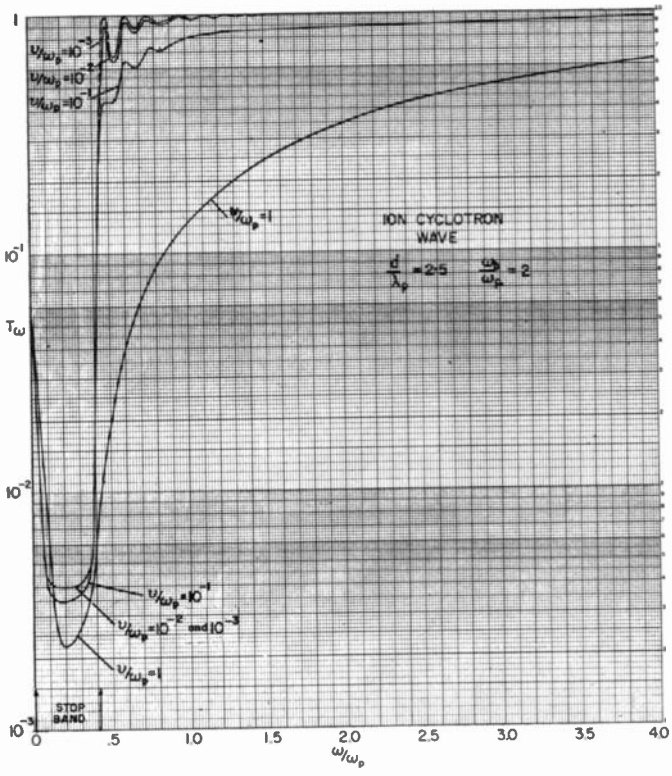

(a)

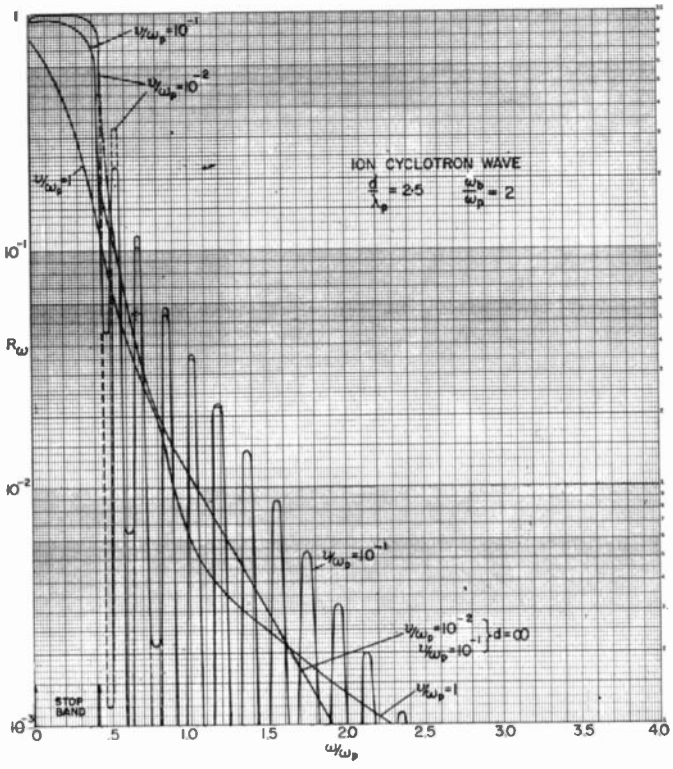

(b)

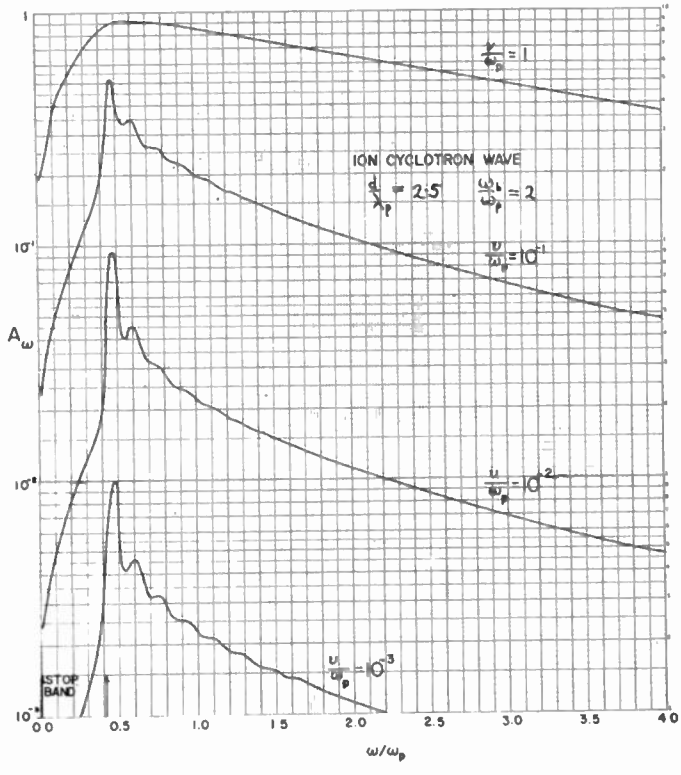

(c)

Fig. 6—(a) Transmissivity (T_ω) of an anisotropic plasma slab as a function of RF frequency for the ion cyclotron wave ($d/\lambda_p=2.5$, $\omega_h/\omega_p=2$) for various electron collision frequencies. (b) Reflectivity (R_ω) of an anisotropic plasma slab as a function of RF frequency for the ion cyclotron wave ($d/\lambda_p=2.5$, $\omega_h/\omega_p=2$) for various electron collision frequencies. (c) Absorptivity (A_ω) of an anisotropic plasma slab as a function of RF frequency for the ion cyclotron wave ($d/\lambda_p=2.5$, $\omega_h/\omega_p=2$) for various electron collision frequencies.

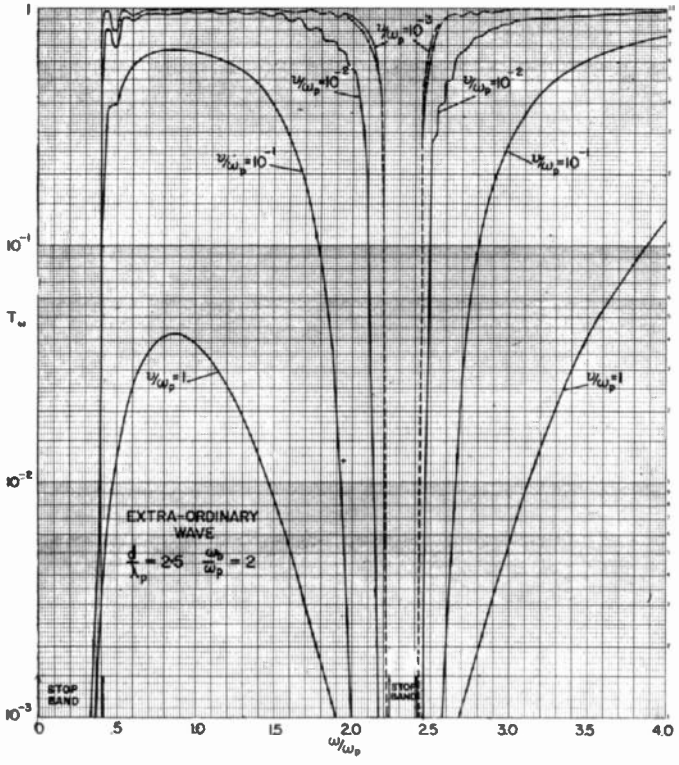

(a)

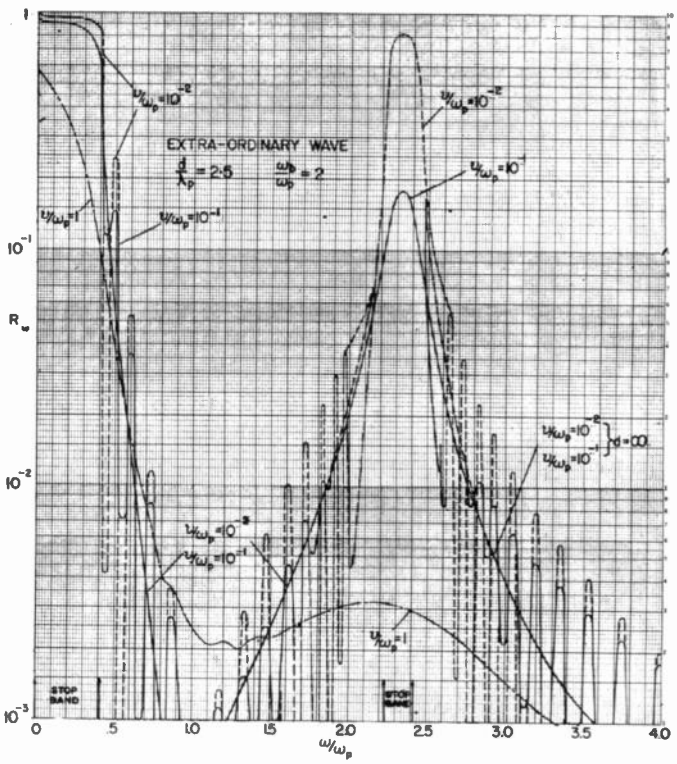

(b)

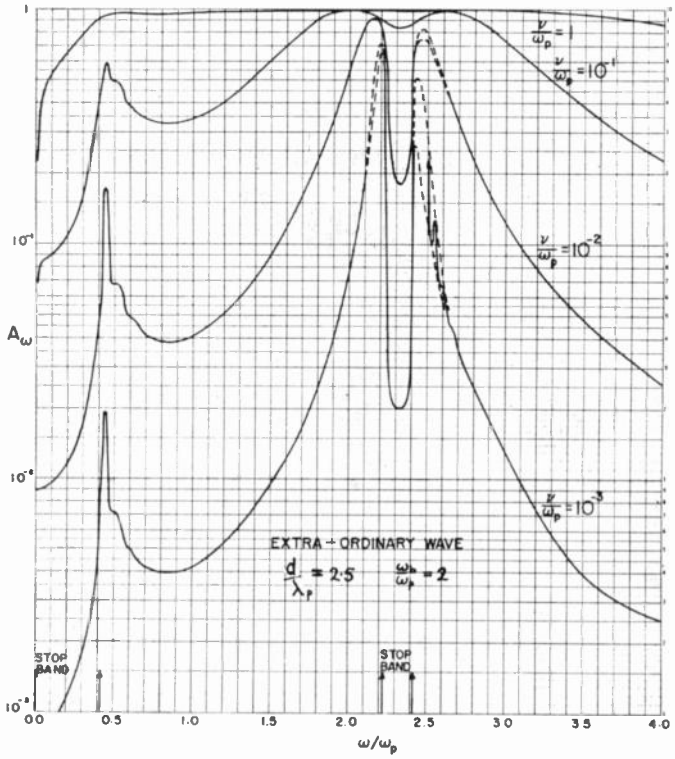

(c)

Fig. 7—(a) Transmissivity (T_ω) of an anisotropic plasma slab as a function of RF frequency for the extraordinary wave ($d/\lambda_p = 2.5$, $\omega_h/\omega_p = 2$) for various electron collision frequencies. (b) Reflectivity (R_ω) of an anisotropic plasma slab as a function of RF frequency for the extraordinary wave ($d/\lambda_p = 2.5$, $\omega_h/\omega_p = 2$) for various electron collision frequencies. (c) Absorptivity (A_ω) of an anisotropic plasma slab as a function of RF frequency for the extraordinary wave ($d/\lambda_p = 2.5$, $\omega_h/\omega_p = 2$) for various electron collision frequencies.

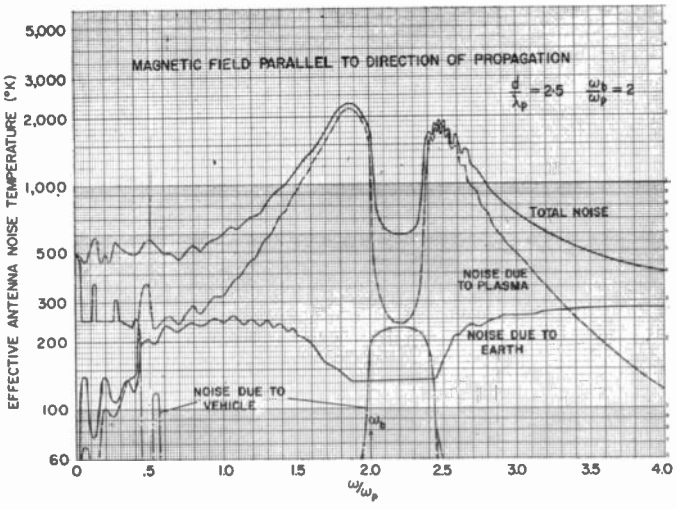

(a)

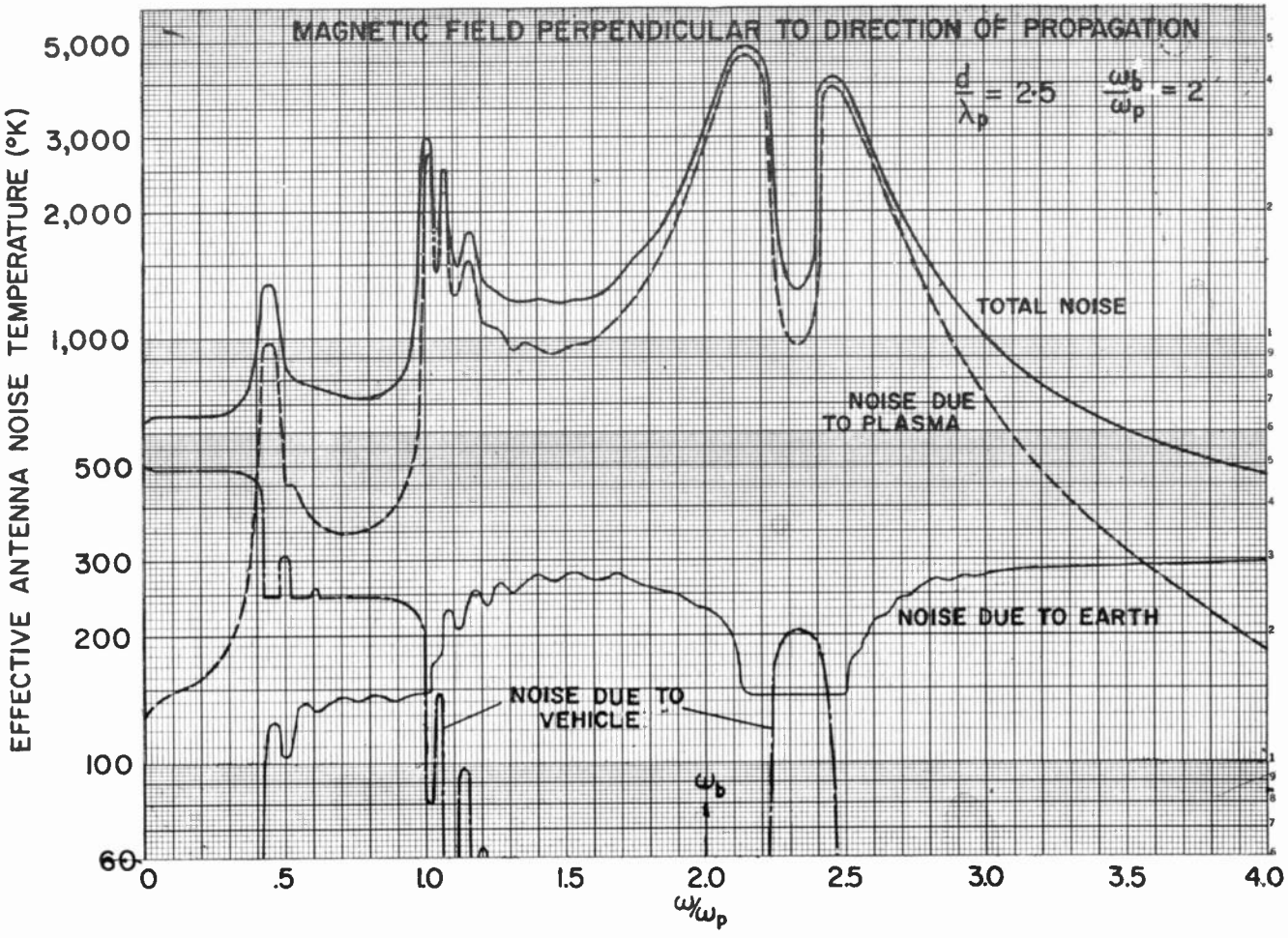

(b)

Fig. 8—(a) Effective noise temperature for a hypersonic space vehicle (anisotropic plasma—longitudinal propagation with $\nu/\omega_p=10^{-2}$, $d/\lambda_p=2.5$, $\omega_b/\omega_p=2$). (b) Effective noise temperature for a hypersonic space vehicle (anisotropic plasma—transverse propagation with $\nu/\omega_p=10^{-2}$, $d/\lambda_p=2.5$, $\omega_b/\omega_p=2$).

VI. Conclusions

The total noise power available at a receiving antenna on a hypervelocity space vehicle has been determined by treating the engulfing plasma sheath as a uniform slab of plasma. The noise emission from the plasma can then be evaluated in terms of a boundary-value problem which for this simple model can be completely solved. The effect of high temperatures of the vehicle surface and of noise sources external to the vehicle and plasma sheath are included in the analysis.

When the plasma sheath is isotropic, the main noise power is due to emission from the vehicle surface if the RF frequency is much lower than the plasma frequency; it is due to sources outside both the vehicle and plasma for RF frequencies much greater than the plasma frequency and results from direct emission from the plasma for RF frequencies in the neighborhood of the plasma frequency. The noise power from the plasma itself is the most significant and exhibits a sharp maximum at an RF frequency just above the plasma frequency. This enhances the suggestion[8] of the value of noise emission measurements as a diagnostic tool for the exploration of the hypersonic environment of a space or re-entry vehicle.

The effects of an anisotropic plasma sheath (due to an auxiliary magnetic field) have also been investigated for the two cases of the magnetic field normal to the sheath and parallel to the sheath. The effect of the anisotropy is to alter completely the spectral characteristics of the available noise power at the receiving antenna. Several regions of both weak and intense noise emission are now possible, depending upon magnetic field strength and orientation.

Generalized Appleton-Hartree Equation for Any Degree of Ionization and Application to the Ionosphere*

I. P. SHKAROFSKY†, MEMBER, IRE

Summary—**A generalized Appleton-Hartree equation is derived, applicable to any variation of electron collision frequency with electron speed and any degree of ionization. Regions of the parameters where simplification occurs are given. Results are shown for the ionosphere (60 to 320 km) and compared with experimental data. Good agreement is obtained for the *D* layer. Experimental data for the *E* layer can also be explained by assuming an electron temperature several times the gas temperature. This is consistent with rocket data and a measurement by Sputnik III. It is shown that the classic Appleton-Hartree equation should be applicable with no corrections necessary for the F_2 layer, provided the collision frequency is averaged appropriately.**

I. Introduction

Most investigations on the propagation of an electromagnetic wave in a magnetized plasma are based on the concept of a constant value for the electron collision frequency, independent of electron speed. The classic Appleton-Hartree equation, used for propagation in the ionosphere, has this inherent assumption. Because the electron elastic collision frequency with the nitrogen molecules in the atmosphere varies as the square of the electron speed,[1] a large discrepancy between classic theory and ionospheric experiments can be expected. An accurate analysis must include these effects. Several corrections to include this speed variation have appeared in the literature.[2–4] These references only account for the neutral particle effects, under the assump-

* Received by the IRE, April 6, 1961. The work reported in this paper was done under Contract GX9-998054-0001-70-Q82 to RCA, Missile and Surface Radar Div., Moorestown, N. J.

† RCA Victor Co., Ltd., Research Labs., Montreal, Canada.

[1] A. V. Phelps and J. L. Pack, "Electron collision frequencies in nitrogen and in the lower ionosphere," *Phys. Rev. Lett.*, vol. 3, pp. 340–342, October, 1959; "Drift velocities of slow electrons in helium, neon argon, hydrogen, and nitrogen," *Phys. Rev.*, vol. 121, pp. 798–806, February, 1961.

[2] R. Jancel and T. Kahn, "Théorie du couplage des ondes électromagnetiques ordinaire et extraordinarie dans un plasma inhomogène et anisotrope et conditions de reflexion. Applicâtions à l'ionosphere," *J. Phys. Radium*, vol. 16, pp. 136–145, February, 1955; "Théorie non Maxwellienne des plasmas homogènes et anisotropes," *Nuovo Cim.*, vol. 12, pp. 573–612; November, 1954.

[3] H. K. Sen and A. A. Wyller, "On the generalization of the Appleton-Hartree magnetoionic formulas," *J. Geophys. Res.*, vol. 65, pp. 3931–3950; December, 1960.

[4] A. V. Phelps, "Propagation constants for electromagnetic waves in weakly ionized dry air," *J. Appl. Phys.*, vol. 31, pp. 1723–1729; October, 1960.

tion that the gas is very slightly ionized. This may be a good approximation to conditions in the D layer, but not in the F layers of the ionosphere. In the following, a generalized Appleton-Hartree equation, valid for *any* variation of the collision frequency with electron speed and *any* degree of ionization, is derived. The results are then applied to the ionosphere. Various domains of the parameters where simplification may result are investigated.

A method for calculating the electronic conductivity for any degree of ionization has been developed.[5] In this method, the usual series expansion of Laguerre polynomials is substituted into the Fokker-Planck equation for Coulomb (electron-ion and electron-electron) collisions,[6] and into the Boltzmann equation for electron collisions with neutral particles. A Maxwellian distribution in electron velocity is assumed. For Coulomb collisions, the expressions are the same as those derived by Landshoff.[7] Collisions of electrons with neutral particles and ions, ac electric fields, as well as static magnetic fields, are treated in this analysis. In the limit of a completely ionized gas, the results agree with those of Spitzer and Harm.[8] For a slightly ionized gas, no expansion is necessary and the results are identical with those of Allis.[9] The conductivity can be calculated by using the Dingle tabulations,[10] if the electron collision frequency varies as an integral power (between -3 and 3) of velocity. This method, to be reviewed in Section II, is utilized here to yield the proper averages (or multiplying factors) for the collision frequency and multiplying factors for the angular frequency.

II. Basis of Analysis

In this analysis, existing gradients and fluctuations in the dielectric coefficient, ion motion and thermal motion of the electrons which give rise to plasma waves, are all neglected. The limit for the convergence of the theory, if thermal motions are neglected, is that the ratio of the thermal velocity of the electrons $\sqrt{kT/m}$ to the phase velocity of the wave c/n is small. That is, $n^2kT/mc^2 \ll 1$, where n is the refractive index and c is the velocity of light.

The electronic conductivity matrix (σ) for any degree of ionization and any variation of electron-neutral particle collision frequency ν_m with electron velocity v can be represented as[5]

$$(\sigma) = \begin{pmatrix} b+c & j(b-c) & 0 \\ -j(b-c) & b+c & 0 \\ 0 & 0 & d \end{pmatrix}, \tag{1}$$

with

$$d = \frac{Ne^2}{m} \frac{1}{\langle \nu_0 \rangle g_0 + j\omega h_0} \tag{2}$$

$$2c = \frac{Ne^2}{m} \frac{1}{\langle \nu_0 \rangle g_+ + j(\omega + \omega_b) h_+} \tag{3}$$

$$2b = \frac{Ne^2}{m} \frac{1}{\langle \nu_0 \rangle g_- + j(\omega - \omega_b) h} \tag{4}$$

where

N,e,m are respectively electron density, charge, and mass,

ω is the RF angular frequency,

ω_b is the cyclotron angular frequency, $\omega_b = |eB/m|$ where B is the magnitude of the dc magnetic field. The magnetic field is taken parallel to the z-axis of a Cartesian or cylindrical system of coordinates.

Also

$\langle \nu_0 \rangle$ is the averaged electron collision frequency with neutrals plus ions and will be defined below.

$g_{0,+,-}$ and $h_{0,+,-}$ are correction factors to account for the variation with velocity of the electron-neutral particle collision frequency and for electron-ion and electron-electron effects.

The averaged collision frequency is defined so as to make g and h equal to 1 at high angular frequencies. This requires[5] that

$$\langle \nu_0 \rangle = -\frac{4\pi}{3N} \int_0^\infty \frac{\partial f_0^0}{\partial v} v^3 \nu_0 dv \tag{5}$$

where

f_0^0 is the distribution function of electron velocity,

v is the electron velocity,

ν_0 is the unaveraged total electron collision frequency —a function of electron speed.

Let the contributions to ν_0 be ν_m from neutrals, whose variation with velocity depends on the constituent gases, and ν_{ei} from ions, known[6] to be of the form

$$\nu_{ei} = \frac{N_+ Y}{v^3}$$

where

$$Y = 4\pi \left(\frac{Ze^2}{4\pi\epsilon_0 m} \right)^2 \ln \Lambda, \qquad \Lambda = \frac{3(4\pi\epsilon_0 kT)^{3/2}}{2Ze^3(\pi N)^{1/2}}, \tag{6}$$

[5] I. P. Shkarofsky, "Values of the transport coefficients in a plasma for any degree of ionization based on a Maxwellian distribution," *Canad. J. Phys.*, vol. 39; November, 1961.

[6] M. P. Bachynski, I. P. Shkarofsky and T. W. Johnston, "Plasmas and the Electromagnetic Field," McGraw-Hill Book Co., Inc., New York, N. Y.; in press.

[7] R. Landshoff, "Transport phenomena in a completely ionized gas in presence of a magnetic field," *Phys. Rev.*, vol. 76, pp. 904–909; October 1, 1949.

[8] L. Spitzer and R. Harm, "Transport phenomena in a completely ionized gas," *Phys. Rev.*, vol. 89, pp. 977–981; March 1, 1953.

[9] W. P. Allis, "Motions of ions and electrons," in "Handbuch der Physik," S. Flügge, Ed., Springer-Verlag, Berlin, Ger., vol. 21; 1956.

[10] R. B. Dingle and D. Arndt, "The integrals $\mathfrak{A}p(x)$ and $\mathfrak{B}p(x)$ and their tabulation," *Appl. Sci. Res.*, vol. 6-B, no. 3, pp. 144–154, 1957; "The integrals $\mathfrak{C}p(x)$ and $\mathfrak{D}p(x)$ and their tabulation," pp. 155–164; "The integrals $\mathfrak{E}p(x)$ and $\mathfrak{F}p(x)$ and their tabulation," no. 4, pp. 245–252; 1957.

where

k is Boltzmann's constant,
T is the electron temperature,
N_+ is the ion density,
Z is the ion charge number, and
ϵ_0 is the permittivity of free space.

For the temperatures considered here, $N_+ = N$ and $Z = 1$. Thus

$$\nu_g = \nu_m(v) + \nu_{ei}(v). \tag{7}$$

Suppose that one can express ν_m as a power index of velocity, not necessarily an integer, *viz.*,

$$\nu_m = cv^r. \tag{8}$$

In most cases, this can be done over the velocity range where the largest contribution to the integral in (5) occurs. Also, if the magnitude of the electric field is sufficiently small, one can let f_0^0 be a Maxwellian distribution

$$f_0^0 = N\left(\frac{m}{2\pi kT}\right)^{3/2} \epsilon^{-mv^2/2kT}. \tag{9}$$

With these assumptions, substitution of (7) into (5) yields

$$\langle \nu_g \rangle = \langle \nu_m \rangle + \langle \nu_{ei} \rangle, \tag{10}$$

with

$$\langle \nu_{ei} \rangle = \frac{4(2\pi)^{1/2}}{3} N_+ \left(\frac{Ze^2}{4\pi\epsilon_0 kT}\right)^2 \left(\frac{kT}{m}\right)^{1/2} \ln \Lambda \tag{11}$$

and

$$\langle \nu_m \rangle = \frac{c\Gamma\left(\frac{5+r}{2}\right)}{\Gamma(5/2)} \left(\frac{2kT}{m}\right)^{r/2} \tag{12}$$

where Γ is a Gamma function.

The (g_0, h_0), (g_+, h_+) and (g_-, h_-) factors are respectively functions of $\omega/\langle \nu_g \rangle$, $(\omega+\omega_b)/\langle \nu_g \rangle$ and $(\omega-\omega_b)/\langle \nu_g \rangle$. They are also functions of $\langle \nu_m \rangle/\langle \nu_{ei} \rangle$, of Z, and depend on the variation of ν_m with velocity. These functions are tabulated in a recent article by the author[5] for $Z = 1$, power law variations of $r = -3, -2 \cdots 3$, various ratios of $\langle \nu_m \rangle/\langle \nu_{ei} \rangle$ and continuous $(\omega \pm \omega_b)/\langle \nu_g \rangle$ values. In a slightly ionized gas, when $\langle \nu_m \rangle/\langle \nu_{ei} \rangle$ becomes quite large, the values of g and h can be obtained from simple analysis, using the tabulations of the Dingle[10] functions.

The g and h functions are monotonic; g increases from an asymptotic value less than unity at small values of $(\omega \pm \omega_b)/\langle \nu_g \rangle$ to unity at large $(\omega \pm \omega_b)/\langle \nu_g \rangle$ values, and h decreases from a limiting value greater than unity to unity. If the power index r in (8) is less than or equal to zero, g and h also vary monotonically as $\langle \nu_m \rangle/\langle \nu_{ei} \rangle$ increases. When r is equal to 0, g and h are identically unity at large ratios of $\langle \nu_m \rangle/\langle \nu_{ei} \rangle$, that is for the slightly ionized gas. However, when r is greater than or equal to 1, g and h vary from the values for the slightly ionized gas to approximately unity, at $\langle \nu_m \rangle/\langle \nu_{ei} \rangle$ between 1 and 10, and then g and h deviate more from unity as $\langle \nu_m \rangle/\langle \nu_{ei} \rangle$ decreases, until they approach the limits for the completely ionized gas. The explanation for this variation is the fact that ν_g, equal to $(\nu_m + \nu_{ei})$, is approximately constant[5,6] when $\langle \nu_m \rangle \approx \langle \nu_{ei} \rangle$ and when ν_m varies as a positive power of speed. In other words, since ν_{ei} decreases with electron speed as $1/v^3$ and ν_m increases as v^r, there exists a ratio, $\langle \nu_m \rangle/\langle \nu_{ei} \rangle$, for which the sum of the decreasing and increasing velocity function results in a more or less constant ν_g with respect to velocity, and when this occurs, g and h are approximately 1. Consequently, g and h shift towards 1 and then deviate from 1 as the degree of ionization in the gas increases.

III. Generalized Equation for the Refractive Index

From Maxwell's curl equation, we can write

$$\Delta x \boldsymbol{H} = [\sigma + j\omega\epsilon_0] \cdot \boldsymbol{E} = j\omega\epsilon_0 \kappa \cdot \boldsymbol{E} \tag{13}$$

where

$\boldsymbol{H}$ is the magnetic field vector, and
σ and κ are respectively the conductivity and dielectric coefficient matrices.

If the elements of the dielectric tensor are denoted by

$$(\kappa) = \begin{pmatrix} \epsilon_{11} & j\epsilon_{12} & 0 \\ -j\epsilon_{21} & \epsilon_{22} & 0 \\ 0 & 0 & \epsilon_{33} \end{pmatrix} \tag{14}$$

then one can write

$$\epsilon_{22} = \epsilon_{11} = 1 - \xi - \psi \tag{15}$$

$$\epsilon_{12} = \epsilon_{21} = -\xi + \psi \tag{16}$$

$$\epsilon_{33} = 1 - \gamma. \tag{17}$$

Note that the ξ, ψ, γ coefficients are equal to $(j/\omega\epsilon_0)$ times the b, c and d coefficients represented in (2) to (4). For any degree of ionization and any variation of ν_m with velocity, ξ, ψ, γ are related to the g and h functions by

$$\xi = \frac{\omega_p^2}{2\omega^2} \frac{j\omega}{\langle \nu_g \rangle g_- + j(\omega - \omega_b)h_-} = \frac{x/2}{h_- - jg_- z - h_- y} \tag{18}$$

$$\psi = \frac{\omega_p^2}{2\omega^2} \frac{j\omega}{\langle \nu_g \rangle g_+ + j(\omega + \omega_b)h_+} = \frac{x/2}{h_+ - jg_+ z + h_+ y} \tag{19}$$

$$\gamma = \frac{\omega_p^2}{\omega^2} \frac{j\omega}{\langle \nu_g \rangle g_0 + j\omega h_0} = \frac{x}{h_0 - jg_0 z} \tag{20}$$

where

$\omega_p = (Ne^2/m\epsilon_0)^{1/2}$ is the plasma frequency,
$\langle \nu_g \rangle$ is the average collision frequency of electrons

In terms of the ξ, ψ and γ coefficients, this is

$$n^2 = 1 - \frac{\dfrac{4\xi\psi}{\alpha} - \dfrac{4\xi\psi - \gamma\alpha}{\alpha(\gamma - 1)}\sin^2\theta}{1 + \dfrac{\alpha - \gamma + 4\xi\psi - \alpha\gamma}{2\alpha(\gamma - 1)}\sin^2\theta \pm \left\{\left[\dfrac{\alpha - \gamma - 4\xi\psi + \alpha\gamma}{2\alpha(\gamma - 1)}\sin^2\theta\right]^2 + \left(\dfrac{\xi - \psi}{\alpha}\right)^2\cos^2\theta\right\}^{1/2}} \tag{29}$$

with neutrals plus ions and is defined in (5) and (10), and[11]

$$x = \omega_p^2/\omega^2 \qquad y = \omega_b/\omega \qquad z = \langle\nu_g\rangle/\omega. \tag{21}$$

The following equation results[2,6] for n, the magnitude of the refractive index, from Maxwell's equations, assuming a plane-wave solution of the form $\exp(-j(\omega/c)\boldsymbol{n}\cdot\boldsymbol{r})$.

where $\alpha = \xi + \psi$. This expansion follows after considerable algebraic manipulation from (28) and after $2(A - B + C)$, $(2A - B)$ and $(B^2 - 4AC)^{\frac{1}{2}}$ have been divided by $2\alpha(\gamma - 1)$.

Let us further manipulate the equations with the values of ξ, ψ and γ given in (18) to (20). Again, after considerable algebra, one finds[12]

$$n^2 = 1 - \frac{x + \left[\dfrac{jx(z\mathfrak{S}_1 + j\mathfrak{S}_3)}{h_0 - x - jg_0 z}\right]\sin^2\theta}{\mathfrak{g}_1 - jz\mathfrak{g}_2 + \left\{\left(\dfrac{-y^2\mathfrak{g}_3 + z^2\mathfrak{S}_5 + j\mathfrak{S}_4 z + jx(z\mathfrak{S}_1 + j\mathfrak{S}_3)}{2(h_0 - x - jg_0 z)}\right)\sin^2\theta \pm \left[\left(\dfrac{-y^2\mathfrak{g}_3 + z^2\mathfrak{S}_5 + j\mathfrak{S}_4 z - jx(z\mathfrak{S}_1 + j\mathfrak{S}_3)}{2(h_0 - x - jg_0 z)}\right)^2\sin^4\theta + (y\mathfrak{g}_4 - jz\mathfrak{S}_2)^2\cos^2\theta\right]^{1/2}\right\}} \tag{30}$$

$$n^4[\epsilon_{11}\sin^2\theta + \epsilon_{33}\cos^2\theta] - n^2[(\epsilon_{11}^2 - \epsilon_{12}^2)\sin^2\theta + \epsilon_{11}\epsilon_{33}(1 + \cos^2\theta)] + \epsilon_{33}(\epsilon_{11}^2 - \epsilon_{12}^2) = 0 \tag{22}$$

where

$$\tan^2\theta = (n_x^2 + n_y^2)/n_z^2. \tag{23}$$

That is, θ is the angle between the direction of propagation and the dc magnetic field, assumed along the z axis. Eq. (22) can be written as

$$An^4 - Bn^2 + C = 0 \tag{24}$$

where, according to (22) and (15) to (17), the coefficients are given by

$$A = \epsilon_{11}\sin^2\theta + \epsilon_{33}\cos^2\theta = 1 - (\xi + \psi)\sin^2\theta - \gamma\cos^2\theta \tag{25}$$

$$B = (\epsilon_{11}^2 - \epsilon_{12}^2)\sin^2\theta + \epsilon_{11}\epsilon_{33}(1 + \cos^2\theta) = 2 - \xi(2 + \sin^2\theta) - \psi(2 + \sin^2\theta) - \gamma(1 - \xi - \psi)(2 - \sin^2\theta) + 4\xi\psi\sin^2\theta \tag{26}$$

$$C = \epsilon_{33}(\epsilon_{11}^2 - \epsilon_{12}^2) = 1 - 2(\xi + \psi) + 4\xi\psi - \gamma[1 - 2(\xi + \psi) + 4\xi\psi]. \tag{27}$$

The solution of the quadratic equation for the square of the refractive index, is usually, in ionospheric theory, written with the square root in the denominator. That is,

$$n^2 = \frac{B \pm \sqrt{B^2 - 4AC}}{2A} = 1 - \frac{2(A - B + C)}{2A - B \pm \sqrt{B^2 - 4AC}}. \tag{28}$$

where

$$x = \omega_p^2/\omega^2 \qquad y = \omega_b/\omega \qquad z = \langle\nu_g\rangle/\omega$$

$$2\mathfrak{S}_1 = 2g_0 - g_- + g_+ \qquad 2\mathfrak{S}_2 = g_+ - g_- \tag{31)(32}$$

$$2\mathfrak{S}_3 = 2h_0 - h_- - h_+ - y(h_+ - h_-) \tag{33}$$

$$2\mathfrak{S}_4 = g_0(h_- + h_+) + h_0(g_- + g_+) - 2g_-h_+ - 2g_+h_- + y(-g_0h_- + g_0h_+ - 2g_-h_+ + 2g_+h_-) \tag{34}$$

$$2\mathfrak{S}_5 = g_0g_- + g_0g_+ - 2g_-g_+ \tag{35}$$

$$2\mathfrak{g}_1 = h_+ + h_- + y(h_+ - h_-) \qquad 2\mathfrak{g}_2 = g_+ + g_- \tag{36)(37}$$

$$2y^2\mathfrak{g}_3 = h_0(h_- + h_+) - 2h_-h_+ + yh_0(h_+ - h_-) + 2h_-h_+y^2 \tag{38}$$

$$2y\mathfrak{g}_4 = h_+ - h_- + y(h_+ + h_-) \tag{39}$$

and where

g_0, h_0 are the values of g and h for argument $\omega/\langle\nu_g\rangle$,
g_+, h_+ for argument $(\omega + \omega_b)/\langle\nu_g\rangle$, and
g_-, h_- for argument $|\omega - \omega_b|/\langle\nu_g\rangle$.

In (31) to (39), two sets of functions, 5$\mathfrak{S}$ and 4$\mathfrak{g}$ functions, are defined. The $\mathfrak{S}$ ones are identically zero, and the $\mathfrak{g}$'s are 1, when the g and h parameters are all equal to 1 (which occurs for constant collision frequency in a slightly ionized gas).

The complicated equation can also be written as

$$n^2 = 1 - \frac{x(1 + jS)}{\mathfrak{g}_1 - jz\mathfrak{g}_2 - y_L R}, \tag{40}$$

[11] In ionospheric theory, the usual notation is capital X, Y, Z instead of the lower-case letters adopted here.

[12] Since the g and h parameters are defined to be corrections in the *denominators* of ξ, ψ and γ, these correction factors combine readily in the following evaluation, and this fact justifies the original definition.

where

$$S = \frac{y_T^2}{h_0 - x - jg_0 z}\left(\frac{z\Theta_1 + j\Theta_3}{y^2}\right)$$

$$y_L = y\cos\theta \qquad y_T = y\sin\theta$$

$$R = V - jxS/2y_L \mp \left[(g_4 - jz\Theta_2/y)^2 + (V + jxS/2y_L)^2\right]^{1/2}$$

$$V = \frac{y_T^2\left[g_3 - (z^2\Theta_5 + j\Theta_4 z)/y^2\right]}{2y_L(h_0 - x - jg_0 z)}. \tag{41}$$

θ is arbitrary). Obviously, in this case $g_0 = g_+ = g_- = 1$, $h_0 = h_+ = h_- = 1$, and consequently

$$4\xi\psi = \gamma(\xi + \psi)$$

$$\Theta_i = 0 \qquad g_i = 1 \qquad S = 0 \qquad z = \nu_m/\omega$$

$$V = y_T^2/[2y_L(1 - x - jz)] \qquad R = V \mp \sqrt{1 + V^2}. \tag{46}$$

The equation for the square of the refractive index becomes the Appleton-Hartree equation, namely:

$$n^2 = 1 - \frac{x}{1 - jz - \dfrac{y_T^2}{2(1 - x - jz)} \pm \left[\dfrac{y_T^2}{4(1 - x - jz)^2} + y_L^2\right]^{1/2}}. \tag{47}$$

IV. Particular Cases

Let us now consider particular cases, when simplification results.

1) Propagation along the magnetic field, *i.e.*, $\theta = 0$:

One obtains two transverse cyclotron waves, according to the $\pm$ sign in the denominator, given by

$$n^2 = 1 - \frac{x}{h_+ - jg_+ z + h_+ y} = 1 - 2\psi = \epsilon_{11} - \epsilon_{12} \tag{42}$$

and

$$n^2 = 1 - \frac{x}{h_- - jg_- z - h_- y} = 1 - 2\xi = \epsilon_{11} + \epsilon_{12}. \tag{43}$$

The wave with h_- and g_- corresponds to the electron cyclotron wave (sometimes called the extraordinary wave for $\theta = 0$), and displays a resonance at $y = 1$ or $\omega = \omega_b$. The wave with h_+ and g_+ corresponds to the ion cyclotron wave (sometimes called the ordinary wave for $\theta = 0$). The terminology of "ion cyclotron wave" is adopted, because this wave would also display a resonance at the ion cyclotron frequency (at $\omega = eB/M_+$) if ion motions were included in the analysis.[6]

2) Propagation perpendicular to the magnetic field, *i.e.*, $\theta = 90$:

One obtains the ordinary and extraordinary waves. The ordinary wave results from choosing the minus sign in the denominator,

$$n^2 = 1 - \frac{x}{h_0 - jg_0 z} = 1 - \gamma = \epsilon_{33}, \tag{44}$$

and the extraordinary wave results from the plus sign in the denominator,

$$n^2 = \frac{(1 - 2\psi)(1 - 2\xi)}{1 - \psi - \xi} = \frac{(\epsilon_{11} - \epsilon_{12})(\epsilon_{11} + \epsilon_{12})}{\epsilon_{11}}. \tag{45}$$

3) Constant collision frequency and a slightly ionized gas:

The classic Appleton-Hartree equation, usually applied to ionospheric work, results. Note the simplification for this case namely that the angular term in the numerator is zero and so are several factors in the denominator. (Here, and in the following cases, the angle

4) High collision frequencies, when $(\langle\nu_u\rangle) \gg \omega_b$ and $(\langle\nu_u\rangle) \gg \omega$:

In a recent article by the author[5] it is shown that $h_0 = h_+ = h_- = h(0)$ and $g_0 = g_- = g_+ = g(0)$, where $h(0)$ and $g(0)$ are the values of the functions for zero argument. Let us define an effective normalized collision frequency for this case as

$$z_1 = zg(0)/h(0) = \langle\nu_u\rangle g(0)/\omega h(0) \tag{48}$$

and a reduced plasma frequency x_1 as

$$x_1 = x/h(0) = \omega_p^2/\omega^2 h(0). \tag{49}$$

The simplification in the Θ and g functions is given in Table I, Column 2. The refractive index satisfies the Appleton-Hartree equation (47), with x_1 and z_1 defined in (48) and (49), replacing x and z. The correction factors, $g(0)$ and $h(0)$, depend on the degree of ionization and on the variation with electron speed of ν_m, the electron collision frequency with neutrals. For example,[5] in very slightly ionized nitrogen, $g(0) = 0.6$ and $h(0) = 3.0$, since in nitrogen, $\nu_m \propto v^2$.

5) High RF angular frequencies, when

$$\text{a) } \omega \gg (\langle\nu_u\rangle) \quad \text{and} \quad \text{b) } \omega \gg \omega_b$$

or

$$\text{a) } \omega \gg (\langle\nu_u\rangle) \quad \text{and} \quad \text{b) } \omega_b \gg \omega$$

or

$$\text{a) } \langle\nu_u\rangle \cong 0 \quad \text{and} \quad \text{b) } \omega \neq \omega_b.$$

As discussed in Section II, all the g and h functions approach 1, and hence, the usual Appleton-Hartree equation (47) results, with $z = \langle\nu_u\rangle/\omega$. Note, that the collision frequency to be applied is that defined in (5), and results quoted in the literature must be checked to determine whether they refer to the same average.

6) High magnetic fields, satisfying

$$\text{a) } \omega_b \gg (\langle\nu_u\rangle) \qquad \text{b) } \omega_b \gg \omega.$$

In this case, $h_+ = h_- = g_+ = g_- = 1$, but g_0 and h_0 depend on $\omega/\langle\nu_u\rangle$. If one also has $\omega \gg (\langle\nu_u\rangle)$, case 5) results. If on the other hand, $\omega \ll (\langle\nu_u\rangle)$, then $g_0 = g(0)$ and $h_0 = h(0)$.

TABLE I

SIMPLIFICATION OF THE Θ AND g FUNCTIONS IN THE GENERALIZED APPLETON-HARTREE EQUATION FOR PARTICULAR CASES (SEE TEXT)

Function	a) Case 3 ν_m constant and neutral dominated b) Case 5 $\omega \gg \langle \nu_g \rangle$ and $\omega \gg \omega_h$ c) Case 5 $\omega \gg \langle \nu_g \rangle$ and $\omega \ll \omega_h$ d) Case 5 $\langle \nu_g \rangle \cong 0$ and $\omega \neq \omega_h$ e) Case 8 $\nu_g = \nu_m + \nu_{ei}$ constant
$g_0, \pm$	1
$h_0, \pm$	1
$\Theta_{1,2,3,4,5}$	0
$g_{1,2,3,4}$	1
S	0
V	$\dfrac{yz^2}{2y_L(1-x-jz)}$

Function	Case 4 $(\langle \nu_g \rangle) \gg \omega_h$ and $(\langle \nu_g \rangle) \gg \omega$	Case 6 $\omega_h \gg \omega$ and $\omega_h \gg (\langle \nu_g \rangle)$	Case 7 $y=1$ and $(\langle \nu_g \rangle) \ll \omega = \omega_h$
g_0	$g(0)$	g_0	1
g_-	$g(0)$	1	$g(0)$
g_+	$g(0)$	1	1
h_0	$h(0)$	h_0	1
h_-	$h(0)$	1	$h(0)$
h_+	$h(0)$	1	1
Θ_1	0	g_0-1	$[1-g(0)]/2$
Θ_2	0	0	$[1-g(0)]/2$
Θ_3	0	h_0-1	0
Θ_4	0	g_0+h_0-2	$3[1-g(0)]/2$
Θ_5	0	g_0-1	$[1-g(0)]/2$
g_1	$h(0)$	1	1
g_2	$g(0)$	1	$[1+g(0)]/2$
g_3	$\lvert h(0)\rvert^2$	$1+(h_0-1)/y^2 \cong 1$ since $y \gg 1$	1
g_4	$h(0)$	1	1
S	0	$\left(\dfrac{z(g_0-1)+j(h_0-1)}{h_0-x-jg_0z}\right)\sin^2\theta$	$\dfrac{z[1-g(0)]\sin^2\theta}{2(1-x-jz)}$
V	$\dfrac{\lvert h(0)\rvert^2 y_T^2}{2y_L(h(0)-x-jg(0)z)}$	$\dfrac{[h_0-1-jz(g_0-1)](1-jz)\sin^2\theta}{2(h_0-x-jg_0z)}$	$\left(\dfrac{2-jz[1-g(0)](3-jz)}{2(1-x-jz)}\right)\sin^2\theta$

The general equation for the refractive index reduces to

$$n^2 = 1 - \frac{x - x\left[-jz(g_0-1)+(h_0-1)\right]\sin^2\theta/(h_0-x-jg_0z)}{1-jz-\left\{\left(\dfrac{y^2+(1-jz+x)[h_0-1-jz(g_0-1)]}{2(h_0-x-jg_0z)}\right)\sin^2\theta \pm \left[\left(\dfrac{y^2+(1-jz-x)[h_0-1-jz(g_0-1)]}{2(h_0-x-jg_0z)}\right)^2 \sin^4\theta + y^2\cos^2\theta\right]^{1/2}\right\}}. \tag{50}$$

7) Cyclotron resonance ($y=1$) with $\omega = \omega_h \gg (\langle \nu_g \rangle)$:

We now have $g_- = g(0)$, $h_- = h(0)$ and $g_0 = g_+ = 1$, $h_0 = h_+ = 1$, $y = 1$. The modified Appleton-Hartree equation is (see Column 4 of Table I)

$$n^2 = 1 - \frac{x + jxz(1-g(0))\sin^2\theta/[2(1-jz-x)]}{1-jz\dfrac{(1+g(0))}{2}+\left\{\left(\dfrac{jz(1-g(0))(3-jz+x)-2}{4(1-x-jz)}\right)\sin^2\theta \pm \left[\left(\dfrac{jz(1-g(0))(3-jz-x)-2}{4(1-x-jz)}\right)^2 \sin^4\theta + \left(1-jz\dfrac{(1-g(0))}{2}\right)^2\cos^2\theta\right]^{1/2}\right\}}. \tag{51}$$

Note that the results, exactly at resonance, are independent of $h(0)$.

8) Constant total collision frequency:

We consider the situation when over a reasonable velocity range, ν_g, given by (7),

$$\nu_g = \nu_m(v) + \nu_{ei}(v) = \nu_m(v) + \frac{4\pi N_+}{v^3}\left(\frac{Ze^2}{4\pi\epsilon_0 m}\right)^2 \ln\Lambda, \tag{52}$$

is constant with respect to velocity. If ν_m varies as v^2, then ν_g is nearly constant[5] when $\langle \nu_m \rangle / \langle \nu_{ei} \rangle$ is between 2.25 and 3.7, since in this range $0.92 \leq g \leq 1$ and $1 \leq h \leq 1.038$. If ν_m varies as v, then $0.96 \leq g \leq 1$ and $1 \leq h \leq 1.035$, when $\langle \nu_m \rangle / \langle \nu_{ei} \rangle$ is between 3 and 15. Assuming that the error in taking g and h equal to 1 is small, the relationship for n reduces to the Appleton-Hartree equation (47), with z denoting ν_g/ω.

V. Application to the Ionosphere

In general, one can plot from the calculated g and h curves, the Θ and $\mathcal{G}$ functions vs $\langle\nu_u\rangle/\omega$ for various ω_b/ω and $\langle\nu_m\rangle/\langle\nu_{ei}\rangle$. The investigation that follows is for ν_m proportional to v^2. This applies up to about 120 km in the ionosphere, where electron collisions with the nitrogen species are predominant over collisions with the oxygen atoms. The usual assumption that the atmosphere is dry (contains no water vapor) is made throughout this discussion. Typical graphs are shown in Figs. 1–9 (pp. 1864–1868) for degrees of ionization corresponding to 1) a weakly ionized gas ($\langle\nu_m\rangle/\langle\nu_{ei}\rangle\to\infty$), 2) equal frequencies of electron collisions with neutrals and ions ($\langle\nu_m\rangle/\langle\nu_{ei}\rangle\cong 1$), and 3) an ion-dominated plasma ($\langle\nu_m\rangle/\langle\nu_{ei}\rangle\to 0$). Values of ω_b/ω equal to 10^4 or 10^3, 10^2, 10, 1 or 0.999, 10^{-1}, 10^{-2}, 10^{-4} are used.

Note the following characteristics in the figures:

1) For large $\langle\nu_u\rangle/\omega$, the Θ curves approach zero and the $\mathcal{G}$ curves approach the values given in Column 2 of Table I. Also, the lower the value of ω_b/ω, the quicker the curve attains its limit.

2) For negligible $\langle\nu_u\rangle/\omega$ and $\omega\neq\omega_b$, the Θ and $\mathcal{G}$ curves are respectively equal to 0 and 1, which should be so according to Column 1 of Table I. At cyclotron resonance, the curves assume the values tabulated in the last column of Table I. Note that if $\omega_b/\omega=0.999$, deviations towards zero or 1 occur for extremely small $\langle\nu_u\rangle/\omega$.

3) In the limit of $\omega_b\gg\langle\nu_u\rangle\gg\omega$, which, for example, occurs when $\omega_b/\omega=10^4$ and $10<(\langle\nu_u\rangle/\omega)<10^3$, some curves flatten out and tend towards the values given in Column 3 of Table I. If ω_b/ω is lower than 10^4, they never actually attain these limits.

4) The largest deviations are present in the curves for the slightly ionized gas, and the least in the partially ionized gas, $\langle\nu_m\rangle\approx\langle\nu_{ei}\rangle$. As the ionization increases, the $\mathcal{G}$ curves shift towards 1 and the Θ curves towards zero, and then they deviate more when $\langle\nu_m\rangle/\langle\nu_{ei}\rangle$ becomes less than 3. Finally, the limiting values for a completely ionized gas are attained.

The graphs show that the approach to the limiting values is slow in most cases, and hence the use of equivalent collision frequencies in the Appleton-Hartree equation must be justified by investigating curves such as illustrated here.

The curves in Figs. 1–9 are not sufficiently accurate to calculate the refractive index. As an example of the difficulty, consider the magnitude of the $(-y^2\mathcal{G}_3+z^2\Theta_5)$ combination in the generalized Appleton-Hartree equation (30). In many cases, one cannot obtain reasonable values, simply because of the inaccuracy in the $\mathcal{G}_3$ and Θ_5 functions. One can conclude that the Θ and $\mathcal{G}$ functions are only useful for illustrating the physical fact that large deviations from zero and unity can occur, and for providing regions where their replacement by limiting constants can be justified.

Values for the electron collision frequency with nitrogen molecules will now be given, and applied to the D layer of the ionosphere, or in general to heights below 85 km. Basically, the formula used for nitrogen is identical to that given by Huxley.[13,14] The cross section for nitrogen, Q_{N_2}, is[15]

$$Q_{N_2}=3.29\times 10^{-23}v\ \text{cm}^2\ (v\ \text{in cm/sec}) \tag{53}$$

and 0.8 times this value for air.

$$Q_{\text{air}}=2.63\times 10^{-23}v\ \text{cm}^2. \tag{54}$$

If N_M is the number density of air molecules, the collision frequency is

$$\nu_m=N_m vQ=2.63\times 10^{-23}v^2(\rho/\rho_0)L_0 \tag{55}$$

where

ρ is the density,
ρ_0 is the density at standard temperature and pressure, and
L_0 is Loschmidth's number
$L_0=p_0/kT_0=2.687\times 10^{19}$ molecules/atm.cm^3.

Hence for air

$$\begin{aligned}\nu_m&=7.073\times 10^{-4}(\rho/\rho_0)v^2(v\ \text{in cm/sec})\\&=7.073(\rho/\rho_0)v^2(v\ \text{in m/sec}).\end{aligned} \tag{56}$$

The high-frequency average is calculated from (12) to be equal to

$$\begin{aligned}\langle\nu_m\rangle&=5.359T\rho/\rho_0\times 10^8\\&=1.9944N_M T\times 10^{-17}(N_M\ \text{in}\ 1/m^3).\end{aligned} \tag{57}$$

Three different average collision frequencies are currently in use in the literature, namely $\langle\nu_m\rangle$, $\bar{\nu}_m$ and ν_P, defined, for a variation of $\nu_m\propto v^2$

respectively by $\langle\nu_m\rangle=(\overline{1/v^2})\overline{d/dv}(\overline{v^3\nu_m/3})=5\overline{\nu_m}/3$,

$$\nu_m=\nu_m$$

and $\nu_P=0.4\langle\nu_m\rangle$. A bar denotes the following average for a scalar quantity ϕ

$$\bar{\phi}=(1/N)\int\phi f_0 4\pi v^2 dv.$$

[13] L. G. H. Huxley, "A discussion of the motion in nitrogen of free electrons with small energies with reference to the ionosphere," *J. Atm. and Terr. Phys.*, vol. 16, pp. 46–58; October, 1959.

[14] I. P. Shkarofsky, *et al.*, "Collision frequency associated with high temperature air and scattering cross-sections of the constituents," in "Electromagnetic Effects of Re-entry," Pergamon Press, New York, N. Y.; 1961.

[15] Phelps in a recent article[1] uses values for nitrogen which are 15 per cent larger than these. In a footnote, he quotes measurements, which should read, "are 10–12 per cent smaller" than given in his paper, so that his new values are 3–5 per cent larger than given here. For consistency, the analysis here is based exclusively on the cross sections plotted in Shkarofsky.[14] Also, for simplicity, the contribution from oxygen is neglected, since the additional error introduced is less than 15 per cent.

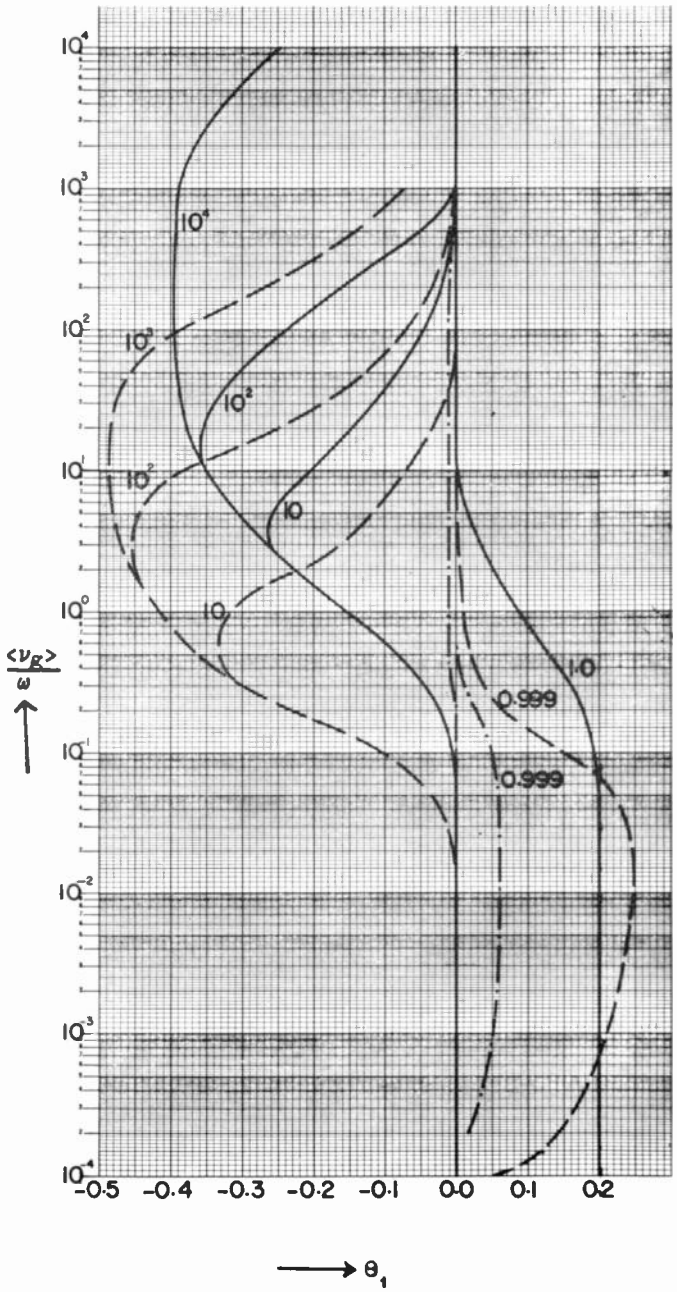

Fig. 1—The function Θ_1. The numbers beside the curves are values of ω_b/ω.
The set ——— corresponds to $\langle \nu_m \rangle / \langle \nu_{ei} \rangle = \infty$
—·—·— $\langle \nu_m \rangle / \langle \nu_{ei} \rangle = 1$
— — — $\langle \nu_m \rangle / \langle \nu_{ei} \rangle = 0$

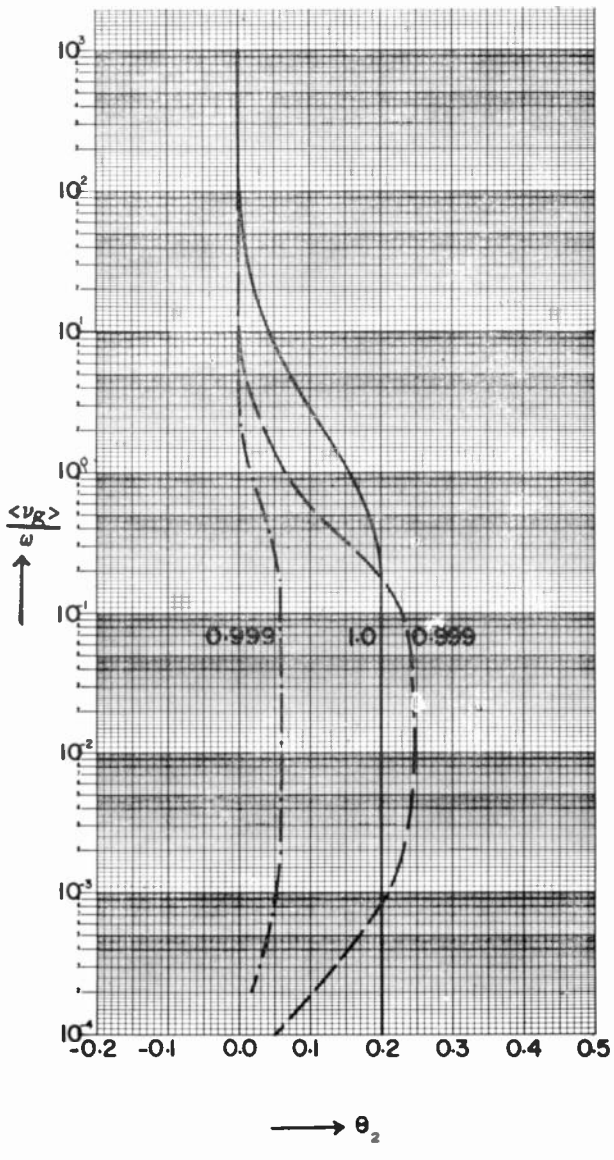

Fig. 2—The function Θ_2. The numbers beside the curves are values of ω_b/ω.
The set ——— corresponds to $\langle \nu_m \rangle / \langle \nu_{ei} \rangle = \infty$
—·—·— $\langle \nu_m \rangle / \langle \nu_{ei} \rangle = 1$
— — — $\langle \nu_m \rangle / \langle \nu_{ei} \rangle = 0$

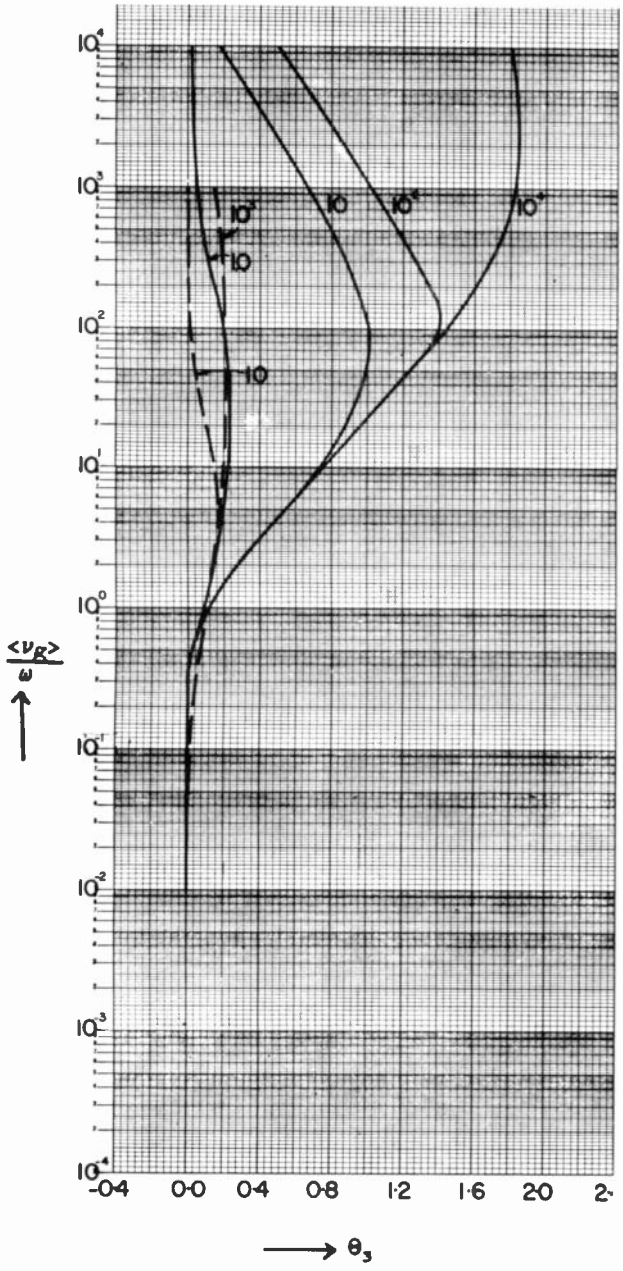

Fig. 3—The function Θ_3. The numbers beside the curves are values of ω_h/ω.
The set ——— corresponds to $\langle \nu_m \rangle / \langle \nu_{ei} \rangle = \infty$
Take $\Theta_3 = 0$ for $\langle \nu_m \rangle / \langle \nu_{ei} \rangle = 1$
— — — $\langle \nu_m \rangle / \langle \nu_{ei} \rangle = 0$

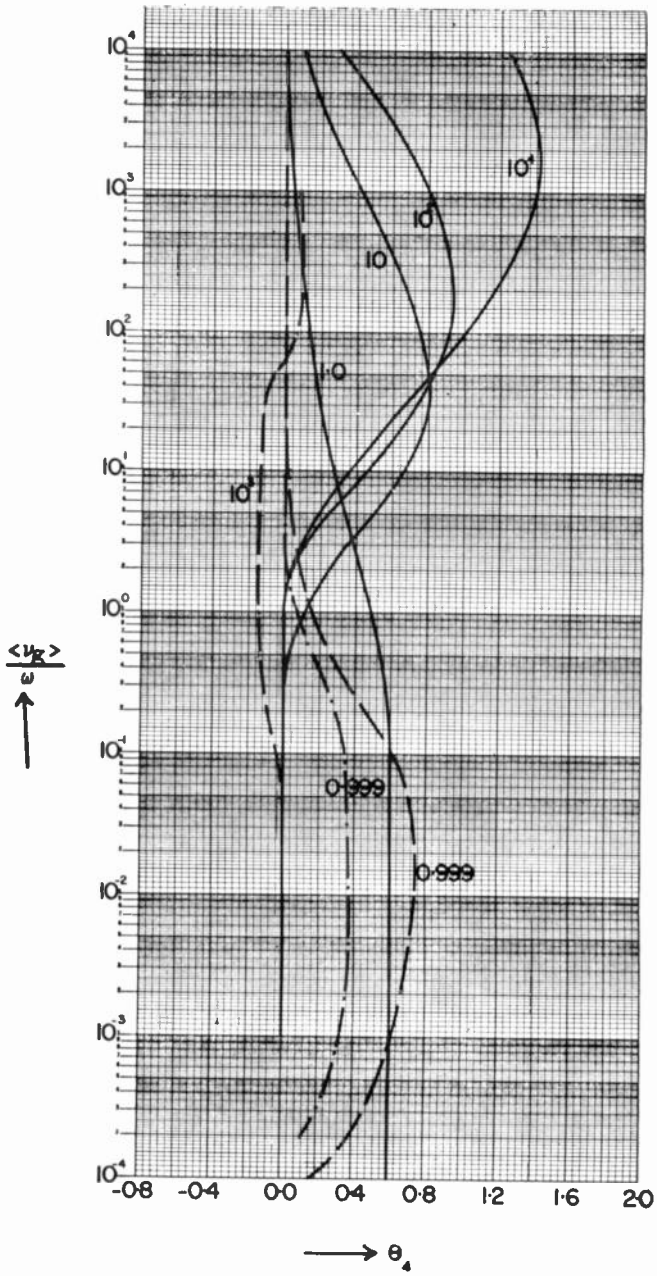

Fig. 4—The function Θ_4. The numbers beside the curves are values of ω_h/ω.
The set ——— corresponds to $\langle \nu_m \rangle / \langle \nu_{ei} \rangle = \infty$
—·—·— $\langle \nu_m \rangle / \langle \nu_{ei} \rangle = 1$
— — — $\langle \nu_m \rangle / \langle \nu_{ei} \rangle = 0$

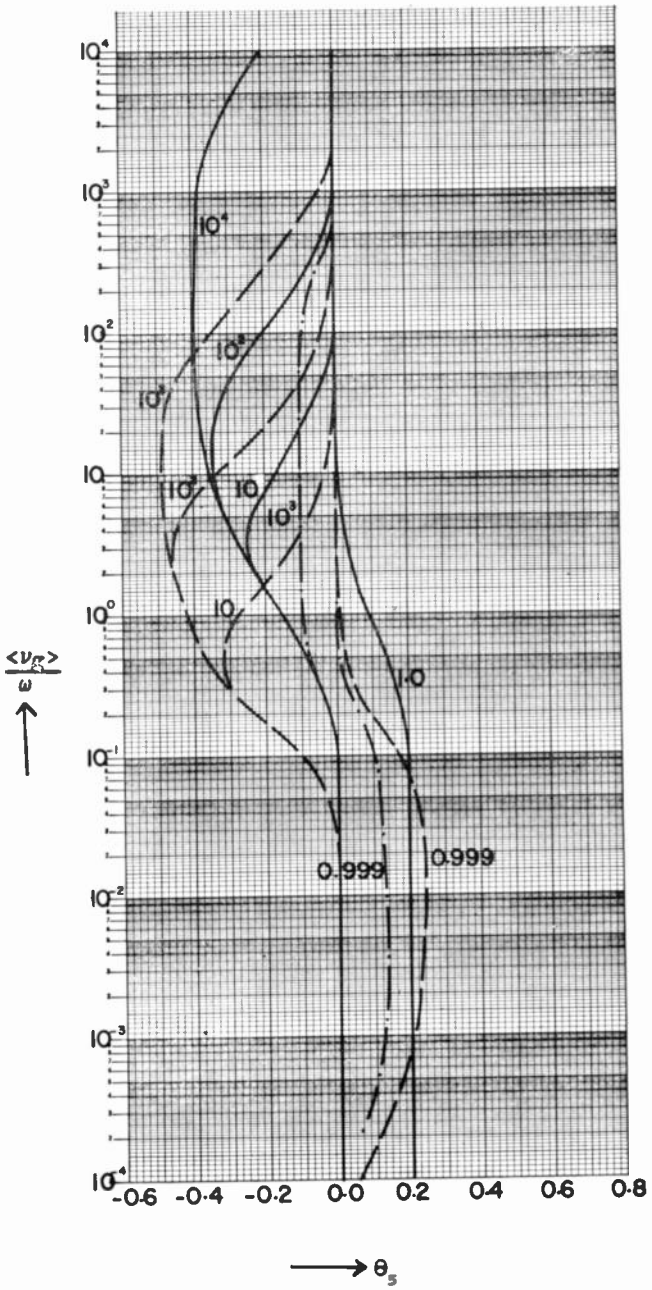

Fig. 5—The function Θ_b. The numbers beside the curves are values of ω_b/ω.
The set ———— corresponds to $\langle \nu_m \rangle / \langle \nu_{ei} \rangle = \infty$
—·—·— $\langle \nu_m \rangle / \langle \nu_{ei} \rangle = 1$
— — — $\langle \nu_m \rangle / \langle \nu_{ei} \rangle = 0$

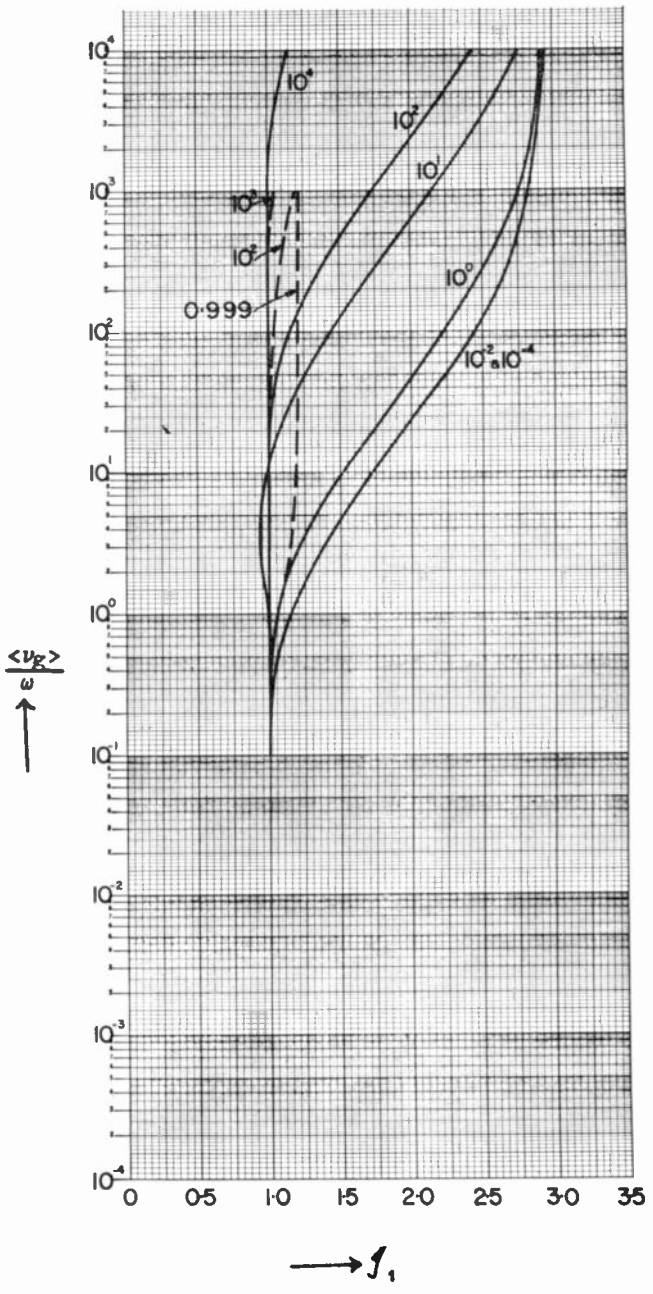

Fig. 6—The function ϑ_1. The numbers beside the curves are values of ω_b/ω.
The set ———— corresponds to $\langle \nu_m \rangle / \langle \nu_{ei} \rangle = \infty$
Take $\vartheta_1 = 1$ for $\langle \nu_m \rangle / \langle \nu_{ei} \rangle = 1$
— — — $\langle \nu_m \rangle / \langle \nu_{ei} \rangle = 0$

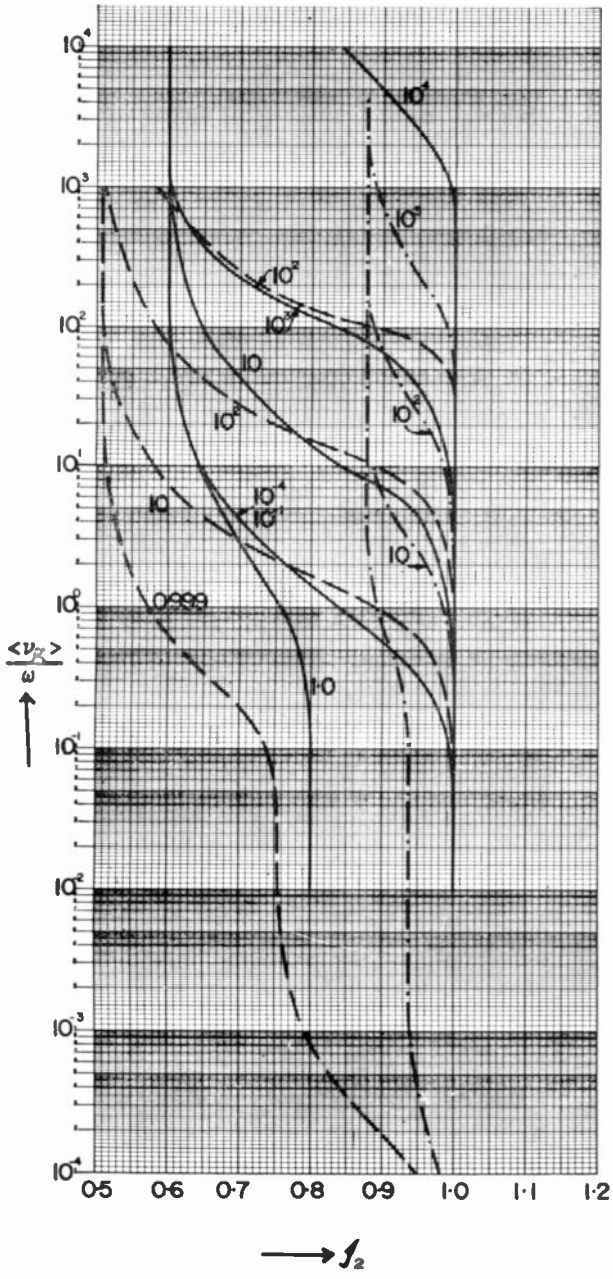

Fig. 7—The function g_2. The numbers beside the curves are values of ω_b/ω.
The set ——— corresponds to $\langle \nu_m \rangle / \langle \nu_{ei} \rangle = \infty$
—·—·— $\langle \nu_m \rangle / \langle \nu_{ei} \rangle = 1$
— — — $\langle \nu_m \rangle / \langle \nu_{ei} \rangle = 0$

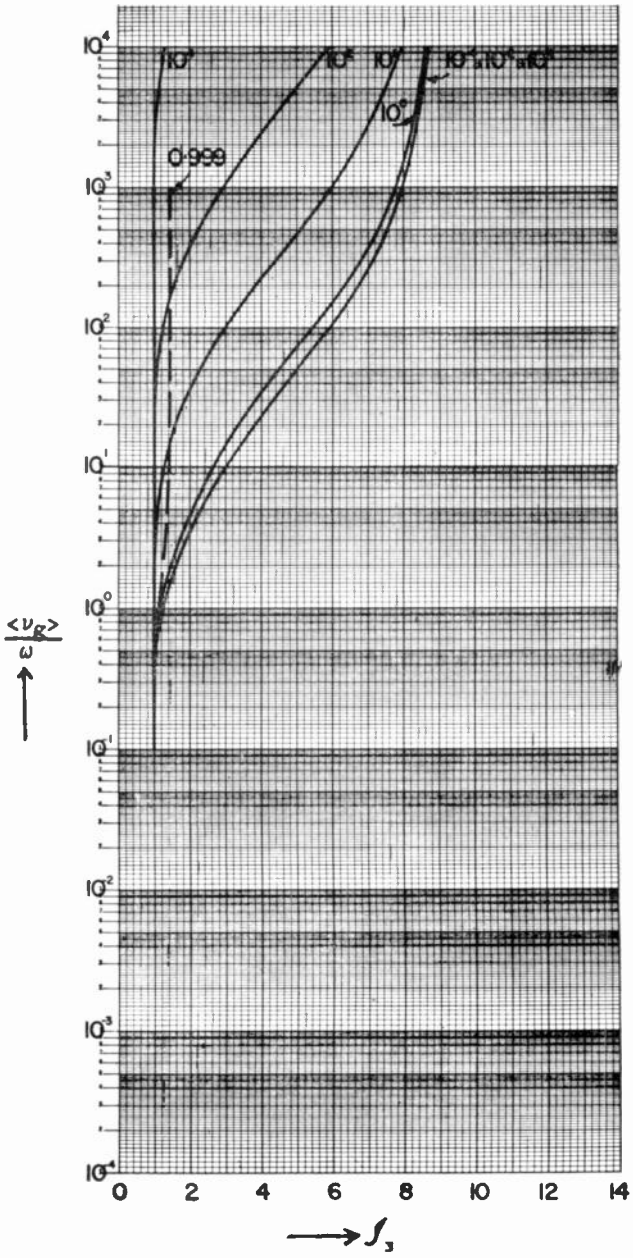

Fig. 8—The function g_3. The numbers beside the curves are values of ω_b/ω.
The set ——— corresponds to $\langle \nu_m \rangle / \langle \nu_{ei} \rangle = \infty$
Take $g_3 = 1$ for $\langle \nu_m \rangle / \langle \nu_{ei} \rangle = 1$
— — — $\langle \nu_m \rangle / \langle \nu_{ei} \rangle = 0$

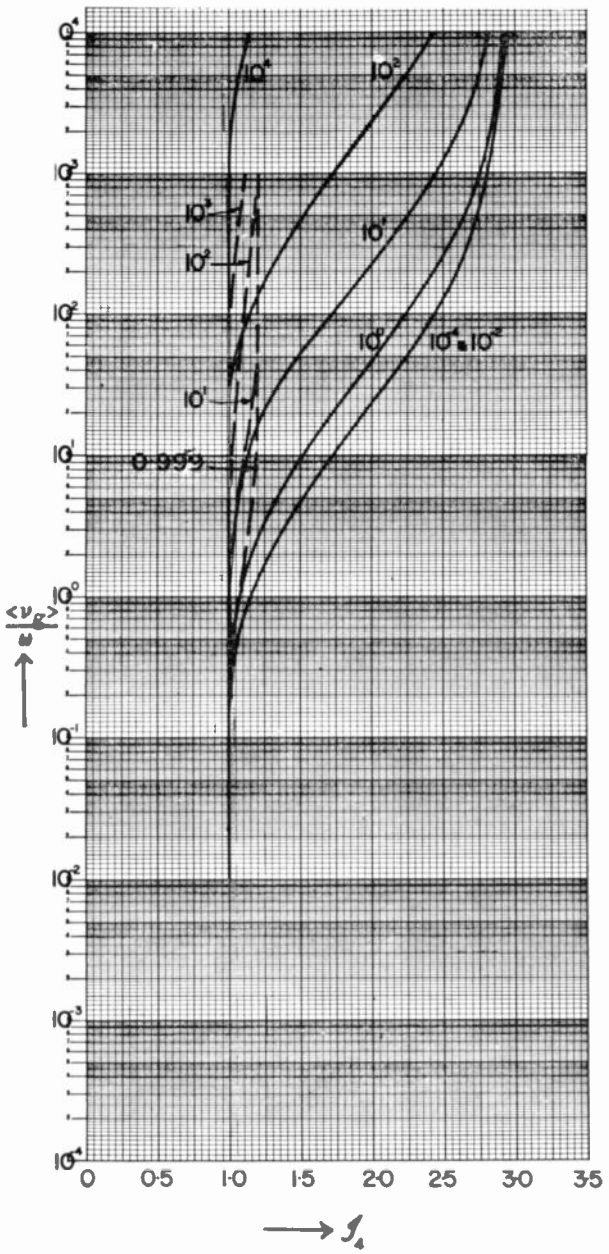

Fig. 9—The function g_4. The numbers beside the curves are values of ω_h/ω.
The set ——— corresponds to $\langle \nu_m \rangle / \langle \nu_{ei} \rangle = \infty$
Take $g_4 = 1$ for — — — $\langle \nu_m \rangle / \langle \nu_{ei} \rangle = 1$
— — — $\langle \nu_m \rangle / \langle \nu_{ei} \rangle = 0$

Many discrepancies between quoted values, such as those of Huxley,[13] who uses the second average, and those of Phelps and Pack[1,4] and Seddon,[16] who adopt the third average, vanish, if this point is remembered. Here, the first average $\langle \nu_m \rangle$ is adopted. As a result, *the values of the collision frequency $\langle \nu_m \rangle$ here are 2.5 times larger than those plotted by Phelps, Pack and Seddon.* Another point to note[14] is that the measurements of the collision cross section of electrons with nitrogen molecules by Huxley,[13] by Phelps, *et al.*,[17] and by Phelps and Pack,[1] using different respective methods, all practically coincide numerically.

An attempt is now made to plot for the ionosphere the quantities $\langle \nu_g \rangle$ and $\langle \nu_m \rangle / \langle \nu_{ei} \rangle$ vs altitude up to 340 km, which is above the F_2 layer. One is immediately faced with three unknowns.

1) The electron density profile depends on local time, season, solar activity and latitude.

2) Although nitrogen is the basic constituent of air below 90 km, electron collisions with oxygen atoms become important at higher altitudes and comparable to that with nitrogen molecules in the F_2 layer. The exact relative proportion of nitrogen molecules and oxygen atoms vs height is unknown.

3) The electron temperature is unknown; it may be quite different, by as much as a factor of 5, than the temperature of the neutral particles. Furthermore, the velocity distribution of the electrons may also be non-Maxwellian.

For discussion, one can assume an average daytime profile[16,18,19] of electron density, shown in Fig. 10. A plasma frequency scale is also shown. We will also adopt the 1959 ARDC model of the atmosphere,[20] which provides values for the molecular weight, as well as for the gas temperature T_0 and neutral particle density N_M. Electron collisions with neutral oxygen molecules are neglected as being small compared with collisions with nitrogen molecules.

Below 90 km, effects due to oxygen atoms[20] can also be neglected, and (57) applies for $\langle \nu_m \rangle$ in air.

Above 180 km, oxygen is assumed to be completely dissociated, and air can be considered to consist only of N_2 and O. Then the relative number densities are given in terms of the molecular weight of air

$$M = (28.016 N_{N_2} + 16 N_0)/N_M \tag{58}$$

by

$$N_{N_2} = N_M(M - 16)/12.016 \text{ and } N_0 = N_M - N_{N_2} \tag{59}$$

where N_{N_2} is the number density of nitrogen, whose molecular weight is 28.016, N_0 is the number density of oxygen atoms (molecular weight = 16), and N_M is the number density of air (molecular weight = M). From the tabulated data[20] for N_M and M, the quantities N_{N_2} and N_0 can be obtained. Let $\langle \nu_{N_2} \rangle$ and $\langle \nu_0 \rangle$ be the averaged collision frequencies for N_2 and O. Then we know (see Section II) that the averages can be added to yield

[16] J. C. Seddon, "Summary of Rocket and Sate lite Observations Related to the Ionosphere," Natl. Aeronautics and Space Admin., Goddard Space Flight Ctr., Washington, D. C., NASA Note D-667; 1961.

[17] A. V. Phelps, *et al.*, "Microwave determination of the probability of collision of slow electrons in gases," *Phys. Rev.*, vol. 84, pp. 559–562; November 1, 1951.

[18] See "The Ionosphere"—IGY issue of PROC. IRE, vol. 47, pp. 167, 169, 273, 281, 292; February, 1959.

[19] J. A. Ratcliffe, Ed., "Physics of the Upper Atmosphere," Academic Press, New York, N. Y., pp. 409–411, 442–445; 1960.

[20] R. A. Minzner, *et al.*, "The ARDC Model Atmosphere, 1959," A.F. Cambridge Research Ctr., Cambridge, Mass., Rep. AFCRC-TR-59-267; August, 1959.

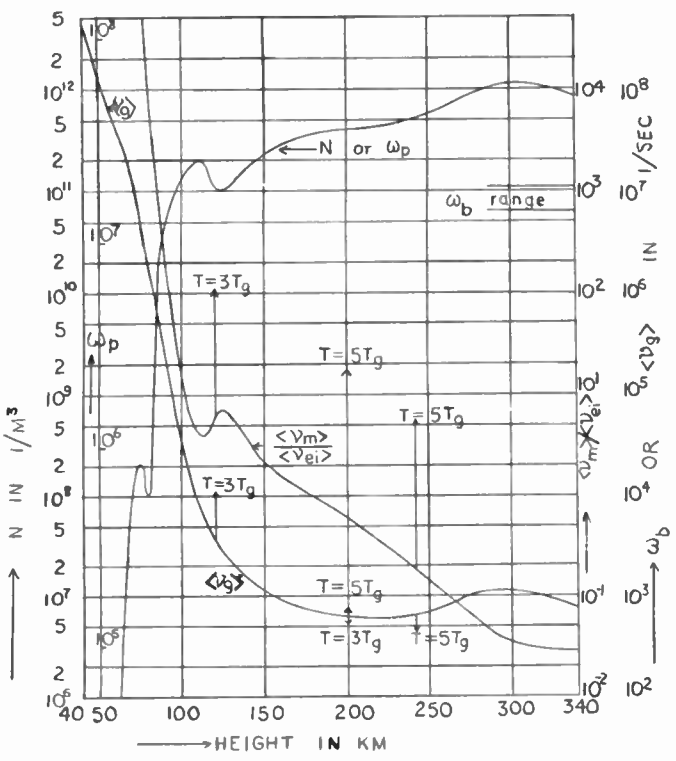

Fig. 10—The ratio $\langle\nu_m\rangle/\langle\nu_{ei}\rangle$ and the total collision frequency $\langle\nu_g\rangle$, vs height for an assumed average daytime profile of electron density (N) or plasma frequency (ω_p), if the electron and neutral particle temperatures are equal. The range in value of the cyclotron frequency (ω_b) is also shown. The arrows indicate possible deviations if the electron temperature is larger than the neutral particle temperature by the amount shown.

the average collision frequency with all neutrals, $\langle\nu_m\rangle$, *viz.*,

$$\langle\nu_m\rangle = \langle\nu_{N_2}\rangle + \langle\nu_0\rangle. \tag{60}$$

The value of $\langle\nu_{N_2}\rangle$ is (1/0.8) times that in (57), since $\langle\nu_m\rangle$ was assumed there to be 80 per cent that of $\langle\nu_{N_2}\rangle$. Thus,

$$\langle\nu_{N_2}\rangle = 2.492 N_{N_2} T \times 10^{-17}. \tag{61}$$

This equation applies if the electron temperature is less than about 1500°K, which would be true[20] up to 400 km, if the electron and gas temperatures are equal ($T \cong T_g$). For higher temperatures, $\langle\nu_{N_2}\rangle$ does not vary as T, since[14] ν_{N_2} is not proportional to v^2. It is known[11] that the cross section of electron collisions with oxygen atoms, based on the analyses of Klein and Brueckner,[21] is nearly constant with speed and equal to 10^{-19} m^2. The analyses of Mitra, Yamanouchi, Robinson, Hammerling, *et al.*, and Lamb and Lin, which predict large cross sections at low electron energies, have been shown[14] to be questionable. A low cross section was also found experimentally by Lin and Kivel.[22] We therefore write

$$\nu_0 = N_0 v \times 10^{-19} \tag{62}$$

and averaging according to (12) yields

$$\langle\nu_0\rangle = 0.8282 \times 10^{-15} T^{1/2} N_0. \tag{63}$$

Adding, (60) becomes (for $T \leq 1500$°K)

$$\langle\nu_m\rangle = 0.8282 \times 10^{-15} N_0 T^{1/2} + 2.493 \times 10^{-17} N_{N_2} T. \tag{64}$$

For reference, the value of ν_m before averaging is, according to (55) and (62), given

$$\nu_m = N_0 v \times 10^{-19} + N_{N_2} v^2 3.29 \times 10^{-25} (v \text{ in } m/s). \tag{65}$$

Between 90 km and 180 km, the relative proportions of N_2, O_2 and O are quite uncertain.[23] However, it is easy to show, from the values[20] of the molecular weight of air as a function of height and from (59), that up to 180 km, the number density of atomic oxygen is certainly not greater than 10 per cent that of nitrogen. Further evidence that this is so is given by Johnson.[24] Assuming that for lower altitudes $N_{N_2} \leq 10\ N_0$, one can neglect the contribution of atomic oxygen given by (63) to the averaged collision frequency and extend the range of (57) up to 180 km, as a first approximation. The error is less than 12.5 per cent.

Most of the uncertainty in the calculation arises from a lack of knowledge of the electron temperature and electron distribution function. The results, to be shown, are based on the ideal assumptions of a Maxwellian distribution and equal electron and gas temperatures. Some calculations based on higher electron temperatures are also shown. The electron and ion densities are assumed equal, and negative ions are neglected. Ions with charge numbers greater than one are assumed to be insignificant.

In Fig. 10, $\langle\nu_g\rangle$, the sum of electron collisions with all neutrals plus ions ($\langle\nu_m\rangle + \langle\nu_{ei}\rangle$) is also plotted where $\langle\nu_m\rangle$ is given by (57) up to 180 km and by (64) above 180 km, and where $\langle\nu_{ei}\rangle$ is given by (11). In MKS units,

$$\langle\nu_{ei}\rangle = 8.375\ N \log \Lambda \times 10^{-6}/T^{3/2}$$

and

$$\Lambda = 1.24 \times 10^7 (T^3/N)^{1/2}. \tag{66}$$

The ratio $\langle\nu_m\rangle/\langle\nu_{ei}\rangle$ is also given vs height. Both are based on the assumption that the electron and gas temperatures are equal. No attempt is made to calculate the conductivity functions g and h, mainly because of the uncertainties in the atomic oxygen concentration and electron temperature, and also because it is shown below that there are regions where g and h are 1.

Several calculations obtained by assuming a higher electron temperature are shown by arrows in Fig. 10.

[21] M. M. Klein and K. A. Brueckner, "Interaction of slow electrons with atomic oxygen and atomic nitrogen," *Phys. Rev.*, vol. 111, pp. 1115–1120; August, 1958.

[22] S. C. Lin and B. Kivel, "Slow-electron scattering by atomic oxygen," *Phys. Rev.*, vol. 114, pp. 1026–1027; May 15, 1959.

[23] Ratcliffe, *op cit.*, p. 34.

[24] C. Y. Johnson, "Aeronomic Parameters from Mass Spectrometry," presented at the Symposium on Aeronomy, Copenhagen, Denmark; July, 1960.

One point is based on measurements with Sputnik III. Krassovsky[25] reports an effective electron temperature of about 7000°K at 242 km, whereas the ARDC value[20] for the air temperature is 1415°K. As a result of $T \cong 5T_g$, the value of $\langle \nu_m \rangle / \langle \nu_{ei} \rangle$ is raised and $\langle \nu_g \rangle$ is decreased at this height. The decrease in $\langle \nu_g \rangle$ is due to the smaller value of $\langle \nu_{ei} \rangle$ which decreases faster with temperature than $\langle \nu_m \rangle$ increases. At heights below 200 km, the ratio $\langle \nu_m \rangle / \langle \nu_{ei} \rangle$ would also be larger, but $\langle \nu_g \rangle$ would be increased rather than decreased. This is because $\langle \nu_m \rangle$ is now the main term in $\langle \nu_g \rangle$ and it increases with temperature. At 200 km, there is only a small change in $\langle \nu_g \rangle$, first a decrease as $T \rightarrow 3T_g$ and then an increase as $T \rightarrow 5T_g$. This result is obtained by plotting $\nu_m = \nu_{N_2} + \nu_O$ vs velocity up to 1 ev, using the collision cross-section data in Shkarofsky, *et al.*,[11] and using the values $N_{N_2} = 7.220 \times 10^{15}$ and $N_O = 1.186 \times 10^{15}$ deduced from Minzner[20] for 200 km. Note that the exact cross-section data for nitrogen is required for these higher temperatures and that ν_{N_2} does not vary as v^2. One finds approximately that ν_m obeys the following power law,

$$\nu_m = 1.265 \times 10^{-5} v^{1.3224} \tag{67}$$

so that

$$\langle \nu_m \rangle = 1.965 T^{.6612}. \tag{68}$$

The sum of $\langle \nu_m \rangle$ and $\langle \nu_{ei} \rangle$ varies little with temperature for 200 km.

The magnetic field of the earth varies between 0.365 and 0.575 gauss, depending on latitude and height. The cyclotron frequency $\omega_b = e\mathcal{B}/m$ is then between 6.42×10^6 and 1.01×10^7, and this is indicated in Fig. 10. We thus see that the largest corrections in the conductivity occur in the D layer (at about 70 km), since $\omega_b \cong \langle \nu_g \rangle$. Above 110 km, in the E and F layers, $\omega_b \geq (10^2 \langle \nu_g \rangle)$, even if $T \cong 5T_g$ or $\langle \nu_g \rangle$ is five times that shown at 110 km. Also, the plasma frequency $\omega_p = (Ne^2/m\epsilon_0)^{1/2}$ is indicated in the figure, and obviously, above 110 km ω_p is much greater than $\langle \nu_g \rangle$. Thus both $x = \omega_p^2/\omega^2$ and $y = \omega_b/\omega$ are much greater than $z = \langle \nu_g \rangle / \omega$. Let us look at Table I. At cyclotron resonance, the last column (case 7) applies. Otherwise, depending on whether $\omega_b \gg \omega$ or $\omega_b \ll \omega$, the third (case 6) or first column (case 5) can be used. Note that provided ω_b is not too near to ω, all the g functions can be taken as one; the Θ functions, however, do not behave as nicely. In the general equation (30), one can neglect Θ_5 since $y^2 g_3 \gg z^2 \Theta_5$.

In the region where $\omega_b \geq (6 \times 10^3 \langle \nu_g \rangle)$, which occurs in the ionosphere above 150 km if $T = T_g$, and above 190 km if $T = 5T_g$, investigation of the g and Θ curves, Figs. 1–9, indicates that it is safe to use the ordinary Appleton-Hartree equation with $\langle \nu_g \rangle$ as the collision frequency, provided the RF angular frequency ω satisfies $\omega_b/\omega \leq 0.9$ or $100 \leq (\omega_b/\omega) \leq 2$. The limit $\omega_b \geq 6 \times 10^3 \langle \nu_g \rangle$, may in fact be less, since as (67) indicates ν_m varies as a power much less than 2, whereas the g and Θ functions are for $\nu_m \propto v^2$. Thus in the F_2 layer, except at cyclotron resonance, it should always be possible to let the g and h correction functions be 1, and the ordinary Appleton-Hartree equation should be applicable.

The region where ν_g is constant with respect to speed depends on $\langle \nu_m \rangle / \langle \nu_{ei} \rangle$. This ratio is quite uncertain because T is unknown. Assuming $T \approx T_g$, the region starts in the E layer and extends to 150 km. If T is five times greater than T_g, then ν_g is constant in the F_2 layer. (See arrow in Fig. 10 and limits for constant ν_g, if $\nu_m \propto v^2$ or $\nu_m \propto v$, given in Section IV, case 8.) This fact provides another justification for letting g and h be 1 in the F_2 layer. In any case, there exists a region where no correction need be applied to the Appleton-Hartree equation, as discussed in case 8. It also seems from the single point of Krassovsky[25] that one has to go to altitudes above the F_2 layer before electron-ion collisions will dominate neutral collisions, since, above 340 km, the neutral particle density decreased more rapidly than the electron density.[26]

VI. Comparison with Experiments

The values of $\langle \nu_g \rangle$ are compared in Fig. 11 with experimental data of Kane,[27] Schlapp,[28] Whitehead[29] and Ataev.[30] Kane's data, plotted here, are those reevaluated[1,31] with the proper v^2 relation for the collision frequency. Recall that the $\langle \nu_g \rangle$ defined here is 2.5 times ν_p, the collision frequency used by Phelps.[1] The values of $\langle \nu_g \rangle$ agree very favorably with Kane's experimental results for the D layer. Ratcliffe[19] also finds good agreement with other experimental data. However, above 90 km, Ratcliffe, Schlapp and Whitehead note that the theoretical values for $\langle \nu_g \rangle$ are appreciably smaller than those obtained experimentally. Ratcliffe and Schlapp suggest that this may be due to atomic oxygen, which they neglect theoretically. In these calculations, however, it is found that the influence of atomic oxygen is small as far as values of $\langle \nu_g \rangle$ are concerned, provided the three assumptions in the analysis are true, namely:

1) atomic oxygen is less than 1/10 the nitrogen concentration below 180 km,

[25] V. I. Krassovsky, "Exploration of the upper atmosphere with the help of the third soviet sputnik," PROC. IRE, vol. 47, pp. 289–296; February, 1959.

[26] Y. L. Albert, "State of the outer ionosphere," *Priroda*, vol. 6, pp. 85–87; 1958. Translated by E. R. Hope, DRB Canada, no. T304R; September, 1958.

[27] J. A. Kane, "Arctic measurements of electron collision frequencies in the D-region of the ionosphere," *J. Geophys. Res.*, vol. 64, pp. 133–139; February, 1960.

[28] D. M. Schlapp, "Some measurements of collision frequency in the E-region of the ionosphere," *J. Atmos. Terr. Phys.*, vol. 16, pp. 340–343; November, 1959.

[29] J. D. Whitehead, "The absorption of short radio waves in the D-, E- and F-regions of the ionosphere," *J. Atmos. Terr. Phys.*, vol. 16, pp. 283–290; November, 1959.

[30] O. M. Ataev, "The determination of the number of collisions in the ionosphere," *Radio Engineering and Electronics*, (Translation of *Radiotekhnika i elektronika* by Pergamon Press, New York, N. Y.), vol. 4, no. 9, pp. 37–45; 1959.

[31] J. A. Kane, "Re-evaluation of ionospheric electron densities and collision frequencies derived from rocket measurements of refractive index and attenuation," Natl. Aeronautics and Space Admin., Goddard Space Flight Ctr., Washington, D. C., NASA TN- D-503; November, 1960.

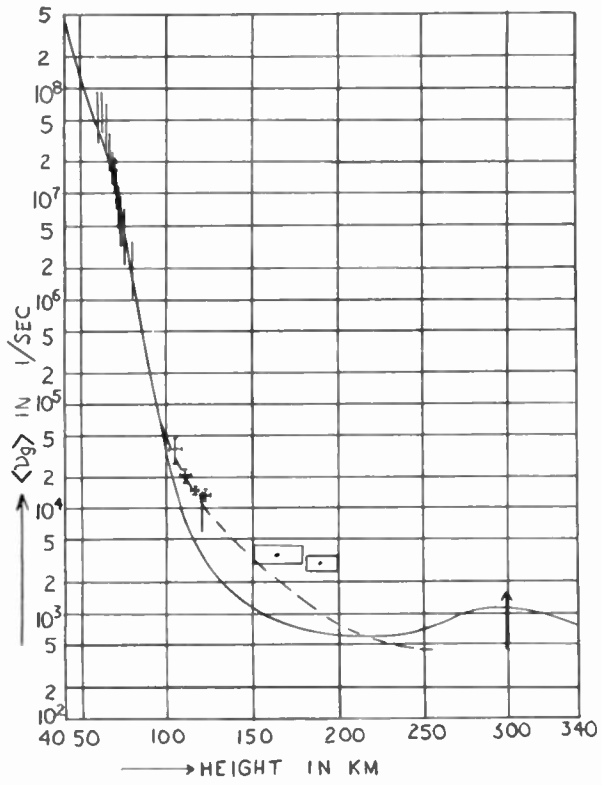

Fig. 11—Comparison of experimental data with the theoretical total collision frequency $\langle \nu_g \rangle$ vs height, replotted from Fig. 10, when $T = T_g$ (solid curve) and T is greater than T_g (dashed curve). The experimental points indicated by vertical lines are those of Kane, by arrows are those of Ataev, by crosses are those of Schlapp and by squares are those of Whitehead.

2) the collision cross section of atomic oxygen is not much greater than that given by Klein and Brueckner[21],
3) the electron and gas temperatures are equal.

Suppose that the electron temperature is greater than the gas temperature above 110 km. Note that at 110 km the gas temperature starts to increase rapidly from about 287°K and reaches 1031°K at 150 km, after which it increases at a slower rate to 1404°K at 200 km. Assume that the electron temperature is much greater at the high temperatures. In Fig. 12, a possible variation is shown, which includes the electron temperatures of 7000°K at 242 km and 15,000°K at 795 km, given by Krassovsky.[25] The latter point has been reevaluated by Whipple[32] to be near 9000°K. If, in the E layer, the electron temperature is about three times the gas temperature (see Fig. 11), the theoretical electron collision frequencies, based on the higher temperature, agree with the experimental values of Schlapp and Ataev in the E layer. Boggess, *et al.*, report rocket data[33] of electron temperatures in the E layer, which indeed indicate a

[32] E. C. Whipple, Jr., "Ion-trap results in 'Exploration of the upper atmosphere with the help of the third Soviet Sputnik,' " PROC. IRE (Correspondence), vol. 47, pp. 2023–2025; November, 1959.

[33] R. L. Boggess, *et al.*, "Langmuir probe measurements in the ionosphere," *J. Geophys. Res.*, vol. 64, pp. 1627–1630; October, 1959.

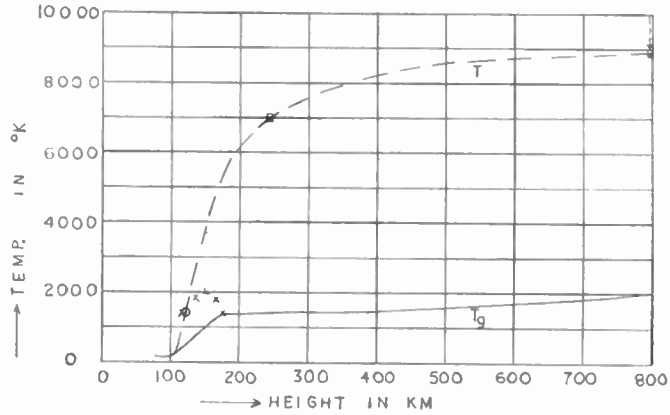

Fig. 12—The temperature of air T_g vs height according to the 1959 ARDC model, and the assumed electron temperature T (dashed curve) vs height. The points at 242 and 795 km are those from Krassovsky. The arrow at 795 km indicates Whipple's interpretation of the Russian measurement, initially deduced to be 15,000°K. The crosses indicate values given by Boggess *et al.* The point ⊙ at 120 km is deduced from Schlapp's and Ataev's values of $\langle \nu_g \rangle$, shown in Fig. 11.

high electron temperature (see Fig. 12), but also a surprising minimum at 175 km. Recent measurements by Boggess[34] indicate that the electron temperature rises to a maximum of 2800°K and becomes isothermal near the F_2 layer (no decline in temperature observed). Whitehead's result for 190 km still remains inexplicable, since, as discussed above, a large change in electron temperature produces a small change in collision frequency at 200 km. Theoretically, the new curve for the collision frequency, shown dashed in Fig. 11, is above the original curve for heights less than 200 km and below the original curve for heights greater than 200 km. Ataev's result for the F_2 layer seems to favor the original curve based on $T = T_g$. However, measurements of collision frequency in the F_2 layer are widely scattered[30] in value and inconclusive.[19] More accurate and systematic measurements, possibly sounding by satellites from above the ionosphere, will check the hypothesis that $T > T_g$ in the F_2 layer, since the hypothesis predicts smaller collision frequency values than given by letting $T = T_g$. This effect is reversed in the E layer where higher temperatures give higher collision frequencies, and, indeed, Schlapp and Ataev find the collision frequency to be higher than expected. One may also suggest that if the hypothesis proves to be correct a measurement of electron collision frequency in the ionosphere may be a sensitive method for determining the electron temperature, especially in the E layer.[35]

Acknowledgement

It is a pleasure to thank Dr. T. W. Johnston and Dr. M. P. Bachynski for stimulating and fruitful discussions.

[34] R. L. Boggess, private communication; March 13, 1961.

[35] A similar suggestion has been made by M. Nicolet, "Collision frequency of electrons in the terrestrial atmosphere," *Phys. Fluids*, vol. 2, pp. 95–99; March–April, 1959, in connection with the electron-ion collision frequency in the F_2 layer.

The Electrical Conductivity of a Partially Ionized Gas*

DIPAK L. SENGUPTA†, MEMBER IRE

Summary—**The electrical conductivity of a low density and partially ionized gas where both electron-neutral particle and Coulomb type collisions play important roles is discussed. The effects of inelastic collisions and a steady magnetic field are not considered. We assume that the ionized gas is perturbed by a weak electric field, and obtain the velocity distribution function for the electrons by solving the Boltzmann equation; the collision between neutral and charged particles is accounted for by the hard sphere model for the particles, while the collision between the charged particles is taken care of by the Fokker-Planck terms. Explicit expressions for ac and dc conductivity are given for various cases. To the extent that the assumptions made for the collision models are valid, the expressions for conductivity given here are quite general and can be used for any degree of ionization.**

Introduction

THE purpose of this paper is to derive expressions for the electrical conductivity of a low-density and partially ionized gas where both electron-neutral particles and Coulomb type collisions between the charged particles play important roles. During the past, considerable work has been done along this line. Margenau[1] and his group published a series of papers dealing mostly with low-intensity fields and weakly ionized gases. Spitzer and his co-workers[2] on the other hand dealt with the small signal static conductivity of low density fully ionized gases. In a weakly ionized gas, Coulomb collisions between charged particles are neglected. In the fully ionized gas it is the Coulomb collisions which determine the electron velocity distribution function.

The present paper deals with an intermediate case of the interaction between a low-intensity electromagnetic field and a partially ionized gas where neither the electron-neutral particles nor the Coulomb collisions can be neglected. The effects of inelastic collisions and a steady magnetic field are neglected in the present analysis. The elastic collision between electrons and neutral particles is explained by the standard binary collision process[3,4] with a hard sphere model for the particles. The Coulomb collisions between the charged particles are accounted for by using the model derived from the Fokker-Planck equation as given by Dreicer.[5] After assuming that the interacting electromagnetic field is of low intensity, an expression for the electron velocity distribution function is derived by solving Boltzmann's equation with the above two models for the collision terms. Expressions for the ac electrical conductivity in various cases are then derived. To the extent that the assumptions for the collision models are valid, the expressions derived here for the conductivity are quite general in nature; they reduce to the well-known relations for both the limiting cases of fully and weakly ionized gases.

Basic Formulation of the Problem

In this section we shall formulate the problem in general terms. The basic parameter which has to be determined before one can obtain any information about the ionized gas is the electron velocity distribution function. Let us define the electron velocity distribution function $F(v, t)$ such that Fd^3v gives the number of electrons whose velocities lie in the element of volume d^3v situated around the point v in the velocity space. It is assumed that the macroscopic properties of the gas do not vary from point to point. Then the distribution function F satisfies Boltzmann's equation:

$$\frac{\partial F}{\partial t} + \mathbf{a}(t)\cdot\nabla_v F = \left(\frac{\partial F}{\partial t}\right)_{\text{coll.}}, \tag{1}$$

where

$\mathbf{a}(t)$ is the force per unit mass on the electrons,

∇_v is the gradient operator in velocity space,

and

$(\partial F/\partial t)_{\text{coll.}}$ is the rate of change of the distribution function due to various types of collisions. At present we assume,

$$\left(\frac{\partial F}{\partial t}\right)_{\text{coll.}} = \left(\frac{\partial F}{\partial t}\right)_{cn} + \left(\frac{\partial F}{\partial t}\right)_{cc}, \tag{2}$$

where the subscript cn means collision between electron and neutral particles, and cc means Coulomb collisions between the charged particles. Explicit expressions for the collision terms depend on the type of model one assumes for the collision process. In general there should be considered two other equations similar to (1) in order to account for the velocity distributions of the heavy

* Received by the IRE, September 5, 1961. The research reported in this paper was sponsored by the Advanced Research Projects Agency and the Air Force under ARPA Order 147-60 and Air Force Contract No. AF 19(604)-7428.

† Radiation Lab., University of Michigan, Ann Arbor.

[1] H. Margenau, "Conduction and dispersion of ionized gases at high frequencies," *Phys. Rev.*, vol. 69, pp. 508–513; May, 1946. Also, "Conductivity of plasmas to microwaves," *Phys. Rev.*, vol. 109, pp. 6–9; January, 1958.

[2] R. Cohen, L. Spitzer and P. Routly, "The electrical conductivity of an ionized gas," *Phys. Rev.*, vol. 80, pp. 230–238; October, 1950.

[3] T. Holstein, "Energy distribution of electrons in high frequency gas discharges," *Phys. Rev.*, vol. 70, pp. 367–384; February, 1946.

[4] S. Chapman and T. G. Cowling, "The Mathematical Theory of Nonuniform Gases," Cambridge University Press, Cambridge, England, ch. 18; 1939.

[5] H. Dreicer, "Electron velocity distributions in a partially ionized gas," *Phys. Rev.*, vol. 117, pp. 343–354; January, 1960.

neutral particles and positive ions. However, for simplicity of analysis it is assumed here that the heavy particles are stationary relative to the motions of the electrons.

In the present problem the acceleration of the electrons is assumed to be of the form:

$$\mathbf{a}(t) = -\frac{eE_0 \cos \omega t}{m}. \tag{3}$$

where

E_0 is the amplitude of the incident electric field and polarized along the z axis,
ω is the angular frequency of the incident field,
$-e$ is the charge of an electron,
m is the mass of an electron.

The effect of the alternating magnetic field is neglected. After the distribution function F is determined from (1), the current produced in the gas may be obtained from

$$J_z = -n_0 e \bar{v}_z = -e \int F d^3v v \cos \theta, \tag{4}$$

where

J_z is the z-component of the current, assumed positive along the positive direction of the z axis,
$\bar{v}_z$ is the mean velocity of the electrons along the positive z-direction,
θ is the angle between the z axis and the velocity vector v,
n_0 is the electron density.

Discussion of the Collision Terms

As mentioned in the Introduction we shall consider only two types of elastic collisions—between electron-neutral particles and electron-heavy positive ions. If the gas is fully ionized and of high density, then collisions between charged particles of the same kind (for example electron-electron, ion-ion) should also be considered. For a low-density ionized gas the latter two collision effects may be neglected in comparison with the first two. The electron-neutral particle interaction is a short-range phenomenon and explicit expression for this is taken from the standard analysis.[3,4] Since Coulomb force is a long-range phenomenon, the cumulative effects of small deflections suffered by the electrons at large distances due to the interaction with the ions become very important,[2] and they cannot be accounted for in the same way as is done in the first case. This type of interaction is in general explained by the Fokker-Planck equation. The detailed derivation of the collision term from the Fokker-Planck equation is given by Dreicer.[5] Here, we take our collision term after applying the relevant approximations to the general Coulomb collision term given by Dreicer.

Evaluation of the Electron Distribution Function

In the analysis we shall make use of the Lorentz approximation which states that the collisions between various particles produce a spherically symmetric velocity distribution—small deviations from spherical symmetry are then explained accurately enough by the coefficient $F^1(v)$ in the spherical harmonic expansion of F:

$$F(\cos \theta, v) = \sum_{n=0}^{\infty} F^n(v) P_n(\cos \theta) \doteq F^0(v) + \cos \theta F^1(v), \tag{5}$$

where

the polar axis is chosen to be the z axis,
P_n's are the Legendre polynomials.

The approximation made in (5) is valid if $F^1 \ll F^0$. This condition physically means that the average velocity of the electron gas is small compared to the root mean square electron speed. This is a reasonable assumption if the perturbing field is small.

Using the orthogonality property of spherical harmonics the following two relations are obtained for the macroscopic quantities of the gas:

$$\text{electron concentration } n_0 = \int_0^{\infty} F^0 4\pi v^2 dv, \tag{6}$$

$$\text{electric current } J_z = -\frac{4\pi e}{3} \int_0^{\infty} F^1 v^3 dv. \tag{7}$$

After expanding the term $\mathbf{a}(t) \cdot \nabla_v F$ in (1) into its spherical harmonic components in the velocity space, substituting (5) into (1), and equating the terms independent of $\cos \theta$ and those dependent on $\cos \theta$, the following relations are obtained:

$$\frac{\partial F^0}{\partial t} - \frac{\gamma \cos \omega t}{3v^2} \frac{\partial}{\partial v} (v^2 F^1) = \left(\frac{\partial F^0}{\partial t}\right)_{cn} + \left(\frac{\partial F^0}{\partial t}\right)_{cc}, \tag{8}$$

$$\frac{\partial F^1}{\partial t} - \gamma \cos \omega t \left(\frac{\partial F^0}{\partial v}\right) = \left(\frac{\partial F^1}{\partial t}\right)_{cn} + \left(\frac{\partial F^1}{\partial t}\right)_{cc}, \tag{9}$$

where

$$\gamma = \frac{eE_0}{m}.$$

The contributions due to electron-neutral particle collisions are,[3,4]

$$\left(\frac{\partial F^0}{\partial t}\right)_{cn} = \frac{1}{v^2} \frac{m}{M} \frac{\partial}{\partial v} (v^3 F^0 \nu_e(v)) + \frac{KT}{Mv^2} \frac{\partial}{\partial v} \left(v^2 \nu_e(v) \frac{\partial F^0}{\partial v}\right), \tag{10}$$

$$\left(\frac{\partial F^1}{\partial t}\right)_{cn} = -F^1 \nu_e(v), \tag{11}$$

where

$$\nu_e(v) = 2\pi N v \int_0^{\pi} (1 - \cos\beta) \sin\beta \cdot \sigma_e(\beta, v) d\beta, \tag{12}$$

N = the number density of neutral particles,
$\sigma_e(\beta, v)$ = differential cross section for elastic scattering through the angle β,
M = the mass of the neutral particles,
T = temperature of the electron gas,
K = Boltzmann constant.

The factor $\nu_e(v)$ may be identified with the frequency of electron-neutral particle collisions. In general $\nu_e(v)$ is a function of v.

The Coulomb collision terms, subject to the Lorentz approximation and the condition $m/M \ll 1$, are given by[5]

$$\left(\frac{\partial F^1}{\partial t}\right)_{ee} = -\frac{n_0 \Gamma_{ei}}{v^3} F^1, \tag{13}$$

$$\left(\frac{\partial F^0}{\partial t}\right)_{ee} = 0, \tag{14}$$

where

$$\Gamma_{ei} = 4\pi \left(\frac{e e_i}{m}\right)^2 \ln(\lambda/p_0), \tag{13a}$$

p_0 = the average impact parameter (distance of closest approach between the two colliding particles),
e_i = charge on a heavy ion,
λ = the Debye shielding distance.

After substituting (10), (11), (13), and (14) into (8) and (9) the following two equations are obtained:

$$\left(\frac{\partial F^0}{\partial t}\right) - \frac{\gamma \cos\omega t}{3v^2} \frac{\partial}{\partial v}(v^2 F^1) = \frac{1}{v^2} \frac{m}{M} \frac{\partial}{\partial v}(v^3 F^0 \nu_e(v)) + \frac{KT}{Mv^2} \frac{\partial}{\partial v}\left(v^2 \nu_e(v) \frac{\partial F^0}{\partial v}\right), \tag{15}$$

$$\frac{\partial F^1}{\partial t} - \gamma \cos\omega t \left(\frac{\partial F^0}{\partial v}\right) = -\left[\nu_e(v) + \frac{n_0 \Gamma_{ei}}{v^3}\right] F^1. \tag{16}$$

In order to solve (15) and (16), we assume that the isotropic part of the distribution function is independent of time. Thus the solution F^1 of (16) in terms of F^0 is given by the following:

$$F^1 = F^1(\text{at } t = 0) \exp -\left[\nu_e(v) + \frac{n_0 \Gamma_{ei}}{v^3}\right] t + \gamma \left(\frac{\partial F^0}{\partial v}\right) \left[\frac{\omega}{\omega^2 + \left\{\nu_e(v) + \frac{n_0 \Gamma_{ei}}{v^3}\right\}^2} \sin\omega t + \frac{\nu_e(v) + n_0 \Gamma_{ei}/v^3}{\omega^2 + \left\{\nu_e(v) + \frac{n_0 \Gamma_{ei}}{v^3}\right\}^2} \cos\omega t - \frac{\nu_e(v) + n_0 \Gamma_{ei}/v^3}{\omega^2 + \left\{\nu_e(v) + \frac{n_0 \Gamma_{ei}}{v^3}\right\}^2} \cdot \exp -\left\{\nu_e(v) + n_0 \Gamma_{ei}/v^3\right\} t\right]. \tag{17}$$

It can be seen from (17) that the combined collision effect (electron-neutral particle and Coulomb) relaxes the perturbed distribution function F^1 to the following steady-state value:

$$F^1 = \gamma \left(\frac{\partial F^0}{\partial v}\right) \left[\frac{\omega}{\omega^2 + \left\{\nu_e(v) + \frac{n_0 \Gamma_{ei}}{v^3}\right\}^2} \sin\omega t + \frac{\nu_e(v) + n_0 \Gamma_{ei}/v^3}{\omega^2 + \left\{\nu_e(v) + \frac{n_0 \Gamma_{ei}}{v^3}\right\}^2} \cos\omega t\right]. \tag{18}$$

After substituting (18) into (15) and taking the time average, we obtain:

$$-\frac{\gamma^2}{6v^2} \frac{\partial}{\partial v}\left[v^2 \frac{\partial F^0}{\partial v} \frac{\nu_e(v) + n_0 \Gamma_{ei}/v^3}{\omega^2 + \left\{\nu_e(v) + \frac{n_0 \Gamma_{ei}}{v^3}\right\}^2}\right] = \frac{1}{v^2} \frac{m}{M} \frac{\partial}{\partial v}(v^3 F^0 \nu_e(v)) + \frac{KT}{Mv^2} \frac{\partial}{\partial v}\left(v^2 \nu_e(v) \frac{\partial F^0}{\partial v}\right). \tag{19}$$

From (19), F^0 can be expressed as:

$$F^0 = A \exp -\int_0^v \frac{mv dv}{\frac{M\gamma^2}{6\nu_e(v)} \frac{\nu_e(v) + n_0 \Gamma_{ei}/v^3}{\omega^2 + \left\{\nu_e(v) + \frac{n_0 \Gamma_{ei}}{v^3}\right\}^2} + KT}, \tag{20}$$

where A is a constant of integration. If Coulomb collisions are neglected the distribution function (20) reduces to the one given by Margenau[1] for the constant mean free path case. If the thermal energy of the electrons is large and the electric field E_0 is sufficiently small, then the term KT in the denominator of the integrand in (20) is predominant and F^0 reduces to the Maxwellian distribution,

$$F^0 = n_0 \left(\frac{m}{2\pi KT}\right)^{3/2} e^{-mv^2/KT}, \tag{21}$$

where the constant A has been determined by using (6). Eq. (20) indicates that, strictly speaking, F^0 cannot be assumed Maxwellian and independent of the field intensity E^0. As we shall see later this fact makes the electrical conductivity of the ionized gas a nonlinear function of the field intensity. We are now in a position to calculate the conductivity of the gas. This is done in the next section.

Expressions for the Electrical Conductivity

After using (7) and (18), the following relation is obtained for the electric current:

$$J_z = -\frac{4\pi e^2 E_0}{3m}\int_0^\infty\left[\frac{\omega v^3}{\omega^2 v^6+\{v^3\nu_e(v)+n_0\Gamma_{ei}\}^2}\sin\omega t + \frac{\{\nu_e(v)+n_0\Gamma_{ei}\}}{\omega^2 v^6+\{\nu_e(v)v^3+n_0\Gamma_{ei}\}^2}\cos\omega t\right]v^6\left(\frac{\partial F^0}{\partial v}\right)dv. \quad (22)$$

Defining complex conductivity as $\sigma=\sigma_r-i\sigma_i$, it can be shown that the real and imaginary parts of the electrical conductivity of a partially ionized gas are given by

$$\sigma_r = -\frac{4\pi e^2}{3m}\int_0^\infty \frac{\nu_e(v)v^3+n_0\Gamma_{ei}}{\omega^2 v^6+\{\nu_e(v)v^3+n_0\Gamma_{ei}\}^2}v^6\cdot\left(\frac{\partial F^0}{\partial v}\right)dv, \quad (23)$$

$$\sigma_i = -\frac{4\pi e^2}{3m}\int_0^\infty \frac{\omega v^3}{\omega^2 v^6+\{\nu_e(v)v^3+n_0\Gamma_{ei}\}^2}v^6\cdot\left(\frac{\partial F^0}{\partial v}\right)dv. \quad (24)$$

For the dc case $\omega=0$, $\sigma_i=0$, $\sigma_r=\sigma_{\text{D.C.}}$ If Coulomb collisions are neglected, and F^0 is assumed to be given by (21), then (23) and (24) can be written in the following forms after introducing the dimensionless parameter $x^2=mv^2/2KT$:

$$\sigma_r = \frac{4\pi e^2 n_0}{3m}\frac{2}{(\pi)^{3/2}}\int_0^\infty \frac{\nu_e(x)}{\omega^2+\nu_e^2(x)}e^{-x^2}x^4dx, \quad (25)$$

$$\sigma_i = \frac{4\pi e^2 n_0}{3m}\frac{2}{(\pi)^{3/2}}\int_0^\infty \frac{\omega}{\omega^2+\nu_e^2(x)}e^{-x^2}x^4dx. \quad (26)$$

For constant ν_e, σ_i and σ_r as given above reduce to the familiar forms.[1] In general $\nu_e(x)$ is a complicated function of x, and the integrals in (25) and (26) are not always amenable to integration in closed forms.

Conductivity of a Fully Ionized Gas

In this section we shall derive expressions for the ac conductivity of a fully ionized gas. In order to simplify the analysis it is assumed that the isotropic part of the the distribution function is Maxwellian and is given by (21). Since the gas is fully ionized, $\nu_e(v)=0$ and hence, (23) and (24) may be written as follows:

$$\sigma_r = \frac{\sigma_{\text{D.C.}}}{3}\int_0^\infty\left[1-\frac{\omega_0^3x^6}{\omega_0^3x^6+1}\right]x^7e^{-x^2}dx, \quad (27)$$

$$\sigma_i = \frac{\sigma_{\text{D.C.}}}{3n_0\Gamma_{ei}}\frac{\omega}{\omega_0^3}\int_0^\infty\frac{x^{10}e^{-x^2}}{x^6+\frac{1}{\omega_0^3}}dx, \quad (28)$$

where

$$\omega_0^3 = \frac{\omega^2\left(\frac{2KT}{m}\right)^3}{n_0^2\Gamma_{ei}^2}. \quad (29)$$

and

$$\sigma_{\text{D.C.}} = \frac{4\pi e^2}{m\Gamma_{ei}}\frac{2}{(\pi)^{3/2}}\left(\frac{2KT}{m}\right)^{3/2}. \quad (30)$$

For the dc case $\omega=0$, we obtain $\sigma_i=0$ and $\sigma_r=\sigma_{\text{D.C.}}$ since in (27)

$$\int_0^\infty x^7e^{-x^2}dx = 3.$$

The dc conductivity as given by (30) is the same as given by Spitzer.[6]

We shall now evaluate explicitly σ_r as given by (27). Let us denote the integral in (27) by I. After a change of variable $t=x^2$, I may be written as follows:

$$I = \frac{1}{2}\int_0^\infty\frac{t^6e^{-t}}{t^3+1/\omega_0^3}dt. \quad (31)$$

Using the known result

$$\int_0^\infty\frac{t^ne^{-t}}{t_1+t}dt = K_n(t_1),$$

where K_n is the usual notation for the modified Bessel function of the second kind and order n, the following is obtained for I:

$$I = \frac{\omega_0^2}{6}K_6(1/\omega_0) - \frac{\omega_0^2}{12}\left[K_6\left(\frac{e^{\pi i/3}}{\omega_0}\right)+K_6\left(\frac{e^{-\pi i/3}}{\omega_0}\right)\right] - i\frac{\sqrt{3}}{12}\omega_0^2\left[K_6\left(\frac{e^{\pi i/3}}{\omega_0}\right)-K_6\left(\frac{e^{-\pi i/3}}{\omega_0}\right)\right]. \quad (32)$$

Eq. (32) may also be written in the following form:

$$I = \frac{\omega_0^2}{6}K_6(1/\omega_0) + \frac{\omega_0^2}{12}\frac{\pi i}{2}\left[H_6^{(1)}\left(\frac{e^{\pi i/6}}{\omega_0}\right)-H_6^{(2)}\left(\frac{e^{-\pi i/6}}{\omega_0}\right)\right] + \frac{\sqrt{3}}{12}\omega_0^2\pi/2\left[H_6^{(1)}\left(\frac{e^{\pi i/6}}{\omega_0}\right)+H_6^{(2)}\left(\frac{e^{-\pi i/6}}{\omega_0}\right)\right], \quad (33)$$

[6] L. Spitzer, "Physics of Fully Ionized Gases," Interscience Publishers, Inc., New York, N. Y., p. 63; 1956.

where $H_6^{(1)}$ and $H_6^{(2)}$ are the notations for the Hankel functions of the sixth order and of the first and second kind respectively. Using the property of the Hankel functions[7] that $H_6^{(1)}(e^{\pi i/6}/\omega_0)$ is the complex conjugate to $H_6^{(2)}(e^{-\pi i/6}/\omega_0)$, the value of the integral I as given in (33) may be written in the following form:

$$I = \frac{\omega_0^2}{6} K_6(1/\omega_0) - \frac{\omega_0^2}{12}\pi\rho \sin\phi + \frac{\sqrt{3}}{12}\omega_0^2\pi\rho\cos\phi, \quad (34)$$

where

$$H_6^{(1)}\left(\frac{e^{\pi i/6}}{\omega_0}\right) = \rho\cos\phi + i\rho\sin\phi. \quad (35)$$

After substituting (34) in (27) the following is obtained for the real part of ac conductivity of a fully ionized gas:

$$\sigma_r = \frac{\sigma_{D.C.}}{3}\left[3 - \frac{\omega_0^2}{6}\left\{K_6(1/\omega_0) - \frac{\pi\rho}{2}\sin\phi + \frac{\sqrt{3}}{2}\pi\rho\cos\phi\right\}\right]. \quad (36)$$

The integration involved in (28) may be evaluated similarly, and we obtain formally the following expression for σ_i,

$$\sigma_i = \sigma_{D.C.}\left(\frac{\omega}{n_0\Gamma_{ei}}\right)^{1/3}\left(\frac{m}{2KT}\right) \cdot\left[\frac{K_{9/2}(1/\omega_0)}{6} - \frac{K_{9/2}\left(\frac{-e^{\pi i/3}}{\omega_0}\right) + K_{9/2}\left(\frac{-e^{-\pi i/3}}{\omega_0}\right)}{12} + i\frac{K_{9/2}\left(\frac{-e^{\pi i/3}}{\omega_0}\right) - K_{9/2}\left(\frac{-e^{-\pi i/3}}{\omega_0}\right)}{4\sqrt{3}}\right]. \quad (37)$$

It can be seen from (36) and (37) that for $\omega = 0$, $\sigma_r = \sigma_{D.C.}$ and $\sigma_i = 0$.

Eqs. (36) and (37) are analytically too complicated to discuss. They can be greatly simplified and brought into more tractable forms if one approximates the Bessel functions involved by the first terms of their corresponding asymptotic expansions. In order to obtain a simplified expression for σ_r we shall work with (32). After using the asymptotic series for the K functions, as given in Watson,[8] and making some algebraic manipulations, the following is obtained for σ_r:

$$\sigma_r = \frac{\sigma_{D.C.}}{3}\left[3 - \frac{\omega_0^2}{12}\left(\frac{\pi\omega_0}{2}\right)^{1/2} \cdot\left\{e^{-1/\omega_0} - e^{-1/2\omega_0}\cos\left(\frac{\pi}{6} - \frac{3}{2\omega_0}\right)\right\}\right]. \quad (38)$$

This expression is valid for the range of frequencies for which the values of ω_0 lie in the range $1/\omega_0 > 6$, where ω_0 is as given by (28). Similarly the asymptotic expression for σ_i is obtained in the following form:

$$\sigma_i = \sigma_{D.C.}\frac{\omega}{\omega_0}\left[\left(\frac{\pi\omega_0}{2}\right)^{1/2} e^{-1/\omega_0} + \frac{1}{3}\left(\frac{\pi\omega_0}{2}\right)^{1/2} e^{1/2\omega_0}\cos\left(\frac{\sqrt{3}}{2\omega_0}\right)\right], \quad (39)$$

which should be used for the range of frequencies for which $1/\omega_0 > 4.5$.

Using (38) and (39), the conductivity of a fully ionized gas has been computed at a few frequencies. It is assumed that the ionized gas has the following characteristics:

$$n_0 = 10^{15}/\text{cm}^3$$
$$T = 10^4 \text{ degrees Kelvin.}$$

The calculated normalized values of σ_r and σ_i are as shown below:

frequency (in kilomegacycles)	$\frac{\sigma_r}{\sigma_{D.C.}}$	$\frac{\sigma_i}{\sigma_{D.C.}} \times 10^{-10}$
1	1	—
10	0.9992	4.3
20	0.9978	18.4

For the ionized gas under consideration the real part of the ac conductivity does not change appreciably from the dc conductivity up to the frequency 1 kMc. The imaginary part of the conductivity increases with frequency. For the values of σ_r and σ_i at frequencies higher than those shown above, one should use (36) and (37).

Discussion

In the above the electrical conductivity of a partially ionized gas has been discussed in detail. It has been assumed that the gas is of low density and that the incident electrical field is very weak. The general expressions derived for the conductivity may be applied to specific cases keeping in mind the assumptions made in the analysis. For non-Maxwellian distribution for the isotropic part of the velocity distribution function and for velocity-dependent collision frequency, the conductivity expressions become very complicated and are to be evaluated by numerical methods. Depending on the type of gas and the degree of ionization, one can make some reasonable physical assumptions which will greatly simplify the calculation.

Acknowledgment

The author wishes to express his thanks to Prof. K. M. Siegel for encouragement during the course of this work, and to Dr. R. Goodrich and Dr. R. Kleinman for reading the manuscript.

[7] E. Jahnke and F. Emde, "Tables of Functions," Dover Publications, New York, N. Y., p. 134; 1945.
[8] G. N. Watson, "Theory of Bessel Functions," Cambridge University Press, Cambridge, England, p. 102; 1952.

Interaction of Microwaves in Gaseous Plasmas Immersed in Magnetic Fields*

K. V. NARASINGA RAO†, STUDENT MEMBER, IRE, J. T. VERDEYEN†, STUDENT MEMBER, IRE, AND L. GOLDSTEIN†, FELLOW, IRE

Summary—**The phenomenon of radio frequency electromagnetic wave interaction in gaseous plasmas is reviewed. The application of microwave interaction to the study of plasmas immersed in magnetic fields is discussed. Attention is focused on the effects produced in such plasmas when one of the simultaneously propagating microwaves is in electron-cyclotron resonance. It is demonstrated that, for relatively modest amplitudes of the resonating wave, the kinetic energy of the electrons increases considerably, which in turn affects 1) the electron collision frequency and 2) the magnetic field control of the plasma confinement.**

I. Introduction

IT is now well known that the phenomenon of wave interaction was first observed in 1933 between low-frequency radio waves which were propagated in a common region of the ionosphere [1]. Since it was possible to trace the effect to a region of the ionosphere which was strongly irradiated by the powerful waves (150–200 kw) transmitted by the Radio Station of Luxemburg, the phenomenon became known as the Luxemburg Effect.

The theory explaining this effect was first proposed in 1934 by Bailey and Martyn [2]. Later (1937) Bailey [3] extended this theory taking into account the influence of the earth's magnetic field on the propagation of the ionospheric radio waves involved. This theory predicted, in particular, that when the frequency of one of the interacting waves is in the vicinity of, or at the gyrofrequency of the electrons in the ionospheric region of interest, the wave interaction will be enhanced. These predictions have since been borne out by direct experimental observations [4].

In 1953 the simple phenomenon of radio wave interaction was extended [5] to (guided) microwaves propagated in laboratory gaseous plasmas under readily controlled conditions with a consequent generalization and close check of the (1955) theory [6]. Based on the generalized theory it was then possible to develop a method of rather detailed investigations of high RF EM wave interaction with gaseous plasmas, which in turn enabled the detailed study of the interaction processes taking place among the charged constituents as well as among the charged and neutral constituents of gaseous plasmas [7], [8].

This paper deals with an experimental investigation of the interaction of two or more electromagnetic waves guided through a magneto plasma medium. The magneto plasma referred to here is a plasma obtained in the afterglow of a pulsed gas discharge (degree of ionization less than 10^{-4}) which is immersed in an external dc magnetic field, variable from 0 to 0.3 webers/m^2. The gases used are primarily the inert gases in the pressure range 0.5 to 10.0 mm Hg. The EM waves utilized are in the frequency range 4.0 to 10.0 Gc and are guided along the external magnetic field. The general topic of investigation is the transfer of EM energy to the electron gas in the plasma and the effects of this transfer of energy on 1) the plasma parameters and 2) the associated wave propagation characteristics of the plasma. This has been investigated, in particular, when the frequency of one EM wave is at or in the vicinity of the cyclotron frequency of the electrons.

This paper is divided into six sections: In Section II, a qualitative description of the interaction of EM waves of radio frequency is given. Section III deals with a description of the plasma medium and a quantitative treatment of the wave interaction phenomenon in gaseous plasmas. The experimental apparatus used in this investigation is described in Section IV. Section V is devoted to the experimental results and Section VI contains the conclusions and the possible implications of these results.

II. Interaction of Electromagnetic Waves in a Plasma

It is known that the propagation of electromagnetic waves in material media is different from the propagation in free space because there is energy exchange between the media and the waves. A plasma, being a material medium, will alter the propagation of electromagnetic waves, and this fact has been used to determine those plasma parameters which influence electromagnetic wave propagation. Usually these techniques have been used to study the plasma in any given time-independent energy state. The probing electromagnetic wave which is used in such a study must be of sufficiently small amplitude so that it does not appreciably disturb the plasma.

If the amplitude of the electromagnetic wave propagating in a plasma does not satisfy this condition, a change in the energy state of the electron gas of the plasma results, which in turn affects the propagation of any succeeding wave packet. This means that each wave packet propagates in a slightly different plasma than the preceding one. This phenomenon is generally referred to as self-modulation or as self-distortion.

* Received by the IRE, August 7, 1961. This work is sponsored by the AFCRC, Geophysics Research Directorate, Bedford, Mass.
† Dept of Elec. Engrg., University of Illinois, Urbana, Ill.

While the change of the energy state of the electron gas thus affects wave propagation in a plasma, it also affects those processes occurring in the plasma which are dependent upon the energy state of the electron gas, such as recombination, diffusion, production rate, etc.

We have considered above the effect of only one electromagnetic wave on a plasma and the resulting reaction of the plasma on the electromagnetic wave in the two cases: 1) negligible perturbations corresponding to small-wave amplitudes and 2) significant disturbances corresponding to large-wave amplitudes. The next step is to combine the two effects by applying two electromagnetic waves to the plasma. One wave will be of sufficiently small amplitude so as to be capable of probing the plasma—hence the name *sensing wave;* the other will be of sufficient amplitude and of different frequency so as to disturb the plasma—hence the name *disturbing wave.* The effect which the disturbing wave causes on the plasma, as detected by the sensing wave, is generally referred to as wave interaction and, when modulation is involved, as cross-modulation.

Let us consider the processes by which energy is transferred from an electromagnetic wave to the electron gas of a plasma. When a high-frequency electromagnetic wave impinges upon a plasma, it causes an ordered oscillatory motion of the electrons which is superimposed onto the existing disordered thermal motion. The ordered electron velocity is 90° in time phase with respect to the driving force of the E field of the wave. The energy associated with this ordered motion, if not interfered with, is taken from the EM wave in $\frac{1}{2}$ cycle, and returned to the wave in the following $\frac{1}{2}$ cycle so that the average power transferred to the electron gas is zero. When, however, the electrons collide with other constituents of the plasma, the ordered momentum is scattered, and consequently the velocities of the electrons no longer have a definite phase relationship to the driving force. Following such collisions, the previous ordered energy of the electron gas is not returned to the electromagnetic wave and hence represents RF power transferred into the electron gas. The electron gas loses, however, a fraction of this energy to the heavy constituents of the plasma.

These momentum-transfer collisions between electrons and the heavy particles of a plasma constitute one mechanism by which EM energy is transferred into disordered thermal energy of the electrons. There exists however, under particular conditions, another mechanism of EM energy transfer to a plasma, in which the collisions, by interrupting the ordered motion of the electrons, hinder the energy transfer. Such conditions occur when resonance prevails between a proper frequency of the plasma electrons, such as their cyclotron frequency, and the particular frequency of the EM waves. In this case, an initial value problem must be considered and the solution of which indicates that the energy of an electron grows, in between collisions, as $(Et)^2$ where E is the applied electric field and t is the time elapsed since its last collision. In the study reported here we are concerned mainly with the effects of this electromagnetic energy transfer from one of the EM waves whose frequency is at or in the vicinity of the cyclotron frequency of electrons.

III. Characteristics of an Afterglow Plasma

As mentioned earlier, the plasma considered here is that obtained in the afterglow of a partially ionized rare gas whose degree of ionization is less than 10^{-4}. We shall assume that only three types of constituent gases are present in the afterglow, namely the gas of the electrons, that of the positive ions and that of the neutral molecules. The fundamental parameters of interest are essentially: 1) the number density of the charged particles, 2) the temperature of the constituent gases, and 3) the type of neutral molecules in which the plasma is formed. Upon removal of the external plasma-excitation source the constituent particles undergo mainly elastic collisions among themselves and with the walls of the reservoir, and thereby attain thermodynamic equilibrium at the temperature of the reservoir ($T_e = T_i = T_g = T_r$). This plasma tends, however, towards a neutral gas state by means of various loss mechanisms of the charged particles. These mechanisms are 1) volume recombination of electrons and ions, 2) diffusion of electrons to boundaries and 3) attachment of electrons to neutral particles. The absence of any electronegative gases in these experiments permits us to neglect the attachment process, and hence the rate of loss of the charged particles is given by

$$\frac{dn}{dt} = -\alpha n_e \cdot n_i + D\nabla^2 n, \tag{1}$$

where α = the recombination coefficient of electrons and ions whose densities are, respectively, n_e, n_i, and D = the diffusion coefficient.

If we assume that only elastic collisions of electrons with other constituents of the plasma take place in the afterglow, it is possible to define certain fundamental quantities which describe the interactions of the electrons with other constituents of the plasma. The probability of electron-molecule collision for momentum transfer, P_{em} is related to the effective cross section of molecules, Q_m and to the corresponding electron-molecule collision frequency ν_{em} by the equation

$$P_{em}(v)p = N_m Q_{em}(v) = \frac{\nu_{em}}{v}. \tag{2}$$

where N_m = number density of molecules, v = velocity of electrons, p = pressure (at 0°C). Analogous quantities for electron-ion collisions are

$$N_s Q_{ei} = \frac{\nu_{ei}}{v}. \tag{3}$$

If Q_{em} does not vary appreciably with electron velocity,

then the collision frequencies mentioned above may be reduced to the following functional forms:

$$\nu_{em} = AT_e^{1/2}, \tag{4}$$

$$\nu_{ei} = \frac{BN_i}{T_e^{-3/2}} \ln \left[CN_i^{-1/2}T_e^{1/2}\right], \tag{5}$$

where A, B, C are constants and T_e is electron temperature. In any case, the total effective collision frequency defined by

$$\nu_t = \nu_{em}(T_e) + \nu_{ei}(T_e) \tag{6}$$

is thus dependent upon the number density of the charged particles, pressure of the gas, kind of gas, and electron temperature. To facilitate the interpretation of the experimental results on the interaction of microwaves, a plot of N_iQ_{ei} and P_{em} as a function of electron temperature is shown in Fig. 1. It can be seen from this figure that an enhancement in electron temperature may cause either a decrease or an increase in the total electron collision frequency ν_t depending on whether *e-i* or *e-m* collisions are predominant. If we neglect the slow variation of the logarithmic term in (5), then the total collision frequency will *increase* with electron temperature provided $\nu_{em} > 3\nu_{ei}$ or *decrease* if $\nu_{ei} > \frac{1}{3}\nu_{em}$. This result is obtained by differentiating (6) with respect to T_e. In certain gases, like Xe, Kr, or Ar, an increase in electron temperature from ~300°K causes a decrease in ν_t, even without any Coulomb collisions. The variation of ν_{em} in these gases with increasing T_e is similar to the variation of ν_t in a low pressure high density neon plasma as can be inferred from Fig. 1. These aspects of the total collision frequency dependence on electronic energy have been demonstrated in this investigation using the technique of wave interaction, and are discussed in Section V.

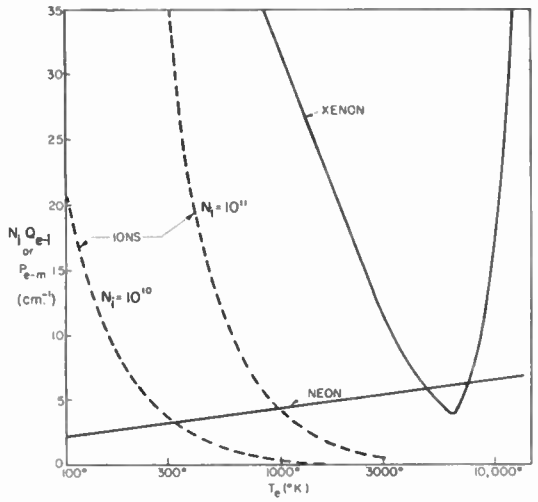

Fig. 1—Probability of electron-molecule collision for momentum transfer P_{em} or N_iQ_{ei} vs electron temperature (°K). The dashed curves represent N_iQ_{ei} for two electron densities 10^{11}/cc and 10^{10}/cc. The solid curves represent P_{em} in neon and xenon gases. Data for solid curves is obtained from [20] and dashed curves are plotted using (5), as given by [6].

Now we shall consider briefly the dependence of the electron-loss mechanisms in a nonmagnetized, decaying, rare gas plasma upon the electron temperature It is known that the volume recombination decreases with increasing electron temperature since α, the recombination coefficient, is inversely proportional to some power ($\sim 3/2$) of T_e [9]. However, if "free" diffusion of electrons occurs in a plasma, it will be enhanced when T_e increases. In a plasma of high-charge densities, interactions among the charges of opposite sign results in the ambipolarity of the diffusion. The ambipolar diffusion coefficient is given by the equation

$$D_a = D_+\left(1 + \frac{T_e}{T_i}\right), \tag{7}$$

where D_+ is the diffusion coefficient of the positive ions. It is seen that D_a increases with T_e.

The ambipolar diffusion in a magneto plasma depends upon the direction of the magnetic field. The diffusion coefficients parallel and perpendicular to the direction of the magnetic field are given [10], [11] in terms of the magnetic field intensity by

$$D_\perp = \frac{D_\parallel}{1 + \dfrac{\omega_H}{\nu_e}\cdot\dfrac{\Omega_H}{\nu_i}}, \tag{8a}$$

$$D_\parallel = D_a, \tag{8b}$$

where ω_H, and Ω_H are the cyclotron frequencies of the electrons and ions, respectively, and ν_e, ν_i are the total electron and ion collision frequencies.

It can be seen from (8a) and (8b) that in plasmas where the condition

$$\frac{\omega_H}{\nu_e}\cdot\frac{\Omega_H}{\nu_i} \gg 1$$

is satisfied, the diffusion of charged particles in the transverse direction is negligible compared to that in the parallel direction, *i.e.*, $D_\perp/D_\parallel \ll 1$. However, the absorption of EM waves under electron-cyclotron resonance conditions results in a considerable heating of the electron gas only. In the plasma considered here, it is possible to chage ν_t appreciably by this process which results in making the ratio $D_\perp/D_\parallel$ approach unity. The implication of this statement is that the transverse diffusion of the plasma can be enhanced considerably by the heating of the electron gas. In other words, the external magnetic field, which impedes the transverse diffusion of the cool electrons and thus delays plasma disintegration, loses its control over the diffusion process when the electrons become energetic.

A. Electromagnetic Description of the Plasma

A mathematical description of the influence of the electromagnetic wave upon a plasma consists of the

simultaneous solution of Maxwell's equations and Boltzmann's equation:

$$\nabla \times H = J + \epsilon_0 \frac{\partial E}{\partial t}, \tag{9}$$

$$\nabla \times E = -\mu_0 \frac{\partial H}{\partial t}, \tag{10}$$

$$\frac{\partial f}{\partial t} + v \cdot \nabla_r f + (E + v \times B) \cdot \nabla_v f = \left.\frac{\partial f}{\partial t}\right|_{\text{coll.}}, \tag{11}$$

$$J = -e \iiint v f d^3v. \tag{12}$$

However, a somewhat less rigorous but a more easily solved set of equations is the combination of Maxwell's equations with the Langevin equation:

$$\frac{\partial v}{\partial t} + \nu v = \frac{q}{m}(E + v \times B), \tag{13}$$

$$J = -nev. \tag{14}$$

In (13), ν is responsible for viscous damping and is related to the average momentum-transfer collision frequency of the electrons with the other constituents of the plasma. The restrictions and assumptions, which are inherent in the usage of (13) rather than (11), have been discussed by several authors [12], [13], [14] and will not be considered here. Suffice it to say that the use of (13) and (14) leads to an expression for the current density which is reasonably accurate for our purposes.

Eqs. (13) and (14) can be solved for the current density in terms of the plasma parameters and the electromagnetic fields.

$$\begin{bmatrix} J_x \\ J_y \\ J_z \end{bmatrix} = \begin{bmatrix} \sigma_{xx} & \sigma_{xy} & 0 \\ -\sigma_{xy} & \sigma_{yy} & 0 \\ 0 & 0 & \sigma_{zz} \end{bmatrix} \begin{bmatrix} E_x \\ E_y \\ E_z \end{bmatrix}, \tag{15}$$

where

$$\sigma_{xx} = \sigma_{yy} = \omega_p^2 \epsilon_0 \left[\frac{\nu + j\omega}{(\nu + j\omega)^2 + \omega_H^2}\right],$$

$$\sigma_{xy} = \omega_p^2 \epsilon_0 \left[\frac{\omega_H}{(\nu + j\omega)^2 + \omega_H^2}\right],$$

$$\sigma_{zz} = \omega_p^2 \epsilon_0 \left[\frac{1}{\nu + j\omega}\right],$$

$$\omega_p^2 = \frac{n_e e^2}{m\epsilon_0},$$

$$\omega_H = \frac{eB_0}{m},$$

$B = B_0 \hat{i}_z$, the external magnetic field.

In principle we could now use (15) in conjunction with (9) and (10) to solve for the propagation constant of the electromagnetic waves in the guiding structures used for this experiment. However, this procedure leads to a transcendental equation which must be solved numerically for the propagation constant [15], and an interpretation of the experiments which follow would be difficult. In order to facilitate the interpretation of our experiments, we use Poynting's Theorem for the average power (per unit of volume) input to the plasma.

$$\langle \mathcal{P} \rangle = \tfrac{1}{2} \operatorname{Re} \sigma_{xx} [|E_x|^2 + |E_y|^2] + \frac{j}{2} \operatorname{Im} \sigma_{xy} [E_x^* E_y - E_x E_y^*] + \tfrac{1}{2} \operatorname{Re} \sigma_{zz} |E_z|^2, \tag{16}$$

where (*) denotes complex conjugate.

Most of the experiments which are described in this paper were performed on plasmas located in the center of a rectangular waveguide as shown in Fig. 6(b). We note that when the magnetic field is not present, then $\sigma_{xy} = 0$, hence E_y and E_z are zero for the TE_{10} mode of propagation. In addition to this fact, E_y and E_z must go to zero at the x walls even in the presence of the magnetic field. Hence the products $\sigma_{xy} E_y E_x$ and $\sigma_{zz} E_z^2$ are of second order and are neglected. Under these assumptions, (16) may be written as

$$\langle \mathcal{P} \rangle = \tfrac{1}{2} \operatorname{Re} \sigma_{xx} |E|^2. \tag{16a}$$

It is seen that the absorption is proportional to the real part of the main diagonal component of the conductivity matrix. This conductivity is plotted as a function of ω_H/ω for various values of ν/ω in Fig. 2. It is interesting to note that the absorption increases with increasing collision frequency for values of the magnetic field variable $(\omega_H/\omega) \neq 1$, whereas at cyclotron resonance $\omega_H = \omega$ the absorption decreases with increasing collision frequency. This is consistent with our earlier observation that the collisions cause the transfer of energy from an electromagnetic wave to the electron gas of the plasma in the absence of resonance conditions, and impede the energy transfer in the close vicinity of resonance.

Fig. 3 illustrates the variation of Re σ_{xx} with ν/ω, where the magnetic field is a fixed parameter. This is the case which corresponds to most of the experiments described here. It is noticed in this figure that for a fixed value of the magnetic field variable $(\omega_H/\omega) \neq 1$, σ_{xx} first increases, reaches a maximum and then decreases as the quantity (ν/ω) increases. The effect of such behavior on the absorption of an electromagnetic wave will be shown in the experimental section. If the statement can be made that the E field inside the plasma is related to the applied E field by a function which is weakly dependent upon the collision frequency, then the point at

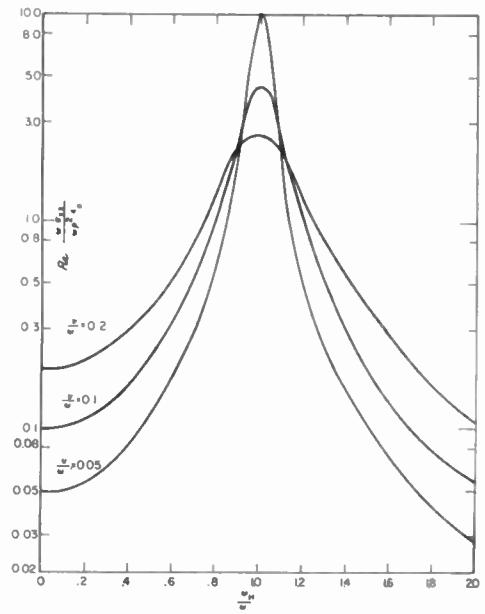

Fig. 2—Normalized electrical conductivity, *i.e.*, real part of σ_{xx} as a function of magnetic field (ω_H/ω), with collision frequency as a parameter.

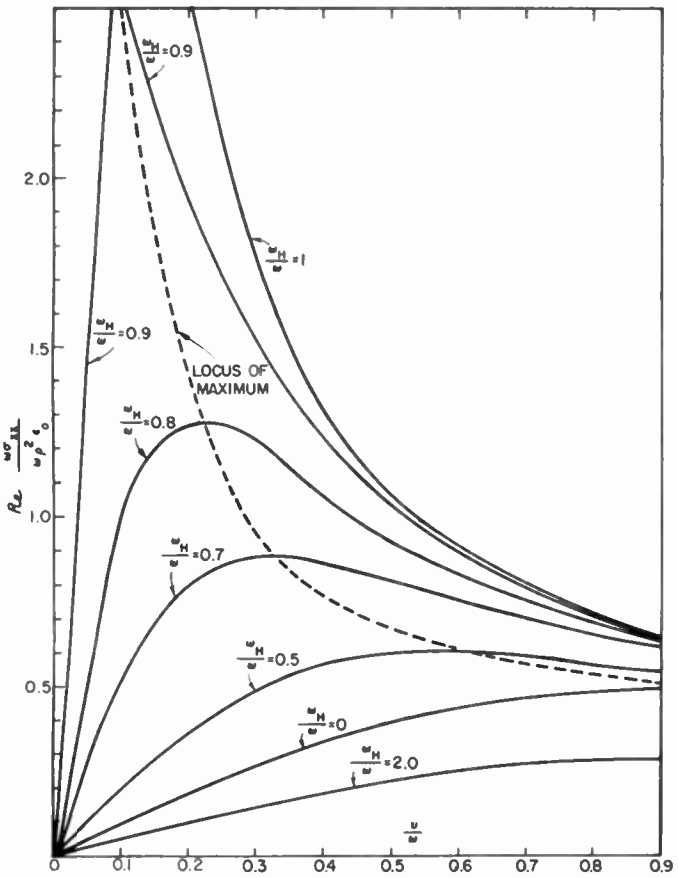

Fig. 3—Normalized electrical conductivity, *i.e.*, real part of σ_{xx} as a function of collision frequency (ν/ω), with magnetic field (ω_H/ω) as a parameter.

which the absorption reaches a maximum, as the collision frequency is varied, is the point at which σ_{xx} is a maximum. This point was used to measure the effective electron collision frequency in both disturbed and unperturbed plasmas.

So far we have only considered the attenuation of an electromagnetic wave, which is one of the two characteristic quantities in wave propagation. The other measurable quantity is the phase velocity of the electromagnetic wave in the plasma. However, the phase velocity does not lend itself to dynamic measurement as easily as the absorption. For this reason, phase velocity measurements will be presented by static point-by-point measurements.

In order to correlate attenuation and phase measurements to the plasma parameters, an analytic expression for the propagation constant γ must be obtained. It was mentioned earlier that a rigorous solution of Maxwell's equations in the guiding structures considered here leads to a transcendental equation which must be solved numerically for the propagation constant. However, in many cases, approximate techniques can be fruitfully used to obtain admittedly less rigorous, but useful, solutions.

One such approximation technique is to use an integral equation which expresses the propagation constant in terms of the fields inside the plasma. This is the approach which is used for the study of magneto plasmas located in a rectangular waveguide as illustrated in Fig. 6(b). It is shown in the Appendix that the propagation constant in this guiding system can be approximated by

$$\gamma^2 + \beta_0^2 = j\omega\mu_0\sigma_{xx}g, \tag{17}$$

where β_0 = phase constant in the structure without a plasma, g = geometrical factor. Experiments which will be described in Section V have shown that (17) is qualitatively correct, and appear to justify the assumptions which are listed in the Appendix.

Another possible approximate method of solving for the propagation constant is to assume that the plasma is unbounded and is subjected to a uniform plane wave. This approach is especially useful in discussing the experiments performed in circular waveguides. For the case when the electromagnetic wave is propagating along the direction of the magnetic field, the propagation constant for circularly polarized waves can be simply expressed by [16], [17]

$$\gamma_{e,i}^2 = -\frac{\omega^2}{c^2}\left[1 - \frac{\omega_p^2/\omega^2}{\left(1 \pm \frac{\omega_H}{\omega}\right) - j\frac{\nu}{\omega}}\right], \tag{18}$$

where $\gamma = \alpha + j\beta$, α = attenuation constant and β = phase constant.

In (18) the minus sign is associated with γ_e, the propagation constant of the extraordinary wave (which rotates in the same sense as the electrons); the positive sign is associated with γ_i, the propagation constant of the ordinary wave (which rotates in the same sense as the positive ions). The decomposition of a linearly-polarized wave into two contrarotating circular waves leads to the well-known Faraday rotation of the plane of polarization of the linear wave. The angle of rotation θ is proportional to the difference of the phase constants β_i and β_e and the length of the path

$$\frac{2\theta}{L} = \beta_i - \beta_e. \tag{19}$$

The waveguide Faraday rotation [18] in a magneto plasma does not appear to differ in the first approximation from that of the unbounded case. The angle of rotation of a linearly-polarized wave propagating in an unbounded plasma is plotted in Fig. 4. It is seen from this figure that the angle of rotation per unit length is proportional to the number density of the electrons, and is nearly independent of the collision frequency for values of ω_H/ω much different than unity.

For ω_H/ω close to 1, the rotation angle is dependent upon both n and ν. The phenomenon of Faraday rotation is used here to study the enhancement of plasma disintegration resulting from a significant rise in the electron temperature following EM-energy transfer at cyclotron resonance to the electron gas of the plasma.

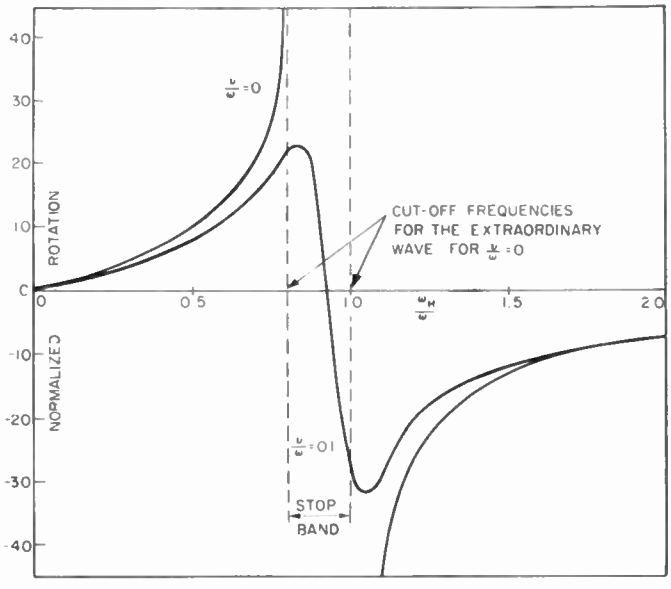

Fig. 4—Normalized Faraday rotation, *i.e.*,

$$\frac{2\theta}{\beta_0 L}\cdot\frac{360}{2\pi} = \left(\frac{\beta_i}{\beta_0} - \frac{\beta_e}{\beta_0}\right)\frac{360}{2\pi}$$

dependence on magnetic field (ω_H/ω) shown for $\nu/\omega=0$ and $\nu/\omega=0.1$. These curves are plotted for the particular value of the parameter $\omega_p^2/\omega^2=0.2$.

IV. Experimental Techniques and Apparatus

The technique of interaction of guided microwaves in a nonmagnetized plasma developed in our laboratory [5] has been extended in this study to investigate the above phenomena in magneto plasmas. The main problems associated with this technique can be broadly divided into three categories: 1) production of a suitable gyromagnetic plasma, 2) propagation of microwaves of proper characteristics through the magneto plasma and 3) investigation of the mutual interaction of these waves and the plasma. In addition to the method of probing the plasma by microwave-interaction techniques the visible light intensity emitted by the afterglow was simultaneously observed, and yielded valuable information concerning the plasma behavior. The general experimental procedure can be described best by referring to the schematic diagram in Fig. 5. A pulsed discharge plasma is obtained in a cylindrical tube which is placed either in a cylindrical or a rectangular waveguide assembly. This assembly is located in the core of a solenoid which provides the external dc-magnetic field. Two pulsed microwave signals of different frequencies and amplitudes are propagated nearly simultaneously through the decaying plasma. The transmission and reflection characteristics of these two waves and their mutual interaction in the plasma is studied under varied experimental conditions, which will be described later.

For the investigation of magneto plasmas located in rectangular waveguides the experimental arrangement shown in Fig. 6 was used. Fig. 6(b) shows the waveguide assembly containing the magneto plasma. A 2.5 or 5.0 cm long pyrex glass tube, with OD 1 cm and wall thickness 0.7 mm is used as a discharge tube in which the magneto plasma is produced. This discharge tube is located at the center of a WR 137 rectangular waveguide, such that the E field of the wave is approximately uniform across the discharge tube. The waveguide assembly containing the discharge tube is in a nearly uniform magnetic field (variation 1 per cent), which can be varied from 0 to 3000 gauss. The plasma is produced in the discharge tube by a recurrent electrical discharge through the gas. The microwave apparatus is shown schematically in Fig. 6(a). Two klystrons generate microwave power at frequencies f_d and f_s. The microwave signal of frequency f_d has a peak power of 100 mw. This signal is designated as the *disturbing signal* and is in resonance with the electrons in the magneto plasma, *i.e.*, $f_d=f_H=eB/2\pi m$. The second microwave signal, $f_s>f_d$ is of sufficiently low amplitude ($\lesssim 10$ μw) and is designated as the *sensing wave*, detected by D_2; D_1 receives only the *disturbing wave* f_d. The microwave signals reflected by the 3-stub tuners are absorbed in the ferrite isolators I_1 and I_2, so as not to re-enter the plasma. Before presenting the experimental results, the sequence of events occurring in a typical experiment is described in a timing diagram shown in Fig. 7. A

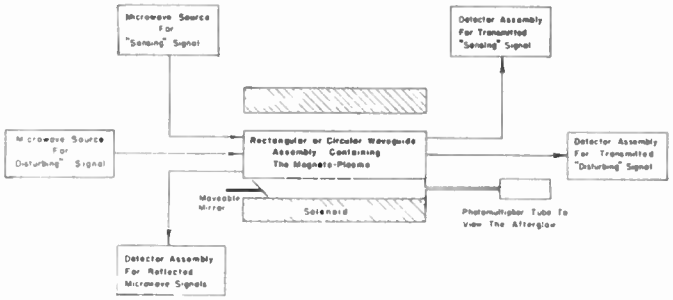

Fig. 5—Schematic diagram illustrating the technique for the study of wave-interaction phenomenon in laboratory magneto plasmas.

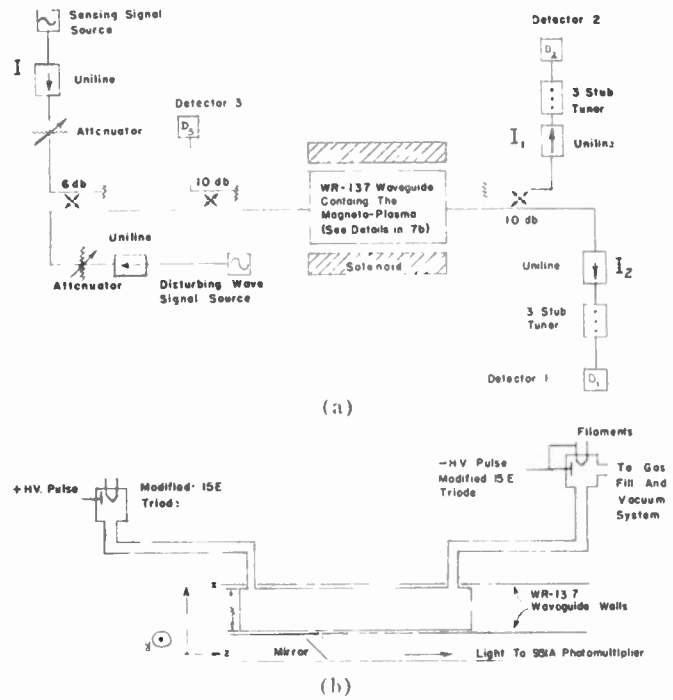

Fig. 6—(a) Block diagram of the experimental arrangement used for the study of magneto plasmas located in rectangular waveguides. (b) A cross-sectional view of the waveguide assembly containing the discharge tube

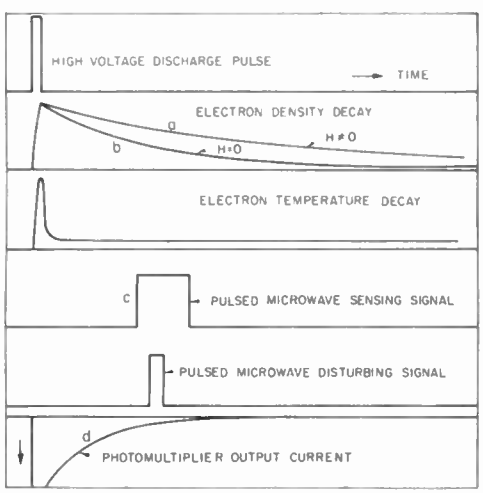

Fig. 7—Timing diagram of the sequence of events in a typical wave-interaction experiment.

2-μsec-wide, 5-kv dc-discharge pulse, repeated at the rate of 100 pps establishes a plasma which then decays as represented by *a* and *b* of Fig. 7. The pulsed microwave signals of controllable widths are propagated at the desired times during the afterglow. The visible light intensity emitted by the afterglow as recorded by a photomultiplier is also sketched in trace *d*. The RF envelopes of the transmitted and reflected microwave signals can be displayed on a dual-beam oscilloscope.

V. Experimental Results

In order to show the general validity of the simple theory of wave interaction in gaseous plasmas and to verify the discussions given in Section III, we report here the results of experiments performed in plasmas produced in neon and xenon gases. The gas pressures are chosen so as to achieve an efficient transfer of electromagnetic energy to the electron gas under cyclotron resonance condition; hence the quantity ν/ω_H should be much smaller than unity. Xenon was chosen as a typical gas whose collision frequency exhibits the Ramsauer behavior for low-energy electrons as opposed to that of neon. The presence of electron-ion collisions in a neon plasma of appropriate charge densities results in the fact that the total collision frequency in such a plasma varies with electronic energy in a manner similar to that of ν_{em} in xenon (see Fig. 1). In the following paragraphs, the propagation characteristics of an electromagnetic wave in a low temperature isothermal (300°K) plasma is studied and this is followed by a similar study in a perturbed plasma.

A. Propagation Characteristic of Sensing Signal Guided Through a Magneto Plasma

A low-power-pulsed microwave signal $f_s = 4.566$ Gc is guided through a decaying magneto plasma obtained in neon at a pressure of 1.6 mm Hg. The experimentally measured attenuation and phase shift undergone by this sensing signal are plotted as a function of the magnetic field in Fig. 8(a). The solid curve represents the measured attentuation and the dotted curve the measured phase constant. The theoretical attenuation and phase constants, α and β, obtained from the expression given by (17) are plotted in Fig. 8(b). A comparison of the theoretical and experimental curves shows the similarity in the general shape of the curves. It is known that the fundamental parameters such as electron density and effective collision frequency can be determined from such experimental data. The technique is also applicable to the determination of these parameters in a plasma which is perturbed, for example, by another electromagnetic wave. If the two EM waves are propagated in the time sequence shown in Fig. 7, then this technique provides information on the state of the plasma prior to, during, and in the wake of the disturbance.

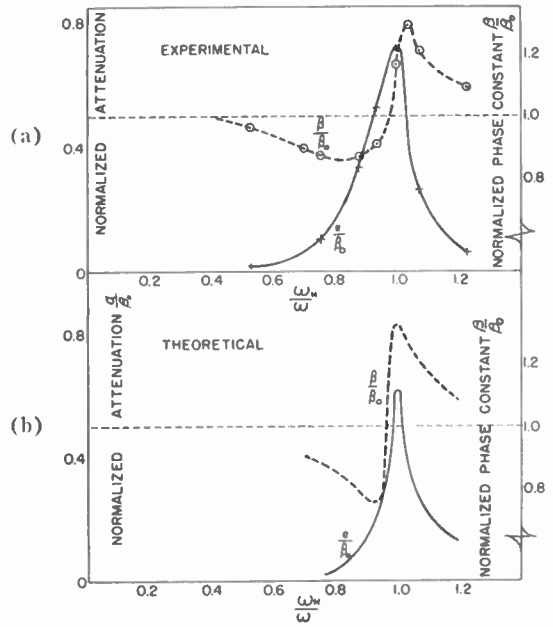

Fig. 8—(a) Experimental values of the normalized attenuation and phase constants as a function of (ω_H/ω). $f_s=4.96$ Gc. Peak power 150 μw. The pulsed probing signal is transmitted 1.0 msec after the termination of a 2-μsec wide, 5-kv discharge pulse through neon gas (1.6 mm Hg). (b) theoretical plot of normalized attenuation and phase constants for $\omega p^2/\omega^2=0.1$ and $\nu/\omega=0.04$.

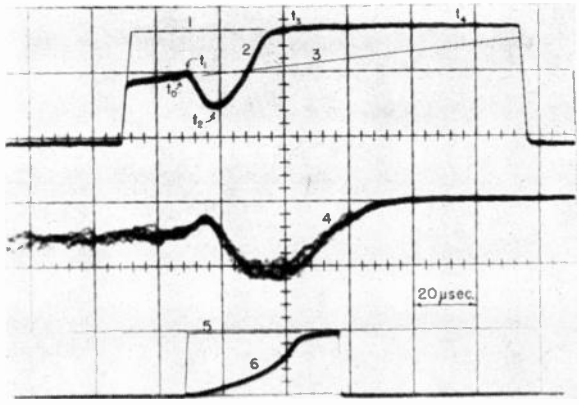

Fig. 9—Wave-interaction in the afterglow of a neon magneto plasma (pressure (1 mm Hg). $f_H=eB/2\pi m=f_D=4.80$ Gc. Peak power 75 mw. Pulsed disturbing signal is propagated 1.0 msec after the termination of 2-μsec wide, 5-kv discharge pulse. $\nu_{ei}>\nu_{em}$ $f_s=6.2$ Gc. Peak power 20 μw. Traces 1 and 5 are the RF envelopes of the transmitted sensing and disturbing pulses in the absence of the plasma. Trace 3 is the envelope of f_s when f_d is shut off. When f_D is incident on the plasma, traces 2 and 6 are transmitted RF envelopes of f_s and f_D, respectively. Trace 4 is the photomultiplier output representing the light intensity emitted in the afterglow. Downward deflection indicates increased light output.

B. Cross-Modulation in a Neon Afterglow

The experiments, which are described below, were performed in a decaying neon plasma under two different conditions: 1) $\nu_{ei}>\frac{1}{3}\nu_{em}$ and 2) $\nu_{em}>3\nu_{ei}$. These conditions determine whether the total collision frequency decreases with energy of the electrons as in case 1, or increases with the energy of the electrons as in case 2. In the early part of a 1 mm Hg-neon afterglow, the electron density is in the range 10^{12} to 10^{10} electrons/cc and $T_e\sim300°K$. Hence, the first condition is prevalent as can be seen from Fig. 1. Of course, as the plasma continues to decay condition 2) becomes prevalent.

Fig. 9 displays the oscilloscope traces of the transmitted microwave signals and the photo-multiplier output for a typical experiment in which condition 1) prevails. Notice that the amplitude of the transmitted sensing wave initially increases, reaching a maximum at the point denoted by t_1, even though the electron energy is increasing from $t=t_0$ to t_1. Since the absorption of the sensing signal is proportional to ν_t for this value of the magnetic field

$$\left(\omega_H=\omega_d,\ i.e.,\ B=\frac{m}{e}\omega_d\right),$$

the increased transparency indicates that the total collision frequency has decreased. At $t=t_1$, the derivative of ν_t with respect to T_e is zero, or $\nu_{ei}=\frac{1}{3}\nu_{em}$. An independent measurement of the number density of the electrons would then yield the temperature T_e. As the energy of the electron gas is further increased, the electron collisions with the neutrals predominate over those with ions so that now the absorption of the sensing wave increases.

At the point $t=t_2$, the absorption reaches a maximum despite the continued energy rise of the electron gas. This point corresponds to the maximum value of σ_{xxs} as a function of ν/ω_s as seen in Fig. 3. This interpretation is correct provided that it is assumed that the number density of the electrons does not vary appreciably in the time interval (t_2-t_0).

If this assumption is correct, then the product of the disturbing power P_d and the time interval t_2-t_0 should be a constant, provided that the rate of energy increase of the electron gas is large compared to the rate of energy loss. This is the case, even for relatively modest values of electric field, when the frequency of the disturbing wave is close to cyclotron resonance. Fig. 10 is a plot of log P_d as a function of log (t_2-t_0) and verifies that $P_d(t_2-t_0)$ is a constant whose value depends on the initial value of ν/ω_d. Hence it is reasonable to neglect the variation of n_e in the time interval t_2-t_0 and assign an energy state to the electron gas such that at $t=t_2$, ν/ω_s has the value which maximizes σ_{xxs}. For the frequencies used here, $\nu/\omega_s\sim0.2$. This is about a 100-fold rise in collision frequency.

This large rise in the collision frequency is also indicated by the amplitude of the transmitted disturbing wave itself. Since the absorption of the disturbing wave is proportional to $1/\nu_t$, this large increase of ν_t results in a decreased absorption.[1] This is the phenomenon which was referred to earlier as self-modulation.

[1] The experiment described here illustrates insertion loss only. However, reflection measurements have shown that the absorption is very closely approximated by the insertion loss.

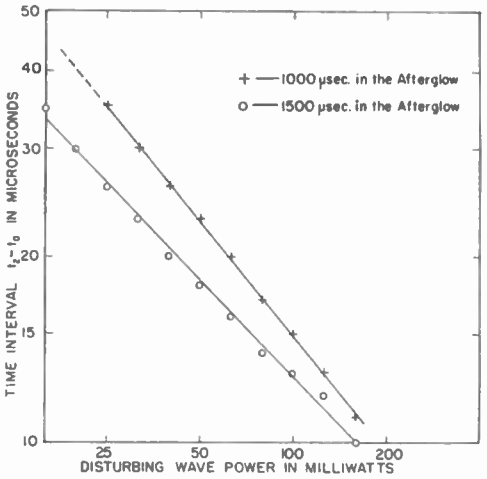

Fig. 10—Time elapsed since the initiation of the disturbing microwave pulse to establish a constant energy state of the electron gas (*i.e.*, corresponding to $\nu/\omega_s \sim 0.2$ at $t=t_2$), as a function of the amplitude of the disturbing wave. The two curves correspond to two different values of n_e and ν_c. Neon gas 1.0 mm Hg. $f_H = eB/2\pi m = 4.86$ Gc; $f_s = 6.2$ Gc.

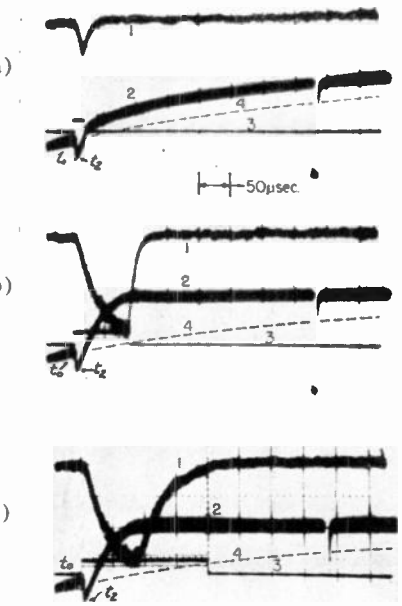

Fig. 11—Wave-interaction phenomena, when the amplitude of disturbing wave is constant, but whose pulse duration is varied. Neon 0.8 mm Hg. $f_H = eB/2\pi m = 4.97$ Gc. Peak power 100 mw. $f_s = 5.86$ Gc. Trace 4 represents the amplitude of the transmitted sensing signal (CW) in the absence of the pulsed disturbing signal. Trace 3 shows the duration for which the disturbing pulse is applied. The effect of the disturbing signal on the plasma "seen" by the sensing signal is represented in trace 2. Trace 1 is the photomultiplier output.

It is also noted in Fig. 9 that the amplitude of the transmitted sensing wave reaches its unattenuated value at the point $t=t_3$. In view of the above discussion, this is possible if the number density of the electrons in the plasma has decayed considerably in the time interval t_3-t_2. This will later be shown to be the case. This fact indicates that the plasma is being rapidly destroyed due to the drastic heating of the electron gas by the resonating disturbing wave. The variation of the visible light intensity, as seen in Fig. 9 also shows the effect of the disturbing wave on the plasma. Immediately after the initiation of the disturbing pulse, the light intensity decreases due to a reduction in the electron-ion recombination coefficient. This reduction in light intensity is known [19], [5] as quenching of the afterglow. Having decreased the collision frequency of the electrons, the rate of transfer of electromagnetic energy to the electrons is thus accelerated. Electrons reach energies high enough to undergo inelastic collisions with neon atoms in their ground state (~18.5 ev) or certainly with neon atoms which are in metastable states (~2 ev). Such collisions result in a net increase of light intensity following the termination of the initial quenching. The decrease in photomultiplier current after the removal of the disturbing pulse is most likely due to the decreasing number of inelastic collisions as well as the reduction in recombination light intensity which in the prevailing charge density range is approximately proportional to n^2.

We shall now describe effects produced at constant amplitude when the width of the disturbing pulse is varied. Figs. 11(a), (b), (c) show the oscilloscope traces of the transmitted microwave signals and photomultiplier current, for three different pulse widths of the disturbing wave under the condition $\nu_{cm} \gg 3\nu_{ei}$. It should be noted that the sensing microwave signal is operated in this instance as a continuous wave pulsed-off for a short duration in order to obtain a reference level. In the absence of the disturbing signal, trace 4 in all these figures shows that the attenuation of the sensing signal decreases as a function of time due to the normal decay of the electron density. For a narrow pulse of the disturbing wave, only the increasing absorption of the sensing signal and immediate relaxation is seen on trace 2 of Fig. 11(a). However, for wider disturbing pulses (width $>t_2-t_0$) it is observed that the amplitude of the transmitted sensing signal reaches a value corresponding to its original unattenuated level even before the conclusion of the disturbing pulse [trace 2 of Fig. 11(b), (c)]. This is again attributed to the rapid loss of electrons from the plasma when they are subjected to resonant heating for the time intervals indicated above. One of the possible reasons for this phenomenon is that it appears necessary to keep the electrons energetic for such a time interval so that they are capable of diffusing to the walls with a very considerably enhanced diffusion coefficient. In addition to the enhanced collisional diffusion, a second possible reason for the rapid disintegration of the plasma might be due to some instability which can develop when considerable selective heating of the electron gas occurs, which is the case at cyclotron resonance. When the cross-modulation experiment was performed in neon (0.5 mm Hg), as shown in Fig. 12, a low-frequency (140 kc) amplitude modulation was observed on the amplitude of the transmitted sensing signal, during the time interval of the disturbing wave pulse. However such variations in the transmitted am-

plitude of the sensing wave were not observed at higher pressures or for lower electron densities.

The phenomena are considerably different at later times in the afterglow (Fig. 13) but are readily understood on the basis of the previous experiments. It is seen that the absorption of the sensing wave increases immediately with increasing electron energy. This is understood upon the basis of the expression of the total collision frequency $\nu_t = \nu_{ei} + \nu_{em}$. Since the electron density is much lower at these times in the afterglow, the contribution of ν_{ei} to the total collision frequency is negligible. Hence, an increase of the energy of the electrons can only increase their collision frequency as contrasted with the initial decrease which was observed in Fig. 9.

It is also seen that the increase in photomultiplier current occurs almost immediately (<1 μsec) after the start of the disturbing pulse. This occurs because the electrons are accelerated to high energies (from about 0.04 ev to at least 2 ev) within very few collision times.

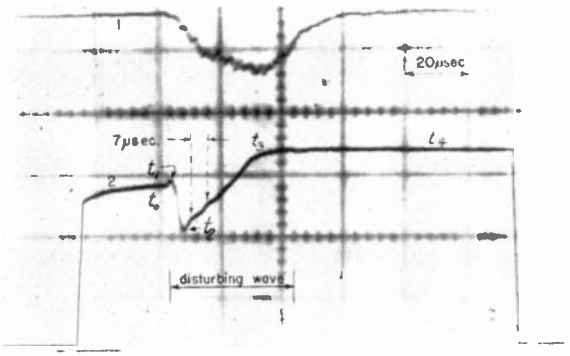

Fig. 12—The low-frequency ($\sim$140 kc) amplitude modulation which was observed on the transmitted amplitude (trace 2) of the sensing signal, when plasma electrons are accelerated by the resonating disturbing wave. Trace 1 is the photomultiplier output. Neon gas 0.5 mm. Hg $f_H = eB/2\pi m = f_D = 5.1$ Gc. Peak power 100 mw; $f_s = 5.86$ Gc.

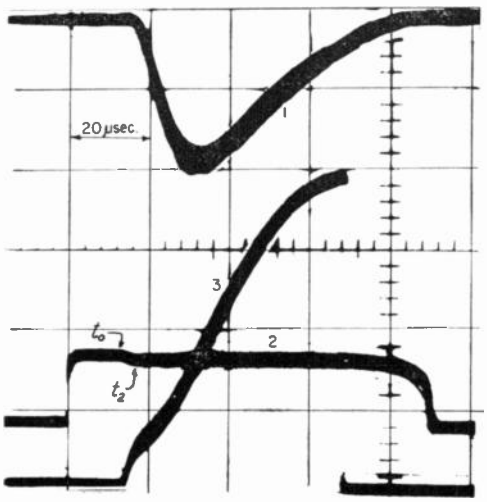

Fig. 13—Wave-interaction in the afterglow of a neon plasma for the condition $\nu_{em} \gg 3\nu_{ei}$. Neon 1.0 mm Hg. $f_D = 4.78$ Gc $= f_H$. $f_s = 6.47$ Gc. Trace 1 shows photomultiplier output. Trace 3 represents the amplitude of transmitted disturbing signal and trace 2 that of the sensing signal. Peak power of $f_D = 100$ mw.

This rapid acceleration is attributed to the fact that the power absorbed from the disturbing wave is inversely proportional to $1/\nu_t$ for $\omega_H = \omega_d$. The total collision frequency at $t = t_0$ is, of course, smaller than in the experiment described in Fig. 9, since the contribution of ν_{ei} to the total collision frequency is here insignificant. Hence the energy rise when only ν_{em} is present is more rapid than in the case when $\nu_t = \nu_{ei} + \nu_{em}$.

This rapid rise in the electronic energy is also evidenced by the self-modulation of the transmitted disturbing wave. It is seen that the transmitted disturbing wave increases more rapidly in Fig. 13 than in Fig. 9. This is consistent with the above discussion.

Additional experiments were performed to verify the fact that the point t_2 of Figs. 9, 11, and 13 is in every case the point where Re σ_{xx_s} reaches its maximum. Two sensing frequencies, ω_{s1} and ω_{s2}, are used such that $\omega_{s1} > \omega_{s2} > \omega_d = \omega_H$. Thus, as predicted by Fig. 3, the point of maximum absorption (t_2) as sensed by ω_{s2} is closer to t_0 than the corresponding point sensed by ω_{s1}. This is seen in Fig. 14.

This figure also illustrates the enhanced disintegration of the plasma in the time interval $t_4 - t_2$. All other quantities being equal, the propagation of ω_{s2} is affected by a smaller electron density than that of the higher frequency ω_{s1}, because ω_{s2} is closer to cyclotron resonance than ω_{s1}. Hence the plasma becomes completely transparent to ω_{s1} at an earlier time than to ω_{s2}.

The enhanced disintegration of the plasma as a result of the rapid rise of electron energy has been studied in greater detail by using Faraday rotation [18] of guided electromagnetic waves through plasmas. In this experiment, the plasma (same dimensions as in the rectangular guide experiments) is centrally located in a circular waveguide immersed in a longitudinal magnetic field. By measuring the angle of rotation of a linearly-polarized TE_{11} pulsed sensing wave as a function of time in the late afterglow, during and in the wake of a pulsed disturbing wave, ($\omega_d = \omega_H$) information is obtained on the influence of the resonance heating of the electrons on the phase velocities of the extraordinary and ordinary sensing waves.

Fig. 15 shows typical results of such an experiment for several amplitudes of the disturbing wave. Notice that at any time $t > t_1$, the angle of rotation does not return to its unperturbed value for large amplitudes of the disturbing wave. However, for smaller amplitudes of the disturbance, the angle tends to relax towards the undisturbed value. Since the rotation angle is directly proportional to the total number of electrons in the magnetized plasma, the difference in angles at $t = t_3$ (after the plasma electron gas has relaxed to its initial temperature) represents the loss of electrons. Notice the correspondence of the experimentally obtained dependence of Faraday rotation upon collision frequency in the interval ($t_1 - t_0$) to that predicted theoretically from (18) and plotted in Fig. 16.

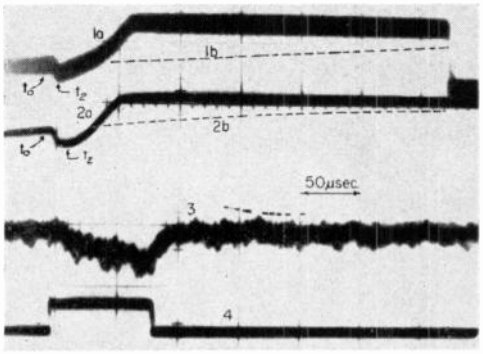

Fig. 14—Effect caused by the disturbing microwave signal ($f_D = 5.05$) on two sensing signals. $f_{s1} = 6.0$ Gc. $f_{s2} = 6.7$ Gc. Trace 1b and 2b represent the amplitudes of transmitted f_{s1} and f_{s2} respectively in the absence of the disturbing signal, whereas 1a and 2a represent the corresponding trace in the presence of the disturbing signal. Trace 4 shows the duration for which the pulsed signal is present. Trace 3 represents the photomultiplier output. Neon gas 0.9 mm Hg.

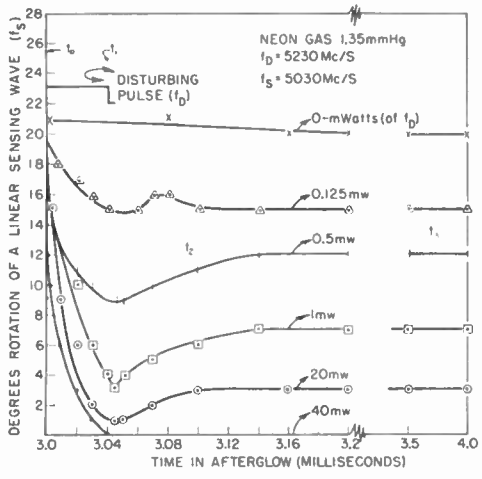

Fig. 15—Faraday rotation of 1 μsec wide sensing signal (f_s) as a function of time in the afterglow, during and in the wake of the pulsed disturbing signal (f_D). The Faraday rotation is shown for different amplitudes of the disturbing signal.

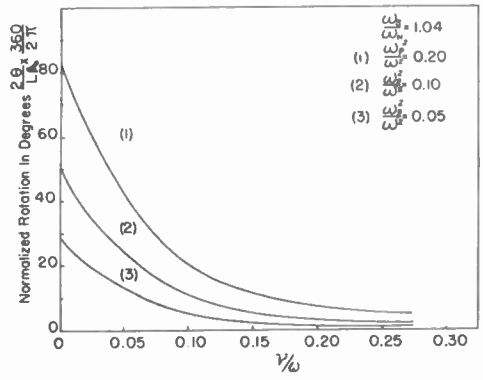

Fig. 16—Normalized Faraday rotation as a function of ν/ω for different values of ω_p^2/ω^2, and constant $\omega_s/\omega_H = 1.04$.

C. Cross-Modulation in a Ramsauer Gas (Xenon)

It was shown in the previous experiments that it was possible for the total collision frequency in a neon plasma to decrease with increasing electronic energy despite the fact that the cross section for momentum transfer between electrons and neon atoms is a slowly increasing function of electron temperature. The decreasing collision frequency with increasing electron energy is due to the coulomb collisions between the electrons and ions which are dominant when the degree of ionization is greater than 10^{-5} and at low electron temperatures ($\lesssim 300°K$).

As is well known, the cross section for momentum transfer of electrons with xenon atoms decreases very rapidly with increasing T_e from ~300°K reaching a minimum and then increasing as shown in Fig. 1. In view of the large absolute values of xenon cross section for slow (~300°K) electrons, the electron-ion collision frequency contributes little, if any, to the total collision frequency at the xenon pressure indicated, even at the maximum electron densities used in these experiments (~10^{11}/cc). At these electron densities however, a neon (1 mm Hg, 300°K) plasma is already completely coulomb-interaction dominated, as just mentioned. Therefore, in view of the falling cross sections with increasing electron energy in both cases, the phenomena of wave interaction will be completely similar.

Fig. 17 shows the oscilloscope traces of the amplitudes of the transmitted signals obtained from the experiment performed in a xenon afterglow. These photographs [Fig. 17(a), (b), (c)] show the effects for three different amplitudes of the disturbing wave ($\omega_d = \omega_H$). It is seen that immediately after the application of the disturbing microwave signal, the absorption of the sensing signal decreases in the time interval $t_1 - t_0$. This is, of course, due to the decreasing collision frequency with increasing electron energy, as is the case in a coulomb-interaction dominated neon plasma. At the instant t_1, the electron energy corresponds to that energy for which Q_{em} and therefore ν_{em} is a minimum (Ramsauer). In the time interval t_1 to t_2 [Fig. 17(a)] the absorption of the sensing signal increases reaching a maximum at $t = t_2$ despite the increasing collision frequency. The interpretation of this point is identical with the corresponding point in the neon plasma discussed earlier and shown in Fig. 9. It is also seen in Fig. 17(c), as opposed to (a) and (b), that as a result of the relatively high level (100 mw) of the disturbing wave and immediately following its conclusion, the complete unattenuated amplitude of the sensing wave signal is transmitted. In the case of a passive plasma this could occur only as a result of a drastic loss of electron density in the short time interval observed.

The results of these experiments led to a simple method of determination of electron collision frequencies in a magneto plasma. This method will now be described.

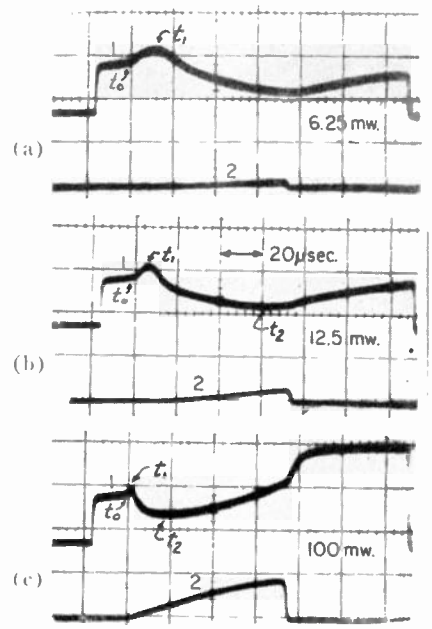

Fig. 17—Wave-interaction phenomena in xenon. Pressure 0.4 mm Hg. Trace 1 is the transmitted amplitude of the sensing signal in the presence of a disturbing signal. Trace 2 is the transmitted amplitude of the disturbing signal. $f_s=6.1$ Gc. $f_H=eB/2\pi m=f_D=5.2$ Gc. The three photographs show the effects for three amplitudes of the disturbing pulse.

D. Cross-Modulation Technique for Determining Collision Frequency

The method is based upon the interpretation of the point $t=t_2$ in Fig. 9. At this point $\partial\sigma_{xxn}/\partial\nu=0$. If the magnetic field intensity is adjusted to a value such that

$$\left.\frac{\partial\sigma_{xxn}}{\partial\nu}\right|_{t=t_0}=0, \tag{20}$$

then the value of ν at $t=t_0$ is a solution to (20). The condition given by (20) is obtained experimentally by varying the magnetic field and observing the cross modulation as shown in Fig. 18. Notice that for both $\omega_H/\omega_s\ll 1$ and $\omega_H/\omega_s\gg 1$, the sensing wave undergoes increased absorption for increasing collision frequency. However, for $\omega_H/\omega_s=1$, the absorption decreases. It appears obvious that there are two values of the magnetic field, for which the cross modulation disappears: these fields are solutions of (20). The value of ν is given to a good approximation by

$$\nu \doteq \omega_s\left|1-\frac{\omega_H}{\omega_s}\right|, \tag{21}$$

where ω_H corresponds to these values of the magnetic field for which the cross modulation disappears.

The validity of this method is limited by the range of validity of (16a). Basically, the use of this equation requires that the electron density be small enough so that the electromagnetic fields inside the plasma can be well approximated by the applied fields. It is for this reason that the experiments were performed with very low electron-density plasmas ($n_e<10^8$/cc). Furthermore,

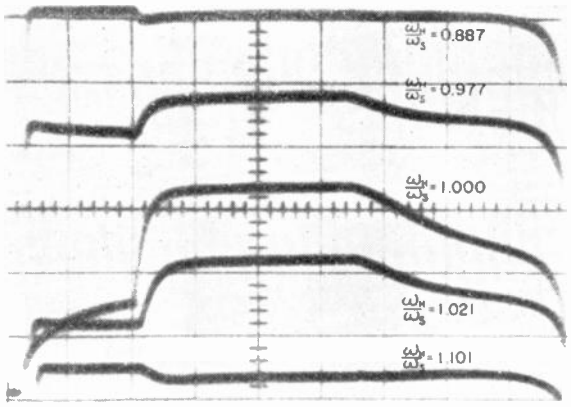

Fig. 18—Variation of the cross-modulation as a function of the magnetic field. Neon gas 12.0 mm Hg. $f_d=4.764$ Gc. $f_s=6.72$ Gc.

experiments have shown that only the value $\omega_H/\omega_s>1$ can be used in (21). For $\omega_H/\omega_s<1$, both α, the attenuation constant, and β, the phase constant, are dependent upon ν, whereas for $\omega_H/\omega_s>1$, β is almost independent of ν. Since attenuation is used for this measurement, the condition $\omega_H/\omega_s>1$ must be used.

This method yielded collision frequencies in good agreement with published results.

VI. Conclusion

In summary, the typical experimental results reported above illustrate adequately the general phenomenon of RF wave interaction in magneto plasmas. The theory on which these experimental results are based can be considered as a generalization of Bailey's [3] theory of interaction of radio waves in the ionosphere. It was shown here that the phenomenon of interaction of microwaves in a magneto plasma constitutes a useful method for investigating plasma behavior. This method is applied here to study some of the detailed aspects of electromagnetic energy transfer into kinetic energy of a charged constituent of the plasma. Particular emphasis was placed here on the transfer of electromagnetic energy to the electron gas of a plasma under cyclotron-resonance condition. The consequent fast rate of kinetic energy increase of the electrons is evidenced by the corresponding change in their collision frequency and also in the magnetic field control of plasma confinement.

Appendix

Derivation of (17)

In order to derive an approximate expression for the propagation constant for waves propagating as exp $(-\gamma z)$ in an anisotropic medium, let us consider Maxwell's equations with and without the plasma:

$$\nabla_t\times \boldsymbol{H}_0-\gamma_0\hat{a}_z\times\boldsymbol{H}_0=j\omega\epsilon_0\boldsymbol{E}_0, \tag{22}$$

$$\nabla_t\times \boldsymbol{E}_0-\gamma_0\hat{a}_z\times\boldsymbol{E}_0=-j\omega\mu_0\boldsymbol{H}_0, \tag{23}$$

$$\nabla_t\times \boldsymbol{H}-\gamma\,\hat{a}_z\times\boldsymbol{H}=\boldsymbol{J}+j\omega\epsilon_0\boldsymbol{E}, \tag{24}$$

$$\nabla_t\times \boldsymbol{E}-\gamma\,\hat{a}_z\times\boldsymbol{E}=-j\omega\mu_0\boldsymbol{H}. \tag{25}$$

where

$\boldsymbol{E}_0$, $\boldsymbol{H}_0$ = electromagnetic fields in the empty structure,

$\boldsymbol{E}$, $\boldsymbol{H}$ = electromagnetic fields in the structure,

$\nabla_t = \hat{a}_x(\partial/\partial_x) + \hat{a}_y(\partial/\partial_y)$,

$\hat{a}$ = unit vector,

γ, γ_0 = propagation constant of a wave with and without the plasma,

J = conduction current density as defined by (15).

The following sum is formed: $\boldsymbol{E}\cdot 22 + \boldsymbol{E}_0\cdot 24 - \boldsymbol{H}\cdot 23 - \boldsymbol{H}_0\cdot 4$; this is integrated over the volume enclosed by the guiding structure. The application of the divergence theorem leads to the following equation:

$$\oint\!\!\oint_S (\boldsymbol{H}_0 \times \boldsymbol{E} - \boldsymbol{H} \times \boldsymbol{E}_0)\cdot d\boldsymbol{S} - (\gamma + \gamma_0)\iiint (\boldsymbol{E}\cdot\hat{a}_z \times \boldsymbol{H}_0 + \boldsymbol{E}_0\cdot\hat{a}_z \times \boldsymbol{H})dV = 2j\omega\iiint(\epsilon_0\boldsymbol{E}\cdot\boldsymbol{E}_0 + \mu_0\boldsymbol{H}\cdot\boldsymbol{H}_0)dV + \iiint \boldsymbol{E}_0\cdot\boldsymbol{J}\cdot dV. \quad (26)$$

The first integral of (26) is zero because of the boundary conditions on E and E_0. Further simplification is possible if the fields in the absence of the plasma are TE. We can solve (23) and (25) for $\boldsymbol{H}$ and $\boldsymbol{H}_0$ and substitute this in (26):

$$\gamma + \gamma_0 = \frac{\iiint \boldsymbol{E}_0\cdot\boldsymbol{J}dV + 2j\omega\iiint(\epsilon_0\boldsymbol{E}\cdot\boldsymbol{E}_0 + \mu_0\boldsymbol{H}\cdot\boldsymbol{H}_0)dV}{\frac{1}{j\omega\mu_0}\iiint(\boldsymbol{E}_0\cdot\nabla_t E_z + (\gamma+\gamma_0)\boldsymbol{E}\cdot\boldsymbol{E}_0)dV}. \quad (27)$$

The fields which were assumed for the plasma partially filling the waveguide as shown in Fig. 6(b) were

$$\boldsymbol{E} = A\sin\left(\frac{\pi y}{a}\right)\hat{a}_x + B\sin\left(\frac{\pi x}{b}\right)\hat{a}_y + C\sin\left(\frac{\pi x}{a}\right)\sin\left(\frac{\pi y}{b}\right)\hat{a}_z. \quad (28)$$

This assumption leads to a solution for the propagation constant given by

$$\gamma^2 - \gamma_0^2 = j\omega\mu_0\sigma_{xx}\left(\frac{W}{a} + \frac{1}{2\pi}\sin\left(\frac{\pi W}{2a}\right)\right) + \frac{8}{\pi^2}\frac{B}{A}\sigma_{xy}\sin\left(\frac{\pi W}{2a}\right). \quad (29)$$

The choice of the ratio B/A was made in the following manner. The dominant mode in the waveguide is the TE_{10} mode in the limit of low electron densities; in addition, the amplitude B arises because σ_{xy} is nonzero. Hence the product of $\sigma_{xy}B$ is considered to be of second order in importance and is neglected.

Bibliography

[1] B. D. H. Tellegan, "Interaction between radio waves?" *Nature*, vol. 131, p. 840; June, 1953.

[2] V. A. Bailey and D. F. Martyn, "The influence of electric waves on the ionosphere," *Phil. Mag.*, vol. 18, pp. 369–386; August, 1934.

[3] ——, "The motions of electrons in a gas in the presence of variable electric fields and a constant magnetic field," *Phil. Mag.*, vol. 23 (suppl), pp. 774–781; April, 1937.

[4] ——, *et al.*, "Resonance in gyro-interaction of radio waves," *Nature*, vol. 169, pp. 911–913; May, 1952.

[5] L. Goldstein, *et al.*, "Interaction of microwaves propagated through a gaseous discharge plasma," *Phys. Rev.*, vol. 90, pp. 151–152, April, 1953; "Quenching of afterglow in gaseous discharge plasmas by lower power microwaves," *Phys. Rev.*, vol. 90, pp. 486–487, May, 1953.
L. Goldstein and J. M. Anderson, "Interaction of microwaves in gaseous discharge plasmas and the Ramsauer effect," in "Record of the Fourteenth Annual Conference on Physical Electronics," Res. Lab. of Electronics, Mass. Inst. Tech., Cambridge; March, 1954.

[6] J. M. Anderson and L. Goldstein, "Interaction of electromagnetic waves of radio-frequency in isothermal plasmas: Collision cross-section of helium atoms and ions for electrons," *Phys. Rev.*, vol. 100, pp. 1037–1046; November, 1955.

[7] A. A. Dougal and L. Goldstein, "Energy exchange between electron and ion gases through coulomb collisions in plasmas," *Phys. Rev.*, vol. 109, pp. 615–624; February, 1958.

[8] L. Goldstein and T. Sekiguchi, "Electron-electron interaction and heat conduction in gaseous plasmas," *Phys. Rev.*, vol. 109, pp. 625–630; February, 1958.

[9] C. L. Chen, *et al.*, "Electron temperature dependence of the recombination coefficient in pure helium," *Phys. Rev.*, vol. 121, pp. 1391–1400; March, 1961.

[10] L. Tonks, "Theory of magnetic effects in the plasma of an arc," *Phys. Rev.*, vol. 56, pp. 360–373; August, 1939.

[11] W. P. Allis and E. L. Gordon, "Microwave Gaseous Discharges," Quart. Progr. Rept. of Res. Lab. of Electronics, Mass. Inst. Tech., Cambridge; July, 1957 (unpublished).

[12] ——, "Motions of ions and electrons," in "Handbuch der Physik," S. Flugge, Ed., Springer-Verlag, Berlin, Germany, vol. 21; 1957.

[13] P. Molmud, "Langevin equation and the ac conductivity of non-Maxwellian plasmas," *Phys. Rev.*, vol. 114, pp. 29–32; April, 1959.

[14] I. P. Shkarofsky, "Values of Transport Coefficients in a Plasma for any Degree of Ionization on a Maxwellian Distribution," Res. Labs., RCA Victor, Ltd., Montreal, Canada, Res. Rept. No. 7-801; December, 1960.

[15] H. Suhl and L. R. Walker, "Topics in guided wave propagation through gyromagnetic media," *Bell Sys. Tech. J.*, vol. 33, pp. 579–659; May, 1954.

[16] E. C. Jordan, "Electromagnetic Waves and Radiating Systems," Prentice Hall, Inc., New York, N. Y.; 1950.

[17] L. Goldstein, "Electrical discharge in gases and modern electronics," in "Advances in Electronics and Electron Physics," L. Marton, Ed., Academic Press, Inc., New York, N. Y., vol. 7; 1955.

[18] ——, "Nonreciprocal electromagnetic wave propagation in ionized gaseous media," IRE Trans. on Microwave Theory and Techniques, vol. MTT-6, pp. 19–29; January, 1958.

[19] C. Kenty, "The recombination of argon ions and electrons," *Phys. Rev.*, vol. 32, pp. 624–635; October, 1928.

[20] S. C. Brown, "Basic Data on Plasma Physics," The Technology Press, John Wiley and Sons, Inc., New York, N. Y.; 1959.

Frequency Conversion in a Microwave Discharge*

J. R. BAIRD† AND P. D. COLEMAN†, MEMBER, IRE

Summary—One nonlinear property of a microwave discharge located between two closely spaced parallel plates whose dimensions are small compared to the wavelength is analyzed. This discharge geometry, with its small volume, permits the attainment of CW microwave power densities in the discharge of the order of 0.1 to 1 Mw/cm³. It is concluded that the high power density coupled with the high diffusion rate of the closely spaced parallel plates results in a modulation of the electron density at the microwave frequency. The source of this nonlinearity is postulated to be a modulation of the ionization frequency ν_i whose functional form is taken to be $\nu_i = \alpha |v_d|$ where v_d is the ordered drift velocity and α is a proportionality factor constant in time. The theoretical analysis is compared to experimental results obtained by approximating the assumed geometry in an *X*-band and *K*-band frequency multiplier and in an *X*-band mixer. Harmonics up through the seventh at *X* band and up through the fourth at *K* band have been studied. Frequency mixing of 9- and 11-kMc signals to obtain a 20-kMc signal has yielded predictable results. Parametric amplification in a discharge is briefly considered.

I. Introduction

NONLINEAR properties are known to be possessed by microwave discharges. However, few paper exist on this subject, perhaps because it is difficult to isolate or restrict the discharge conditions such that a single effect can be studied and quantitatively analyzed.

In this paper the discharge geometry chosen is that of two closely spaced parallel plates having dimensions which are small compared to the operating wavelength. This restriction reduces the description of the discharge to a one-dimensional, lumped circuit element.

The small volume condition on the discharge permits the system to be operated at large CW power densities and field strengths for very modest absolute input power. Typical volumes considered are of the order of 10^{-5} cm³. Hence with a power input of 10 watts, the power density approaches 1 Mw/cm³. Field strengths are typically of the order of 0.5 to 3 kv/cm. Thus the discharge is being driven sufficiently hard for nonlinear effects to become useful and important.

The large electron densities and close spacing of the discharge plates permit diffusion losses to become dominant. The large power densities permit ionizations at fast rates. Hence the possibility exists for generating and losing electrons in times comparable to the RF period.

For the discharge geometry in this paper, it is postulated that the ionization frequency ν_i can be appreciably modulated by the microwave drive frequency. The functional form assumed is that ν_i is proportional to the absolute value of the ordered drift velocity v_d in the direction of the applied microwave field. Since this function is even, the ionization frequency will be modulated twice during each RF cycle.

By first solving for the linear drift velocity solution v_d of the momentum transfer equation, then determining ν_i, and, third, solving the continuity equation for the electron density $n(x, t)$, the harmonic current response of the discharge can be readily computed. It has been found convenient to include along with the microwave field a dc field for diagnostic purposes.

The analysis has been experimentally verified with a 3-cm frequency multiplier and mixer, and an 8.6-mm frequency multiplier. The variation of harmonic power as a function of a dc bias field is shown experimentally to be in close agreement with theory up through the 7th harmonic in the *X*-band device. Conversion losses were also found to be accurately predictable.

The performance of the 35-kMc multiplier was checked through the 4th harmonic. Here the electron density is varying at a 70-kMc rate. Just how far in frequency one can extend this type of device has yet to be determined.

II. Description of the Nonlinearity

If the microwave discharge is assumed to have a parallel plate geometry, then all quantities will involve only one space variable x. Neglecting the ionic current, the current density $J(x, t)$ of $n(x, t)$ electrons per unit volume having an average velocity $v_d(x, t)$ is given by the scalar expression

$$J(x, t) = qn(x, t)v_d(x, t) \tag{1}$$

where $-q = e$ is the electronic charge.

If the discharge is nonlinear, then the current density $J(x, t)$ response to the application of a combined dc and microwave electric field will have harmonic current components in addition to the fundamental and dc components. This will require, as seen from (1), that the electron density $n(x, t)$ and/or the average drift velocity $v_d(x, t)$ be expressible in a Fourier series.

In the linear analysis[1] of a microwave discharge in a parallel plate geometry where a combined dc and ac electric field E_T of the form

$$E_T = E_0 + E\left[\cos \omega t - \frac{\omega}{\nu_c} \sin \omega t\right] \tag{2}$$

* Received by the IRE, August 28, 1961. The work described was performed under the sponsorship of the AEC Res. Div., Thermonuclear Branch, under Contract AT(11-1)-392 and WADD Electronic Tech. Lab., under Contract AF33(616)-7043.

† Ultramicrowave Group, University of Illinois, Urbana, Ill.

[1] E. Everhart and S. C. Brown, "The admittance of high frequency gas discharges," *Phys. Rev.*, vol. 76, pp. 839–842; September, 1949.

is applied in the x direction, the solution of the momentum transfer equation

$$\frac{\partial v_d}{\partial t} + \nu_c v_d = \frac{qE_T}{m} \tag{3}$$

for the velocity v_d is given by

$$v_d = \frac{q}{m\nu_c}[E_0 + E\cos\omega t] = \frac{qE}{m\nu_c}[\beta + \cos\omega t], \tag{4}$$

where ν_c is the collision frequency for momentum transfer, m is the electron mass, and β is defined as

$$\beta = E_0/E. \tag{5}$$

The continuity equation for the case where diffusion is the dominant loss mechanism is

$$\frac{\partial n}{\partial t} = \nu_i n + D\frac{\partial^2 n}{\partial x^2}. \tag{6}$$

where ν_i is the ionization frequency and D the diffusion constant.

A linear solution (electron density independent of time) of (6) for the condition $n(x, t)$ is zero at the metal plate boundaries located to $x = \pm l$ is

$$n(x, t) = n(x) = n_0 \cos\left(\frac{\pi x}{2l}\right), \tag{7}$$

with

$$D = \left(\frac{2l}{\pi}\right)^2 \nu_i. \tag{8}$$

To account for a nonlinear effect using the momentum transfer and continuity equations, it could be assumed that the collision frequency ν_c and/or the ionization frequency ν_i are not constant in time.

Margenau and Hartman[2] have treated the case of a low power level microwave discharge wherein diffusion has been neglected and the electron density has been assumed to be constant in time. The nonlinearity of the discharge has been accounted for by having the collision frequency ν_c a function of time. This assumption leads to harmonic component terms in the average drift velocity $v_d(x, t)$.

In the discharge geometry of this paper, diffusion will be the dominant loss mechanism for electrons as opposed to attachment and recombination since the density gradient between the two closely spaced electrodes is extremely high. Also the power level (0.1 to 1 Mw/cm³) and field strength (0.5 to 3 kv/cm) are quite large so that electrons can be generated and lost at a very rapid rate. This leads to the possibility that the ionization frequency ν_i could be a function of time and hence, the electron density $n(x, t)$ could be modulated by the microwave drive field. The problem is to find the appropriate functional form of $\nu_i(t)$ that will explain the experimental facts.

In his study of dc gas discharges, Townsend assumed that the ionization frequency ν_i was proportional to the average dc drift velocity.[3] A corresponding assumption for the microwave discharge would be to make the ionization frequency proportional to the absolute value of the ordered drift velocity since ionizations are equally probable for both positive and negative velocities;

$$\nu_i = \alpha|v_d|. \tag{9}$$

While the utility of the assumption made in (9) will have to be determined by the agreement between computed and experimental results, some intuitive arguments can be made to support this assumption.

The microwave field strengths used in the experiments described in this paper, while far in excess of the minimum required to sustain the discharge, are not sufficient to give an electron-ionizing energy in one oscillation. To provide a net transfer of energy, collisions must exist. The energy which the electrons gain is largely in the form of random thermal motion with only a small part contributed by ordered RF motion. Thus, it is expected that the electron energy or temperature is at best only slightly modulated by the RF field.

Except for high velocity electrons, the electron velocity distribution in velocity space is probably not too different from a Maxwell distribution as shown in Fig. 1(a). However, consider next the distribution of velocities in the x, y and z directions. The curves of Fig. 1(c) and (d) are close to equilibrium distributions since there are no applied fields in these directions. All velocities in the y and z directions are a result of energy gained in the x direction and scattered into the y and z directions by elastic and inelastic collisions. The most probable x component of velocity will not be zero, as indicated by Fig. 1(b), but will vary with the RF ordered velocity as shown by curves a and c.

The number of electrons Δn with velocities exceeding the ionizing velocity v_i due to the RF modulation will be given approximately by

$$\Delta n \simeq \int_{v_i}^{\infty} N\left[\frac{m}{2\pi kT}\right]^{-1/2} \cdot \left[\epsilon^{-(m/2kT)(v_x - |v_d|)^2} - \epsilon^{-(m/2kT)v_x^2}\right]dv_x. \tag{10}$$

Since $|v_d| \ll v_i$, the first exponential term can be expanded in a series wherein only the first two terms are retained, yielding

$$\Delta n \simeq |v_d| \int_{v_i}^{\infty} \frac{mv_x}{2kT} N\left(\frac{m}{2\pi kT}\right)^{-1/2} \epsilon^{-(mv_x^2/2kT)}dv_x. \tag{11}$$

Thus assuming the ionization frequency ν_i proportional to the number of electrons Δn having an x com-

[2] H. Margenau and L. M. Hartman, "Theory of high frequency gas discharges II," *Phys. Rev.*, vol. 73, pp. 309–315; February, 1948.

[3] S. C. Brown, "Basic Data of Plasma Physics," John Wiley and Sons, Inc., New York, N. Y., p. 137; 1959.

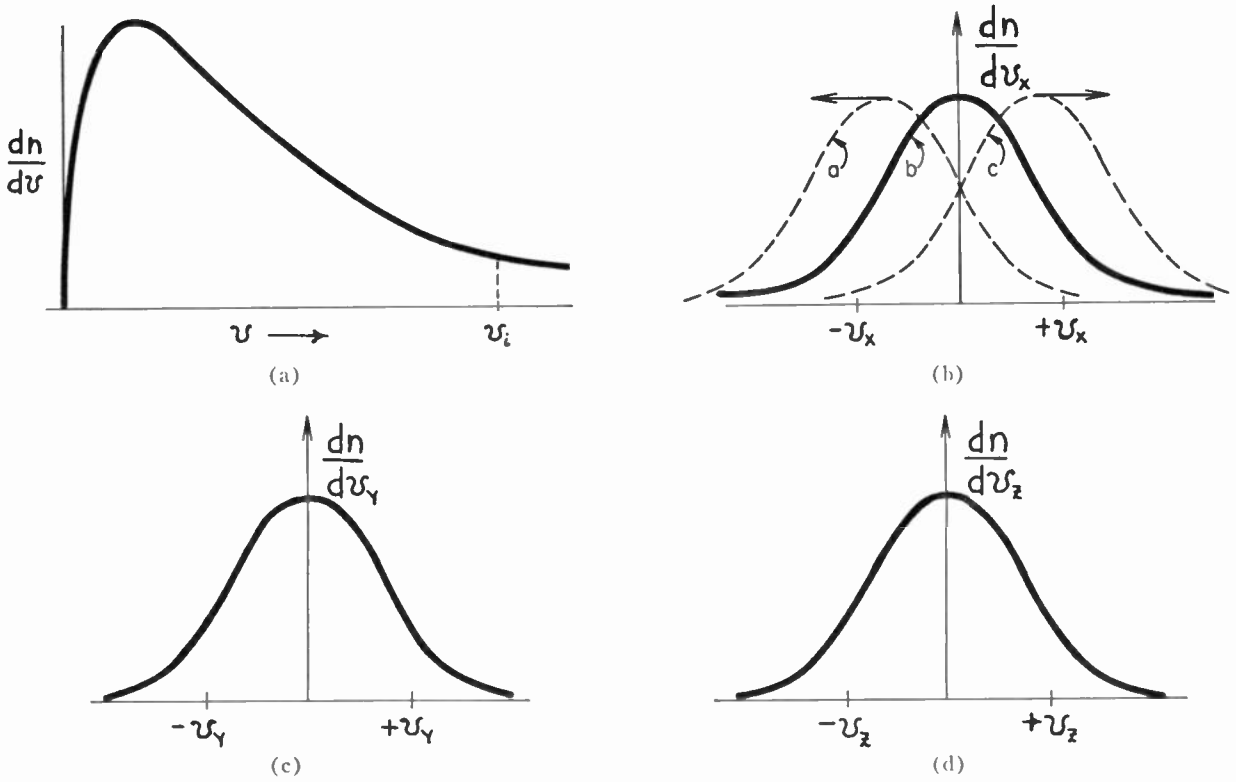

Fig. 1—Maxwell distribution of velocity components. (a) Velocity distribution. (b) Distribution of x component of velocity. (c) Distribution of y component of velocity (d) Distribution of z component of velocity.

ponent of velocity exceeding the ionization velocity v_i appears to be compatible with (9).

For the discharge geometry and power levels stated in this paper, it will be assumed that the principal source of nonlinearity arises from an RF modulation of the ionization frequency ν_i and that its functional form can be sufficiently described by the relationship given in (9).

III. Calculation of Current Density Function $J(x, t)$

The current density function $J(x, t)$ will be calculated assuming that the average drift velocity $v_d(x, t)$ in the x direction can be represented by the linear solution given by (4) and that the electron density function $n(x, t)$ contains harmonic terms because of the RF modulation of the ionization frequency ν_i. The calculation of $n(x, t)$ involves solving (6) and (9).

Substituting the linear drift velocity value given by (4) into (9), the result is

$$\nu_i = \frac{q\alpha E}{m\nu_c} \left| \beta + \cos \omega t \right|, \tag{12}$$

where α is a constant of proportionality independent of the time t.

Since ν_i is seen to be an even function of $\theta = \omega t$, it can be expanded in the following Fourier cosine series:

$$\nu_i = \frac{q\alpha E}{m\nu_c} \left[\frac{a_0}{2} + \sum_{k=1}^{\infty} a_k \cos (k\theta) \right], \tag{13}$$

where the Fourier coefficient a_k are given by

$$a_k = \frac{1}{\pi} \int_{-\pi}^{\pi} \left| \beta + \cos \theta \right| \cos (k\theta) d\theta = a_k(\beta). \tag{14}$$

The boundary condition that the electron density is zero at $x = \pm l$ will require that the space variation of $n(x, t)$ is given by the factor $\cos(\pi x/2l)$ as in the linear case. The appropriate functional form for $n(x, t)$ is

$$n(x, t) = n_0 \left[1 + \sum_{s=1}^{\infty} B_s \sin (s\theta) \right] \cos \left(\frac{\pi x}{2l} \right), \tag{15}$$

where the coefficients B_s are yet to be determined. It will be observed that the expression for $n(x, t)$ as given by (15) reduces to the linear solution when the coefficients B_s are set equal to zero. Since the modulation of $n(x, t)$ is not expected to be large, all the B_s coefficients are small compared to one.

The various terms in the continuity equation, as given by (6), can now be readily computed. First, the term $\nu_i n$ is seen to be

$$\nu_i n \simeq \frac{\alpha q n_0 E}{m\nu_c} \left[\frac{a_0}{2} + \sum_{k=1}^{\infty} a_k \cos (k\theta) \right] \cos \left(\frac{\pi x}{2l} \right), \tag{16}$$

where the coefficients B_s have been neglected. Next, the diffusion term is approximated by

$$D \frac{\partial^2 n}{\partial x^2} \simeq - \frac{n_0 D \pi^2}{4l^2} \cos \left(\frac{\pi x}{2l} \right). \tag{17}$$

Finally, by differentiating $n(x, t)$ as given by (15), one obtains

$$\frac{\partial n}{\partial t} = n_0\omega \sum_{s=1}^{\infty} sB_s \cos(s\theta) \cos\left(\frac{\pi x}{2l}\right). \tag{18}$$

Equating coefficients of like terms in the continuity equation yields

$$B_s = \frac{\alpha q E}{m\omega\nu_c} \frac{a_s}{s}. \tag{19}$$

The current density $J(x, t)$ can now be readily computed from (4) and (15):

$$J(x, t) \simeq \frac{n_0 q^2 E}{m\nu_c} \left\{ |\beta + \cos\omega t| + \frac{\pi q\alpha a_0 E}{m\omega\nu_c} \sum_{s=2}^{\infty} A_s \sin s\omega t \right\} \cos\left(\frac{\pi x}{2l}\right), \tag{20}$$

where the small term multiplying $\sin \omega t$ has been neglected, and A_s is given by

$$A_s = \frac{1}{2\pi a_0}\left[2\beta \frac{a_s}{s} + \frac{a_{s-1}}{s-1} + \frac{a_{s+1}}{s+1}\right] = A_s(\beta). \tag{21}$$

The harmonic terms in (20) are those involving the coefficients A_s. Hence the linear solution is obtained by setting A_s equal to zero.

At this point in the analysis, all the coefficients can be calculated in terms of β, the ratio of dc electric field amplitude E_0 to the RF field amplitude E; however, the proportionality constant α is still to be determined.

IV. Physical Realization of Assumed Discharge Geometry

Assuming the preceding analysis to be valid, it should be possible to predict the nonlinear behavior of any microwave discharge system in which the discharge takes place between closely spaced parallel plates whose dimensions are small compared to the wavelength. The conditions imposed are that the system can be described essentially in terms of one dimensional, lumped circuit elements as opposed to a distributive system.

A convenient way to meet the prescribed conditions in a microwave waveguide system is shown in Fig. 2. In this structure, the adjustable center conductors of two dc isolated coax lines meet in the center of a rectangular waveguide to form a small gap discharge region. If the gap spacing is small compared to the discharge post diameter, a uniform field assumption in the gap region is a good approximation. The coax lines are dc isolated by mica washers, while a vacuum seal is maintained by O rings positioned as shown.

The basic structure of Fig. 2 has been used for both a frequency multiplier and a frequency mixer. With some modification it might also be useful in a microwave discharge, parametric amplifier system.

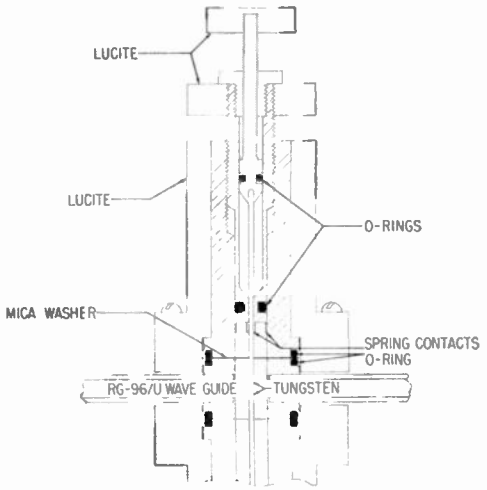

Fig. 2—Cross-sectional view of microwave gas discharge structure.

V. Frequency Multiplication

Any nonlinear element capable of being driven at high power levels with microwave frequencies of the order of 10 to 70 kMc is of considerable interest for the possible production of low millimeter and submillimeter wave signals; therefore, the first application of the preceding analysis will be made to a microwave frequency multiplier.

To evaluate the harmonic power output of the microwave discharge system shown in Fig. 2, the current I flowing in the discharge posts due to the motion of the electrons in the discharge gap must be computed. This current is given by the well known expression

$$I = \frac{A}{2l}\int_{-l}^{l} qnv_a dx = \frac{A}{2l}\int_{-l}^{l} J dx, \tag{22}$$

where A is the area of the discharge plates.

Substituting for J from (20) and performing the integration over x, the current is found to be

$$I \simeq \frac{2n_0 q^2 AE}{\pi m\nu_c} \left\{ |2\beta + \cos\omega t| + \frac{\pi q\alpha a_0 E}{m\omega\nu_c} \sum_{s=2}^{\infty} A_s \sin(s\omega t) \right\}. \tag{23}$$

The factor 2 multiplying β has been added in the dc term in an attempt to account for the positive ion current. At microwave frequencies this positive ion current is negligible.

From (23) it is seen that the various current amplitudes are

$$I_0 \simeq \frac{4n_0 q^2 AE_0}{\pi m\nu_c}, \tag{24}$$

$$I_1 \simeq \frac{2n_0 q^2 AE}{\pi m\nu_c}, \tag{25}$$

The block diagram of Fig. 6 shows the experimental set-up. Here the first slotted line is used to insure that the tuned impedance of the discharge is at least close to an impedance match, while the second slotted line is used to measure the real part of the input impedance of the discharge, R_1, as introduced in (28).

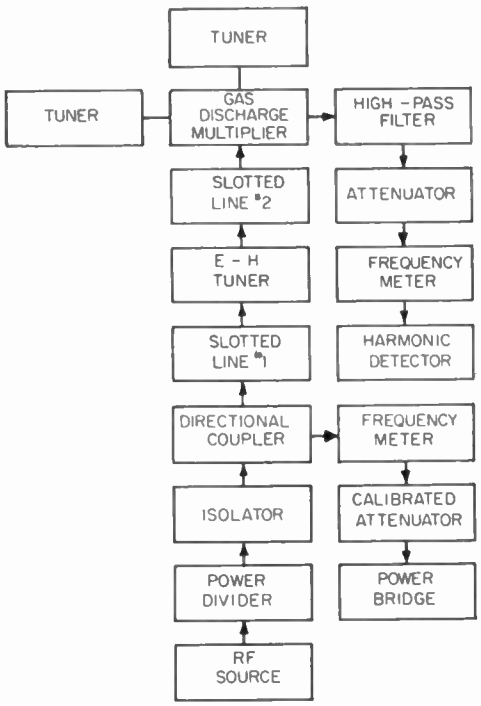

Fig. 6—Block diagram of experimental set-up.

To experimentally observe this variation of harmonic power with bias voltage, a 60-cycle sweep voltage is connected directly to the two discharge posts and to the horizontal input of an oscilloscope so that the horizontal deflection of the oscilloscope trace is proportional to the bias voltage. The vertical input of the oscilloscope is fed by the output of a crystal detector used to monitor a selected harmonic power. Hence the vertical deflection of the oscilloscope trace is proportional to the harmonic power P_n. The oscilloscope traces in the top half of Figs. 3–5 show the results of this measurement made on a microwave discharge multiplier driven by an X-band signal. The input power level was in the range 20 to 40 watts CW at a frequency of 9 kMc.

Similar experiments were done using 25 watts of CW power at 35 kMc with almost identical curves being obtained for the second, third, and fourth harmonic power.

Both theory and experiment show that all even harmonic powers are zero at zero bias voltage ($\beta = 0$), while all odd harmonic powers are maximum. This assumes that both discharge posts are identical in size. If the two posts are not identical, electron diffusion to one post will exceed that to the other resulting in an "effective dc bias voltage" thereby permitting some even harmonic power to appear. It is believed that the results of Uenohara[4] on an S-band multiplier of similar geometry can be explained on the basis of this discharge post geometry effect since the two posts in his experiment were of different sizes.

VII. Absolute Value of Harmonic Power

To further investigate the harmonic power conversion ratio given in (31), the resistance ratio (R_n/R_1) and electron ratio (N_R/N_T) must be computed and/or measured.

It can be seen from (13) that the value of the ionization frequency averaged over an RF cycle can be related to (N_R/N_T) as follows:

$$\langle \nu_i \rangle = \frac{1}{2\pi}\int_0^{2\pi} \nu_i d\theta = \frac{q\alpha a_0 E}{2m\nu_c} = \frac{\omega}{2\pi}\left(\frac{N_R}{N_T}\right). \tag{32}$$

The value of $<\nu_i>$ can also be expressed as

$$\langle \nu_i \rangle = \zeta D E_m^2, \tag{33}$$

where ζ is the ac ionization coefficient,[5] D the diffusion constant, and E_m is the amplitude of the ac electric field. Thus if ζ is known for the gas used, the ratio (N_R/N_T) could be computed. Unfortunately, detailed data of this type is scarce, so it is desirable to look for another method of estimating the electron ratio.

Experimentally, N_T can be measured by applying a dc voltage $V_0 = 2lE_0$ to the discharge posts and observing the dc current given by (24). Combining (24) and (30), it is seen that

$$N_T = \frac{2ml^2\nu_c}{q^2}\left(\frac{I_0}{V_0}\right), \tag{34}$$

where all quantities on the right side of (34) are now known or measured.

Of the total power P dissipated in the microwave discharge, a certain amount (aP) will go into creating ionization. Thus, if ω is the RF angular frequency and V_i the average ionization potential for the gas, then the total number of electrons N_R produced during one RF cycle is given by

$$N_R = \frac{2\pi a P}{\omega V_i}. \tag{35}$$

As a typical example in using the above technique for determining the ratio of N_R/N_T, consider the 35 kMc gas discharge structure previously given in Fig. 2, wherein air is used for the gas. The gap spacing $2l$ in this structure is 0.010 inch, and the post diameter 0.025 inch, resulting in a gas volume of 8×10^{-5} cm^3. The input CW power P used was 25 watts; hence the power density was 300 kw/cm^3. The gas pressure was

[4] M. Uenohara, "A new high-power frequency multiplier," PROC. IRE, vol. 45, pp. 1419–1420; October, 1957.
[5] S. C. Brown, "Basic Data of Plasma Physics," John Wiley and Sons, Inc., New York, N. Y., 1959.

TABLE I

HARMONIC OUTPUT FROM 8.6-MM FREQUENCY MULTIPLIER

Harmonic Number s	β_{max}	$A_s^2(\beta_{max})$	R_1/Z_0	R_s/Z_0	N_R/N_T	Power Input (watts)	Theoretical Power (watts)	Measured Power (watts)
2	0.75	7.8×10^{-3}	0.25	0.5	0.2	25	15.5×10^{-3}	15×10^{-3}
3	0	0.57×10^{-3}	0.25	0.5	0.2	25	1.14×10^{-3}	1×10^{-3}
4	0.4	16×10^{-6}	0.25	0.5	0.2	25	32×10^{-6}	24×10^{-6}

TABLE II

HARMONIC OUTPUT FROM 3-CM FREQUENCY MULTIPLIER

Harmonic Number s	β_{max}	$A_s^2(\beta_{max})$	R_1/Z_0	R_s/Z_0	N_R/N_T	Power Input (watts)	Theoretical Power (watts)	Measured Power (watts)
2	0.75	7.8×10^{-3}	0.03	0.5	0.25	40	0.330	0.1
3	0	0.57×10^{-3}	0.03	0.5	0.25	40	24×10^{-3}	40×10^{-3}
4	0.4	16×10^{-6}	0.03	0.5	0.25	40	0.67×10^{-3}	1×10^{-3}
5	0	3.6×10^{-6}	0.03	0.5	0.25	40	0.15×10^{-3}	0.3×10^{-3}
6	0.25	0.58×10^{-6}	0.03	0.5	0.25	40	24×10^{-6}	—
7	0	0.196×10^{-6}	0.03	0.5	0.25	40	8.2×10^{-6}	—

adjusted to approximately 44 mm Hg so that the collision frequency ν_c was approximately equal to ω. The field strength was in the range 1 to 3 kv/cm. For these conditions, it is estimated[6] that the fraction a is of the order of $\frac{1}{3}$. Finally assuming an average ionization potential V_i for air of 14 electron volts, we compute the value of N_R to be 1.1×10^8. The measured value of N_T obtained from (34) was determined to be 5×10^8, giving the approximate ratio of N_R/N_T the value 0.2.

The radiation resistance R_r of a uniform filament of current of length c across the center of a rectangular waveguide of dimensions a and b has the value[7]

$$R_r = \frac{c^2}{ab} Z_0 \tag{36}$$

where Z_0 is the characteristic impedance of the guide. In the structure considered in this paper, the harmonic current on the discharge posts is not uniform but has a sinusoidal distribution. If the electrical length of the current filament exceeds 180°, as it will for high harmonics, destructive interference will result so that in general the effective length of posts is about equal to λ_s, the harmonic free-space wavelength. This nonuniform sinusoidal current distribution will reduce the value of R_r by a factor of two; hence the value of R_s appearing in (27) will be taken to be

$$R_s \simeq \frac{\lambda_s^2}{2ab} Z_0. \tag{37}$$

Using the above technique, Tables I and II for an 8.6-mm and a 3-cm frequency multiplier were compiled. The agreement between theoretically computed and experimentally measured harmonic power is considered satisfactory.

The R_1/Z_0 ratios tabulated in Tables I and II are determined from slotted line measurements taken directly at the input to the discharge device. The tuned VSWR is more commonly of the order of 2. It might be assumed that an impedance match would be desirable. However, this is not true if a stable discharge is to be maintained. Suppose an impedance match did exist. Next, suppose a slight reduction in average electron density occurs. This density reduction would necessarily cause a change in the RF impedance of the discharge and hence change the impedance match. This in turn would cause a power reflection with less power dissipated in the plasma, which would mean a further reduction in electron density and so on until the discharge disappears. Thus to sustain a discharge by microwave energy alone, some mismatch must occur, such that a reduction in plasma density improves the VSWR.

Most of the experiments performed with the multiplier used air as the gas. However, nitrogen, neon, argon, helium, xenon, and carbon dioxide were also used. As might be expected, a discharge in nitrogen was found to have almost the same behavior as a discharge in air. For other gases the input power level could not be maintained at the same value as that for air without the discharge expanding out of the gap region and into the waveguide. Hence for these cases the ratio N_R/N_T was less than that associated with air. However, when an external dc magnetic field was applied along the axis of the discharge posts to retard transverse diffusion of the plasma, the power conversion efficiency was improved to the point where argon, for example, could be made to yield superior results to air. Also, each different gas had to be used at the pressure necessary to make the collision frequency approximately equal to the drive frequency ω.

[6] S. C. Brown and W. P. Allis, "Basic Data of Electrical Discharges," Mass. Inst. Tech., Cambridge, Tech. Rept. No. 283, pp. 172–173; June 1958.

[7] J. C. Slater, "Microwave Transmission," McGraw-Hill Book Co., Inc., New York, N. Y., p. 288; 1942.

VIII. Frequency Mixing

The preceding analysis can readily be extended to include the process of frequency mixing by including a second field in (2).

Let the new applied electric field be of the form

$$E_T = E_0 + E_1\left[\cos \omega_1 t - \frac{\omega_1}{\nu_c} \sin \omega_1 t\right] + E_2\left[\cos \omega_2 t - \frac{\omega_2}{\nu_c} \sin \omega_2 t\right], \tag{38}$$

where $E_2 \ll E_1$, so that the discharge is maintained by means of the microwave power P_1 at angular frequency ω_1.

Corresponding to (4), the new linear solution to the momentum transfer equation for the drift velocity is

$$v_d(x, t) = \frac{q}{m\nu_c}\left[E_0 + E_1 \cos \omega_1 t + E_2 \cos \omega_2 t\right]. \tag{39}$$

Since it has been assumed that $E_2 \ll E_1$, the expression for $n(x, t)$ will essentially be the same as that determined previously in (15);

$$n(x, t) \simeq n_0\left[1 + \frac{\alpha q E_1}{m\omega_1\nu_c} \sum_{s=1}^{\infty} \frac{a_s}{s} \sin (s\omega_1 t)\right] \cdot \cos\left(\frac{\pi x}{2l}\right). \tag{40}$$

Following the same procedure used in obtaining (23), the new current I, flowing in the discharge posts, will contain sum and difference frequencies as indicated below:

$$I \simeq \frac{2n_0 q^2 A l}{\pi m \nu_c}\left\{\left[2E_0 + E_1 \cos \omega_1 t + E_2 \cos \omega_2 t\right] + \left[\frac{\pi q \alpha a_0 E_1^2}{m\omega_1\nu_c} \sum_{s=2}^{\infty} A_s \sin (s\omega_1 t)\right] + \frac{\alpha q E_1 E_2}{m\omega_1\nu_c}\left[\sum_{s=1}^{\infty} \frac{a_s}{2s}\left[\sin (s\omega_1 + \omega_2)t + \sin (s\omega_1 - \omega_2)t\right]\right]\right\}. \tag{41}$$

The current amplitude I_2 at frequency ω_2 is seen to be

$$I_2 = \frac{2n_0 q^2 A E_2}{\pi m \nu_c}. \tag{42}$$

while the current amplitude I_3 at the sum or difference freqency $\omega_3 = \omega_1 \pm \omega_2$ is

$$I_3 = \frac{n_0 \alpha q^3 A l E_1 E_2}{\pi m^2 \nu_c^2 \omega_1} a_1. \tag{43}$$

A mixer efficiency can now be defined as the ratio of the power output P_3 at frequency ω_3 to the power input P_2 at frequency ω_2; thereby we can obtain an expression similar to that given by (28).

$$\frac{P_3}{P_2} = \frac{I_3^2 \Re_3}{I_2^2 R_2} = \left(\frac{\alpha q a_1 E_1}{2m\omega_1\nu_c}\right)^2\left(\frac{\Re_3}{R_2}\right) = \left(\frac{\Re_3}{R_2}\right)\left(\frac{N_R}{N_T}\right)^2\left(\frac{a_1}{2\pi a_0}\right)^2; \tag{44}$$

In this ratio, $\Re_3$ is the interaction resistance at frequency ω_3, while R_2 is the resistance associated with frequency ω_2.

If $\omega_1 \simeq \omega_2$ and $\omega_3 = \omega_1 + \omega_2 \simeq 2\omega_1$, then $R_2 \simeq R_1$ and $\Re_3$ will be approximately equal to the interaction resistance of the second harmonic frequency considered in the frequency multiplier. In (21), for the case $s = 2$, a_1 will contribute the most to the value of A_2, so that

$$A_2 \simeq \frac{a_1}{2\pi a_0}. \tag{45}$$

Hence, for these conditions, the mixer conversion efficiency should be approximately the same as the second harmonic conversion efficiency. Also, the variation of P_3 with β should be similar to the variation of the second harmonic power. A comparison of the curves given in Figs. 3 and 7 shows this to be true.

To investigate experimentally the mixing properties of the plasma, the parallel-plate discharge-gap geometry was built into the crossed X-band structure shown in Fig. 8. This arrangement permits the introduction of: a 20-watt CW 9-kMc signal through one waveguide port; a sliding short tuning element in a second waveguide to adjust for maximum electron density modulation; a third waveguide containing a filter to block the 9-kMc signal but pass a 0.1-watt, 1-kc square wave modulated, 11-kMc mixing signal; and finally, a fourth waveguide which tapers down from the X-band waveguide to an RG 53/U K-band waveguide to pass the 20-kMc sum frequency. A 20-kMc band-pass filter was also included in the RG 53/U waveguide section to reject the 18-kMc, second harmonic of the 9-kMc drive frequency. This filter arrangement, plus the square wave modulation of the 11-kMc mixing frequency, makes certain that other frequencies in the system are not mistaken for the desired 20-kMc sum frequency.

The power P_3 as a function of β or bias voltage was observed by again applying a 60-cps sweep voltage to the discharge posts and to the horizontal input of an oscilloscope. The crystal detected, 20-kMc output power was fed to the vertical input of the oscilloscope to obtain the oscilloscope trace shown in the top of Fig. 7. The base line in this picture is caused by the square wave modulation of the 11-kMc signal which is not synchronized with the 60-cps sweep voltage.

A measurement of the 20-kMc sum frequency power

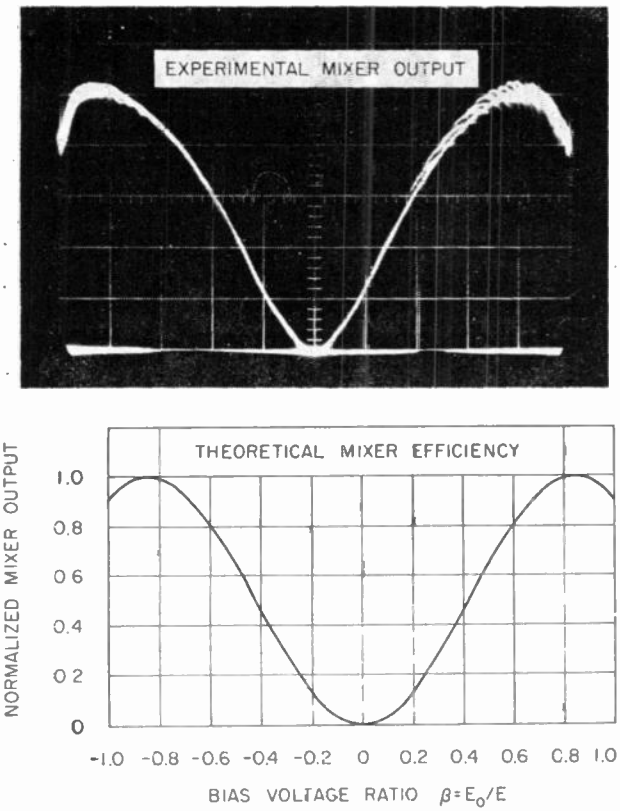

Fig. 7—Mixer output vs bias voltage.

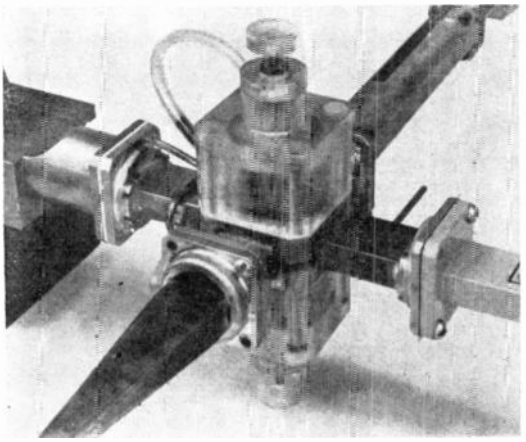

Fig. 8—Gas discharge structure.

yielded a signal 28 db down from the 100-mw 11-kMc power. This conversion ratio to the sum frequency compares favorably to the value one could obtain with a crystal diode operating at the same frequencies. It is believed that if a different structural arrangement were made to observe the difference frequency rather than the sum frequency, this conversion loss could be substantially reduced especially if the difference frequency was placed at 60 Mc where $\mathcal{R}_3$ in (44) could be made quite large.

IX. Parametric Amplification

Modulation of the electron density at a microwave frequency implies that the discharge has time-varying properties which may be exploited in a parametric amplifier. It was seen in Section VIII on frequency mixing that the application of the low level, complex field

$$e_2 = E_2\left(1 + j\frac{\omega_2}{\nu_c}\right)\epsilon^{j\omega_2 t} \tag{46}$$

along with the high level pump field e_1 gave rise to a complex current,

$$i_3 = -jI_3\epsilon^{j\omega_3 t} = -j\frac{q^2N_R}{2lm\nu_c}\left(\frac{a_1}{2\pi a_0}\right)E_2\epsilon^{j\omega_3 t} \tag{47}$$

at the difference frequency $\omega_3 = \omega_1 - \omega_2$.

If the power P_3 radiated by the current i_3 is reflected back into the discharge, it will in turn produce an e_3 field to mix with the pump field e_1. This power relationship can be expressed as

$$P_3 = \tfrac{1}{2}\left|\, i_3\right|^2\mathcal{R}_3 = \tfrac{1}{2}\left|\, 2le_3\right|^2/R_3, \tag{48}$$

where $\mathcal{R}_3$ is the radiation resistance associated with the current i_3, while R_3 is the real part of the discharge impedance at frequency ω_3.

Eq. (48) will determine the magnitude of the field e_3, but not its phase. However, it will be assumed that the fields at ω_3 were reflected to make e_3 have the following complex form:

$$e_3 = E_3\left(1 + j\frac{\omega_3}{\nu_c}\right)\epsilon^{j\omega_3 t}. \tag{49}$$

This field e_3 will now combine with the pump field e_1 to produce a current Δi_2 at the signal frequency ω_2;

$$\Delta i_2 = -j\frac{q^2N_R}{2lm\nu_c}\left(\frac{a_1}{2\pi a_0}\right)E_3\epsilon^{j\omega_2 t}. \tag{50}$$

The original current i_2 produced by the field e_2 was given by (42). In complex form the expression is

$$i_2 = \frac{q^2N_T}{2lm\nu_c}E_2\epsilon^{j\omega_2 t}. \tag{51}$$

Since the discharge is a lossy element, further effects of Δi_2 will be neglected. Hence the power P_2 at the signal frequency is seen to be

$$P_2 \simeq \tfrac{1}{2}\,\mathrm{Re}\,(i_2 + \Delta i_2)(2le_2)^*$$
$$= \frac{q^2N_TE_2^2}{2m\nu_c}\left[1 - \frac{\omega_2}{\nu_c}\left(\frac{N_R}{N_T}\right)\left(\frac{E_3}{E_2}\right)\left(\frac{a_1}{2\pi a_0}\right)\right]. \tag{52}$$

The choice of the phase of e_3 in (49) is now apparent since it leads to the desired negative power term in (52). The first term in (52) is the power dissipated in the discharge at frequency ω_2.

In order to have gain in the device,

$$G = \frac{\omega_2}{\nu_c}\left(\frac{N_R}{N_T}\right)\left(\frac{E_3}{E_2}\right)\left(\frac{a_1}{2\pi a_0}\right) \tag{53}$$

must be greater than unity. This expression contains the unknown field ratio E_3/E_2.

To evaluate E_3/E_2, first note that the power dissipated in the discharge at frequency ω_2 can also be written as

$$\frac{q^2 N_T E_2^2}{2m\nu_c} = \frac{|\,2Ie_2\,|^2}{2R_2}, \tag{54}$$

where R_2 is the real part of the discharge impedance at ω_2.

Solving (54) for R_2, the result is

$$R_2 = \frac{4l^2 m\nu_c}{q^2 N_T}\left[1 + \left(\frac{\omega_2}{\nu_c}\right)^2\right]. \tag{55}$$

From (48), it can be shown that

$$\frac{E_3}{E_2} = \frac{q^2 N_R}{4l^2 m\nu_c}\left(\frac{a_1}{2\pi a_0}\right)\left[\frac{\Re_3 R_3}{1 + \left(\frac{\omega_3}{\nu_c}\right)^2}\right]^{1/2}. \tag{56}$$

Finally, the gain G expression becomes, with the use of R_2 from (55),

$$G = \frac{\omega_2}{\nu_c}\left(\frac{N_R}{N_T}\right)^2\left(\frac{a_1}{2\pi a_0}\right)^2\left(\frac{\Re_3 R_3}{R_2^2}\right)^{1/2} \cdot \frac{\left[1 + \left(\frac{\omega_2}{\nu_c}\right)^2\right]}{\left[1 + \left(\frac{\omega_3}{\nu_c}\right)^2\right]^{1/2}}. \tag{57}$$

This equation shows that it would be desirable to make the signal frequency ω_2 considerably greater than the collision frequency ν_c, indicating that the gas pressure should be reduced in order to make the discharge extremely reactive. This is analogous to the high Q or high "cutoff" frequency requirements for crystal diodes used as parametric amplifiers.

An important problem in the design of a possible gas discharge parametric amplifier would be achieving the desirable impedance levels to maximize the resistance ratio term in (57) while at the same time maintaining impedance matches in the microwave circuits.

Assuming that a parametric amplifier would operate in the manner described, it may have two interesting features: 1) the saturated power output could be high, perhaps the order of one watt and 2) the gain could be controlled by changing the bias voltage.

X. Conclusions

It is concluded that the nonlinear behavior of a microwave discharge located between two closely spaced parallel plates whose dimensions are small compared to the wavelength can be accurately analyzed using the assumption that the ionization frequency ν_i is proportional to the absolute value of the drift velocity v_d.

Using straightforward Fourier expansions for ν_i and the electron density $n(x, t)$, the momentum transfer and continuity equations can be solved readily for the current $J(x, t)$ response to applied microwave fields.

The discharge geometry and analysis has a somewhat universal aspect in that it can be applied with little change in form to frequency multipliers, frequency mixers, and parametric amplifiers.

Experimentally, CW power densities of the order of 0.3 Mw/cm^3 were obtained using 25 watts of 35-kMc power. Modulation of the electron density the order of 5 per cent at 70 kMc (twice the drive frequency) was believed to have been achieved.

The microwave gas discharge, with its relatively large CW and pulsed power capabilities, combined with its predictable performance at high harmonics, make it an attractive element for further study in the low millimeter wave region.

A Plasma Microwave Energy Detector*

R. L. TAYLOR† AND S. B. HERSKOVITZ†, MEMBER, IRE

Summary—**A detector of microwave energy employing a gaseous discharge is described. The principle of operation is based upon the temperature sensitivity of the electron-ion recombination rate. By photomultiplier observations of the decaying plasma afterglow, short pulses of microwave energy can be detected. At present, the minimum discernible signal strength is about one microwatt peak.**

The theory, experimental configuration, and prospects for improved sensitivity are discussed.

LARGELY overshadowed by space age and controlled fusion programs are the efforts of numerous researchers into the more prosaic area of electronic applications of the plasma state of matter. One such activity deals with the use of a gaseous discharge as the detection element in radar receivers.

The ability to detect minute amounts of microwave energy is the prime function of a radar system. To perform this task, a typical radar receiver employs an extremely sensitive semiconducting crystal rectifier as its sensing element. This very sensitivity, however, places a burden upon the user in the form of protecting the crystal rectifier from accidental exposure to incident energies of more than a few ergs. This exposure must be guarded against, not only when the rectifier is actually in operation in a radar receiver, but even while the element is being stored or transported.

For several years, various groups of investigators have explored the use of an ionized gas as a detector element to provide a means of minimizing this problem.[1–5] In this application an ionized gas possesses several noteworthy properties: namely, the element does not act as a detector until activated, and second, it can be exposed to megawatts of energy without permanent damage. These advantages, however, are not gained without a corresponding sacrifice in sensitivity.

Detectors which use ionized gases have usually been based upon changes in electrical conductivity. The detector to be described, however, is quite different from its predecessors in that it makes use of changes in the light output of a decaying plasma.

Light from a Decaying Plasma

The mechanisms involved with the emission of light from a gas during ionization and subsequent afterglow are numerous and form the subject of several phases of physics, *e.g.*, emission spectroscopy, quantum mechanics, metastable determination, etc. Of fundamental interest to the present discussion, however, is the alteration of the total light emitted from a gaseous afterglow, or decaying plasma, with the addition of microwave energy to the system.

In 1928, Kenty observed a quenching of certain spectral lines in an emission spectrum with the addition of dc energy.[6] That the light output of a gaseous afterglow could similarly be altered by microwave energy was first demonstrated and is being extensively investigated by the Goldstein group[7,8] at the University of Illinois.

If a gas is ionized by a pulse of electrical energy, a typical afterglow is observed upon removal of the pulse. The characteristic light output of a pure noble gas shows several interesting features. (See Fig. 1.) Initially, at time zero (the moment of removal of the ionizing pulse), an extremely high level of light output is observed which rapidly decreases to a minimum in perhaps 40 microseconds (μsec). The abscissa represents volts output of

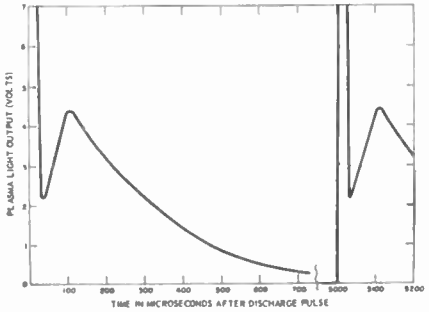

Fig. 1—Light output from pulsed plasma.

* Received by the IRE, August 28, 1961.

† Air Force Cambridge Research Laboratories, Office of Aerospace Research, Electronics Research Dir., Laurence G. Hanscom Field, Bedford, Mass.

[1] D. H. White, "Microwave Detection with Gas Tubes," Fed. Telecommun. Labs., Nutley, N. J., Contract DA-36-039-SC-15512, Final Rept.; 1953.

[2] H. Farber, "Study of Microwave Detection in Gaseous Discharge Tubes," Polytech. Inst. Brooklyn, N. Y., Contract DA-36-039-SC-5670, Final Rept.; 1955.

[3] L. Gould, "Microwave Detection by a dc Gaseous Discharge," Signal Corps Engrg. Labs., Belmar, N. J., Tech. Memo No. M-1836; October, 1956.

[4] M. Mentzoni, "The Detection of Microwaves by Glow Discharges," Polytechnic Institute of Brooklyn, Brooklyn, N. Y., Contract AF 30(602)-1448; 1957.

[5] H. Farber and M. Mentzoni, "The Long Rise Times Associated with Gaseous Detection of Microwaves," Polytechnic Institute of Brooklyn, Brooklyn, N. Y., Contract AF 19(604)-4143; February, 1959.

[6] C. Kenty, "The Recombination of argon ions and electrons," *Phys. Rev.*, vol. 32, pp. 624–635; October, 1928.

[7] J. M. Anderson and L. Goldstein, "Interaction of Microwaves in Gaseous Discharge Plasmas," University of Illinois, Urbana, Contract AF 19(604)-524, Tech. Rept. No. 7; 1955.

[8] A. A. Dougal and L. Goldstein, "Energy between electrons and ion gases through coulomb collisions in plasmas," *Phys. Rev.*, vol. 109, pp. 615–624; February, 1958.

a photomultiplier viewing the total light output, and the ordinate time, in μsec. The next feature of note is a secondary build-up of light output to a maximum value at about 100 to 120 μsec. A monotonic decay of light which will be referred to as the afterglow period is then traced out. At the right, the initiation of another pulse and afterglow period occurs.

The initial intense light output is a result of energy loss by the many excited atoms. As electrons now rapidly lose energy through inelastic collision processes, fewer excited atoms are created and the light output falls. A condition is finally reached such that the electron temperature and density are appropriate for optimum electron-ion recombination. A second light output maximum is then observed. It is at this point, the inception of the characteristic afterglow, that the plasma performs as a microwave detector.

The effect of impinging microwave energy, such as a radar echo, on the afterglow luminosity is now considered. At sufficiently high frequencies, such as those commonly employed in radar systems, only the electrons, by virtue of their minute mass, are greatly affected by the alternating electric field of the radar echo. Thus incident electromagnetic energy acts almost exclusively as an energy source for the electrons in the gas. Fig. 2 represents this situation diagrammatically. The incident electromagnetic signal, represented by a circle at the center, supplies energy almost exclusively to the electrons of the plasma system. The electrons, in turn, through collisional processes, impart this energy to the ions, neutral species, and container walls.

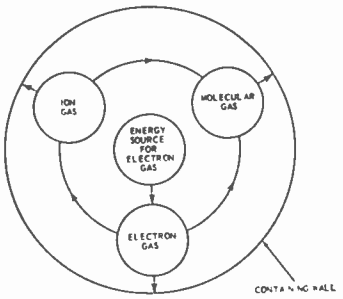

Fig. 2—Energy distribution processes.

To postulate a simple working picture of the light-producing mechanisms germane to the detection application, the assumption is made that electron-ion recombination is the principal source of visible light emitted from the decaying discharge. This assumption ignores certain other conceivable emitting processes such as metastable decays, wall fluorescence, multibody collisions, etc. These omissions, however, do not materially alter the detection mechanism.

Despite this simplifying assumption, the electron-ion recombination phenomenon is unfortunately still beclouded by additional complexities. The recombination process may take numerous forms.[9] Certain of these are light producers; others are not. Since methods of independently determining the coefficients of various electron-ion recombination processes are rather fragmentary, the following discussion will deal with the "bulk" coefficient. This recombination coefficient, which is ordinarily measured, will be understood to be representative of the various independent light-producing mechanisms.

Many measurements of electron-ion recombination have been made.[10] The inconsistency of data from investigator to investigator leaves much to be desired. Notwithstanding the spread of experimental data, it can be stated that the recombination coefficient is a decreasing function of temperature. Representative of these values is the data of Chen, *et al.*, yielding an experimental temperature dependence of $T_e^{-3/2}$ for electron-ion recombination coefficient over a pressure range of 7–29 mm Hg in pure helium.[11] Thus, as electrons are heated, the recombination coefficient decreases. From assumptions above, this decrease also results in a lowering of the afterglow light output. This quenching of the afterglow forms the basis of the described detector.

Enhancement of Afterglow Quenching

To optimize the performance of a microwave energy detector based upon quenching of the afterglow, two general criteria must be considered: 1) the detector must be in a condition to efficiently convert incident energy, *e.g.*, a radar echo, into afterglow light quenching and 2) the incident signal must be delivered efficiently to the detector.

For optimum performance as a detector, loss of electrons by means other than recombination must be minimized. Diffusion losses can be suppressed by operation at higher gas pressures, the use of magnetic fields, and appropriate container geometry. Electron losses by attachment are eliminated by the use of noble or other gases with unfavorable attachment rates.

The remaining electron loss process, recombination, may be controlled, within bounds, to optimize the detector for specific application. The recombination rate, as previously mentioned, is a decreasing function of temperature. The rate of cooling of electrons can be affected by four parameters:

1) number density of neutral atoms (pressure),
2) collision probability,
3) mass of the neutral atom,
4) metastable atom concentration.

For a given electron density and incident signal, electrons with lower temperatures, hence greater recombination rate, will yield a greater quench in afterglow.

[9] L. B. Loeb, "Basic Processes of Gaseous Electronics," University of California Press, Berkeley, pp. 477–594; 1955.
[10] *Ibid.*, pp. 560–562.
[11] C. L. Chen, C. C. Leiby and L. Goldstein, "Electron temperature dependence of the recombination coefficient in pure helium," *Phys. Rev.*, vol. 121, pp. 1391–1400; March, 1961.

Rapid cooling of electrons can be achieved by using higher pressures of parent atoms with large collision cross sections and small atomic masses. Destruction of metastable states by the use of Penning mixtures[12] also accelerates cooling. Under these conditions, a high-sensitivity short-duration afterglow would be produced.

To extend the afterglow period, and hence increase the range of detection between pulses, it is desirable to cool the plasma electrons more slowly. This action is accompanied by a decrease in optimum sensitivity. In the particular experiments described, in order to prolong the interpulse period, electrons were cooled at a slower rate than that which would have yielded maximum sensitivity.

Techniques for insuring the efficient delivery of the incident signal to the detector are based upon common microwave techniques and physical electronics principles. Microwave techniques include such obvious expedients as maintaining low-loss transmission lines and power-multiplication approaches. Further techniques for enhancing the increase of electron energy due to an incident signal by cyclotron resonance will also enhance the detection abilities.[13,14]

Consideration of the above requirements, to a large extent, dictates the choice of parent gas and experimental configuration. Practical considerations, however, somewhat modify this idealized picture, and necessitate compromise.

Experimental Configuration

From the foregoing criteria, the general experimental configuration may be surmised. The choice of a rare gas as the parent medium is evident. For a compromise between maximum sensitivity and duration of afterglow, neon, with its moderate mass, low probability of collisions, and ease of ionization, was chosen as the parent gas. The gas is contained in a simple discharge tube, the diameter of the glass envelope being chosen so as to be as large as possible—for diffusion considerations—without imposing serious microwave mismatch problems.

The gas bottle is inserted into an *S*-band waveguide line. The plasma is established by a pulse of dc power, typically 1000 volts, and the light output monitored by a gated photomultiplier. A pulse of *S*-band energy is then introduced into the waveguide system to serve as a simulated radar echo. This simulated echo is monitored by use of a crystal probe in a slotted line. The entire system is synchronized by a master trigger generator and the output displayed on an oscilloscope. To permit variation of the gas fill, the detector tube is attached to a vacuum and gas back-fill system. Fig. 3 represents the experimental situation diagrammatically.

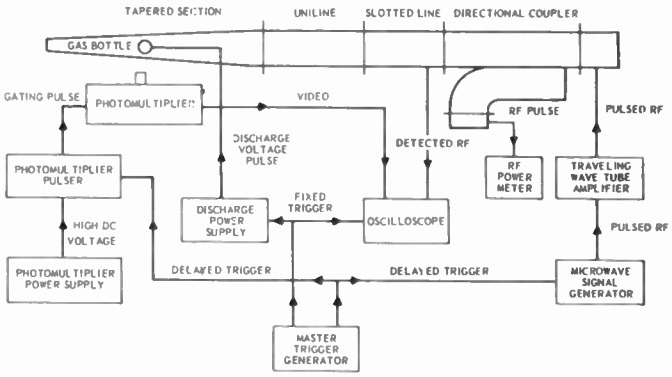

Fig. 3—Block diagram of plasma microwave detector.

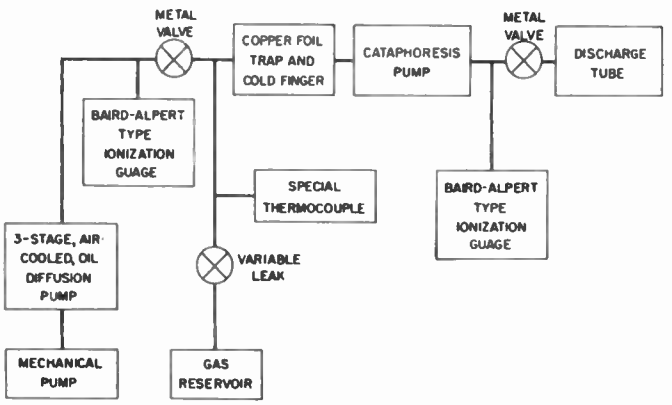

Fig. 4—Block diagram of vacuum system.

The vacuum and gas back-fill system (see Fig. 4) is of conventional design, employing a three-stage oil diffusion pump capable of attaining vacua of 10^{-7} mm Hg. Of special interest is the use of a cataphoresis pump[15] in the form of a glass helix consisting of about 72 inches of $\frac{1}{2}$-inch outside-diameter tubing wound into 7 loops. This pump allows noble gases to be ultrapurified. A special wide-range thermocouple[16] is employed to measure gas pressures without the possibility of contamination from manometric fluids.

The plasma detector itself consists of a simple discharge tube $\frac{3}{4}$-inch outside diameter, with tungsten rod electrodes spaced about 12 inches apart. The detector is placed diagonally through the *H*-plane of a 2:1 tapered

[12] A mixture of gases in which the ionization potential of one constituent is below the metastable potential of the other. Thus, the metastable level is continuously destroyed by collisions between the two species.

[13] J. E. Etter and L. Goldstein, "Guided Wave Propagation in Gyromagnetic Gaseous Discharge Plasmas," University of Illinois, Urbana, Contract AF 19(604)-524, Tech. Rept. No. 3; 1954.

[14] L. P. McGrath, A. D. Chatterjee and J. P. Monier, "Further Studies of Resonance Phenomena at Microwave Frequencies in Gyromagnetic Gaseous Discharge Plasmas," University of Illinois, Urbana, Contract AF 19(604)-2152, Sci. Rept. No. 2; 1957.

[15] R. Riez and G. H. Dieke, "The analysis and purification of rare gases by means of electric discharges," *J. Appl. Phys.*, vol. 25, pp. 196–201; February, 1954.

[16] Consolidated Vacuum Corp. Autovac Vacuum Gauge Type LKB-3294. Ranges from 1 micron to 100 mm Hg.

section (see Fig. 5). In this configuration, the detector tube essentially fills the cross section of the microwave line. During detection the afterglow electron densities as measured by standard cavity techniques[17–19] are in the range of 1×10^{10} to 4×10^{10} electrons per cubic centimeter.

The most satisfactory performance of the plasma detector in respect to minimum detectable signal resulted from the use of pure neon gas in the pressure range of from 2 to 10 mm Hg.

In Fig. 6 the typical detection phenomenon is represented. The upper trace represents a 150-μsec portion of the light output from the decaying plasma contained within the gas tube. The photomultiplier is gated so as to protect it from the extremely high light output typical at the inception of the plasma (see Fig. 1), and thus prevents fatiguing of the photocathode. Light output is displayed as amplitude in arbitrary units on the vertical axis and time (50 μsec per major division) on the horizontal. In the lower curve, the quenching of light output due to a 5-μsec, 20-mw peak pulse at 3000 Mc is displayed.

Caution must be used in assigning a sensitivity figure to the plasma microwave detector. In semiconductor crystal detector nomenclature, sensitivity deals with a voltage output resulting from a given power input. The crystal is generally used to detect, rectify, and mix the incoming signal with the output of a local oscillator. The resultant IF frequency is then amplified, rectified, and reamplified before being measured. The plasma detector is not analogous to a crystal in this function. A crystal, however, can also be used directly to rectify microwave signals, the output being fed into a video amplifier. In this function, a closer comparison to the plasma detector may be made. The plasma detector acts essentially as an energy transducer, converting incident microwave energy into an alteration of light intensity. This function is so dissimilar to the function of a crystal detector that comparison of sensitivity by semiconductor crystal nomenclature is meaningless. More useful, therefore, is the specification of a minimum detectable signal, one which will produce an alteration of the light output curve by an amount equal to twice the value of the average noise, or thickness, of the light output curve. In this context, maximum sensitivities of the plasma detector are from 1 to 5 microwatts peak power.

Fig. 7 shows the effect of various signal strengths on the amount and character of the typical afterglow quench. Here input pulses vary from one to 128 mw in

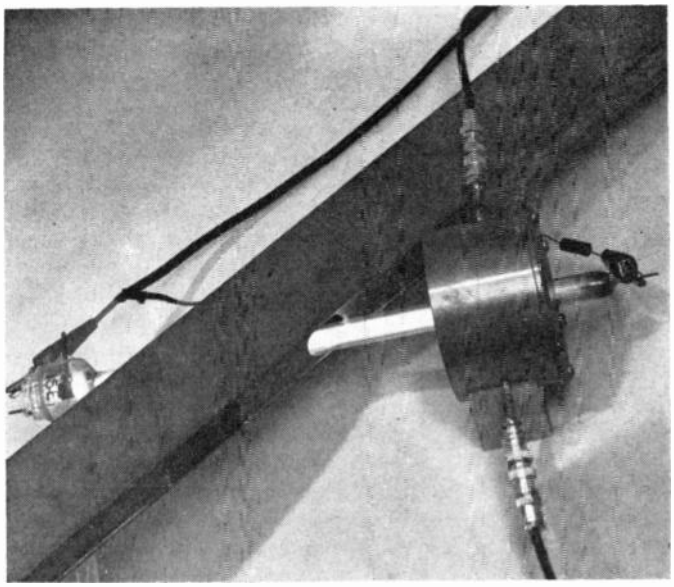

Fig. 5—Plasma microwave detector. The diode detector is inserted into the *H*-plane of a tapered waveguide section. The cylindrical cavity to the right is used to determine electron densities.

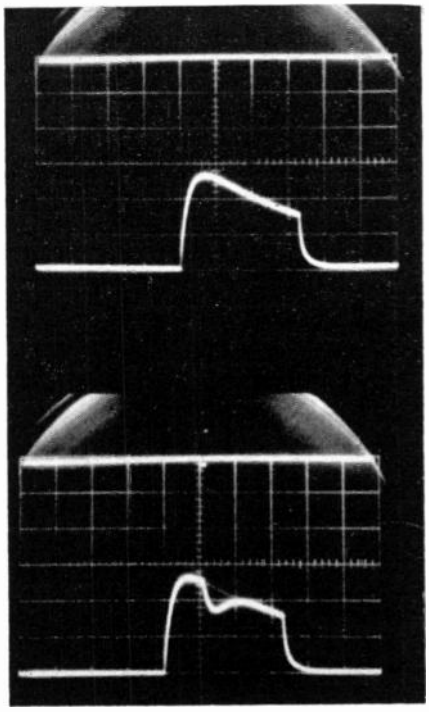

Fig. 6—Typical detection phenomenon. *Upper portion*: Afterglow of 5-μsec duration pulsed discharge (1 kv, about 0.5 amp) in neon (p = 10 mm Hg), 250 μsec after pulse. Time scale: 50 μsec per division. *Lower portion:* same discharge conditions as above. Quenching pulse is 5 μsec wide, 20 mw peak power. Photomultiplier gated RCA 6217.

[17] S. C. Brown and D. J. Rose, "Methods of measuring the properties of ionized gases at high frequencies. I—Measurements of *Q*," *J. Appl. Phys.*, vol. 23, pp. 711–718; July, 1952.

[18] S. C. Brown and D. J. Rose, "Methods of measuring the properties of ionized gases at high frequencies. II—Measurement of electric field," *J. Appl. Phys.*, vol. 23, pp. 719–722; July, 1952.

[19] D. J. Rose and S. C. Brown, "Methods of measuring the properties of ionized gases at high frequencies, III—Measurement of discharge admittance and electron density," *J. Appl. Phys.*, vol. 23, pp. 1028–1032; September, 1953.

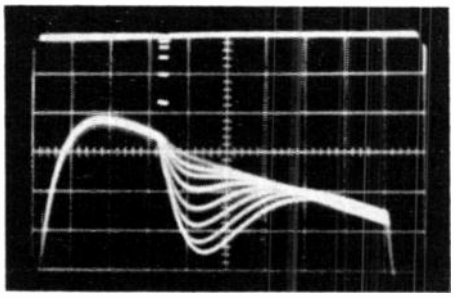

Fig. 7—Variation of quench with signal strength. Input pulses of 5-μsec duration varying from 1 to 128 mw in 3-db steps. Time scale: 20 μsec per division. Discharge conditions identical to those of Fig. 6.

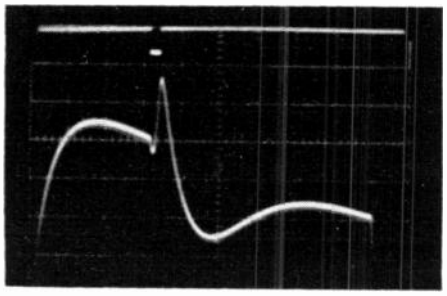

Fig. 8—Ionization due to large input signal. Input pulse of 5-μsec duration, 500-mw peak power. Time scale: 20 μsec per division. Discharge conditions identical to those of Fig. 6.

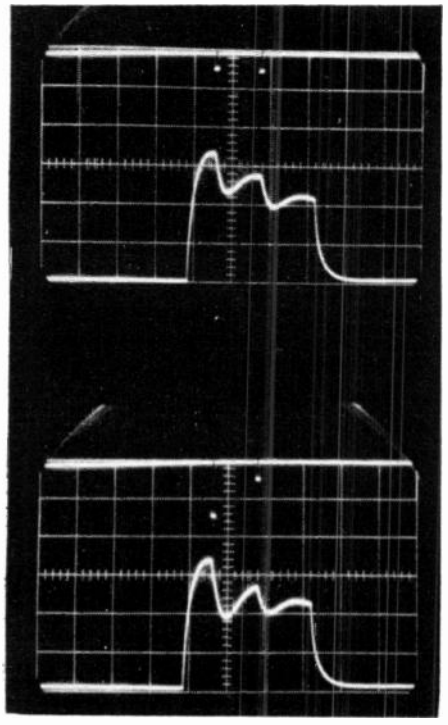

Fig. 9—Multiple pulse response. *Upper portion:* input pulses of 5-μsec duration, 20-mw peak power. *Lower portion:* input pulses of 5-μsec duration, 90 mw followed by 20-mw peak power. Discharge conditions identical to those of Fig. 6.

3-db steps. The stronger signals produce more profound alterations of the light output but also prolong the "recovery time," or interval before normal light output is resumed. Each major division on the horizontal scale represents 20 μsec.

By continuously increasing the microwave signal strength, a point is reached where energy input is sufficient to cause further ionization in a manner similar to the plasma originating pulse. Fig. 8 illustrates this effect with an input pulse of 500 mw. On the lower trace, an initial small decrease of light, followed by a building up to an increased value and subsequent decay is seen.

In Fig. 9, the effects of multiple input pulses are illustrated. In the upper portion, two pulses of 20 mw each cause similar decreases in light output. In the lower portion, an input signal of 90 mw followed by a signal of 20 mw results in quenches of different magnitude. It is readily apparent that the plasma detector is not a square law device.

A typical response curve of input power to light quenching in arbitrary units is illustrated in Fig. 10.

The plasma detector is inherently a broad-band device. The unit employed in these experiments operates over the entire usable range of *S*-band (2.84″×1.34″) waveguide. Fig. 11 depicts the frequency response of a typical 10-mm neon gas fill. Curves are plotted for

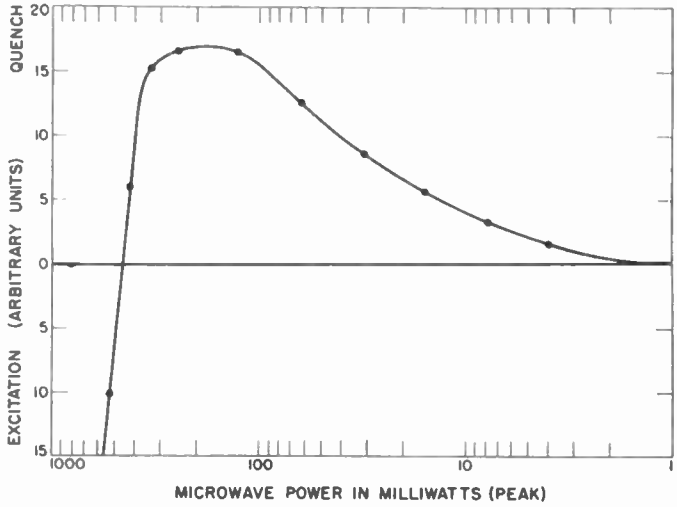

Fig. 10—Light output alteration as a function of input signal level.

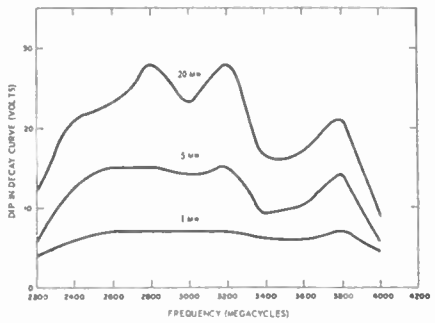

Fig. 11—Frequency response of plasma microwave detector.

three power inputs; 20, 5, and 1 mw peak. The fine structure, particularly evident in the 20-mw curve, is related to the standing wave ratio of the microwave line. At points of poorer matching (*i.e.*, at 3000 and 3400 Mc), the incident power upon the detector is diminished, with a consequent lowering of the amount of light quenching.

The Future of the Plasma Detector

The plasma microwave detector, as it exists today, does not rival the crystal rectifier as an envelope detector. A standard crystal rectifier can detect signals with strengths in the order of 10^{-8} watts. In the present state of development, the plasma detector under optimum conditions can respond to about 10^{-6} watts of incident energy. A crystal semiconductor used as a mixer can detect microwave signals as small as 10^{-13} watts. The plasma microwave detector has not been investigated for any mixing properties.

There are, however, several approaches available to improve the present minimum detectable signal level. An obvious method of increasing the plasma detector sensitivity is to employ a dc magnetic field so as to cause the plasma electrons to execute cyclotron motion. In this condition, the electrons are more efficient absorbers of microwave energy at particular microwave frequencies, and will produce more profound quenching of light output. The relationship of magnetic field to applied microwave frequency may be related simply by $B=0.357f$, where B is the magnetic field in Gauss and f is the applied microwave frequency in Mc per second. Thus, to produce maximum signal enhancement at 3000 Mc, a 1070-Gauss magnetic field would be employed. Such operation will narrow the bandwidth of the device.

Practical difficulties may prevent full utilization of the advantages expected from operation at cyclotron resonance. These difficulties concern the compromise necessary in optimum gas pressure to satisfy the conflicting requirements of minimizing pressuring broadening effects on cyclotron resonance, maintaining a stable discharge, and minimizing unwanted electron loss through diffusion. The magnetic field required for cyclotron resonance, however, yields the advantage of restraining electron diffusion.

Methods to enhance or multiply the incident microwave signal offer other sensitivity increasing techniques. The use of "squeezed" waveguide sections, resonant cavities, and similar structures effectively multiplies the incident power density upon the detector. These manipulations also narrow the bandwidth of operation.

Finally, it should be remembered that we can measure only what we can see. The present method of display, presentation, and observation leaves much to be desired as far as determining the ultimate sensitivity of this device.

Interaction of a Modulated Electron Beam with a Plasma*

G. D. BOYD†, MEMBER, IRE, R. W. GOULD‡, MEMBER, IRE, AND L. M. FIELD‖, FELLOW, IRE

Summary—**The results of a theoretical and experimental investigation of the high-frequency interaction of an electron beam with a plasma are reported. An electron beam, modulated at a microwave frequency, passes through a uniform region of a mercury arc discharge after which it is demodulated. Exponentially growing wave amplification along the electron beam was experimentally observed for the first time at a microwave frequency equal to the plasma frequency. Approximate theories of the effects of 1) plasma-electron collision frequencies, 2) plasma-electron thermal velocities and 3) finite beam diameter, are given.**

In a second experiment the interaction between a modulated electron beam and a slow electrostatic wave on a plasma column has been studied. A strong interaction occurs when the velocity of the electron beam is approximately equal to the velocity of the wave and the interaction is essentially the same as that which occurs in traveling-wave amplifiers, except that here the plasma colum replaces the usual helical slow-wave circuit. The theory predicting rates of growth is presented and compared with the experimental results.

* Received by the IRE, August 7, 1961. This work was supported by the Office of Naval Research, Contract NONR 220(13).
† Bell Telephone Labs., Inc., Murray Hill, N. J.
‡ California Inst. of Tech., Pasadena, Calif.
‖ Microwave Tube Div., Hughes Aircraft Co., Culver City, Calif.

I. Introduction

IN 1929 Tonks and Langmuir[1] reported on experiments involving electron-plasma oscillations and defined the electron-plasma oscillation frequency

$$\omega_p^2 = \frac{n_0 e^2}{m\epsilon_0} \tag{1}$$

where e is the magnitude of the electronic charge, m its mass, n_0 the density of plasma electrons per unit volume, and ϵ_0 the permittivity of free space. (MKS units are used throughout this paper.)

When the electron thermal velocities are small compared to the velocity of waves being considered, the plasma can be characterized by a dielectric constant

$$\frac{\epsilon}{\epsilon_0} = 1 - \frac{\omega_p^2}{\omega(\omega - i\nu)}. \tag{2}$$

where ω is the angular signal frequency and ν is an effective collision frequency for the plasma electrons. For the experiments described in this paper the effect of the massive positive ions may be neglected.

In 1948 Haeff[2] suggested that plasma oscillations excited by a directed beam of charged particles might be responsible for certain types of RF energy received from the sun, and he discussed the mechanism of two-stream amplification. Bohm and Gross[3] have given a more extensive discussion of the interaction of an electron beam and a thermal plasma. Complex propagation constants were found for waves whose frequency is approximately equal to the plasma frequency defined in (1). The significance of the complex propagation constant is that small disturbances are amplified as the beam drifts through the plasma. In an earlier paper Pierce[4] had noticed a similar instability when an electron beam passed through a positive ion cloud and had attempted to relate this to positive ion oscillations observed in vacuum tubes. These discoveries have stimulated a very great amount of theoretical study of instabilities in plasmas with non-Maxwellian velocity distribution. The amplification mechanism, however, is essentially that of the double-stream amplifier invented by Haeff[5] and independently by Pierce and Hebenstreit.[6] In the case of the plasma, one group of charged particles is stationary.

Several experiments have been performed in which directed electron beams are passed through the plasma region of a gas discharge. Looney and Brown's[7] early experiment is representative. A beam of high-energy electrons (several hundred volts) was injected into the plasma of a dc discharge from an auxiliary electron gun. RF signals were detected by a small wire probe placed in the beam. The probe was movable and showed the existence of standing-wave patterns of oscillatory energy. Nodes of the pattern coincided with electrodes which bound the plasma. The thickness of the ion sheaths at these electrodes determined the standing-wave pattern. The frequencies of oscillation seemed to be related to the transit time effects of the electrons between the sheaths and did not appear to verify the theory of Bohm and Gross.[3] Later Gordon[8] investigated the energy exchange mechanism which was involved and showed that the results of Looney and Brown might be understood in terms of reflex klystron oscillations due to the electron beam being reflected by the sheaths. He found that the radiation detected by the probe was due to the fields of the bunched beam and not primarily due to plasma oscillations. Wehner[9] had previously built a plasma oscillator using this klystron bunching principle.

Very recently Kofoid[10] found oscillations very similar to those of Looney and Brown when two oppositely directed electron beams were passed through the plasma. This result tends to support Gordon's conclusion.

The dispersion equation for small amplitude waves in a system consisting of a beam and a collisionless plasma has been derived by a number of investigators.

$$1 = \frac{\omega_p^2}{\omega^2} + \frac{\omega_b^2}{(\omega - \gamma v_b)^2} \tag{3}$$

where ω_p is the plasma frequency of the plasma, ω_b is the plasma frequency of the beam, and v_b is the drift velocity of the beam. A number of simplifying assumptions have been made in obtaining this result:

1) Only small sinusoidal waves have been considered.
2) The electric vector and the direction of propagation of waves have been taken parallel to the direction of the beam (longitudinal waves).
3) All quantities were independent of the coordinates

[1] L. Tonks and I. Langmuir, "Oscillations in ionized gases," *Phys. Rev.*, vol. 33, pp. 195, 990; 1929.
[2] A. V. Haeff, "Space-charge wave amplification effects," *Phys. Rev.*, vol. 74, pp. 1532–1533; 1948. Also, "On the origin of solar radio noise," *Phys. Rev.*, vol. 75, pp. 1546–1551; 1949.
[3] D. Bohm and E. P. Gross, "Theory of plasma oscillations. A. Origin of medium-like behavior," *Phys. Rev.*, vol. 75, pp. 1851–1864; 1949. Also, "Theory of plasma oscillations. B. Excitation and damping of oscillations," *Phys. Rev.*, vol. 75, pp. 1864–1876; 1949. Also, "Effects of plasma boundaries in plasma oscillations," *Phys. Rev.*, vol. 79, pp. 992–1001; 1950.
[4] J. R. Pierce, "Possible fluctuations in electron streams due to ions," *J. Appl. Phys.*, vol. 19, pp. 231–236; 1948.
[5] A. V. Haeff, "The electron-wave tube," PROC. IRE, vol. 37, pp. 4–10; January, 1949.
[6] J. R. Pierce and W. B. Hebenstreit, "New type of high-frequency amplifier," *Bell Sys. Tech. J.*, vol. 28, pp. 33–51; 1949.
[7] D. H. Looney and S. C. Brown, "The excitation of plasma oscillations," *Phys. Rev.*, vol. 93, pp. 965–969; 1954.
[8] E. I. Gordon, "Plasma Oscillations, Interactions of Electron Beams with Gas Discharge Plasmas," Ph.D. dissertation, Mass. Inst. Tech., Cambridge; 1957.
[9] G. Wehner, "Plasma oscillator," *J. Appl. Phys.*, vol. 21, pp. 62–63; 1950.
[10] M. J. Kofoid, "Experimental two-beam excitation of electron oscillations in a plasma without sheaths," *Phys. Rev. Lett.*, vol. 4, pp. 556–557; 1960.

perpendicular to the direction of the beam and the effective beam boundaries were neglected; *i.e.*, the problem was considered one-dimensional.

4) Thermal velocities and collisions of the plasma electrons were neglected.
5) The plasma and the beam were assumed spatially uniform.

One may interpret this dispersion relation as giving either the propagation constant γ of waves whose frequency is ω, or the frequency of oscillation of disturbances whose wave number is γ. It is the former interpretation which we employ in this paper.

In the absence of a secondary electron beam or alternative feedback path, we expected the system of an electron beam interacting with a plasma over a finite length to be inherently stable; that is, we did not expect spontaneous oscillations.[11] On the other hand, small perturbations in current (shot noise) or velocity of the incoming electron beam or fluctuations arising in the plasma would increase in amplitude along the electron beam. In the first[12] of the two experiments described below (Fig. 1) we deliberately introduced a modulation of the electron beam at a microwave frequency and observed the amount by which this modulation was increased after having passed through the plasma. This experiment verified some of the early predictions. Kharchenko, *et al.*,[13] examined the modulation of the beam as it emerged from the plasma when no microwave modulation had been applied initially. They found a noise modulation whose frequency spectrum was sharply peaked at the plasma frequency, presumably due to the selective amplification of wide band fluctuation noise. Finally, Bogdanov,[14] and very recently, Allen and Kino,[15] repeated our first experiment with a longitudinal magnetic field and observed several interesting new effects.

During the course of the first experiment it was shown[16] that a cylindrical plasma column was capable of supporting electrostatic waves whose velocity could be made slow compared with the velocity of light. This suggested the second experiment[17] described below (Fig. 4) in which traveling-wave interaction occurred between such a slow wave and an electron beam which passed down the axis of the plasma at a velocity about equal to the wave velocity.

II. Interaction at Plasma Resonance

The first experiment utilized devices of the type shown in Fig. 1. An electron beam was modulated by a short helix, passed along the axis of the plasma column, and then upon emerging was demodulated by a second helix. The plasma density could be varied by changing the arc current, and strong amplification was found to occur[12] only when the plasma frequency was very close to the modulation frequency.

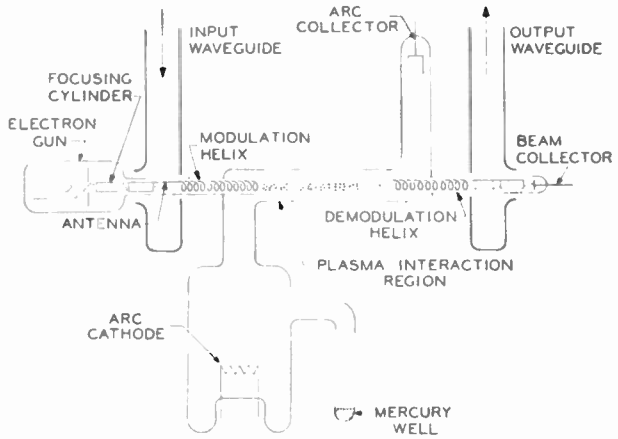

Fig. 1—Helix modulation experiment.

A. The Effect of Thermal Velocities of the Plasma Electrons—One-Dimensional Theory

Bohm and Gross[3] have derived the dispersion equation, including the effect of the thermal distribution of velocities of the plasma electrons, for a broad electron beam passing through a stationary plasma. The effect of short-range collisions of the plasma electrons may also be included in an approximate manner through the introduction of a velocity-independent collision frequency[18] ν. We now give a discussion of the solutions of this equation for the conditions of our first experiment.

All waves were assumed to have exponential spatial and time dependence $e^{i(\omega t-\gamma z)}$, where $\gamma=\beta-i\alpha$ was the complex propagation constant and α and β were both real. A beam plasma frequency was defined in terms of the beam electron density n_b by $\omega_b^2=n_b e^2/m\epsilon_0$. The thermal distribution of velocities of the electron beam about their mean velocity v_b was neglected since their

[11] P. A. Sturrock, "Excitation of plasma oscillations," *Phys. Rev.*, vol. 117, pp. 1426–1429; 1960.

[12] G. D. Boyd, L. M. Field, and R. W. Gould, "Excitation of plasma oscillations and growing plasma waves," *Phys. Rev.*, vol. 109, pp. 1393–1394; 1958. (This article contains a preliminary account of the first experiment described here.)

[13] I. F. Kharchenko, *et al.*, "Experimental and theoretical investigation of the interaction of an electron beam with a plasma," *Proc. Conf. on Ion Phenomena in Gases*, Uppsala, Sweden, vol. II, pp. 671–680; 1959.

[14] E. V. Bogdanov, V. J. Kislov, and Z. S. Tchernov, "Interaction between an electron stream and a plasma," *Proc. Symp. on Millimeter Waves*, Polytechnic Inst. of Brooklyn, N. Y., vol. 9, pp. 57–71; April, 1959.

[15] M. A. Allen and G. S. Kino, "Interaction of an electron beam with a fully ionized plasma," *Phys. Rev. Lett.*, vol. 6, pp. 163–165; 1961.

[16] A. W. Trivelpiece, "Slow Wave Propagation in Plasma Waveguides," Ph.D. dissertation, Calif. Inst. Tech., Pasadena; 1958. Also, A. W. Trivelpiece and R. W. Gould, "Space charge waves in cylindrical plasma columnes," *J. Appl. Phys.*, vol. 30, pp. 1784–1793; 1959. Also, "Electro-mechanical modes in plasma waveguides," *Proc. IEE*, vol. 105, pt. B, pp. 516–519; 1958.

[17] G. D. Boyd and R. W. Gould, "Travelling wave interaction in plasmas," *J. Nuclear Energy*, vol. 2, pt. C, pp. 88–89; 1961. (This article contains a preliminary account of the second experiment described here.)

[18] R. W. Gould, "Plasma Oscillations and Radio Noise from the Disturbed Sun," Calif. Inst. of Tech., Pasadena, Calif., Tech. Rept. 4, Contract NONR 220 (13); September, 1955.

random energy of approximately 0.1 ev was small compared to the random energy of 4.7 ev of the plasma electrons.

With these definitions the one-dimensional dispersion relation may be written

$$1 = \omega_p^2 \frac{(\omega - i\nu)}{\omega} \int_u \frac{f_0(u)du}{(\omega - \gamma u_z - i\nu)^2} + \frac{\omega_b^2}{(\omega - \gamma v_b)^2}, \quad (4)$$

where $f_0(u)$ was the normalized unperturbed distribution function of velocities of the plasma electrons and $du = du_x du_y du_z$. We assumed a Maxwellian velocity distribution

$$f_0(u) = \left(\frac{m}{2\pi kT}\right)^{3/2} \exp\left\{-\frac{m}{2kT}(u_x^2 + u_y^2 + u_z^2)\right\}, \quad (5)$$

where T is the equivalent "temperature" of the plasma electrons, and u is their random velocity vector.

The integral which resulted when (5) was substituted into (4) may be expressed in terms of the error function of complex argument. A large-argument asymptotic expansion of this function was easily obtained by expanding the denominator of the integral in (4) in powers of $\gamma u_z/(\omega - i\nu)$ and integrating term by term. The dispersion relation became

$$1 = \frac{(\omega_p/\omega)^2}{1 - i\frac{\nu}{\omega}}\left\{1 + \frac{\Gamma^2}{R\left(1 - i\frac{\nu}{\omega}\right)^2} + \frac{5}{3}\frac{\Gamma^4}{R^2\left(1 - i\frac{\nu}{\omega}\right)^4} + \cdots\right\} + \frac{(\omega_b/\omega)^2}{(\Gamma - 1)^2}, \quad (6)$$

where

$$R = \frac{mu_b^2}{3kT}. \quad (7)$$

is the ratio of the beam energy to the mean energy of a plasma electron and

$$\Gamma = \frac{\gamma v_b}{\omega} \quad (8)$$

is a normalized propagation constant. For the first experiment $R \approx 100$ and $|\Gamma| \approx 1$.

Neglecting collisions, there was a range of frequencies for which Γ was complex and a range for which it was real. Since $R \gg 1$, only the first two terms of the above series were considered. Eq. (6) then reduced to

$$(\Gamma - 1)^2(\Gamma^2 + \Lambda) + \sigma = 0, \quad (9)$$

where

$$\sigma = R\left(\frac{\omega_b}{\omega_p}\right)^2, \qquad \Lambda = R\left(1 - \frac{\omega^2}{\omega_p^2}\right) \quad (10)$$

Fig. 2 shows the locus of the roots of this equation in the complex Γ plane with Λ and σ as parameters. The growth constant is $-\alpha = (\omega/v_b)$ Im Γ. Alternatively, the gain is -8.68α db per cm, if α has units cm^{-1}. For a growing wave α is negative. This figure reveals that the maximum growth rate α occurs when the frequency ω is within a few per cent of the plasma frequency, provided $0.003 \leq \sigma \leq 3.0$ and $R \geq 30$. Thus maximum interaction occurs close to plasma resonance. In Fig. 3 we plot the normalized growth rate vs ω_p^2/ω^2 for representative beam energies (R) and beam densities (ω_b^2/ω_p^2).

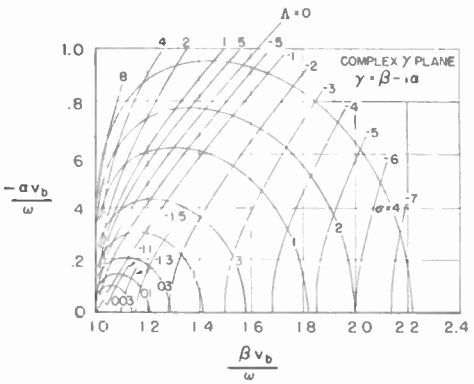

Fig. 2—Solution of (9) for the complex propagation constant

$$\Gamma = \frac{\gamma v_b}{\omega} = \frac{\beta v_b}{\omega} - i\frac{\alpha v_b}{\omega}$$

over a range of values of the parameters σ and Λ.

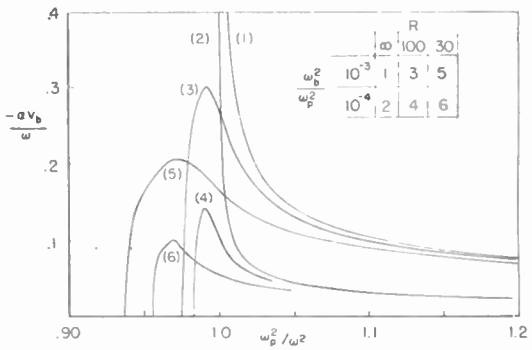

Fig. 3—Growth parameter $-\alpha$ vs the normalized plasma frequency squared. R is the ratio of the electron-beam energy to the average random energy of the plasma electrons. ω_b^2/ω_p^2 is the ratio of the beam-electron density to the plasma-electron density.

The effect of collisions is to reduce the growth rate, and it is convenient to evaluate this effect when $\omega = \omega_p$ ($\Lambda = 0$) since this is the condition for maximum growth rate (approximately). If it is also assumed that collisions are infrequent ($\nu \ll \omega$), (6) may be written as

$$\Gamma = 1 + i\sqrt{\frac{\sigma}{\Gamma^2 + iR\frac{\nu}{\omega}}}. \quad (11)$$

This equation is easily solved by iteration, taking Γ^2 equal to unity on the right-hand side as the first step. (Results are given in Tables I and II of Sections V and VI.)

B. The Effect of Finite Electron-Beam Diameter

In the Appendix we derive the dispersion equation for waves which can exist upon an electron beam of radius b passing through an infinite plasma. Thermal velocities and collisions of the plasma electrons are neglected. It is shown that the effect of the finite beam diameter is to introduce a beam-plasma reduction factor into (3), so that it can be written as

$$1 = \frac{\omega_p^2}{\omega^2} + \frac{(\omega_b')^2}{(\omega - \gamma v_b)^2} \tag{12}$$

where

$$\left(\frac{\omega_b'}{\omega_b}\right)^2 = \frac{1}{1 + \dfrac{I_0(\gamma b) K_1(\gamma b)}{I_1(\gamma b) K_0(\gamma b)}} . \tag{13}$$

In the thin beam limit ($\gamma b \to 0$), the above becomes

$$\left(\frac{\omega_b'}{\omega_b}\right)^2 \simeq \frac{1}{2}(\gamma b)^2(0.11593 - \ln \gamma b) \qquad \gamma b \ll 1, \tag{14}$$

which is similar to that obtained by Sturrock.[11]

We note from (13) that, if γ is real, the effect of finite beam size is simply to reduce the effective beam density and hence the rate of growth. When the growth per wavelength is small ($-\alpha \ll \beta$), it is sufficient to evaluate (13) by setting $\gamma = \omega/v_b$. Fig. 3 shows that this is not always a good approximation, and a complete discussion of the solutions of (12) and (13) has not been given. The solutions of the corresponding dispersion equation which results when the beam and plasma are subjected to a very strong axial magnetic field is given in Bogdanov, *et al.*[14]

III. Slow-Wave Interaction

During the course of the first experiment (Fig. 1), an interaction of the electron beam with the plasma was obtained when the plasma frequency was several times the modulation frequency imposed on the beam.

In this case the electron beam interacts with one of the slow space-charge waves which propagates along the plasma column. These propagating waves are electromechanical in nature and result from the interplay of kinetic energy of the plasma electrons and the energy stored in the electric field. In the special case of no axial magnetic field these waves are surface waves. They have been studied in detail by Trivelpiece and Gould.[16] Synchronism between an electron beam and such a slow wave results in familiar traveling-wave interaction. (See Pierce and Field[19] for a physical description of traveling-wave interaction.)

The second experiment described in this paper was designed to investigate more completely this traveling-wave interaction. A different configuration, shown in Fig. 4, was employed. In order to enhance the traveling-wave interaction, the diameter of the plasma column was made smaller than in the first experiment, and the electron-beam diameter was made larger. Modulation and demodulation of the electron beam was accomplished with cavity resonators (at a fixed frequency) so as to allow a variable beam velocity.

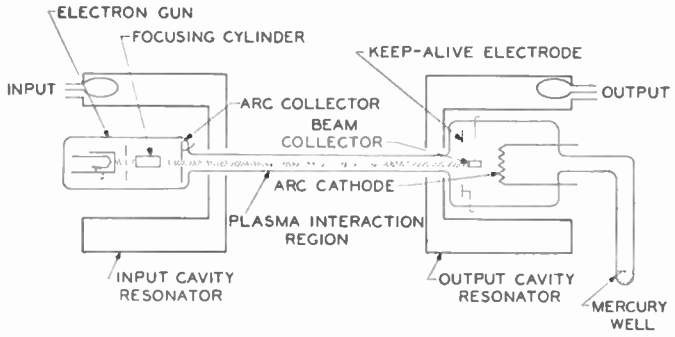

Fig. 4—Cavity-modulation experiment.

A. Slow-Wave Mode of Propagation

We now give a short theoretical discussion of the electrostatic waves which propagate along a nondrifting plasma column of radius a which fills a glass tube whose outer radius is c. Two cases will be considered: 1) a perfectly-conducting surface at radius c, and 2) the glass tube in free space. Thermal velocities and collisions of the plasma electrons will be neglected.

The electric fields of these modes are derivable from a potential if their phase velocity is small compared to the velocity of light.[16] In this approximation the potential satisfies the Laplace equation. First let there be a conducting surface at radius c. Field are assumed to vary as $e^{i(\omega t - n\theta - \beta z)}$. In the absence of the electron beam and neglecting collisions, the propagation constant is real, so β is used for the propagation constant instead of $\gamma(\alpha = 0)$.

The time-varying potential in each region is given by

$$\phi_1 = \frac{I_n(\beta r)}{I_n(\beta a)} e^{i(\omega t - n\theta - \beta z)} \qquad r \leq a$$

$$\phi_1 = \frac{I_n(\beta r) K_n(\beta c) - I_n(\beta c) K_n(\beta r)}{I_n(\beta a) K_n(\beta c) - I_n(\beta c) K_n(\beta a)} e^{i(\omega t - n\theta - \beta z)}$$

$$a \leq r \leq c. \tag{15}$$

Matching tangential electric field and normal displacement at $r = a$, and using (2) for the plasma dielectric permittivity and κ as the relative dielectric constant of the glass, one obtains the dispersion equation

$$\left(1 - \frac{\omega_p^2}{\omega^2}\right)\frac{1}{\kappa} = \frac{I_n(\beta a)}{I_n'(\beta a)} \left\{ \frac{I_n'(\beta a) K_n(\beta c) - I_n(\beta c) K_n'(\beta a)}{I_n(\beta a) K_n(\beta c) - I_n(\beta c) K_n(\beta a)} \right\}, \tag{16}$$

where the primes denote derivatives of the Bessel functions with respect to the argument. In the limit of

[19] J. R. Pierce and L. M. Field, "Traveling-wave tubes," PROC. IRE, vol. 35, pp. 108–111; February, 1947.

large βa the asymptotic frequency of propagation is

$$\frac{\omega}{\omega_p} = \frac{1}{\sqrt{1+\kappa}}. \tag{17}$$

The solution of this equation for the circularly symmetrical mode ($n=0$) is shown in Fig. 5 by the lower dashed curve, where we plot ω/ω_p vs βa. The phase and group velocities are given by ω/β and $\partial\omega/\partial\beta$, respectively. Angular dependent modes are not of particular interest in the second experiment since their fields vanish on the axis where the electron beam passes and, in addition, the excitation cavities are cylindrically symmetric.

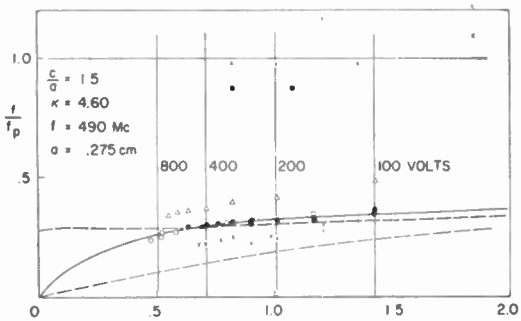

Fig. 5—Frequency vs propagation constant βa for the surface-wave mode of propagation on a plasma-glass column in free space (solid curve), and when covered with a conducting surface (dashed curve). In the latter case, the upper dashed curve represents the $n=1$ mode, and the lower dashed curve represents the $n=0$ mode. The ○, ● and △ correspond to measurements on the plasma-glass column in free space, and should lie on the theoretical solid curve. The × data was obtained with the glass coated with a conducting layer, and such points should lie on the lower dashed curve.

Where the glass tube is in free space rather than being surrounded by a metallic conductor, expressions for the potential in three separate regions—1) plasma $r \leq a$, 2) glass $a \leq r \leq c$, 3) free space $c \leq r < \infty$—must be joined so that the tangential field and normal displacement are continuous. This leads to a dispersion equation for the circularly symmetric mode ($n=0$)

$$\left(1-\frac{\omega_p^2}{\omega^2}\right)\frac{I_1(\beta a)}{I_0(\beta a)} = \frac{-\kappa}{be\coth(\beta c,\beta a)} \cdot \frac{\kappa + \dfrac{K_1(\beta c)}{K_0(\beta c)}\dfrac{1}{be\tanh(\beta c,\beta a)}}{\kappa + \dfrac{K_1(\beta c)}{K_0(\beta c)}\,Be\tanh(\beta c,\beta a)}, \tag{18}$$

where the functions

$$be\coth(\beta c,\beta a) = \frac{I_1(\beta c)K_0(\beta a) + I_0(\beta a)K_1(\beta c)}{I_1(\beta c)K_1(\beta a) - I_1(\beta a)K_1(\beta c)}$$

$$be\tanh(\beta c,\beta a) = \frac{I_1(\beta c)K_1(\beta a) - I_1(\beta a)K_1(\beta c)}{I_0(\beta c)K_1(\beta a) + I_1(\beta a)K_0(\beta c)}$$

$$Be\tanh(\beta c,\beta a) = \frac{I_0(\beta c)K_0(\beta a) - I_0(\beta a)K_0(\beta c)}{I_1(\beta c)K_0(\beta a) + I_0(\beta a)K_1(\beta c)} \tag{19}$$

are defined and tabulated by Birdsall.[20] Solution of this equation is depicted by the solid line in Fig. 5. The horizontal line in Fig. 5 at $\omega/\omega_p=1$ corresponds to plasma oscillations which are independent of the wavelength of the disturbance.

The vertical lines labeled 800, 400, 200, and 100 volts correspond to constant phase velocity lines when the frequency is fixed and the plasma density is varied. The intersection of these curves with any of the propagation constant curves specifies the operating point at which the electron beam velocity is synchronous with the phase velocity of the surface wave.

B. Interaction Impedance

An electron beam traveling in synchronism with the slow surface wave will interact with the axial electric field of the wave. Under these conditions a spatially growing wave will result (the propagation constant becomes complex), so that the RF energy traveling along the plasma column increases with distance. This energy is supplied by the conversion of the beam kinetic energy.

Pierce[21] has shown that an approximate value of the growth constant in a traveling-wave amplifier can be expressed in terms of an *interaction impedance*, which is proportional to the square of the axial electric field at the position of the beam per unit power flow in the slow wave. Calculations[22] of this impedance for the circularly symmetric mode of the plasma-glass column in free space (ω-β diagram is given by the solid curve of Fig. 5) are approimately 800 ohms in the range $0.5<\beta a<1.5$.

IV. Characteristics of the Plasma and the Electron Beam

A. Mercury Arc Discharge

The positive column of an arc discharge in mercury vapor was the plasma. The mercury gas pressure was regulated by maintaining the temperature of the mercury "well" at 300 ± 0.1°K. The vapor pressure at this temperature was 2.1×10^{-3} mm Hg (2.1 microns), and the density of mercury atoms was 6.8×10^{13} per cm³. The electron density n_0, corresponding to an electron plasma frequency of 3000 Mc, was 1.12×10^{11} per cm³. The random energy of the plasma electrons was characterized by an equivalent temperature T_e. Measurements of T_e by Langmuir probes gave $T_e=35{,}000$°K, or 4.7 electron volts. The energy corresponding to the axial drift velocity which is necessary to carry the discharge current was about 0.2 ev and was therefore small compared with the random energy. The collision

[20] C. K. Birdsall, "Memorandum for File ETL-12," Hughes Aircraft Co., Malibu, Calif.; July 1, 1953.
[21] J. R. Pierce, "Traveling Wave Tubes," D. Van Nostrand Co., New York, N. Y.; 1950.
[22] G. D. Boyd, "Experiments on the Interaction of a Modulated Electron Beam with a Plasma," Ph.D. dissertation, Calif. Inst. Tech., Pasadena; 1959. Also, "Power Flow and Gap Coupling to Slow Wave Plasma Modes," Electron Tube and Microwave Lab., Calif. Inst. Tech., Pasadena, Tech. Rept. 12, NONR 220 (13); June, 1959.

frequency of plasma electrons with the sheath at the tube wall was approximately 129×10^6 sec^{-1} for a plasma column diameter of 1.04 cm (as in the first experiment). The collision frequency of electrons with un-ionized mercury atoms was 37×10^6 sec^{-1} corresponding to a mean-free path of the plasma electrons through mercury atoms of approximately 3.5 cm, which was somewhat greater than the tube diameter.

The mean-free path for beam electrons of 100 to 1000 volts in the plasma ranged from about 26 to about 65 cm at the vapor pressure used throughout these experiments.

B. Electron Beam

The electron-beam gun was of the conventional type used in traveling-wave tubes. Beam focusing was possible with an electron lens (focusing cylinder, Figs. 1 and 4) and ion space-charge forces. *L* cathodes were found to be the most satisfactory in resisting the adverse effects of mercury ion bombardment. Arcing between gun electrodes due to the presence of ions did not seem to occur in the voltage range employed. The cathode button diameters were 0.045 and 0.090 inch in the helix modulation tube of Fig. 1 and in the cavity modulation tube of Fig. 4, respectively.

V. Helix Modulation Experiment

A. Interaction at Plasma Resonance

A schematic of the helix modulation tube is shown in Fig. 1. The plasma interaction length between helices was about 5 cm. The inner radius of the glass tube was 0.52 cm. The *S*-band coupling waveguides were tapered to 1 cm in height. The input and output helices were each 3 cm long. The helix-synchronous voltage was 400 volts.

In the operation of the experiment the electron beam was modulated with a microwave frequency between 2.2 and 4.0 kMc, and the output signal from the demodulation helix was observed as the arc current was swept. The plasma density, and thus the square of the plasma frequency, is approximately proportional to arc current in low-pressure arc discharges.[23] According to the theory presented in Section II, the output signal level should be a maximum when the arc current is such that plasma frequency ω_p equals the modulation frequency ω. This value of arc current for maximum interaction should change as the input frequency is changed. For convenience, the arc current was swept at a 60-cps rate, so that the result could be displayed on an oscilloscope.

The output signal level was displayed on the *y* axis of the oscilloscope, while a signal proportional to the discharge current was used to drive the *x* axis. Fig. 6 shows the resulting display for six different modulating frequencies. The arc current zero line is the heavy vertical line on the extreme left. From these and similar traces the current for maximum interaction was obtained, and the result is shown in Fig. 7.

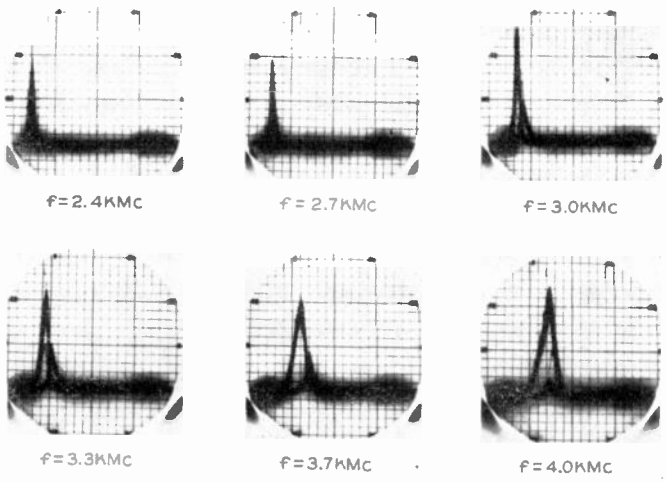

Fig. 6—Detected output signal vs arc current as obtained from the helix-modulation tube. Horizontal calibration: 20 divisions equal 0.40 ampere.

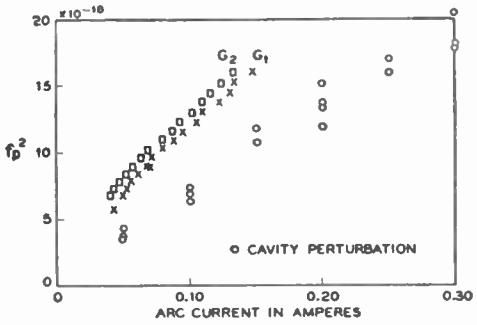

Fig. 7—G_1 and G_2 give the axial plasma frequency squared as obtained from Fig. 6. The circles represent measurements of the average plasma frequency squared over the plasma interaction region as obtained by the cavity perturbation method.

The observation that points G_1 and G_2 lie on relatively straight lines passing nearly through the origin is strong evidence that the interaction observed corresponds to plasma resonance. Approximate equality of the modulation frequency and the plasma frequency must be ascertained from an independent measurement of plasma density. The fact that the straight lines when extrapolated to zero frequency do not pass exactly through the origin may be explained in terms of part of the plasma being produced by beam collisions. Differences in beam focusing probably accounts for the difference between the intercepts of curves G_1 and G_2, taken with different electrode potentials.

To obtain a measurement of electron density by an independent method, the cavity-perturbation tech-

[23] B. Klarfeld, "Characteristics of the positive column of gaseous discharge," *J. Phys. USSR*, vol. 5, pp. 155–175; 1941.

nique[24–26] which measured the average plasma electron density over the cross section, was applied to the plasma interaction region of the helix tube. The average square of plasma frequency was also plotted vs arc current in Fig. 7. The difference in slopes (a factor of 1.4) between the cavity data and G_1 or G_2 may be explained by the fact that electron density on the axis, where interaction occurs, is higher than the average density for a specific current. Assuming a parabolic dependence of density on radius,[27] it was estimated from the ratio of the slopes that the edge plasma density was about 0.4 of the plasma density on the axis, which was in reasonable accord with Klarfeld.[23]

B. Rate of Growth

Table I presents theoretical growth constants in db per cm for different values of the electron-beam current. All rates of growth are for 3000 Mc, assume a 400-volt beam, include a beam-reduction factor of 0.4 [from (25)], a beam diameter of 3 mm, and a value of $R=100$. The first column gives the maximum rate of growth (such as that taken from the peak of the curves in Fig. 3) and neglects collisions. The second column also neglects collisions and gives the growth at the plasma frequency $\omega=\omega_p$. The remaining columns are also for $\omega=\omega_p$, but include collision frequencies ν of 30, 100, and 300 Mc, respectively.

TABLE I

THEORETICAL GROWTH CONSTANTS AT PLASMA RESONANCE FOR THE HELIX MODULATION TUBE

I_b	Max G db per cm	G at $\omega=\omega_p$ db per cm			
ma	$\nu=0$	$\nu=0$	$\nu=30\times10^6$	$\nu=100\times10^6$	$\nu=300\times10^6$
0.25	17.2	11.1	10.74	9.68	6.95
0.5	22.05	15.5	14.93	13.4	9.71
1.0	27.55	21.4	20.55	18.38	13.5
2.0	34.0	29.2	27.9	24.96	18.68

Experimentally, the maximum net gain observed between the input and output waveguides was about +25 db. Under this condition the cathode current was 2.0 ma, and the current reaching the beam collector was 0.48 ma. When the arc was turned off but the beam left on, the net loss between waveguides was as little as 10 db if the beam remained well focused. This implies an electronic gain of 35 db in the 5-cm interaction length or a growth constant of 7 db per cm. The theoretical prediction, assuming a beam current of 0.5 ma and a collision frequency of 100 Mc (Table I), was about 13.4 db per cm. On many occasions the helix modulation tube showed a net *loss* of 10 db or so. Adjusting electrode potentials of the device so as to show net gain was sometimes difficult.

The theoretical bandwidth of this amplification device is less than 1 per cent. The experimentally observed bandwidths of 25 per cent or so seen in Fig. 6, together with the reduced gains, are likely to be explained by the variations in the plasma density *along* the path of the beam. When the plasma frequency varies along the path of the electron beam, it can be shown that the effect is to reduce the gain at any one frequency and to increase the range of frequencies over which amplification is possible. The density is probably lowest where the beam enters and where it emerges because of diffusion losses.

It is difficult, for two reasons, to observe the growing waves at plasma resonance by moving an antenna along the outside of the glass column. First, the fields decay exponentially away from the surface of the beam and the decay factor is large, since $\beta a=8.2$ for the helix tube at 3000 Mc and 400 volts. Secondly, as may be seen from the following argument, plasma oscillations ($\omega=\omega_p$) produce very little field outside the plasma column. The dielectric constant (2) is zero in the plasma, and hence the normal component of the displacement vector vanishes at the edge of the plasma. Therefore, the normal component of the electric field vanishes outside the plasma column. Of course this argument neglects the effect of random energy of the plasma electrons, but it does serve to indicate that the field outside should be small. The first argument does not apply to the cavity modulation tube to be discussed in Section VI, since βa is approximately unity and the electron beam passes closer to the edge of the plasma column in that tube. The growing wave at plasma resonance *was* detectable in the cavity modulation tube using a traveling probe.

C. Slow-Wave Interaction

When the electron beam was defocused so badly that it filled most of the plasma column, being reflected from the sheath from the edge of the plasma column and then partially collected at the second helix, an interaction was observed when the plasma frequency was greater than the modulation frequency. Fig. 8 shows the detected output signal vs arc current. The arc current increases from left to right and is zero at the heavy vertical line at the far left. Two interactions may be seen, the one at lower current occurring when

[24] M. A. Biondi and S. C. Brown, "Measurements of ambipolar diffusion in helium," *Phys. Rev.*, vol. 75, pp. 1700–1705; 1949.
[25] K. B. Persson, "Limitations of the microwave cavity method of measuring electron densities in a plasma," *Phys. Rev.*, vol. 106, pp. 191–195; 1957.
[26] S. J. Buchsbaum and S. C. Brown, "Microwave measurements of high electron densities," *Phys. Rev.*, vol. 106, pp. 196–199; 1957.
[27] R. M. Howe, "Probe studies of energy distributions and radial potential variations in a low pressure mercury arc," *J. Appl. Phys.*, vol. 24, pp. 881–894; 1953.

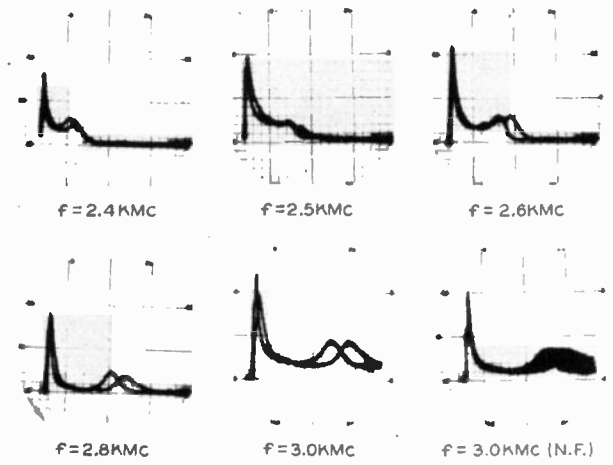

Fig. 8—Detected output signal vs arc current as obtained from the helix tube. Calibration as in Fig. 6. The interaction peak at the larger current is with the surface wave mode of propagation. NF is with the output unfiltered.

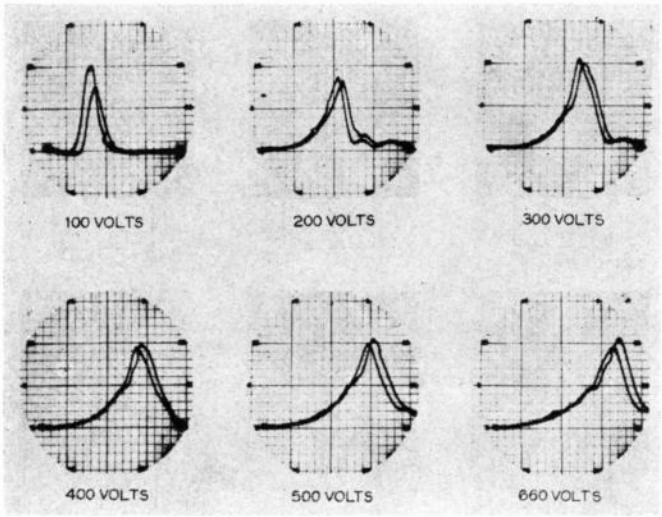

Fig. 9—Detected output signal vs arc current as obtained from the cavity-modulation tube. Horizontal calibration: 20 divisions equal 0.050 ampere. The beam is interacting with the angularly independent surface-wave mode of propagation.

$\omega_p = \omega$, and the one at higher current presumably due to the axially symmetric surface wave mode of propagation. The subsidiary maxima in Fig. 2 of the preliminary report[12] were probably also due to the surface-wave interaction. If the beam were not deliberately defocused, interaction with the surface wave could not be observed since the fields are strong only at the surface of the plasma column.

Also shown in Fig. 8 are two photographs at the same frequency taken with the detected output signal both filtered and nonfiltered (NF). Appreciable noise is present in both interactions, some of which may be associated with moving striations.[28]

In Figs. 6, 8 and 9 hysteresis is evident. This may be due to space-charge buildup and decay or to nonequilibrium heating effects. The hysteresis phenomena is not completely understood.

VI. Cavity Modulation Experiment

A. Slow-Wave Interaction

A larger beam and smaller plasma column were necessary to obtain strong interaction with the surface-wave mode of propagation, thus the device shown in Fig. 4 was constructed. By varying the beam voltage (approximately 1000 to 100 volts) βa could be made to fall between 0.5 and 1.5. By operating with a significantly smaller value of βa than in the helix tube, the surface-wave fields are much stronger near the axis where the electron beam passes. By employing an axial magnetic field it would be possible to have the fields on the axis stronger than at the surface.[16]

The detected output signal 490 Mc is shown in Fig. 9 vs arc current at six different electron-beam voltages. The zero of current is the numbered heavy line at the far left. As the beam velocity increases, the phase velocity of the slow surface wave must also increase to fulfill the synchronism condition. From Fig. 5 it is seen that βa and f/f_p decrease as the velocity increases. Thus as the beam velocity increases the plasma frequency must increase if synchronism is to be maintained. Fig. 9 shows that, indeed, as the beam voltage is increased, the arc current for maximum gain increases.

The electron density in the plasma column of the cavity-modulation tube was measured by the cavity-perturbation technique.[24–26] as a function of arc current. From the arc current corresponding to the peak interaction in Fig. 9 one may obtain the *experimental* ω-β diagram as shown by the data points in Fig. 5. The result is seen to correspond well to the theoretical curves. Any errors in the cavity measurements of plasma density would tend to shift the vertical scale.

Interaction was also observed at the plasma resonance with the cavity tube. This interaction occurred near the value of the current at which the arc extinguished, and stable operation was difficult. Nevertheless, the values of the interaction-arc current at which this interaction occurred were used to determine the plasma frequency $f_p = \omega_p/2\pi$, and the results (f/f_p) are plotted in Fig. 5 near the horizontal line at $f/f_p = 1$.

B. Growing Surface Waves

The surface-wave fields are strongest at the surface of the plasma column. A traveling probe at the surface of the glass column was used to detect a growing standing-wave pattern (Fig. 10). The standing-wave pattern is a result of the interference between the growing surface wave and the wave which is reflected by the output cavity resonator. From the standing-wave pattern one may measure the electronic wavelength on the plasma column. This is in agreement with the value predicted from the beam voltage.

[28] L. Pekarek, "Theory of moving striations," *Phys. Rev.*, vol. 108, pp. 1371–1372; 1957.

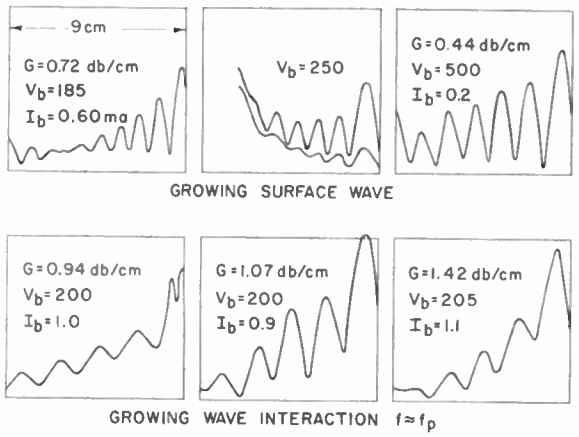

Fig. 10—Growing wave strength vs distance as obtained by a traveling probe at the surface of the glass column of the cavity-modulation tube.

The 250-volt case in Fig. 10 is of particular interest. The lower curve was taken with the beam current greatly reduced by lowering the cathode temperature. The signal then decayed along most of the interaction region because of collisional attenuation in the surface-wave propagation. The upper curve is with a normal beam current and shows a growing wave.

Theory[21] predicts a growth constant of 2.75 db per cm when an interaction impedance of 800 ohms (Section III-B) and a 200-volt beam at 1-ma current are assumed, and when space charge in the beam, plasma random energy, and collisions are neglected. A representative experimental value at 1 ma and 200 volts is about 0.8 db per cm. The discrepancy between the theoretical and experimental growth constants may be due possibly to the neglect of loss along the plasma column in the theoretical calculation.

C. Interaction at Plasma Resonance

Because of the smaller value of βa (approximately 1) for the cavity tube (as compared with $\beta a \approx 8$ in the helix tube), it was found that a growing standing-wave pattern could be observed with a traveling probe outside the plasma column (see Fig. 10). A representative growth constant was found to be 1 db per cm at 1-ma beam current.

Measurements on the growing standing-wave pattern indicated that the interfering wave had a large phase velocity compared to the forward-beam velocity, and thus the standing-wave pattern was probably due to stray radiation in free space from the signal source. The standing-wave pattern could not have been a result of the reflected surface wave since the latter does not propagate when $f=f_p$.

Table II gives theoretical growth constants in db per cm, assuming a 200-volt beam, a beam reduction factor of 0.21 from (25) a beam diameter of 4.8 mm, and a value of $R=200/4.7=42.6$. The presentation of the data is similar to that in Table I.

TABLE II

THEORETICAL GROWTH CONSTANTS AT PLASMA RESONANCE FOR THE CAVITY-MODULATION TUBE

I_b	Max G db per cm	G at $\omega=\omega_p$ db per cm			
ma	$\nu=0$	$\nu=0$	$\nu=30\times10^6$	$\nu=100\times10^6$	$\nu=300\times10^6$
0.25	6.61	5.32	4.72	3.58	2.11
0.5	8.27	7.23	6.38	4.92	2.96
1.0	10.32	9.62	8.52	6.70	4.16
2.0	12.72	12.52	11.20	9.05	5.78

The experimentally measured growth rate of 1 db per cm was considerably less than the theoretical value of about 6.7 db per cm (assuming 100-Mc collision frequency), and this discrepancy is most likely due to variations of the axial plasma density or to an incorrect estimate of the beam diameter in the plasma.

VII. Summary and Conclusions

Experiments have been performed substantiating two types of interaction between a modulated electron beam and a plasma. In one case the plasma acts as a resonant, nonpropagating medium and in the other as a slow traveling-wave structure with which synchronism between it and the electron beam is observed.

Exponential growth constants along the beam were measured with a traveling probe for both interactions. The experimental rates of growth were considerably less than that predicted theoretically. For the traveling-wave interaction, the neglect of loss and the random energy of the plasma electrons in the theory are probably of most importance.

Trivelpiece and Gould[16] have shown that immersing the plasma column in an axial magnetic field converts the nonpropagating plasma resonance into a backward-wave propagating mode (phase and group velocities in opposite directions) with which backward-wave interaction (and thus oscillation) is possible. Recently Targ and Levine[29] have observed such backward-wave oscillations. Structureless slow-wave propagating circuits are intriguing and deserve further investigation.

Appendix

Three-Dimensional Theory Neglecting the Random Energy of the Plasma Electrons

If in a plasma the wavelength of the disturbance is small compared to the free-space wavelength at that frequency, the magnetic field associated with plasma oscillations may be neglected. Under this quasi-static approximation the time-varying potential and charge

[29] R. Targ and L. P. Levine, "Backward-wave microwave oscillations in a system composed of an electron beam and a hydrogen gas plasma," *J. Appl. Phys.*, vol. 32, pp. 731–737; 1961.

density are related by Poisson's equation

$$\nabla^2\phi_1 = -\rho_1/\epsilon_0. \tag{20}$$

In the one-dimensional case analyzed in Section II-A the quasi-static *approximation* is unnecessary since the time-varying magnetic field vanishes identically ($\nabla \times \boldsymbol{E}_1 = -\gamma \mathbf{e}_z \times \boldsymbol{E}_1 = 0$).

The three-dimensional problem considered here consists of an electron beam of finite radius b passing through a nondrifting infinite cold plasma. To obtain the dispersion equation for growing waves, one computes the sum of the ac charge densities of the beam and of the plasma from the linearized small-signal continuity and force equations. Substituting this sum into (20) and rewriting slightly, one obtains

$$\nabla \cdot \left\{ 1 - \frac{\omega_p^2}{\omega^2} - \frac{\omega_b^2}{(\omega - \gamma v_b)^2} \right\} \nabla\phi_1 = 0, \tag{21}$$

where a z dependence of $e^{-i\gamma z}$ has been assumed. This is the appropriate differential equation for the beam and plasma together. In the region outside the beam the same equation can be used by setting $\omega_b = 0$.

Note that (21) is written in the form $\nabla \cdot \boldsymbol{D}_1 = 0$, where $\boldsymbol{D}_1$ is the displacement vector. In this form the boundary condition at the interface between the region containing plasma alone and that containing plasma plus beam is evident: the normal component of the quantity $\boldsymbol{D}_1$ is continuous between regions. The potential must also be continuous.

The solutions to (21) are either

$$1 = \frac{\omega_p^2}{\omega^2} + \frac{\omega_b^2}{(\omega - \gamma v_b)^2} \qquad r \leq b, \tag{22}$$

or

$$\nabla^2\phi_1 = 0 \qquad 0 \leq r \leq \infty. \tag{23}$$

Eq. (22) is identical to (3). This represents the one-dimensional solution and is independent of beam radius. Eq. (22) was derived by Pierce,[1] except that he was considering the interaction of beam electrons with ions. The solution of this equation is plotted in Fig. 3 under the designation of $R = \infty$.

For the three-dimensional case the solutions are obtained from (23). Note that (23) implies that $\rho_{1b} + \rho_{1p} = 0$, and therefore that the system consisting of the electron beam and the plasma has no density modulation; only a "rippled boundary" form of modulation at $r = b$ which is the interface between the two regions.

Circularly symmetric solutions of (23) contain modified Bessel functions and are, respectively, $I_0(\gamma r)e^{-i\gamma z}$ and $K_0(\gamma r)e^{-i\gamma z}$ for the radius less than or greater than the beam radius. The potential has been taken to be finite at the origin and zero at infinity. Matching the above boundary conditions results in

$$1 = \frac{\omega_p^2}{\omega^2} + \frac{(\omega_b')^2}{(\omega - \gamma v_b)^2}, \tag{24}$$

where

$$\left(\frac{\omega_b'}{\omega_b}\right)^2 = \frac{1}{1 + \dfrac{I_0(\gamma b)K_1(\gamma b)}{I_1(\gamma b)K_0(\gamma b)}}. \tag{25}$$

The only quantitative effect in (24) compared to (3), which neglects the random energy of the plasma electrons, is to replace the electron-beam plasma frequency by a *reduced*-beam plasma frequency ω_b'. This is a result of the difference between *rippled boundary* modulation and density modulation.

Inclusion of the effects of the random energy of the plasma electrons into the finite geometry problem is more difficult due to the complexity of the boundary conditions. As an approximation to the three-dimensional problem it is assumed that one may take the one-dimensional dispersion relation (6) and replace the beam plasma frequency by the reduced-beam plasma frequency of (25). This results in an approximate dispersion relation, including the random energy and collisions of the plasma electrons, for a finite diameter beam in an infinite plasma.

If the electron beam were immersed in a finite axial magnetic field both rippled boundary and density modulation would occur.

Acknowledgement

A great deal of credit for the success of these experiments is attributable to A. F. Carpenter, whose skill and patience in the fabrication of the glass tubes is gratefully acknowledged. Fruitful discussions were enjoyed with Dr. A. W. Trivelpiece.

The continuing support of the Office of Naval Research is very gratefully acknowledged.

A Method of Measurement of Flame Attenuation at 200 Mc*

ALBERT W. BIGGS†, MEMBER, IRE

Summary—**This paper presents a simple method for the determination of the attenuation encountered by a VHF signal as it passes through a flame or the exhaust trail produced by a flame. The measurements are made of the VSWR and the shift of the minimum electric field as the ionized gases pass between two parallel plates of a short-circuited, two-bar transmission line. The relative dielectric constant and the conductivity of an ionized gas are plotted for several electron densities and collision frequencies for a frequency of 200 Mc. Another set of curves is derived from these for attenuation and minimum shift due to ionized gases in a predetermined length of transmission line. Characteristic impedance curves are also plotted. Simple Smith chart techniques are used to determine the VSWR and minimum shift when ionized gases pass through a length of shorted transmission line. The length corresponds to a half wavelength of the wave in the line with no ionized gases present. Calibration was accomplished with the use of distilled water.**

Introduction

SEVERAL methods are available[1] for the measurements of attenuation in a radio signal when it passes through an ionized gas. The selection of 200 Mc as the frequency for attenuation measurements precluded the use of microwave horns[2] or helix antennas[3] because of their large physical size. The transmission line proved to be the simplest mechanism. When it has a short-circuited load, the VSWR is high (infinitely when losses in the system are absent, but this is impossible). The minimum is also quite sharply defined.

When a slightly ionized gas passes between the two conductors of a short-circuited transmission line, the wave is attenuated as it passes to and from the short circuit. The VSWR is reduced with the increase of electron density and the increase of collision frequency. The wavelength of the wave is also increased in the ionized plasma region. Both of these can be measured with a slotted line and a standing wave detector.

Analytical Determination of VSWR and Minimum Shift

The relative dielectric constant K of an ionized gas is a function of the collision frequency ν of electrons with gas molecules, the plasma frequency ω_p, and the frequency ω of the radio signal passing through the medium. It is given by

$$K = 1 - \frac{1}{(\nu/\omega_p)^2 + (\omega/\omega_p)^2}, \tag{1}$$

with the plasma frequency equal to

$$\omega_p = e\sqrt{\frac{n}{\epsilon_0 m}} \times 10^3, \tag{2}$$

where n is the electron density in electrons per cubic centimeter, e is the electron charge, m is the electron mass, and ϵ_0 is the dielectric constant of free space (MKS units). This is shown in Fig. 1 for a frequency of 200 Mc. The range of collision frequencies is selected because it is typical[4] for flames.

The conductivity σ is given by the expression

$$\sigma = \epsilon_0 \nu \frac{1}{(\nu/\omega_p)^2 + (\omega/\omega_p)^2}. \tag{3}$$

This is shown in Fig. 2 for a 200 Mc signal.

The attenuation α and phase constant β are derived from K and σ in terms of collision frequency and electron density from[5]

$$\alpha = \frac{\omega}{c}\sqrt{K}\sqrt{\sqrt{1+\left(\frac{\omega\sigma}{K\epsilon_0}\right)^2} - 1} \tag{4}$$

$$\beta = \frac{\omega}{c}\sqrt{K}\sqrt{\sqrt{1+\left(\frac{\omega\sigma}{K\epsilon_0}\right)^2} + 1} \tag{5}$$

The curve for α is shown in Fig. 3.

* Received by the IRE, August 21, 1961.

† Aero-Space Div., Boeing Co., Seattle, Wash.

[1] A. G. Gaydon and H. G. Wolfhard, "Flames—Their Structure, Radiation, and Temperature," Chapman & Hall, Ltd., London, Eng.; 1953.

E. Sanger, P. Goercke and I. Bredt, "Ionization and Luminescence in Flames," NACA Tech. Memo 1305; April, 1951.

H. Belcher and T. M. Sugden, "Studies on the ionization produced by metallic salts in flames. I. The determination of the collision frequency of electrons in coal-gas/air flames," *Proc. Roy. Soc. (London) A*, vol. 201, pp. 480–488; May, 1950.

T. M. Sugden and B. A. Thrush, "A cavity resonator method for electron concentration in flames," *Nature*, vol. 158, pp. 703–704; October, 1951.

H. Smith and T. M. Sugden, "Ionization produced in metallic salts in flames. I. Ionic equilibrium in hydrogen/air flames containing alkali metal salts," *Proc. Roy. Soc. (London) A*, vol. 211, pp. 31–58; February, 1952.

T. M. Sugden, "The use of microwaves in the study of ionic and chemical equilibrium at high temperature," *Discussion, Faraday Soc.*, vol. 19, pp. 68–76; January, 1955.

F. P. Adler, "Measurement of the conductivity of a jet flame," *J. Appl. Phys.*, vol. 25, pp. 903–906; July, 1954.

[2] W. C. King and W. Gordy, "One-to-one millimeter wave spectroscopy. IV. Experimental methods and results for OCS ClH_3F, and H_2O," *Phys. Rev.*, vol. 93, pp. 407–412; February, 1954.

K. E. Shuler and J. Weber, "A microwave investigation of the ionization of hydrogen-oxygen and acetylene-oxygen flames," *J. Chem. Phys.*, vol. 22, pp. 491–502; February, 1954.

[3] A. Dauguet, "Etude de l'ionisation des gaz de propulseurs a reaction," *Ann. Télécommun.*, vol. 12, pp. 234–244; June, 1957.

[4] J. Schneider and F. W. Hofmann, "Absorption and dispersion of microwaves in flames," *Phys. Rev.*, vol. 116, pp. 244–249; October, 1959.

[5] E. C. Jordan, "Electromagnetic Waves and Radiating Systems," Prentice-Hall, Inc., New York, N. Y., p. 672; 1955.

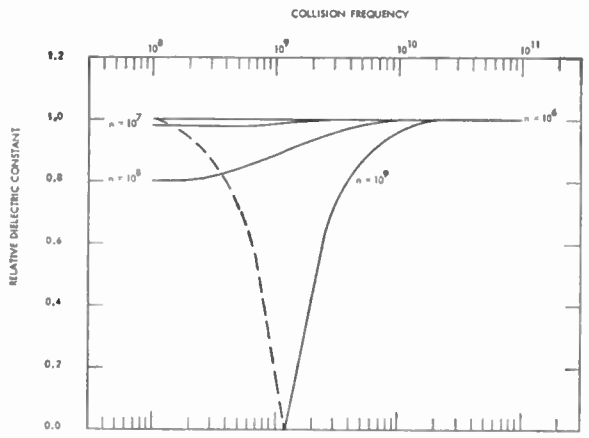

Fig. 1—Relative dielectric constant in an ionized gas for different electron densities.

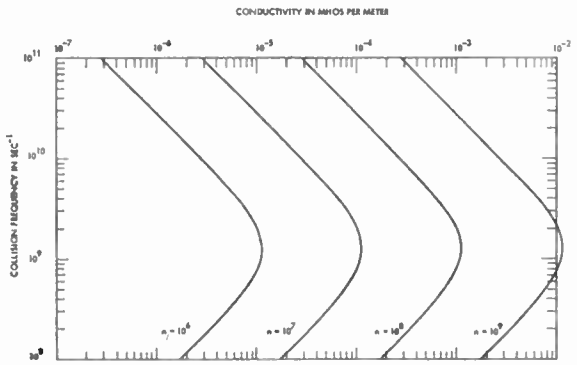

Fig. 2—Conductivity of an ionized gas for different electron densities.

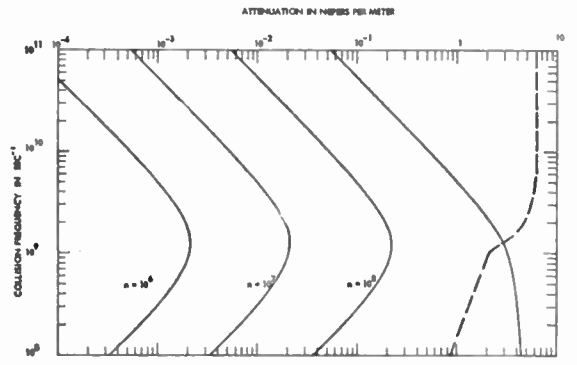

Fig. 3—Attenuation in an ionized gas for different electron densities.

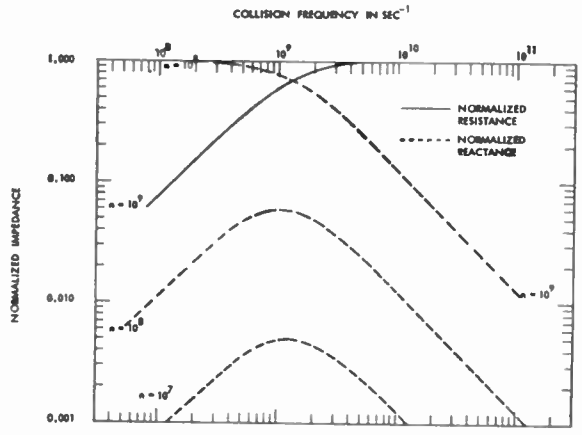

Fig. 4—Characteristic impedance of an ionized gas for different electron densities.

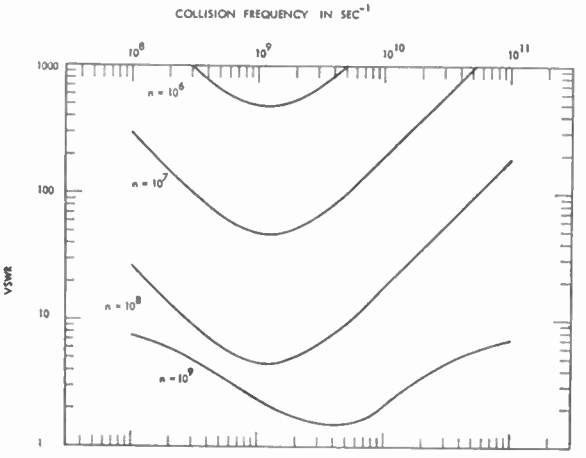

Fig. 5—VSWR with lossless coaxial cable in an ionized gas for different electron densities.

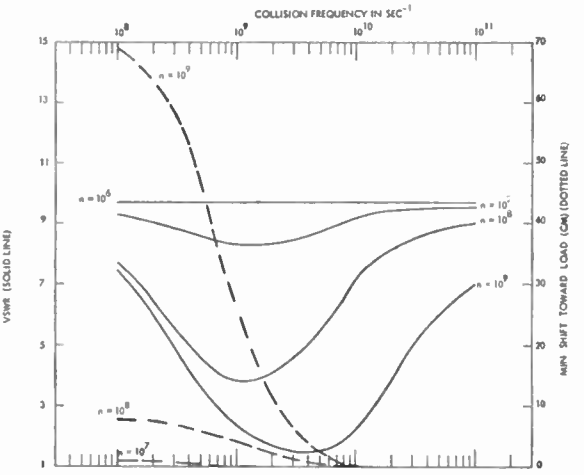

Fig. 6—VSWR and shift of minimum for 25 ft PF RG87A coaxial cable in an ionized gas for different electron densities.

In terms of σ and K, the characteristic impedance Z_1 is

$$Z_1 = Z_1' - jZ_1'' \tag{6}$$

with

$$Z_1' = \frac{0.707 Z_0}{\sqrt{K[1 + (\omega\sigma/K\epsilon_0)^2]}} \sqrt{\sqrt{1 + (\omega\sigma/K\epsilon_0)^2} + 1} \tag{7}$$

$$Z_1'' = \frac{0.707 Z_0}{\sqrt{K[1 + (\omega\sigma/K\epsilon_0)^2]}} \sqrt{\sqrt{1 + (\omega\sigma/K\epsilon_0)^2} - 1}. \tag{8}$$

These are shown in Fig. 4. The characteristic impedance Z_0 is that for a two-bar transmission line with air dielectric:[6]

$$Z_0 = 120\pi \frac{a}{b}, \tag{9}$$

where a is the separation between plates and b is the width of the plates.

The VSWR for a transmission line with no losses is given in Fig. 5. The actual installation uses 25 feet of RG87A coaxial cable. The attenuation of this cable and 56 in of brass two-bar line is 0.012 neper per meter. The attenuation lowers the VSWR to those shown in Fig. 6. Also shown is the shift in the minimum electric field measured from the load. A shorter length of cable would yield higher VSWR readings.

Interpretation of VSWR and Minimum Shift

At high values of electron density, for n greater than 10^8, the minimum shift and the VSWR yield both electron density and collision frequency. For low values of electron density, two possibilities exist for collision frequency. More sensitive measurements are needed, but the attenuation can be determined with the aid of Fig. 6 and Fig. 3.

[6] S. Ramo, and J. R. Whinnery, "Fields and Waves in Modern Radio," John Wiley and Sons, Inc., New York, N. Y., p. 364; 1953.

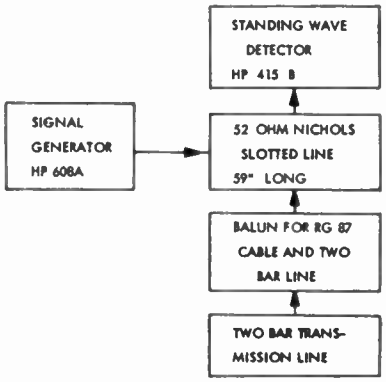

Fig. 7—Block diagram of measurement equipment.

Calibration

Distilled water was used to calibrate the two-bar transmission line. A block diagram showing the instrumentation is in Fig. 7.

The two-bar line was constructed with two waveguides so that cooling water could flow in the line when hot ionized gases passed between the bars. One end of the line was short-circuited. The other end was matched to a coaxial cable by a quarter wavelength balun. The line was immersed in distilled water at depths measured in wavelengths of the wave in water. The VSWR with three-quarter wavelengths of line in water was 1.04. For a half wavelength, it was 26. The corresponding conductivity was 3×10^{-2} mhos per meter, while the relative dielectric constant was 82. This compares with 10^{-2} and 78 from Von Hippel.[7] A one molar solution of sodium chloride gave a VSWR of 13 for all depths of liquid in the two-bar line. The attenuation for a one molar solution of salt water is so large for six or more inches of liquid that the wave is lost. The solution takes on the character of a metallic surface. Eqs. (6) and (7) reduce to

$$Z_1' = Z_1'' = 0.707 Z_0 \left(\frac{\epsilon_0}{\omega\sigma}\right). \tag{10}$$

The conductivity is readily obtained with the help of a Smith chart. The shift in the minimum can also be used with liquids of conductivities greater than that of distilled water.

[7] A. Von Hippel, "Dielectric Materials and Applications," John Wiley and Sons, Inc., New York, N. Y., p. 361; 1954.

Electrical Characteristics of a Penning Discharge*

J. C. HELMER† AND R. L. JEPSEN†, SENIOR MEMBER, IRE

Summary—**The uniform-space-charge theory of the high-vacuum, Penning discharge has been tested and supported in two experiments. In one experiment a measurement of ion energies verifies the existence of a large space-charge depression of potential along the axis of the anode cylinder. In another, the frequency of body rotation of the electron cloud is verified by allowing the cloud to interact with the structure of a split-anode magnetron. Spontaneous oscillation is obtained. The avalanche theory of the cold-cathode discharge is tested by a measurement of the noise spectrum of the discharge current. Partial confirmation is obtained, although it is finally concluded that the discharge may be dominated by other processes, such as plasma instabilities. Evidence for plasma instabilities is presented in the form of star-shaped, ion-sputtering patterns. Three possible instability mechanisms are discussed, by means of which such sputtering patterns could be formed. A useful by-product of this investigation is the discovery that a Penning "ion-gun" produces a naturally collimated, intense ion beam of sharply defined energy.**

I. Introduction

PENNING discharges have been used for ion sources, vacuum gauges, and small vacuum pumps. More recently it has been possible to construct high-speed, high-vacuum pumps containing thousands of small Penning discharge cells operating in parallel. In this respect the state of the art has reached a high degree of refinement,[1] although the electronic characteristics of the discharge itself are not too well defined. The purpose of this paper is to describe some recent experiments on the Penning discharge and to discuss the results in relation to existing theories of the discharge.

It is important to note that many different types of discharges can exist in the Penning cell, depending on the operating pressure. Much of the available literature on this discharge is concerned with a low-voltage, glow-type discharge which is observed at relatively high pressures. In the following discussion we will be concerned only with a high-voltage, high-impedance discharge which is characteristic of the cell for all pressures *below* approximately 10^{-4} mm Hg. Operation in this region is distinguished by the fact that there is little or no trapping of positive ions in the discharge so that the body of the discharge consists of a dense, negative cloud of electrons.

II. Physical Principles of the Penning Discharge

The electrode configuration for a Penning cell is shown in Fig. 1. A cylindrical anode is mounted between two cathodes and immersed in a magnetic field parallel to the axis of the cylinder. It is most easy to visualize the operation of the cell by supposing that the anode contains a cloud of electrons in perfect vacuum. The electrons are supposed to have energy less than the applied potential, so they cannot reach the cathodes. In addition the magnetic field is supposed to be so strong that the cycloidal electron orbits in the transverse plane are much smaller in diameter than the anode. Then the electrons cannot reach the anode. Consequently, the electron cloud is contained without losses, except for radiation which we neglect.

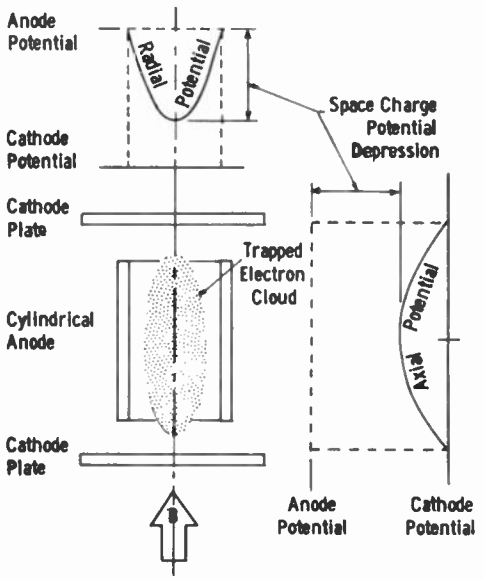

Fig. 1—Configuration of a Penning discharge.

Now suppose that a neutral molecule enters the system. This molecule will eventually be ionized by the energetic electron cloud. The ionizing electron will recover the energy it has lost by moving closer to the anode, while the ion is driven into one of the cathodes by a strong electric field, giving rise to secondary emission of electrons. In steady state, the process is described by a Townsend avalanche equation. If the mechanism of trapping secondaries is independent of pressure, then we may predict the following measurable behavior:

1) The current drawn by the cell is proportional to pressure.
2) The pumping speed of the cell in liters per second is independent of pressure.

The second conclusion really depends on another assumption, *i.e.*, that the pumping speed in molecules per second is proportional to the current. In any case these predictions have been verified over the pressure range 10^{-5} to 10^{-8} mm Hg for a cell of approximately the following dimensions and operating conditions:[1]

* Received by the IRE, August 21, 1961.
† Varian Associates, Palo Alto, Calif.
[1] R. L. Jepsen, "Important characteristics of a new type Getter-ion pump," *Le Vide*, vol. 80, pp. 80–94; March-April, 1959.

anode diameter	$\frac{1}{2}$ in
anode length	$\frac{7}{8}$ in
cathode spacing	$1\frac{1}{4}$ in
magnetic field	1200 gauss
anode voltage	3000 v.

Thus it is reasonable to state that the principal feature of the discharge is a trapped cloud of electrons whose charge is approximately constant and independent of pressure. By virtue of its motion this cloud sweeps out the volume of the system at a constant rate, in a manner analogous to the rotor of a mechanical forepump, disposing of the molecules by ionization. To consider what happens to the molecules after ionization would involve the description of pumping mechanisms which are described elsewhere and are outside the scope of this article.[2]

An additional confirmation of this viewpoint is that for different gasses at the same pressure, the current drawn is approximately proportional to the ionization cross section. Thus the charge of the electron cloud is substantially independent of gas type, as well as of pressure.

In order to account for the current drawn at a given pressure, in a given gas, one of the authors has shown that the number of trapped electrons must be such as to cause a space-charge depression of potential along the axis of the anode cylinder that is a substantial fraction of the applied voltage.[3] The maximum number of trapped electrons is determined by the condition that the potential depression on the axis of the anode shall not exceed the applied voltage, otherwise electrons will drain to the cathodes. In the absence of a detailed knowledge of the potential profile within the anode, we may assume the existence of uniform charge density. For this case the maximum amount of negative charge Q that may be trapped in a cylindrical anode at a voltage V relative to the cathodes is given by

$$Q = 1.11V \times 10^{-12} \tag{1}$$

coulombs per centimeter of anode length. This charge is independent of the anode diameter. The value of the magnetic field depends on the anode diameter, since the condition for constant cycloidal orbit energy is $V/Bd = \text{constant}$, where V is the anode voltage, d is the anode diameter, and B is the magnetic field strength. On the other hand, the number of ionizations required for an electron to reach the anode remains invariant only if V and Bd are separately held constant. This is the condition for invariance of the Townsend avalanche equation.

The large space-charge depression of potential along the axis of the Penning cell results in strong radial electric fields within the anode which are transverse to the dc magnetic field. Consequently, the device has many of the characteristics of a crossed-field, smooth-bore magnetron. Furthermore, experiments by the authors on magnetron geometries have disclosed that magnetron cells and Penning cells have very similar characteristics. Therefore, in the interests of simplicity, it is reasonable to approach the theory of the Penning cell by way of the theory of the cold-cathode magnetron which has a simple, two-dimensional field configuration. Theories for the striking potentials of cold-cathode magnetrons have been developed by Haefer[4] and by Redhead,[5] but no theory exists for the current-voltage characteristic of a cold-cathode magnetron discharge under space-charge dominated conditions. This is the case of interest to us.

The difficulty in analyzing the space-charge limited discharge is illustrated by a discussion of the planar magnetron, shown in Fig. 2. Two planes are separated in the x direction by an amount a. The planes lie in the yz plane and are immersed in a magnetic field in the z direction. Across the planes is applied a potential V. The charge distribution is assumed to be a function of x alone. An avalanche, starting from one secondary electron at the cathode, works its way towards the anode so that the charge of electrons in an avalanche at position x is given by

$$q = e \exp \int_0^x \alpha(E)dx, \tag{2}$$

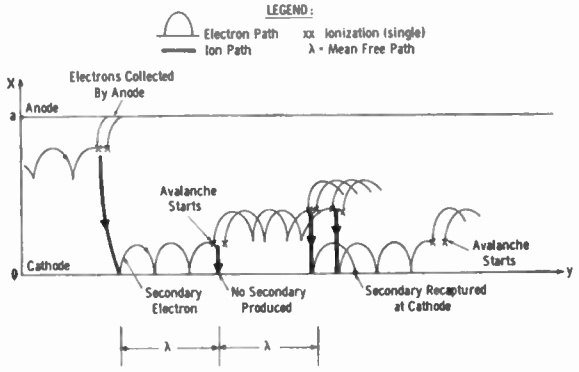

Fig. 2—Discharge in a planar magnetron.

which defines $\alpha(E)$. Multiplying this by the number of avalanches per second initiated at the cathode gives the average current at position x. The average charge density is obtained by dividing the average current by the drift velocity $v(e)$ in the x direction. Thus for the divergence equation $\nabla \cdot E = \rho/\epsilon$ we get

$$\frac{dE}{dx} = \frac{i_0}{\epsilon v(E)} \exp \int_0^x \alpha(E)dx, \tag{3}$$

[2] S. L. Rutherford, *et al.*, "On pumping mechanisms in Getter-ion pumps employing cold-cathode gas discharges at low pressures," in "Vacuum Symposium Transactions," Pergamon Press, London, Eng., p. 380; 1960.

[3] R. L. Jepsen, "Magnetically confined cold-cathode gas discharges at low pressures," submitted to *J. Appl. Phys.*

[4] R. Haefer, "Die Strom-Spannungscharakteristiken einer selbstandigen Gasentladung im transversalen Magnetfeld," *Acta Phys. Austriaca*, vol. 8, pp. 213–224; 1954.

[5] P. A. Redhead, "The Townsend discharge in a coaxial diode with axial magnetic field," *Canad. J. Phys.*, vol. 36, pp. 255–270; March, 1958.

where i_0 is the current at the cathode ($x=0$). The solution of this equation is constrained by the condition

$$\int_0^a Edx = V = \text{constant}. \tag{4}$$

In addition we must satisfy the Townsend avalanche equation

$$\Gamma(P)\left[\exp \int_0^a \alpha(E)dx - 1\right] = 1, \tag{5}$$

where $\Gamma(P)$, a function of the pressure P, is the average probability per ion of generating a secondary electron at the cathode *which succeeds in getting away from the cathode by collision with a neutral molecule*. We may expect in (3) that for every value of E at the cathode E_0 there is an i_0 such that (4) is satisfied. However, there is only one combination E_0, i_0 such that (5) is satisfied also. The solutions to (3)–(5) may be obtained with a computer if the functions $\alpha(E)$, $v(E)$, and $\Gamma(P)$ are known. The trouble is that these functions are not well known. If an electron has neither much greater nor much less than ionizing energy, then $v(E)$ is approximately the radius of the cycloidal electron orbit divided by the time between collisions, while $\alpha(E)$ is the inverse of the radius of the cycloid orbit. In our case this approximation is *not* valid, since the electric field at the cathode may be very weak due to space-charge depression. Then electrons in traversing the space between cathode and anode pass through a wide range in energy, beginning with elastic collisions and progressing through the energy required for excitation, ionizing, and multiple ionizing collisions. An additional limitation to this approach is that we have neglected cooperative phenomena, such as plasma oscillations and instabilities, which in the past have played a major role in the explanation of current drawn by magnetrons under below cutoff conditions.

In the absence of an analytic solution for the potential distribution in the interior of the magnetron or the Penning cell, we have found it convenient to assume a uniform charge distribution, leading in the case of Penning cells to a parabolic potential well in the radial direction. The radial electric field E_r gives rise to an azimuthal drift velocity equal to E_r/B such that a parabolic potential well produces a uniform rotation of the electron cloud. The measurements to be described bear in part on the assumption of uniform charge distribution. In addition we will consider the effects produced by avalanche noise and plasma instabilities.

III. The Energies of Ions Produced in a Penning Cell

If a hole is drilled in a cathode on the axis of a Penning cell, the ions that are normally incident on the area of the hole emerge and form a useful ion beam. The ion energies and the beam definition may be analyzed by collecting the beam in a Faraday cup preceded by a small aperture for exploring the transverse dimensions of the beam. When a positive voltage is applied to the Faraday collector, some of the ions may not be energetic enough to overcome the potential barrier and are turned away. Thus, the current-voltage characteristic of the collector serves to measure the energy distribution of the ion beam. Experiments of this type have produced the following results:

1) Ion Energies: The ion energy is sharply defined, with a spread of less than 10 per cent of the mean ion energy. In a standard cell, such as that described in Section II, with an anode voltage of 3000 volts, the mean ion energy is about 1000 electron volts. These ions originate along the axis of the cell and, consequently, their energy is a measure of the potential along the axis. In this case we have a space-charge depression of potential of 2000 volts, thus confirming the earlier prediction of the magnitude and importance of this depression. A typical current-voltage collector characteristic is shown in Fig. 3. The depression of the curve below the zero current axis is caused by the collection of secondary electrons which are present in copious numbers.

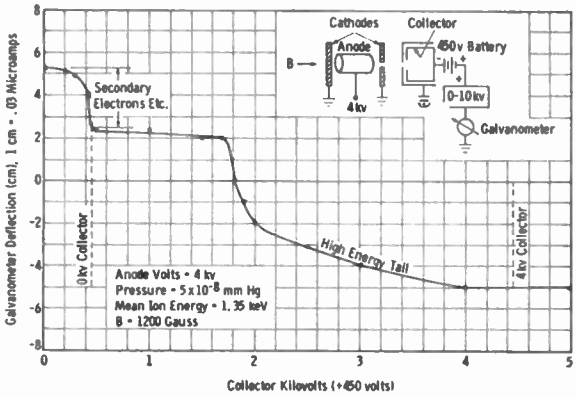

Fig. 3—Measurement of ion energy.

2) Beamwidth: The beamwidth, which was not aperture limited, generally lies between 5 and 10° as determined by the angle subtended by the half-intensity points at the beam aperture. This measurement was made in a plane about 2 in from a $\frac{1}{8}$-in diameter beam aperture. The unusual degree of self-collimation may be caused in part by beam neutralization from secondary electrons produced on the edges of the beam aperture.

3) Voltage Dependence of Ion Energies: Below an anode voltage of 4000 volts the ion energy dependence is complicated, as shown in Fig. 4. In this region the space charge is approaching the theoretical maximum given by (1). Above an anode voltage of 4000 volts the ion energy increases linearly with voltage so that relation to (1) is violated. This violation must occur since there is a limit to the space charge that can be contained by a given magnetic field strength. The condition for containment, derived from orbit analysis, is simply that

$$\frac{\omega_p^2}{\omega_c^2} \ll 1, \tag{6}$$

where ω_p is the plasma frequency and ω_c is the cyclotron frequency of the electrons. Thus, as the anode voltage increases, the axial potential depression adjusts itself so that (6) is always satisfied. This measurement points up a unique feature of the Penning discharge, *i.e.*, that as a magnetron it is able to adjust the potential of its virtual axial cathode to whatever value is best suited to the needs of the discharge.

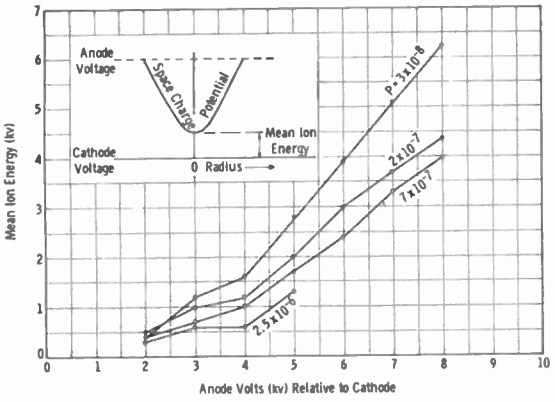

Fig. 4—Voltage and pressure dependence of ion energy.

Allis has shown that (6) is just the ratio of the mc^2 energy density of the electrons to the energy density of the magnetic field.[6]

4) Pressure Dependence of Ion Energies: It is shown in Fig. 4 that at constant anode voltage, a decrease in pressure is accompanied by an increase in ion energy, perhaps reflecting a reduction in space charge. This brings up the interesting question of whether there is some low pressure at which the discharge will go out. It is well known, for example, that Penning structures employing ring anodes tend to go out at pressures in the neighborhood of 10^{-6} mm Hg. The explanation of this behavior may be that at low pressures too many secondary electrons are recaptured at the cathodes before making the ionizing collisions which allow them to be trapped in the cloud. This is the origin of the pressure dependence of (5). On the other hand, the cylindrical anode Penning cell we have described is known to maintain a discharge to pressures as low as 10^{-12} mm Hg.[7] Our electrode configuration may be especially favorable for the generation of two-stream instabilities between the secondary electron streams and the trapped electron cloud.[8,9] Such an instability would be an efficient mechanism for the trapping of secondary electrons. In our case the instability would occur near the plasma frequency of the electron cloud, and the condition for instability is that the secondary electrons shall oscillate between the cathodes at approximately the same frequency. This condition may be met with an electron cloud of high density, such as we obtain, but perhaps not with a cloud of lower density.

5) Ion Current: A $\frac{1}{8}$-in diameter hole in a $\frac{1}{2}$-in diameter cell occupies 1/16 of the cross-sectional area of the cell. It is found, however, that the ion beam contains $\frac{1}{5}$ of the total ion current to the cathode from which it emerges. This shows that the ion current is most intense at the center of the cathode, which may be deduced easily by visual examination of the cathode sputtering pattern. Through some mechanism, about which we can only speculate, many of the ions produced throughout the volume of the cell ultimately emerge along the axis of the cell with axially directed velocities, thereby producing a narrow beam of very high intensity and well-defined energy. At a pressure of 10^{-6} mm Hg a beam current of about 1 microamp is obtained.

IV. Rotation of the Electron Cloud

A distinguishing feature of uniform charge distribution is that the electron cloud within the anode rotates with uniform angular velocity. If the space-charge depression of potential along the axis, relative to the anode potential, is equal to V_0 then the shape of the parabolic potential well is given by $V' = V_0(r/a)^2$, where a is the anode radius. Consequently, the radial electric field E_r and the angular frequency of rotation ω_r are given by

$$E_r = 2V_0 r/a^2, \qquad \omega_r = E_r/rB = 2V_0/Ba^2. \tag{7}$$

On the other hand the plasma and cyclotron angular frequencies are given respectively by

$$\omega_p^2 = 4eV_0/ma^2, \qquad \omega_c^2 = \left(\frac{eB}{m}\right)^2, \tag{8}$$

and we note that there is a simple relation among the three angular frequencies, given by

$$\omega_p^2 = 2\omega_c\omega_r. \tag{9}$$

On the basis of this uniform space-charge theory we estimate that in our standard cell, described in Section II, we have a plasma frequency of about 1000 Mc, a cyclotron frequency of 3300 Mc, and a rotational frequency of 150 Mc.

The frequency of rotation of the electron cloud was measured by splitting the anode lengthwise into two halves to form the plates of a split anode magnetron, as shown in Fig. 5. To these two plates was connected a Lecher wire resonator. Spontaneous oscillation was observed in the neighborhood of 150 Mc, and the frequency of oscillation varied in approximate proportion to V/B, where V is the anode voltage and B is the applied magnetic field, as one would predict from (7). Therefore this measurement verifies the predictions of the uniform space-charge theory.

A unique feature of this oscillator is that the electron

[6] W. P. Allis, "Motion of Ions and Electrons," *Handbuch der Physik*, Springer-Verlag, Berlin, Gottingen, Heidelberg, Germany, vol. 21, p. 386; 1956.
[7] A. Klopfer, "Die Erzeugung Von Hockstvakua mit Getter-Ionenpumpen und das Messen von sehr tiefen Drucken," *Vakuum-Tech.*, vol. 10, pp. 113–118; May, 1961.
[8] J. R. Pierce, "Increasing space charge waves," *J. Appl. Phys.*, vol. 20, pp. 1060–1066; November, 1949.
[9] A. V. Haeff, "The electron-wave tube—a novel method of generation and amplification of microwave energy," Proc. IRE, vol. 37, pp. 4–10; January, 1949.

supply is produced by ionization, the rate of which is proportional to pressure. Starting current is obtained by raising the pressure until oscillation starts in the region of 10^{-6}–10^{-5} mm Hg. The power output does not exceed a few milliwatts and further increases in pressure destroy the oscillation by collision broadening. The linewidth of the oscillation is a few megacycles.

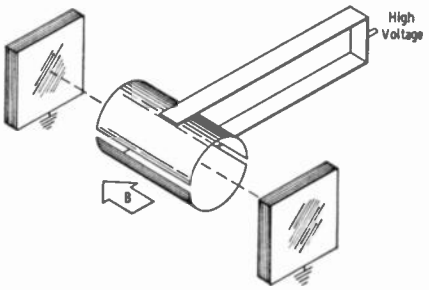

Fig. 5—Gas discharge, split-anode magnetron.

V. Avalanche Noise

If the current drawn by the Penning cell is due to the random formation of electron avalanches, as described in Section II, then this process will give rise to a Schrot noise. In the cell current a fluctuation ΔI will be observed, whose magnitude is given by the following equation

$$\Delta I/I = \sqrt{2qf/I}, \tag{10}$$

where I is the cell current, q is the charge in each avalanche, and f is the bandwidth of the noise. Furthermore, the noise spectrum will have a high-frequency cutoff given by

$$f_c \simeq 1/2\pi\tau, \tag{11}$$

where τ is roughly the width of an avalanche in time. In one set of measurements, noise of this type was found. These measurements indicated that on the average there were 10^6 electrons in each avalanche and that over the pressure range 10^{-8}–10^{-6} mm Hg the time width τ of the avalanche was given by the equation

$$\tau = 10^{-10}/P_{mm} \text{ seconds}, \tag{12}$$

where P_{mm} is the pressure in mm Hg. Eq. (12) is exactly what one would expect, since the radial rate of electron diffusion is proportional to pressure.

Unfortunately, additional work has shown that noise of this type is generally obscured by other processes, and avalanche noise seems to be an incidental rather than a characteristic feature of the discharge.

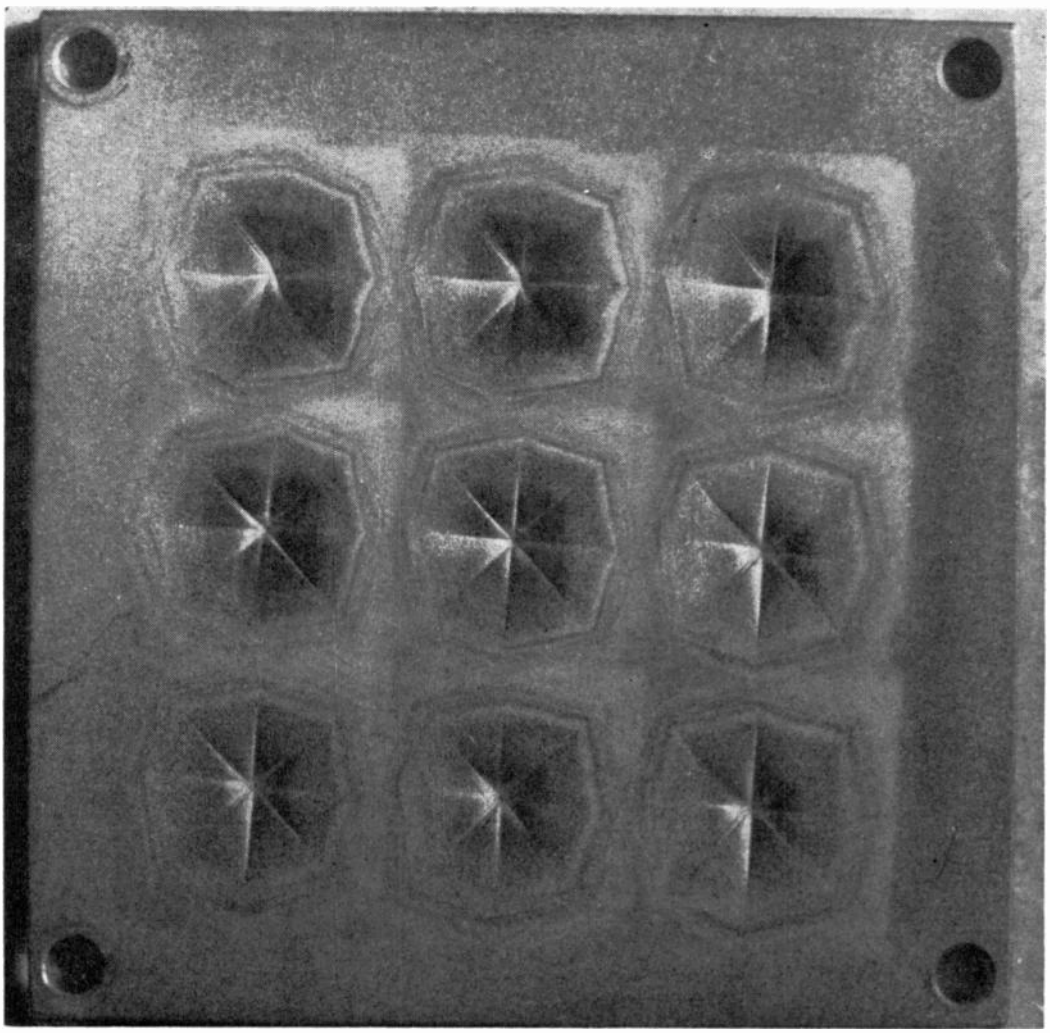

Fig. 6—Cathode sputtering pattern produced by 9 cells.

VI. Instabilities

Observation of the ion sputtering patterns on the cathodes of a Penning cell frequently show the existence of crossed or star-shaped sputtering patterns, particularly if the anode is not cylindrical. In Fig. 6 is shown a photograph of a cathode that has been bombarded by a set of nine $\frac{1}{2}$-inch-square anodes in a parallel array. An eight pointed star is sputtered out of the cathode opposite each cell with the center of the star on the cell axis. The sharp lines of the star are well-defined indentations formed by the removal of cathode material. Cylindrical cells produce only a pit in the center of the cathode, as noted in Section III, 5). If, however, a slightly elliptical cell is used, a cross is formed in the cathode such that the lines of the cross coincide with the major and minor axes of the ellipse. Visual observation has shown that these sputtering patterns are, in fact, images of an identical pattern appearing in the discharge itself. In Fig. 7 is shown a photograph of the discharge as it appears in a 2-in-square anode. This shows a pattern identical in form with the sputtering pattern from a $\frac{1}{2}$-in-square anode in Fig. 6. The luminous lines of the discharge lie in radial planes containing the axis and can be observed only by looking through a transparent screen cathode directly along the axis of the cell.

These remarkable patterns are believed to arise from an instability of the discharge which occurs in the pressure range 10^{-5}–10^{-4} mm Hg. We may speculate on the mechanism of such an instability.

Instabilities may arise from electrostatic oscillations of the electron cloud of the form discussed by Trivelpiece and Gould.[10] In this case the Penning anode will act as an open-circuited section of waveguide containing an electron cloud. Oscillations may be set up with a sinusoidal variation in amplitude along the longitudinal axis and a distribution of radial nodes not unlike those formed in a vibrating plate. The frequencies of such oscillations will lie somewhat below the plasma frequency. The star-shaped sputtering patterns may be the images of such radial nodes, where the image itself is formed by RF gradient focusing of the ions. In general, the function of anode asymmetry is to lock the azimuthal position of the instability to the laboratory coordinates.

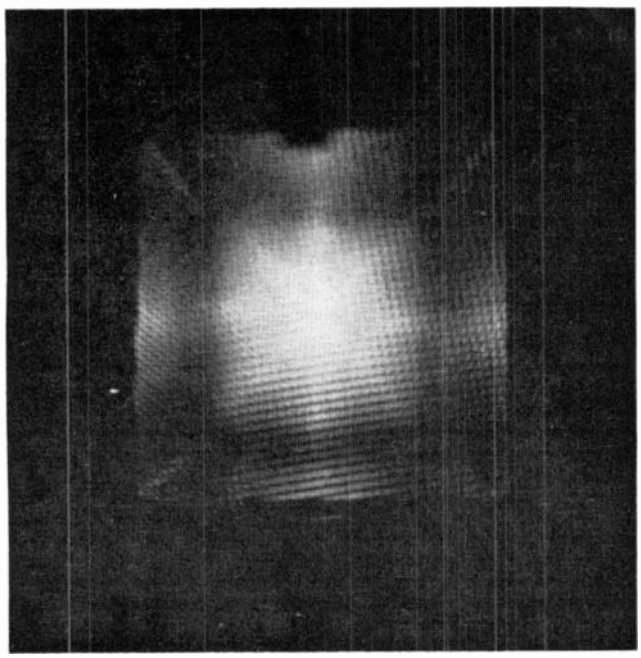

Fig. 7—Appearance of the discharge as viewed along the axis of a 2-in-square anode. Pressure $\simeq 10^{-4}$ mm Hg.

Another form of instability which arises in crossed field devices has been discussed by Bunemann,[11] and by MacFarlane and Hay.[12] This instability gives rise to the formation of radial spokes in the discharge which may or may not be rotating. If, as in our case, the spokes are not rotating, the instability condition is approximately that the electron cloud rotates through these spokes at a rate such that the frequency of perturbation in the frame of reference of the electron is equal to the local plasma frequency.

Pease[13] discussed a third form of instability, giving rise to radial spokes of oscillating amplitude. In one form of his instability the radial-oscillation frequency is equal to the cyclotron frequency/$\sqrt{2}$ and the resulting spokes would produce a cross-shaped sputtering pattern such as we observe in elliptical cells. At this time, however, the true mechanism for our instability is unknown.

VII. Conclusions

The large space-charge depression of potential on the axis of a Penning discharge has been measured. This measurement verifies the prediction that the anode traps a very dense cloud of electrons and that space-charge fields play a dominant role in the behavior of the discharge. The theory of uniform distribution of space charge has been supported by a measurement of the angular drift frequency of the electron cloud. A Schrot type of avalanche noise may occur in Penning discharges, but it is not essential to the existence of the discharge. Therefore the operation of the discharge cannot be explained by simple diffusion theory alone. Radial instabilities of unknown origin appear in the high-pressure end of the high-vacuum discharge region. These are responsible for the star-shaped sputtering patterns that have been observed on the cathodes of the discharge cell. The high-vacuum Penning discharge may be used as an ion gun, in which case it produces a naturally collimated, very intense ion beam of well-defined energy.

VIII. Acknowledgment

The authors are particularly indebted to S. L. Rutherford, S. L. Mercer, and E. Hodges for their assistance in the completion of this work.

[10] A. W. Trivelpiece and R. W. Gould, "Space charge waves in cylindrical plasma columns," *J. Appl. Phys.*, vol. 30, pp. 1784–1793; November, 1959.

[11] O. Bunemann, "A small amplitude theory for magnetrons," *J. Electronics and Control*, vol. 3, pp. 1–50; July, 1957.

[12] G. G. MacFarlane and H. G. Hay, "Wave propagation in a slipping stream of electrons," *Proc. Phys. Soc. (London) B*, vol. 63, pp. 409–427; May, 1950.

[13] M. C. Pease, "Time dependent electron flow," *J. Appl. Phys.*, vol. 31, pp. 70–76; January, 1960.

Generation and Application of Highly Ionized Quiescent Cesium Plasma in Steady State*

J. Y. WADA†, MEMBER, IRE, AND R. C. KNECHTLI†, MEMBER, IRE

Summary—**A method of generating highly ionized quiescent plasmas in steady state is presented. Plasma densities in excess of 4×10^{12} ions/cm^3 at greater than 90 per cent ionization have been obtained. The validity of double probe measurements of plasma density and temperature in the presence of a dc magnetic field up to about 1500 gauss has been established. The recombination coefficient α of highly ionized cesium plasmas up to densities exceeding 4×10^{12} ions/cm^3 has been found to be equal to or less than 3×10^{-11} cm^3/sec, at least an order of magnitude smaller than the lowest value published to date. A valuable technique for basic as well as applied plasma research has thus been developed and directly applicable results obtained.**

I. Introduction

THE most commonly used method of generating a laboratory plasma is by means of electrical discharges. Typical characteristics of such plasmas are low percentage ionization, instabilities, and oscillations. Furthermore, a thermal equilibrium condition of the electrons and ions is not normally obtained in steady-state operation. For these reasons, a need for a new method of generating highly ionized quiescent plasmas of useful density in steady state has long been recognized. The possibility of generating a quiescent plasma by means of thermionic electron emission combined with resonance ionization (contact ionization) of cesium vapor was reported a number of years ago.[1] The plasma produced by this new method overcomes the aforementioned difficulties encountered with electrical discharges; such a plasma then makes possible a systematic and conclusive investigation of the properties of fully ionized quiescent plasmas. More recently, the results of experimental investigations of such a cesium plasma at a number of laboratories have been reported.[2–5] A brief account of the experimental results obtained at our laboratory was published earlier.[6] The purpose of the present paper is to give a more extensive and detailed description of the apparatus and of those experimental results obtained since the earlier publication.

* Received by the IRE, September 5, 1961. Part of this work was supported by the Office of Naval Research and by the Advanced Project Research Agency.

† Hughes Research Labs., Malibu, Calif.

[1] R. C. Knechtli and W. Knauer, "Low-temperature high-density plasmas," *Bull. Am. Phys.*, ser. 2, vol. 3, p. 81; January, 1958.

[2] R. C. Knechtli and J. Y. Wada, "Generation and measurement of highly ionized quiescent plasmas in steady state," *Bull. Am. Phys.*, ser. 2, vol. 5, p. 366; June, 1960.

[3] R. B. Hall and G. Bekefi, "Cesium plasma," *Bull. Am. Phys.* ser. 2, vol. 5, p. 314; April, 1960.

[4] G. S. Kino, "Thermal Generation of a Fully Ionized Plasma," LMSD Fifth Annual Symp.; December 16–17, 1960.

[5] N. Rynn and N. D'Angelo, "Device for generating a low temperature highly ionized cesium plasma," *Rev. Sci. Instr.*, vol. 31, pp. 1326–1333; December, 1960.

[6] R. C. Knechtli and J. Y. Wada, "Generation and measurement of highly ionized quiescent plasmas in steady state," *Phys. Rev. Letters*, vol. 6, pp. 215–217; March, 1961.

II. Generation of Highly Ionized Quiescent Plasma

A quiescent highly ionized cesium plasma is generated and maintained in steady state in the apparatus sketched in Fig. 1. This apparatus consists of two plasma emitters facing one another and immersed in a homogeneous axial uniform magnetic field as shown by B_0 in Fig. 1. Each plasma emitter consists of a tantalum disk heated to thermionic emission temperature by electron bombardment from an auxiliary cathode. In order to ensure an electric field free plasma region, the auxiliary cathode is completely isolated from the plasma. The whole device, including the hot tantalum plates, is placed in a vacuum tight enclosure and thoroughly outgassed at an elevated temperature. The pressure of background gases other than cesium vapor is kept at all times on the order of 10^{-7} mm Hg or less in order to keep the effect of these gases negligible. Such a condition is maintained with the use of a vac-ion pump attached to the apparatus. Although this vac-ion pump is operated only when the cesium vapor pressure is lowered by cooling the enclosure wall to subzero temperatures, and though it is turned off during experiments to avoid pumping of cesium, the background gas pressure does not exceed the order of 10^{-7} mm of Hg at any time. The cesium vapor pressure is controlled by admitting an excess of cesium metal into the apparatus after a thorough outgassing, and by accurately controlling the temperature of the enclosure walls. A direct measurement of the cesium vapor pressure is made during the operation by measuring the saturation Cs^+ ion emission from a hot tungsten filament installed in the enclosure.

In the apparatus of Fig. 1, ions are emitted by contact ionization of the cesium on the hot tantalum disks; simultaneously, electrons are emitted thermionically from the same disk. Thus, plasma is continuously generated at both ends of the plasma column at a rate controlled by the neutral cesium vapor pressure. Since these hot tantalum disks facing each other act as plasma emitters, there is no loss of plasma at either end of the plasma column. Further, a relatively modest dc magnetic field (of the order of a few hundred gauss) is sufficient to make plasma diffusion in the radial direction negligible. This technique results in a well-defined quiescent plasma column, as indicated in Fig. 1.

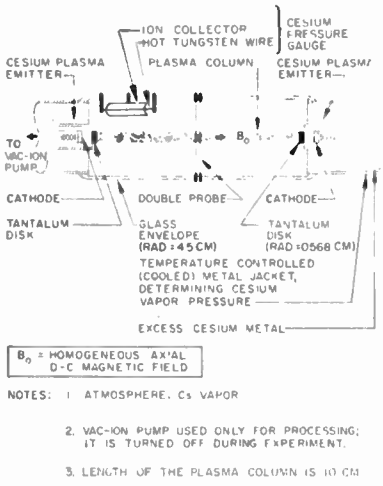

Fig. 1.

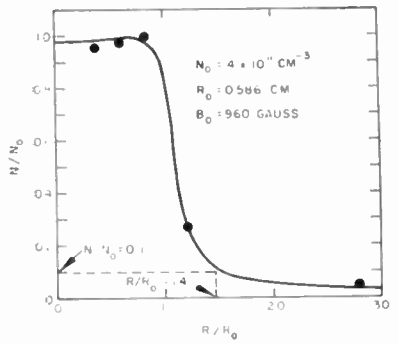

Fig. 2.

Langmuir probes were used to measure the plasma characteristics (ion density, electron temperature) because of the inherent simplicity of the probe technique. These probes were used as double probes, in order to minimize the perturbation introduced by them in the plasma; their dimensions also were kept relatively small. Such double probes were installed at the midplane between the two emitters. Each set consists of two 0.025-mm-diameter tungsten wires spaced approximately 3 mm apart and connected with small springs to the tungsten pins sealed on through the glass envelope. One set is placed near the axis of the plasma column; the other set is located a short distance away from the main plasma column. Because of the presence of a dc magnetic field, the validity and interpretation of this double probe method of measurement could be subject to question. Our experimental results described in Section IV did, however, substantiate our theoretical expectation that double probe measurements, even in the presence of a dc magnetic field up to at least 1500 gauss, are reliable under the conditions of our measurements (probe dimensions, spacing, and sheath thickness—all smaller than the ion cyclotron radius).

Using these probes, the characteristics of the emitter and some properties of the cesium plasma generated in this apparatus have been investigated. The results are summarized below.

A. Radial Density Distribution

For a first-order evaluation of the radial density distribution of the plasma column generated in the apparatus shown in Fig. 1, this apparatus was used with one plasma emitter operating, the other being kept cold. The angle of the dc magnetic field with respect to the axis of the tube was then continuously changed so as to sweep the plasma column across the probes (three fixed probes at different radial positions were used in this experiment). The probe measurements of plasma density as a function of magnetic field orientation yielded the profile shown in Fig. 2. Typically, the plasma density at the radial distance beyond $1.4R_0$ (R_0 is the radius of the emitter) is smaller than one-tenth the density near the center of the plasma column.

B. Effect of Emitter Temperature on Stability of Plasma

In Fig. 3 the effect of the emitter temperature on the plasma density is shown for a fixed neutral cesium vapor pressure. At sufficiently high emitter temperatures, the rate of the thermionic electron emission exceeds the rate of ion generation; then the plasma density is dependent only on the cesium vapor pressure and is nearly independent of the emitter temperature. On the other hand, if the emitter temperature is made lower, so that the rate of ion generation is greater than the thermionic emission rate, then the rate of plasma generation will be limited by the rate of electron emission. This is borne out by the measurement of plasma density vs emitter temperature shown in Fig. 3. This measurement indeed indicates that for $J_- < J_+$ (*i.e.*, $T < 2000°$K in Fig. 3),

$$n_+ = n_- = \frac{2J_-}{ev_+},$$

where J_+ and J_- are respectively the electron saturation current density[7] and ion saturation current density available at each plasma emitter. (The factor two arises from the fact that two plasma emitters are operating.)

At relatively low temperatures, a positive space-charge sheath on the thermionic emitter surface is formed as a result of excess ion generation. Then the thermionic electrons are accelerated across the positive ion space-charge sheath and are therefore expected to gain energy. This excess energy may manifest itself either in form of noise, fluctuations, oscillations, excess electron velocity, or excess electron temperature. In our experiments, fluctuations of the potential of a floating

[7] H. A. Jones and I. Langmuir, "The characteristics of tungsten filament as functions of temperature," *GE Rev.*, vol. 30, Part I, pp. 310–319; June, 1927; Part II, pp. 354–361, July, 1927; Part III, pp. 408–412, August, 1927.
The experimental data given in Section II-B has been obtained with a tungsten plasma emitter. The general discussion and conclusion of this section, however, also do apply to tantalum emitters with an appropriate translation of the temperature scale by approximately 120°K towards lower temperatures.

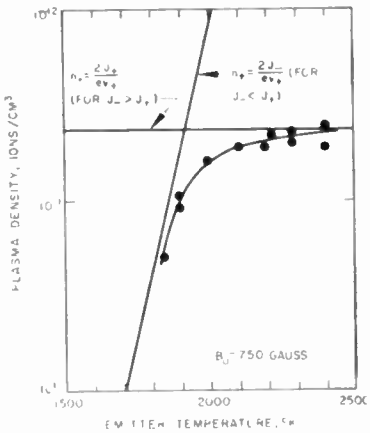

Fig. 3.

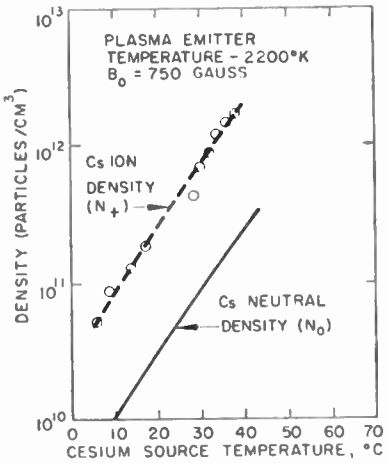

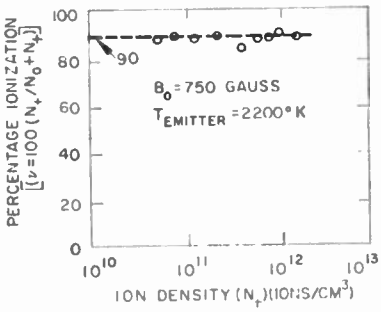

Fig. 4.

probe were actually observed when an ion sheath was present at the plasma emitters (excess ion emission; $T<1900°K$ in Fig. 3). These fluctuations were observed with a high frequency and sensitive oscilloscope connected to the probe. They occurred at frequencies approximately in the range of 10 to 100 kc with an amplitude on the order of 0.04 v, decreasing as the temperature increased. These fluctuations disappeared when the emitter temperature was raised to the point where no more ion sheath was formed at the emitter ($J_{-sat} > J_{+sat}$: $T>1900°K$ in Fig. 3).

C. Measurement of Degree of Ionization

The results of a typical set of measurements of cesium plasma density and neutral cesium density are shown in Fig. 4. The corresponding values of the degree of ionization ν of the plasma are shown on the same figure. It may be observed that up to a density higher than $n_+ = 10^{12}$ ions/cm³, a plasma with a degree of ionization $\nu \approx 90$ per cent has been obtained. It is interesting to point out that the value $\nu = 90$ per cent corresponds approximately to the degree of ionization expected by taking into account the plasma loss on the probes as long as the volume recombination is negligible. At higher densities volume recombination should be more pronounced and reduce the degree of ionization of the plasma with increasing plasma density. In fact, by the measurement of the percentage ionization, the value of the recombination coefficient may be determined experimentally. The discussion of this experiment and the results obtained will constitute the next section.

It should be noted that a highly ionized quiescent plasma can easily be generated with the technique described here. Such a plasma in steady state constitutes a valuable experimental tool to the investigation of the properties of highly ionized plasma in basic as well as applied plasma research. In the following sections, two of many possible applications of such quiescent cesium plasmas are considered in some detail.

III. Measurement of Recombination Coefficients

An immediate application of our highly ionized quiescent cesium plasma is the measurement of the recombination properties of ionized cesium ions, *viz.*, the coefficient of recombination. As was mentioned earlier, the plasma diffusion in the radial direction may be made negligible with the application of a dc magnetic field. Thus, in the presence of an axial dc magnetic field, the first-order cause for plasma loss in this plasma column is volume recombination, together with plasma losses on the small probes used to measure the plasma density and temperature. The plasma loss on the probes is readily taken into account, and its effect on the degree of ionization of the plasma is, to a first-order approximation, independent of plasma density. The degree of ionization of the plasma then is determined by the condition that the rate of cesium ion generation on the plasma emitters be equal to the rate of cesium ion loss by volume recombination and by surface recombination on the probes. Since the rate of volume recombination is proportional to the recombination coefficient, the latter is found directly from the measurement of the degree of ionization as a function of plasma density. More specifically, we can write the rates of plasma generation and plasma surface and volume recombinations in the following manner:

$$\left(\frac{\partial N_+}{\partial t}\right)_{\text{gen}} = (2A_e)\left(\frac{\bar{v}_0}{4}\right)n_0 \text{ (rate of plasma generation)}$$

$$\left(\frac{\partial N_+}{\partial t}\right)_{\text{probe}} = (A_p)\left(\frac{\bar{v}_+}{4}\right)n_+ \text{ (rate of plasma losses to probes)}$$

$$\left(\frac{\partial N_+}{\partial t}\right)_{\text{volume}} = \alpha n_- n_+ A_e L = \alpha n_+^2 A_e L \text{ (total volume recombination),}$$

where

$n_- = n_+ =$ plasma density
$n_0 =$ cesium neutral density
$2A_e =$ total combined area of two emitters (A_e is approximately equal to the plasma column cross-sectional area)
$A_p =$ total effective area of probes (including the ion sheath effects)
$\bar{v}_0/4 =$ average thermal velocity of neutral cesium directed toward the plasma emitter surface
$\bar{v}_+/4 =$ average thermal velocity of the positive cesium ion directed toward the effective probe surface
$L =$ distance between two plasma emitters.

Equating the rate of cesium ion generation on the emitter to the rate of cesium ion losses by volume recombination and on the probes, the recombination coefficient can be obtained explicitly in terms of measurable quantities,

$$\alpha = \frac{\bar{v}_0}{2Ln_+}\left[\frac{1-\nu}{\nu} - \frac{A_p\bar{v}_+}{2A_e\bar{v}_0}\right],$$

where $\nu = n_+/(n_+ + n_0)$ is the measured degree of ionization.

In an apparatus of the type sketched in Fig. 1, a plasma column with density up to about 4×10^{12} ions/cm^3 has been generated and sustained between two hot tantalum emitters which are spaced 10 cm apart. The corresponding degree of ionization (as shown in Fig. 4) at the density of 4×10^{12} ions/cm^3 yielded with the above relation an upper limit for the volume recombination coefficient α of

$$\alpha \leq 3\times10^{-11}\ \frac{\text{cm}^3}{\text{sec}}.$$

To evaluate the significance of this result, it is appropriate to compare it with the measured values of α reported to date in the literature[8,9] and with the values which may theoretically be expected.

The values published to date[8,9] for α all are larger than our measured limit $\alpha \leq 3\times10^{-11}$ cm^3 sec^{-1}. (The lowest reported value is that of 3×10^{-10} cm^3 sec^{-1} given by Mohler.[8]) Insofar as dissociative recombination was invoked in the published experiments[8,9] to explain these relatively high values of α, the fact that our experiment leads to lower values of α is not too surprising. In our experiment, the high degree of ionization and low prevalent neutral density should greatly reduce the probability of formation of molecular ions and, therefore, of dissociative recombination.

The minimum value of a α to be theoretically expected corresponds to pure radiative recombination and is about equal to 10^{-12} cm^3 sec^{-1} at an electron temperature of 2000°K. This is not inconsistent with the result of our measurements.

Finally, considering the collision of two electrons with one ion in a highly ionized plasma leads to the recombination theory recently proposed by D'Angelo.[10] This should apply to our experimental conditions; for an electron temperature $T = 2000$°K and an electron density of $n_- = 4\times10^{12}$ cm^{-3}, this theory predicts $\alpha \cong 10^{-11}$ cm^3 sec^{-1}, a value which is also consistent with our measurements so far.

To gain a better understanding of recombination in a highly or fully ionized plasma, a measurement of the actual value of α rather than a determination of an upper limit still is called for. This means a modification of our apparatus for measurements at higher plasma densities and cesium vapor pressures. These modifications are presently being undertaken. At the same time, because of the apparently very low value of α, the generation of a highly ionized quiescent plasma in steady state up to densities of the order of 10^{14} cm^{-3} in large volumes may be expected with the type of apparatus shown in Fig. 1. Even higher densities may be feasible in smaller volumes.

IV. Validity of Double Probe Measurements in a DC Magnetic Field

Because double probes are convenient to use with the quiescent cesium plasmas considered here, it was found desirable to verify the validity of double probe measurements in presence of a dc magnetic field. Indeed, while the double probe methods of plasma density and temperature measurements in the absence of magnetic

[8] F. L. Mohler, "Recombination of ions in the afterglow of a cesium discharge," *J. Res. NBS*, vol. 19, pp. 447–456; 1937.
[9] P. Dandurand and R. B. Holt, "Electron density and light intensity decay in cesium afterglows," *Phys. Rev.*, vol. 82, pp. 278–279; April, 1951.
[10] N. D'Angelo, "Recombination of ions and electrons," *Phys. Rev.*, vol. 121, pp. 505–507; January, 1961.

field are commonly accepted,[11] their interpretation in the presence of a dc magnetic field has been subject to question.[12] It is reasonable to assume, however, that as long as the ion cyclotron radius is larger than sheath thicknesses and probe dimensions, the effect of the magnetic field on double probe characteristics may be neglected in a double probe measurement. This statement is based upon the following consideration. As long as the ion cyclotron radius is relatively large, neither the shape of the ion sheath around the floating double probes, nor the ion saturation current to these probes should be greatly affected by the magnetic field; hence, the plasma (ion) density measurements should, to first order, remain unaffected. The rate of electron collection in the retarding field of the floating probes should not be greatly affected by the magnetic field either; even though the electron cyclotron radius may be small, one degree of freedom (in the direction of the magnetic field) remains unperturbed for the electron motion. Hence, the double probe measurement of electron temperature (obtained from the rate of electron collection) should not be greatly affected by the magnetic field. The experimental results presented here substantiate these assumptions.

In the present measurements, plasma density and temperature are measured by means of double probes and interpreted according to classical double probe theory[11] as if no dc magnetic field were present. The plasma density thus obtained from the double probes is then compared with that obtained from a microwave cavity (resonant frequency shift) measurement; the electron temperature from the probes is compared with the pyrometrically measured temperature of the plasma emitter. The prior comparison of the plasma electron temperatures with the plasma emitter temperature by measurements of the mean cyclotron radius had shown these two temperatures to be the same within measuring accuracy for the conditions of the experiment described below.[13]

The cesium plasma used in the present measurements was generated in the apparatus sketched in Fig. 5. A drifting cesium plasma column was formed which extended through the length of a tubular glass envelope up to an end plate. The latter was used mainly to properly align the dc magnetic field. Two sets of double probes are mounted on the glass envelope. The distance between the two sets of probes is sufficient for insertion of an appropriate microwave cavity between them; however, this distance is small compared with the total length of the plasma column in order to a have uniform

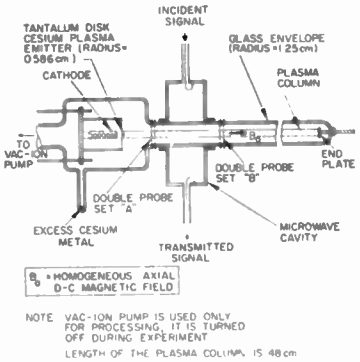

Fig. 5.

density over the measured region. Since the plasma considered was well defined and in steady state, the instrumentation was very simple. For the microwave density measurements, as shown in Fig. 5, an *S*-band microwave cylindrical cavity with a proper TM_{010} resonant mode was placed in between the two sets of double probes, over the glass envelope which contained the steady-state plasma column. Since the TM_{010} mode contained only axial and no radial electrical fields (except for the fringe field due to the holes on the cavity end plates), the microwave plasma density measurement would be essentially independent of the applied magnetic field strength.

Each set of double probes consisted of two 0.025-mm-diameter tungsten wires spaced approximately 3 mm apart and welded on to the tungsten pins sealed on through the glass envelope. Two sets of probes were used to determine whether an axial density gradient existed in the plasma column along the cavity interaction region. The double probe plots obtained from these two sets of probes are practically identical for magnetic fields above 300 gauss, thus showing, as expected, negligible plasma density gradient along the microwave cavity.

The measurements were made over the range of magnetic field extending from 300 gauss to 1500 gauss with a plasma emitter temperature (pyrometrically measured temperature of hot tantalum disk) at about 2100°K and with plasma densities between 10^{10} and 10^{11} electrons /cm^3. The emitter temperature was made sufficiently high so that 1) the rate of thermionic electron emission would exceed the rate of ion emission; 2) the possible formation of a positive ion-space charge is eliminated; and 3) the temperature of electrons in the plasma is essentially equal to the emitter temperature. Under these conditions, and with the probe dimensions and spacings given above, sheath thickness, probe dimensions, and probe spacings were small compared with ion cyclotron radius. Double probe characteristics were recorded on an *x-y* recorder; a typical characteristic is shown in Fig. 6. These probe characteristics were interpreted according to the classical theory of double

[11] E. O. Johnson and L. Malter, "A floating double probe method for measurements in gas discharges," *Phys. Rev.*, vol. 80, pp. 58–68; October, 1950.
[12] A. Gutherie and R. K. Wakerling, "The Characteristics of Electrical Discharges in Magnetic Fields," McGraw-Hill Book Co., Inc., New York, N. Y., p. 30; 1949.
[13] W. Knauer, private communication.

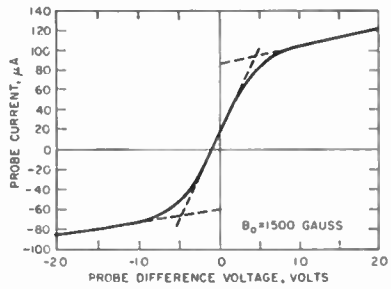

Fig. 6.

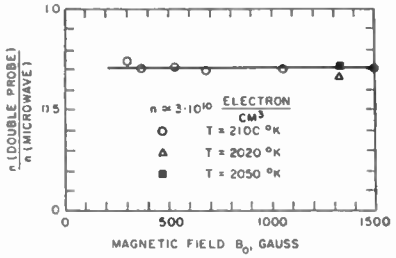

Fig. 7.

probes in absence of magnetic fields.[11] Because of the small probe diameter, the effect of sheath thickness had to be taken into account;[11] this was also done under the assumption that the effect of magnetic field on sheath thickness was negligible, the sheath being an ion sheath controlled by ion current flow over a distance small compared with ion cyclotron radius. The radius of the plasma column was assumed to be the same as the emitter radius.

The plasma density measurements performed simultaneously with the double probes and with the microwave technique are compared in Fig. 7. Agreement within 30 per cent is shown throughout the entire range of magnetic field used in the experiment. The fact that the discrepancy of 30 per cent between the two measurements is independent of magnetic field indicates a systematic rather than magnetic field dependent error.

The electron temperature of the plasma obtained from the probe measurements was compared with simultaneous pyrometric measurements of the plasma emitter temperature (hot tantalum disk), the latter having already been found equal to the electron temperature of the plasma. The result is given in Table I and shows agreement within 10 to 20 per cent.

The results shown in Fig. 7 and Table I lead to the conclusion that double probe measurements of plasma density and temperature are reliable and are not noticeably affected by the presence of a dc magnetic field, at least under the conditions of the experiments reported above where sheath thickness, probe dimensions, and probe spacing were small compared with ion cyclotron radius.

TABLE I

PLASMA TEMPERATURE MEASUREMENTS

Magnetic Field	Plasma Temperature, °K	
B_0, gauss	Double Probe	Pyrometric
300	2450	2100
375	2300	2100
525	2450	2100
675	2300	2100
1050	2360	2100
1350	2170	2020
1350	2250	2120
1500	2450	2100

V. Conclusion

In conclusion it may be stated that the usefulness of a simple technique for generating highly ionized quiescent plasmas of reasonably high density in steady state has been demonstrated, that the validity of double probe measurements in the presence of dc magnetic fields up to at least 1500 gauss has been verified, that a novel and direct technique for the measurement of the recombination coefficient of cesium plasmas has been developed, and that this coefficient has been found so far to be $\leq 3\times10^{-11}$ cm^3 sec^{-1} up to plasma densities on the order of 4×10^{12} ions/cm^3.

VI. Acknowledgment

The writers wish to thank W. Bernstein, Drs. A. Fafarman and W. Knauer for helpful discussions, and Dr. A. Fafarman for his contribution to the earlier part of this work. Acknowledgment is extended also to A. W. Robertson for his able assistance in the construction and operation of the experimental apparatus.

A New Approach to Thermionic Energy Conversion: Space Charge Neutralization by an Auxiliary Discharge*

W. BERNSTEIN† AND R. C. KNECHTLI†, MEMBER, IRE

Summary—**The characteristics of an auxiliary discharge thermionic energy converter are derived and compared with experimental results. It is shown that the power expended in the auxiliary discharge can be as low as 10 per cent of the power generated by the converter. Thus, efficiencies of about 25 per cent and power output densities as high as 10 w/cm² can be obtained at temperatures of about 1500°K provided that low work function anodes are developed. The specific advantages of the auxiliary discharge technique over the conventional cesium converters are discussed.**

Introduction

THE development of practical thermionic converters is under active investigation at many laboratories. Desirable requirements for a useful converter include a conversion efficiency of at least 20 per cent, a power output of at least 5 w/cm², a life of at least 1000 hours, and operation in a temperature range consistent with the intended heat source. The usual heat sources include combustion, solar, nuclear, and radioisotope; therefore, a reasonable upper limit to the operating temperature appears to be about 1800°K. In this paper, it will first be shown that it should be possible to realize the desired efficiency and power output density requirements at cathode temperatures of about 1500°K; secondly, that the techniques which have been most intensively investigated do not appear capable of satisfying all the converter requirements; finally, a new technique will be presented which appears to represent a solution to many of these problems.

Simplified expressions for the efficiency and power output density of a converter are given by

$$\eta = \frac{\phi_c - \phi_A - J_0\rho d}{\phi_c + \frac{A_r}{A_e}\sigma\frac{\epsilon T^4}{J_0}} \qquad P_0 = J_0(\phi_c - \phi_A - J_0\rho d),$$

where

ϕ_c and ϕ_A = the cathode and anode work functions, respectively,
J_0 = collected current density in a/cm²,
ρ = plasma resistivity, if a plasma is present in the interelectrode space,
d = interelectrode spacing in cm,
A_r/A_e = ratio of radiating to emitting areas,
ϵ = emissivity of the cathode, given by

$$1\Big/\left(\frac{1}{\epsilon_c} - \frac{1}{\epsilon_a} - 1\right),$$

σ = Stefan-Boltzmann constant,
T = absolute temperature.

In this expression we have obviously neglected losses associated with the heat conductivity and electrical resistance of the leads, and have assumed that the total current per diode is sufficiently small so that effects of the self-magnetic field can be ignored.

The plasma resistivity arises from interaction of the emitted electrons with ions and neutral particles in the interelectrode space. The charged particle resistivity can be evaluated from the equation derived by Spitzer,[1]

$$\rho_1 = \frac{6.53 \times 10^3 \ln \Lambda}{T^{3/2}} \Omega \text{ cm},$$

and can be reduced only by an increase in the electron temperature. The resistivity due to electron-neutral collisions is evaluated, in the temperature range, by

$$\rho_2 = \frac{(1.3 \times 10^{11})\sigma_c \Omega \text{ cm}}{f},$$

where

σ_c = electron-neutral cross section,
f = fractional ionization,

and can be reduced significantly by an increase in the fractional ionization and an increase in the electron temperature for certain gases.

In order to conveniently determine the optimum performance of a thermionic converter, the equations for efficiency and power output density have been evaluated as functions of cathode temperature in Figs. 1 and 2 for anode work functions of 1.0 and 1.8 ev respectively, under the following assumptions:

1) The output current density is 10 a/cm² at all temperatures and is equal to the temperature limited (saturation) emission current density of the cathode.

* Received by the IRE, August 16, 1961.
† Hughes Research Labs., Malibu, Calif.

[1] L. Spitzer, Jr., "Physics of Fully Ionized Gases," Interscience Publishers, Inc., New York, N. Y.; 1956.

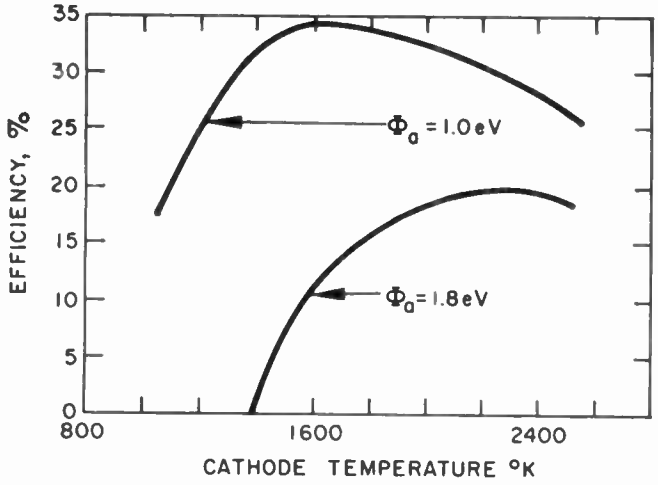

Fig. 1—Converter efficiency as a function of cathode temperature for 1.0- and 1.8-ev anode work functions.

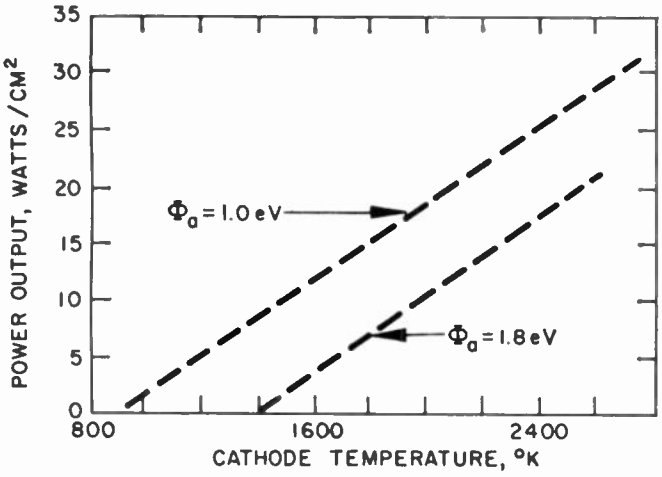

Fig. 2—Converter power output density as a function of cathode temperature for 1.0- and 1.8-ev anode work functions.

2) The cathode thermionic emission obeys the Richardson equation $J = 120T^2 \exp(-e\phi_c/\kappa T)$.
3) Therefore, the value of cathode work function is that which gives 10 a/cm² at the specified temperature.
4) The plasma resistivity is taken to be 0.2 Ω cm; at an interelectrode spacing of 0.2 cm, this corresponds to 0.04 Ω, and a resistive drop of 0.4 volt at 10 a/cm².
5) A conservative value of 0.3 is taken for the effective cathode emissivity.
6) The ratio A_r/A_c is taken to be unity.

As can be seen from Figs. 1 and 2, the desired efficiencies and power output densities are easily obtained at temperatures between 1500 and 1800°K, provided low work function anodes can be developed. The use of higher work function anodes obviously requires a shift toward higher temperature for comparable characteristics. It should be pointed out that this analysis is based on the use of the theoretical emission constant of 120 a/cm² in the Richardson equation. Since almost all materials have experimentally determined emission constants smaller than this value, it is necessary to shift all the curves to slightly higher temperatures.

At present, two approaches to the development of a practical converter have been extensively investigated. In the vacuum converter,[2] which is a low temperature device, the effects of the electron space charge are reduced by the use of very small (0.0005 inch) interelectrode spacings; even at these small spacings the current densities are only about 1 a/cm², and thus the power output density is limited to at most 1 w/cm². The second approach utilizes a plasma in the interelectrode space to eliminate the effects of the electron space charge; the plasma is produced by contact ionization of cesium vapor at the hot cathode.[3] Since the ionization efficiency of cesium vapor at a hot surface falls rapidly for values of surface work function below the cesium ionization potential (3.9 volts), the amount of cesium vapor must be increased in order to maintain the desired plasma density. This leads to a high plasma resistivity, since cesium has a large electron-neutral cross section (3×10^{-14} cm²) at these temperatures; thus, very small interelectrode spacings are required. Under certain conditions, volume ionization related to the current flow in a cesium diode has been observed to far exceed contact ionization, thus significantly reducing this resistance and the small electrode spacing requirement. The mechanism of this "arc mode" is as yet not well understood. No measurements have been published yet to indicate that this process of space charge neutralization could be acceptably economic to permit efficient converter operation at low cathode temperature. At high cesium pressures, cathodes produced by formation of partial cesium monolayers on tungsten appear to represent a solution to the cathode problem. However, the anode is then completely covered with cesium; control of the anode temperature may yield a reduction in anode work function to 1.6 ev, but further reduction appears difficult.

The use of a cesium plasma triode in which the plasma is produced by contact ionization of cesium vapor at a third high work function electrode has been described by Hernqvist.[4] Here, operation at cathode temperatures of about 1500°K at lower cesium pressures and reasonable interelectrode spacings appears possible; however

[2] H. F. Webster, "Calculation of the performance of a high-vacuum thermionic energy converter," *J. Appl. Phys.*, vol 30, pp. 488–492; April, 1959.
[3] R. L. Hirsh, "Effect of interelectrode spacing on cesium thermionic converter performance," *J. Appl. Phys.*, vol. 31, p. 2064; November, 1960.
[4] K. G. Hernqvist, "Plasma synthesis and its application to thermionic power conversion," *RCA Rev.*, vol. 22, pp. 7–20; March, 1961.

anode work functions less than 1.6 ev do not appear possible. In all cesium devices the problem of containment of high cesium pressures at high temperatures still remains serious and may lead to a significant limitation to the life of converters.

Theoretical Discussion

To escape the difficulties and limitations associated with contact ionization of cesium vapor, we have considered other methods for the production of the plasma in the interelectrode space. The use of an auxiliary discharge appears to represent an attractive method for the production of the required high density plasmas.[5] It will be shown that, in the proposed device, the power required in the auxiliary discharge to maintain the plasma represents only a small fraction of the output power of the converter. Thus, this technique offers many advantages over the cesium techniques, particularly in the temperature range below 2000°K. These advantages include: 1) that both the cathode and anode materials may be independently selected for optimum performance, 2) that the plasma resistivity is low and very small interelectrode spacings are not required, 3) that the problems associated with cesium containment are eliminated, and 4) that standard tube construction techniques can be used throughout. Consequently, the major research effort at this laboratory has been directed toward the development of auxiliary discharge thermionic converters.

One particular auxiliary discharge thermionic converter is shown schematically in Fig. 3; other configurations are obviously possible.[6] Electrons are thermionically emitted from the wires, are accelerated by the applied voltage and ionize the gas in the interelectrode space. As the plasma density increases, a positive ion sheath forms about each wire the thickness of the sheath decreases as the plasma density increases. Since the entire applied voltage appears across the sheath, which is thin at high plasma densities, the electrons are accelerated in passage through the sheath without any interactions, and enter the gas region as a monoenergetic stream. Only those positive ions which randomly strike the ion sheath will be collected to the wires; the remaining ions diffuse to both anode and cathode of the converter. The detailed analysis of this mode of discharge

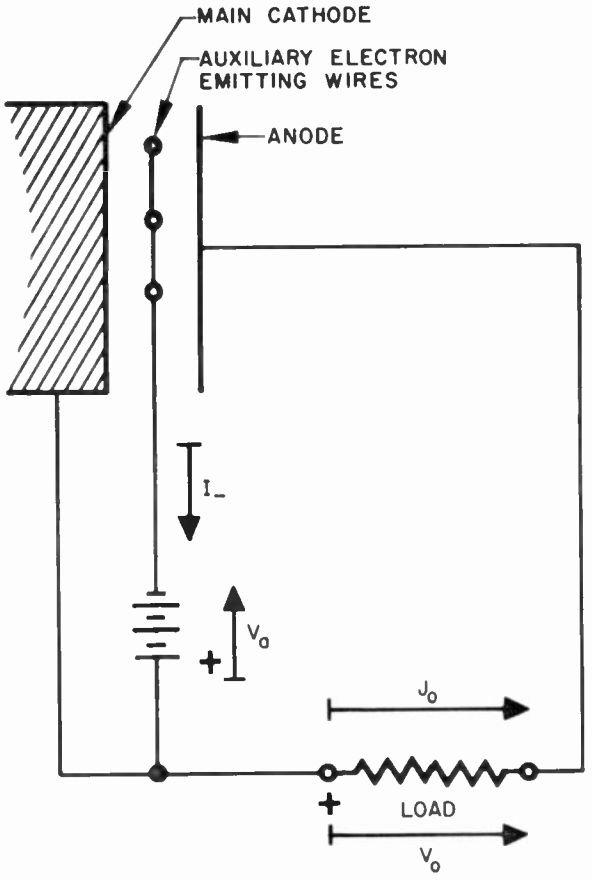

Fig. 3—Schematic of an auxiliary discharge thermionic converter.

(Langmuir mode) will be found in Langmuir and Jones.[7]

Langmuir has shown that the electron current density emitted from a surface which can be neutralized by a positive-ion current to that surface is given by

$$J_0 = \sqrt{\frac{M_+}{m_e}}\, J_+.$$

In the present configuration, the positive-ion current density at the cathode, neglecting recombination losses, is given by $J_+ = (\gamma/2) I_-$, where

γ = ionization efficiency,

I_- = wire emission current/cm² of cathode area.

The neutralized current density possible in the converter is therefore

$$J_0 = \gamma/2 \sqrt{\frac{M_+}{m_e}}\, I_-,$$

and the power required to maintain the discharge is

$$P_a = V_a I_-,$$

where

V_a = auxiliary discharge voltage.

[5] The technique of neutralizing large electron currents by an auxiliary discharge produced plasma was first investigated by I. Langmuir (I. Langmuir, "The interaction of electron and positive ion space charges in cathode sheaths," *Phys. Rev.*, vol. 33, pp. 954–989; June, 1929) and later practically demonstrated by Johnson and Webster in the Plasmatron (E. O. Johnson and W. M. Webster, "The Plasmatron, a continuously controllable gas-discharge developmental tube," Proc. IRE, vol. 40, pp. 645–659; June, 1952). Since the requirements for low-power consumption in an auxiliary discharge thermionic converter are far more stringent than in a Plasmatron, it remains necessary to use a mode of auxiliary discharge and a geometry leading to more efficient operation.

[6] While this work was in progress, an auxiliary discharge thermionic converter was described by D. Gabor, "A new thermionic generator," *Nature*, vol. 189, pp. 868–872; March 18, 1961. Although the general concepts and predicted results are similar to those described in this paper, it should be emphasized that the discharge geometry and conditions are quite different.

[7] I. Langmuir and H. A. Jones, "Collisions between electrons and gas molecules," *Phys. Rev.*, vol. 31, pp. 357–404; March, 1928.

In order to conserve the power spent in the auxiliary discharge, a high ionization efficiency, heavy ion, low operating voltage, and low recombination rate are desirable. Each of these parameters will now be discussed in detail.

It appears difficult to obtain a high ionization efficiency in pure noble gases, at electron energies only slightly above the ionization threshold. At these energies, the excitation cross section is about three times as large as the ionization cross section.[8] Since those electrons which produce excitations no longer have sufficient energy to produce ionization, only 25 per cent of the emitted electrons are available for production of the plasma. The probability of cumulative ionization appears small at the electron temperatures expected in these discharges. Thus, at pressures where the mean free path for ionization is comparable to the average path length of the electrons in the device, values of the ratio J_0/I_- of 35 for argon and 70 for xenon may be expected.

The ionization thresholds for the noble gases are 15.7 volt, 13.3 volts and 11.5 volts for argon, krypton, and xenon, respectively. It is, therefore, obvious that higher ratios of J_0/I_- can be obtained at lower voltages for Xe than for A. It should be pointed out, that at applied voltages in excess of about 25 volts, sputtering of the wires by the positive ions, which randomly strike the sheath, will occur.

Recombination may result in a serious plasma loss at high plasma densities. If the recombination process is entirely radiative, the recombination coefficients are sufficiently small that no significant loss can occur. However, dissociative recombination with large recombination coefficients has been observed to occur for all noble gases at pressures of 1 mm Hg in discharge afterglows.[9] Since the electron temperature was only about 300°K and the electron density only about $10^9/cm^3$ in these measurements, it is uncertain whether this process will occur under the present discharge conditions.

The use of mixtures which demonstrate the Penning effect,[10] such as Xe—0.1 per cent A and A—0.1 per cent Hg, appears to represent a method for improving the ionization efficiency and eliminating the possibility of dissociative recombination. In these mixtures, the energy lost in excitation is available for ionization of the contaminant gas; this can result in a significant improvement in the ionization efficiency at electron energies corresponding to the energy required for excitation of the metastable state (11.6 volts in argon). On the other hand, the total pressure of the contaminant gas is sufficiently low that the probability of formation of the molecular ion, required for dissociative recombination, is small and therefore radiative recombination should be the only important recombination process.[9] Thus, in A—0.1 per cent Hg, the ratio J_0/I_- should be about 300, at an applied voltage at 12 volts.

Experiments and Results

A series of experiments was performed to demonstrate the validity of these concepts and specifically to determine the value of J_0/I_- at low voltages and the value of plasma resistance at reasonably high density. An auxiliary discharge converter was constructed using 1 cm^2 Phillips Type B dispenser cathodes as both cathode and anode. The interelectrode spacing is 0.3 cm. For most measurements, the anode is not heated except by radiation from the hot cathode. Three 0.0008-inch tungsten wires, spaced about 0.2 cm apart, are centered in the interelectrode space and are heated by a battery. The measurements are made at a pressure of about 1 mm Hg of A; the base pressure with the cathode at operating temperature is about 2×10^{-7} mm Hg.

A typical current voltage characteristic is shown in Fig. 4. Ratios of J_0/I_- of about 100 and as high as 120 are usually observed at about 1 mm Hg, for J_0 values up to 5 a/cm^2. The ratio decreases at both higher and lower pressures presumably because of a decrease in the ionization efficiency. 500-kc oscillations, which have not been studied in detail, are sometimes observed in the saturation current region.

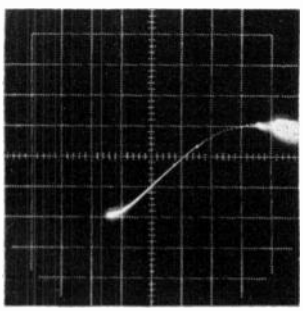

Fig. 4—Current-voltage characteristic of auxiliary discharge thermionic converter.

The current-voltage characteristic is obviously dominated by resistance; the work function difference appears to be about 0.5 volt. The contribution of the plasma resistance is determined in the following manner: It has been shown that the resistance is inversely proportional to the fractional ionization and consequently to the wire emission current. Therefore, the resistance, determined from the slope of the current-voltage characteristic, is plotted against the reciprocal of the emission current in Fig. 5. An intercept, corresponding to a fixed resistance of 0.43 Ω is found; subsequent measurements showed that 0.3 Ω is present in the leads and 0.1 Ω can easily be attributed to poor contacts in the cathode and anode structures. Under these conditions, the plasma resistance at a wire emission current of 100 ma (which should yield a density sufficient to neutralize

[8] H. S. W. Massey and E. H. S. Burhop, "Electronic and Ionic Impact Phenomena," Oxford University Press, London, Eng.; 1956.
[9] S. C. Brown, "Basic Data of Plasma Physics," John Wiley and Sons, Inc., New York, N. Y.; 1959.
[10] M. J. Druyvesteyn and F. M. Penning, "The mechanism of electrical discharges in gases of low pressure," *Rev. Moden Phys.*, vol. 12, pp. 87–174; April, 1940.

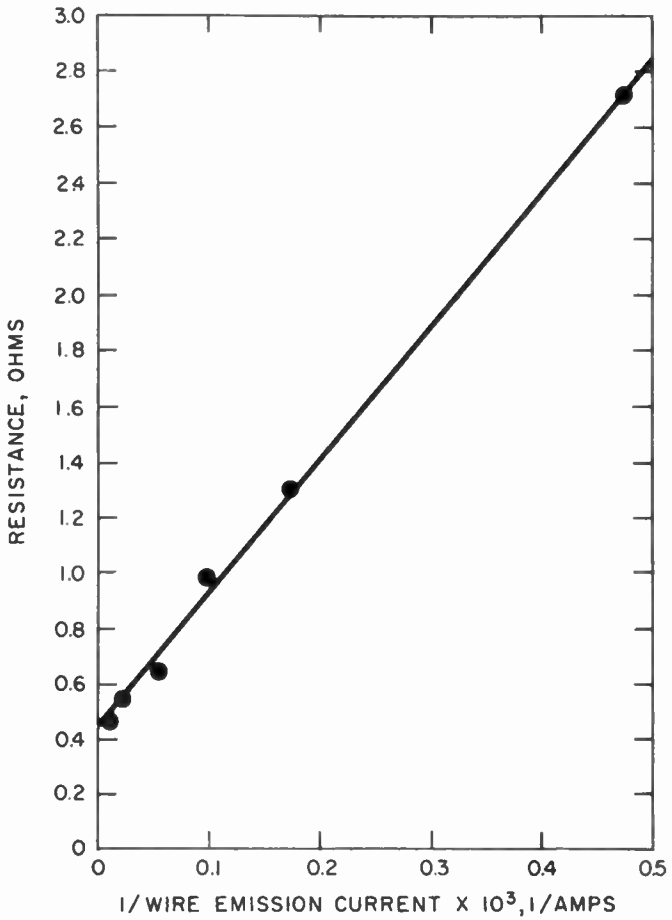

Fig. 5—Total auxiliary discharge converter resistance as a function of the reciprocal of the wire emission current. Saturation current is 3 a/cm², pressure about 1 mm Hg argon, and the auxiliary discharge voltage is 20 volts.

10 a/cm²) is only about 0.04 Ω, an entirely acceptable value. It should, of course, be pointed out that since the plasma resistance is determined by the wire emission current, the resistive drop $J_0\rho d$ is constant for all values of cathode saturation current if J_0/I_- is held constant. It is thus desirable to use as high cathode current densities as possible.

It is not clear, at present, how ratios J_0/I_- as high as 120 are possible in pure argon. It is possible that ions may be reflected from both the cathode and anode with relatively high probability, thus yielding higher plasma densities than expected. Also, the formation of the molecular ion will result in an increase of $\sqrt{2}$ in the ratio; at these densities, dissociative recombination will not introduce a serious loss for argon. It is also possible that the electron temperature may be sufficiently higher than expected so that cumulative ionization is possible. A more detailed study of the discharge processes is in progress.

It should be pointed out that the plasma density is probably not uniform across the cathode surface. The use of rectangular rather than circular cathodes will result in a more efficient use of the wire emission current and will probably lead to even larger ratios of J_0/I_-.

It is obvious that large amounts of power are required to heat the tungsten wires to the temperature required for the emission of 100 ma. However, it is believed that suitable low work function materials may be used to permit emission of this current at temperatures comparable to that provided by radiation and conduction from the hot surface of the main cathode. Direct generation of ac, at any frequency up to 10 kc, is achieved by pulsing the accelerating voltage; no change in the converter characteristics is observed in this mode of operation.

In summary, neutralized currents of 5 a/cm² have been attained at an expenditure of about 1 watt in the auxiliary discharge. If a cathode with a work function of about 2.3 ev is used in conjunction with a 1.0 ev work function anode, then an output power of 4 w/cm² at an over-all efficiency of about 25 per cent is possible at a temperature of about 1500°K. Further reduction of the power consumption in the auxiliary discharge and improvement of over-all efficiency still are possible by selecting a gas mixture more favorable than argon. In conclusion, because high efficiencies seem attainable and because the necessity for cesium vapor is obviated, it is believed that this approach represents an attractive solution to the development of long-life, efficient and practical thermionic converters capable of operating at relatively low temperatures, and capable of direct generation of ac.

Acknowledgment

The authors have had many interesting discussions with W. Knauer. The devices were constructed by E. J. Haag and E. L. Nezgoda.

Correspondence

Stability Criteria for a Tunnel-Diode Amplifier*

It is often necessary when designing tunnel-diode amplifiers to keep the generator and load isolated from direct currents. This can be accomplished with the circuit of Fig. 1 which employs the blocking capacitor C_B to isolate the simulated generator and load R_L from the bias supply. The bias supply is isolated from the tunnel diode by the inductance L_B. If L_B is large there will exist some critical value of C_B below which the circuit becomes unstable. This circuit is suited to amplification at frequencies where L_B has a high impedance. Hines[1] has treated the stability of a similar circuit at high and low frequencies. The criteria developed here are general for all frequencies.

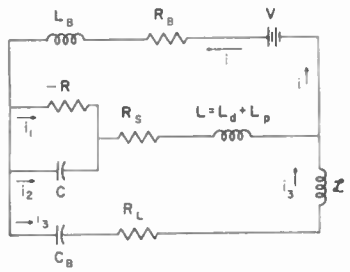

$-R$: negative resistance of tunnel diode
C: tunnel-diode junction capacitance
R_S: tunnel-diode series resistance
$L=L_d+L_p$: tunnel-diode lead inductance plus external "peaking inductance" of the shorted length of line used in the amplifier
C_B: coupling capacitance (dc blocking condenser)
L_B: bias T inductance (RF choke)
R_B: battery circuit resistance
V: bias voltage
R_L: load resistance seen by tunnel diode
$\mathcal{L}$: inductance in the load circuit

Fig. 1—Equivalent circuit of bias circuit, tunnel diode, and generator/load.

The differential equations for i, i_1, i_2, i_3 as a function of time are (see Fig. 1):

$$-Ri_1 = \frac{q_2}{C} \quad \text{or} \quad -R\frac{di_1}{dt} = \frac{i_2}{C}. \tag{1}$$

$$-Ri_1 + R_S(i_1+i_2) + L\frac{d}{dt}(i_1+i_2) = V - R_B i - L_B\frac{di}{dt}, \tag{2}$$

$$\mathcal{L}\frac{di_3}{dt} + R_L i_3 + \frac{q_3}{C_B} = V - R_B i - L_B\frac{di}{dt}, \tag{3}$$

$$i_1 + i_2 + i_3 = i. \tag{4}$$

We try solutions in which the currents i, i_3, and i_1 vary as $ae^{\lambda t}$, $be^{\lambda t}$, and $ce^{\lambda t}$, respectively. Stability is achieved if the real part of λ is negative, instability if the real part of λ is positive. We then find from (1)–(3)

$$i_1 = \frac{R_B\lambda + L_B\lambda^2}{(R_S - R)\lambda + (L - RR_SC)\lambda^2 - LRC\lambda^3}\cdot i$$

$$i_2 = -RC\frac{di_1}{dt} = \frac{RC(R_B\lambda + L_B\lambda^2)\lambda}{(R_S - R)\lambda + (L - RR_SC)\lambda^2 - LRC\lambda^3}\cdot i$$

$$i_3 = \frac{-R_B\lambda + L_B\lambda^2}{\mathcal{L}\lambda^2 + R_L\lambda + \dfrac{1}{C_B}}\cdot i. \tag{5}$$

When (5) is used in (4) we find

$$a_4\lambda^4 + a_3\lambda^3 + a_2\lambda^2 + a_1\lambda + a_0 = 0, \tag{6}$$

where

$$\begin{aligned}
a_4 &= RC[L_B(\mathcal{L}+L) + L\mathcal{L}]\\
a_3 &= RC[L_BR_L + \mathcal{L}R_B + L(R_B+R_L)]\\
&\quad - L_B\mathcal{L} - (L - RR_SC)(L_B+\mathcal{L})\\
a_2 &= RC\left[R_BR_L + \frac{L_B+L}{C_B}\right] + (L_B+\mathcal{L})\\
&\quad\cdot(R-R_S) - L_BR_L - R_B\mathcal{L}\\
&\quad - (L - RR_SC)(R_B+R_L)\\
a_1 &= \frac{1}{C_B}[(R_B+R_S)RC - (L+L_B)]\\
&\quad + (R-R_S)(R_B+R_L) - R_BR_L\\
a_0 &= \frac{1}{C_B}[R - R_S - R_B].
\end{aligned} \tag{7}$$

The Routh-Hurwitz criteria that the solutions λ of (6) all have their real parts less than zero are the following:[2]

$$a_0, a_1, a_2, a_3, a_4 > 0 \tag{8a}$$

$$a_1a_2 - a_3a_0 > 0 \tag{8b}$$

$$a_1(a_3a_2 - a_4a_1) - a_0a_3^2 > 0. \tag{8c}$$

Thus, for example, one can see that $a_1<0$ if

$$C_B < C_B^* = \frac{L + L_B - RC(R_S+R_B)}{(R-R_S)(R_B+R_L) - R_BR_L} \tag{9}$$

and that $a_3<0$ if

$$R < R^* = \frac{L_B(L+\mathcal{L}) + L\mathcal{L}}{R_SC(L_B+\mathcal{L}) + C[L_BR_L + (L+\mathcal{L})R_B + LR_L]}. \tag{10}$$

Thus if either C_B or R is less than C_B^* and R^*, respectively, instability results. Eqs. (9) or (10) are sufficient, but not necessary, conditions for instability.

In experimental test of these stability criteria, the following circuit parameters were chosen: $R_B=10\ \Omega$, $L_B=0.3\times10^{-6}$ henries, $R=100\ \Omega$, $C=7\times10^{-12}$ farads, $L=3\times10^{-9}$ henries, $\mathcal{L}=3\times10^{-9}$ henries, $R_S=2\ \Omega$, $R_L=50\ \Omega$ (the tunnel diode used was the GE 1N2939). For these circuit values, the quantities a_4, a_3, a_2 and a_0 are all >0 for all values of C_B. The quantities a_1, $a_1a_2-a_3a_0$, and $a_1(a_3a_2-a_4a_1)-a_0a_3^2$ are plotted as functions of C_B in Fig. 2. We see there that instability will result if $C_B<66$ $\mu\mu$f. It was observed experimentally that stability occurred for $C_B=90$ $\mu\mu$f and instability for $C_B=25$ $\mu\mu$f.

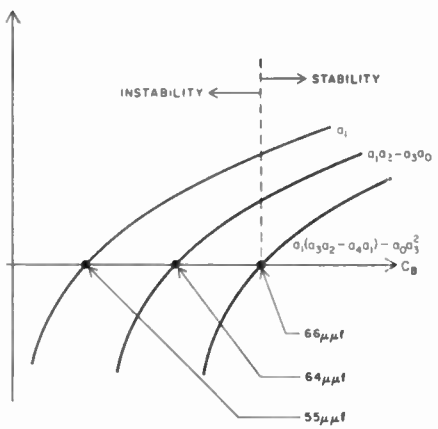

Fig. 2—Plot of left sides of (8a) (8c) vs C_B. Values of circuit elements used in this example are given in the text.

The stability calculation could be performed with respect to any other circuit parameter.

The circuit analyzed here must be considered only as a laboratory model. In a real system R_L is replaced by $Z(\omega)$ depending on the actual generator and load used. A similar analysis will then have to be carried out for a differential equation which is at least one degree higher and possibly also nonlinear.

The authors would like to thank Dr. I. Gerst (State University of New York) for several cogent remarks concerning the Analysis.

* Received by the IRE, October 10, 1961. This work was performed for the Rome Air Dev. Center under Contract No. AF 30(602) 2184.

[1] M. E. Hines, "High-frequency negative resistance circuit principles for Esaki diode applications," *Bell Sys. Tech. J.*, vol. 39, pp. 477–513; May, 1960.

[2] E. A. Guillemin, "The Mathematics of Circuit Analysis," John Wiley and Sons, Inc., New York, N. Y., ch. 6; 1949.

H. Boyet
D. Fleri
C. A. Renton
Defense Electronic Products
RCA
New York, N. Y.

Discussion of a Deflection System for a Flat Television Picture Tube*

Ramberg[1] has given a very interesting analysis of a novel focusing scheme originally proposed by Aiken for a flat television picture tube. The computation of the electron trajectories is based on formulas for the potential distribution given in the Appendix for a basic electrode configuration. The potential distribution in the actual horizontal and vertical deflection systems can then be obtained by superposition from this basic solution.

It is the purpose of this note to give some alternate solutions for the basic configuration of Fig. 15 in Ramberg's paper which appear to have certain computational advantages over that given in the paper. For convenience, the relevant figure is reproduced below as Fig. 1.

Ramberg obtains his basic solution by adding four partial results: a constant, two Fourier integrals which converge rather rapidly for small values of $|z|$, and a closed-form expression. The last part is somewhat complex and requires the solution of a transcendental equation, evaluation of a number of constants and four series. An alternate solution for this part is

$$\frac{1-x}{2} - \frac{1}{\pi}\sum_{m=1}^{\infty}\frac{\cosh m\pi y}{m\cosh m\pi b}\sin m\pi x. \quad (1)$$

It is easily seen that this solution reduces to $\frac{1}{2}$ at $x=0$ and to zero at $x=1$. The coefficients in the series are chosen to make the solution vanish at $y=|b|$ also. For aspect ratios b considered by Ramberg ($b\geqq 1$), the above series converge extremely rapidly. In the central plane ($y=0$), two or three terms of the series are sufficient for the computation of ϕ and the electric field components.

In spite of their rapid convergence, the other terms in Ramberg's expression are also rather cumbersome. In or near the central plane ($y=0$), we can obtain an approximate solution by conformal transformations. The result can then be made accurate by the addition of small correction terms.

For $b\to\infty$, the problem reduces to a two-dimensional one in the xz plane (see Fig. 2) which can be solved by two transformations of the Schwarz-Christoffel type. The result is

$$\phi_\infty = 1 - \frac{1}{\pi}\cot^{-1}\left(\frac{e^{-\pi z}+\cos\pi x}{\sin\pi x}\right). \quad (2)$$

If we replace the last part of Ramberg's expression by (1) and then let $y=0$ and $b\to\infty$, we obtain

$$\phi_\infty = 1 - \frac{x}{2} - \frac{1}{\pi}\int_0^\infty \frac{\sinh lx}{\sinh l}\,\frac{\sin lz}{l}\,dl \quad (3)$$

which must be identical with the closed-form expression given by (2). Making use of this identity, we find that for any aspect ratio b,

$$\phi(x,0,z) = 1 - \frac{1}{\pi}\cot^{-1}\left(\frac{e^{-\pi z}+\cos\pi x}{\sin\pi x}\right) - \frac{1}{\pi}\sum_{1}^{\infty}\frac{\sin m\pi x}{m\cosh m\pi b} - \frac{4}{\pi^2}\int_0^\infty\sum_{0}^{\infty}\cdot\frac{\sin(2n+1)\pi x}{(2n+1)\cosh\left\{b\sqrt{l^2+(2n+1)^2\pi^2}\right\}}\cdot\frac{\sin lz}{l}\,dl$$

$$+\frac{1}{\pi}\int_0^\infty\left\{\frac{\sinh lx}{\sinh l} - \frac{4}{\pi}\sum_{n=0}^{\infty}\frac{(-1)^n}{2n+1}\,\frac{\sinh x\sqrt{l^2+[(2n+1)\pi/2b]^2}}{\sinh\sqrt{l^2+[(2n+1)\pi/2b]^2}}\right\}\frac{\sin lz}{l}\,dl \quad (4)$$

$$\phi = 1 - \sum_{m=1}^{\infty}\sum_{n=0}^{\infty}A_{mn}\sin m\pi x\cdot\cos[2n+1)\pi y/2b]e^{k_{mn}z} \quad (5)$$

for $z\leqq 0$, and

$$\phi = 1 - x - \frac{2}{\pi}\sum_{1}^{\infty}\frac{\cosh m\pi y}{m\cosh m\pi b}\sin m\pi x + \sum_{m=1}^{\infty}\sum_{n=0}^{\infty}B_{mn}\sin m\pi x\cdot\cos[(2n+1)\pi y/2b]e^{-k_{mn}z} \quad (6)$$

for $z\geqq 0$. Here,

$$k_{mn}^2 = (m\pi)^2 + [(2n+1)\pi/2b]^2. \quad (7)$$

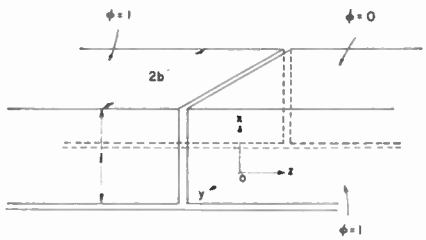

Fig. 1.

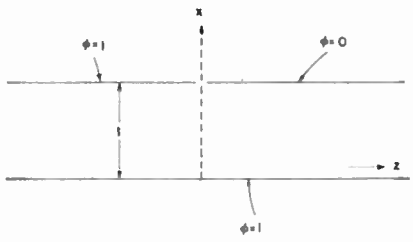

Fig. 2.

Again, for aspect ratios $b\geqq 1$, the series converge very rapidly so that one or two terms will suffice in most computations. In fact, it is easily estimated that all correction terms account for less than five per cent of the solution. Additional correction terms can be introduced when $y\neq 0$. The closed-form expression in (2) can also be used for the vertical deflection system.

Alternate series expressions for ϕ, that converge rapidly for $|z|>0$, can also be given. We note that ϕ must tend to unity for large negative values of z. For large positive values of z, the potential must approach the distribution given in (1). This suggests the solutions

Matching ϕ and $\partial\phi/\partial z$ at $x=0$, we obtain

$$A_{mn} = B_{mn} = \frac{-4(-1)^{m+n}}{\pi^2 m(2n+1)}\cdot\left\{1 - \frac{(-1)^m(2n+1)^2}{(2n+1)^2+(2mb)^2}\right\}. \quad (8)$$

These series are very good for the computation of ϕ as long as $|z|$ is not too small, but even at $z=0$ the convergence is quite satisfactory because of the sign alternations. For the computation of the electric field components, however, this solution is not very satisfactory near $z=0$.

HARRY GRUENBERG
Syracuse University
Syracuse, N. Y.

Author's Comment[2]

Unquestionably, Gruenberg's series expression (1) for my closed-form elliptic-function expression as well as his closed-form expression (2) for the series corresponding to $b=\infty$[3] can contribute materially to the ease of computation. I had omitted the series representation with respect to z, given by his (5)–(8), since the contribution of the series at values of z sufficiently large to make this representation preferable in the calculation of the field components is of smaller importance.

EDWARD G. RAMBERG
Institut für theoretische Physik
Technische Hochschule Darmstadt
Germany

* Received by the IRE, February 13, 1961.

[1] E. G. Ramberg, "Electron-optical properties of a flat television picture tube," PROC. IRE, vol. 48, pp. 1952–1960; December, 1960.

[2] Received by the IRE, March 16, 1961.

[3] In the corresponding expression for the vertical deflection field given by Ramberg at the bottom left of page 1959, an additive term $(1-y)$ has been omitted on the right side.

A Resonant Slot Parametric Amplifier*

A C-band degenerate parametric amplifier has been constructed in which the varactor diode is incorporated as an integral part of a resonant slot or iris. The present configuration is shown in Fig. 1 and uses a Microwave Associates 4254X varactor diode mounted in an end-plate resonant iris. The diode used is self-resonant above the operating frequency and, therefore, inductive irises were employed to resonate the residual capacitance of the diode. Capacitive irises could be used for operating frequencies above the self-resonant frequency of the diode, and in fact, the dam[1] structure is one variation of such a configuration. While the present structure employs an end-plate iris, similar operation could be achieved with guide wall slots as might be applicable in iterative array antennas.

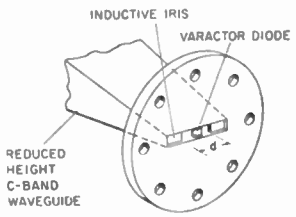

Fig. 1—C-band resonant slot amplifier (biasing arrangement not shown).

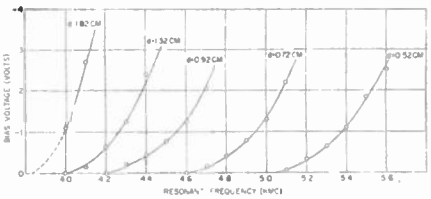

Fig. 2—Tuning range of resonant slot amplifier.

Current results are quoted on the device operating in a reflecting mode with pump power incident on the opposite face. Different pump arrangements would make possible the operation of this device in the transmission mode. Passive measurements on the device clearly show that its equivalent circuit is essentially the same when the iris is radiating into space as it is when connected to X-band waveguide.

The operating or resonant frequency of the iris is dependent, of course, on the parameters of the particular diode in use. The operating frequency, however, can be tuned by either adjusting the slot width (and hence equivalent parallel inductance) or the diode bias (and hence capacitance of the junction). The former adjustment covers a broader range of frequencies, but requires mechanical tuning; the latter is a simple electrical adjustment which may, however, affect operating bandwidth and noise figure if carried too far. In Fig. 2 are plotted resonant frequencies of the structure as a function of bias voltage with slot width as the parameter. It can be seen that either adjustment can effectively control the resonant frequency over a small range of frequencies, and in any practical case the particular application and accessibility of the amplifier would determine the tuning method employed.

Operating in the frequency range of 4.3 to 4.9 kMc, the device has been made to operate at stable gains of up to 20 db. Gain-bandwidth products over this frequency range varied with slot width from 50 to greater than 250 Mc. The values given are for the device operated as a single tuned structure, and additional irises or tuning screws can be used to broaden the response.

By proper diode bias adjustment, the elements can be made to oscillate with the same pump power used in the amplifying mode. In an antenna array, the elements could thus serve dual transmit-receiver functions controlled through diode programming.

The device reported in this letter is similar in concept to a tunnel-diode[2] amplifier recently reported as the result of an independent study.

J. W. Amoss
G. P. Rodrigue
Sperry Microwave Electronics Co.
Clearwater, Fla.

* Received by the IRE, October 13, 1961.

[1] B. C. DeLoach, "Waveguide parametric amplifiers," presented at the Internatl. Solid-State Circuits Conf., Philadelphia, Pa., February 15–17, 1961; *Digest of Technical Papers*, pp. 24–25, February, 1961.

[2] M. E. Pedinoff, "A tunnel-diode slot transmission amplifier," Proc. IRE (Correspondence), vol. 49, p. 1315; August, 1961.

Low-Frequency Noise in Backward Diodes*

The noise temperature of backward diodes was measured over the frequency range from 300 cps to 20 kc. For bias voltages much less than the valley voltage,[1] the noise temperature exhibits the familiar $1/f$ characteristic at frequencies below 1 kc, and is substantially constant at frequencies above 1 kc. Using these devices, a 100-Mc balanced mixer, converting to 5 kc, has exhibited a double-channel noise figure of less than 7 db. This is a 30-db improvement over what would be expected from present day mixers using point contact devices.

Noise Temperature Measurement

Measurements were made using matched pairs of wire wound precision resistors as noise sources. The hot noise source was operated at room temperature (290°K), and the cold noise source at liquid nitrogen temperature (77°K).

The noise temperature of the device under test was obtained in the following manner:

1) The noise output with the 290°K noise source, E_h, was recorded over the desired frequency range.

2) The noise output with the 77°K noise source, E_c, was recorded over the desired frequency range.

3) The operating point of the diode was adjusted so that its dynamic resistance was equal to the hot (and cold) resistance. For this operating point, the noise output of the diode, E_d, was plotted over the desired frequency range.

4) The noise temperature, $\bar{t}$, was calculated from the following expression:

$$\bar{t} = \left(1 + \frac{T_c}{T_h}\right)\left[\frac{\left(\frac{E_d}{E_h}\right)^2 - 1}{1 - \left(\frac{E_c}{E_h}\right)^2}\right],$$

where T_c and T_h are the cold and hot temperatures in degrees Kelvin respectively.

These tests indicate that at bias voltages much less than the valley voltage, the backward diode has no appreciable $1/f$ noise above 1 kc.

Applications and Experimental Results

Comparison of the noise temperature of backward diodes and point contact diodes[2,3] indicates that the backward diode will provide superior performance in mixing applications requiring a low IF frequency, or in detector applications requiring a video output. Although standard junction diodes may have low noise figures at low frequencies, they are not suitable for microwave applications. Their limitations in this area are due to storage time, and due to the parasitic losses associated with the series resistance, r_s. The backward diode has no storage effects, since it operates on the principle of quantum mechanical tunneling, which is a majority carrier phenomenon. In addition, the series resistance associated with it is much smaller than that obtained with normal junction devices, since extremely low resistivity semiconductor material is used in its fabrication.

In order to test the performance of the backward diode in an operational circuit, a 100 Mc mixer was designed for direct down-conversion to 5 kc. A balanced structure was chosen in order to suppress any local oscillator noise that would otherwise degrade the mixer performance. Using a temperature-limited noise diode, a double-channel noise figure of under 7 db was obtained. A similar mixer, using point contact devices, will normally result in a 30–40-db noise figure.

The effect of operation with a high-input frequency was evaluated in a single diode mixer. This circuit was chosen for its simplicity of construction and ease of adjustment. A 30-Mc IF was chosen in order to considerably simplify the measurement of noise figure, and avoid the effects of local

* Received by the IRE, August 18, 1961; revised manuscript received, August 31, 1961.

[1] L. Esaki and T. Yajima, "Excess noise in narrow germanium p-n junctions," *J. Phys. Soc.*, (Japan), vol. 13, p. 1281; November, 1958.

[2] B. G. Bosch *et al.*, "Excess noise in microwave mixer crystals," Proc. IRE (Correspondence), vol. 19, pp. 1226–1227; July, 1961.

[3] I. L. Newberg, "Video Frequency Noise Measurements on Microwave Crystal Mixers," Radar Res. Group Electronic Sys. Lab., Dept. Elec. Engrg, M.I.T., Cambridge, Mass., No. 7848-TM-3 and 7848-TM-6, Contract AF 33(616)-5489, Task 50688; May, 1959 and November, 1959.

oscillator noise. The results obtained with this IF frequency should be comparable to those obtained with an audio IF frequency, since both frequencies are beyond the range where $1/f$ noise is important.

A coaxial noise source and double-stub tuner were used from 500 Mc to 2 kMc. Measurements were taken at 8.9 kMc using a waveguide noise source and a sliding probe tuner, coupled to the diode through a waveguide to coaxial transition.

Double-channel noise figures were obtained, ranging from 5 db at 500 Mc, to 14 db at 8.9 kMc. These noise figure measurements were about 2 db lower than anticipated because of the increased local oscillator drive used during this test.

The results of these experiments have indicated that it is possible to operate backward diodes as low noise mixers up to approximately one-tenth the cutoff frequency associated with the valley capacitance and the parasitic series resistance. The experimental data was taken on backward diodes with a cutoff frequency of approximately 20 kMc. With present fabrication techniques, it is feasible to extend the cutoff frequency of these devices to a value in excess of 100 kMc. Indeed, tunnel diodes with cutoff frequencies of twice this value have been reported[4] in the literature.

In conclusion, it should be noted that whereas the performance of the backward diode in this application can be duplicated by the tunnel diode,[5] a backward diode mixer is unconditionally stable for all values of source and load conductances. In addition, the device is less susceptiable to damage from accidental mechanical or electrical overloads than the point contact diode. The combination of these advantages makes the device near-ideal for applications of the type discussed in this note.

The author wishes to thank Dr. S. K. Ghandi and Dr. S. T. Fisher for their helpful suggestions and comments in preparing this material.

W. C. Follmer
Philco Research Center
Blue Bell, Pa.

[4] C. A. Burrus, "Millimeter wave Esaki diode oscillators," Proc. IRE (Correspondence), vol. 48, p. 2024; December, 1960.
[5] M. D. Montgomery, "The tunnel diode as a highly sensitive microwave detector," Proc. IRE (Correspondence), vol. 49, pp. 826–827; April, 1961.

An Extremely Wideband Tunable S-Band Parametric Amplifier*

An S-band nondegenerate parametric amplifier has been developed that can be tuned continuously across a 1000-Mc band from 2100 to 3100 Mc by mechanically tuning the pump circuit, and frequency shifting the pump source. The amplifier can be electronically tuned over a 260-Mc band from 2470 to 2730 Mc by frequency shifting the pump source only.

* Received by the IRE, October 9, 1961.

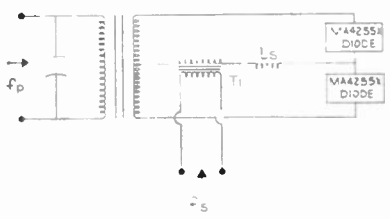

Fig. 1—Circuit diagram of a parametric amplifier.

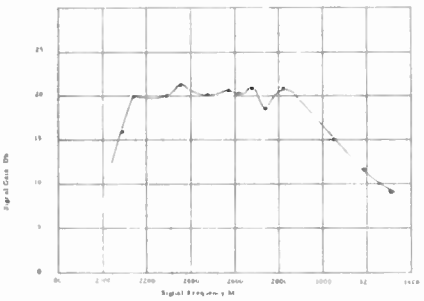

Fig. 2—Signal gain vs signal frequency.

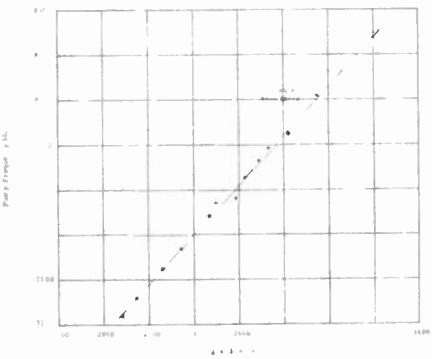

Fig. 3—Pump frequency vs signal frequency.

The amplifier uses two commercially available varactors in a balanced circuit configuration similar to that used by Kliphuis[1] (see Fig. 1). The zero bias capacitances of the two varactors were matched to within 10 per cent. At the signal frequency the two varactors appear in parallel, and the inductance Ls is chosen to resonate with the total diode capacitance. The signal circuit bandwidth is very wide, due to the stagger tuning effect of the two diodes in parallel. The self-resonant frequency of the two diodes in series is chosen as the idler frequency. Since there is very little external loading, the idler circuit bandwidth is determined by the Q of the varactors at the idler frequency. Because of the low ratio of idler to signal bandwidth, the voltage gain bandwidth product ($G^{1/2}BW$) is relatively low. With the availability of better varactors that have a higher self-resonant frequency (*e.g.*, "Sharpless Varactors") one will be able to get greater idler bandwidths thereby increasing the $G^{1/2}BW$ product. The wideband transformer T_1 is adjusted to give the desired gain. The use of a fixed tuned idler circuit requires that the pump frequency be varied to tune the signal frequency across the specified signal band. The pump power is introduced through a low Q resonant slot that can be mechanically tuned over 1600 Mc at X band.

Fig. 2 shows the measured midband gain as function of signal frequency, with the pump optimized. The minimum gain across the 1000 Mc tuning range was 15 db. The instantaneous gain bandwidth product was 130 Mc minimum, and was as high as 240 Mc at parts of the signal band. The noise figure of the amplifier was 2.8 db at 2400 Mc and 3.0 db at 2900 Mc. Fig. 3 is the plot of the pump frequency for optimum operation vs signal frequency.

The amplifier may also be electronically tuned for signal frequencies between 2470 Mc and 2730 Mc by varying the pump frequency only. The minimum gain was 18.5 db and the instantaneous $G^{1/2}BW$ was 100 Mc minimum. Such an amplifier can be rapidly tuned across the specified band by using a backward wave oscillator as the pump tube. The total pump power necessary for operation was approximately 50 mw. The diodes were operated with a negative bias of 0.4 volt.

Further work is presently in progress to extend this type of operation to higher frequencies.

Martin Grace
Airtron
Div. of Litton Industries
Morris Plains, N. J.

[1] J. Kliphuis, "C-band nondegenerate parametric amplifier with 500-Mc bandwidth," Proc. IRE (Correspondence), vol. 49, p. 961; May, 1961.

A Tunnel-Diode Frequency Multiplier with Gain*

A frequency multiplier which exhibits a voltage gain for the second and third harmonics has been constructed using the nonlinear negative resistance characteristics of a tunnel diode.

The possibility of using a nonlinear negative resistor to generate harmonics has been discussed by R. H. Pantell.[1] He arrives at an expression for the power gain in the mth harmonic of the form

$$\frac{W_m}{W_0} = \frac{1}{m^2}\left[\frac{h_m}{W_0} - 1\right], \qquad (1)$$

where W_0 = power input from the source, W_m = power output at the mth harmonic.

$$h_m = \frac{1}{4\pi^2}\int_0^{2\pi} dy \int_0^{2\pi} dx \frac{\partial i}{\partial v}\left(\frac{\partial v}{\partial x}\right)^2, \qquad (2)$$

i is the instantaneous current, v is the instantaneous voltage, $x=\omega_m t$ and $y=\omega_0 t$, ω_0 is the source frequency in radians, ω_m is the harmonic frequency in radians, and t is the time.

From (1) it can be seen that when h_m is negative, the right-hand side of (1) may have a magnitude greater than one, and harmonic generation is achieved with a

* Received by the IRE, October 2, 1961.

[1] R. H. Pantell, "General power relationships for positive and negative resistors," Proc. IRE (Correspondence), vol. 46, p. 1958; December, 1958.

power gain. Eq. (2) shows that h_m is negagive only when $\partial i/dv$ is negative.

The tunnel-diode characteristic in Fig. 1 exhibits an appropriately large nonlinear negative conductance region. Using the circuit in Fig. 2 we observed second harmonic generation with a voltage gain of 3.7. Both source and second harmonic voltages were measured across the tunnel diode and the corresponding waveforms are shown in Fig. 3.

With a circuit of this type the best results are obtained with a low amplitude drive when the circuit is biased just beyond the region of self oscillation. Additionally, a small value of $\sqrt{L/C}$ improves the waveform.[2]

Although much work remains to be done on reliability and cascading circuits, it appears that a tunnel-diode frequency multiplier could be a reasonable means for translating stable signals from a quartz crystal oscillator from 1 kc up into the 100 kMc region. A frequency translator of this type may have the advantages of working at a constant low signal level and being all solid state.

The authors appreciate the financial support of the University Council on Research and Creative Work.

F. S. Barnes
L. Morris
Elec. Engrg. Dept.
University of Colorado
Boulder, Colo.

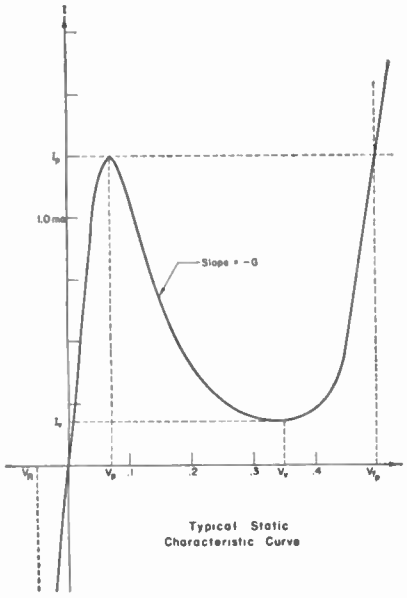

Fig. 1—A typical characteristic curve for a tunnel diode.

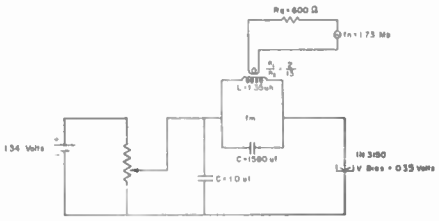

Fig. 2—The circuit diagram for a second harmonic frequency multiplier.

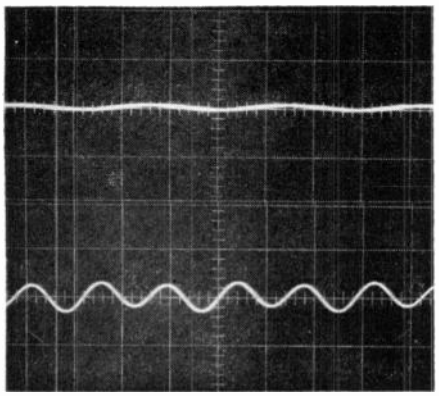

Fig. 3—The fundamental and second harmonic waveforms as viewed across the tunnel diode.

[2] W. A. Edson, "Vacuum Tube Oscillators," John Wiley and Sons, Inc., New York, N. Y., pp. 42–63; 1953.

Generation of Microwave Harmonics in an Electrodeless Discharge at Low Pressure*

The possibility of RF harmonic power being produced in an ionized gas was considered more than a decade ago [1], [2]. In these studies it was shown that, under special conditions, appreciable harmonic power may be generated in the ionosphere. An early attempt to produce RF harmonics in ionized gases was made by Hanley and Ruhlig [3]. With primary power at 200 Mc they achieved a conversion efficiency of 23 per cent for the second harmonic; however, to the author's knowledge, their technique has not been attempted at microwave frequencies. The main feature of their device appears to be that the coaxial discharge geometry used results in large electric field gradients.

Several workers have produced harmonics using a microwave discharge in a gap in a waveguide post [4]–[7]. Baird [8] has found that these results can be explained by electron density modulation during the RF cycle.

Whitmer [9], [10] and Hill and Tetenbaum [11] have investigated harmonic generation in cyclotron resonant plasmas at microwave frequencies. In the latter case a 15-db conversion loss was obtained for the second harmonic. Conversion to higher harmonics was very inefficient.

In the U. K. harmonics have been produced with arcs in high pressure gas [12]. In recent work using argon at 100 atmospheres, Froome [13] has produced submillimeter harmonics having power of the order of one microwatt. About 3 watts of fundamental power at 35 Gc were used in this experiment.

* Received by the IRE, August 16, 1961.

Bierrum and Walsh [14], also in the U. K., have used a point to plane geometry with pulsed power at 10 cm. Although poor efficiencies were obtained, this group has conclusively established that the harmonic output power is coherent [15].

It seems that several different mechanisms may be operating in these various experiments. The discouraging fact is that all the experiments at microwave frequencies have had very high conversion losses, at best comparable to that obtainable with low power nonlinear resistance diodes. This note reports another approach by which the author has obtained an order of magnitude improvement in efficiency for 10 cm fundamental power. This efficiency equals that achieved by Hanley and Ruhlig [3] at UHF.

The most successful arrangement is shown in Fig. 1 where the discharge vessel is either cylindrical or spherical. For generating the second harmonic the conventional cross-guide arrangement was used with coaxial coupling. A coaxial choke prevented the harmonic power from radiating into the fundamental guide. A sliding short and a tuner were used to match the second harmonic power into the harmonic waveguide. A similar arrangement was used to generate the fourth harmonic using an *X*-band guide. A choke was used to prevent the fourth harmonic from radiating into the *S*-band guide. Other harmonics, however, could radiate into the *S*-band guide. Tuning was provided for these harmonics by the arrangement shown in Fig. 2. The narrow branch of the shunt Tee does not propagate the fundamental, hence movement of the sliding short provides tuning only at harmonics other than the fourth. By this adjustment the fourth harmonic power could be improved by 3 to 4 db.

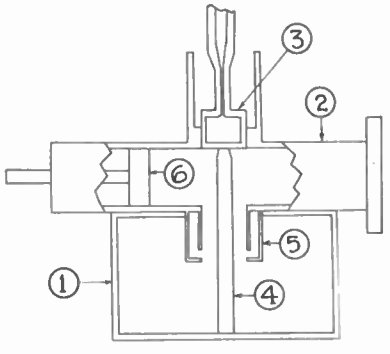

Fig. 1—Hamonic generator. 1) *S*-band guide, 2) *C*-band guide, 3) quartz discharge vessel, 4) brass post, 5) coaxial choke, and 6) adjustable waveguide short.

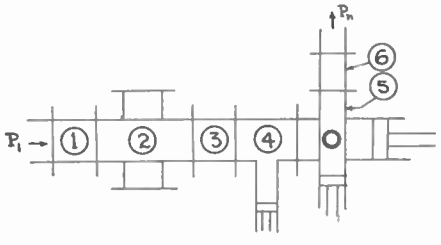

Fig. 2—Waveguide arrangement for harmonic generator. 1) *S*-band isolator, 2) directional coupler, 3) *E*/*H* tuner, 4) adjustable tee, 5) harmonic generator (Fig. 1), and 6) harmonic guide tuner.

The experimental conditions are summarized:

Fundamental Power:	10–50 watts CW at 2.9 Gc
Gas used:	air at 0.1 to 0.3 mm of Hg.
Discharge Vessel:	fused quartz, inside diameter 8 mm
Post Diameter:	0.10 to 0.15 inch.

The following conversion efficiencies were observed:

Harmonic:	Conversion Efficiency:
2	− 6.4 db
3	−13.2 db
4	−16.6 db.

All powers were measured with an FXR temperature compensated power meter using Weinschel attenuators. No allowance was made for losses in the fundamental and harmonic tuners.

By studying the effect on the fourth harmonic power it became evident that the best adjustment of the sliding short on the cutoff branch of the shunt Tee probably was one that satisfactorily terminated both the second and third harmonics (*i.e.* reduced the radiation of these harmonics down the fundamental guide).

A special interaction region was not made for the third harmonic. The third harmonic power was measured using each of the second and fourth harmonic generators with an appropriate band-pass filter. Similar results were obtained for both arrangements.

It is noteworthy that the pressures used are considerably below that for optimum breakdown. It is thought that these low pressures reduce the efficiency of the ionizing process and the resulting lower electron density is consistent with a higher electric field strength for a given fundamental power. Too low a pressure results in an unstable discharge and difficult tuning. Preliminary tests with Argon, which is more easily ionized than air, indicate that the most efficient operation occurs in the pressure range 30 to 40 microns of mercury. Further measurements have yet to be completed. In all cases it is important to have a very small capillary in the discharge tube. Capillaries larger than one-half mm in diameter resulted in a jet of plasma extending a few cm up the neck of the discharge tube. The efficiency of conversion under such conditions is reduced.

The operating mechanism in these experiments is not fully understood. It is believed that the very large electric field gradients result in a nonsinusoidal motion for the electrons. A preliminary analysis shows that the energy can be coupled from the fundamental fields to the harmonic fields by this process. It is interesting that such a process, which requires collisions only for the maintenance of the discharge, would be essentially that of a nonlinear reactance. The conversion efficiency consequently is not restricted by the $1/n^2$ limit for the nonlinear resistance.

In these experiments appreciable power may have been absorbed by the tuners. The efficiency of the discharge itself in generating the second harmonic may well have been better than 6 db, the theoretical limit for the nonlinear resistance.

This research is being continued in an attempt to gain a better understanding of the process, and to test the usefulness of this process at higher frequencies.

The author is grateful to Prof. J. L. Yen, who supervised this research and to the National Research Council of Canada for financial assistance.

C. B. Swan
University of Toronto
Toronto, Canada

References

[1] J. Feinstein, "Higher order approximations in ionospheric wave propagation," *J. Geophys. Res.*, vol. 55, pp. 161–170; June, 1950.
[2] K. Försterling and H. O. Wüster, "Über die Entstehung vor oberwellen in der Ionospäre," *J. Atmospheric and Terrest. Phys.*, vol. 2, pp. 22–31; 1951.
[3] T. E. Hanley and A. J. Ruhlig "Harmonic Power from an RF Discharge," Naval Res. Lab., Wash., D. C., NRL Progress Rept.; November, 1953.
[4] M. Uenohara, *et al.*, "*A new high-power frequency multiplier.*" Proc. IRE, vol. 45, pp. 1419–1420; October, 1957.
[5] K. Inada, M. Uenohara, and T. Masutani, "On the harmonics radiating from microwave discharge in air," *Proc. of the 4th Internatl. Conf. on Ionization Phenomena in Gases*, North Holland, vol. 2, pp. 768–773; 1960.
[6] J. R. Baird and P. D. Coleman, "High power gas discharge frequency multiplier," *Proc. of the Symp. on Millimeter Waves*, New York, N. Y., April, 1959, Polytechnic Press, Brooklyn, N. Y.; 19 0.
[7] G. S. Kino, *et al.*, "Millimeter Wave Generation and Amplification in Plasmas," W. W. Hansen Physics Lab., Stanford Univ., Stanford, Calif., Sci. Rept. No. 6, Contract No. AF 19 (604)-5226; December, 1959.
[8] J. R. Baird, "Frequency Conversion in a Plasma," source, University of Illinois, Urbana, Ill. Tech. Rept. No. 6, AEC Contract No. AT 11-1-392; June, 1961.
[9] R. F. Whitmer, "The nonlinear interaction of an electromagnetic wave with an anisotropic plasma," *Proc. of the Symp. on Electronic Wave-Guides*, New York, N. Y., April, 1958, Polytechnic Press, Brooklyn, N. Y.; 1958.
[10] R. F. Whitmer and E. B. Barrett, "Nonlinear interaction of an electromagnetic wave with a plasma layer in the presence of a static magnetic field. I—Theory of harmonic generation," *Phys. Rev.*, vol. 121, pp. 661–668; February 1, 1961.
[11] R. M. Hill and S. J. Tetenbaum, "Harmonic generation in a cyclotron resonant plasma," *J. Appl. Phys.*, vol. 30, pp. 1610–1611; October, 1959.
[12] K. D. Froome, "An 8-volt cold cathode mercury arc emitting microwaves," *Nature*, vol. 179, pp. 267–268, February, 1957; "A new microwave harmonic generator," *Nature*, vol. 184, p. 808, September, 1959; "Millimeter waves from mercury arc harmonic generator," *Nature*, vol. 186, p. 959, June, 1960; "Sub millimeter waves by harmonic generation from cold cathode arcs," *Nature*, vol. 188, p. 43, October, 1960.
[13] K. D. Froome, private communication.
[14] N. R. Bierrum and D. Walsh, "Harmonics from a microwave gas discharge," *J. of Electronics and Control*, vol. 8, pp. 81–90; February, 1960.
[15] N. R. Bierrum, D. Walsh, and J. C. Vokes, "Coherence and bandwidth of a gas discharge harmonic generator," *Nature*, vol. 186, pp. 626–626; May 21, 1960.

A Ruby Laser Exhibiting Periodic Relaxation Oscillations*

A ruby optical maser, with confocal ends[1,2] and an optical axis oriented 90 degrees to the cylinder axis, has been constructed by the Orlando Division of The Martin Company. This maser demonstrates some interesting properties applicable to optical radars.

A ruby measuring 2 inches in length and ¼ inch in diameter, was centered in a GE FT-524 flash tube within a magnesium oxide reflector. Threshold energy required was 1350 joules as opposed to 2030 joules required for a zero-degree oriented ruby with flat ends[3] under the same conditions. Total pulse duration realized was approximately 700 μsec. The pulse, exhibiting an initial rise time of less than 0.2 μsec, is depicted in Fig. 1. As would be expected, the output of the 90 degree oriented ruby crystal is linearly polarized. Because of the spherical ends, the half power beamwidth is 7.6 degrees. It should be noted, however, that collimation may be obtained by means of a simple lens system. These measurements were obtained with one of the faces 2 per cent transmitting and the other heavily silvered.

An important and interesting property of this optical maser is reflected in the nature of the relaxation oscillations generated. Part of an output pulse, displayed on an expanded time scale, is shown in Fig. 2. The periodic structure of the output is evident when compared with a similar sampling of the output of a zero-degree oriented ruby on the same time scale, as indicated in Fig. 3. The pulse period, referring again to Fig. 2, varied from 3.5 μsec at 3200 joules input power to 10 μsec just above threshold.

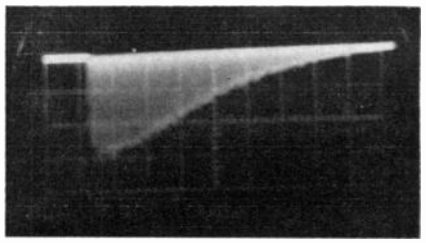

Fig. 1—Envelope of output pulse from 90° oriented ruby with confocal ends.

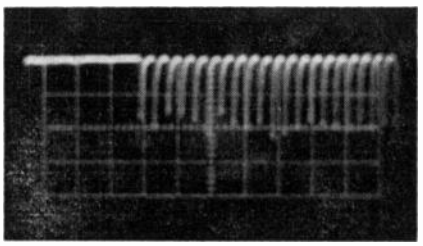

Fig. 2—Relaxation oscillations of 90° confocal ruby.

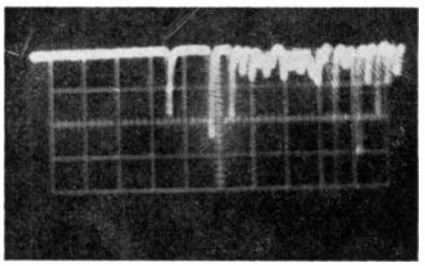

Fig. 3—Relaxation oscillations of 0° ruby with flat ends.

* Received by the IRE, September 25, 1961.

[1] G. D. Boyd and J. P. Gordon, "Confocal multinode resonator for millimeter through optical wavelength masers," *Bell Sys. Tech. J.*, vol. 40, pp. 489–508; March, 1961.

[2] A. G. Fox and T. Li, "Resonant modes in a maser interferometer," *Bell Sys. Tech. J.*, vol. 40, pp. 453–488; March, 1961.

[3] T. H. Maiman, "Optical maser action in ruby," *British Commun. and Electronics*, vol. 7, pp. 674; September, 1960. An optical maser using a zero-degree oriented ruby with flat ends was first reported in this article.

This periodic characteristic of the output pulse should greatly enhance the usefulness of an optical maser in an optical ranging application using correlation techniques. In addition, possible application in Doppler ranging, using a ruby laser, is suggested.

R. E. Johnson
W. H. McMahan
F. J. Oharek
A. P. Sheppard
Microwave Laboratory
The Martin Co.
Orlando, Fla.

Broad-Band S-Band Parametric Amplifier*

A nondegenerate *S*-band parametric amplifier has been constructed that has a 400-Mc bandwidth and a 2.1-db noise figure. Peak gain of the amplifier, as shown in Fig. 1, is 13 db with a 3-db ripple in the band-pass.

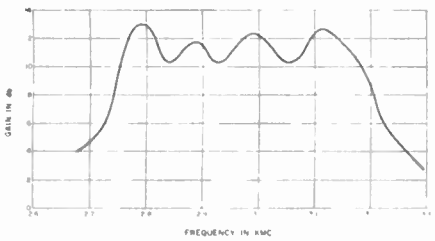

Fig. 1—13-db gain, 425 Mc, per cent $G^{1/2}B = 64$ per cent.

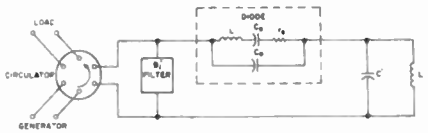

Fig. 2—Parametric amplifier equivalent circuit.

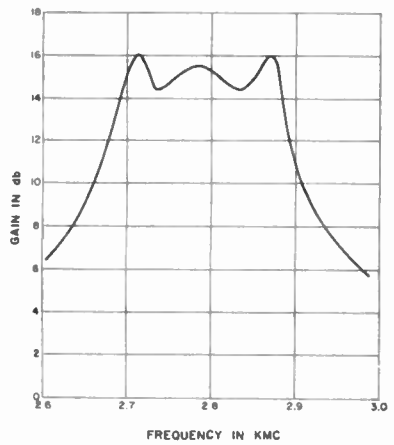

Fig. 3—16-db gain, 202 Mc, per cent $G^{1/2}B = 44.2$ per cent.

* Received by the IRE, October 9, 1961. This work was performed for the Bureau of Naval Weapons, Washington, D. C., Contract No. NOw 61-0283-d.

The amplifier utilizes a gallium arsenide pill varactor with a 0.4-pf capacitance.

The equivalent circuit for the amplifier is shown in Fig. 2. The values of L' and C' were chosen so that the idler frequency occurred at essentially the diode self-resonant frequency, and so that a triple-tuned response was achieved. By use of tuning screws appropriately placed on the line, the bandwidth can be shaped to obtain the type of response desired. Two typical responses are shown in Figs. 1 and 3; pump frequency in these instances was about 14.8 Gc. Two hundred milliwatts pump power was used to reverse bias the diode to -3.5 volts. This gave rise to a large value of C_1/C_0, which was necessary to obtain the broad bandwidth.

The author is indebted to B. Vincent for his interesting discussions and helpful suggestions.

Kenneth M. Johnson
Apparatus Div.
Texas Instruments, Inc.
Dallas, Tex.

Magnetoresistive Effect as a Possible Memory Device*

The change of resistance of a material in a magnetic field (Gauss effect) has been utilized primarily as a means of measuring magnetic fields. However, this effect in ferromagnetic materials might be applied in computer storage devices. Characteristics of these devices would be fast switching times and nondestructive readout.

The mechanism of the magnetoresistive effect is an extremely complex one, involving changes in the mean free path.[1] From a phenomenological standpoint, in the ferromagnetic materials, this involves an increase in the resistance when the current and magnetization are in the same direction, and a decrease when they are perpendicular to each other. The potential difference between these two states is then

$$\Delta V = IR_0 \cdot (\delta_1 + \delta_2),$$

where R_0 is the resistance in the demagnetized state and

$$\delta_i = \frac{\Delta R_i}{R_0}.$$

Values of δ_i as high as 0.16 have been reported.[2]

In our work, no attempt was made to optimize our materials; most samples were evaporated films of iron or nickel-iron, approximately one inch long by 0.050 inch wide.

Fig. 1 shows the dependence of magnetoresistive output on the magnetic field for a typical iron film approximately 5000 Å thick. Note the critical field necessary before

* Received by the IRE, October 13, 1961.

[1] E. N. Adams and T. D. Holstein, Jr., *J. Phys. Chem. Solids*, vol. 10, p. 254; 1959.

[2] Y. Shirakawa, Tohoku Imperial University, Sci. Rept. No. 27, 532.

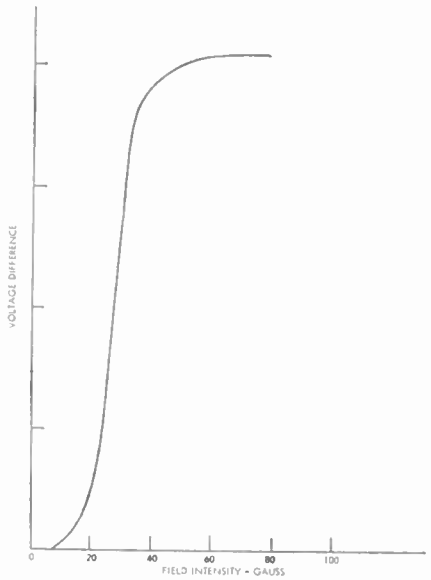

Fig. 1—Voltage difference vs field intensity for a typical iron film.

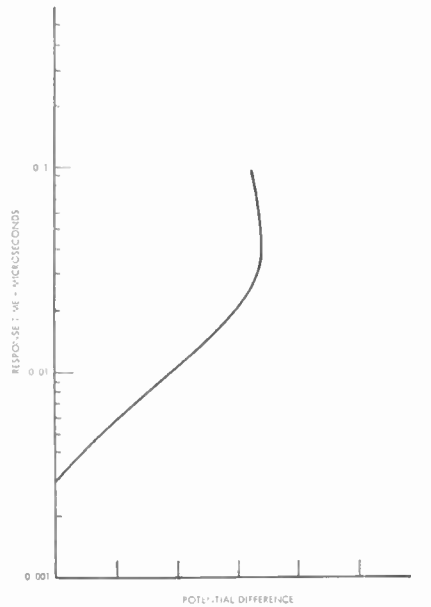

Fig. 2—Response time vs potential difference for a typical thin film.

the film begins to switch. Fig. 2 is a plot of response time vs potential difference for a typical film. This was obtained by calculating the decay time of the discharge network used to switch the film. Care was taken to ensure that the maximum field was always sufficient to saturate the material. The curve (Fig. 2) was plotted as the time constant of the discharge circuit was varied. Note that in both curves, the potential difference is in arbitrary units since it is directly dependent on the current and the resistance.

The feasibility of the magnetoresistive effect memory application was successfully demonstrated by evaporating a nine-element test array. Writing was accomplished by pulse drive lines. Readout was in a cyclic mode at a 10-kc rate.

One additional advantage of a magnetoresistive storage device over other thin film memories might be expected. The most

critical parameter in an array of this type would be its resistance which is easier to control than the magnetic properties of other thin films.

C. PETTUS
T. YOUNG
General Products Div.
Development Lab.
IBM Corp.
Endicott, N. Y.

A Generalized Hildebrand's Method for Nonuniform Transmission Lines*

Second-order ordinary linear differential equations (LDE) with variable coefficients are, in general, solved approximately. However, there is an exact technique to convert the above-mentioned LDE into an LDE having constant coefficients originally developed by Hildebrand,[1] requiring a certain interrelationship among variable coefficients. This communication outlines his method and generalizes it so that the interrelationship among variable coefficients is completely eliminated.

The propagating voltage $V(x)$ of the nonuniform transmission line, having known arbitrary and continuous functions of x for impedance $Z(x)$ and admittance $Y(x)$, gives the following LDE:

$$V''(x) - (Z'/Z)V'(x) - YZV(x) = 0, \quad (1)$$

where the primes are used for derivatives with respect to x in this communication. Introduce a new independent variable w in place of x such that

$$w = f(x), \quad (2)$$

where the precise form of $f(x)$ is to be determined later. Combine (1) and (2),

$$f'^2\ddot{V}(w) + [f'' - (Z'/Z)f']\dot{V}(w) - YZV(w) = 0, \quad (3)$$

where the dots over the symbol represent the derivatives with respect to the newly introduced independent variable w.

Hildebrand's idea is to convert (3) into an LDE with constant coefficients,

$$\ddot{V}(w) + a\dot{V}(w) + bV(w) = 0, \quad (4)$$

where a and b are arbitrary constants. A comparison of (3) and (4) reveals that the coefficients of $\dot{V}(w)$ give a Bernoulli's nonlinear differential equation (NDE) for $f'(x)$, while the coefficients of $V(w)$ give another equation for $f'(x)$. These two $f'(x)$'s must be the same. In order to realize this identity, $Y(x)$ and $Z(x)$ must be interrelated through

$$Y(x) = -bZ(x) \Big/ \left[c + a\int Z(x)dx\right]^2, \quad (5)$$

where c is any constant and $Z(x)$ is arbitrary. The undetermined $f(x)$ becomes

$$f(x) = \int Z(x)\left[d - (a/b)\int Y(x)dx\right]dx, \quad (6)$$

where d is also any constant. The voltage $V(x)$ is given by

$$V(x) = A_1 \exp\left[\left(-\frac{a}{2} + \frac{\sqrt{a^2 - 4b}}{2}\right)\int f(x)dx\right] + A_2 \exp\left[\left(-\frac{a}{2} - \frac{\sqrt{a^2 - 4b}}{2}\right)\int f(x)dx\right], \quad (7)$$

where constants A_1 and A_2 are to be specified uniquely by the imposed boundary conditions on $V(x)$.

The preceding method lacks in generality as $Y(x)$ and $Z(x)$ are interrelated. Past exact analyses[2-5] of nonuniform transmission lines required similar interrelationships between $Y(x)$ and $Z(x)$. In this respect, the approximate method[1] seems to relax the interrelationship between $Y(x)$ and $Z(x)$.

Using the well-known Cayley's factorization technique[6] (3) can be rewritten as

$$[D + p(w)][D + q(w)]V(w) = 0, \quad (8)$$

where the differential operator D is used for (d/dw), and $p(w)$ and $q(w)$ are two undetermined functions of w. The comparison between (3) and (8) gives

$$f'^2(p + q) = f'' - (Z'/Z)f', \quad (9)$$

$$f'^2(\dot{q} + pq) = -YZ. \quad (10)$$

Eliminate p from (9) and (10) so that a generalized Riccati's NDE for q is obtained, and

$$f'q'(x) + q(x)[f'' - (Z'/Z)f'] - f'^2q^2(x) = -YZ, \quad (11)$$

where (12) has been used,

$$\dot{q} = \frac{dq(w)}{dw} = \frac{dq(x)}{dx}\frac{dx}{dw} = \frac{q'(x)}{f'(x)}. \quad (12)$$

A curious thing is that (11) is also a Riccati's NDE for $f'(x)$. This peculiarity happens to be a mere coincidence.[7] The recent communication[3] has shown how to solve (11) if variable coefficients are properly interrelated. Using the form of $(P_1/R_1)' = Q_1$, the following equation is derived easily:

$$f'' - (Z'/Z)f' = +(f + B_1)YZ, \quad (13)$$

where B_1 is a constant of integration.

If $f(x)$ is to be determined from (13), this becomes an impossible problem for variable and independent $Y(x)$ and $Z(x)$. It is proposed to use (13) in a different fashion. If $Z(x)$ and $f(x)$ are independent functions, $Y(x)$ should be given by (13). The remaining task to retrieve the propagating voltage $V(x)$ is a mechanical routine, and it is omitted here.

It is interesting to observe a simple example for which $Z(x) = 1$ (const.) and $Y(x) = x$. This *assumed* nonuniform line gives a nonhomogeneous Airy's differential equation,

$$f'' - xf = xB_1. \quad (14)$$

Using Airy's functions, $Ai(x)$ and $Bi(x)$, (14) is readily solved. This example was chosen intentionally for using an Airy's equation. However, in practical situtations for tapered lines or matchings, $f(x)$ will not be solved with ease for given independent $Z(x)$ and $Y(x)$. It would be of value if $f(x)$ and $Z(x)$ were systematically varied so that the minimum reflection coefficient would be realized for a given taper length. A substitution of (13) into (1) provides

$$V''(x) - \frac{Z'}{Z}V'(x) - \left[\frac{\frac{Z'}{Z}f' - f''}{f + B_1}\right]V(x) = 0. \quad (15)$$

The end result has shown that (15) is solved exactly for arbitrary $Z(x)$ and $f(x)$ which are independent of each other, provided $f'(x)$ is not zero.

The author wishes to express his deep gratitude to Prof. F. B. Hildebrand, Dept. of Math, M.I.T., for the help received in the literature search of the mathematical method involved in this note.

IWAO SUGAI
ITT Federal Labs.
Nutley, N. J.

* Received by the IRE, June 16, 1961; revised manuscript received, August 10, 1961.

[1] F. B. Hildebrand, "Advanced Calculus for Engineers," Prentice-Hall Inc., New York, N. Y., p. 50; 1948.

[2] I. Sugai, "The solutions for nonuniform transmission line problems," PROC. IRE (Correspondence), vol. 48, pp. 1489–1490; August, 1960.

[3] I. Sugai, "A new exact method of nonuniform transmission lines," PROC. IRE (Correspondence), vol. 49, pp. 627–628; March, 1961.

[4] I. Sugai, "D'Alembert's method for nonuniform transmission lines," PROC. IRE (Correspondence), vol. 49, pp. 823–824; April, 1961.

[5] I. Sugai, "Riccati's and Bernoulli's equations for nonuniform transmission lines," IRE TRANS. ON CIRCUIT THEORY (Correspondence), vol. CT-8, September, 1961.

[6] E. L. Ince, "Ordinary Differential Equations," Dover Publications Inc., New York, N. Y., pp. 128–129; 1956.

[7] I. Sugai, "A class of solved Riccati's equations," *Elec. Commun.*, vol. 37, pp. 56–60; May, 1961.

The Radar Cross Section of the Moon*

Our theory[1,2] on the scattering from the moon's surface has been criticized in many places.[3,4] We were interested in determining

* Received by the IRE, September 18, 1961.

[1] T. B. A. Senior and K. M. Siegel, "A theory of radar scattering by the moon," *J. Res. NBS*, vol. 64D, pp. 217–229; May–June, 1960.

[2] K. M. Siegel, "Radio Characteristics of Lunar Surface Materials," presented at 12th Internatl. Astronautical Congress, Washington, D. C.; October 4, 1961.

[3] V. A. Hughes, "Roughness of the moon as a radar reflector," *Nature*, vol. 186, pp. 873–874; June 11, 1960.

[4] H. S. Hayre, "Radar scattering cross section—applied to moon return," PROC. IRE (Correspondence), p. 1433; September, 1961.

the electromagnetic constants and the thermal constants of the lunar surface. We were not interested in determining, unless it could be determined easily, the topography of the lunar surface. We recognized that under various propagation conditions the moon's return faded and, in fact, looked like something which was very difficult to analyze on a point-by-point basis or on a slip-of-film-by slip-of-film basis. We recognized very early that significant efforts could be made by radar to map the surface of the moon. Pettingill has made an excellent start in this direction. It was not our concern when analyzing the early lunar radar data to pick out any scattering centers on the surface of the moon, but simply to state that the key scattering centers could be found and to point out that the data we had analyzed suggested that they were approximately 5–10, which number was later increased to "of order 30." We stated that by using the experimental results of modulation loss as determined by Trexler and Youmans and by analyzing the experiments of Aarons, we could predict the maximum radar returns under good propagation conditions at all wavelengths between 100 and 10,000 Mc, and at all pulse lengths. We have been successful,[1,2] in showing that all radar data of the lunar surface were, in fact, in agreement with our predictions as far as this maximum return under optimum propagation conditions is concerned.

Apparently our operational definition of smooth as opposed to rough has not been well understood, and it would appear that the criticisms of our work (for example, by Hughes[3] and Hayre[4]) have been mainly because of this. We were interested in finding out if there was a significant number of perturbations the order of magnitude of a wavelength contributing to the returns from the key scattering centers on the surface of the moon, and we pointed out that a direct measure of the roughness effect could be obtained from a comparison of orthogonal polarizations. We stated that if the differences between orthogonal polarizations were large (10–40 db), then there could not be a significant number of such perturbations dominating the return; we also stated that if the returns from the key scattering centers showed differences of this magnitude, there could be no significant returns from perturbations the order of a wavelength for all radar wavelengths, *e.g.*, 100 Mc to 10,000 Mc, and as a result the moon could be considered a quasi-smooth surface in those regions. We went on to determine the electromagnetic constants for the first key scattering center, and later work showed these values to be in reasonable agreement with the average values obtained for the total lunar surface by radiation data.[5,6] Authors have used other definitions of rough and smooth to criticize our results which, in fact, we feel are not comparable. For example, at long pulse lengths under usual propagation conditions, if there are many scattering centers in the beam, one would expect a good approximation of the return to come from the random phase addition of these many scatterers. If, then, one analyzes the addition function and finds the phase variation is such as to agree with what one could have derived from random phase conditions from earth, then one has a tendency in this phase sense to state that if there are many scatterers present the surface is "rough." Under our definition the surface polarization-wise could still be smooth. For long pulse length returns we would expect to obtain, under normal propagation conditions, typical maximum cross sections which would be associated with the random phase additions from 30 scattering centers, for example. We therefor feel that the statistical evidence presented[3,4,7,8] does not bear on our definition for quasi-smooth. In other words, 30 smooth scattering areas which were in the beam simultaneously and whose phase was such as to vary in a random fashion with height, could agree with the definitions of rough as given[3,4,7,8] but simultaneously would be smooth under our definition. We hope this may clear up some of the arguments that have existed in this field, particularly those arguments which are more concerned with nomenclature than with physics.

T. B. A. Senior
K. M. Siegel
The University of Michigan
Ann Arbor, Mich.

[5] A. E. Salomonovich presented at IAU Symp. No. 14, Leningrad, USSR; December 9, 1960. (To be published by Cambridge University Press, Cambridge, England.)

[6] V. S. Troitskii, presented at IAU Symp. No. 14, Leningrad, USSR December 9, 1960. (To be published by Cambridge University Press, Cambridge, England.)

[7] W. E. Brown, "A lunar and planetary echo theory," *J. Geophys. Res.*, vol. 65, pp. 3087–3095; October, 1960.

[8] F. B. Daniels, "A theory of radar reflection from the moon and planets," *J. Geophys. Res.*, vol. 66, pp. 1781–1788; June, 1961.

WWV and WWVH Standard Frequency and Time Transmissions*

The frequencies of the National Bureau of Standards radio stations WWV and WWVH are kept in agreement with respect to each other and have been maintained as constant as possible with respect to an improved United States Frequency Standard (USFS) since December 1, 1957.

The nominal broadcast frequencies should for the purpose of highly accurate scientific measurements, or of establishing high uniformity among frequencies, or for removing unavoidable variations in the broadcast frequencies, be corrected to the value of the USFS, as indicated in the table below. The corrections reported have been arrived at by means of improved measurement methods based on LF and VLF transmissions.

The characteristics of the USFS, and its relation to time scales such as ET and UT2, have been described in a previous issue,[1] to which the reader is referred for a complete discussion.

The WWV and WWVH time signals are also kept in agreement with each other. Also they are locked to the nominal frequency of the transmissions and consequently may depart continuously from UT2. Corrections are determined and published by the U. S. Naval Observatory. The broadcast signals are maintained in close agreement with UT2 by properly offsetting the broadcast frequency from the USFS at the beginning of each year when necessary. This new system was commenced on January 1, 1960. A retardation time adjustment of 20 msec was made on December 16 1959; another retardation adjustment of 5 msec was made at 0000 UT on January 1, 1961; and a time advancement of 50 msec was made at 0000 UT on August 1, 1961.

WWV Frequency
With Respect to U. S. Frequency Standard

1961 September	Parts in 10^{10}†
1	−152.0
2	−152.1
3	−152.1
4	−152.0
5‡	−151.9
6	−150.6
7	−150.5
8	−150.5
9	−150.5
10	−150.6
11	−150.6
12	−150.5
13	−150.5
14	−150.5
15	−150.3
16	−150.3
17	−150.4
18	−150.3
19	−150.2
20	−150.3
21	−150.2
22	−150.1
23	−150.0
24	−150.0
25	−149.9
26	−149.8
27	−149.7
28	−149.6
29	−149.5
30	−149.5

† A minus sign indicates that the broadcast frequency was low. The uncertainty associated with these values is $\pm 5\times10^{-11}$.
‡ Frequency adjusted $+1\times10^{-10}$ on September 5.

National Bureau of Standards
Boulder, Colo.

[1] Refer to "National Standards of Time and Frequency in the United States," Proc. IRE (Correspondence), vol. 48, pp. 105–106; January, 1950.

Notice of Frequency Adjustment WWV/WWVH

During 1960 and 1961 the nominal frequency of WWV was offset from the U. S. Frequency Standard by −150 parts in 10^{10} in order to establish a unit in close agreement with the value of the unit of UT2.

In 1962 the nominal frequency offset will be −130 parts in 10^{10} for the same reason. The frequency of WWV and WWVH will be higher by 20 parts in 10^{10} beginning at 0000 UT, January 1, 1962.

National Bureau of Standards
Boulder, Colo.

* Received by the IRE, October 26, 1961.

Received by the IRE, November 17, 1961.

Rebuttal to "A Note on Sugai's Class of Solutions to Riccati's Equation"*

The author would like to express his sincere appreciation for Dr. Stickler's interest[1] in his letter.[2] His work is undoubtedly a worthy contribution. However, there are a few interesting items which he did not consider. The purpose of this letter is to mention them briefly and also to discuss the aspect of "generalization" which he seems to have claimed.

Besides the required condition of $Q_1+Q_4=0$, there are four cases of interest as follows:

1) If Q_1 alone is zero, (3)[3] gives a quadratic expression

$$Q_4h^2 + Q_3h + Q_2 = 0,$$

where $h=v'/v$. This says that the condition $Q_1=0$ requires that $c_i(i=1, 2, 3, 4)$ must satisfy the above quadratic expression in order to provide a particular solution for Riccati's equation. Stickler says that Q_1 is not zero but he does not give a reason.

2) If Q_2 alone is zero, (3) yields a solvable Bernoulli's equation,

$$h'Q_1 - Q_1h^2 = Q_3h.$$

3) If Q_3 alone is zero, (3) results in another equation of Riccati:

$$h'Q_1 - Q_1h^2 = Q_2.$$

This has essentially two variable coefficients, as both sides can be divided by Q_1. Fourteen transforms which convert such Riccati equations into first-order linear differential equations are reported.[1] At this point an excellent work by Murphy[5] should be cited, which solved many Riccati and other nonlinear differential equations.

4) If Q_4 alone is zero, (3) gives a first-order linear differential equation,

$$h'Q_1 - Q_3h = Q_2.$$

All of these four cases also require "interrelated" variable coefficients since Q's are related to seven independent variable functions (except Q_1, which is related to four variable functions). It is possible to generate a much more complicated transform in place of (2) such that many combinations of exponential, trigonometric and polynomial functions are included. Yet such a complicated transform of the dependent variable introduces much more complicated interrelationships among variable coefficients with much decreased practical applications.

The basis of Dr. Stickler's generalization seems to have originated from the author's two transforms,[2] $r(x)=R_1s(x)/[s'(x)+P_1s(x)]$ and $r(x)=[s'(x)-P_1s(x)]/[Q_1s(x)]$. On the other hand, they had been derived from two transforms,[6] $y(x)=f(x)g(x)$ and $y(x)=1/[f(x)g(x)]$, where $f(x)$ and $g(x)$ were arbitrary functions of x. It was unfortunate that this background of the two transforms was not mentioned in the previous note,[2] and also that the paper[6] which derived them in detail was not published until May, 1961. These circumstances might have given the impression to readers that those two new transforms were generated by the so-called mathematicians' trick.

The fact that at least two functions $f(x)$ and $g(x)$ are needed, as they are to be related to each other, should be pointed out. Therefore, it is not possible to replace $y(x)$ by $z(x)$ as in $y(x)=z(x)$, which is not a transform but a change of symbols. It is also impossible to replace $y(x)$ by $f(x)\pm g(x)$, for such an expression yields Riccati's equations for $f(x)$ and $g(x)$. The key point is to obtain a solvable equation (linear or nonlinear) by using properly the products of two of the four following variables: $f(x)$, $f'(x)$, $g(x)$, and $g'(x)$, developed by $y'(x)$ and $y^2(x)$. The most compact form of transformations in nonlinear fashions that can be considered is a product or a division of two functions $f(x)$ and $g(x)$. Stickler uses five functions; four of $c_i(x)$'s and $v(x)$. In this respect it should be noted that almost all available books published in the past have mentioned the transform of the type $y(x)=f(x)/g(x)$. These books develop elegant theorems for the general solutions of Riccati's equations after their particular solutions are *somehow* obtained, and they do not mention how these particular solutions can be obtained. In contrast, my other paper[6] was motivated to secure these particular solutions exactly by using the three above-mentioned elementary and compact transforms.

A similar idea to Stickler's for converting Riccati's equations directly into Bernoulli's equations with the requirement of interrelated variable coefficients has been published[7] for the exact solutions of nonuniform transmission lines.

All these works have the common denominator, inter-relationship among variable coefficients. Therefore, any step forward which dispenses with this common denominator is a more "general" method. A small improvement has been published.[8] It combines the original method of Hildebrand, the Cayley factorization technique, and the new transform.[2]

The author would like to explain this slight improvement by taking an example of a practical problem of nonuniform transmission lines. The past exact solutions rigidly interrelated $Z(x)$ and $Y(x)$, even though these line parameters were "arbitrary." What the latest note[2] seems to have proved is that, if the independent variable x (the length of the nonuniform line) is changed to a newly-introduced independent variable w through $w=f(x)$, where $f(x)$ is arbitrary, we can have three arbitrary functions in one equation such as

$$f''(x) - [Z'(x)/Z(x)]f'(x) = [f(x) + B_1]Y(x)Z(x),$$

where B_1 is any constant. The author proposed, in general, *not* to solve for $f(x)$ when $Z(x)$ and $Y(x)$ are given independently and arbitrarily. What he proposed was to assign two independent functions such as $f(x)$ and $Z(x)$ to specify $Y(x)$, or $f(x)$ and $Y(x)$ to determine $Z(x)$, from the above equation, in order to realize the optimum performance of nonuniform lines in terms of its reflection coefficient or its minimum length. To the best knowledge of the author, this approach of having two independent variable parameters for nonuniform lines seems never to have been cited in the literature. This is a slight generalization of Hildebrand's method. For this reason the title "A Generalized Hildebrand's Method for Nonuniform Transmission Lines" was used.

IWAO SUGAI
ITT Federal Laboratories
Nutley, N. J.

* Received by the IRE, August 23, 1961.

[1] D. C. Stickler, "A note on Sugai's class of solutions to Riccati's equation," PROC. IRE (Correspondence), vol. 49, p. 1320; August, 1961.

[2] I. Sugai, "A new exact method of nonuniform transmission lines," PROC. IRE (Correspondence), vol. 49, pp. 627–628; March, 1961.

[3] All equation numbers refer to Stickler.[1] All equations in this article are unnumbered, in order to avoid confusion.

[4] I. Sugai, "A class of solved Riccati's equations," *Elec. Comm.*, vol. 37, pp. 56–60; May, 1961.

[5] G. M. Murphy, "Ordinary Differential Equations and Their Solutions," D. Van Nostrand Co., Inc., Princeton, N. J.; 1960.

[6] I. Sugai, "Exact solutions for ordinary nonlinear differential equations," *Elec. Commun.*, vol. 37, pp. 47–55; May, 1961.

[7] I. Sugai, "Riccati's and Bernoulli's equations for nonuniform transmission lines," IRE TRANS. ON CIRCUIT THEORY (Correspondence), vol. CT-8; September, 1961.

[8] I. Sugai, "A generalized Hildebrand's method for nonuniform transmission lines," PROC. IRE (Correspondence), vol. 49, p. 1945; December, 1961.

On the Hues Seen in Fox-Color Images*

Kallmann[1] has described his observations on a two-color system. The authors have worked in the same field,[2] and would like to draw attention to the following point.

The contrast γ of color separation slides is of crucial importance for obtaining satisfactory tri-color projection. It is therefore very probable that it is important for two-color projection too. E. H. Land used slides with $\gamma=1$ and so did we. H. E. Kallmann does not mention the value of γ of his slides. The contrast of black and white film is generally not equal for different colors. One usually corrects this by choosing different developing times for the green and red separation slides. The exact procedure we used is described in our article.[3] If one does not adjust the developing times to the desired value of γ, one is very likely to get red and green separation slides of unequal contrast and $\gamma\neq 1$. Pictures such as these, combined with additional blue separation slides, yield unsatisfactory tri-color projection.

Although we do not think that this point changes H. E. Kallmann's observations substantially, it might well change the quality judgment of an observer.

C. BURCKHARDT
M. J. O. STRUTT
Swiss Federal Inst. Tech.
Zürich, Switz.

* Received by the IRE, September 18, 1961.

[1] H. E. Kallmann, "On the hues seen in fox-color images," PROC. IRE, vol. 49, pp. 1228–1229; July, 1961.

[2] C. Burckhardt and M. J. O. Strutt, "Experiments with E. H. Land's two-color projection," IRE TRANS. ON BROADCAST AND TELEVISION RECEIVERS, vol. BTR-7, pp. 34–40; April, 1961.

[3] C. Burckhardt and M. J. O. Strutt, "Versuche mit Landscher Zweifarbenprojektion," *Scientia Electrica*, vol. 7, pp. 66–76; June, 1961.

A Stability Test for Linear Discrete Systems in Table Form*

In this note a simple stability test[1,2] similar to Routh's table is being introduced for linear discrete systems. The proof, discussions, and extension of this method will be presented in detail in the future.[3] This test is an alternate to the stability criterion recently developed by Jury[4,5], and it shows that these two criteria are identically equal.[2]

A necessary and sufficient condition for the roots of

$$F(z) = a_0 + a_1 z + a_2 z^2 + \cdots + a_k z^k + \cdots + a_n z^n, \quad \text{with} \quad a_n > 0$$

to have all its roots inside the unit circle in the $z = e^{Ts}$ plane, or equivalently, for the linear discrete system to be stable is obtained as follows.

1) Form the following table: [It should be noted that the elements of row $2k+2$ consist of the coefficients of the row $2k+1$ written in reverse order ($k = 0, 1, 2, \cdots$).]

"Stability Test Table"

Row	z^0	z^1	z^2	$\cdots\cdots$	z^{n-k}	$\cdots$	z^{n-1}	z^n
1	a_0	a_1	a_2	$\cdots\cdots$	a_{n-k}	$\cdots$	a_{n-1}	a_n
2	a_n	a_{n-1}	a_{n-2}	$\cdots\cdots$	a_k	$\cdots$	a_1	a_0
3	b_0	b_1	b_2	$\cdots\cdots$	$\cdots$	$\cdots$	b_{n-1}	
4	b_{n-1}	b_{n-2}	b_{n-3}	$\cdots\cdots$	$\cdots$	$\cdots$	b_0	
5	c_0	c_1	c_2	$\cdots\cdots$	$\cdots$	c_{n-2}		
6	c_{n-2}	c_{n-3}	c_{n-4}	$\cdots\cdots$	$\cdots$	c_0		
$\vdots$	$\vdots$	$\vdots$	$\vdots$	$\vdots$	$\vdots$			
$2n-5$	s_0	s_1	s_2	s_3				
$2n-4$	s_3	s_2	s_1	s_0				
$2n-3$	r_0	r_1	r_2					

where,

$$b_k = \begin{vmatrix} a_0 & a_{n-k} \\ a_n & a_k \end{vmatrix} \qquad d_k = \begin{vmatrix} c_0 & c_{n-2-k} \\ c_{n-2} & c_k \end{vmatrix}$$

$$c_k = \begin{vmatrix} b_0 & b_{n-1-k} \\ b_{n-1} & b_k \end{vmatrix} \qquad r_0 = \begin{vmatrix} s_0 & s_3 \\ s_3 & s_0 \end{vmatrix}$$

$$r_2 = \begin{vmatrix} s_0 & s_1 \\ s_3 & s_2 \end{vmatrix}.$$

2) Check for the constraints inequalities by noting the elements of the first column and the following:

$$F(1) > 0, \qquad F(-1) \begin{matrix} > 0 & n \text{ even} \\ < n & \text{odd} \end{matrix}$$

$$\left.\begin{array}{l} |a_0| < a_n \\ |b_0| > |b_{n-1}| \\ |c_0| > |c_{n-2}| \\ |d_0| > |d_{n-3}| \\ \vdots \\ |r_0| > |r_2| \end{array}\right\} (n-1) \text{ constraints.}$$

The above constraints constitute the necessary and sufficient conditions for stability of any order linear discrete systems.

It is noticed from the table that a certain computation involved in dotted entry in in row $2n-3$ becomes redundant. Therefore, the corresponding second-order determinant to be calculated in entries $2n-4$, and $2n-5$ is also redundant.

Examples

1) $F(z) = 3 - 2z - \frac{3}{2}z^2 + z^3, \qquad n = 3.$

By applying the first constraints, we notice $F(1)>0$, $F(-1)>0$, and, since $n=3$, the system is unstable and the test could be discontinued. However, for the sake of illustration we form the table for this case as follows:

Row	z^0	z^1	z^2	z^3
1	3	-2	$-\frac{3}{2}$	1
2	1	$-\frac{3}{2}$	-2	3
3	8	$\frac{9}{2}$	$-\frac{5}{2}$	

For the remainder of the stability constraints,

$$3 > 1, \qquad |a_0| < a_n,$$

violated

$$8 > \frac{5}{2}, \qquad |b_0| > |b_{n-1}|.$$

Therefore, the system is unstable. It should be added that by certain combinations of variation of signs one can obtain information on the number of roots inside the unit circle.[3] In this case, all the roots are outside the unit circle and no root is inside the unit circle.

2) $F(z) = 0.0025 + 0.08z + 0.4126z^2 - 1.368z^3 + z^4, \quad n = 4.$

Row	z^0	z^1	z^2	z^3	z^4
1	0.0025	0.08	0.4126	-1.368	1
2	1	-1.368	0.4126	0.08	0.0025
3	$\simeq -1$	1.368	-0.4116	-0.0834	
4	-0.0834	-0.4116	1.368	-1	
5	0.9936	-1.402	0.5256		

* Received by the IRE, August 21, 1961.

[1] M. Marden, "The geometry of the zeros of a polynomial in a complex variable," *Am. Math. Soc.*, pp. 148–161; 1949.

[2] Y. Tyspkin, "Theory of Pulse Systems," State Press for Physics and Mathematical Literature, Moscow, USSR, pp. 423–427; 1958. (In Russian.)

[3] E. I. Jury and J. Blanchard, "On the roots of a real polynomial inside the unit circle and a stability criterion for linear discrete systems," to be published in *Trans. AIEE.*

[4] E. I. Jury, "A Simplified Stability Criterion for Linear Discrete Systems," University of California, Berkeley, ERL Rept. No. 373; June, 1961.

[5] E. I. Jury, "Discussion on 'The stability of sampled-data systems,' by Van J. Tschauer," *Regelungstechnik*, Münich, Germany, RT8, pp. 42–46; 1960.

Stability test:

$$F(1) = 0.1271 > 0, \quad F(-1) = 2.703 > 0$$
$$0.0025 < 1, \quad |a_0| < a_n$$
$$1 > 0.0834, \quad |b_0| > |b_{n-1}|$$
$$0.9936 > 0.5256, \quad |c_0| > |c_{n-2}|$$

The system is stable.

In conclusion, this criterion is particularly useful if the coefficients of $F(z)$ are given in numbers, for in this case the stability computation involves only second-order determinants which is very simple for hand computations.

E. I. Jury
J. Blanchard
Dept. of Elec. Engrg.
University of California
Berkeley, Calif.

A Stability Test for Linear Discrete Systems Using a Simple Division*

In a preceding note [1] a stability test has been presented for linear discrete systems using table form. In this discussion an alternate procedure for the table form is indicated in which the test involves simple division of polynomials.

The stability test will be presented first and its validity second, shown by using the preceding criterion [1].

A necessary and sufficient condition for the polynomial

$$F(z) = a_0 + a_1 z + a_2 z^2 + \cdots + a_k z^k + \cdots + a_n z^n, \quad \text{with} \quad a_n > 0 \tag{1}$$

to have all its roots inside the unit circle in the $z = e^{Ts}$ plane, or equivalently, for the linear discrete system to be stable, is obtained as follows:

1) Form the inverse polynomial of $F(z)$ as follows:

$$F^*(z) = z^n F(1/z) = a_n + a_{n-1} z + a_{n-2} z^2 + \cdots + a_{n-k} z^k + \cdots + a_0 z^n. \tag{2}$$

2) Obtain the stability constraints α_k by simple division as shown

$$\frac{F(z)}{F^*(z)} \to \alpha_0 + \frac{F_1(z)}{F_1^*(z)} \to \alpha_0 + \alpha_1 + \frac{F_2(z)}{F_2^*(z)} \to \alpha_0 + \alpha_1 + \alpha_2 + \frac{F_3(z)}{F_3^*(z)} + \cdots \to \alpha_0 + \alpha_1 + \alpha_2 + \cdots + \alpha_{n-2} + \frac{F_{n-1}(z)}{F_{n-1}^*(z)}, \tag{3}$$

where $F_1(z)$, $F_2(z) \cdots$ are the remainder polynomials obtained from the division and $F_1^*(z)$, $F_2^*(z) \cdots$ are their inverses, as defined in (2).

* Received by the IRE, August 31, 1961.

In this case it is only necessary to obtain α_0 and α_1.

$$\frac{F(z)}{F^*(z)} \to \frac{a_0}{a_3} + \frac{\frac{a_1a_3 - a_0a_2}{a_3} z + \frac{a_2a_3 - a_0a_1}{a_3} z^2 + \frac{a_3^2 - a_0^2}{a_3} z^3}{\frac{a_3^2 - a_0^2}{a_3} z + \frac{a_1a_3 - a_0a_1}{a_3} z^2 + \frac{a_1a_3 - a_0a_2}{a_3} z^3} \to \frac{a_0}{a_3} + \frac{a_1a_3 - a_0a_2}{a_3^2 - a_0^2} + \cdots.$$

3) Satisfy the following constraints for the stability test:

$$F(1) > 0, \quad F(-1) \begin{cases} > 0, & n \text{ even} \\ < 0, & n \text{ odd} \end{cases}, \quad |\alpha_k| < 1, \quad k = 0, 1, 2, \cdots, n-2. \tag{4}$$

The proof of the above test lies in the use of the preceding stability criterion, for it can be easily established that the identity of α_k's and the stability constants, a_0, b_0, c_0, $\cdots$, are as follows [1]:

$$\alpha_0 = \frac{a_0}{a_n}, \quad \alpha_1 = \frac{b_{n-1}}{b_0}, \quad \alpha_2 = \frac{c_{n-2}}{c_0}, \quad \cdots, \quad \alpha_{n-2} = \frac{r_2}{r_0}.$$

Thus

$$\alpha_0 = \frac{a_0}{a_3}, \quad \alpha_1 = \frac{a_1a_3 - a_0a_2}{a_3^2 - a_0^2}.$$

The stability constraints are

$$F(1) > 0, \quad F(-1) < 0, \quad \frac{|a_0|}{a_3} < 1, \quad \left|\frac{a_1a_3 - a_0a_2}{a_3^2 - a_0^2}\right| < 1.$$

3) $F(z) = 0.0025 + 0.08z + 0.4126z^2 - 1.368z^3 + z^4$

$F^*(z) = 1 - 1.368z + 0.4126z^2 + 0.08z^3 + 0.0025z^4.$

In this case we need obtain α_0, α_1, α_2 as follows:

$$1 - 1.368z + 0.4126z^2 + 0.08z^3 + 0.0025z^4 \Big) \underline{0.0025 + 0.08z + 0.4126z^2 - 1.368z^3 + z^4} \Big(0.0025$$
$$0.0025 - 0.0034z + 0.001z^2 - 0.002z^3 + \simeq 0z^4$$

$$z - 1.368z^2 + 0.4116z^3 + 0.0834z^4 \Big) \underline{0.0834z + 0.4116z^2 - \sim 1.368z^3 + z^4} \Big(0.0834$$
$$0.0834z - 0.114z^2 + 0.0342z^3 + 0.007z^4$$

$$0.993z^2 - 1.4022z^3 + 0.5256z^4) 0.5256z^2 - 1.4022z^3 + 0.993z^4 \Big(0.53$$

From the stability constraints imposed previously on the a's, b's, $\cdots$, the constraints to be imposed on the α_k's are readily established, as explained in (4).

Examples

To illustrate the procedure to be followed, we establish the constraints in general terms for $n = 2$, $n = 3$, and provide a stability test for $n = 4$ when the coefficients of the latter polynomial are given in numbers:

1) $F(z) = a_0 + a_1 z + a_2 z^2, \quad a_2 > 0.$

In this case $F^*(z)$ is given as

$$F^*(z) = a_2 + a_1 z + a_0 z^2.$$

α_0 is obtained from

$$\frac{F(z)}{F^*(z)} \to \alpha_0 + \cdots, \quad \alpha_0 = \frac{a_0}{a_2}.$$

The stability contraints are

$$a_0 + a_1 + a_2 > 0, \quad a_0 - a_1 + a_2 > 0, \quad |\alpha_0| < 1, \quad \frac{|a_0|}{a_2} < 1.$$

2) $F(z) = a_0 + a_1 z + a_2 z^2 + a_3 z^3, \quad a_3 > 0$

$$F^*(z) = a_3 + a_2 z + a_1 z^2 + a_0 z^3.$$

It should be noted that in obtaining α_0, α_1, and α_2, the terms encircled in dotted lines as above need not be calculated. Similarly, such simplification could also be obtained from the previous examples.

In this case,

$$\alpha_0 = 0.0025, \quad \alpha_1 = 0.0834, \quad \alpha_2 = 0.53.$$

For stability constraints:

$$F(1) = 0.1271 > 0 \quad F(-1) = 2.703 > 0, \quad 0.0025 < 1, \quad 0.0834 < 1, \quad 0.53 < 1.$$

The system is stable as also shown in the preceding note[1].

In conclusion, one may notice that this test is similar to the preceding test, except that it is written in a different form. The advantages of this procedure are twofold: 1) This form is easier to remember. 2) One may not need knowledge of determinants; this form also provides a minor simplification. This procedure is equivalent to the continued fraction expansion method used for stability test of linear continuous systems.

ACKNOWLEDGMENT

The author would like to thank Dr. M. A. Pai for a discussion which was helpful in writing this note.

E. I. JURY
University of California
Berkeley, Calif.

REFERENCES

[1] E. I. Jury and J. Blanchard, "A stability test for linear discrete system in table form," PROC. IRE, vol. 49, pp. 1947–1948; December, 1961.
[2] E. I. Jury, "Additions to 'Notes on the stability criterion for linear discrete systems'," IRE TRANS. ON AUTOMATIC CONTROL, vol. AC-6 pp. 342–343; September, 1961.
[3] E. I. Jury, "A Simplified Stability Criterion for Linear Discrete Systems," University of California, Berkeley, ERL Rept. No. 373; June, 1961.

Duality of Planar Networks*

A recent communication[1] describes a method of forming the dual of a planar network which contains transformers. In this note I would like to describe a slightly different approach to duality and show how it clarifies certain controversial issues. In this respect it is suggested that this new approach may be more fundamental and may, in fact, be the basic law governing the duality of networks.

SIGNIFICANCE OF EIGENVALUES

The dual of a planar network is usually acquired by dualizing each term of the mesh or nodal equations, or by operating on the network matrices as described in the literature.[2] For instance, if (Z_1) is the Z matrix of a network, then $(1/r^2)(Z_1)$ is the Y matrix, and $r^2(Z_1)^{-1}$ is the Z matrix of the dual network. Thus, dual networks can be formed by matrix inversion. It follows, therefore, that the product of the Z (or Y) matrices of two mutually dual networks is equal to the unity matrix I, multiplied by a scalar factor r^2 (or $1/r^2$ in the case of Y matrices).

$$(Z_1)(Z_1)^{-1} = I = (Z_1)^{-1}(Z_1)$$
$$r^2(Z_1)(Z_1)^{-1} = r^2 I = (Z_1)r^2(Z_1)^{-1}$$

Therefore, if (Z_1) and (Z_2) are the Z matrices of two dual networks,

$$(Z_1)(Z_2) = r^2 I \qquad (1)$$
$$\left| (Z_1)(Z_2) - r^2 I \right| = 0. \qquad (2)$$

Eq. (1) resembles the usual definition of dual impedances z_1 and z_2, where $z_1 z_2 = r^2$ and r^2 is a frequency independent positive constant with the dimensions of resistance squared. Since (2) is the characteristic equation of the product $(Z_1)(Z_2)$, the following definition of duality is prompted.

Two networks are dual if the characteristic equation of the matrix product of their Z (or Y) matrices has equal, positive eigenvalues whose dimensions are those of resistance (or conductance) squared.

Before applying this definition, it is instructive to consider the simplest dual networks with one element as shown in Fig. 1. Obviously, the inverse matrix method breaks down in this simple case, while the well-used mesh and nodal operation does not. The reason is very clear; the Z matrix of network 1 and the Y matrix of network 2 do not describe the single impedance element in any way. Therefore, when using the inverse matrix method, it is a necessary condition that the matrices fully describe the networks concerned.

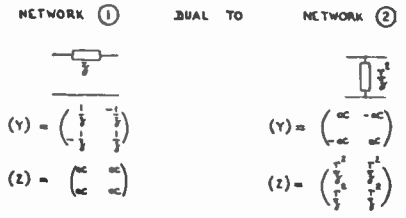

Fig. 1—Simple dual networks.

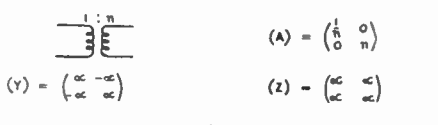

(a)

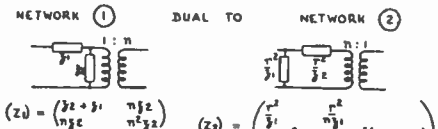

(b)

Fig. 2—(a) Ideal transformer. (b) Network and an ideal transformer.

A. The Transformer

Consider the ideal transformer with descriptive matrices as in Fig. 2(a). Apart from the fact that a dual is not indicated by taking inverse matrices, the matrix elements are dimensionless and therefore, any solution to the characteristic equation previously mentioned cannot have the dimensions of resistance squared. This requirement of the eigenvalues would indicate that there is no dual network for an ideal transformer, thus explaining much past controversy. Since a transformer operates on networks, it seems natural to absorb a transformer into the Z or Y matrix of an accompanying network before attempting to find the dual of the network. Any transformers in the dual network can then be extracted. As an example of this procedure consider a practical transformer with leakage inductance z_1 and magnetizing inductance z_2 as shown in Fig. 2(b) (where these effects have been separated from the ideal transformer $1:n$). The details in Fig. 2(b) substantiate the findings in the literature[1] and indicate how an ideal or a practical transformer may be treated.

B. The Gyrator

The fictitious circuit element called a gyrator has found great use in duality studies[3] and apparently, unlike the transformer, has presented no controversy. It is easily shown that gyrators fulfill the eigenvalue requirements.

C. Transistors and Vacuum Tubes

The synthesis[4,5] of active devices suggests the existence of their duals. The duality between present-day active devices will now be dealt with. This subject has been discussed in the literature,[2,3] where the arguments have been mainly descriptive. It has been stated that the junction transistor (common-emitter) is the dual of the vacuum-tube triode (common cathode). Yet it is an undisputable fact that junction transistor circuitry is analogous, and not dual, to its vacuum-tube counterpart. In fact, most vacuum-tube circuits can be transistorized by simply lowering the impedance levels of interconnecting networks.

Let (Y_{ij}) and (y_{ij}) be the Y matrices of the junction transistor (common-emitter) and triode (common-cathode), respectively. To test for duality, (3) is inspected.

$$\left| \begin{pmatrix} Y_{11} & Y_{12} \\ Y_{21} & Y_{22} \end{pmatrix} \begin{pmatrix} y_{11} & y_{12} \\ y_{21} & y_{22} \end{pmatrix} - \frac{1}{r^2} \cdot I \right| = 0. \qquad (3)$$

On substituting practical values in (3), it is very obvious that duality between these devices is most unlikely. For instance, at low frequencies it is usual to take y_{11}, y_{12} and Y_{12} as zero, in which case (3) becomes (4).

$$\frac{1}{r^2}\left(\frac{1}{r^2} - y_{22} Y_{22} \right) = 0. \qquad (4)$$

The eigenvalues are 0 and $y_{22}Y_{22}$; therefore, the proposed conditions for duality are not fulfilled.

In searching for duality among active devices it is interesting to note that it is most strongly exhibited within the configurations of one type of device. For instance, let (Y_{ij}') and (y_{ij}') be the Y matrices of a junction transistor in the common-base and common-collector configurations, respectively. The characteristic equation is (5)

$$\left| \begin{pmatrix} Y_{11}' & Y_{12}' \\ Y_{21}' & Y_{22}' \end{pmatrix} \begin{pmatrix} y_{11}' & y_{22}' \\ y_{21}' & y_{22}' \end{pmatrix} - \frac{1}{r^2} \cdot I \right| = 0. \qquad (5)$$

At low frequencies it is valid to put $Y_{12}' = y_{12}' = 0$; for identical bias conditions Y_{11}', Y_{21}', y_{22}' and $-y_{21}'$ are all approximately equal to g_m, the forward transconductance. Eq. (5) becomes (6):

$$\left(y_{11}' g_m - \frac{1}{r^2} \right)\left(Y_{22}' g_m - \frac{1}{r^2} \right) = 0. \qquad (6)$$

In practice, y_{11}' and Y_{22}' are very small and of similar order, thus yielding eigenvalues $y_{11}'g_m$ and $Y_{22}'g_m$ which are approximately equal, positive, and of the dimensions conductance squared. It could be said,

* Received by the IRE, August 21, 1961.
[1] P. G. Griffith, "Duality as applied to transformers," PROC. IRE (Correspondence), vol. 49, pp. 816–817; April, 1961.
[2] R. F. Shea, "Principles of Transistor Circuits," John Wiley and Sons, Inc., New York, N. Y.; 1954.
[3] R. L. Wallace, Jr., and G. Raisbeck, "Duality as a guide in transistor circuit design," *Bell Sys. Tech. J.*, vol. 30, pp. 381–417; April, 1951.
[4] J. Shekel, "The gyrator as a three-terminal element," PROC. IRE, vol. 42, pp. 1014–1016; August, 1953.
[5] H. J. Carlin, "Theory and Application of Gyrator Networks," Polytechnic Inst. of Brooklyn, N. Y., Res. Rept. 289; March, 1954.

then, that these two basic configurations of a transistor tend to be dual. (Similar results apply to the two vacuum-tube configurations, common-grid and common-anode.) The existence of this approximate duality is certainly suggested by the details of Fig. 3, where the networks of (a) are dual to those in (b) and the impedance levels are consistent with the transistor configurations.

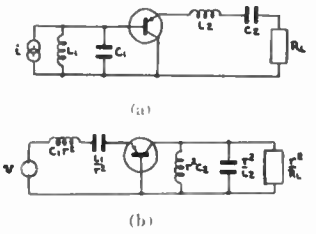

Fig. 3. (a) Common-collector amplifier. (b) Common-base amplifier.

Conclusion

The above examples suggest that consideration of the eigenvalues gives a deeper insight into the existence of duality. In this light the duality of networks could be defined as follows:

Definition: Let (Z_1) and (Z_2) be the Z matrices which fully describe two active or passive networks Z_1 and Z_2. Then Z_1 and Z_2 are dual if the characteristic equation of $(Z_1)(Z_2)$ has eigenvalues which are positive, equal, and have the dimensions of resistance squared (or conductance squared in the case of Y matrices).

J. R. James
Radar and Telecommun. Branch
Royal Military College of Science
Swindon, Eng.

Schwarz's Lemma and Linear Passive Systems*

The physical interpretation of some basic mathematical theorems often leads to equally interesting results concerning the performance of a class of physical systems. Sometimes the situation is the other way around, that is, a relatively sophisticated mathematical fact has a physically trivial counterpart.

The subject of this note is to derive a physical interpretation of one of the fundamental theorems of Function Theory known as Schwarz's lemma. It turns out that this lemma suggests a basic inequality between active and reactive power of a linear passive one-port. The inequality is far from being trivial.

Schwarz's lemma is one of the basic theorems of Function Theory which has been subjected to many generalizations and ramifications for more than half a century. It appears as though the lemma comprises some fundamental thought which is not to be disposed of by the mode du jour. The statement of the lemma in its simplest form is given below.

Schwarz's lemma: Let $f(z)$ be a function analytic in the region $|z|<1$ and let

i) $|f(z)| \leq 1$ for $|z| < 1$

ii) $f(0) = 0$.

Then,

$$|f(z)| \leq |z| \quad \text{in} \quad |z| < 1. \qquad (1)$$

and the inequality can hold only when $f(s)=e^{j\alpha}z$, α being a real constant. In geometric language, the lemma states that the euclidean distances to the origin are not increased by this very general class of analytic mapping functions. (See Fig. 1.)

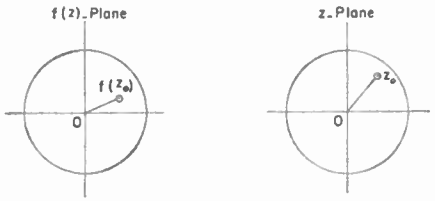

Fig. 1.

Schwarz's basic lemma, as expected, has penetrated in numerous branches of physical sciences. When the function describing a physical problem is properly normalized in the reference frame of the unit disk, one can infer from the lemma a fundamental upper limit for the performance of the associated linear system. Furthermore, with the proper mathematical manipulations, one may derive more informative bounds at the price of being confined to a more restrictive family of linear systems.

The electrical engineering profession has had its own share of benefit in the use of this lemma. The theorem appears, I believe, since 1930 in the literature of the circuit theory. The reader interested in some of the applications of this theorem to Network Synthesis may wish to refer to one of several existing books on the subject or to the literature.[1-5]

As an example of the use of Schwarz's lemma, we apply the theorem to $Z(s)$ the driving-point impedance or admittance function of a bilateral linear passive network. For the complex frequency $s=\alpha+j\beta$, the active and reactive powers under the above steady-state regime are, respectively,

$$U(\alpha,\beta) = \operatorname{Re} Z(\alpha+j\beta),$$
$$V(\alpha,\beta) = \operatorname{Im} Z(\alpha+j\beta). \qquad (2)$$

In order to apply the lemma, one may use a well known linear transformation of the frequency and the impedance function, that is,

$$\frac{Z(s)-Z(s_0)}{Z(s)+\overline{Z(s_0)}}; \qquad \frac{s-s_0}{s+\bar{s}_0} \qquad \operatorname{Re} s_0 > 0. \qquad (3)$$

Since the conditions of the lemma are now satisfied, one can derive a suitable generalization of (1) for driving-point impedance or admittance functions. (These functions are generally referred to as Positive Real Functions, or PRF in abbreviated form.)

Theorem: For any PRF we have

$$\left|\frac{Z(s)-Z(s_0)}{Z(s)+\overline{Z(s_0)}}\right| \leq \left|\frac{s-s_0}{s+\bar{s}_0}\right|$$
$$\operatorname{Re} s > 0, \ \operatorname{Re} s_0 > 0. \qquad (4)$$

A geometric interpretation of this inequality is rather interesting. Fig. 2 suggests that for a physically realizable one-port we have

$$\frac{A'B'}{A'C'} \leq \frac{AB}{AC}. \qquad (4a)$$

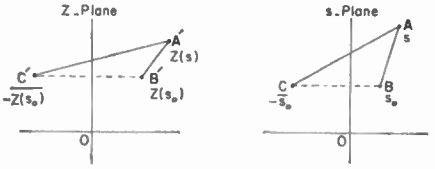

Fig. 2.

We note with interest that the ratio of two euclidean distances appears in our calculation. (There are other forms of the theorem expounding on noneuclidean distances. See for instance G. Pick's theorem in Caratheodory[6] which has been employed in the well-known paper of O. Brune. See also Bolinder.[4])

To translate this inequality in physical language, we let

$$Z(s_0) = Z(\alpha+j\beta) = U_0 + jV_0,$$

and write

$$\left|\frac{(U-U_0)+j(V-V_0)}{(U+U_0)+j(V-V_0)}\right| \leq \left|\frac{(\alpha-\alpha_0)+j(\beta-\beta_0)}{(\alpha+\alpha_0)+j(\beta-\beta_0)}\right| \qquad (5)$$

$$\frac{(U-U_0)^2+(V-V_0)^2}{(U+U_0)^2+(V-V_0)^2} \leq \frac{(\alpha-\alpha_0)^2+(\beta-\beta_0)^2}{(\alpha+\alpha_0)^2+(\beta-\beta_0)^2}. \qquad (6)$$

This is a general inequality which illustrates the Schwarz's lemma for PRF.[7] The inequal-

* Received by the IRE, August 30, 1961. This work was partially supported by the Rome AF Dev. Center.

[1] P. I. Richards, "A special class of functions with positive real parts in a half-plane," *Duke Math. J.*, vol. 14, pp. 777–786; month, 1947.
[2] A. Fialkow and I. Gerst, "Impedance synthesis without minimization," *J. Math. Phys.*, vol. 34, pp. 160–168; October, 1955.
[3] N. Balabanian, "Network Synthesis," Prentice-Hall, Englewood Cliffs, N. J.; 1958.
[4] E. F. Bolinder, "Impedance and Power Transformations by the Isometric Circle Method and Non-Euclidean Hyperbolic Geometry," Res. Lab. of Electronics, Mass. Inst. Tech., Cambridge, Tech. Rept. No. 312; June 24, 1957.
[5] F. M. Reza, "A supplement to the Brune synthesis," *Trans. AIEE*, vol. 74, pp. 85–90; March, 1955.
[6] C. Caratheodory, "Theory of Functions of a Complex Variable," Chelsea Publishing Co., New York, N. Y., vol. 2, ch. 1; 1959.
[7] The reader is assumed to be familiar with the physical meaning of applying an excitation with $s=\alpha+j\beta$ which requires the introduction of resistors along with all inductors and capacitors.

ity (4) can be further employed for obtaining more specialized results if desired so. For example, if we let $s_0=a>0$, we find as a corollary for any PRF

$$\frac{Z(s)}{s} \leq \frac{Z(a)}{a} \qquad s>a>0. \tag{7}$$

(7) is one of many results which can be derived from (4). Other results and interpretation of other forms of this lemma such as Jensen's theorem have been derived by the author. The latter being perhaps of more interest to the professional circuit theorists will be given elsewhere.

F. M. Reza
Dept. of Elec. Engrg.
Syracuse University
Syracuse, N. Y.

Discussion of "Forward Scattering by Coated Objects Illuminated by Short Wavelength Radar"*

In the course of a theoretical study on bistatic scattering measurements, I came across what appears to be an experimental error published in Proceedings.[1] As shown in Fig. 6 of the article by Hiatt, Siegel, and Weil, forward-scatter cross sections are measured by placing the test target between transmitting and receiving horns in a transmission path which has been nulled out via a secondary circuit. This interpretation is verified by the "Experimental Procedures" sec- of the article.

The fallacy of this procedure can be seen by measuring the forward-scattering characteristics of:

1) a matched termination or attenuator,
2) a short circuiting wall between horns, or
3) a matched phase shifter.

In each case a substantial scattering cross section dependent on transmitting antenna gain will be measured where, in fact, none exists at all.

In a more recent article,[2] another experimenter displays a similar arrangement of equipment in Fig. 21 for the same purpose. However, since the latter paper conspicuously avoids any measurements in the region of 180° direct forward scatter, it may be assumed that the error was not repeated. It must be recognized that forward scattering cannot be rigorously defined or measured at a bistatic angle of 180°.

J. Fisch
20 Elmwood Lane
Syosset, N. Y.

* Received by the IRE, July 20, 1961.
[1] R. E. Hiatt, K. M. Siegel, and H. Weil, "Forward scattering by coated objects illuminated by short wavelength radar," Proc. IRE, vol. 48, pp. 1630–1635; September, 1960.
[2] R. J. Garbacz and D. L. Moffatt, "An experimental study of bistatic scattering from some small, absorber coated, metal shapes," Proc. IRE, vol. 49, pp. 1184–1192; July, 1961.

Authors' Comment[3]

Fisch states that it is an utter fallacy to measure the forward-scattering characteristics of an object by the method used by the authors,[1] where the test target is placed between the transmitting and receiving horns in a transmission path which has been nulled out via a secondary circuit. We are at a loss to understand his defense of this position. Fisch proposes to disprove our procedure by measuring the forward-scattering characteristics of certain transmission line components, *i.e.*, a matched termination. He has stated that "a substantial scattering cross section dependent on transmitting antenna gain will be measured where, in fact, no forward-scattering cross section exists." This statement is untrue in two ways. First, the measured scattering cross section will not depend on antenna gain (it is assumed that the target is placed in a region of plain wave illumination); it will depend only on the degree to which the field incident on the receiving horn is changed by the energy absorbed and scattered by the test target. It is common practice to determine the amount of change by introducing a known scatterer such as a sphere. Second, Fisch is wrong when he states that his proposed test targets have no (forward) scattering cross section. This statement hardly warrants a rebuttal. Any object that changes the incident energy, whether it be a perfect piece of radar absorbing material, a matched antenna or one of Fisch's test targets will have a forward-scattering cross section. We[1] have shown by an approximate method, and Logan[4] has shown by consideration of the exact sphere solution, that the leading term in the asymptotic expansion of the forward-scattering cross section for high frequencies is precisely $4\pi A^2/\lambda^2$, where A is the area outlined by the boundary between the lit region and the shadow region of the target. The close agreement between our experimental results, our theoretical results, and Logan's theoretical results, shown in Fig. 1 of reference 1, should have convinced Fisch that no glaring experimental error had been committed. The method we use, and for which we take full responsibility, is very similar to that used by Hamren[5] in measuring forward-scatter cross-section areas. The block diagram describing his method is almost indentical to our block diagram. Hamren's method and other methods are described by King and Wu.[4]

It is almost amusing to hear "that forward scattering cannot be rigorously defined or measured at a bistatic angle of 180°." In saying this Fisch has discarded much of theoretical diffraction theory in electromagnetics and most of nuclear scattering theory, as the optics theorem relates the total cross section to the imaginary part of the forward-scattering amplitude. Since according to Fisch the forward-scattering amplitude is beyond definition, then by the above theorem so is the total cross section; again working backwards Fisch has "shown" that we can't define conservation of energy for all scattering systems in all branches of physics. Luckily for those of us working in physics Fisch is wrong, and most of our physical laws will last a good deal longer. Apparently, more work should be published explaining the bright line behind the penny, so that forward-scattering answers will be no longer the mystery some people now believe them.

We would like to take this opportunity to point out the good agreement between the experimental results of Garbacz and Moffatt[2] and the theoretical predictions in reference 1. We are happy to see this agreement in the resonance region.

K. M. Siegel
R. E. Hiatt
Radiation Laboratory
University of Michigan
Ann Arbor, Mich.

[3] Received by the IRE, August 9, 1961.
[4] R. W. P. King and T. T. Wu, "Scattering and Diffraction of Radio Waves" (Appendix for Logan's work), and pp. 192–194 of Hamren's work (see reference 5 below), Harvard University Press, Cambridge, Mass.; 1959.
[5] S. D. Hamren, "Scattering from Spheres," Elec. Engrg. Dept., University of California, Berkeley, Rept. 171; June 15, 1950.

Inductive Probability as a Criterion for Pattern Recognition*

Consider a sequence of length n composed of elements from the set $\{A_j\}$. Then the inductive probability that the next member of the sequence will be A_p is

$$P^*(A_p) = \frac{n_p + \omega_p}{n + \sum_p \omega_p}, \tag{1}$$

where n_p is the number of times A_p appears in the sequence, and ω_p is the logical width of A_p.[1] If there are m elements and the logical widths are the same, this reduces to

$$P^*(A_p) = \frac{n_p + 1}{n + m}. \tag{2}$$

To extend this measure to pattern recognition consider, as an example, the case in which there are only two elements A_1 and A_2. Suppose, for example, the sequence is

$$A_1A_2A_1A_2A_1A_2A_1A_2.$$

The inductive probability that the next element of the sequence will be A_1 is given by relation 2, in which

$$\left.\begin{aligned} n &= 8 \\ n_p &= 4 \\ m &= 2 \end{aligned}\right\} \qquad \therefore\ P^*(A_1) = 1/2.$$

The probability that the next elements will A_1A_2 is given by

$$\left.\begin{aligned} n &= 4 \\ n_p &= 4 \\ m &= 4 \end{aligned}\right\} \qquad \therefore\ P^*(A_1A_2) = 5/8.$$

* Received by the IRE, August 14, 1961.
[1] R. Carnap, "Logical Foundations of Probability," University of Chicago Press, Chicago, Ill.; 1950.

In this case, the pairs (A_1A_1), (A_1A_2), (A_2A_1) and (A_2A_2) are considered as the basic blocks. Similarly,

$$P^*(A_1A_2A_1A_2) = \frac{2+1}{2+16} = \frac{3}{18}$$

$$P^*(A_1A_2A_1A_2A_1A_2) = \frac{1+1}{1+64} = \frac{2}{65}.$$

Note that the prediction (A_1A_2) has the largest measure. This is because not only does it match the pattern, but it does so with the fewest possible elements. The extension to nonbinary cases is obvious.

However, there is an objection to this application of inductive probability. What can be done if the sample sequence is not composed of complete period? In the above example, how do we test for repetitions over three elements?

BERNARD HARRIS
College of Engrg.
New York University
New York, N. Y.

Law for Noise Loading of Multivoice-Channel FD Systems*

The concept of using a white noise signal with uniform power density over the baseband for the analysis and testing of multivoice-channel systems using FD multiplex has now become well-established in the art.

The rms level of this signal is made to correspond to the level expected of the complex baseband signal when voice traffic is actually present. Normally the level is that which is not expected to be exceeded for more than 1 per cent of the busy hour, based on the classic work of Holbrook and Dixon.[1] Curve A, of Fig. 1, is scaled from their Fig. 6, Curve B, which is usually used for this purpose.

In pursuance of this approach, the CCIR has suggested the rms level of the white noise signal should be

$$[-15 + 10 \log N] \text{ dbm0}, \qquad N > 240$$

$$[-1 + 4 \log N] \text{ dbm0}, \qquad 240 > N > 60.$$

These relations are shown by Curves B and C respectively.

The Holbrook and Dixon curve did not include the effect of normal channel limiting, allowance for this being applied to their "instantaneous load capacity" data. As shown by Jacobsen,[2] this factor introduces a significant discrepancy. For this reason, it was suggested by the writer[3] that the rms level could be approximated with sufficient accuracy for design purposes by a law of the form

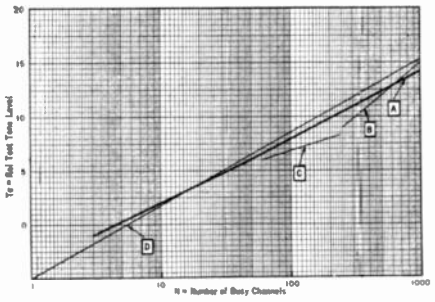

Fig. 1.

$$T_c = AN^{\alpha}, \tag{1}$$

where

T_c = rms power level of complex signal relative to single-channel test tone.
N = number of busy channels.
A, α = constants depending on the busy hour statistics.

Subrizi[4] later indicated that speech volumes had tended to decrease since Holbrook and Dixon carried out their work, thereby reducing the composite rms level. On the other hand, some allowance must be made in the operative system for carrier leak, dialing impulses, and the like.

Taking these into account, the writer[5] subsequently suggested the rms level for the "1 per cent of the busy hour" criterion, could be expressed satisfactorily by the relation

$$T_c = 0.315N^{0.67} \tag{2}$$

or in db,

$$(-5 + 6.7 \log N)1000 > N > 3.$$

This is shown as our Curve D. As can be seen, this is a closer fit to the original data than the CCIR values over most of the range.

The concept of a single law to represent rms loading is particularly valuable in comparative studies of systems, in terms of both performance and economics.

The number of teletype channels used varies considerably from system to system. Consider, however, a typical case of one voice channel in eight used for this purpose. On the basis of 18 FSK telegraph channels per voice channel and CCIR levels, the average power per voice channel so allocated will be -7.5 dbm0.

The composite N channel system level will then be

$$T_c' = A\left(\frac{7N}{8}\right)^{\alpha} + \left(\frac{N}{8}\right)\frac{1}{5.7}. \tag{3}$$

(Similar equations can of course be derived for other telegraph channel densities.)

The ratio γ between this power and that obtained from (2) (assuming all channels are used for voice) is

$$\delta = (0.875)^{\alpha} + \frac{N^{(1-\alpha)}}{14.5}.$$

Thus, there is only a small error in using (1) to represent the loading for voice plus telegraph channel densities up to the value indicated.

A further factor to be considered is that all the curves shown here are based on N busy channels. When the data are applied to an N channel capacity system, it is implied that all channels are "busy"; *i.e.*, the trunk occupancy is unity, a condition which never applies in sound engineering design. For small numbers of channels this may be as low as 0.4, or less, so that an rms level based on N channels rather than that expected from the trunk occupancy, tends to be somewhat conservative. On the other hand, this further supports the use of (2), for nominal ratios of voice-to-telegraph channels, since the increased loading due to the latter tends to be offset by the reduced occupancy.

C. A. PARRY
Page Communications Engineers, Inc.
Washington, D. C.

Reliability Factors in Thermoelectric Generator Design*

A multitude of semiconductor thermocouple elements are required in large-scale thermoelectric generators. Ideally the thermocouples may be series-paralleled in any manner to achieve the required load voltage and current. However, from a practical standpoint, the mean-time-to-failure of a thermocouple will place limits on the permissible series-parallel arrangement.

Consider the schematic generator circuit of Fig. 1; a total of S subsystems, each with n thermocouples in series, are operating in parallel. Assuming identical operating conditions and performance for each thermocouple, the line current, I_L, is simply SI, where I_e is the current through any single thermocouple. Failure of an individual thermocouple (failure is considered to be an open circuit) will interrupt the output of an entire subsystem with a consequent reduction in power delivered to the load. It may be desirable to maintain n as high as possible since the load voltage will vary directly as n; however, it is not desirable that a large number of thermocouples be eliminated as effective generators by a single failure. What then is the tolerable number of thermocouples in a subsystem?

If the failure process obeys what is sometimes described in the physical literature as a "chance" breakdown mechanism (*i.e.*, if the instantaneous probability of failure at

* Received by the IRE, July 28, 1961; revised manuscript received, August 11, 1961.

[1] B. D. Holbrook and J. T. Dixon, "Load rating theory for multichannel amplifiers," *Bell Sys. Tech. J.*, vol. 18, pp. 624–644; October, 1939.

[2] B. B. Jacobsen, "The effect of nonlinear distortion in multichannel amplifiers," *Elec. Commun.*, vol. 19, pp. 29–54; 1940.

[3] C. A. Parry, "Design factors for the optimization of multichannel radio systems," *Trans. AIEE, (Commun and Electronics)*, no. 233, pp. 606–620; November, 1957.

[4] V. Subrizi, "A speech volume survey on telephone message circuits," *Bell Labs. Rec.*, pp. 292–295; August, 1953.

[5] C. A. Parry, "A formalized procedure for the prediction and analysis of multichannel tropospheric scatter circuits," IRE TRANS. ON COMMUNICATIONS SYSTEMS, vol. CS-7, pp. 211–221; September, 1959.

* Received by the IRE, July 24, 1961; revised manuscript received, September 5, 1961. The work reported in this letter was supported in part by Alco Products, Inc.

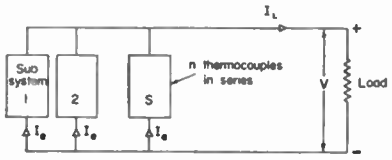

Fig. 1—Schematic thermoelectric generator circuit.

time τ, conditional upon nonfailure prior to time τ, is constant), then the fraction f, of the original number of thermocouples which are intact after an operating period τ is

$$f = \exp(-\tau/M), \tag{1}$$

where M is the mean-time-to-failure of the subsystem. For n identical thermocouples in series, we have $1/M = n/m$, where m is the mean-time-to-failure of an individual thermocouple. Thus the probability that a subsystem of n thermocouples is in operation after time τ is

$$f = \exp(-n\tau/m). \tag{2}$$

The most probable line current I_L can be determined with the aid of the binomial distribution

$$b = \frac{S!}{k!(S-k)!} f^k (1-f)^{S-k}, \tag{3}$$

where b is the probability that in S repeated independent trials with probability f for success and $(1-f)$ for failure there will occur k successes and $(S-k)$ failures $(0 \le k \le S)$. For the generator under consideration, S, the number of parallel subsystems, represent the number of independent trials. "Successes" imply the subsystem is still intact and contributing to the line current. It is interesting to note that by using two or more subsystems in parallel we are decreasing the probability that the line current is 100 per cent of its rated value

$$b_{100\%} = f^S(1-f)^0 = f^S. \tag{4}$$

Since $f < 1$, f^S is largest when $S = 1$. However, the addition of parallel subsystems also decreases the probability that the line current is zero.

It is a property of the binominal distribution that the mean or expected number of successes[1] is $E(r_s) = fS$, where r_s is a random variable representing the number of successes observed among S trials. Thus, the mean or expected fraction of the initial line current from S subsystems which remains after τ is simply $f = E(r_s)/S$. Since the load voltage is constant, the mean or expected remaining fraction of the original power is also f, as given in (2).

Consider a thermoelectric generator with power rating P, which is to be operated unattended for a specified period. There is no provision for automatic switching or replacement of open-circuited thermocouples. In the most simple analysis under matched load conditions the load voltage V is

$$V = ne\Delta T/2 = P/I_L, \tag{5}$$

where

e = thermoelectric power of a thermocouple, volts/°C
ΔT = operating temperature interval, °C.

Combining (2) and (5), we have

$$I_L = \frac{2P}{ne\Delta T} = \frac{-2P\tau}{e\Delta T m \ln(f)} = \frac{P}{V}. \tag{6}$$

As an example, see Table I where some series-parallel combinations for a 100 kw generator required to operate 10,000 hours are presented. The resistance of a thermocouple has been arbitrarily taken as 0.01 ohm, corresponding to $I_e = 5$ amperes. Carbon composition resistors under stabilized operating conditions can have a mean failure time of the order of 10^8 hours. In the absence of quantitative data on thermocouple reliability, the assumption of a mean failure time longer than 10^8 hours is hardly justified. Thus, this simplified analysis serves to partially indicate the role reliability factors must play in thermoelectric generator design. As systems of progressively larger capacity are envisioned without comparable improvement in material figure of merit, greater emphasis must be placed upon reliability and associated problems of power distribution from low voltage-high current sources.

TABLE I

SERIES-PARALLEL COMBINATIONS FOR TWO CHOICES OF MEAN-FAILURE-TIME

(Power output 10^5 watts, operating period 10^4 hours, $e\Delta T = 0.1$ v, thermocouple resistance = 0.01 Ω)

Permissible Fraction of Original Power After 10,000 hrs, f	Allowed Number of Series Thermocouples, n	Load Current I_L, amps	Required Number of Parallel Subsystems $S = I_L/5$	Load Voltage V, volts
		$m = 10^6$ *hours**		
0.95	5	3.9×10^5	7.8×10^4	0.25
0.80	22	$9.0 = 10^4$	1.8×10^4	1.1
0.50	70	2.9×10^4	5.8×10^3	3.5
		$m = 10^8$ *hours*		
0.95	510	3.9×10^3	$7.8 = 10^2$	25.5
0.80	2230	9.0×10^2	1.8×10^2	111
0.50	6930	2.9×10^2	5.8×10^1	346

* Mean time for thermocouple failure (open circuit).

The authors are indebted to Dr. Arthur E. Mace for helpful interpretations and constructive criticisms of the text.

M. R. SEILER
T. S. SHILLIDAY
Battelle Memorial Inst.
Columbus, Ohio

[1] See, for example, W. Feller, "An Introduction to Probability Theory and Its Applications," John Wiley and Sons, Inc., New York, N. Y., pp. 104–110, 173–174; 1950.

A Proposed Test of the Constancy of the Velocity of Light*

The experiment recently suggested by Rapier,[1] interesting and ingenious though it is, cannot demonstrate the isotropy of space to light propagation. The fallacy results from the impossibility of *empirically* establishing the absolute synchronization of clocks located in different regions of space. This is closely allied to the impossibility of empirically establishing the absolute simultaneity of events occurring in separate locations in space. The results follow from the assumption of a finite upper bound on the velocity of signal propagation.

Suppose one wished to establish the absolute simultaneity of a pair of events occurring in two different locations such as a flash of light in the distance and the reading of a clock *here* at that time. Presumably, knowing the distance separating the clock from the flash and the velocity of propagation of light, the transit time may be subtracted from the present clock reading to find the time at which the flash occurred. The temptation is to conclude that the hands of the clock stood at a certain reading simultaneously with the occurrence of the flash. Unfortunately, this *cannot be verified experimentally*. How is the velocity of light, used for the above "correction," determined? Simply by dividing the distance separating the occurrence of a flash by the time elapsed between that occurrence and an observer's reception of it. In other words, the velocity determination necessitates a *second* clock, one located at the site of the flash. Moreover, if the time interval (of transit) is to be meaningful, then the two clocks, at the two locations, must be synchronized. That is, we must know that the hands of the one clock simultaneously read the same as the hands of the other clock. In short, the establishment of the simultaneity of two events in two different regions of space requires the synchronization of a pair of clocks at these locations, and the synchronization of the clocks at these locations of space presupposes that it has been established that their hands occupy the same positions at the same time, *i.e.*, simultaneously.

It should be emphasized that the logical difficulties inherent in this and allied *Gedanken* experiments can *not* be circumvented by synchronizing a pair of clocks together and then transporting one of them to a new location. This obviously begs the question. Furthermore, it presupposes that the time indication of a clock is independent of its path and velocity. In other words, it presupposes some such proposition to the effect that two clocks in synchrony at one place will still be in synchrony when brought to different places along different paths with different speeds. Aside from the impossibility of ever empirically verifying such a proposition, even were it true (whatever that may mean, in the light of our never being able to verify it), it is a proposition that is specifically denied by relativity.

It may not be inapposite to point out

* Received by the IRE, August 25, 1961; revised manusript received, September 5, 1961.

[1] P. M. Rapier, PROC. IRE (Correspondence), vol. 49, p. 1322; August, 1961.

that time measurement in general is fraught with dilemmas. Problems arise in the case of clocks in the same region of space and even in the case of individual clocks. When two clocks are in the same region of space we can, of course, synchronize them. That is, we can arrange matters so that the hand of one clock will be at position A simultaneous with the hand of another clock being at position A', and so that the hand of one is at B, C, and so on, simultaneously with the other clock's hand being at B', C', and so on. But we have no way of ascertaining whether a particular clock is measuring off equal time *intervals*, *i.e.*, we cannot verify empirically that the interval A–B is the same as the interval B–C, nor that the interval A'–B' is the same as the interval B'–C'. In the case of an individual clock, how do we know it is accurate? By an appeal to astronomical observations and the laws of mechanics, of course. But the accurate verification of these laws and facts presupposes the existence of accurate clocks to begin with.

C. K. Gordon, Jr.
Applied Science Div.
Litton Systems, Inc.
Woodland Hills, Calif.

Narrow-Band and Wide-Band Noise Figures*

Introduction

There are at present two generally used methods of specifying transistor low-frequency noise figure (NF): a wide-band and a narrow-band method. The wide-band method[1,2] averages noise over a wide audio range in a carefully controlled roll-off amplifier, while the narrow-band method[3] measures noise over a very narrow band at a spot frequency, usually 1 kc. In the hope of removing some of the confusion regarding the relative merits of each measurement, they will both be very briefly discussed.

Discussion

A transistor noise spectrum is shown in Fig. 1. For a high-gain planar transistor f_1 may be in the region of 200–500 cps, while for a more conventional type it may lie in the region of a few kc. The upper frequency f_2 occurs above audio frequencies[4] and will not be discussed here. The average ("wide-band") NF is also shown plotted in Fig. 1. An examination will clearly indicate whether a spot NF or a wide-band NF will be higher at a certain frequency.

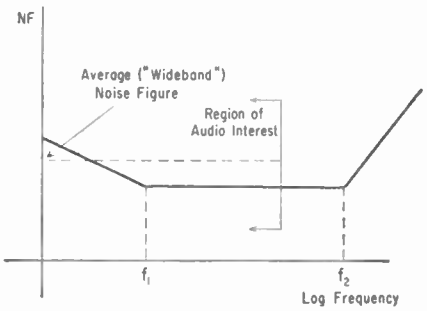

Fig. 1—Transistor noise spectrum.

Generally, a planar transistor is about out of the $1/f$ region at 1 kc; therefore, a 1-kc NF will generally be lower than the wide-band NF. Other transistors are generally in the $1/f$ region at 1 kc, and therefore the 1-kc NF will generally be higher than the wideband NF. A 1-kc NF will indicate the degree that the transistor is in or out of the $1/f$ region and is therefore an excellent indication of its quality; a wide-band NF, while still useful, does not indicate directly the f_1 of a transistor. A complete specification would have both, but if only one is to be chosen, the 1 kc NF is very much the more desirable. This is particularly true when its ease of measurement is considered.

Paul J. Bénéteau
Fairchild Semiconductor Corp.
Mountain View, Calif.

* Received by the IRE, August 25, 1961.

[1] J. J. Davidson, "Transistor noise factor tester," *Semiconductor Products*, vol. 2, pp. 15–20; February, 1959.

[2] P. J. Bénéteau and L. Blaser, "The Measurement of Noise Figures of Transistors," Fairchild Semiconductor Corp., Mountain View, Calif., APP-13.

[3] L. Blaser, "1 kc Narrow-Band Automatic Transistor Noise Figure Test," Fairchild Semiconductor Corp., Mountain View, Calif., APP-29.

[4] H. F. Cooke, "Transistor upper noise corner frequency," Proc. IRE (Correspondence), vol. 49, p. 648; March, 1961.

Design of a Helium-Neon Gaseous Optical Maser*

A gaseous optical maser[1] has been designed and built at Raytheon. The aim of this communication is to provide construction information concerning this version of the gaseous optical maser.

This device, which is shown in Fig. 1, was operated successfully for the first time on June 26, 1961. The main frame consists of four Invar rods joined by stainless steel rings at each end. The Fabry-Perot mirrors, which are made of quartz, are so placed that their outermost surfaces are in the same plane as the ends of the Invar rods (see Fig. 2). By using stainless steel for all connecting parts, this placement of the quartz mirror plates assures that their innermost faces, which bear the reflecting coatings, remain a relatively constant distance (one micron per degree centigrade) apart during moderate variations in ambient temperature.

* Received by the IRE, August 18, 1961; revised manuscript received, September 1, 1961.

[1] A. Javan, W. R. Bennett, Jr. and D. R. Herriott, *Phys. Rev. Lett.*, vol. 6, pp. 106; 1961.

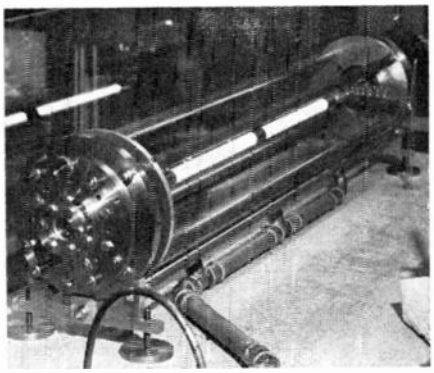

Fig. 1—Photograph of gaseous optical maser.

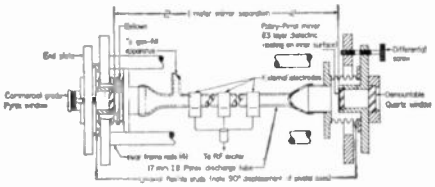

Fig. 2—Raytheon gaseous optical maser. (Details of copper gaskets and loading springs for vernier adjustment of parallelism not shown.)

The movement of the stainless steel end plates which carry the Fabry-Perot mirrors is controlled by differential screws threaded into the end plates and the end rings. Vernier adjustment is obtained by varying the spring pressure tending to squeeze the end plates and end rings together. This spring loading also takes up backlash in the threads of the differential screws. Hinge action is accomplished by deforming two studs in the hinge line at each end. These studs are stainless rods milled so that they will flex about one preferred axis. These uniaxial flexible studs have no backlash and cannot become frozen by corrosion if bakeout is required. The differential screws are thinned down in the portion between the two threaded sections to accommodate misalignment as the end plates are swung through a small arc.

The various sections of the optical maser are vacuum sealed with thin annealed copper gaskets. As the flange bolts are tightened at each joint, sharp cornered shoulders bite into the soft copper to accomplish the seal. A commercial quartz optical flat is sealed in this manner to provide an output window. A shoulder structure suitable for standard Varian Pyrex windows is also provided.

The Pyrex glass discharge tube is sealed to Kovar sleeves on the ends of the bellows assemblies. Only one bellows is required at each end.

The RF discharge is maintained by connecting a simple "ham" transmitter to three sheet brass electrodes wrapped around the discharge tube. The end electrodes are grounded and the center electrode goes to a pi section matching circuit in the transmitter. A rating of 60 watts is more than adequate to sustain maser action.

The quartz Fabry-Perot mirrors are made from 1/20 wavelength optical flats available from a precision gauge manufac-

turer. Dr. Turner of Bausch and Lomb, Inc., coated these plates with 13-layer dielectric coatings with maximum reflectivity peaked at approximately 1.2 microns.

After the maser was put into operation, a group of concentric rings was observed in the output from each end. Subsequent examination of quartz flats similar to the ones installed within the maser revealed a concentric ring pattern intrinsic in the quartz itself. Fringes formed by pressing two such flats together show that the ring pattern is not due to the surfaces. The Schlieren technique shows that the rings are due to regular optical density variations. A coarse granular structure is superimposed on the ring pattern. Since the maser resonator is actually formed between the coatings on the innermost surfaces of the flats, these density variations do not affect the optical maser operation of the device. They act only as filters inserted between the maser and the detector. These variations are the result of the way the quartz manufacturer accomplishes the fusion operation. Not all quartz blanks have the rings, and in the future an attempt will be made to pick ring-free optical flats.

Although the optical maser was designed to withstand a moderate bakeout, this operation has not been necessary. Internal clean-up was accomplished by ion bombardment within the maser filled with the correct gas mixture (0.1 mm. Hg of neon and 1.0 mm of helium obtained from commercial lecture bottles). Three evacuation and refill cycles were required before the scouring action of the gas discharge cleaned up practically all of the residual contaminants so that the maser could be operated continuously for long periods of time.

When either end plate is tilted slightly from perfect parallelism, the observed beam spot breaks up into two areas separated by a dark band. Further tilting produces a more complex pattern. The nature of these patterns is being investigated by means of interference experiments. The position of the dark nodal bands is constant throughout the maser as indicated by simultaneous examination of the outputs from the two ends.

A study in progress at Raytheon has indicated that the $2s_2$ neon level should be excited very much more strongly than the other $2s$ levels because the $2s_2$ level lies closest to the ^3S level in helium. The transition probabilities of the $2s \rightarrow 2p$ transitions have been calculated by Koster and Statz.[2] The transition having the highest probability which originates with a $2s_2$ level is the $2s_2 \rightarrow 2p_4$ transition which has a wavelength of 1.15259 microns. The $2p_4$ level has a large transition probability to the $1s_2$ level. Since the $1s_2$ level is not metastable, there should be relatively little blockage in the return of the atoms to the ground state via this route. Our only observed output to date, measured with a Perkin-Elmer 98G monochromator, has a wavelength of 1.153 microns. Javan and his co-workers also report that the 1.153 micron line is the strongest.[1]

[2] G. Koster and H. Statz, *J. Appl. Phys.*, vol. 32, p. 2054; 1961.

Now that the practical details of operation have been solved, an extensive program of research is contemplated. Experimental observations on the transient effects of switching the excitation on and off, the effects of a magnetic field, and several interesting interference phenomena will be reported shortly.

C. F. Luck
R. A. Paananen
H. Statz
Research Division
Raytheon Company
Waltham, Mass.

A Critical Note on "Steady-State Analysis of Circuits Containing a Periodically Operated Switch"*

In the above paper,[1] Fettweis obtains the frequency components of the current in and the voltage across a periodic ideal switch in series with an arbitrary time-dependent impedance and a cisoidal voltage source. He further shows that if any parameter in a circuit is switched periodically between two finite nonzero values, the problem can be treated by means of an equivalent series circuit incorporating an ideal switch. Now, in practice, 1) "switches" are seldom if ever ideal, *i.e.*, they generally have a noninfinite impedance when open and a nonzero impedance when closed (*e.g.*, a rectifier bridge in a series or shunt modulator); and 2) stepwise variation of reactive elements is seldom desired, let alone achieved, since it demands impulse functions of power unless synchronized with the instants of zero stored energy. It follows that the main practical interest in step-wise variation of parameters lies in resistance variation.

It is the purpose of this note to show that a direct approach to the problem of a circuit containing a resistance varying step-wise between finite nonzero values, (which may always be reduced to a simple series circuit by Thévenin's theorem) has the following advantages over Fettweis' suggested equivalent circuit approach: 1) no equivalent circuit is required; 2) as a result the current and voltage analysed are directly those in and across the periodic resistance and not in and across a mythical ideal switch; 3) no impulse functions occur, whatever the nature of the impedance in series with the periodic resistance; and 4) the tendency to impulse functions, which are solely due to idealising the switching process (*i.e.*, making the upper resistance value tend to infinity or the lower tend to zero), emerges clearly from the general analysis.

In Fig. 1, r varies step-wise between r_1 in the ranges $(N-\frac{1}{2})T < t < NT$ and r_2 in the ranges $NT < t < (N+\frac{1}{2})T$ (N = any integer, $0 < r_2 < r_1 < \infty$). The equivalent series circuit containing an ideal switch is shown in Fig. 2. Attention is drawn to the following relations between the two circuits:

$$Z(s) = \frac{r_1^2}{r_1 - r_2} \cdot \frac{r_2 + Z'(s)}{r_1 + Z'(s)}, \tag{1}$$

$$i = I + \frac{V}{r_1}, \qquad v = V + \frac{r_1 r_2}{r_1 - r_2} i. \tag{2}$$

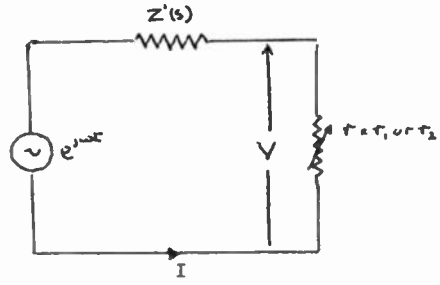

Fig. 1.

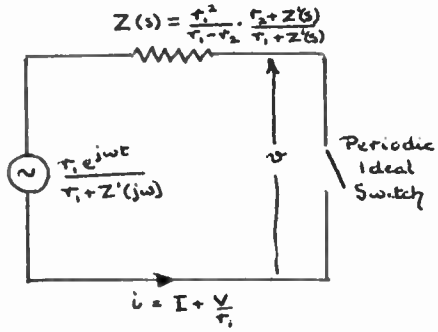

Fig. 2.

Considering the current I as the sum of steady-state and transient terms, we postulate

$$I = \frac{1}{r_1 + Z'(j\omega)} \left\{ e^{j\omega t} + \sum_1^m c_k e^{\gamma_k t} \right\},$$

$$V = -r_1 I, \quad -\frac{T}{2} < t < 0, \tag{3}$$

$$I = \frac{1}{r_2 + Z'(j\omega)} \left\{ e^{j\omega t} + \sum_1^m d_k e^{\delta_k t} \right\},$$

$$V = -r_2 I, \quad 0 < t < \frac{T}{2}, \tag{4}$$

in which the γ_k and δ_k are the finite zeros of $r_1 + Z'(s)$ and $r_2 + Z'(s)$, respectively. The number of these is clearly the same (m) being either the number of zeros or poles of $Z'(s)$, whichever is the greater.

The known periodicity of $Ve^{-j\omega t}$ and $Ie^{-j\omega t}$ with period $T \equiv 2\pi/\Omega$ justifies

$$V = e^{j\omega t} \sum_{-\infty}^{\infty} V_n e^{jn\Omega t},$$

$$I = e^{j\omega t} \sum_{-\infty}^{\infty} I_n e^{jn\Omega t}, \tag{5}$$

* Received by the IRE, August 21, 1961; revised manuscript received, September 11, 1961.

[1] A. Fettweis, IRE Trans. on Circuit Theory, vol. CT-6, pp. 252–260; September, 1959.

where

$$V_n = \frac{1}{T}\int_{-T/2}^{T/2} V e^{-j(\omega+n\Omega)t}dt,$$

$$I_n = \frac{1}{T}\int_{-T/2}^{T/2} I e^{-j(\omega+n\Omega)t}dt. \qquad (6)$$

Finally the circuit ohmic equation, from Fig. 1, gives

$$V_n = I_n Z'\{j(\omega + n\Omega)\}, \quad n \neq 0$$

but

$$V_0 = I_0 Z'(j\omega) + 1. \qquad (7)$$

Substituting the values of V and I from (3) and (4) in (6), and carrying out the integrations and substituting the resulting values of V_n and I_n in (7) gives the infinite set of equations

$$\frac{r_2 + Z_0'}{r_1 + Z_0'}\sum_1^m c_k \frac{1-(-1)^n e^{-X_k}}{X_k - jn\pi} + \frac{r_2 + Z_n'}{r_1 + Z_n'}\sum_1^m d_k \frac{(-1)^n e^{Y_k} - 1}{Y_k - jn\pi} = \frac{1-(-1)^n}{jn\pi}\left\{\frac{r_2 + Z_0'}{r_1 + Z_0'} - \frac{r_2 + Z_n'}{r_1 + Z_n'}\right\} \qquad (8)$$

in which

$$X_k \equiv \frac{T}{2}(\gamma_k - j\omega), \qquad Y_k \equiv \frac{T}{2}(\delta_k - j\omega),$$

$$Z_n' \equiv Z'\{j(\omega + n\Omega)\}, \qquad (9)$$

(8) being valid for all integral n, the RHS vanishing with n.

It may be noted that, if (8) is multiplied by $r_1^2/r_1 - r_2$, and (1) is used, (8) is *identical* with Fettweis' (16). Indeed it is clear from (1) that the zeros of $r_1 + Z'(s)$ are the poles of $Z(s)$ and the zeros of $r_2 + Z'(s)$ are the zeros of $Z(s)$, *i.e.*, that the γ and δ in (8) are identical with Fettweis' α and β. It then follows that the c and d in (8) are identical with Fettweis' a and b.

Any $2m$ independent equations of the infinite set (8) suffice the find the unknown c_k's and d_k's. Following Fettweis, however, (8) may be manipulated to give two sets of m equations for the c_k and d_k separately:

$$\sum_{l=1}^m c_l \frac{1 - e^{-(X_l + Y_k)}}{X_l - Y_k} = \frac{1 - e^{Y_k}}{Y_k} \qquad (10)$$

$$\sum_{l=1}^m d_l \frac{1 - e^{X_k + Y_l}}{X_k - Y_l} = \frac{e^{X_k} - 1}{X_k} \qquad (11)$$

$k = 1, 2, \cdots, m.$

A knowledge of the c_k and d_k at once allows V_n, I_n to be computed. Note that no restrictions have been applied to $Z'(s)$.

Impulse Functions in I and V

Let p', z', be the number of finite poles and zeros of $Z'(s)$. *If* $r_1 \to \infty$, the zeros of $r_1 + Z'(s)$ approximate to the poles of $Z'(s)$, p' in number, whereas if r_1 is finite and nonzero, the zeros of $r_1 + Z'(s)$ are p' or z' in number, whichever is the greater. Further, if Z' is passive, p' and z' cannot differ by more than unity. It follows that if Z' is passive and if $z' = p' + 1$, making $r_1 \to \infty$ reduces the number of finite zeros of $r_1 + Z'(s)$ from z' to $p' = z' - 1$, *i.e.*, one of these zeros moves to infinity, necessarily along the negative real axis since $r_1 + Z'(s)$ is also passive, *i.e.*, one of the γ_k, say γ_1, $\to -\infty$, *i.e.*, from (9), $RX_1 \to -\infty$. The terms involving c_1 in (10) become $-c_1 e^{-X_1 - Y_k}/X_1$, the other terms remaining finite. Hence $-c_1 e^{-X_1}/X_1$ tends to some finite limit C_1, which, with coefficient e^{-Y_k} replaces c_1 as the unknown in these equations. The contribution to V in the interval $-T/2 < t < 0$ is, from (3),

$$-\frac{r_1 c_1 e^{\gamma_1 t}}{r_1 + Z_0'} \to C_1 X_1 e^{X_1} e^{\gamma_1 t} \to \frac{C_1 T}{2}\gamma_1 e^{\gamma_1(t+T/2)} e^{-j\omega T/2} \to -\frac{C_1 T}{2} e^{-j\omega T/2}\delta\left(t + \frac{T}{2}\right),$$

namely an impulse function at $t = -T/2$ of amplitude $-C_1 T/2$ times the applied voltage at that instant. There is no corresponding impulse in I since $I = -V/r_1$ in the relevant interval.

The effect on (11) is trivial, the equation for the case $k = 1$ degenerating to

$$1 + \sum_1^m d_l = 0,$$

which, using (4), shows that when $t \to 0$ in the range $0 < t < T/2$, $V \to 0$ and I also $\to 0$ unless $r_2 = 0$.

A similar analysis shows that *if* $r_2 \to 0$ and Z' is passive with $p' = z' + 1$ then one of the δ_k, say δ_1, $\to -\infty$, *i.e.*, $RY_1 \to -\infty$. The terms involving d_1 in (11) approximate to $-d_1/Y_1$ for all k. Thus $-d_1/Y_1$ tends to some finite limit D_1 which, with coefficient unity, replaces d_1 as the unknown. The relevant contribution to I in the interval $0 < t < T/2$ is, from (4),

$$\frac{d_1 e^{\delta_1 t}}{r_2 + Z_0'} \to -\frac{D_1 T}{2Z_0'}\delta_1 e^{\delta_1 t} \to \frac{D_1 T}{2Z_0'}\delta(t),$$

an impulse at $t = 0+$ of amplitude $D_1 T/2Z_0'$ times the applied voltage at this instant. This is not reflected in the voltage since $V = -r_2 I$ in the relevant interval. The effect on (10) is trivial: the case $k = 1$ degenerates to

$$\sum_{l=1}^m c_l e^{-X_l} + 1 = 0,$$

i.e.

$$\sum_{l=1}^m c_l e^{-\gamma_l T/2} + e^{-j\omega T/2} = 0$$

showing, by comparison with (3), that $I = 0$ when $t \to -T/2$ in the range $-T/2 < t < 0$ and V also $\to 0$ unless $r_1 \to \infty$.

J. M. Layton
Elec. Engrg. Dept.
Univ. of Birmingham
Birmingham, Eng.

Cyclic Codes and Transition Coding*

Data transmission systems often operate by making a binary decision at each bit time on the state of the signal during the previous interval. That is, the receiver decides which of two voltage levels, frequencies, phases, or amplitudes (depending on the modulation used) was representative of the signal during the interval under consideration.

After the decisions concerning the successive states of the line have been made, it remains only to recover the binary data. There are two ways in which this is usually done.

In the first system, a 1 is identified with one state and a 0 with the other. For example, in an FM system, f_1 could represent a 1 and f_2 a 0. Such a system could be called "state" coding (it has also been called NRZ coding). The recovery of the binary data from the succession of states on the line in this case is a trivial operation.

Alternatively, a 1 can be identified with a change of state and a 0 with no change of state. Such a system has been called "transition" coding (it has also been called NRZI and NRZ1 coding). The interpretation to be used, "state" or "transition," depends, of course, on the technique used to encode the data.

It is interesting to compare the resulting error patterns with the two interpretations. If $E_s(x)$ is the error polynomial with state coding, then, with a few assumptions, the error polynomial with transition coding, $E_T(x)$, can be shown to be

$$E_T(x) = (1 + x)E_s(x). \qquad (1)$$

The following are the required assumptions:

1) The polynomials are obtained by forming the sum

$$\sum_{i=0}^{n-1} A_i x^i. \qquad (2)$$

where n is the number of bits in the message, and $A_i = 0$ if the $(i+1)$th bit of the message is received correctly and 1 if that bit is in error.

2) End-effects are negligible for a reasonably long message. This can be stated in many ways. One of these is to say that an error in the decision on the last state is impossible and that there exists a state known without error before the first state considered as a bit of information in "state" coding. The latter is justified in most practical cases and implies that the jth "transition" bit is between the states that represent $(j-1)$th and jth "state" bits.

If one chooses to change (2) to the form

$$\sum_{i=0}^{n-1} A_i x^{n-1-i}, \qquad (3)$$

then (1) becomes

$$E_T(x) = (1 + x)E_s(x)x^{-1}. \qquad (4)$$

This does not change materially the discussion at hand.

* Received by the IRE, September 5, 1961.

Let us suppose that the same cyclic code is being used for detection with the "transition" interpretation and with the "state" interpretation. From (1) and the work of Peterson and Brown,[1] it is evident that $E_T(x)$ is undetected if, and only if, $E_s(x)$ is undetected, providing only that the characteristic polynomial $P(x)$ of the cyclic code does not contain $(1+x)$ as a factor.

Furthermore, if $(1+x)$ is a factor of $P(x)$ and $P(x)$ is used in the "state" case and $(1+x)P(x)$ in the "transition" case, one can state that $E_T(x)$ is undetected if, and only if, $E_s(x)$ is undetected.

The foregoing does not apply to those cases where "transition" coding is used and the decision for each bit is made in the receiver by examining two consecutive states of the received signal simultaneously. It applies only where the decision for each state is made separately.

FRANCIS CORR
Compagnie IBM France
Nice, France

[1] W. W. Peterson and D. T. Brown, "Cyclic codes for error detection," PROC IRE, vol. 49, pp. 228–235; January, 1961.

A Transistor Equivalent Circuit*

Brunn[1] has developed an equivalent circuit for use in the design of video amplifiers which proves to be very useful. The devices of concern were alloy-fused so that no electric field was present in the base region. With the use of diffusion process and development of various graded base structures, the frequency range of the transistors was extended to hundreds of Mc ranges. But the electric field present in the base region introduced excess-phase shifts, which are especially effective in the common emitter configuration. Therefore, it will be useful to have an equivalent circuit which includes the excess-phase shift associated with the diffused base structures. It can be shown that if the impurity in the base region is exponential in form, a constant electric field exists in the base region. Under this condition, the transport factor of the device can be approximated by

$$\text{T.F.} = \frac{\alpha_0 e^{-jm\omega/\omega_\alpha}}{1 + j\omega/\omega_\alpha}, \qquad (1)$$

which is approximately equal to α (common-base short-circuit-current gain). In this expression m is the excess-phase shift at the 3-db point (radians in excess of 45°). The input impedance of a transistor, neglecting for the moment r_b', is given by

$$Z_{in} = \frac{r_e}{1-\alpha}. \qquad (2)$$

Substituting (1) into (2) we have

$$Z_{in} = \frac{r_e}{1 - \alpha_0 + j\omega/\omega_\alpha[1+\alpha_0 m]}, \qquad (3)$$

assuming $\omega \ll \omega\alpha$.

Eq. (3) can be written as

$$Z_{in} = \frac{r_e/1-\alpha_0}{1 + j\omega/\omega_\alpha\left(\frac{1+\alpha_0 m}{1-\alpha_0}\right)}. \qquad (4)$$

Eq. (4) can be used to realize the hybrid equivalent circuit shown in Fig. 1. Here the current source has been represented in terms of V_1, which is valid for frequencies $\omega \ll \omega_T$ where ω_T is given by $\beta_0\omega_\beta$, the gain bandwidth product of the common emitter configuration. Now r_b' and C_c have to be added as extrinsic circuit parameters. As in vacuum tubes, C_c can be treated as the Miller effect capacitance, in which case its effect to the input is given by

$$C_c' = C_c\left(1 + \frac{R_L}{r_e}\right), \qquad (5)$$

where R_L/r_e is the low-frequency voltage gain (V_L/V_1).

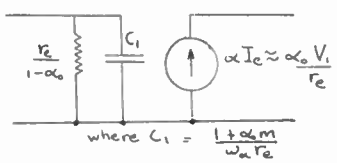

Fig. 1.

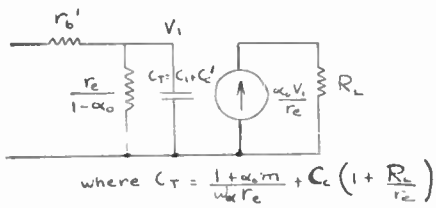

Fig. 2.

The final equivalent circuit is shown in Fig. 2. With m over one in the present mesa and planar structures, its effect is evident from Fig. 2. Further, under the condition

$$\omega \ll \omega_T,$$

all effects are lumped into one pole which simplifies considerably the circuit design.

VASIL UZUNOGLU
Solid State Lab.
Westinghouse Electric Corp.
Baltimore, Md.

* Received by the IRE, June 19, 1961; revised manuscript received, September 8, 1961.

[1] G. Brunn, "Common-emitter transistor Video amplifiers," PROC. IRE, vol. 44, pp. 1561–1572; November, 1956.
See also D. O. Pederson and R. S. Pepper, "An evaluation of transistor low pass broadbanding technique," 1959 IRE WESCON CONVENTION RECORD, pt. 2, pp. 111–126.

A DC Pumped Amplifier with a Two-Dimensional Field Structure*

A number of structures exist for amplifying cyclotron waves on electron beams by interaction with periodic electrostatic or magnetic fields. These include the electrostatic quadrupole structure[1] and the magnetic ring structure,[2] both of which have field components which vary spatially in three dimensions.

Amplification is also possible in periodic structures of the type shown in Fig. 1 whose fields vary in two dimensions only (see also Gould and Johnson[3]). These structures would be particularly suited to use with strip beams in conjunction with Cuccia couplers and may have advantages for high power amplification. The potential distribution in the structure is given by

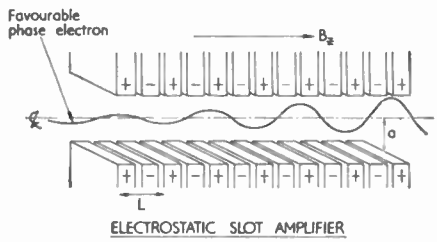

Fig. 1

$$V_s = V + \sum A_n V_E \frac{\cosh \beta_n x}{\cosh \beta_n a} \sin \beta_n z. \qquad (1)$$

$|V_E|$ is the electrode potential, A_n is an amplitude coefficient and $\beta_n = 2\pi(2m+1)/L$. Considering only the fundamental in the structure β_1, the equations of motion for a paraxial electron are

$$\frac{d^2x}{d\theta^2} + \frac{dy}{d\theta} - \mu x \sin \beta_1 z = 0 \qquad (2a)$$

$$\frac{d^2y}{d\theta^2} - \frac{dx}{d\theta} = 0 \qquad (2b)$$

$$\frac{d^2z}{d\theta^2} - \frac{\mu}{\beta_1} \cos \beta_1 z = 0. \qquad (2c)$$

$$\theta = \frac{B_z t}{\eta} = \omega_c t \quad \text{and} \quad \mu = \frac{\beta_1^2 A_1 V_E}{B_z^2 \eta \cosh \beta_1 a}.$$

For amplification, electrons must traverse a structure period in half an electron cyclotron period. Hence for small pump strengths $\sin \beta_1 z = \sin 2\theta$ in (2a) and (2b). Integrating (2b) and substituting for $dy/d\theta$ in (2a) gives an unstable Mathieu equation in x. This may be solved to give the subsequent dis-

* Received by the IRE, September 14, 1961.

[1] E. I. Gordon, "A transverse-field traveling-wave tube," PROC. IRE (Correspondence), vol. 48, p. 1158; June, 1960.
[2] T. Wessel-Berg and K. Blötekjaer, "Some Aspects of Cyclotron Wave Interaction in Time Periodic and Space Periodic Fields," presented at Internatl. Conf. on Microwave Tubes, Munich, Ger.; June 7–11, 1960.
[3] R. W. Gould and C. C. Johnson, "Coupled mode theory of electron-beam parametric amplification," *J. Appl. Phys.*, vol. 32, pp. 248–258; February, 1961.

placement of an electron in an input fast or slow wave entering the structure at (r, ϕ) as

$$x = r\left[\cosh\frac{\mu\theta}{4}\cos(\theta+\phi) - \sinh\frac{\mu\theta}{4}\cos(\theta-\phi)\right], \quad (3a)$$

$$y = r\left[\cosh\frac{\mu\theta}{4}\sin(\theta+\phi) - \sinh\frac{\mu\theta}{4}\sin(\theta-\phi)\right]. \quad (3b)$$

These equations show that its motion is that of an electron in the input fast or slow wave growing as $\cosh \mu\theta/4$ coupled with that in a slow or fast wave growing as $\sinh \mu\theta/4$.

The wave-coupling characteristics of this device are therefore the same as that of the dc quadrupole amplifier. The gain in decibels is given by

$$20 \log_{10} \cosh\left[\frac{A_1 V_E N\pi}{4V_0 \cosh \beta_1 a}\right];$$

N is the number of sections in the structure and V_0 the synchronous beam voltage for zero structure voltage.

Since there is a periodic electric field along the axis, electrons entering the structure at a velocity $u_0 = L\omega_r/\pi$ will have their average velocity over a structure period reduced and so synchronism will be lost. The velocity u (voltage V) required to maintain synchronism is found by integration of (1c) as

$$\frac{2u_0}{\pi} K\left[\frac{\pi}{2}, \sqrt{\frac{2A_1V_E}{A_1V_E + V\cosh\beta a}}\right] \cdot\left[1+\frac{A_1V_E}{V\cosh\beta a}\right]^{-1/2};$$

K is a complete elliptic integral. This expression increases with increasing $|V_E|$.

Like the dc quadrupole amplifier, synchronous waves are to a first order unaffected in the structure, and hence beam spread effects are small. In this tube they will be governed by the beam thickness, and so for a given beam this effect can be minimized by making it as thin and wide as possible.

The condition where the transit time over a structure period is a full cyclotron period can be investigated by writing $\sin\theta$ for $\sin 2\theta$ in (2a). It is then found that wave growth of order μ^2 may take place. This is generally negligible. The experimental results were obtained in a tube operating at 1100 Mc incorporating Cuccia couplers and a structure with 16 pairs of electrodes whose synchronous voltage was 450 v. A strip beam was used. Gain curves for various beam voltages in this range are shown in Fig. 2 together with the theoretical structure curve. Beam interception on the structure produced the turnover of the gain curves. For beam velocities corresponding to the ω_r-pumping region, both small gain ($\sim$3 db) and attenuation effects can be produced by increasing the pumping electrode voltages. The precise effect seems to depend on beam velocity and may be due to coupling between the fast cyclotron wave and the longitudinal space-charge waves produced by the axial fields in the structure.

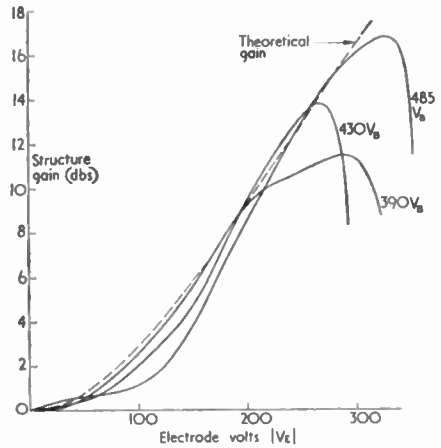

Fig. 2

The author wishes to thank Dr. T. E. Allibone, Director of this Laboratory, for permission to publish this letter and P. Jeffree for tube construction and the experimental work.

J. C. Bass
Research Laboratory
Associated Electrical Industries,
Aldermaston Court, Berkshire England

Miniaturized *S*-Band Isolator*

As earlier reported,[1] the use of a different concept in strip transmission-line isolators resulted in a compact isolator for the VHF and UHF range. It is also possible to utilize a similar-type structure at the higher frequencies with the expected large improvement in physical size and weight of such devices. This note reports some results of an isolator in the *S*-band frequency region. The evident size advantage can be seen in Fig. 1. The dimensions were $2\frac{1}{2}\times\frac{7}{8}\times1$ inch and the weight is 3 ounces.

A cross-sectional view of the isolator is shown in the inset of Fig. 2. Here, as in the UHF version, the ferromagnetic material is placed asymmetrically on the center conductor and magnetized perpendicular to the direction of propagation.

The same general characteristics noted in the low-frequency isolators were also observed at frequencies up to *C* band. The most useful characteristic was that for a particular ferrite geometry, the operating frequency could be lowered by a sizeable amount by sliding the ferrite slabs to a more symmetrical position on the center strip. This is evidenced in Fig. 2. Curve 2 represents the results with the ferrite slabs in one position and curve 1 shows the results of the ferrite being moved 0.030 inch to a more symmetrical position. Thus the operating frequency was conveniently shifted downward by approximately 400 Mc.

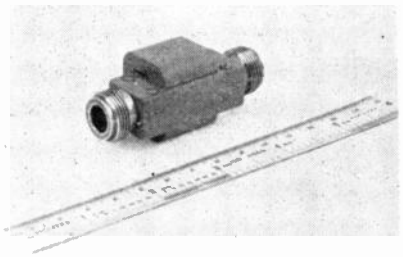

Fig. 1—Miniaturized isolator.

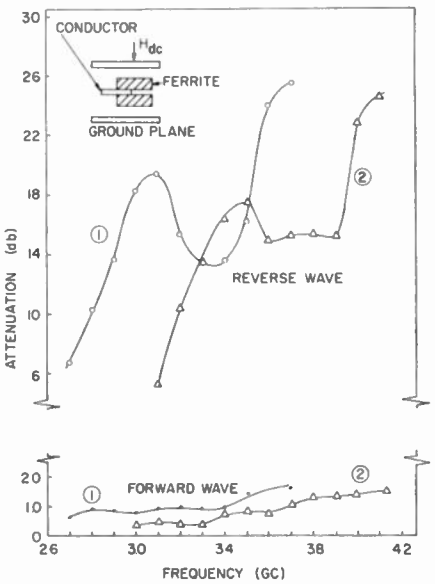

Fig. 2—Electrical characteristics of isolator.

The electrical results were notable; better than 10-to-1-db isolation-to-insertion-loss ratio was achieved from 2.8 to 3.4 Gc or a bandwidth of approximately 20 per cent. As curve 2 in Fig. 2 shows, the same nonreciprocal ratio was obtained from 3.2 to 3.7 Gc. The input VSWR was low in both cases.

The material used in this case was a common magnesium manganese ferrite. For greater power-handling capacity, it is possible to use a temperature-compensated material such as yttrium-gadolinium garnet.[2]

Acknowledgment

The author wishes to thank M. Liberman for his aid in the construction of this device.

D. Bruce Swartz
Applied Physics Sec.
Sperry Microwave Electronics Co.
Clearwater, Fla.

* Received by the IRE, September 11, 1961.

[1] D. B. Swartz, "Compact UHF isolator," *J. Appl. Phys.*, vol. 32, pp. 319–320; March, 1961.

[2] G. R. Harrison and L. R. Hodges, "Microwave properties of polycrystalline hybrid garnets," *Microwave J.*, vol. 4, pp. 53–65; June, 1961.

Pole-Zero Sensitivity Relationships*

Several interesting and useful relationships between the sensitivities of critical frequencies to element variations can be derived from the well-known relationships for frequency and magnitude scaling of network functions.[1] Thus, if s_0 is a critical frequency (either a pole or a zero) of a network containing l inductors, r resistors, and c capacitors:

$$\frac{ds_0}{s_0} = \sum_{i=1}^{l} S_{L_i}^{s_0} \frac{dL_i}{L_i} + \sum_{i=1}^{r} S_{R_i}^{s_0} \frac{dR_i}{R_i} + \sum_{i=1}^{c} S_{C_i}^{s_0} \frac{dC_i}{C_i}, \quad (1)$$

where

$$S_x^{s_0} \equiv \frac{x}{s_0} \cdot \frac{\partial s_0}{\partial x}.$$

If all elements of a kind vary together, (1) may be written in the form

$$\frac{ds_0}{s_0} = \frac{dL}{L} \sum_{i=1}^{l} S_{L_i}^{s_0} + \frac{dR}{R} \sum_{i=1}^{r} S_{R_i}^{s_0} + \frac{dC}{C} \sum_{i=1}^{c} S_{C_i}^{s_0}. \quad (2)$$

To accomplish frequency scaling such that $s_0 = as_0'$, the elements are varied according to: $L = (1/a)L'$, $C = (1/a)C'$, $R = R'$. Therefore,

$$\frac{ds_0}{s_0} = \frac{da}{a} = -\frac{dL}{L} = -\frac{dC}{C} \quad \text{and} \quad \frac{dR}{R} = 0. \quad (3)$$

Substituting (3) into (2) gives

$$\sum_{i=1}^{l} S_{L_i}^{s_0} + \sum_{i=1}^{c} S_{C_i}^{s_0} = -1. \quad (4)$$

To scale the magnitude of a network impedance by a factor b:

$$L = bL', \quad C = \frac{1}{b} C', \quad R = bR' \text{ while } s_0 = s_0'.$$

Therefore,

$$\frac{dL}{L} = \frac{db}{b} = -\frac{dC}{C} = \frac{dR}{R} \quad \text{and} \quad \frac{ds_0}{s_0} = 0. \quad (5)$$

Substituting (5) into (2) gives

$$\sum_{i=1}^{l} S_{L_i}^{s_0} + \sum_{i=1}^{r} S_{R_i}^{s_0} - \sum_{i=1}^{c} S_{C_i}^{s_0} = 0. \quad (6)$$

Since the sensitivities are phasors which depend on the network configuration and element values but *not* on the particular type of element variation, (4) and (6) give relationships which are valid for any kind of variation. However, unless the variation of all elements of a kind is uniform, (2) is not valid and the more general form, (1), must be used.

Often RC circuits containing no inductance are of interest, in which case $S_{L_i}^{s_0} = 0$, and (4) and (6) may be combined to yield

$$\sum_{i=1}^{r} S_{R_i}^{s_0} = \sum_{i=1}^{c} S_{C_i}^{s_0} = -1. \quad (7)$$

As an example of the application of (7), consider a parallel-T null circuit which is built into a functional electronic block so that environmental effects (temperature, etc.) cause a uniform variation on all elements of a kind. Then from (2) and (7),

$$\frac{ds_0}{s_0} = -\left(\frac{dR}{R} + \frac{dC}{C}\right). \quad (8)$$

Since the value given by (8) is real, the variation of the transmission zero will take place in a radial direction in the s plane. Therefore the null frequency will shift, but the Q of the null will remain unaffected. It can then be concluded that the Q is changed only when individual elements of a kind vary by different amounts. Eq. (8) also emphasizes the well-known fact that if the resistances and capacitances can be so compensated as to vary by equal amounts in opposite directions, the critical frequencies are unaffected. Eq. (7) serves as a useful check on the accuracy of calculated sensitivities, and also shows that regardless of the circuit configuration or the number of elements, the combined sensitivities remain constant. Therefore it would be fruitless to attempt to devise passive circuits with low sensitivities to the uniform type of variation that has been assumed. As pointed out, however, the uniform variation of one type of element can be made to compensate for the uniform variation of another type of element.

W. E. Newell
Semiconductors Devices Sec.
Electronics Dept.
Westinghouse Res. Labs.
Pittsburgh, Pa.

* Received by the IRE, September 25, 1961.

[1] M. E. Van Valkenburg, "Introduction to Modern Network Synthesis," John Wiley and Sons, Inc., New York, N. Y., Sec. 2.5; 1960.

A Waveguide In-Line Ferrite Rotary Joint*

Most waveguide rotary joints utilize the principle of converting the RF energy either to the TEM mode in coaxial or the TM_{01} mode in cylindrical line. The object of the conversion is to obtain a circularly symmetric transmission mode which is not effected by the physical orientation of the transmission line about the axis of propagation. A technique has been developed which essentially removes the effect of the transmission line altogether by means of confining the propagation in a circular mode within a rod of ferrite placed axially in the waveguide. The orientation of the waveguide walls then have little effect on the transmission, and one section of waveguide can be axially rotated with respect to a succeeding section. The VSWR and insertion loss can be made quite small and, although the device uses ferromagnetic principles, it is completely reciprocal.

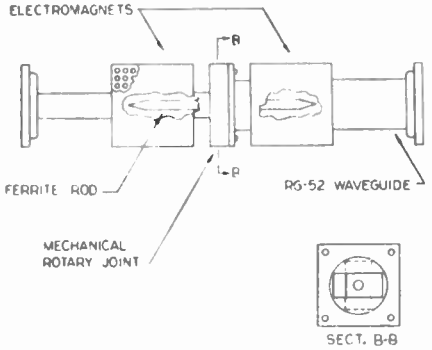

Fig. 1 Experimental ferrite rotary joint.

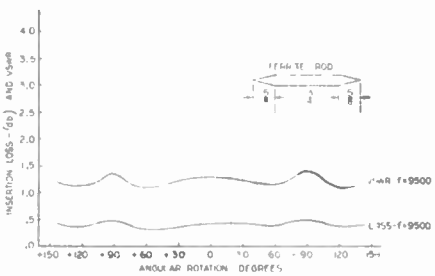

Fig. 2—Plot of insertion loss and VSWR vs rotation. Field = 900 oe.

An experimental X-band model of the rotary joint is shown in Fig. 1. A quarter-inch diameter rod of R-151 ferrite is supported axially in RG-52 waveguide with polystyrene supports. The rod is 3 in long with $\frac{3}{4}$ in tapers at each end for matching. Experimental electromagnets are around the waveguide for application of a longitudinal magnetic field.

A plot of the measured VSWR and insertion loss is shown in Fig. 2. It is seen that the VSWR is less than 1.4 and the insertion loss less than 0.5 db for all angles of rotation. It should be noted that no particular attempt was made in this model to optimize the VSWR or insertion loss other than placing the simple taper at each end; nor was an optimum length chosen other than which gave reasonably low VSWR and insertion loss as shown. The purpose of the model was mainly to prove the concept of the rotary joint.

The reciprocity of the joint was checked by reversing the input and output connections. Also, the direction of the magnetic field was reversed by changing the polarity of the magnetizing current. In both cases the values of VSWR and insertion loss were the same.

The principle of operation of the device is the conversion of the dominant mode linearly-polarized field in the rectangular guide into a circularly-polarized field contained primarily within the ferrite rod and reconversion into linear polarization past the junction of the rotating sections. In order to effect these polarization changes, two ferromagnetic principles are utilized. One is the

* Received by the IRE, September 1, 1961.

usual Faraday rotation effect and the other a "variable dielectric waveguide" effect. The latter effect[1] is brought about by the change in the permeability of the ferrite due to the applied magnetic field. As the permeability increases, larger portions of the RF field in the waveguide will be contained within the ferrite rod. The high dielectric constant of the ferrite causes large phase shifts. At the same time, the field which enters the rod is Faraday rotated in polarization such that the field is now in two orthogonal components, one parallel to the broad wall and the second parallel to the narrow wall of the waveguide. In the absence of the ferrite rod, the parallel component would not propagate at frequencies below the cutoff as determined by the narrow wall dimension (for RG-52, below 14.75 Gc). However, since most of the field is within the ferrite, cutoff is at a much lower frequency. In the limiting case, where all the RF field is within the rod, cutoff would be determined by the propagation of the circular TE_{11} mode in a rod of dielectric constant ϵ and diameter d. This frequency is

$$f_c = \frac{c}{\lambda_c} = \frac{1.841c}{\pi d\sqrt{\epsilon}} \cong 8 \text{ Gc}.$$

If we assume that the major portion of the field is contained within the ferrite, the actual cutoff is somewhere close to, but slightly above, 8 Gc.

Because of the rectangular geometry, the phase velocities of the two orthogonal components will differ, and at some point along the rod, they will be in quadrature. This will give rise to an elliptically-polarized field, or if the field magnitudes are equal, to circular polarization. At this point along the rod, the walls of the waveguide have little or no effect on the propagation and the joint can be effectively placed here. Beyond this joint, a reverse process as described above takes place, reconverting the field back to the dominant linear mode in the waveguide.

In order to support the above, a test was performed to prove the circularity of the field at the junction. This consisted of measuring the circularity of the radiated field of the second half of the rod unbounded by the waveguide. A circular field with an ellipticity of only 1.4 db was measured.

In its final form, this joint will offer a convenient means for the embodiment of an end-on rotary joint in a very short length. With the electromagnets replaced with small permanent magnets, the length of the joint proper should be of the order of 2 to 2½ in. The complexity of the mechanics of the joint is reduced since no choking is required as with usual joints and the bearing mechanism can be quite simple. In addition, this technique offers a simple means of transforming from linear to circular polarization which could be useful in many other component or antenna applications.

H. Saltzman
Douglas Research Corp.
Mount Vernon, N.Y.
A. Rossero
GPL Div.
General Precision, Inc.
Pleasantville, N. Y.

[1] J. A. Weiss, "A phenomenological theory of the Reggia Spencer phase shifter," Proc. IRE, vol. 47, pp. 1130–1137; June, 1959.

Signal-to-Noise Ratios in Photoelectric Mixing*

Quantum mechanical analyses[1] have shown that even an ideal linear amplifier has an inherent noise of $h\nu$ watts/cps referred to the input, *i.e.*, the total noise power spectral density $\psi(\nu)$ is given by

$$\psi = \frac{h\nu}{\exp(h\nu/kT) - 1} + h\nu. \qquad (1)$$

The first term is the thermal noise (one-dimensional black-body radiation) from the source at temperature T. The second term represents the minimum additional noise due to quantum effects, and is usually ascribed entirely to spontaneous emission in the amplifying medium.

For $h\nu \gg kT$, thermal noise virtually disappears, and $\psi \to h\nu$. Thus if an ideal amplifier has a pass band B cps wide centered at a frequency $\nu \gg kT/h$, and if the input signal power is $\bar{P}_s$, the output signal-to-noise ratio (SNR) will be

$$\frac{S}{N} = \frac{\bar{P}_s}{\int_{\nu-B/2}^{\nu+B/2} \psi(\nu)d\nu} = \frac{\bar{P}_s}{h\nu B}. \qquad (2)$$

The SNR does not become infinite in the absence of thermal noise: instead the familiar kT is replaced by $h\nu$. At room temperature and optical frequencies $h\nu/kT \approx 90$, so that (2) applies and gives the performance of an ideal coherent light amplifier.

A photocell is a perfect square-law device in the sense that the current is proportional to the incident light power. If two similarly polarized coherent, coincident beams of light of slightly different frequency fall on a photocell, the power, and hence the photocurrent, will vary at the difference frequency. Photocells can thus be used as mixers having conversion gain, and it is interesting to compare their signal-to-noise performance with that of the ideal amplifier.

Fig. 1 shows a balanced mixer consisting of two photocells and a half-reflecting half-transmitting mirror, $M/2$, which serves as a hybrid junction. For such a mirror, the reflection and transmission coefficients are $e^{i\pi/4}/\sqrt{2}$ and $e^{-i\pi/4}/\sqrt{2}$, respectively, and so if we write the instantaneous signal power as

$$P_s = [A_s \cos(\omega_s t + \pi/4)]^2$$

and the instantaneous local oscillator power as

$$P_0 = [A_0 \cos(\omega_0 t - \pi/4)]^2$$

we find

$$P_1 = \tfrac{1}{2}(A_0 \cos\omega_0 t + A_s \cos\omega_s t)^2,$$
$$P_2 = \tfrac{1}{2}(A_0 \sin\omega_0 t - A_s \sin\omega_s t)^2. \qquad (3)$$

(We have complicated the expressions for P_s and P_0 to simplify those for P_1 and P_2. The relative phase of signal and local oscillator is significant only when $\omega_0 = \omega_s$.)

Now, if η is the quantum efficiency of a photocell, *i.e.*, the average number of electrons produced per photon absorbed, then the photocurrent is given by $i = \eta q P/h\nu$, where q is the charge on the electron. Thus we find, ignoring any frequency components higher than $\delta \equiv \omega_s - \omega_0$, that

$$i_1 + i_2 = \frac{\eta q}{2h\nu}(A_0^2 + A_s^2), \qquad (4)$$

while the signal current i_s is given by

$$i_s = i_1 - i_2 = \frac{\eta q}{h\nu} A_0 A_s \cos\delta t, \qquad (5)$$

and has the mean-square value

$$\overline{i_s^2} = \left(\frac{\eta q}{h\nu}\right)^2 \frac{A_0^2 A_s^2}{2}. \qquad (6)$$

If the bandwidth of the circuits following the mixer is B cps, the mean-square shot noise affecting the output will be

$$\overline{i_n^2} = 2qB(i_1 + i_2) = \frac{\eta q^2 B}{h\nu}(A_0^2 + A_s^2). \qquad (7)$$

Taking the ratio of (6) to (7), we have

$$\frac{S}{N} = \frac{\eta}{2h\nu B} \frac{A_0^2 A_s^2}{A_0^2 + A_s^2}. \qquad (8)$$

As A_0 is increased, both the signal current (5) and the SNR (8) increase, the former without limit, the latter approaching the value

$$\left.\frac{S}{N}\right|_{\max} = \frac{\eta}{h\nu B} \frac{A_s^2}{2} = \eta \frac{\bar{P}_s}{h\nu B}, \qquad (9)$$

where $\bar{P}_s$ is the average value of P_s.

Comparing this result with (2), we see that if the quantum efficiency were unity, the photoelectric heterodyne converter would have the same signal-to-noise performance as the ideal amplifier, which is perhaps not too surprising.

But now let us consider the performance of the device as a homodyne converter, or synchronous detector. To do this we merely set $\omega_0 = \omega_s$ so that $\delta = 0$, and we now find from (5) that i_s has a mean-square value twice as great as before, $\cos\delta t$ having been replaced by unity. The output noise in the band from 0 to B cps will still be given by (7). As a result, we now find in the limit, as $(A_0/A_s) \to \infty$:

$$\left.\frac{S}{N}\right|_{\max} = \eta \frac{\bar{P}_s}{\left(\frac{h\nu}{2}\right)B}. \qquad (10)$$

With unity quantum efficiency the perform-

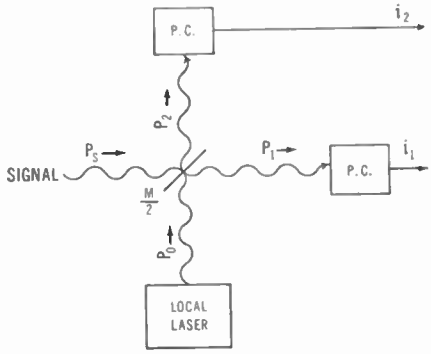

Fig. 1—A balanced photoelectric mixer.

* Received by the IRE, August 10, 1961; revised manuscript received September 19, 1961.

[1] See, *e.g.*, M. W. P. Strandberg, "Inherent noise of quantum-mechanical amplifiers," *Phys. Rev.*, vol. 106, pp. 617–620; May 15, 1957.

ance is now twice as good as that of an *ideal* amplifier, which does seem surprising.

The two-fold improvement with homodyne as against heterodyne mixing occurs because the signal conversion gain is doubled while the noise (which arises after mixing) is unaffected. This improvement is not found in the usual RF mixer where the noise enters with the signal and changes in conversion gain affect both equally.

It should be noted that the result (10) *cannot* be obtained by later synchronous detection of the IF resulting from an initial optical heterodyne mixing. In order to obtain the base-band B as in (10), the IF band would have to extend from $\delta-B$ to $\delta+B$ and so have twice the width assumed in (7). This doubles the total IF noise power, but only half of this total, *i.e.*, the amount given by (7), is demodulated along with the signal to produce base-band power. Thus the ratio (9) is again obtained.

The results (9) and (10) include only the usual Poisson distributed shot noise of the photocurrent. If one assumes a noise power of $h\nu/2$ watts/cps associated with the input signal due to the zero-point energy of the electromagnetic field, then (10) becomes

$$\left.\frac{S}{N}\right|_{\max} = \frac{\overline{P}_s}{\left(1+\frac{1}{\eta}\right)\left(\frac{h\nu}{2}\right)B} \qquad (11)$$

which for $\eta=1$ agrees with the SNR for an ideal linear amplifier. However, one must then assume this same $h\nu/2$ noise to be present in the input to any linear amplifier which leaves only $h\nu/2$ for additional noise due to spontaneous emission.

Additional noise might also result from statistical fluctuations in η, but this component, if it exists, should vanish as $\eta\to 1$. The quantum efficiency of good silicon photodiodes is probably close enough to unity to test experimentally whether (10) or (11) holds.

In any event, photoelectric mixing appears very promising as a means for linear amplification and frequency conversion of coherent optical signals.

B. M. Oliver
Hewlett-Packard Co.
Palo Alto, Calif.

Efficiency of Frequency Multipliers Using Charge-Storage Effect*

The disadvantage of the basic circuit for harmonic generation using the charge-storage effect of a p-n junction, treated by Leenov and Uhlir,[1] is that unwanted power is dissipated in both load and generator resistors. The basic circuit is shown in Fig. 1(a). By referring to the ideal current waveform shown in Fig. 2, it is seen that if both the input and output are resonated to allow only sinusoids at two frequencies to exist across the junction, no discontinuity and hence no harmonic generation, can occur due to the charge-storage effect; the circuit is as shown in Fig. 1(d).

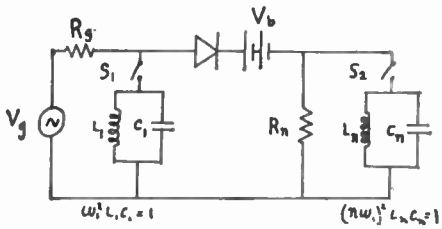

Fig. 1—Practical circuits.
(a) S_1 and S_2 open—untuned case.
(b) S_1 open, S_2 closed—tuned output.
(c) S_1 closed, S_2 open—tuned input.
(d) S_1 and S_2 closed—tuned input and output (basic circuit for multiplication using depletion-layer effect).

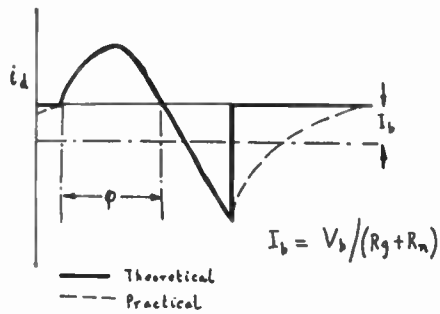

Fig. 2—Current waveforms for untuned cases.

In contrast to the untuned case treated by Leenov and Uhlir, that of the output load being resonant at $n\omega_1$ has been analysed; the circuit is as shown in Fig. 1(b). The results for a $\times 2$ and a $\times 10$ generator are shown in Fig. 3(a) and (b), respectively. It is seen that there is a value of R_n/R_g which gives a minimum loss for a given angle of forward drive. To illustrate the behavior, an angle of 120° was chosen for the calculation; in fact, this angle is not the optimum one and a slight improvement can be obtained by increasing the conduction angle to about 140° (approximately 1 db for the $\times 2$ circuit and 4 db for the $\times 10$ circuit). The important point to note is that the efficiency is inherently limited by the nature of the nonlinearity being utilized. From the curves it is seen that the theoretical limiting value of power loss for the $\times 2$ multiplier is 7.2 db and for the $\times 10$ multiplier 25 db, giving an improvement in each case of about 3 db over the untuned circuit. The discrepancy between these values obtained theoretically and the measured results may be accounted for by the deterioration in waveform due to the slow recovery time of the diode used (collector-base junction of OC44, input at 350 kc). The actual waveform obtained is shown in Fig. 2.

The alternative to resonating the load is to prevent harmonic currents from flowing in the generator resistance. In this case, if the generator is matched to the input impedance of the multiplier, theory predicts

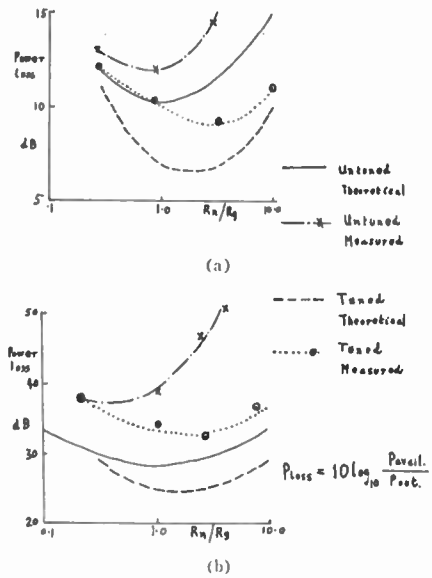

Fig. 3—Results for tuned output circuit.
(a) $\times 2$ circuit. (b) $\times 10$ circuit.

that an over-all improvement of 5.0 db may be obtained compared with the untuned circuit for $\phi=120°$. The arrangement used is shown in Fig. 1(c) and measurements on this circuit closely confirmed the theoretical figure of 5.0 db. The matching conditions for this circuit can be obtained from the Fourier coefficients for the fundamental frequency and yield the result $R_n \doteq \frac{1}{3}R_g$ for $\phi=120°$ (see Fig. 2).

To give some idea of the relative merits of an optimized charge-storage type multiplier compared with a depletion layer nonlinearity multiplier, consider each type when multiplying by 10. The charge-storage type has a limiting efficiency of -23 db (tuned and matched input, $\phi=120°$). For a similar loss, theoretical calculations indicate that using depletion layer nonlinearity, the circuit being as shown in Fig. 1(d), a diode with a Q factor $\doteq 100$ at the fundamental frequency is required, (estimated for the case of $V_1=0.95\ V_b$, where V_1 is the peak applied voltage and V_b is the bias voltage, assuming $\gamma=\frac{1}{2}$, *i.e.*, abrupt junction).[2] It should be noted that if three $\times 2$ stages using the depletion-layer effect are cascaded (giving approximately the same order of multiplication, *i.e.*, $\times 8$ compared with $\times 10$), an over-all efficiency of about -5 db should be obtained, if a diode of similar Q is available, (*i.e.*, $Q=100/n$ at the output frequency $n\omega_1$).

It may thus be concluded that, in general, the highest efficiency may be obtained by cascading lower order (*e.g.*, $\times 2$) multipliers using the depletion-layer effect. For high order single-stage multipliers (having the obvious advantage of simplicity) it may be advantageous to use the charge-storage effect, depending upon whether or not a high Q diode is available. The important point to note is that the efficiency of the

* Received by the IRE, July 24, 1961; revised manuscript received, September 25, 1961.

[1] D. Leenov and A. Uhlir, "Generation of harmonics and subharmonics at microwave frequencies with p-n junction diodes," Proc. IRE, vol. 47, pp. 1724–1729; October, 1959.

[2] The optimum value of V_1/V_b, and hence the value of Q factor, depends critically upon the forward conduction characteristics of the diode.

charge-storage type multiplier is inherently limited. It may also be relevant in practical applications that the power handling capabilities of this type of multiplier are considerably greater than those of the depletion-layer type. It should also be borne in mind that in practical circuits it is of course possible that harmonic generation may occur due to a combination of the two mechanisms, (as in the simple two frequency depletion-layer multiplier, with finite loss resistance).

The author gratefully acknowledges the many helpful discussions he had with Dr. A. R. Boothroyd and Dr. D. F. Page.

D. J. Roulston
Dept. of Elec. Engrg.
Imperial College of Science and Tech.
London, England

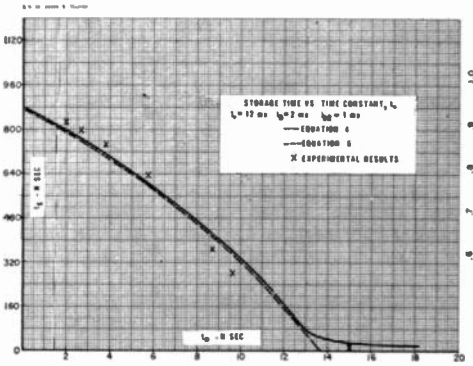

Fig. 2.

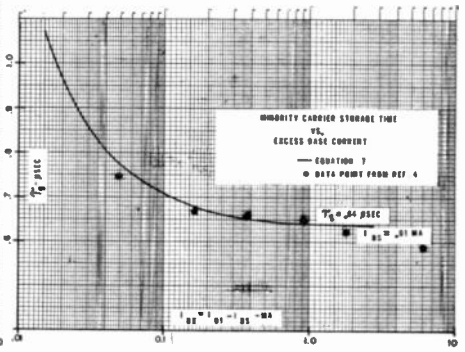

Fig. 3.

Transistor Storage Time in Circuits with Speed-Up Capacitors*

Base speed-up capacitors have been treated in connection with storage time primarily to calculate τ_s.[1] Presented here are expressions which have been obtained for storage time using arbitrary values of speed-up capacitance C for the circuit shown in Fig. 1.

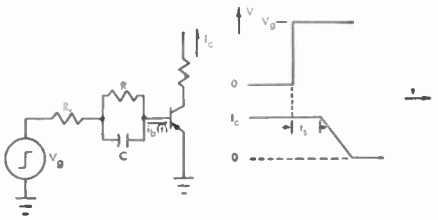

Fig. 1—Experimental circuit and associated waveforms.

When the transistor is saturated and when τ_s, an effective minority carrier lifetime, is used in place of the usual τ, the continuity equation can be integrated once in a field-free base region. Use of the divergence theorem then leads to the following first-order differential equation:

$$I_{Bs} - i_b(t) = K_s p_c(t) + k_s \frac{dp_c(t)}{dt}, \qquad (1)$$

where

I_{Bs} = base current at saturation threshold,
K_s = proportionality factor between p_c and saturated base current,
k_s = proportionality factor between charge stored and p_c for the diode with emitter and collector tied together,
$i_b(t)$ = instantaneous base current,
$p_c(t)$ = instantaneous minority carrier density in base at the collector junction.

Eq. (1) is valid for storage-time calculations only because it relates the excess current necessary to maintain the excess charge, Q_{Bx} (*i.e.*, the additional charge over and above that required for the threshold of saturation) in the base. By using the initial condition

$$p_c(0) = \frac{1}{K_s}\{I_{Bs} - I_{B1}\}, \qquad (2)$$

(1) can be integrated recalling that p_c is zero at time t_s. Thus,

$$I_{Bs} = e^{-t_s/\tau_s}\left[\frac{1}{\tau_s}\int_0^{t_s} i_b(t)e^{t/\tau_s}dt + I_{B1}\right], \qquad (3)$$

where

I_{B1} = final equilibrium "on" base current with device in saturation.

For a step voltage V_g, (3) yields for storage time

$$t_s = \tau_s \ln\left[\frac{(I_{B1} - I_{B2})\left(1 + \frac{R}{R_s}\frac{t_0}{t_0 - \tau_s}\right)}{I_{Bs} - I_{B2} + \frac{R}{R_s}\left(\frac{t_0}{t_0 - \tau_s}\right)(I_{B1} - I_{B2})e^{-t_s/t_0}}\right], \qquad (4)$$

where

I_{B2} = "off" generator voltage divided by the total series resistance ($R+R_s$),

and

$$t_0 \equiv \frac{RR_sC}{R + R_s}. \qquad (5)$$

When C and, hence, t_0, is set equal to zero, (4) degenerates to the frequently used expression for storage time.[1-3] Eq. (4) is plotted in Fig. 2.

An approximation to (4) also appears in Fig. 2. This approximation is valid when $t_s \gg t_0$, and is described by

$$t_s = \tau_s \ln\frac{(I_{B1} - I_{B2})\left(1 + \frac{R}{R_s}\frac{t_0}{t_0 - \tau_s}\right)}{I_{Bs} - I_{B2}}. \qquad (6)$$

Because of practical experimental limitations, the experimental value of τ_s determined may correspond to the value predicted by (6). In view of this, τ_s may be calculated from (6) under the condition $t_0 \ll \tau_s$. For the experimental procedure outlined by Sparkes and Beaufoy (*i.e.*, $I_{B2}=0$, $R_s \ll R$), (6) simplifies to

$$\tau_s = \frac{RC}{1 - \frac{I_{Bs}}{I_{B1}}}. \qquad (7)$$

Fig. 3 is a plot of (7) and the experimental data (i_c=3 ma) from Fig. 11 of Sparkes.[4] Note that (7) describes the initial variation of τ_s with excess base current. At large values of I_{Bx}, the deviation of experimentally observed data may be explained by effects due to high injection levels. Fig. 3 is similar to Fig. 11 of Sparkes.[4] The explanation given in this reference for the initial variation in τ_s (the change in charge due to collector depletion region narrowing) is a contributing factor. However, it is believed that an important contributing factor to this variation is given by (7).

Expressions for t_s have also been derived for ramp and exponential forms of the generator V_g output. It is anticipated that the work described here will be published in detail in the near future.

R. P. Nanavati
Syracuse Univ.
Syracuse, N. Y.
R. J. Wilfinger
General Products Div.
Development Lab.
IBM Corp.
Endicott, N. Y.

* Received by the IRE, September 7, 1961; revised manuscript received, September 15, 1961.

[1] R. Beaufoy and J. J. Sparkes, "The junction transistor as a charge controlled device," *ATE J.*, vol. 13, pp. 310–327; October, 1957.

[2] J. J. Ebers and J. L. Moll, "Large signal behavior of junction transistors," Proc. IRE, vol. 42, pp. 1761–1772; December, 1954.

[3] J. A. Ekiss and C. D. Simmons, "Junction transistor response characterization," *Solid State J.*, vol. 2, pp. 17–24; January, 1961.

[4] J. J. Sparkes, "A study of the charge control parameters of transistors," Proc. IRE, vol. 48, pp. 1696–1705; October, 1960.

Improvement in the Performance of an Automatic Noise Figure Meter with a Liquid-Nitrogen-Cooled Termination*

NOMENCLATURE

B = amplifier bandwidth
F = noise figure meter reading
F' = actual noise figure of amplifier
G = amplifier gain
k = Boltzmann's constant (1.38×10^{-23} watt-sec/°K)
L = directional coupler insertion loss
N = available noise power from amplifier when noise generator is off
N^* = available noise power from amplifier when noise generator is on
t_1 = coupling power coefficient of directional coupler
t_2 = resistive power transmission coefficient of the direct path through coupler
T = termination temperature
T_0 = defined ambient temperature (290°K)
T_0' = actual ambient temperature
T_e = rated excess noise of noise generator
T_e' = actual excess noise of noise generator
T_R = excess-noise temperature of amplifier.

In the measurement of the noise figure of low-noise (less than 6-db) amplifiers, it is difficult to obtain an accurate scale reading on standard automatic noise figure meters. One method of expanding the scale and increasing the measurement accuracy employs a directional coupler and cooled termination,[1] as shown in Fig. 1.

The definition of noise figure[2] is the ratio of the available noise power from the amplifier to the available noise power from an ideal amplifier, both with input termination temperature T_0. In the case of the normal automatic noise figure meter where a noise source is connected directly to the amplifier input, the available output noise power with the noise source not turned on is

$$N = kT_0BGT. \tag{1}$$

The available output noise power with the noise generator on is

$$N^* = kT_0BGF + kT_eBG. \tag{2}$$

The noise power ratio is

$$\frac{N^*}{N} = 1 + \frac{T_e}{FT_0}. \tag{3}$$

The noise power ratio for the amplifier under evaluation (Fig. 1) is

$$\frac{N^*}{N} = \frac{T_R + (T_0' + T_e')t_1 + [T_0'(1 - t_2) + Tt_2](1 - t_1)}{T_R + T_0't_1 + [T_0'(1 - t_2) + Tt_2](1 - t_1)}. \tag{4}$$

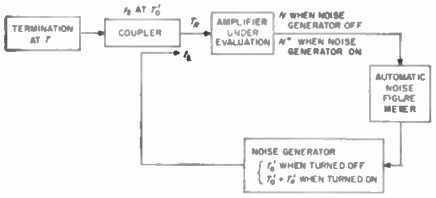

Fig. 1.

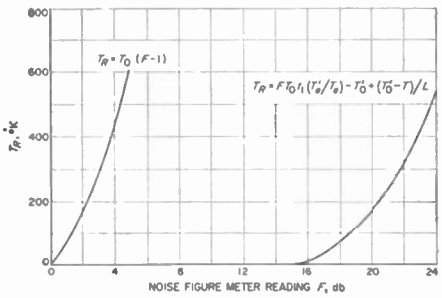

Fig. 2.

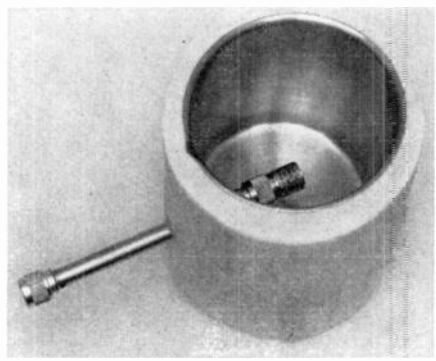

Fig. 3.

Setting (3) and (4) equal to each other and substituting $t_2(1-t_1) = 1/L$ gives

$$T_R = FT_0t_1\frac{T_e'}{T_e} - T_0' + \frac{T_0' - T}{L}. \tag{5}$$

Noise figure is related to receiver noise temperature by

$$F' = 1 + \frac{T_R}{T_0}. \tag{6}$$

Eq. (5) is plotted on the right-hand side of Fig. 2 for a typical example.

The following parameters were measured at 2388 Mc using a Narda directional coupler Model 3003-30 and a Bendix noise tube Model TD-40:

$$L = 1.026(0.11\text{ db})$$
$$t_1 = 0.0107(-19.70\text{ db})$$
$$T_e'/T_e = 0.794(-1\text{ db})$$
$$T_0 = T_0' = 290°\text{K}$$
$$T = 77.5°\text{K}.$$

For comparison, a plot of noise figure (as conventionally measured) vs receiver temperature is shown on the left-hand side of Fig. 2. Reading accuracy is better with the new technique, particularly in the measurement of low noise temperatures. Values of L and t_1 were obtained with the Weinschel dual-channel insertion test set (accurate to 0.02 db), and T_e'/T_e was evaluated with a 2388-Mc mixer and recorder system calibrated to about 1 per cent using a liquid-nitrogen-cooled termination, room-temperature termination, and ATL precision attenuator.

The coupling value for the directional coupler is best chosen to give a noise figure reading on the meter near the center of the scale (the most accurate portion of the scale). A noise figure meter reading of 18 db for the above example is obtained with an amplifier noise temperature of 72°K.

This improved measurement technique also slightly reduces the sensitivity to excess-noise temperature error.[3]

Fig. 3 shows a typical liquid-nitrogen-cooled termination, 50-ohm transmission line, and container as used in the method described. The container and transmission line are constructed from stainless steel to reduce thermal heat loss. The Stoddart Aircraft Company termination has a special insert selected to have a VSWR of less than 1.05 at the operating frequency when cooled to the temperature of liquid nitrogen (77.5°K).

This technique of noise figure measurement extends the range of an automatic noise figure meter for use with low-noise amplifiers, increases the accuracy, and is relatively simple to implement.

C. T. STELZRIED
Jet Propulsion Lab.
California Inst. Tech.
Pasadena, Calif.

* Received by the IRE, August 7, 1961; revised manuscript received, September 18, 1961. This paper presents the results of one phase of research carried out at the Jet Propulsion Lab., California Institute of Technology, under Contract No. NASw-6, sponsored by NASA.

[1] M. Negrete, "Additional conveniences for noise figure measurements," *Hewlett Packard J.*, vol. 10; February–March, 1959.

[2] H. T. Friis, "Noise figures of radio receivers," PROC. IRE, vol. 32, pp. 419–422; July, 1944.

[3] *Research Summary No. 36-7*, Jet Propulsion Lab., Calif. Inst. Tech., Pasadena, Calif., vol. 1, p. 85; February 5, 1961.

A Tunnel-Diode Wide-Band Frequency Doubling Circuit*

A typical tunnel-diode volt-ampere characteristic shows a marked similarity to a parabola in the region of its peak current operating point. If a sinusoidal voltage is applied to a diode biased at its maximum current point, the diode current variations will be at twice the frequency as the applied voltage. See Fig. 1. If the selected region of the diode provides a transfer function of Ke^2 and $e = \sin\omega t$; then

$$i = K\sin^2\omega t = K\frac{(1 - \cos 2\omega t)}{2}.$$

The steady-state component is removed by ac coupling.

* Received by the IRE, September 25, 1961.

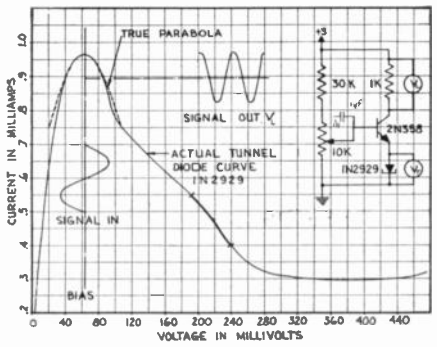

Fig. 1.

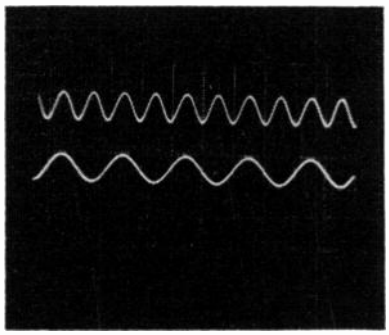

Fig. 2.

The waveforms from the circuit of Fig. 1 show a 2-kc voltage variation being derived from a 1-kc signal source. See Fig. 2. The sweep speed in Fig. 2 is 50 μsec/cm and the vertical sensitivity is 50 mv/cm.

FRANK D. NEU
Lawrence Radiation Lab.
University of California
Berkeley, Calif.

A Note on Antenna Breakdown*

INTRODUCTION

The fact that the breakdown potential for an antenna varies with pressure and that the recovery potential is somewhat lower than the breakdown potential is well treated in the literature. The general shape of the curves are shown in Fig. 1.

The temptation is to devote primary attention to the breakdown curve. The researcher concentrates on determining and improving the breakdown curve. The designer concentrates on providing an antenna that operates below the breakdown curve. The recovery curve is, for the most part, ignored. This reasoning makes an apparently logical assumption that there is no need to be concerned with antenna recovery characteristics if the antenna does not break down. There are some circumstances, however, that cause antenna breakdown from an external stimulus, and then the antenna will remain in this condition as long as the antenna operating point is above the recovery curve.

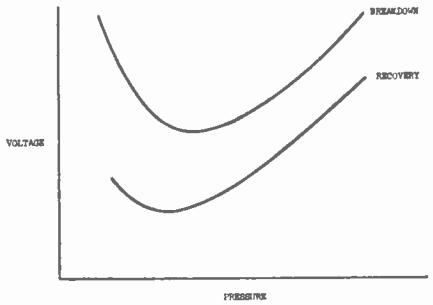

Fig. 1.

DISCUSSION

An excellent example of the breakdown stimulus is missile staging, which was demonstrated during the Titan missile program. Some Titan missiles that successfully staged suffered breakdown of the telemetry antenna, operating at about 200 Mc, while Titan missiles that had not staged passed through the identical altitude region without incurring breakdown. The antenna breakdown began at the time of missile staging.

An explanation for this series of events can be deduced by reviewing a few simple factors associated with the staging of the Titan. The first stage is jettisoned, and the second stage is ignited while the two stages are close to each other. The highly ionized exhaust from the second stage is deflected from the first stage. Some of this plasma finds its way to the telemetry antenna. Curves similar to Fig. 1 exist for the antenna operating in the plasma. However, the curves are at a much lower voltage level than those for antenna operation in air. If the plasma breakdown voltage drops below the antenna operating point, breakdown occurs. The antenna operates in the plasma for a short period of time as the missile accelerates away from the first stage. The change from antenna operation in plasma to operation in air is a continuous time function. As the effect of the plasma decreases, the breakdown and recovery curves once more return to the original values. But if the antenna has broken down, it will stay in that condition until the operating point goes below the recovery curve. Now the performance of the Titan telemetry antenna can be explained. When the Titan did not stage, there was no stimulus and thus no breakdown. Some of the missiles that staged did not incur antenna breakdown. For these missiles, the plasma breakdown voltage did not drop below the antenna operating point. In the case of the remaining missiles, the plasma breakdown voltage dropped below the operating point causing breakdown in the presence of the plasma. This momentary breakdown became sustained breakdown because the operating point was above the recovery curve.

An additional example is afforded by an analysis of the performance of the telemetry antenna on a nose cone that was used on the Atlas and Thor missiles. Antenna breakdown during powered flight was more common on the Atlas than on the Thor. For our purposes, there are two major differences between the powered flight of the Atlas and Thor missiles: the Atlas achieves higher velocities than the Thor, and the Atlas stages whereas the Thor does not. There has been speculation that some of the Atlas nose-cone antenna breakdown was caused by shock ionization due to the higher velocity. A comparison of the Atlas and Thor velocities through the critical altitude region, 150,000 to 300,000 feet for the frequencies involved, rule out shock ionization. There is no evidence that the Atlas nose cone is subjected to shock ionization during powered flight. An examination of the records reveals that on a substantial percentage of tests, breakdown of the antenna begins at staging. This evidence indicates strongly that on some Atlas test flights, breakdown of the nose-cone telemetry antenna was caused by plasma in the vicinity of the antenna, which in turn was the result of staging.

CONCLUSION AND RECOMMENDATIONS

Much work has been done to improve the antenna characteristics represented by the breakdown curve. The results of this work will certainly be useful on vehicles that do not encounter a stimulus to cause momentary breakdown.

However, antenna performance can be governed by the recovery curve and not the breakdown curve when an external stimulus, such as staging, is encountered. Those engaged in antenna breakdown research should give more consideration to recovery characteristics of antennas.

The antenna designer who is concerned with breakdown must decide whether the breakdown or recovery curve governs for his application. In these cases where the recovery curve governs, he must be extremely careful when he tries to apply theory or experimental data that deals only with the breakdown curve, since some of the techniques developed to improve the breakdown characteristics may have little effect on the recovery characteristics.

E. L. TARCA
Space Systems Technology Group
Siegler Corp.
Inglewood, Calif.

* Received by the IRE, September 25, 1961.

Contributors

Morrel P. Bachynski was born in Bienfait, Saskatchewan, Can., on July 19, 1930. He received the B.E. degree in engineering physics in 1952, and the M.Sc. degree in 1953, both from the University of Saskatchewan, Saskatoon, Can., and the Ph.D. degree from McGill University, Montreal, Can., in 1955.

M. P. Bachynski

Until October 1955, as a member of the staff of the Eaton Electronics Research Laboratory (McGill University), he was engaged in investigations of aberrations in microwave lens systems. Since that time he has been with the RCA Victor Research Laboratories, Montreal, Can., concerned primarily with short-wave propagation and plasma physics problems, where he is now Director of the Microwave Physics Laboratory. In addition, he is connected with the Graduate School of McGill University, teaching classes in antenna and electromagnetic theory in the Extension Department.

Dr. Bachynski is a member of the Canadian Association of Physicists and Commission VI of the Canadian National Committee of URSI.

❖

Jack R. Baird (S'60) was born in Colchester, Ill., on May 1, 1931. He received the B.S. and M.S. degrees in electrical engineering in 1958 and 1959, respectively, from the University of Illinois, Urbana, where he is presently working on the Ph.D. degree.

J. R. Baird

From 1951 through 1954 he served in the U. S. Air Force as an Instructor in the radar school at Lowry Air Force Base, Denver, Colo. He joined the Ultramicrowave Group, at the University of Illinois, in 1956 as an undergraduate technician designing and constructing high-power modulators, waveform generators, and special power supplies for low millimeter wavetubes. He is currently a Graduate Research Assistant. His research interests have included problems in field emission, nonlinear microwave plasmas, megavolt electronics, and submillimeter waves.

Mr. Baird is a member of Tau Beta Pi.

❖

W. Bernstein received the B.S. degree from New York University, N. Y., in 1944. From 1946 to 1948 he did graduate work at the University of Chicago, Ill., and the University of Wisconsin, Madison.

He is a physicist in the Electron Dynamics Department of the Hughes Research Laboratory, Malibu, Calif. Prior to joining Hughes, he was at Project Materhorn, Princeton University, N. J., and at Brookhaven National Laboratory. His fields of specialization are plasma physics and low-energy nuclear physics.

W. Bernstein

❖

Albert W. Biggs (S'56–M'59) was born in Toledo, Ohio, on October 4, 1926. He received the B.S. degree in electrical engineering from Washington University, St. Louis, Mo., in 1948, and the M.B.A. degree from Stanford University, Stanford, Calif., in 1950. He is currently completing his dissertation for the Ph.D. degree in electrical engineering at the University of Washington.

A. W. Biggs

From 1955 to 1957, he was at the University of Washington as an Instructor in Electrical Engineering. Since 1957, he has been with the Boeing Company, Seattle, where he has been engaged in research on microwave and low-frequency propagation.

Mr. Biggs is a member of the American Physical Society.

❖

Gary D. Boyd (S'53–M'60) was born in Los Angeles, Calif., on September 14, 1932. He received the B.S., M.S., and Ph.D. degrees in 1954, 1955, and 1959, respectively, from the California Institute of Technology, Pasadena, where he was engaged in plasma physics research.

G. D. Boyd

He is presently engaged in research on optical masers at the Bell Telephone Laboratories, Inc., Murray Hill, N. J.

Dr. Boyd is a member of the American Institute of Physics.

George R. Brewer was born in New Albany, Ind., on September 10, 1922. He received the B.E.E. degree in electrical engineering in 1943 from the University of Louisville, Ky., and the M.S.E. degree in electrical engineering in 1948, the M.S. degree in physics in 1949, and the Ph.D. degree in electrical engineering in 1951, all from the University of Michigan, Ann Arbor.

G. R. Brewer

From 1943–1944 he worked with the M.I.T. Radiation Laboratory, Cambridge, Mass., where he was concerned with magnetron development. In 1944 he joined the Naval Research Laboratory, where he did research and development on microwave electron tubes and in 1947 he began research on magnetrons, space charge, and associated subjects at the Engineering Research Institute of the University of Michigan. He joined Hughes Research Laboratories, Malibu, Calif., in 1951, where he has worked with traveling-wave tubes, electron guns, electron beam focusing systems, and more recently with ion propulsion. He is currently Head of the Electron Dynamics Department.

Dr. Brewer is a member of the American Rocket Society, the American Physical Society, Sigma Xi, RESA, and Phi Kappa Phi.

❖

Gilles G. Cloutier was born in Quebec City, Canada, on June 27, 1928. He received the B.A. degree in 1949 and the B.Sc. degree in physics in 1953, both from Laval University, Quebec. He was employed in the Research Laboratories of the Defense Research Board of Canada from 1953–1954. He received the M.Sc. and Ph.D. degrees from McGill University, in 1956 and 1959, respectively

G. C. Cloutier

In 1959 he joined the Research Laboratories of the RCA Victor Company, Montreal, where he is carrying out research in the field of microwave physics, plasmas and ionic propulsion.

Dr. Cloutier is a member of the Canadian Association of Physicists, the American Rocket Society and Sigma Xi.

❖

Paul D. Coleman (A'45–M'55) was born in Stoystown, Pa., on June 4, 1918. He received the B.A. degree from Susquehanna

University, Selinsgropve, Pa., in 1940, the M.S. degree in physics from Pennsylvania State University, University Park, in 1942, and the Ph.D. degee in physics from the Massachusetts Institute of Technology, Cambridge, in 1951.

P. D. COLEMAN

He was employed as a physicist with the U. S. Signal Corps and subsequently with the U. S. Air Force at Wright Air Development Center, Dayton, Ohio, from 1942 to 1946. During this period, he was engaged in work on electromagnetic theory, and received the Army Air Force Meritorious Civilian Award in 1946 for his contribution to aircraft antenna theory.

From 1946 to 1951, he was a physicist with the U. S. Air Force at the Cambridge Air Research Center, Mass., and later a Research Associate in physics at the Research Laboratory of Electronics, at M.I.T., where he was concerned with the generation of submillimeter waves.

In 1951, he became an Associate Professor in Electrical Engineering at the University of Illinois, Urbana, where he established the Ultramicrowave Group in the Electrical Engineering Research Laboratory. He is presently a Professor on the graduate electrical engineering staff, teaching and directing research on submillimeter wave generation, detection, and propagation. In 1959, he became a member of the Board of Technological Counselors of FXR, Inc., Woodside, N. Y., and in 1960 was elected Chairman.

He is a member of Sigma Xi, the American Physical Society, and Pi Mu Epsilon.

❖

Frederick W. Crawford was born in Birmingham, England, on July 28, 1931. After four years in industry, during which he obtained the B.Sc. degree in engineering from London University, London, England, he spent four years at Liverpool University, Liverpool, obtaining the Ph.D. degree for research on arc discharges in 1955, and the Diploma in Education in 1956. He obtained the M.Sc. degree in Mathematics from London University in 1958.

F. W. CRAWFORD

During 1956–1957, he worked on electronic instrumentation as a scientist with the Research Department of the National Coal Board. The next two years were spent as a Senior Lecturer in Electrical Engineering at the College of Advanced Technology, Birmingham, England. Since the end of 1959, he has been working on plasma instabilities as a Research Associate at the Microwave Laboratory, Stanford University, Stanford, Calif. He is presently on a temporary leave to study at the Centre des Etudes Nucléaires de Saclay, France.

Dr. Crawford is a member of Sigma Xi, an associate member of the IEE, and an associate of the Institute of Physics of Great Britain.

❖

Malcolm R. Currie (S'52–A'55–SM'58) was born in Spokane, Wash., on March 13, 1927. He received the B.A. degree in physics in 1949, the M.S. degree in 1952, and the Ph.D. degree in 1954, all from the University of California, Berkeley.

M. R. CURRIE

From 1944 to 1947 he served in the U. S. Navy Air Corps. He was associated with the Microwave Laboratory at the University of California from 1949 to 1951. From 1952 to 1954 he was a Research Assistant in the Electronics Research Laboratory. He was an Instructor in the Department of Electrical Engineering during 1953–1954. Since 1954 he has been associated with the Research Laboratories of the Hughes Aircraft Company, Malibu, Calif., where he has been concerned primarily with problems in microwave and millimeter wave tubes, plasma physics, optical masers and ion propulsion. From 1957 to 1959 he was Manager of the Electron Dynamics Department. In 1960 he became Director of the Physics Laboratory, and he is now Associate Director of the Research Laboratories.

Dr. Currie received the Eta Kappa Nu Award (outstanding young electrical engineer) for 1958. He is a member of the American Physical Society, the American Rocket Society, Sigma Xi, RESA, and Phi Beta Kappa.

❖

Daniel G. Dow (S'53–M'57) was born in Ann Arbor, Mich. on April 26, 1930. He received the B.S. degree in engineering physics in 1952 and the M.S.E.E. degree in 1953, both from the University of Michigan, Ann Arbor, and the Ph.D. degree from Stanford University, Stanford, Calif., in 1958.

D. G. DOW

From 1953 to 1955 he was a Project Officer in the Electron Tube Branch at Wright Air Development Center, Dayton, Ohio, responsible for research and development in microwave tubes. From 1955 to 1958, he was a Research Assistant at Stanford and holder of Fellowships from the Sylvania Electric Corporation and the Bell Telephone Laboratories. From 1958 to 1961 he was a member of the faculty of electrical engineering at the California Institute of Technology, Pasadena, and a Consultant to the Physics Laboratory of the Hughes Research Laboratories, Culver City, Calif. In July of 1961 he joined the Central Research Laboratories of Varian Associates, Palo Alto, Calif., where he is currently conducting research in the fields of plasma physics and physical electronics.

Dr. Dow is a member of the American Physical Society and Sigma Xi.

❖

Lester M. Field (M'48–F'52) was born in Chicago, Ill., on February 9, 1918. He received the B.S. degree from Purdue University, Lafayette, Ind., in 1939, and the Ph.D. degree from Stanford University, Calif., in 1943.

L. M. FIELD

Upon receiving his Ph.D. degree, he joined the Electron Dynamics Group of the Bell Telephone Laboratories. After early work in electron optics and magnetrons, he collaborated with Dr. J. R. Pierce to become co-developer of the first stable traveling-wave tubes. This device introduced new principles into the art of microwave amplification which served as the opening wedge to a whole new realm of types of amplifiers and new interaction processes. In 1946 he returned to Stanford University where he was one of the originators of their Electron Tube Laboratory. During this period he invented many modern forms of traveling-wave tube propagating structures, the velocity-jump amplifier (and noise de-amplifier), scanning search-receivers, transverse current amplifiers, and many others. He became Stanford University's youngest full Professor at 32. In 1953 he became a full Professor at the California Institute of Technology, Pasadena, and there established a tube research activity which expanded into a group studying plasma physics and microwave interaction with matter. Here he invented several forms of beam-plasma amplifiers and studied fundamental plasma behavior. During this period he also became the Associate Director of the Hughes Research Laboratories, Los Angeles, Calif., and became Head of its Physics Laboratory in 1955. As Head of the Physics Laboratory, he participated in establishing programs in plasma studies, fusion power, ion propulsion and masers, as well as maintaining a continuing interest in microwave tubes through patents on new forms of high-power tube structures, such as the stub-supported contrawound helix and folded waveguide circuit. In recent years, he has been concerned with monitoring and welding together research, development,

production and business groups to make an over-all microwave tube enterprise.

Dr. Field is a member of Sigma Xi, and the American Physical Society. He is a Wilbur Scholar of Tau Beta Pi, and recipient of the 1949 Eta Kappa Nu Outstanding Young American Engineer Award.

❖

Ian P. French was born in Cuenca, Ecuador, on April 22, 1935. He received the B.Sc. (Hons.) degree in applied physics from St. Andrews University, Scotland, in 1958. He is continuing his studies under the auspices of the Extension Department of McGill University.

I. P. FRENCH

He joined Canadair, where he was engaged in radome design and test in 1958. In 1959 he joined the RCA Victor Research Laboratories, Montreal, Can., where he has spent some time on millimeter-wave studies. Since then he has been engaged in investigations of the electromagnetic properties of plasmas, and is presently associated with experiments on microwave propagation through plasmas and aerospace communication studies.

❖

Ladislas Goldstein (SM'55–F'56) was born in Dombrad, Hungary, on February 6, 1906. He received the B.S. degree in physics from the College of the City of Nagyvarad, and the M.S. degree from the University of Paris, France, in 1928, where he was a Fellow from 1929 to 1934, receiving the D.Sc. degree in nuclear physics in 1937.

L. GOLDSTEIN

From 1934 to 1937 he was an Assistant Instructor at the University of Paris, and from 1937 to 1940 he was a Research Associate and a Fellow of the National Center Research of France. From 1940 to 1942 he was a Research Associate at the Institute of Atomic Physics. He was the Director of the laboratories at the Canadian Radium and Uranium Corporation from 1942 to 1944, and from 1944 to 1945 he was a research worker with the Admiralty Research Laboratories, Teddington, England. From 1945 to 1951 he was a Research Physicist with the Federal Telecommunication Laboratory, and in 1951 he became a Professor of Electrical Engineering at the University of Illinois, Urbana.

He has concentrated his efforts in the field of nuclear physics. He has worked on the use of gas-discharge phenomena in microwave physics, microwave propagation through media containing free electrons, infrared radiation detection, and the application of ionizing radiations of radioactive substances.

Dr. Goldstein is a member of the Physical Society.

❖

Roy W. Gould (S'48–A'51–M'56) was born in Los Angeles, Calif., on April 25, 1927. He received the B.S.E.E. degree from the California Institute of Technology, Pasadena, in 1949, and the M.S. degree from Stanford University, Stanford, Calif., in 1950. He completed the requirements for the Ph.D. degree in physics at the California Institute of Technology in 1955. During his graduate study, he held a National Science Foundation Fellowship and a Howard Hughes Fellowship.

R. W. GOULD

In 1951 and 1952, he was employed at the Caltech Jet Propulsion Laboratory as a Research Engineer and worked on the guidance system of the Corporal missile. Since 1955, he has been on the staff of the California Institute of Technology, where he now an Associate Professor of Electrical Engineering and Physics, teaching and conducting research in the field of plasma physics.

Dr. Gould is a member of Tau Beta Pi, Sigma Xi, and the American Physical Society.

❖

Theodore P. Harley (S'58–M'59) was born in New York, N. Y., on July 25, 1925. He received the B.S.E.E. degree in 1948 from the College of the City of New York, and the M.S.E.E. degree from Colorado University, Boulder, in 1953. He has also completed additional graduate studies at the University of Washington, Seattle, leading to a Ph.D. degree and has taught a course in electronics.

T. P. HARLEY

From 1948 to 1953, he was employed by the Bureau of Reclamation, Denver, Col. In 1953 he joined the staff of the Boeing Company, Seattle, Wash., as an Associate Research Engineer. Currently, he is working in the Aero-Space Division of this company doing work in propagation through plasmas.

❖

John C. Helmer, for a photograph and biography, please see pages 1588–1589, of the October, 1961, issue of these PROCEEDINGS.

Edward W. Herold was born in New York, N. Y., in 1907. He received the B.Sc. degree in physics from the University of Virginia, Charlottesville, in 1930, the M.Sc. degree from the Polytechnic Institute of Brooklyn in 1942, and an honorary D.Sc. degree, also from the Polytechnic Institute of Brooklyn, in 1961.

E. W. HEROLD

From 1924 to 1926 he worked at Bell Telephone Laboratories, and from 1927 to 1929 with E. T. Cunningham, Inc. He was with RCA at Harrison, N. J., from 1930 to 1942 and from 1942 to 1959 at RCA Laboratories, Princeton, N. J., where he became Director, Electronic Research Laboratory. In 1959, he joined Varian Associates, Palo Alto, Calif. as Vice President, Research. He has made his career in research and development, specializing in electron tubes, semiconductor physics and devices, signal-to-noise problems, and plasma physics.

He is a member of Phi Beta Kappa and Sigma Xi, and has been active in IRE affairs including membership on the Board of Directors from 1956 to 1958.

❖

Sheldon B. Herskovitz (S'55–M'56) was born in Brooklyn, N. Y., on March 13, 1930. He received the B.S. degree in chemistry in 1951 from the Massachusetts Institute of Technology, Cambridge. He served in the Air Force for two years with the Vacuum Tubes Group of the Air Force Cambridge Research Center, Cambridge, Mass., and then returned to Harvard University, Cambridge, where he received the M.A. degree in chemistry in 1955. During graduate work, he was employed as an engineer in the Research and Development Group of Microwave Associates, then in Boston, Mass. Since 1955, he has been employed at the Air Force Cambridge Research Laboratories, where he has been concerned primarily with an experimental research program involving the interaction of ionized gases and microwave energy.

S. B. HERSKOVITZ

Mr. Herskovitz is a member of the American Physical Society, the American Vacuum Society, and the Scientific Research Society of America.

❖

Henri Hodara was born in Paris, France, on January 8, 1926. He received the B.S.E.E. degree from the Massachusetts Institute of

Technology, Cambridge, in 1947; the M.S.E.E. degree from Stanford University, Calif., in 1949; and is presently completing his Doctoral dissertation at the Illinois Institute of Technology, Chicago.

H. Hodara

From 1949 to 1956 he was primarily active as a Management Consultant, in both the U.S.A. and abroad. He was a Project Engineer for Cook Research Laboratories from 1956 to 1960. While at Cook, he designed a UHF subminiature transmitter for a recovery package, airborne ferret equipment, and object locators. In 1960 he joined The Hallicrafters Company, Chicago, Ill., as Head of Space Communications and has since then become Associate Director of the Research and Development Division. His work is primarily in the field of communications; he has published extensively on wave propagation in anisotropic plasmas, re-entry blackout, and communications. He is a Hallicrafters' Consultant to the Physical Science Laboratory of the New Mexico State University and Bell Telephone Laboratories on plasma propagation for Nike-Zeus. He has also acted as a Consultant to the Army Corps of Engineers, Fort Belvoir, Va., on various problems of weak signal detection and electromagnetic theory and has taught evening graduate school in the Electrical Engineering Department of the Illinois Institute of Technology.

❖

Robert L. Jepsen (A'52–SM'57) was born in Valley, Wash., on June 16, 1920. He received the B.S. degree in electrical engineering from Washington State College, Pullman, in 1944 and the Ph.D. degree in physics from Columbia University, New York, N. Y., in 1951.

R. L. Jepsen

He was employed by the Radio Corporation of America, Lancaster, Pa., from 1944 to 1946 as a magnetron research and development engineer. Between 1946 and 1951, he was a Research Associate at the Columbia Radiation Laboratory where he was engaged in research on magnetrons. He joined Varian Associates, Palo Alto, Calif., as a Research Physicist in 1951, and served as Director of the microwave tube research until 1957. He was awarded the first Varian Associates Advanced Study Grant and spent the 1957–1958 academic year at Harvard University, Cambridge, as a Research Fellow working in the fields of ferrites and ferromagnetic insulators. Upon returning to Varian Associates, he worked as a Research Physicist in the areas of plasma physics and vacuum physics. He is presently Manager of Research and Development for the Vacuum Products Division.

Dr. Jepsen is a member of Tau Beta Pi and Sigma Xi.

❖

Gordon S. Kino (S'52–A'54) was born in Melbourne, Australia, on June 15, 1928. He received the B.S. and M.S. degrees in mathematics in 1948 and 1950, respectively, from London University, London, England. In 1955 he received the Ph.D. degree in electrical engineering from Stanford University, Stanford, Calif.

G. S. Kino

He joined the Mullard Radio Valve Company, Salfords, Surrey, England, in 1947, where he did research on microwave triodes, traveling-wave tubes, and klystrons. From 1951 to 1955 he was employed as a Research Assistant at the Electronics Laboratory of Stanford University, where he carried out research on traveling-wave tubes and electromagnetic theory. He became a member of the technical staff of the Bell Telephone Laboratories, Murray Hill, N. J., in 1955, where he was associated with the Electron Tube Development Department and did research on magnetrons. He returned to the Stanford Microwave Laboratory in 1957, and is now an Associate Professor in the Electrical Engineering Department. He is in charge of a plasma physics group at Stanford.

Dr. Kino is a member of Sigma Xi, the American Physical Society, and the American Rocket Society.

❖

Ronald C. Knechtli (M'45) was born in Geneva, Switzerland, on August 14, 1927. He received the Diploma in electrical engineering in 1950 and the Ph.D. degree in 1955 from the Swiss Federal Institute of Technology, Zurich.

R. C. Knechtli

From 1951 to 1953 he was a Research Engineer at Brown Boveri, Baden, Switzerland, in the field of microwave tubes and then a Research Assistant at the Massachusetts Institute of Technology, Cambridge. From 1953 to 1958 he worked on low-noise microwave tubes and plasma physics at the RCA Laboratories, Princeton, N. J.; in 1958 he joined the Hughes Research Laboratories, Malibu, Calif., where he now heads the Plasma Research Section.

Dr. Knechtli is a member of the American Physical Society, Sigma Xi, and RESA.

K. V. Narasinga Rao (S'55) was born in Vizagapatam, India, on June 27, 1933. He received the B.Sc. (Hons) degree in physics from Andhra University, Waltair, India, in 1952, and the diploma (D.I.I.Sc.) in electrical technology from the Indian Institute of Science, Bangalore, in 1955.

K. V. Narasinga Rao

He joined the Andhra Electricity Department, Madras, India, as a junior electrical engineer for a short period in 1955. In 1957 he received the M.S. degree in electrical engineering from the University of Illinois, Urbana, where he is currently a Research Assistant in the Gaseous Electronics Laboratory, and where he is finishing his Ph.D. requirements.

Mr. Narasinga Rao is a student member of the American Geophysical Union.

❖

Dipak L. Sengupta (S'55–M'59) was born in Bengal, India, on January 16, 1931. He received the B.Sc. degree in physics and the M.Sc. degree in radiophysics, both from Calcutta University, Calcutta, India, in 1950 and 1952, respectively. He received the Ph.D. degree in electrical engineering from the University of Toronto, Toronto, Ontario, in 1958.

D. L. Sengupta

Until 1954 he worked as a Government of India Senior Research Scholar at the Bengal Engineering College of Calcutta University. At the University of Toronto, he was a part-time Research Assistant in electrical engineering; there he designed and developed the antenna assembly of the University's radio-telescope. During the year of 1959 he worked in the Gordon McKay Laboratory of Harvard University, Cambridge, Mass., as a Research Fellow in electronics in the Division of Applied Physics and Engineering. At present, he is an Associate Research physicist at the Radiation Laboratory of the University of Michigan, Ann Arbor.

Dr. Sengupta is a member of Sigma Xi and the American Physical Society.

❖

Issie P. Shkarofsky (M'58) was born in Montreal, Canada, on July 4, 1931. He graduated in 1952 from McGill University, Montreal, with the B.Sc. degree and first-class honors in physics and mathematics. In the following year, 1953, he obtained the

M.Sc. degree, conducting his research at the Eaton Electronics Research Laboratory, McGill University, in the fields of microwave optics and antennas. He then joined the microwave tube and noise group at the Eaton Electronics Research Laboratory, McGill, and received the Ph.D. degree in 1957 with a dissertation on modulated electron beams in space-charge-wave tubes and klystrons.

I. P. Shkarofsky

After graduation, he joined the Microwave Research Laboratory, RCA Victor Co., Ltd., Montreal, where he has participated in research on microwave diffraction and millimeter waves. He is presently engaged in research on electromagnetic wave interaction with plasmas, plasma kinetics and plasma stability.

Dr. Shkarofsky is an associate member of the Canadian Association of Physicists.

❖

Leonard S. Taylor (A'54–M'56) was born in New York, N. Y., on December 28, 1928. He received the A.B. degree in Physics from Harvard University, Cambridge, Mass., in 1951, and the M.S. and Ph.D. degrees in Physics from New Mexico State University, University Park, in 1956 and 1960, respectively.

L. S. Taylor

From 1951 to 1954 he was employed by the Raytheon Manufacturing Company, where he worked in microwave component development and guided missile flight test analyses. From 1955 to 1959 he was at White Sands Missile Range, N. Mex., where he was engaged in the development of special microwave telemetry equipment and communications systems analysis. Since August, 1960, he has been with the Advanced Aerodynamics Operation of the General Electric Space Sciences Laboratory, Valley Forge, Pa., where he has been engaged in research on the interaction of electromagnetic waves and plasmas.

Dr. Taylor is a member of the American Physical Society and Sigma Pi Sigma.

❖

Richard L. Taylor was born in Milford, N. H., on September 22, 1931. He received the B.S.E.E. degree from the University of New Hampshire, Durham, in 1954.

He was then employed by the Air Force Cambridge Research Center, Cambridge, Mass., where he worked on radar devices. He entered active service with the Army in 1955, during which time he again was connected with radar systems. He returned to the Air Force Cambridge Research Laboratories in 1957, where he is presently employed as an Electronic Engineer in the Gaseous Electronics Section. His present work deals with the measurement of plasma properties by the use of microwave techniques.

R. L. Taylor

❖

George Tyras (S'54–M'57) was born in Czestochowa, Poland, on November 26, 1920. He received the B.S.E.E. degree from Newark College of Engineering, N. J., in 1954 and the M.S.E.E. degree from the University of Washington, Seattle, in 1957.

G. Tyras

From 1952 to 1954, he was affiliated with Charles Engelhard, Inc., Newark, N. J., where he was engaged in research and development of industrial instruments. In 1954 he joined the Boeing Company, Seattle, Wash., where he was engaged in the analysis of fire control systems and radar detection. Later he became involved in analysis of electromagnetic propagation through anisotropic ferrites. Presently he is engaged in research on radio-frequency propagation through ionized gases. He is also doing further graduate work in electrical engineering at the University of Washington under the Boeing Graduate Study Program.

❖

Joseph T. Verdeyen (S'59) was born in Terre Haute, Ind., on August 15, 1932. He received the B.S.E.E. degree from Rose Polytechnic Institute, Terre Haute, in 1954.

J. T. Verdeyen

He then participated in the Communication Development Training Program at Bell Telephone Laboratories, Murray Hill, N. J., until 1955, at which time he entered the Signal Corps for two years. During this time, he participated in the evening graduate program of Rutgers University, Fort Monmouth, N. J. In September, 1957, he became an Assistant Instructor in Electrical Engineering at Rutgers, where he received the M.S.E.E. degree in 1958. He then joined the staff of the University of Illinois, Urbana, as an Instructor in Electrical Engineering, and began work towards the Ph.D degree. He is currently engaged in research in plasma physics.

Mr. Verdeyen is a member of Tau Beta Pi and Blue Key.

❖

Jim Y. Wada (S'56–M'57) was born in Lomita, Calif., on May 15, 1934. He received the B.S. degree in engineering from the University of California at Los Angeles in 1956, and the M.S.E.E. degree from the University of Southern California, Los Angeles, in 1958. Currently he is studying at U.S.C. on a part-time basis for the Ph.D. degree.

J. Y. Wada

In 1956 he joined the technical staff of Hughes Aircraft Company, Malibu, Calif., where he participated in the research and development of radar transmitters and low-noise microwave tubes. Since 1959 he has been engaged in plasma physics research.

Mr. Wada is a member of the American Physical Society and Tau Beta Pi. He was a recipient of the Hughes M.S. Fellowship.

❖

James S. Yee (M'59) was born in Canton, China, on October 24, 1927. He received the B.S. degree in physics and the M.S. degree in electrical engineering in 1952 and 1956, from the University of Washington, Seattle. He has taken graduate courses on electromagnetic theory at the University of Southern California, Los Angeles, and is continuing graduate work on microwave networks and electromagnetic theory at the University of Washington.

J. S. Yee

From 1952 to 1953 he was with the U. S. Geological Survey, Sacramento, Calif. From 1953 to 1954 he was a Research Fellow at the Electrical Engineering Department, University of Washington. He was with the Boeing Company, Seattle, where he worked on radar-tracking error problems from 1954 to 1955, and from 1955 to 1957 he was at the Hughes Research Laboratories, Culver City, Calif., where he conducted research on linear and two-dimensional slot array designs, surface wave antennas and electromagnetic diffraction problems, especially those related to radar cross section of simple and complex shapes. Presently, he is a Research Specialist with the Antennas and Radomes Unit, Boeing, conducting research work on antennas operating in a hypersonic environment, and on microwave and plasma interactions.

Mr. Yee is a member of Phi Beta Kappa, and an associate member of Sigma Xi.

Books

Satellite Environment Handbook, Francis S. Johnson, Ed.

Published (1961) by Stanford University Press, Stanford, Calif. 144 pages+3 index pages+xii pages +references by chapter+5 appendix pages. Illus. 7×10. $5.50.

Although there has not yet been a spate of books on the upper atmosphere, their numbers are certainly beginning to respond to the greatly increased scientific and technological activity in this field. This book, written by authors at the Space Physics Research Group of the Missiles and Space Division of the Lockheed Aircraft Corp., Palo Alto, Calif., is a concise and up-to-date compendium of information "compiled principally in response to numerous questions from engineering projects directed to the Space Physics Research organization."

The editor says: "Many of the phenomena described in this book were not known or even suspected three years ago. Some of our present ideas will undoubtedly have to be altered in varying degrees within the next year or two. It is probable that there are still some major surprises in store for us."

The chapters and authors are:

1) Structure of the upper atmosphere (16 pages): F. S. Johnson
2) Structure of the ionosphere (20 pages): W. B. Hanson
3) Penetrating radiation (26 pages): A. J. Dessler
4) Solar radiation (11 pages): F. S. Johnson
5) Micrometeorites (10 pages): J. F. Vedder
6) Radio noise (6 pages): O. K. Garriott
7) Thermal radiation from the earth (6 pages): F. S. Johnson
8) Geomagnetism (26 pages): A. J. Dessler

The first two chapters describe the upper atmosphere. They are accurate and reasonably adequate except that the chapter on the ionosphere does not contain a section on the propagation of radio waves. Because of the existence in the ionosphere of free electrons, of vertical gradients in the electron concentration, of the pervading magnetic field of the Earth, and of the collisions with other constituents, this is a very complicated matter which certainly is one of the most important aspects of satellite environment. Nearly all of our knowledge of the ionosphere has been obtained from its effect on radio wave propagation. Consequently, there are necessarily numerous references to these effects in this chapter but they require a prior knowledge on the part of the reader for understanding. The chapter should also include such classical things as the Chapman theory of layer formation, and the close relationship of the *E*-region ionization with solar zenith angle, in contrast to the large role of geomagnetic control in *F*-region ionization. Also, some mention should have been made of field-aligned ionization and of estimates and observations of integrated electron content from which it is concluded that there is something like four times as much ionization above hmF2 as there is below it.

The second two chapters describe the particle and electromagnetic radiation environment to which the atmosphere is exposed from without. These chapters are especially interesting because they contain so much new information. As is true with the first two chapters as well, they cannot fail to give even the specialist new perspective and stimulation. The chapter on penetrating radiation treats particles trapped in the Earth's magnetic field, solar flare radiation, and cosmic radiation. The motion of trapped particles and the way in which the motion is controlled by the field, are described very clearly. Although the book does not use the term, it should be mentioned that the geocentric region bove hmF2 in which charged particles move under control of the Earth's magnetic field and essentially without collisions, is now being called the *magnetosphere* (after the suggestion of T. Gold). The chapter on solar radiation includes the latest measurements made from space vehicles and presents a complete picture of what is known of the spectrum of solar radiation incident upon the atmosphere.

The flux of "meteoroids" past the Earth can be estimated from radar and visual data, from the mass-accretion by the Earth as obtained by analyses of deep-sea sediments and dust collected in remote regions, from the zodiacal light, and by direct measurement with space vehicles. The answers obtained from the various methods are spread by a factor of 10^4 so that there is still much to be learned about this feature of the Earth's environment. This problem is presented in the fifth chapter with the same conciseness and clarity which characterizes those on the atmosphere and radiation.

The short chapter on radio noise is useful but it is very brief and has been presented mainly from the point of view of a ground-based observer.

The chapter on thermal radiation from the Earth is also short but will be interesting to nearly all readers because most will not know anything about it although the principal reference is to work published 25 years ago. A one-page description of the airglow is included in this chapter.

Geomagnetism is, of course, of great importance to satellite environment. Although the editor has chosen to place this chapter last, the reader might well be advised to read it first because the magnetic field exercises so much control over the ionized atmosphere and the charged particles which enter it from without. The inclusion of the integral invariant to describe the field, and of hydromagnetic waves to explain sudden perturbations, insures that even the experienced geomagnetician will enjoy reading the chapter. He will note the omission, though, of direct measurements by space vehicles, and of measurements made by the double refraction of radio waves and the possibility of extending these with "top-side sounders."

If you are interested in the upper atmosphere and near planetary-space, this book should be on your shelf beside Mitra and Ratcliffe.[1] Because it is so very concise, it is not the same kind of book that they are. But for that reason, it can accomplish what a 600–700 page, exhaustive treatment cannot: 1) For the expert from another field, it can give a short but advanced and correct introduction; 2) For the upper atmospherici st, it can give a new perspective. For the latter, it is an experience like flying across the United States in clear weather in a jet aircraft for the first time, after crossing it many times since childhood by automobile. One misses a lot of detail but he gains a perspective the automobile could never give him. At the same time, he hates to see a visitor, in making his first trip, do it by jet; but that's how it is these days more often than not.

M. G. Morgan
Dartmouth College
Hanover, N. H.

[1] See review, Proc. IRE, Vol. 48, p. 2045, December, 1960.

Handbook of Thermophysical Properties of Solid Materials, Vol. IV, A. Goldsmith, T. E. Waterman, and H. J. Hirschhorn, Eds.

Published (1961) by the Macmillan Company, 60 Fifth Ave., New York 11, N. Y. 798 pages+vi pages. Illus. 8¼×11¼. $90.00 set of 5 vols.

The stated purpose of this five volume work is to compile, evaluate, and consolidate all original text data on thermophysical properties of solid material published during the period 1940 to 1957 inclusive. The materials contained in these volumes are those which may find application in the design of aircraft, missiles, space vehicles, conventional or nuclear power plants, or allied equipment. A further restriction is that only materials melting above 1000°F are included: exceptions are limited to the categories of plastics or composite materials.

The handbook was prepared by the Heat Transfer Section of the Armour Research Foundation and was based on technical goals and requirements set forth by the Thermophysical Branch, Material Center, Wright Air Development Division.

The properties considered, presented as functions of temperature when applicable, are: density, melting point, latent heat of fusion, latent heat of vaporization, latent heat of sublimation, specific heat at constant pressure, thermal conductivity, thermal diffusivity, emissivity, reflectivity, linear thermal expansion, vapor pressure, and electrical resistivity.

The properties are arranged in a materials index. Volume I covers elements melting above 1000°F and includes 13 different forms of carbon data. Volume II covers alloys and includes the following subsections:

iron-base alloys, copper-base alloys, nickel-base, cobalt-base, and refractory metal-base alloys, light metal alloys including titanium alloys, and other metal alloys. Volume III covers ceramics including glasses. Volume IV, the only volume presented for review, covers cermets, intermetallics, polymeric material including plastics and composite materials. Volume V contains the complete list of references, the alphabetic author index, and the alphabetic list of materials.

The data are presented in graphical form utilizing the absolute temperature scales. A single page contains, on one side, a graph displaying the data and, on the other side, pertinent reference material. The properties, organized by materials, are presented individually under each material section. The readability of the text is, in general, quite adequate; however, in cases where a great deal of data is available concerning a certain property, the identification symbols can be confusing to recognize.

Due to the relatively new surge of interest in materials shown by electronics people, these volumes can be a valuable addition to a reference library. They appear to be most useful to two general types of readers. The first would be those interested in surveying general classes of materials for specific useful properties. The volumes contain a wealth of general knowledge which would be very useful in a survey of this kind. In this light, one feature of the compilation of data is noticeable by its absence. There are no summary graphs comparing the same property for general groups of materials. This type of summary graph would be exceptionally useful to the reader interested in comparing a particular property within a group of materials. The second type of reader for whom the book would be most useful is the preliminary design engineer. Once a material is decided upon for a specific application, many of the important design parameters can be obtained in these volumes. Due to the fact, however, that the volumes include data through 1957 only, it will be necessary for the design engineer further to augment the present information with more recent data. This is particularly true of Volume IV which covers cermets, intermetallics, polymerics, and composite materials in which interest has grown rapidly during the past four years.

There is one example of an outstanding lack of understanding concerning the applicability of some of the data. Presented in Volume IV are electrical resistivity values for some intermetallic semiconducting compounds such as indium antimonide. It is well known that the electrical resistivity depends on the carrier concentration in semiconductors; but, in the section on indium antimonide showing the electrical resistivity, no information is given which details the specific carrier concentration at which the electrical resistivity measurements were made. This type of information is extremely limited in its usefulness.

Two drawbacks to the method of presentation are noted. The first is the organization of the information by the use of a materials index which could be expansible. The idea is an excellent one; however, the binding of the material in book form makes it very inconvenient to insert additional pages into the volumes. Perhaps a presentation in binder form into which additional pages could be easily placed would be more acceptable. The second drawback is the inclusion of all references in the fifth volume. In the reviewer's case, not having been supplied with the reference volume, it was impossible to check the references cited for accuracy. This severely limits the worker who may be interested in the information contained in one volume rather than the whole set.

While it is relatively easy to find fault in an undertaking of this magnitude, these volumes are definitely worthy of inclusion in a library of reference materials and are a vast improvement over existing works of similar nature. They will be particularly useful to the technical person at the survey or preliminary design stage.

James G. Harper
Texas Instruments Inc.
Dallas, Tex.

Static Relays for Electronic Circuits, Richard F. Blake, Ed.

Published (1961) by Engineering Publishers, Div. of The AC Book Co., Inc., Elizabeth, N. J. 198 pages +viii pages. Illus. 6½×9¼. $7.50.

The material in this book was based on the Static Relays Symposium sponsored by the Electronic Components Research Department of the U. S. Army Signal Research and Development Laboratory. There are 18 chapters prepared by various authors covering the general state of the art. The first three are devoted to a statement of the general concept, a useful review of regenerative switching in semiconductors and desirable specifications for static relays.

This book will be particularly interesting to the practicing engineer already in the field of semiconductors who has not kept abreast of developments in static switching. Many new circuits and ideas are presented leading toward a surprisingly wide range of applications where replacement of mechanical contacts with an operationally equivalent static semiconductor device is feasible.

R. P. Burr
Circuit Research Co.
Glen Cove, N. Y.

Thermoelectricity: Science and Engineering, by R. R. Heikes and R. W. Ure.

Published (1961) by Interscience Publishers, Inc., 250 Fifth Ave., New York 1, N. Y. 569 pages +6 index pages +xi pages. Illus. 6½×9¼. $18.50.

The purpose of this book is to provide a systematic treatment of thermoelectricity, and to cover various topics in chemistry physics, and engineering. Many of these topics in themselves could constitute an entire volume and sufficient references are given to prior literature. The key results are presented with clarity. The book also contains some original contributions to the theory of thermoelectric materials and thermoelectric device design.

The first two chapters cover basic definitions and the thermodynamics of thermoelectric phenomena. Next are two chapters on transport processes in semiconductors, semimetals, narrow-band semiconductors, ionic crystals and liquids. The effects of high energy radiation and diffusion are then presented. These subjects are followed by chemical preparation and experimental measurement of material properties.

Following these fundamental topics is a chapter on the relationship between the thermoelectric figure of merit and microscopic properties of various types of materials. It is here that the question of optimum choice of material parameters, such as doping level, is considered. Next, the additional effects which occur at low temperatures, such as the phonon drag effect, are considered. Known thermoelectric materials are then surveyed and their electric, thermal, and chemical properties given in several tables and graphs.

The final four chapters of the book are concerned with devices. The basic principles of thermionic conversion are treated, followed by thermoelectric devices. The subject matter covered includes: approximate and exact calculations of device performance; staged and simple thermocouple designs; heat transfer problems and their effect on device design; technology problems, such as contacts to thermoelectric materials.

This book is a good reference work in the area of thermoelectricity; both the basic principles and advanced topics have been adequately covered. The book is recommended to all those engaged either in basic thermoelectric research or engineering. Particularly, it will serve as an excellent introduction to the field.

W. H. Clingman
Texas Instruments Inc.
Dallas, Tex.

Recent Books

Davis, Sidney A. and Ledgerwood, Byron, K. *Electromechanical Components for Servomechanisms.* McGraw-Hill Book Co., Inc., 330 W. 42 St., New York 36, N. Y. $11.50. A book designed to give practical aid in the selection, specification and application of rotating components. Various components are discussed and their design features analyzed.

Langmuir, D. B., Stuhlinger, E., and Sellen, J. M., Jr., Eds. *Electrostatic Propulsion,* Vol. 5 in *Progress in Astronautics and Rocketry,* M. Summerfield, Series Ed. Academic Press, Inc., 111 Fifth Ave., New York 3, N. Y. $5.75.

Martin, W. T. and Reissner, E. *Elementary Differential Equations.* Addison-Wesley Publishing Co., Inc., Reading, Mass. $6.75. A textbook of differential equations with applications to physical science and engineering, intended primarily for a one-semester course.

Parratt, Lyman G. *Probability and Experimental Errors in Science: An Elementary Survey.* John Wiley and Sons, Inc., 440 Park Ave. S., New York 16, N. Y. $7.25. A book designed to introduce the undergraduate student to the unifying concepts of probability and statistics as they apply in science.

Proceedings of the Second International Conference on Operational Research. John Wiley and Sons, Inc., 440 Park Ave. S., New York 16, N. Y. $15.00.

Scanning the Transactions

Words are essential for communication and even for thought. English-speaking peoples need not be limited in their communicating and thinking by a dearth of words; the new unabridged Webster's contains the forbidding number of 450,000. Of these, approximately 100,000 are claimed to be new additions, words that were not in previous editions of this tome. It is a certainty that the field of electronics has made a not insignificant contribution here, although it would be demanding too much to require lexicographers to be absolutely current in the dynamic electronics vocabulary. Even those most intimately concerned with it have their problems in keeping pace. More difficult than learning accepted terminology is the problem of manufacturing and sorting new terms for new ideas, devices, and requirements. Tunnel diodes are no exception. There is an impressive amount of work in progress on these devices, but discussion is hampered by a lack of standard terminology and definitions. Now a paper has been published which puts forth the important tunnel-diode parameters and includes definitions, symbology, and measurement methods. (C. D. Todd, "Tunnel-Diode Parameters," IRE TRANS. ON INSTRUMENTATION, September, 1961.)

Underwater television is not an entirely new concept. In fact, television "underwater" is occasionally brought rather dramatically to our attention with TV commercials showing that, if we should care to, we can use this pen for writing or that razor for shaving while immersed in the universal solvent. Sometimes the net result of such commercials is an urge to submerge the TV set itself. This is done, but in a much more scientific way, as described in a recent paper on the role of television in underwater weapons testing. Closed-circuit television systems have been used by the Navy to instantaneously obtain valuable data on Polaris Missile launchings and other underwater tests. (O. R. Metzler, "Television in Underwater Weapons Testing," IRE TRANS. ON MILITARY ELECTRONICS, October, 1961.)

Education will continue evolving as long as the subject matter with which it is concerned is undergoing evolution. Nowhere is this more apparent than in engineering education. The trend can be towards more specialization as the subjects become increasingly complex, or the emphasis can be on fundamentals and a broader approach. A plea not for more humanities but for different humanities has been made. The thesis is that a reappraisal of the extent, task, and presentation of the humanities is mandatory. (W. W. Harmon, "The Humanities in an Age of Science," IRE TRANS. ON EDUCATION, September, 1961.) One educator has presented some very cogent arguments for a complete renovation of the engineering curriculum and the awarding of a nonprofessional degree. He maintains that specialized professional training is the proper function of the graduate schools only. (N. Balabanian, "A Case for a Liberal Engineering Education and a Nonprofessional Degree," IRE TRANS. ON EDUCATION, September, 1961.)

Family, genus, and species were categories created by the naturalist Linnaeus to bring order to the near chaos in biological classification. Although not a problem of comparable magnitude, engineers are for convenience usually classified by means of their special interests. Without some of us realizing it, a new "breed" has quite recently joined our ranks: the bio-medical engineer. This interdisciplinary title would have sounded almost absurd not too many years ago, but now the bio-medical engineer is very much—and very appropriately—with us. His appearance has been attended by some unique and challenging problems in education (Symposium on Educational Frontiers in Bio-Medical Engineering, IRE TRANS. ON BIO-MEDICAL ELECTRONICS, October, 1961.)

Radio-electronics originally was concerned with communications and little else, but now each year reveals it ramifying into new and sometimes unexpected areas. Measurements in many fields have been revolutionized in the age of electronics. Two novel applications have recently been discussed. Measurement of the atmospheric temperature field by electromagnetic means is possible. (D. Fryberger and E. Uretz, "Some Considerations Concerning the Measurement of the Atmospheric Temperature Field by Electromagnetic Means," IRE TRANS. ON MILITARY ELECTRONICS, October, 1961.) The atmosphere comes under additional electronic surveillance, this time chemical, with a device for measuring ozone content. (C. R. McCully, *et al.*, "An Instrument for Continuous Analysis of Atmospheric Ozone," IRE TRANS. ON INSTRUMENTATION, September, 1961.)

Round Shoulders on humans are not considered as particular signs of strength. Not so for waveguides. "Round shoulders"—or more exactly, rounded corners—are known to be useful in many high-power microwave components in eliminating breakdown by reducing electric-field concentrations. Conditions in microwave high-power filters are considered in detail in a recent paper. A number of rounded-corner geometries important in microwave-filter structures were analyzed by conformal mapping. The optimum shape is not necessarily an approximation to a circular arc but rather a geometry for uniform field strength over the rounded portion. Smoothness is much more important for evacuated than for pressurized filter structures. Formulas and graphs are presented for use by the designer. (S. B. Cohn, "Rounded Corners in Microwave High-Power Filters and Other Components," IRE TRANS. ON MICROWAVE THEORY AND TECHNIQUES, September, 1961.)

Abstracts of IRE Transactions

The following issues of TRANSACTIONS have recently been published, and are now available from The Institute of Radio Engineers, Inc., 1 East 79 Street, New York 21, N. Y., at the following prices. The contents of each issue and, where available, abstracts of technical papers are given below.

Sponsoring Group	Publication	IRE Members	Libraries and Colleges	Non-Members
Aerospace and Navigational Electronics	ANE-8, No. 3	$2.25	$3.25	$4.50
Bio-Medical Electronics	BME-8, No. 4	2.25	3.25	4.50
Education	E-4, No. 3	2.25	3.25	4.50
Electron Devices	ED-8, No. 5	2.25	3.25	4.50
Engineering Management	EM-8, No. 3	2.25	3.25	4.50
Instrumentation	I-10, No. 2	2.25	3.25	4.50
Microwave Theory and Techniques	MTT-9, No. 5	2.25	3.25	4.50
Military Electronics	MIL-5, No. 4	2.25	3.25	4.50

Aerospace and Navigational Electronics

VOL. ANE-8, NO. 3, SEPTEMBER, 1961

The Evaluation of Error Standard Deviation in the Accuracy Evaluation of the Doppler Navigator—N. Marchand (p. 91)

The standard error deviation for the Doppler navigator is theoretically derived for the general case of both random and systematic errors. It is demonstrated that both the along-course error deviation and across-course error deviation, when expressed on a per unit basis, consist of two terms. One term is independent of the distance traveled and the other is dependent upon the distance traveled. There is a possibility that results of statistical analysis of experimental data, as given in the literarure, may be incomplete since the term in the error standard deviation, per unit distance traveled, which is independent of distance traveled is not included. It is demonstrated how this omission may come about by neglecting the mean errors in the subsets of the population of observations.

Identification and Evaluation of Magnetic-Field Sources of Magnetic Airborne Detector Equipped Aircraft—P. Leliak (p. 95)

A general method for identifying and evaluating magnetic sources associated with the magnetic airborne detector-equipped aircraft is described. It is derived for the compensation of magnetic noise related to the maneuvers of the aircraft. Mathematical formulas are included with a uniform engineering method, that is independent of the type of magnetic source encountered, for analyzing magnetic airborne detector records. A method for calibrating magnetic sources while in flight is also offered.

Correction to "Post-War Developments in Continuous-Wave and Frequency-Modulated Radar"—W. K. Saunders (p. 105)

A Basic Control Equation for Rendezvous Terminal Guidance—L. A. Irish (p. 106)

A basic rendezvous homing control equation, which adjusts the magnitude and direction of the acceleration of an interceptor vehicle in response to sensed interceptor-target relationships, is derived, and the selection of system gain parameters to give a desired dynamic behavior is described. Modifications to the basic control equation for the following system variations are discussed:

1) Rendezvous at a preset relative position or velocity,
2) Landing on the moon (or other extra-terrestrial body),
3) Operation with a propulsion unit having a limited range of thrust variation,
4) Operation with a fixed-thrust pulsed propulsion unit.

Abstracts (p. 114)
Book Reviews (p. 115)
PGANE News (p. 116)

Bio-Medical Electronics

VOL. BME-8, NO. 4, OCTOBER, 1961

Papers from Symposium on Educational Frontiers in Bio-Medical Engineering, University of Vermont; May 5–6, 1960

New Frontiers in Bio-Medical Engineering Education—G. C. Riggle (p. 208)

Biology in Bio-Medical Engineering—R. W. Stacy (p. 209)

Physiology in Bio-Medical Engineering—F. J. Sichel (p. 211)

The Role of the Engineer in Bio-Medical Science—S. A. Talbot (p. 212)

Specialized Courses Required in Bio-Medical Engineering Science—S. A. Talbot (p. 216)

Bio-Medical Engineering Program at Johns Hopkins, Pennsylvania, Rochester and Yale—H. P. Schwan (p. 219)

The Bio-Medical Engineer—J. W. Dow (p. 223)

Informal Training Program in Bio-Medical Engineering at Brooklyn Polytechnic Institute and the Rockefeller Institute—R. L. Schoenfeld (p. 225)

Bio-Medical Engineering Program at Drexel Institute of Technology—D. H. Le Croissette (p. 227)

Medical Electronics at the University of Vermont—H. M. Smith, Jr. (p. 228)

Medically- and Engineering-Oriented Facilities, Instruction and Research in Bio-Medical Electronics—V. W. Bolie, M. J. Swenson, W. B. Boast, and R. Getty (p. 229)

Bio-Medical Electronics—Past and Present—H. P. Schwan (p. 234)

A brief review of the development of the field of bio-medical electronics and its present status is presented. Topics include development, description of the field, industry education and future outlook.

Influence of Light Atmospheric Ions on Human Visual Reaction Time—M. Knoll, J. Rheinstein, G. F. Leonard, and P. F. Highberg (p. 239)

An automatic electronic visual-reaction-time meter has been developed which includes a random-pulse generator controlled by nuclear radiation for starting the subject's light pulse. With this instrument (using radioactive ion generators) several hundred subjects have been investigated in over 12,900 tests. An influence of light atmospheric ions on the human reaction time has been found for ion currents between 10^6 and 10^9 inhaled ions per second or ion densities of about 10^3 to 10^6 ions/cm^3. Inhaling positive or negative ions may increase or decrease the reaction time of different people or even of the same person after several hours. In this respect the influence of ions resembles the effect of many drugs on the human system. The effect disappears when the subject is breathing through the nose instead of the mouth.

Electrical Analog Simulation of Temperature Regulation in Man—R. J. Crosbie, J. D. Hardy, and E. Fessenden (p. 245)

Using the basic equations for heat balance which have been developed to take into account heat losses by radiation, convection and evaporation, an electrical analog has been constructed to simulate the physiological responses to heat and cold in the nude man. As has been previously shown, physiologic temperature regulation involves three of the basic types of control modes, namely, proportional control, rate control, and some of the characteristics of on-off control. The rate and proportionality constants have been determined experimentally on the assumption that the regulated temperature is the average body temperature. Time constants for the various thermal changes can be determined from the thermal constants of tissue and the response times of the physiological variables of sweating, vasomotor activity and change in metabolic rate. The simulator predicts steady-state situations of rectal temperature, skin temperature, metabolic rate, vasomotor state and evaporative heat loss under both resting conditions and exercise. Dynamic responses to sudden shifts in environmental temperature, air velocity, relative humidity and metabolic rate can be simulated to a considerable extent using equations based on the controls outlined above.

Transistorized Pacemaker for Remote Stimulation of the Heart by Radio-Frequency Transmission—L. Eisenberg, A. Mauro, and W. W. L. Glenn (p. 253)

Diverse techniques have been developed for controlling the cardiac rate by external means when normal physiological processes fail to maintain a stable rate. These techniques are presented in a brief summary.

The factors underlying the choice of the radio frequency transmission technique are presented and evaluated, taking into account

control of the stimulus, avoidance of infection, and minimizing the number of electrical components within the body. A set of design specifications is then evolved based upon the physiological needs of the patient, utilizing the philosophy of the RF transmission approach. The design of two transistorized, battery-operated pacemakers is then presented in detail with a description of the constructed units and an evaluation of performance. These units have now been used successfully on five patients.

A Portable Miniature Transistorized Radio-Frequency Coupled Cardiac Pacemaker—D. M. Hickman, L. A. Geddes, H. E. Hoff, M. Hinds, A. G. Moore, C. K. Francis, and T. Engen (p. 258)

A miniature, transistorized radio-frequency-coupled cardiac pacemaker was developed to eliminate wires penetrating the skin when electrodes are placed on the heart to drive it. The design also eliminates the need for totally implanting a pacemaker with its batteries.

The stimulating impulse is transmitted via amplitude modulation to a tuned circuit and detector assembly implanted below the skin. The output of the detector is connected to electrodes directly on the heart, making external control of the heart rate possible.

In operation, the pacemaker transmitter is placed on the surface of the body above the receiver implant. The size of the unit is $4 \times 1\frac{3}{4} \times 1\frac{1}{2}$ inches. It weighs three ounces.

Correction to "The Center for Vital Studies—A New Laboratory for the Study of Bodily Functions in Man"—W. A. Spencer, L. A. Geddes, and H. E. Hoff (p. 262)

Letters to the Editor (p. 263)

Abstracts of Current Bio-Medical Electronic Research Projects (p. 265)

Notices (p. 267)

PGBME Affiliates (p. 268)

Proceedings of the Third International Conference on Medical Electronics (p. 296)

Education

Vol. E-4, No. 3, September, 1961

Acknowledgment—W. R. LePage (p. 83)

Editorial—H. E. Koenig (p. 84)

A Case for a Liberal Engineering Education and a Nonprofessional Degree—N. Balabanian (p. 86)

The traditional four-year engineering program gives neither an adequate professional training nor a liberal education. It is proposed that a four-year program of "liberal engineering" be instituted which synthesizes traditionally compartmentalized disciplines and concentrates on the intellectual components of the profession. Specialized professional training should be the proper function of the graduate school.

The Technology of Information Systems—Another Challenge for Engineering Education—L. E. Saline (p. 91)

The proper functioning of the world in which we live is becoming more and more dependent on information and how we use it. With methodologies and machines that are becoming available to information systems technology, we are, indeed, entering the Age of Information—an age of promise in business, in government, and in the military that can have as profound an effect on the world as the harnessing of the atom, the development of electric power, or the Industrial Revolution of the Nineteenth Century. The purpose of this paper is to delineate the broad technology of information systems in order to provide a basis for estimating the impact of this technology on future engineering education. Suggestions for modifying undergraduate engineering curriculums are made in order that future engineering graduates will be prepared to contribute to the continuing development of the technology and to utilize the technology in performing other engineering work. This paper discusses such topics as: What is an Information System?; Functions of a Generic Information System; Men in Information Systems; Machines in Information Systems; Methods in Information Systems; How Information Systems Are Created; Major Problems Facing Information Systems Technology; and The Challenge for Engineering Education.

Dis-service Courses—T. L. Martin, Jr. (p. 98)

For many years the traditional engineering physics course was the pivotal subject in the engineering curriculum. It provided an adequate basis in macrophysics to support traditional engineering. The course is still offered, virtually unchanged for the past forty years except in minor details; the evolution of microphysics, structural chemistry, and physical metallurgy has made little impact upon this course. Engineering physics is now a sacred cow—a dis-service course.

This course has been cancelled at the University of Arizona and classical macrophysics is taught by the engineering departments in the various and usual subdivisions of mechanics, thermodynamics, electric and magnetic fields, and electric circuits. A new course, at the junior level, has been introduced by the Physics Department to cover Microphysics. It is offered under the title of "Structure of Matter" and covers electrons, atoms, chemical bonds, crystals, the energy band theory of crystals, and other topics from wave, statistical, and quantum mechanics. The course has been offered for three years. While it is under constant revision there is little doubt now that this represents a positive solution to a part of the problem posed to engineering educators by recent advances in contemporary science.

System Theory in a Unified Curriculum—H. K. Kesavan and B. R. Myers (p. 102)

The incessant search for unifying concepts in engineering education has, in recent times, stepped up its pace to match the tempo of our scientific and technological progress. Although a single unified curriculum for all engineering problems would indeed be a utopia, there is hope, nevertheless, that certain apparently diverse areas of engineering can be regrouped with emphasis on the basic disciplines underlying them. System theory, which is briefly exposed here, is one such fundamental discipline with its mainsprings in the mathematical model of linear-graph theory. The chief assertion of this paper is that system theory could very well serve as a basis for unifying the areas of 1) circuit theory, 2) circuit aspects of electronics, 3) rotating machinery, 4) elementary statics and dynamics, and 5) system analysis. The ideas presented here are sufficiently supported by the authors' classroom experiences. In the light of the curriculum proposed, certain of the inevitable implications for Canadian electrical engineering are discussed.

On Some Mathematical Aspects of Magnetohydro- and Plasma-Dynamics—M. Z. V. Krzywoblock (p. 111)

The author presents a review of some mathematical aspects of magnetohydrodynamics and plasma-dynamics, and the fields of mathematics required and used in those domains are briefly discussed. The last section is devoted to the discussion of adjusting the mathematical program of a university, from the point of view of engineering, physics and mathematics, so that a greater number of students in those disciplines will be prepared for graduate courses in magnetohydrodynamics and plasma-dynamics.

The Humanities in an Age of Science—W. W. Harman (p. 118)

Many persons today question the meaningfulness of the traditional formulations of some of the basic questions which have been asked in the humanities, and also the validity of the introspective means by which answers have been sought. These challengers often appear to have behind them the great weight of the scientific progress of recent centuries. The basic issue on which the behavioral scientist and the scientific humanist appear to differ so from the poet, the artist, or the religious philosopher has to do with the physical and the spiritual aspects of reality. Predominately, the scientist tends to operate on the implicit assumption that only the physical or sense-perceived world has reality; the poet and the mystic live in both worlds. The behavioral scientist tends to see values as culturally generated and acquired, the poet, as inherent in the structure of things.

Questions about the nature of reality are not to be decided by disputation among ourselves, but by conducting such experiments as will enable us to discern what that nature really is. The nature of such experiments and suggestions for the possible resolution of this basic issue form the subject matter of this paper.

Correction to "Today's Dilemma in Engineering Education"—G. S. Brown (p. 126)

Correspondence (p. 127)

Contributors (p. 128)

Electron Devices

Vol. ED-8, No. 3, September, 1961

Editorial—E. L. Steele (p. 345)

New Editorial Board (p. 346)

An Integrated Semiconductor Shift Register—J. T. Wallmark and S. M. Marcus (p. 350)

Transition Region Properties of Reverse-Biased Diffused p-n Junctions—J. Cohen (p. 362)

Poisson's equation is solved for two common types of diffused p-n junctions in a manner similar to that of previous authors. By a suitable transformation, the field in the junction and capacitance-voltage relation for all junctions are shown to be presentable as a single family of curves with no approximation other than the assumption of negligible drift field. The abrupt and graded regions are discussed in detail. The zero-bias potential and capacitance are also discussed.

Alloy Diffused Variable Capacitance Diode with Large Figure-of-Merit—A. Shimizu and J. Nishizawa (p. 370)

The product of the cut-off frequency and the capacitance-voltage sensitivity is proposed as a figure-of-merit of the variable capacitance diode.

It is expected from the theoretical results that the high-voltage sensitivity, $(\partial C/\partial V)/C$ of the capacitance is obtained by the "hyper-abrupt" junction in which the impurity concentration decreases with the distance from the p-n boundary. Assuming the exponential decrease of the impurity concentration, the theoretical expression is derived for the capacitance-voltage characteristic of the "hyper-abrupt" junction diode, and is compared with the experiment.

"Hyper-abrupt" structure is easily obtained by the alloy-diffusion technique. The experimental capacitance-voltage characteristics of the germanium alloy-diffused diode agree fairly well with the theoretical results. Diodes changing the capacitance in proportion to the -3 power of the applied voltage have been made, with the tuning ratio to about 100. To date, a diode with the maximum cut-off frequency of 30 kMc and with the figure-of-merit

$F\gamma$ of 5.5 kMc/v, has been made. Further increase of these quantities, however, will be obtained by the reduction of the thickness of the base layer, which is about 15 microns in the above diode.

A Treatment of Diffusion Errors Affecting Junction Depth—J. E. Reynolds (p. 377)

An error treatment of the diffusion variables of time t, temperature T, and starting resistivity ρ, has been made in regard to their effects upon junction depth. An analytical equation has been derived for engineering usage in determining the per cent error in junction depth x:

$$\text{Per cent error in junction depth} = 100\sqrt{\frac{\Delta t^2}{2t} + \frac{Q\Delta T^2}{2RT^2} + \frac{\sqrt{\pi Dt}}{\mu n_0^2 N_{-x}}\Delta\rho \exp\,(x^2/4Dt)^2}$$

A sample calculation using the above equation is presented along with a method of estimating errors in junction depth due to heating and cooling in the diffusion cycle.

Diode Oscillation in High-Voltage Klystrons—K. Tomiyasu and M. P. Forrer (p. 381)

Diode oscillations at frequencies between 1350 and 3700 Mc sometimes occurred in a particular high-voltage pulsed klystron. These frequencies agree closely with those calculated for an inverted spherical diode. The oscillations are often delayed a few microseconds after the electron beam is turned on. Experimental techniques revealed that two of the modes, TE_{41} and TE_{61}, with Q's of about 1000 had their highest electric fields in a region of the electron gun remote from the beam.

Proposed Method for Controlling and Minimizing Reflections from a Surface—R. H. Mattson (p. 386)

This paper proposes a method whereby the reflection of an electromagnetic wave from a surface can be controlled. The idea is to use a p-n junction as the controlling device. The device is made in such a way that the junction is parallel to the surface upon which the electromagnetic radiation is impinging. If the p region is very narrow the wave will penetrate through it into the depletion region. If the n region is hi conductivity, the wave is reflected from it. Then if the depletion layer width is right for the frequency considered, the reflected wave will interact with the impinging wave to give the desired effect. By changing the bias applied to the junction a tuning effect can be obtained.

Detailed analysis of the proposed device is covered in the paper. There are some practical limitations to creating the device described, but the idea and the method of analysis could be useful to individuals interested in creating microwave tuning and control components.

Ceramic Metalizing Tape for Reliable Metal-Ceramic Seals—H. D. Doolittle, K. Ettre, R. F. Spurck, and P. F. Varadi (p. 390)

A ceramic-metalizing method was developed which increases the reliability of hard-soldered metal-ceramic seals and makes production automation possible. The new technique utilizes a "metalizing tape" consisting of a self-supporting plastic tape which contains the metalizing powders and a suitable binder (methacrylic-type). This tape can be manufactured with extremely uniform thickness, density and surface smoothness, all of which qualities can be controlled on the prefabricated tape prior to its usage. The application of the prefabricated metalizing tape to the ceramic surface can be accomplished in a very simple way: by using a suitable solvent to form a bond between the metalizing tape and the ceramic, or by thermal sealing. The materials and the methods used for the preparation of the metalizing tape are described, as well as the methods of application.

The resulting extremely uniform metal coating on the ceramic makes it possible to investigate the effect of metalizing thickness and of different materials on the bond strength and on the vacuum qualities of metal-ceramic butt seals.

Tunnel-Diode Converter Analysis—C. S. Kim (p. 394)

An analysis of tunnel-diode converters is presented for two different conditions of operation. In the first, the converter is self-oscillating; in the second, the local oscillator (LO) voltage is provided from an external source. Two classes of self-oscillating converters are presented. The first operates on the fundamental of the oscillation frequency and the other operates on the second harmonic.

Assuming the dynamic conductance of a tunnel diode changes only as a function of the local oscillator voltage, and expressing this conductance in a Fourier series, a 3×3 conductance matrix is obtained. Utilizing this matrix, expressions for gain, bandwidth, and noise figure are obtained. The analysis includes the image frequency termination. In the expressions for noise figure, the cross-correlation terms, produced by the amplitude change of the dc equivalent shot-noise current due to the LO voltage, are also included.

Correction to "Bridge Measurement of Tunnel-Diode Parameter"—W. H. Card (p. 405)

The Videograph Tube—A New Component for High-Speed Printing—R. W. Crews and P. Rice (p. 406)

A cathode-ray tube having a faceplate penetrated by an array of many fine wires, has been developed for high-speed printing applications. Charge patterns are deposited on moving paper in response to a modulated electron beam which scans the inner ends of the wires in the CRT. The pattern on the paper is dusted with an electroscopic powder to make it visible. Copy having a resolution of 10^4 picture elements/inch^2 can be produced at a rate of 2 feet^2/second.

The tube is being used in high-speed facsimile equipment and in a computer output printer which prints magazine address labels at a speed of 130,000 labels per hour from digital information stored on tape. Television pictures have been reproduced field-by-field at standard rates. The tube has wide application in systems where high-speed, remote print-out or local reproduction of copy is required. The cost of the recording paper is about one-tenth that of light-sensitive materials.

Influence of Velocity Spread on Gain and Efficiency of Klystrons—H. G. Kosmahl (p. 414)

This paper presents the calculation of the effect of velocity spread in electron streams on the gain and efficiency in klystrons. Using the density-function method and assuming a half-Maxwellian velocity distribution, a small-signal theory of a klystron tube was developed. The form of the solution is a power series whose coefficients contain even powers of $\omega q/\omega$. The effect of losses in the cavity has also been included. The results are presented as plots of the ratios of the ac component of the bunched current with velocity spread vs a dimensionless parameter that is a measure of the velocity spread. The plots contain $\omega q/\omega$, the lengths of the drift tube and of the gaps as important design parameters.

Engineering Management

Vol. EM-8, No. 3, September, 1961

Decision Making, Growth, and Failure—S. B. Alpert and H. Weitz (p. 120)

A case study is presented of the changes in the ratio of "administrative" to "productive" personnel in the aircraft engine division of a large industrial firm. The ratio is traced over an eight year period through growth and decline stages. Some contributing factors and consequences of the A/P index are examined.

Designing the Corporate Structure to Combine Small-Company Vitality with Large-Company Strength—A. W. Tyler and A. D. Ehrenfried (p. 125)

The early leaders in corporate organization are found to be the giants of industry today. Following the move of the past decade to corporate decentralization is a new trend toward the recentralizing of management planning and specialized service. The result is a new form of corporate structure toward which both large corporations and groups of small companies can evolve. This structure appears to combine the better features of both the large and the small organization. It is made necessary by the complexity of present-day business management, and is made possible by the new technologies of electronic data processing, business communications, and high-speed transportation.

The Institutional Location of the Scientist and His Scientific Values—R. G. Krohn (p. 133)

Several writers on the history of science have argued that changes in the institutional location of science will be accompanied by several major changes in scientific attitudes and values. A sample of approximately 30 per cent of the working scientists in several disciplines was interviewed in the Minneapolis-St. Paul area. Those interviewed worked in government, industrial, and university laboratories. A number of indicators of scientific attitudes and values were examined.

Special Section on Services for R, D, and E

Development of a Technical Services Department for IBM—F. H. Welsh, Jr. (p. 139)

To develop the highly complex products required of industry today, it is necessary to provide the research and engineering personnel developing these products with an array of highly specialized supporting services. Since these supporting skills are not required by any one engineering group 100 per cent of the time, economics dictates that these services be centralized. Thus, a Technical Services Department is born. The supporting skills provided by such an organization may vary, for example, from the analytical ability of highly-specialized Ph.D.s, to the manipulative ability of highly trained tool and die makers.

IBM has a particular need for such specialized services because of the number of engineering groups which it has working simultaneously on different projects. In this article, it is not possible to cover the development of Technical Services in all the IBM Laboratories. Therefore, the discussion is limited to the IBM General Products Division Development Laboratory at Endicott, N. Y. This is appropriate, as Endicott is typical of other IBM Commercial Laboratories.

A Systematic Procedure for Preparing Specifications on Electronic Instrumentation and Control Systems—H. Olken (p. 143)

This is a report on the development of a systematic procedure for preparing specifications for electronic instrumentation or control systems. This procedure aids in the preparation

of specifications which: 1) make it possible to find any particular specification requirement quickly, and 2) insure that no important requirement has been omitted. Details of this procedure and a discussion of advantages gained through its use are presented. Also discussed is a technique for specification review and revision that helps to improve the proficiency of engineers at specification writing.

The Industrial Engineer's Role in New Product Development—D. W. Karger (p. 155)

Two examples are presented of the kind of contribution industrial or production or methods engineers can make to new product development. The first is a 1.2 volt mercuric oxide battery. The second is a tantalum capacitor. Contributions to analyses of costs and tolerances are cited.

Technical and Management Notes

An Approach to Probabilistic Forecasting of Engineering Manpower Requirements—L. B. Wadel and C. M. Bush (p. 158)

A statistical technique is presented for estimating probable future manpower requirements in the face of uncertainty about the success of outstanding bids.

A Visual Method of Program Balance and Evaluation—L. B. C. Fong (p. 160)

A visual method is presented for providing an overview of the entire program of the Diamond Ordnance Fuze Laboratories. The display indicates relative emphasis of effort at the various levels in the laboratories and permits comparison between fields and specialities.

Instrumentation

Vol. I-10, No. 2, September, 1961

Tunnel Diode Parameters—C. D. Todd (p. 57)

Engineers and technicians concerned with the use of, or the testing of tunnel diodes need to understand the symbology and basic definitions of the various parameters involved. In many cases, a knowledge of simplified measuring techniques is also necessary. It is the purpose of this paper to fulfill these basic needs.

Microwave Theory and Techniques

Vol. MTT-9, No. 5, September, 1961

Microwaves—A Review of Progress in Great Britain During 1960—A. E. Karbowiak (p. 374)

The fields covered by the review are: Electromagnetic theory as applicable to wave propagation, theory of waveguides and components, microwaves in fundamental measurements (such as time and atomic constants), designs of components, measurements, solid-state devices and a summary of utilization. Future trends are also indicated. The review (with some exceptions) does not cover the following fields: Antennas, propagation and microwave tubes. In reviewing technical publications, preference is given to such aspects of work which are novel, fundamental or are of controversial nature or are likely to influence future trends; where appropriate, criticism of the work is given.

A New Type of Circular Polarizer Using Crossed Dipoles—M. F. Bolster (p. 385)

A method of obtaining a circularly-polarized wave by use of two orthogonal dipoles driven in parallel by a common transmission line is shown. The lengths of the dipoles are so chosen that the real part of their input admittances are equal and the angle of the input admittances differ by 90°. When these two conditions are met the resulting radiated wave in a normal direction will be circularly polarized.

The method is applicable both to a circularly-polarized radiating antenna and to the problem of producing a circularly-polarized wave of the TE_{11} mode in a round waveguide. For the first case, an analysis and a method of design are shown, and for the second case an experimentally developed example is given. The second case employs monopoles rather than dipoles for convenience in energizing from a coaxial line.

Rounded Corners in Microwave High-Power Filters and Other Components—S. B. Cohn (p. 389)

Microwave high-power filters must be operated with internal air pressures of at least one atmosphere, or with a good vacuum. Pressures between these extremes result in reduced power-handling ability. The breakdown processes for both high air pressure and vacuum are discussed, and it is made clear that any sharp corner on which the electric field would concentrate must be rounded if high-power operation is to be achieved. For good results in vacuum operation, the surfaces must be especially smooth and free of contamination, while in high-pressure operation, minor irregularities are less important.

Various high-power filter configurations of importance are described, and the structural corners at which electric-field concentrations occur are pointed out. A number of simplified geometries are then shown that can represent the essential portions of the practical structures with sufficient accuracy for ordinary purposes. Formulas and graphs for these simplified geometries are presented that give the ratio of the maximum electric field strength on the boundary to a uniform reference field strength at a point sufficiently removed from the corner. In some cases, the boundary curve is an approximation to a circular arc, while in other cases a boundary shape is derived such that the electric field strength along the curve is constant. These constant-field-strength boundaries are optimum shapes from the standpoint of power-handling ability.

A Periodic Structure of Cylindrical Posts in a Rectangular Waveguide—E. E. Altshuler (p. 398)

The propagation characteristics of a rectangular waveguide loaded with uniformly spaced cylindrical posts (periodic structure) are investigated at a frequency of 2840 Mc. A qualitative discussion on the expected behavior of the effective guide wavelength of this type of periodic structure is presented, and it is shown that the presence of the posts reduces the guide wavelength of the waveguide. The guide wavelength is then measured as a function of post diameter, post depth, and post spacing; and curves enabling one to design periodic structures which have guide wavelengths in the region of the free space wavelength are presented.

Modes in Rectangular Guides Loaded with a Transversely Magnetized Slab of Ferrite Away from the Side Walls—G. Barzilai and G. Gerosa (p. 403)

The characteristic equation describing the general modal spectrum for a rectangular guide partially filled with a slab of ferrite transversely magnetized and situated away from the side walls is derived. This equation is numerically solved for particular cases and for modes of zero and first order with respect to the dependence along the direction of the dc magnetic field. Some experiments to verify the theoretical results are presented and show good agreement with the theory.

Higher-Order Evaluation of Electromaggetic Diffraction by Circular Disks—W. H. Eggimann (p. 408)

The problem of the diffraction of an arbitrary electromagnetic field by a circular perfectly-conducting disk has been solved by using a series representation in powers of $k=2\pi/\lambda$ and the rectangular disk coordinates. The surface current density is given in terms of the field and its derivatives at the center of the disk. General expressions for the electric- and magnetic-dipole moments, the far-field and the scattering coefficient for the case of a plane wave at arbitrary incidence are presented. The calculations agree with results published by other authors. A bibliography of the most recent publications on this problem is included.

Low-Noise Properties of Microwave Backward Diodes—S. T. Eng (p. 419)

This paper describes, for what is believed to be the first time, the low-noise properties of backward tunnel diodes in microwave applications. The physics of the diodes is reviewed together with some of the characteristics and equivalent circuit parameters. The diodes are then considered as mixer diodes with IF in the audio range and also the standard 30-Mc IF. Another promising application considered is the use of the backward diodes in low-level detection.

The results show that the noise figure at 13.5 kMc with a 1-kc IF is around 15 db better than any commercially available mixer diodes. Using 30-Mc IF, the noise figure of backward diode mixers is without special optimum design, comparable to the best mixer diodes on the market. Of great importance, especially in microminiaturization, is the fact that these diodes may be used with a very low local oscillator power (50 μw or less). The high nonlinearity of the I-V characteristic at the origin and the low 1/f noise properties of these diodes are also of benefit in crystal video receivers and other low-level detector applications.

Design Theory of Up-Converters for Use as Electronically-Tunable Filters—G. L. Matthaei (p. 425)

The up-converters discussed use a single diode, a wide-band impedance matching filter at their signal input, a moderately wide-band impedance matching filter at their pump input, and a narrow-band filter at their sideband output. With a narrow-band filter at the sideband output, the frequency which will be accepted by the amplifier can be controlled by varying the pump frequency. Analysis of the impedance matching problem involved shows that tuning ranges of the order of a half-octave to an octave are possible. Theory is presented for both the lower-sideband and upper-sideband types of tunable up-converters and for the design of the required impedance-matching networks. It is shown that, because of the pump input bandwidth required, it will generally be necessary to accept some mismatch at the pump input. But, by use of a properly designed impedance-matching filter, the reflection loss can be kept nearly constant across the pump band, and the incident pump power required is not unreasonable. It is seen that properly designed devices

of this type using voltage-tunable pump oscillators should have wide tuning range, fast tuning capability, a useful amount of gain, no image response, and a low noise figure.

Anisotropic Properties of Strip-Type Artificial Dielectric—N. J. Kolettis and R. E. Collin (p. 436)

Theoretical formulas for the propagation phase constant of a two-dimensional strip medium are presented for general directions of propagation. In addition a number of experimental results are included that verify the validity of the theory. Some of the difficulties encountered in defining equivalent dielectric constants for this medium are also pointed out.

Optimization of Waveguide Tapers Capable of Multimode Propagation C. C. H. Tang (p. 442)

By converting Maxwell's equations, the general case of mode conversion in tapered waveguides is treated by matrix formulation in terms of an infinite set of coupled differential equations with nonuniform coupling coefficients and varying phase constants. An "orthogonalization" or "diagonalization" process is introduced through a nonlinear matrix transformation which is a function of taper length. The general matrix solution of the problem is obtained through a perturbation method in the form of an integral equation of the Volterra type, and the integral equation is solved by an iteration method. In view of the difficulties in finding eigenvalues, the problem is then reduced to the two-mode case, and the mode conversion is obtained in an explicit form revealing certain information which characterizes the choice of "mode-conversion distribution function." Optimization is first obtained through proper choice of the mode-conversion distribution function. In an attempt to approximate a Tchebycheff mode-conversion response, further optimization is realized by creating "new zeros" and thereby changing the density of the distribution of zeros in the vicinity of the origin of the mode-conversion curve and the nature of the optimization procedure essentially becomes that of synthesis. Through using the optimized distribution function, a total reduction of about 50 per cent in taper length is realized (when compared with the cosine-squared distribution) for the case of 50-db prescribed-mode discrimination in a taper connecting a $\frac{7}{8}$-in ID waveguide to a 2-in ID waveguide operating in the circular electric mode up to 75 kmc.

Correspondence (p. 452)
Contributors (p. 455)

Military Electronics

Vol. MIL-5, No. 4, October, 1961

A. G. Waggoner (p. 264)

Guest Editorial—A. G. Waggoner (p. 265)

Microwave Telemetry at U. S. Missile Ranges—G. F. Bigelow, T. B. Jackson, and R. T. Merriam (p. 266)

An orderly plan has been prepared covering the implementation of UHF radio telemetry on the country's missile ranges. Requirements have been drafted for UHF systems to be developed by 1970. Programs have been launched to transfer the requirements into equipment. Preliminary standards have been established.

Today, UHF telemetry links are utilized for a limited number of projects. Currently a high-performance UHF link is expensive, large in size, and complex. One must use a transmitter that may weigh 12 to 50 pounds, that has a volume of 250 to 1000 cu in, and that has an over-all power efficiency of 2 per cent for an 8 to 10 watt output. Its cost may be 10 times that of a 5-watt VHF transmitter. Automatic tracking systems are required but are not generally available. Special preamplifier-converters are also necessary. Because of these factors, UHF telemetry is used, at present, only by a few missile projects.

Obviously, we must continue to advance the state-of-the-art until a spectrum of microwave devices is available to fill the needs of the majority of telemetry users. Economy, as well as technical capability and flexibility, will be the mark of these developments.

Information Bandwidth Problems in Instrumentation of Missile Flight Tests W. E. Mimmack (p. 272)

The operation of missile flight-test instrumentation systems at minimum bandwidth is an important economic consideration. Design of instrumentation systems may become difficult or impossible unless intelligently chosen bandwidth parameters are specified. Since nearly all missile flight-test instrumentation systems operate as sampled data devices, the bandwidth parameter shows up as a sampling rate requirement.

It can be shown, under fairly general conditions involving no highly restrictive assumptions, that the rate of information acquisition of a sampled-data instrumentation system, when considered as a function of sampling interval, has a maximum. This can be readily appreciated intuitively. For a position-measurement system, for instance, if the sampling interval is made very short, the amount of information gained with each subsequent sample is very small because of the large amount of prior information about the position of the object being measured. No information would be gained if a sample were taken an infinitesimally small time after an initial measurement. Also, a very long time interval between samples would permit considerable growth of ignorance about the object's position, but the logarithmic information-gain function would grow slowly compared with t^{-1}; so the information rate for long sampling intervals would also be a small number. Somewhere between these two cases lies at least one maximum in information rate.

The selection of a sampling rate corresponding to the maximum information rate is recommended as a good choice for many types of missile test instrumentation systems. General sampling-rate formulas are developed, as well as specific formulas for certain important types of instrumentation problems.

Some Considerations Concerning the Measurement of the Atmospheric Temperature Field by Electromagnetic Means—D. Fryberger and E. F. Uretz (p. 279)

A system for determining atmospheric temperature structure by using an electromagnetic radiometer probe is described. The relationship between the electromagnetic sensor reading and atmospheric conditions is developed for both the microwave and infrared sensor utilizing a unified approach for the two cases. It is shown that, with the assumption of horizontal homogeneity, several alternate procedures for inversion of sensor readings to yield the spacial-temperature field are possible. One of these procedures which was used to invert theoretical radiometer readings from an assumed atmospheric structure is described in detail. The results of the inversion which was accomplished with the aid of a UNIVAC 1105 computer are included.

Improvement in Tracking Accuracy of Pulse Radar by Coherent Techniques—S. Kazel and J. N. Faraone (p. 286)

The theory of optimum linear prediction and filtering is applied to determine the optimum system response of pulse (noncoherent) and pulse-Doppler (coherent) radars for target motions consisting of 1) random steps of velocity, and 2) random steps of acceleration. The rms error in velocity data is calculated for each system, and the improvement factor of pulse-Doppler over pulse radar is obtained. The improvement factor is considerably greater in the case of random steps of acceleration, demonstrating that the relative accuracy of the two systems depends on the nature of the target motion, as well as on the radar parameters. Although the errors in both systems are reduced somewhat by allowing large delays in output data, the relative accuracy is found to be unchanged.

Integrated Missile Flight Safety System at Vandenberg/Point Arguello—K. E. Bailey and J. K. Moller (p. 294)

The background for the present safety system is outlined in a review of the original Air Force plans and installations and subsequent Navy-Air Force agreements for the coordinated use of the Pacific Missile Range, considering the expanded scope of operations in the area.

A description is given of the ground stations in the unified acquisition and tracking system for range safety as well as the auxiliary equipment for missile monitoring during early parts of its flight trajectory. A review is made of the associated data transmission and processing equipment including operational direct voice circuits. The corresponding safety equipment in different types of missiles is discussed in connection with both command, tracking, and telemetry functions. The implementation of the flight termination command requirements is outlined in the main transmitting station and missile checkout apparatus. The support areas of status reporting, telemetry, timing, and communications are discussed in detail. Finally, new requirements for precise downrange impact prediction and vehicle thrust termination are described.

The Digital Data Processor for the Skytop Static Test Facility—K. M. Roehr and R. D. Coleman (p. 300)

The Digital Data Processor implements a new data-acquisition concept which permits self-adaptive, accurate, real-time digitizing and editing of a large number of high-frequency data channels. The system was designed to meet the constantly changing requirements of a high-energy propulsion engine research and development program.

The centrally located processor basically samples 127 channels of analog information from any one of several 1-million-pound static test stands, and produces a digital tape. Before a new test the sampling scheme of the data channels is quickly set for any desired selection sequence that will best fit the new test situation. During a test the data processor can monitor preselected channels. Based on their performance, sampling priority can be shifted from one channel group to another, thus automatically optimizing the data-acquisition process. Immediate digitizing of the multiplexed analog data preserves its original accuracy. Record lengths on the output tape are programmable, and the tape format is compatible with the IBM 7090 computer.

Determination of Satellite Trajectories from Track-While-Scan Radar Measurements—R. B. Barrar and R. Deutsch (p. 306)

Classical methods for determining satellite orbits were limited to the use of angle information and only rough estimates of distance. With radar, it is possible to obtain good range information, but poor angular accuracy. Three approximate schemes are described which are ideally suited to track-while-scan radar observations. The accuracy obtained with these techniques has been demonstrated by the numerical evaluation of some typical cases.

Infrared Automatic Acquisition and Tracking System—R. C. Barbera (p. 312)

A technique for accumulating airborne visible and infrared spectroradiometric data from missile plumes and re-entry objects establishes the requirements for a precision tracking front surface mirror. The processing of target radiation, reflected by the tracking mirror into an infrared tracker telescope, to derive target coordinate information, is described. The deri-

vation of transformed target error signals to command the motion of the hydraulically driven tracking mirror is outlined. A description of the servo-electronics system, with selected circuitry, is given. The dynamic characteristics of the system, as determined from preliminary field tests, indicate that the system has a tracking rate capability of 10°/sec with an accuracy better than 60 seconds of arc. The detection sensitivity of the infrared tracker telescope is 1.6×10^{-10} w/cm² in the 2- to 6-μ region, and is sufficient to provide 10-mile tracking ranges against a jet target in a sunlit cumulus cloud background.

In a typical installation, aiming of the tracking mirror is provided by a 7×35, 10° field of view sighting telescope which is automatically slaved by the tracking mirror when acquisition and target tracking occurs, thereby providing continuous observation of the target. As an alternative to visual aiming, an automatic search program is generated by an accurate electro-mechanical programmer, which is described.

Target acquisition, in an automatic mode of operation, is accomplished through the use of a simple logic circuit which provides electronic background discrimination by virtue of signal pulse width.

High Precision Angle Determination by Means of Radar in a Search Mode—E. C. Watters, F. L. Rees, and R. A. Enstrom (p. 317)

One of the more difficult requirements to meet in the design of radars is that of accurate angular measurement. In tracking radars the azimuth and elevation of a target can be measured to a high degree of accuracy by a nulling method. Two of the most practical methods for obtaining angular accuracy in search radars are discussed in this paper. The first method is an interferometer technique employing either two receiving antennas for each dimension of angular measurement with two frequencies of transmission for the resolution of ambiguities, or three receiving antennas positioned relative to one another so that the equivalent effect is achieved with only one-frequency transmission. The second method is a combination amplitude comparison and interferometer technique in which the ambiguities are resolved by the amplitude comparison system. An analysis of each of these systems has been made using a statistical approach in which equations are developed relating the probability of error for a specified angular accuracy to SNR power in the receiver. Curves are presented which show this relationship for a 100 to 1 beam-splitting ratio.

An automatic TV Tracking Theodolite for Range Instrumentation—R. Wisnieff (p. 326)

The factors affecting the design of a gated Automatic TV Tracking System are discussed, and a system mechanization to achieve the design objectives is outlined. Only the composite video of a closed-circuit TV system is required as an input. A study of the dynamic performance of typical targets indicates that the unpredictable target motion in a frame period of 1/30 sec must be an extremely small fraction of the field of view required for initial target acquisition. This permits the use of a small tracking gate in the larger acquisition field, since the target coordinates of the previous frame may be used to position the gate. This small gate permits a signal-to-noise enhancement and effectively rejects extraneous targets outside the tracking gate.

The tracking is effected by subdividing the tracking area into equal early and late video gates in each coordinate. The differential video between these gates is applied to an electronic integrator in such a manner that the integrator output voltage, which is also the reference for the generation of the early-to-late gate transition, changes to place this gate transition on the target. The integrator voltages are, therefore, a measure of the target coordinates in the TV field.

The operation of an experimental system fabricated to determine the feasibility of applying this technique to a range-instrumentation system has produced tracking accuracies of better than 0.05 milliradian in an acquisition field of 10×10 milliradians. Current developments and additional applications of the technique are discussed briefly.

The Future of Pulse Radar for Missile and Space Range Instrumentation—D. K. Barton (p. 330)

An account of instrumentation radar development is given, and advantages and disadvantages of radar as compared to other instruments are discussed. Capabilities of present monopulse radars are described, based upon actual test data from the AN/FPS-16. This radar has a range of 200 miles on echo targets of one-square-meter cross section and can track to an accuracy of 0.1 mil in angle and 5 yards in range. The next generation in instrumentation radar is represented by the AN/FPQ-6, now under development, which will extend accurate tracking to ranges in excess of 500 miles on echo targets and will track existing beacons beyond the moon. An important capability not yet exploited in pulsed-instrumentation radars is the coherent pulsed-Doppler velocity-measurement channel which will equal the accuracy of microwave CW systems in radial-velocity data. Provisions for adding this fourth tracking channel to both AN/FPS-16 and AN/FPQ-6 are being made, and suitable beacons are being designed. An important advantage of pulsed-Doppler radar is the ability to share a single coherent beacon in multiple-station operation, providing highly accurate, three-coordinate velocity and position data without special interstation communication links over ground paths.

Beyond the immediate developments of the AN/FPQ-6, there are three major areas of improvement which will greatly extend radar performance. Solid-state maser preamplifiers will increase sensitivity of microwave radars by a factor of nearly one hundred within one or two years. Microwave antennas are already under construction in the 100- and 300-ft diameter class. Multiple-tube transmitters will make available ten to one hundred times the presently used average power, and signal-processing techniques are available to code the transmissions for accurate measurement of range and velocity. As a result of these developments, the improvement in radar performance should proceed at a more rapid pace even than that of the past ten years.

The unique ability of radar in acquiring and tracking uncooperative objects has been appreciated for some years, and examples of actual tracks are presented to show some of the interesting data which can be extracted from satellite echo signals.

Effects of Atmospheric Turbulence on Optical Instrumentation—R. A. Becker (p. 352)

The results of research on optical turbulence at White Sands Missile Range are presented. It has been shown that elevating camera stations 33 feet above ground level can yield nearly a threefold increase in optical resolution during periods of atmospheric turbulence. Early research postulated the existence of thermal-induced air lenses as the cause of optical-turbulence effects. Recent research has shown that air lenses can account for most of the observed effects. The "prism" concept of turbulence appears to be unnecessary for explaining tubulence-induced image motion.

The dependence of the optical effects of turbulence upon exposure time and aperture size are discussed qualitatively. The source of optical turbulence in the atmosphere and a method of measuring the turbulence-generating potential of various terrain surfaces are described on the basis of micrometeorology.

This research has been limited to an investigation of optical turbulence during the period from sunrise to sunset. However, many of the results apply to the nighttime turbulence encountered by astronomers.

Television in Underwater Weapons Testing—A. R. Metzler (p. 357)

At the Naval Ordnance Test Station sea ranges at San Clemente Island, closed-circuit television is used both over and under water for certain phases of underwater weapons testing. The functions of this instrumentation are to provide: real-time data, engineering surveillance, monitoring, underwater launcher positioning, range surveillance, time-event data, trajectory data, and to assist in underwater search and recovery.

At present, 17 closed-circuit systems are in use above and below the surface of the ocean, and more systems are being built. The new systems include an Image Orthicon camera for underwater search and a Vidicon-type system for operations at a depth of 6000 feet.

Programmed Search in Adaptive Systems—N. S. Potter (p. 362)

An investigation is conducted of the programming of search by discrete data systems over a space volume. The distribution of search effort which leads to the greatest attainable information rate on a contact, or probability of its retention by maximizing the probability of a positive interrogation within some designated time interval is determined. An estimate of p, the relative frequency of positive interrogations of an individual contact, is utilized as a basis for adjustment of the sampling rate in accordance with results of the search program optimization study. It is shown that in the case of Rayleigh signal sources, the rate of convergence to a stable estimate of p is greatest if a search program characterized by a rapid sampling rate and a consequent low probability of detection on the individual trial is employed.

If, following a sequence of observations, the statistical distribution of the position of the contact may be ascertained with some confidence, a suitably restricted space volume may be used in the allocation of search. It is shown that, if an extremal exists, the uniformly interrogated search field, which is optimal in the sense that the product of the containment and detection probabilities is greatest, is defined by an equiprobability density of location contour. Further, if a nonuniformly distributed search program is pursued and the errors are determined to be binormally, circularly distributed, the greatest effort should be allocated to the region in the vicinity of the center of the positional distribution, with a parabolic decline to zero in dwell time as the periphery of a bounding, circular region, whose radius is a function of the standard deviation, is approached.

The Design of a CW Passive Missile Trajectory Measuring System—R. A. Voss (p. 370)

Several tests have provided data sufficient to demonstrate the feasibility of tracking missiles with a CW passive Doppler system. Initial experiments utilized a local television station as a target illuminator; later tests examined the capability of such a system as a terminal trajectory measuring device. These latter tests showed that the system could be designed to have a multiple-target capability.

An interim high-power system is being installed to determine if the techniques established for a low-power system can be extended to provide reliable coverage of White Sands Missile Range (WSMR). Some improvement of these techniques is anticipated, and, in addition, certain tests will employ spaced receivers operated as radio interferometers.

Contributors (p. 375)

Abstracts and References

Compiled by the Radio Research Organization of the Department of Scientific and Industrial Research, London, England, and Published by Arrangement with that Department and *Electronic Technology*, Dorset House, Stamford St., London S.E. 1, England

NOTE: The Institute of Radio Engineers does not have available copies of the publications mentioned in these pages, nor does it have reprints of the articles abstracted. Correspondence regarding these articles and requests for their procurement should be addressed to the individual publications, not to the IRE

The number in heavy type at the upper left of each Abstract is its Universal Decimal Classification number. The number in heavy type at the top right is the serial number of the Abstract. DC numbers marked with a dagger (†) must be regarded as provisional.

UDC NUMBERS

Certain changes and extensions in UDC numbers, as published in PE Notes up to and including PE 666, will be introduced in this and subsequent issues. The main changes are:

Artificial satellites:	551.507.362.2	(PE 657)
Semiconductor devices:	621.382	(PE 657)
Velocity-control tubes, klystrons, etc.:	621.385.6	(PE 634)
Quality of received signal, propagation conditions, etc.:	621.391.8	(PE 651)
Color television:	621.397.132	(PE 650)

The "Extensions and Corrections to the UDC" Ser. 3, No. 6, August, 1959, contains details of PE Notes 598–658. This and other UDC publications, including individual PE Notes, are obtainable from The International Federation for Documentation, Willem Witsenplein 6, The Hague, Netherlands, or from The British Standards Institution, 2 Park Street, London, W.1., England.

ACOUSTICS AND AUDIO FREQUENCIES

534.152 3603

Optical Calibration of Vibration Pickups at Small Amplitudes—V. A. Schmidt, S. Edelman, E. R. Smith and E. Jones. (*J. Acoust. Soc. Am.*, vol. 33, pp. 748–751; June, 1961.) A photometric device based on a Fizeau-type interferometer and capable of measuring sinusoidal variations ranging from 72 to 4400 Å in amplitude is described.

534.2:534.88 3604

Horizontal Refraction in a Three-Dimensional Medium of Variable Stratification—D. E. Weston. [*Proc. Phys. Soc. (London)*, vol. 78, pp. 46–52; July, 1, 1961.] The bending of rays caused by reflection at an inclined boundary is discussed, with reference to underwater propagation of sound. See also 2204 of 1959.

534.2–14 3605

The Propagation of Tone Signals in a Plane Water Layer with Agitated Surface—L. N. Zakharov. (*Akust. Z.*, vol. 6, no. 4, pp. 454–461; 1960.) Investigation of the effect of surface agitation on signal amplitude and phase difference. Quantitative correlations are obtained between the fluctuation of the acoustic signal and height of the surface wave.

534.2–14 3606

The Fluctuations of Underwater Acoustic Signals Reflected from a Rough Sea Surface—G. E. Smirnov and O. S. Tonakanov. (*Akust. Z.*, vol. 6, no. 4, pp. 482–490; 1960.) Experiments were carried out in natural conditions and in a model tank at frequencies of 5–25 kc and 70–200 kc respectively. A factor is derived for the amplitude variation and the magnitude of fluctuation of the phase difference of reflected signals corresponding to different values of the roughness coefficient of the water surface.

534.21 3607

Experimental Study of the Influence of Surface Finish on Attenuation of Surface Waves—N. S. Bykov and Yu. G. Shneider. (*Akust. Z.*, vol. 6, no. 4, pp. 501–503; 1960.)

534.232 3608

Computation of Axial Concentration Coefficient of Certain Discrete Receiving-Radiating Groups—R. V. Belyakov. (*Akust. Z.*, vol. 6, no. 4, pp. 499–501; 1960.)

534.232:538.652 3609

Utilization of Magnetostrictive Materials in Generating Intense Sound—R. R. Whymark. (*J. Acoust. Soc. Am.*, vol. 33, pp. 725–732; June, 1961.) The calculating and theoretical sound outputs of a laminated bar of annealed Ni at its resonance frequency agree within ±10 per cent. The bar, resonant longitudinally at 20 kc, gave a measured maximum sound intensity of 167 w/cm².

534.232:621.316.825 3610

Thermoelectric Ultrasonic Pickup with a Semiconductor Thermistor—É. K. Labartkava (*Akust. Z.*, vol. 6, no. 4, pp. 468–471; 1960.) A brief description is given of a point-type transducer consisting of a microthermoresistor with a plexiglas thermosensitizer.

534.232.089.6 3611

Acoustic Measurements under Transient Temperature Conditions—W. L. Paine. (*J. Acoust. Soc. Am.*, vol. 33, p. 816; June, 1961.) A transducer to be calibrated is precooled or warmed to the temperature extreme of interest and its performance is then monitored as it returns to the ambient temperature of the water in an anechoic test tank.

534.283–8:537.311.31 3612

Dynamical Theory of Ultrasonic Attenuation in Metals—N. Takimoto. (*Progr. Theor. Phys.*, vol. 25, pp. 327–352; March, 1961.) A detailed investigation of the ultrasonic attenuation governed by the dynamic properties of conduction electrons.

534.522.1 3613

Optical Measurement of Ultrasonic Fields—R. F. Weeks (*J. Acoust. Soc. Am.*, vol. 33, pp. 741–747; June, 1961.) Passage of an ultrasonic wave train through a transparent solid produces a periodic birefringence within the solid. A photomultiplier scans the transmitted light mechanically to determine sound energy flow in the solid.

534.62 3614

Acoustic Properties of Anechoic Chamber—N. Olson. (*J. Acoust. Soc. Am.*, vol. 33, pp. 767–770; June, 1961.) Results of measurements made in a chamber built for the National Research Council of Canada are given in graphical form.

534.88:621.396.965.4 3615

Multiplicative Receiving Arrays: the Angular Resolution of Targets in a Sonar System with Electronic Scanning—V. G. Welsby. (*J. Brit. IRE*, vol. 22, pp. 5–12; July, 1961.) A theoretical analysis of the effect of cross-product terms on the performance of a multiplicative system is given. Results of practical trials confirm that the system can give an angular resolution approximately twice as good as that of the same array used additively.

621.395.625.3:681.84.083.84 3616

The Modulation Noise of Magnetic Recording Tape—P. A. Mann. (*Arch. elekt Übertragung*, vol. 15, pp. 18–24; January, 1961.) With reference to earlier investigations on unused and erased tape (3385 of 1957) the effect of modulation on tape noise is calculated for sinusoidal and pulse modulation. The spectral

The Index to the Abstracts and References published in the PROC. IRE from February, 1960 through January, 1961 is published by the PROC. IRE, May, 1961, Part II. It is also published by *Electronic Technology* and appears in the March, 1961, issue of that Journal. Included with the Index is a selected list of journals scanned for abstracting with publishers' addresses.

A list of organizations which have available English translations of Russian journals in the electronics and allied fields appears each June and December at the end of the Abstracts and References' section.

distribution of noise power is found to be independent of signal frequency.

681.828.5 3617
Electronic Generation of Sounds using the Principle of Light-Spot Scanning of Stencils—G. Holoch. (*Nachrtech. Z.*, vol. 14, pp. 1–6; January, 1961.) Method and equipment are described for the production of pure and mixed sounds with dynamic structure of almost any desired rate of variation.

ANTENNAS AND TRANSMISSION LINES

621.315.212 3618
Temperature Variation of Primary and Secondary Parameters of 2.6/9.5 mm Coaxial Pairs—A. Payant. [*Câbles & Trans. (Paris)*, vol. 15, pp. 130–147; April, 1961.] A theoretical and experimental study with reference to the experimental Corbeil-Versailles link.

621.315.212:621.372.51 3619
Physically Short High-Power Balun is Continuously Variable—J. T. Coleman. (*Electronics*, vol. 34, pp. 50–52; July 28, 1961.) A coaxial-line capacitively loaded balun for 5 Mw at 10–30 Mc having a physical length $<\lambda°/20$ and using vacuum variable capacitors is described.

621.372.2:621.371 3620
Transmission-Line Model—J. D. Wallace. (PROC. IRE, vol. 49, p. 1324; August, 1961.) A hypothetical infinitely long coaxial line with zero-loss conductors having a ratio between the inner diameter of the outer conductor and the outer diameter of the inner conductor equal to $e^{2\pi}$, when used in a vacuum, can be shown to have the same properties as free space. The line formulas enable various propagation problems to be simulated. Examples are given.

621.372.2:[621.372.51+621.372.814 3621
The Design of n-Step Line Transformers—H. Schreiber. (*Arch. elekt. Übertragung*, vol. 15, pp. 84–90; February, 1961.) Design formulas are derived for noncompensated matching transformers consisting of n sections of homogeneous transmission line. Design methods are compared.

621.372.2:621.372.512 3622
High-Speed Microwave Switch—L. L. Oh and C. D. Lunden. (*Electronics*, vol. 34, p. 60; July 7, 1961.) A noncontacting rotary switch using straight-line and circular-line codirectional couplers for sampling the power in a 24-element linear antenna array is described. It scans at rates up to 5000 rev/min and has a power-coupling efficiency of 80 per cent at 430 Mc.

621.372.2:621.372.512 3623
Zigzag-Line Couplers transfer Microwave Power—L. L. Oh and C. D. Lunden. (*Electronics*, vol. 34, pp. 58–59; July 14, 1961.) Brief details are given of several UHF switches using a zigzag line as the coupling element. An almost constant input impedance is maintained during switching and several advantages, due to the absence of arcing and mechanical contacts, are obtained over conventional switching devices.

621.372.8:537.56 3624
Propagation of Centimetre Waves through Waveguides Filled with Plasma of the Positive Column of a Discharge: Part 1—V. E. Golant, A. P. Zhilinskiĭ, M. V. Krivosheev, and G. P. Nekrutkina. (*Zh. Tekh. Fiz.*, vol. 31, pp. 55–62; January, 1961.) Results of an experimental investigation are compared with theoretical data.

621.372.8:537.56 3625
Propagation of Centimetre Waves through Waveguides Filled with Plasma of the Positive Column of a Discharge: Part 2—V. E. Golant, A. P. Zhilinskiĭ, M. V. Krivosheev, and L. I. Chernova. (*Zh. Tekh. Fiz.*, vol. 31, pp. 63–70; January, 1961.) Results are given of an experimental investigation of the dependence of the wave propagation constant on the high-frequency field strength, for regions in which nonlinear effects occur. Part 1: 3624 above.

621.372.8.09 3626
The Influence of Parasitic Parameters of an Electrical Waveguide Model on the Accuracy of the Solution of the Problem of Field Distribution—N. I. Shtein. (*Radiotekh. Elektron.*, vol. 5, pp. 1417–1425; September, 1960.)

621.372.81 3627
Wave Parameters and Wave Matrices Particularly for Microwave Networks with Multimode Waveguide—H. Brand. (*Arch. elekt. Übertragung*, vol. 15, pp. 48–60; January, 1961.) The relation between vector field quantities and the scalar wave parameters in waveguide networks is analyzed for several types of mode. The use of scattering and transmission matrices for calculations on multimode waveguide systems is described with examples.

621.372.829:621.372.853.2 3628
Propagation of Electromagnetic Waves in Waveguides of Complex Cross-Section with a Cross-Magnetized Ferrite Plate—N. M. Kovtun. (*Radiotekh. Elektron.*, vol. 5, pp. 1426–1430 September, 1960.) Equations are derived defining the propagation constants of a ferrite-loaded waveguide of H-shape cross section and variants of this.

621.372.832 3629
Electromagnetic Waves in Multiterminal Couplings of Rectangular Waveguide—H. Kaden. (*Arch. elekt. Übertragung*, vol. 15, pp. 61–70; February, 1961.) The distribution of H_{01}-mode power at a transition from two parallel waveguides to a single waveguide of double width is considered, and the problem is formulated mathematically by an infinite set of linear equations which are solved approximately by computer. The coupling between two parallel rectangular waveguides coupled by a slot of arbitrary length is calculated and the special case of equal distribution of power in the two waveguide sections is discussed.

621.372.837.1 3630
Waveguide Switch for Microwave Radiometers—M. J. B. Scanlan. (*Electronic Tech.*, vol. 38, pp. 337–339; September, 1961.) The switch, especially useful for large waveguides, is based on the short-slot or Riblet coupler and operates in the range 1–2 Gc. A vane, rotating at half the switching frequency, opens and closes the waveguides joining the two couplers.

621.372.852:621.318.134 3631
Low-Level Garnet Limiters—F. R. Arams, M. Grace, and S. Okwit. (PROC. IRE, vol. 49, pp. 1308–1313; August, 1961.) S- and L-band low-level passive limiters using polished single crystals of narrow-line-width Y-Fe garnet have been developed. Performance data are given. The operation of three novel types of limiter—electronically tunable preselectors and cavity-type and comb-type filters—is described.

621.396.67 3632
The Antenna Constructed by Parallel Wires—K. Nagai, R. Sato, and H. Uchida. (*Sci. Repts. Res. Insts. Tohoku Univ., Ser. B.*, vol. 12, no. 2, pp. 73–96; 1960.) The interchange between normal-phase modes and the zero-phase modes in the case of two asymmetrical or discontinuous parallel wires is considered. The theory developed is applied to radiating systems.

621.396.67:621.397.62 3633
The Permissible Mismatch in Aerial Installations for Television Reception—Fiebranz. (See 3955.)

621.396.67.095 3634
Current Waves in a Thin Cylindrical Conductor: Part 3—Variational Method and its Application to the Theory of an Ideal Conductor and a Conductor with Impedance—L. A. Vaĭnshteĭn. (*Zh. Tekh. Fiz.*, vol. 31, pp. 29–44; January, 1961.) A method of successive approximations is described based on the variational principle. This technique permits a derivation of an expression for waves in thin conductors. An approximate expression is also obtained for the scattering characteristic of a plane EM wave on a semi-infinite conductor. Part 2: 4104 of 1960.

621.396.67.095 3635
Current Waves in a Thin Cylindrical Conductor: Part 4—Input Impedance of an Oscillator and the Accuracy of Formulae—L. A. Vaĭnshteĭn. (*Zh. Tekh. Fiz.*, vol. 31, pp. 45–50; January, 1961.) Values of the complex variable determining the input impedance of an infinite conductor are tabulated, and the significance of this parameter in calculating the impedance of a straight conductor of finite length is clarified. Part 3: 3634 above.

621.396.674.3 3636
The Electromagnetic Fields of a Horizontal Dipole in the Presence of a Conducting Half-Space—J. R. Wait. (*Canad. J. Phys.*, vol. 39, pp. 1017–1028; July, 1961.) Fairly simple expressions for the fields are obtained by three methods and adequately cover all distances.

621.396.676:551.507.362.2 3637
Reconnaisance Satellite Antennas—R. B. MacAskill. (*Electronic Ind.*, vol. 20, pp. 108–115; April, 1961.) Design problems relating to gain, bandwidth and directivity requirements are discussed. Signal resolving techniques and possible types of antenna are outlined.

621.396.677 3638
Circular Aerial Arrays for Radio Astronomy—J. P. Wild. [*Proc. Roy. Soc. (London) A*, vol. 262, pp. 84–99; June 13, 1961.] A theoretical analysis shows that a circular array has a number of advantages over the Mills cross: 1) the length of transmission line between each element and receiver is halved; 2) for the same information, the number of elements required is reduced in the ratio $4:\pi$; 3) the beam possesses circular or elliptical symmetry, and 4) the system can be calibrated directly for phase and amplitude using a transmitter on a central tower.

621.396.677:621–526 3639
Project Echo: Antenna Steering System—Klahn, Norton, and Githens. (See 3937.)

621.396.677.091.22 3640
Maximum Antenna Gain of Shaped Beams—D. Levine. (*J. Franklin Inst.*, vol. 271, pp. 184–191; March, 1961.) The maximum gain of narrow beams can be evaluated within 1 db if it is assumed that 60 per cent of the transmitted energy lies outside the 3-db power contour. If the computed gain exceeds the measured value by more than 1 db, it is probable that the design can be improved.

621.396.677.3 3641
The Theory of a Single-Ring Circular Antenna Array—C. E. Hickman, H. P. Neff, and J. D. Tillman. (*Commun. and Electronics*, no. 54, pp. 110–115; May, 1961.) An examination is made of the currents possible in a circular array, the pattern which results from them and means of producing a specific radiation pattern.

621.396.677.3 3642
Resolution Characteristics of Correlation Arrays—I. W. Linder. (*J. Res. N. Bur. S.*, vol. 65D, pp. 245–252; May/June, 1961.) Analysis of resolution capabilities of correlation arrays shows a marked change in performance in the presence of two or more signal sources. These effects are analyzed for single-frequency signal sources and for randomly varying signal sources. Under optimum conditions a correlation array has twice the directivity of a linear array of the same length.

621.396.677.73 3643
A Method of Determining Phase Centres and its Application to Electromagnetic Horns—Y. Y. Hu. (*J. Franklin Inst.*, vol. 271, pp. 31–39; January, 1961.) The center of a radiating system may be located from the expression for the radiating field. The method is applied to EM horns of different dimensions and flare angles.

621.396.677.833 3644
The Radiation of a Reflector Aerial in the Shadow Region—V. L. Tandit and L. B. Tartakovskiĭ. (*Radiotekh. Elektron.*, vol. 5, pp. 1398–1406; September, 1960.) The radiation field in the shadow region of an infinitely thin, ideally conducting reflector irradiated by a small wide-beam exciter is calculated, taking into account diffraction corrections for the near field of the exciter, the curvature of the reflector, and fringe effects.

621.396.677.833.2 3645
The Condition of Shadowing and the Diffraction Correction to Current Distribution—B. E. Kinber. (*Radiotekh. Elektron.*, vol. 5, pp. 1407–1416; September, 1960.) Theoretical treatment relating to the diffraction field of a paraboloidal radiator.

621.396.677.833.2 3646
Project Echo: A Horn-Reflector Antenna for Space Communication—A. B. Crawford, D. C. Hogg, and L. E. Hunt. (*Bell Syst. Tech. J.*, vol. 40, pp. 1095–1116; July, 1961.) The mechanical construction and electrical properties are described. Gain and pattern measurements at 2390 Mc agree well with the theoretical characteristics.

621.396.677.833.2:621.396.965 3647
Design of Line Feed for World's Largest Aperture Antenna—A. F. Kay. (*Electronics*, vol. 34, pp. 46–47; July 7, 1961.) A description of the design of the feed system for the 1000 ft spherical dish antenna being erected at Arecibo, Puerto Rico.

AUTOMATIC COMPUTERS

681.142 3648
Digital Computers.—K. Mierzowski. (*VDI Z.*, vol. 103, pp. 767–775; June 11, 1961. 4 tables.) Annual review of developments in computer design with descriptions of recent installations and tabulated performance data. 76 references. For previous review see 3381 of 1960 (Schuff).

681.142 3649
Notes on the Structure of Logic Nets—R. M. Stewart. (Proc. IRE, vol. 49, pp. 1322–1323; August, 1961.) An elementary approach to a theory of the role of structure in logic nets.

681.142 3650
The Main Store of a Digital Differential Analyzer—P. L. Owen, M. F. Partridge, and T. R. H. Sizer. (*Electronic Engrg*, vol. 33, pp. 514–520; August, 1961.) A description of the performance and circuits of the main store of CORSAIR.

681.142:621.3.029.6 3651
A Potential Microwave Computer Element—R. W. Couch, A. F. Rashid, and R. Spence. (Proc. IRE, vol. 49, pp. 1338–1339; August, 1961.) A bistable-oscillator frequency-script system is described which uses a tunnel diode as the active element. A switching time of the order of 10 cycles is required for resonance frequencies of 600/735 kc. Operation at 250/375 Mc has been demonstrated, and operation at 10 Gc is suggested.

CIRCUITS AND CIRCUIT ELEMENTS

621.316.825 3652
New, Thermally Variable Bead Resistor—V. J. Tennery and R. G. West. (*J. Appl. Phys.*, vol. 32, p. 1402; July, 1961.) The unique I/V characteristic of ion-doped $BaTiO_3$ is illustrated. A bead 0.075 inch in diameter dissipated 1.5 w in still air.

621.318.4:621.3.011.4 3653
Equivalent Circuits of Coils with Distributed Capacitances—A. Fettweis. (*Rev. HF, Brussels*, vol. 5, no. 2, pp. 19–25; 1961.) The equivalent circuit comprises an ideal coil, a certain number of positive capacitances (two in the case of a coil with one winding) and an additional capacitance which can be either positive or negative depending on the relative magnitude and the exact distribution of the various parasitic capacitances.

621.318.4.042:621.375.3 3654
On the Core Gain of the Magnetic Amplifier Cores—K. Murakami and T. Kikuchi. (*Sci. Repts. Res. Insts. Tohoku Univ., Ser. B*, vol. 12, no. 2, pp. 135–144; 1960.) New definitions, specific core gain and core gain, are suggested and the relation of these to the power gain of an amplifier is discussed.

621.318.435 3655
An Experimental Study on the Ampere-Turn Gain of Ordinary Saturable Reactors—W. A. Geyger. (*Commun. and Electronics*, no. 54, pp. 173–178; May, 1961.) Measurements show the great improvements in performance of dc instrument transformers can be obtained by slightly increasing the effective ratio of primary to secondary turns and applying a properly rated ac bias circuit.

621.318.57:537.312.62 3656
On the Linear Circuit Aspects of Cryotrons—P. M. Chirlian and V. A. Marsocci. (Proc. IRE, vol. 49, p. 1326; August, 1961.) An expression is derived for the gate resistance of a cryotron in the transition region.

621.318.57:621.317.6 3657
Variable-Conductance Sampling Switch—J. E. Taylor. (*Rev. Sci. Instr.*, vol. 32, pp. 754–755; June, 1961.) Weighted sums are produced of discrete samples from continuous voltage waveforms, by varying the rate at which the integrating capacitor can charge. The switch has been operated randomly and cyclically at rates between 20 and 50000/sec.

621.318.57:621.382.23 3658
The Silicon Cryosar—H. Izumi. (Proc. IRE, vol. 49, pp. 1313–1314; August, 1961.) The main difference from the Ge cryosar [3211 of 1959 (McWhorter and Rediker)] is that negative-resistance characteristics are obtained using crystals with uncompensated impurities. As a computer element the device has been switched in about 50 nsec and has a maximum/minimum voltage ratio as high as 7.

621.319.4:621.372.44:621.382 (083.7) 3659
IRE Standards on Solid-State Devices: Definitions of Terms for Nonlinear Capacitors, 1961—(Proc. IRE, vol. 49, pp. 1279–1280; August, 1961.) Standard 61 IRE 28.S1.

621.372.44:621.373 3660
On Some Aspects of Matrix Calculus applied to Local Oscillation in Nonlinear Circuits—F. Bertein. (*J. Phys. Radium*, vol. 21, suppl., *Phys. Appl.*, pp. 137A–148A; November, 1960.) The application of matrix methods to the analysis of oscillating circuits with an impressed signal of low amplitude is considered. The representation of amplitude and phase modulation in coordinate form is illustrated, and examples are given of the use of these methods in problems of oscillator stabilization.

621.372.5:517.7 3661
Elliptic Functions in Network Synthesis—S. D. Bedrosian. (*J. Franklin Inst.*, vol. 271, pp. 12–30; January, 1961.) The Jacobian elliptic functions are used to solve the approximation problem of network synthesis. A unified design chart for image parameter filters, elliptic-function filters and 90°-phase-difference networks is shown and tabular and graphical data emphasizing extreme parameter values are given.

621.372.5:621.3.049.75 3662
Shaping of Distributed *RC* Networks—B. L. H. Wilson and R. B. Wilson. (Proc. IRE, vol. 49, pp. 1330–1331; August, 1961.) An improvement in the attenuation factor of a 180°-phase-shift network from 29 to 7 appears to be possible if the conventional untapered 3-section network is replaced by a tapered distributed network.

621.372.54 3663
Graphical Procedures for Solving the Approximation Problem of Electrical Filters—R. Rubini. (*Alta Frequenza*, vol. 30, pp. 135–155; February, 1961.) Three graphical methods of synthesizing filter response characteristics as the sum and difference of functions of similar geometric form are explained. The methods are theoretically equivalent but have different fields of application. For English version see *ibid.*, vol. 30, pp. 198–215; March, 1961.

621.372.54:621.372.412 3664
Optimum Matching of Symmetrical Low-Pass and High-Pass Filters: Application to Low-Pass and High-Pass Ladder Filters using Piezoelectric Crystals—J. E. Colin and P. Allemandou. [*Câbles & Trans.* (*Paris*), vol. 15, pp. 99–114; April, 1961.] A filter structure is suggested which is especially suitable for use with crystal elements. Advantages and disadvantages of this and similar structures are discussed.

621.372.543.2 3665
Tunable Rejection Filters—L. A. Moxon. (*Electronic Tech.*, vol. 38, pp. 327–330; September, 1961.) An analysis of the requirements for a rejection filter is used in the design of some practical circuits, tunable over half an octave and covering the HF band.

621.372.55:621.396.4:621.376 3666
V.H.F. Broad-Band Variable Group-Delay Equalizers—R. Hamer and R. G. Wilkinson. (*Electronic Engrg*, vol. 33, pp. 506–510; August, 1961.) The two designs described are for links using 1) 960 telephony channels or 405-line subcarrier color television, and 2) 1800 telephony channels or 625-line subcarrier color television.

621.372.6 3667
Application of Graph Theory to the Analysis of Active and Mutually Coupled Networks—W. H. Kim. (*J. Franklin Inst.*, vol. 271, pp. 200–221; March, 1961.) A unified graphical ap-

proach applying the concept of the mathematically equivalent circuit [52 of 1956 (Percival)] as it relates to the indefinite admittance matrix of a multipole.

621.372.632:621.382.23 3668
Stable Low-Noise Tunnel-Diode Frequency Converter—F. Sterzer and A. Presser. (PROC. IRE, vol. 49, p. 1318; August, 1961.) An initial wide-band converter with local-oscillator frequency 780 Mc and intermediate frequency 30 Mc had unity conversion gain and a radiometer noise figure of 2.5 db.

621.373:621.372.2:621.372.44 3669
Self-Oscillation in a Transmission Line with a Tunnel Diode—J. Nagumo and M. Shimura. (PROC. IRE, vol. 49, pp. 1281–1291; August, 1961.) A theoretical analysis of the circuit is given together with experimental results. The self-oscillation can be explained as a periodic solution of the linear wave equation with a nonlinear boundary condition.

621.373:621.391.822 3670
Broadening of the Spectrum of an Oscillator due to Noise—J. Loeb. (*Ann. Télécommun.*, vol. 14, pp. 151–152; May/June, 1959.) A formula is derived for the frequency broadening due to random thermal noise in a nonlinear circuit.

621.373.4 3671
Pulling Phenomena in Valve Oscillators—S. Spiess. (*Nachrtech.*, vol. 10, pp. 452–457 and 540–546; October and December, 1960.) A general theory of pulling effects is derived on the basis of band-filter theory. These effects are calculated as a function of detuning and degree of coupling between similar and dissimilar oscillator circuits. A mechanical analogue of a "pulled" oscillating system is described.

621.373.4.029.4:621.316.86 3672
Varistor Network controls Voltage-Tuned Oscillator—M. Uno. (*Electronics*, vol. 34, pp. 44–47; July 28, 1961.) An AF phase-shift oscillator, with SiC varistors as the variable elements has almost constant output over a range of 10:1 and low harmonic distortion.

621.373.421.11 3673
Locking of a Two-Circuit Oscillator—G. D. Shemanaev and E. N. Ivanova. (*Radiotekh. Elektron.*, vol. 5, pp. 1387–1397; September, 1960.) The addition of a second tuned circuit improves the amplitude/frequency and phase /frequency characteristics of a locked oscillator. The effect of coupling conditions on stability is discussed.

621.373.421.13 3674
Recent Development of Quartz Crystal Units for Telecommunication—K. Takahara. (*Rev. Elec. Commun. Lab., Japan*, vol. 9, pp. 165–206; March/April, 1961.) A new method and equipment devised for manufacture and development of crystal units in the range 1 kc–100 Mc, and associated apparatus are described.

621.373.43:621.382.23 3675
Tunnel-Diode One-Shot and Triggered Oscillator—T. W. Flowerday and D. D. McKibbin. (PROC. IRE, vol. 49, p. 1315; August, 1961.) The one-tunnel-diode flip-flop described by Kaenel (1761 of July) which requires a bidirectional pulse can be made to operate as a triggered oscillator by the addition of an identical circuit with modified bias.

621.373.43:621.382.3 3676
The Switching Mechanism of the Schmitt Trigger Circuit using Transistors—K. Leberwurst. (*Nachrtech.*, vol. 10, pp. 519–524; December, 1960.) Equivalent circuits and characteristic curves are derived; results of measurements are given for comparison.

621.373.431.1:621.382.23 3677
The Tunnel-Diode Pair—D. J. Hamilton and M. J. Morgan. (*Semiconductor Prod.*, vol. 4, pp. 17–23; July, 1961.) The composite V/I characteristic of the twin circuit is considered and its application in the design of astable, monostable and bistable multivibrators is illustrated; trigger requirements and effects of loading can also be determined.

621.374 3678
A Low-Level Linear Rundown Circuit for Pulse Height to Pulse Width Conversion—D. L. Endsley, W. W. Grannemann, and T. Summers. (*Commun. and Electronics*, no. 54, pp. 150–152; May, 1961.) A two-transistor device consisting of a constant-current generator and an emitter follower circuit is described. Experimental and theoretical analysis of the circuit are in good agreement.

621.374:621.382.23 3679
Tunnel-Diode Fast-Step Generator produces Positive or Negative Steps—R. Carlson. (*Electronics*, vol. 34, pp. 48–49; July 28, 1961.) The generator produces pulses of about 2 μsec duration having a rise time of 0.5 nsec at recurrence frequencies up to 100 kc.

621.374:621.382.333 3680
The Collector-Coupled Complementary Pair—V. Spány. (*Electronic Engrg*, vol. 33, pp. 526–527; August, 1961.) The astable mode gives phantastron-type waveforms with peak-to-peak voltages almost equaling the supply voltage. The bistable mode gives thyratron-type characteristics.

621.374.3:621.382.3 3681
Fast Coincidence Circuits using Avalanche Transistors—J. C. Artiges and J. C. Brun. (*J. Phys. Radium*, vol. 22, suppl., *Phys. Appl.*, pp. 53A–58A; February, 1961.) The circuit described has a resolution time of 2 nsec and an efficiency of 90 per cent. Results of tests made with 1) a pulse generator, and 2) a pair of photomultipliers are reported.

621.374.32:621.382.3 3682
An Automatic Self-Checking Transistor Counter with Digital Display—H. I. Messer and W. H. P. Leslie. (*Electronic Engrg*, vol. 33, pp. 484–489; August, 1961.)

621.374.32:681.142 3683
A Fast Binary Counter—E. Taranto. (*J. Brit. IRE*, vol. 22, pp. 31–32; July, 1961.) "A transistor binary counter employing seven flip-flops is described. Its operation is dependent only on the switching time of one flip-flop which may be ~100 nsec."

621.374.4:621.372.44 3684
A Tripler Circuit using a Capacitance Diode—D. Lohrmann and W. Marks. (*Frequenz*, vol. 15, pp. 9–12; January, 1961.) Mathematical analysis of a frequency tripler circuit and deviation of an equivalent circuit. The results of an analysis and of measurements on a practical circuit are compared.

621.374.5 3685
The Pulse Response of a Delay Line—P. Poincelot. [*Câbles & Trans.* (*Paris*), vol. 15, pp. 93–98; April, 1961.] An expression is developed for each element of the network and a solution is obtained in the form of a convergent Neumann series.

621.375.018.756:621.382.23 3686
Zener Diode creates Logarithmic Pulse Amplifier—D. Ophir and U. Galil. (*Electronics*, vol. 34, pp. 68–70; July 14, 1961.) Amplification over three decades is achieved by using as the logarithmic device a Zener diode to which a small resistance has been added to straighten the characteristic curve.

621.375.221 3687
Note on the Series Correction of Wide-Band Amplifiers—A. V. J. Martin. (*Onde élect.*, vol. 41, pp. 258–262; March, 1961.) A variation of the series-inductance correction circuit is considered in which the load resistance is connected across the output, and the circuit designed for either maximally flat transfer impedance or maximally flat input impedance. Inconvenient ratios of input to output capacitance can be avoided by using a cathode-follower stage.

621.375.3 3688
A New Magnetic-Controlled Rectifier Power Amplifier with a Saturable Reactor Controlling 'On' Time—R. E. Morgan. (*Commun. and Electronics*, no. 54, pp. 152–155; May, 1961.)

621.375.4 3689
Problems relating to Transistor Power Amplifiers—G. B. Debiasi. (*Alta Frequenza*, vol. 30, pp. 114–121; February, 1961.) The design of transformerless AF output amplifiers is considered, and a graphical method for determining transistor thermal stability is given.

621.375.4.024 3690
A Circuit for the Compensation of Voltage Drift in the Input Stage of a Direct-Coupled Transistor D.C. Amplifier—U. Hölken. (*Nachrtech. Z.*, vol. 14, pp. 32–36; January, 1961.) In the circuit given the temperature drift of the base/emitter voltage has been compensated almost to the theoretical limit.

621.375.4.024:621.398 3691
Differential Amplifier with Regulator Achieves High Stability, Low Drift—R. D. Middlebrook and A. D. Taylor. (*Electronics*, vol. 34, pp. 56–59; July 28, 1961.) A transistor dc amplifier suitable for missile telemetry systems is described.

621.375.426 3692
Narrow-Band Amplification with Transistors—E. R. Hauri and H. Beneking. (*Nachrtech. Z.*, vol. 14, pp. 37–39; January, 1961.) Contribution to 4149 of 1960 with author's reply.

621.375.9:538.569.4 3693
Field-Swept Maser Oscillation—J. C. Kemp. (*Phys. Rev. Lett.*, vol. 7, pp. 21–23; July 1, 1961.) The application by Singer and Wang (2897 of October) of their analysis of maser oscillations to experimental results of the author is criticized. They attribute the oscillations to energy exchange between cavity and emitting sample. The radiation envelope is, however, largely determined by the Zeeman field sweep rate, due to a different mechanism.

621.375.9:538.569.4:538.222 3694
Paramagnetic Maser Oscillator Analysis—S. Wang and J. R. Singer. (*J. Appl. Phys.*, vol. 32, pp. 1371–1376; July, 1961.) An equation for the output waveform is derived and numerical solutions obtained using a computer. Good agreement with experiment is given for steady-state and field-swept oscillators.

621.375.9:538.569.4:621.396.43 3695
Project Echo: The Dual-Channel 2390-Mc/s Travelling-Wave Maser—R. W. De Grasse, J. J. Kostelnick, and H. E. D. Scovil. (*Bell Syst. Tech. J.*, vol. 40, pp. 1117–1127; July, 1961.) Details of the ruby material isolator and amplifier package construction are given. An instantaneous bandwidth of 13 Mc and effective noise temperature of 8°K were obtained and the gain (>33db) was sufficient to override the noise of the following stage.

621.375.9:621.372.44 3696
Parametric Amplifiers—G. B. Stracca. (*Alta Frequenza*, vol. 30, pp. 98–113; February, 1961.) Theoretical comparison of gain, bandwidth, noise and stability of the negative-resistance amplifier and upper- or lower-sideband converts. Experimental results are also reported. For English version see *ibid.*, vol. 30, pp. 244–254; March, 1961.

621.375.9:621.372.44 3697
The Wide Tuning Range of Backward Travelling-Wave Parametric Amplifiers—H. Hsu and S. Wanuga. (PROC. IRE, vol. 49, pp. 1339–1340; August, 1961.) A method is indicated of increasing the range beyond that suggested by Straus. (IRE TRANS. ON MICROWAVE THEORY AND TECHNIQUES, vol. MTT-9, p. 95; January, 1961.)

621.375.9:621.372.44:621.382.2 3698
Theory of Nonreciprocal Circuits with Equal Input and Output Frequency using Nonlinear Semiconductor Elements—R. Maurer and K. H. Löcherer. (*Arch. elekt. Übertragung*, vol. 15, pp. 71–83; February, 1961.) The quadripole equations and transfer gain are derived for nonreciprocal amplifiers which consist of tunnel-diode or parametric-diode converter stages in cascade connection [see also 93 of February (Maurer *et al.*)]. Matching and decoupling problems are considered for various circuit configurations.

621.375.9:621.372.44:621.382.23 3699
Signal and Noise Characteristics of Diode-Reactance Amplifiers for the U.H.F. Region—R. Maurer. (*Radio Mentor*, vol. 27, pp. 110–113; February, 1961.) Examples are given of mixer circuits, straight amplifiers, and a traveling-wave amplifier using parametric-amplifier techniques. The problem of matching by means of nonreciprocal elements or by bridge circuit is also dealt with.

621.375.9:621.372.44:621.391.822 3700
Noise Figure and Stability of Negative-Conductance Amplifiers—A. C. MacPherson. (PROC. IRE, vol. 49, pp. 1314–1315; August, 1961.) Calculations of lowest noise-figure attainable from stability considerations are in agreement with results of an earlier analysis [2277 of 1960 (Van der Ziel and Tamiya)], but the lowest possible noise figure is obtained at the expense of stability.

621.375.9:621.372.44:621.396.969.3 3701
Project Echo: 961-Mc/s Lower-Sideband Up-Converter for Satellite-Tracking Radar—M. Uenohara and H. Seidel. (*Bell Syst. Tech. J.*, vol. 40, pp. 1183–1205; July, 1961.) The amplifier is pumped at 11.7 Gc and although regenerative it has been made unconditionally stable by careful mechanical and electrical design. The over-all noise figure is 1.6 db, gain 22 db and bandwidth 20 Mc.

621.375.9:621.382.23 3702
A Tunnel-Diode Slot Transmission Amplifier—M. E. Pedinoff. (PROC. IRE, vol. 49, pp. 1315–1316; August, 1961.) A negative-conductance waveguide transmission-type amplifier consisting of a tunnel-diode mounted within an S-band waveguide end-plate slot has been built operating at a frequency of 2.7 Gc with a bandwidth of 21 Mc and 16 db gain. No measurements have yet been made of noise figure.

621.376:621.372.54 3703
The Matching Problem of the Ring-Type and Double Push-Pull Modulator with Filter Termination at Both Ends.—H. Bauch. *Arch. elekt. Übertragung*, vol. 15, pp. 1–17; January 1961.) Detailed discussion of an impedance matching method for obtaining optimum frequency response and minimum attenuation.

621.376.22 3704
A Ring Modulator with Integrated Filters—J. Salzmann. [*Câbles & Trans.*, vol. 15, pp. 148–159; April, 1961.] A lossless four/terminal frequency-translating network is proposed which avoids using a transformer between rectifiers and filters.

GENERAL PHYSICS

535.215 3705
Theory of Phototexcitation in Solids—A. Messen. (*J. Phys. Radium.*, vol. 22, pp. 135–141; March, 1961.) The theory of optical absorption by photoexcitation is reviewed and further investigated. A distinction is made between "oblique" and "vertical" transitions.

537.311.1 3706
Tunnelling from an Independent-Particle Point of View—W. A. Harrison. (*Phys. Rev.*, vol. 123, pp. 85–89; July 1, 1961.) Calculation of wave functions for tunnelling problems, with applications.

537.52:538.63 3707
Radio-Frequency Breakdown Controlled by Drift of Electrons in an Inhomogeneous Magnetic Field—L. T. Shepherd and H. M. Skarsgard. (*Canad. J. Phys.*, vol. 39, pp. 983–992; July, 1961.) Measurements of breakdown RF electron field versus magnetic field were made at pressures between 1.25 and 6×10^{-4} mm in H and He. The breakdown RF field varied as the inverse square root of the magnetic field as predicted by theory.

537.525 3708
Experimental Evidence for Beam-Plasma Interaction in a Low-Pressure Argon Discharge—L. H. Putnam, H. D. Collins, and N. L. Oleson. (*Phys. Rev. Lett.*, vol. 7, pp. 77–79; August 1, 1961.)

537.533 3709
Broadening of a Beam of Electrons by the Space Charge—M. Boivin. (*J. Phys. Radium*, vol. 21, suppl., *Phys. Appl.*, pp. 171A-172A; November, 1960.) A recurrence formula is developed for computing the broadening of the beam.

537.56 3710
Filamentary Structure Produced by an Electric Current in a Plasma—H. Alfvén. (*Ark. Fys.*, vol. 19, pp. 375–378; June 8, 1961.) An electric field parallel to a magnetic field in a plasma at low pressure produces a current which is confined to a filament. Simple formulas are given for the cross-section of the filament and the current in it.

537.56 3711
Space Dispersive Properties of Plasma—J. Neufeld. (*Phys. Rev.*, vol. 123, pp. 1–10; July 1, 1961.)

537.56:537.533 3712
Interaction of Fast Electron Beams with Longitudinal Plasma Waves—Ya. A. Romanov and G. F. Filippov. (*Zh. Eksp. Teor. Fiz.*, vol. 40, pp. 123–132; January, 1961.) Equations are derived for the variation with time of the plasma-wave spectral density and the fast-electron distribution function, for arbitrary velocity distributions.

537.56:538.56 3713
Waves in a Rarefied Ionized Gas Propagated Transverse to an External Magnetic Field—T. Watanabe. (*Canad. J. Phys.*, vol. 39, pp. 1044–1057; July, 1961.) Three modes of plane waves, in which the perturbed magnetic field is parallel to the external magnetic field, can be propagated transverse to the external magnetic field in a collision-free and fully ionized gas. In the HF limit the three modes behave respectively as electromagnetic, electron sound, and ion sound waves.

537.56:538.566:535.43 3714
Concerning the Disturbances Produced by a Body Moving in a Plasma—L. P. Pitaevskiĭ and V. Z. Kresin. (*Zh. Eksp. Teor. Fiz.*, vol. 40, pp. 271–281; January, 1961.) Formulas derived for the disturbance of electron density are used to calculate the effective cross-section for the scattering of electromagnetic waves at this disturbance in particular cases.

537.56:538.6 3715
Electrohydromagnetic Waves in a Fully Ionized Gas: Part 2—K. D. Cole. (*Planet. Space Sci.*, vol. 5, pp. 292–298; August, 1961.) The Appleton-Hartree dispersion formula for magneto ionics is generalized to include the effect of heavy ions. The ratio of particle energy to magnetic field energy in a wave of arbitrary frequency is determined. A band of frequencies around the plasma frequency is found for which waves are attenuated. Location of these bands would enable the interplanetary magnetic field and electron density to be estimated. Part 1: 2305 of 1960.

537.56:538.63 3716
The Statistical Mechanics, Dynamics and Magnetohydrodynamics of Plasmas—R. Jancel and T. Kahan. (*Cah. Phys.*, vol. 15, pp. 57–101; February, 1961.) A system of equations is established in particular to denote the movement, the current and the compression tensor of an ionized gas. These are applied to partially and completely ionized gases and used to obtain the general equations of magnetohydrodynamics. Propagation modes of different types of waves are determined.

537.56:538.63 3717
On Plasma Oscillations with Special Emphasis on the Landau Damping and the Gross Gaps in the Frequency Spectrum—A. Kildal. (*Nuovo Cim.*, vol. 20, pp. 104–122; April 1, 1961. In English.) A linear theory of oscillations of the form exp $[i(\boldsymbol{k}.\boldsymbol{r}-\omega\, t)]$ in a collision-free electron plasma in an external magnetic field is given.

537.56:538.63 3718
Collective Motions in a Plasma due to Magnetic Interaction—G. Kalman. (*Nuovo Cim.*, vol. 20, pp. 198–200; April 1, 1961.) The existence of collective modes due to the static magnetic interaction between the current elements represented by the moving electrons has been investigated.

537.56:538.63 3719
Plasma Density Fluctuations in a Magnetic Field—E. E. Salpeter. (*Phys. Rev.*, vol. 122, pp. 1663–1674; June 15, 1961.) A continuation of earlier work (*ibid.*, vol. 120, pp. 1528–1535; December 1, 1960) in which the frequency spectrum was derived for the spatial Fourier transform of the electron charge density fluctuations in a plasma. The effects of a constant magnetic field in an arbitrary direction are considered. A theoretical basis is provided for analyzing back-scatter experiments, and intensities are derived as a function of the real frequency variable for the case of thermodynamic equilibrium.

538.311:621.318.3 3720
Hydromagnet: a Self-Generating Liquid-Conductor Electromagnet—H. H. Kolm and O. K. Mawardi. (*J. Appl. Phys.*, vol. 32, pp. 1296–1304; July, 1961.) The exciting current is generated by forcing a liquid conductor radially inwards across an axial magnetic field. The tangential current thus generated adds to the initial applied field.

538.561:537.122 3721
Emergence into Vacuum of the Cherenkov Radiation produced by Longitudinal Waves in a Medium—B. L. Zhelnov. (*Zh. Eksp. Teor. Fiz.*, vol. 40 pp. 170–177; January 1961.) The EM radiation of an electron moving into a vacuum from a medium with spatial dispersion is considered. Under certain conditions, in addition to the transition radiation there is Cherenkov radiation from longitudinal waves in the medium. At large distances from the interface this radiation is a spherical wave confined to a narrow range of frequencies near the plasma frequency.

538.561.029.65:537.533 3722
Coherent Generation of Microwave Power by Annihilation Radiation of a Prebunched Beam—B. W. Hakki and H. J. Krumme. (PROC. IRE, vol. 49, p. 1334; August, 1961.) Millimeter-wave radiation at the 100 mw level has been produced by the creation and annihilation of a tightly bunched 0.8 Mev electron beam. A proposed extension of the method, based on optical techniques, is intended to produce power in the submillimeter region.

538.566:535.42 3723
The Problem of Diffraction of Electromagnetic Waves as a Perfectly Conducting Plane Ring—G. A. Grinberg and É. N. Kolesnikova. (*Zh. Tekh. Fiz.*, vol. 31, pp. 13–17; January, 1961.) Theoretical treatment of the diffraction of plane electromagnetic waves assuming a ring of internal radius and width much greater than the wavelength. Integral equations for the "shadow" currents are given, from which the total current flowing in the screen is determined.

538.566:535.42 3724
Diffraction of a Plane Wave by a Unidirectionally Conducting Half-Plane—S. R. Seshadri. [*Proc. Nat. Inst. Sci. (India) Part A*, vol. 27, pp. 1–10; January 26, 1961.] The problem is formulated in terms of an integral equation specifying the screen function, whose solution is obtained by the standard Wiener-Hopf procedure. Expressions for the fields and the current induced on the half-plane are given.

538.566:535.42 3725
A Note on the Diffraction of a Scalar Wave by a Small Circular Aperture—R. A. Hurd. (*Canad. J. Phys.*, vol. 39, pp. 1065–1070; July, 1961.)

538.566:537.56 3726
Kinetic Theory of Reflection of Electromagnetic Waves from a Moving Plasma—V. I. Kurilko. (*Zh. Tekh. Fiz.*, vol. 31, pp. 71–77; January, 1961.) Mathematical analysis of the reflection of electromagnetic waves from a plasma moving in a space in which the phase velocity of the waves is less than the velocity of light.

538.566.029.6:535.43:537.56 3727
Scattering of Microwaves from a Cylindrical Plasma in the Born Approximation: Part 1—Y. Midzuno. (*J. Phys. Soc. Japan*, vol. 16, pp. 971–980; May, 1961.) Formulas are derived for the angular distribution function and the effect of special distributions is considered.

538.569.4 3728
Some Properties of Resonance Line-Shape Functions—D. G. Hughes and D. K. C. MacDonald. [*Proc. Phys. Soc. (London)*, vol. 78, pp. 75–80; July 1, 1961.] Mathematical discussion of the broadening of spectral lines.

538.569.4:537.228.5 3729
Shift of Nuclear Quadrupole Resonance Frequency by Electric Field—T. Kushida and K. Saiki. (*Phys. Rev. Lett.*, vol. 7, pp. 9–10; July 1, 1961.) A linear shift in the Br^{81} line in $NaBrO_3$ is observed when a field of several kv/cm is applied parallel to the (111) crystal axis. The line shape becomes asymmetric, and is attributed to unresolved line splitting.

538.569.4:537.228.5 3730
Linear Effect of Applied Electric Field on Nuclear Quadruple Resonance—J. Armstrong, N. Bloembergen, and D. Gill. (*Phys. Rev. Lett.*, vol. 7, pp. 11–14; July 1, 1961.) A linear Stark effect is observed in the Cl^{35} line in $KClO_3$ and $NaClO_3$ crystalline powders, as predicted theoretically.

538.569.4:537.29 3731
Linear Effect of Applied Electric Field on Magnetic Hyperfine Interaction—N. Bloembergen. (*Phys. Rev. Lett.*, vol. 7, pp. 90–92; August 1, 1961.)

538.569.4:621.375.9 3732
Angular Variation of Axial Spin-Hamiltonian Eigenvalues in Strong Magnetic Field—H. A. Buckmaster. (*Canad. J. Phys.*, vol. 39, pp. 1073–1079; July, 1961.) The expressions for the energies of transitions between levels with strong field quantum numbers M and $M-m$ are given for $m=1, 2, 3$. The tables give the values of the coefficients containing S and M for a range of values of these parameters.

538.569.4:621.375.9:535.61-1/2 3733
A Proposal for a Tunable Source of Radiation for the Far Infrared using Beats between Optical Masers—D. C. Lainé. (*Nature*, vol. 191, pp. 795–796; August 19, 1961.)

538.569.4:621.375.9:535.61-2 3734
Theory of Quantum Oscillators in a Multimode Cavity—W. G. Wagner and G. Birnbaum. (*J. Appl. Phys.*, vol. 32, pp. 1185–1194; July, 1961.) The distribution of power in the various modes in the steady-state operation of an optical maser is studied.

538.569.4:621.375.9:535.61-2 3735
Proposed Technique for Modulation of Coherent Light—A. K. Kamal and S. D. Sims. (PROC. IRE, vol. 49, p. 1331; August, 1961.) A frequency shift of the coherent-light output proportional to the strength of an electric field applied to a ruby laser provides a system for FM of the output.

GEOPHYSICAL AND EXTRATERRESTRIAL PHENOMENA

523.164 3736
Studies in Cosmic Radio Noise at Bangalore—S. Bhagavantum, M. Krishnamurthi and S. Ramakrishna. (*J. Indian Inst. Sci.*, vol. 43, pp. 97–103; April, 1961. The techniques in use at Bangalore for a radio survey of the sky and the disturbed sun at 28.6 Mc and 62 Mc are described.

523.164.3:551.507.362.2 3737
Interpretation of Cosmic-Noise Measurements at 3.8 Mc/s from Satellite 1960 nl—J. H. Chapman and A. R. Molozzi. (*Nature*, vol. 191, p. 480; July 29, 1961.) The analysis given is based on the assumption that observed variations in signal strength were due to three causes: 1) variation of radiation resistance of the antenna with the dielectric constant of the surrounding ionosphere, 2) restriction of the angular aperture at the antenna due to ionospheric refraction and polarization, and 3) variation of cosmic-noise power over the sky.

523.164.32:551.510.535 3738
Oscillations in the Refraction of Radio Waves Emitted by the Sun—B. M. Chikhachev. (*Radiotekh. Elektron.*, vol. 5, pp. 1359–1369; September, 1960.) Radio astronomy observations at sunrise in November and December, 1949, at wavelengths of 1.5 and 2 m showed a periodic variation of ionospheric refraction with uniform change of zenith distance of the sun. This variation is analyzed in terms of sunspot activity and the motion of "cellular" waves in the ionosphere [see 1680 of 1950 (Martyn)].

523.164.34 3739
Lunar Temperature Measurements at 3200 Mc/s—W. J. Medd and N. W. Broten. (*Planet. Space Sci.*, vol. 5, pp. 307–313; August, 1961.)

523.164.4 3740
Distribution of Brightness in Extragalactic Radio Sources—A. T. Moffet and P. Maltby. (*Nature*, vol. 191, pp. 453–454; July 29, 1961.) Measurements have been made at 31.3 cm λ both on N-S and E-W base lines with a resolution of about 1.5′. Interpretations are given of the asymmetry observed in 88 sources.

523.164.4 3741
The Radio Source Hercules *A*—P. J. S. Williams, D. W. Dewhirst, and P. R. R. Leslie. (*Observatory*, vol. 81, pp. 64–68 plate; April, 1961.) Interferometer observations were made at 178 Mc on the two components of the intense source. The separation in declination is $0'.32 \pm 0'.60$.

523.164.4 3742
Central Component of the Radio Source Centaurus *A*—P. Maltby. (*Nature*, vol. 191, pp. 793–794; August 19, 1961.) Observations made with a variable-spacing interferometer at 21.6 and 31.3 cm show that the radiation originates outside the wide dust band.

523.165 3743
Flux and Energy Spectra of the Protons in the Inner Van Allen Belt—J. E. Naugle and D. A. Kniffen. (*Phys. Rev. Lett.*, vol. 7, pp. 3–6; July 1, 1961.)

523.165 3744
Energy Spectrum of Electrons Trapped in the Geomagnetic Field—M. Walt and W. M. MacDonald. (*J. Geophys. Res.*, vol. 66, pp. 2047–2052; July, 1961.) Solutions of the Fokker-Planck equation for the electron distribution function are obtained by reducing the equation to an eigenvalue problem. The spectrum obtained with a source of decaying albedo neutrons is at variance with the observed result.

523.165:551.507.362.2 3745
Characteristics of the Van Allen Radiation Zones as Measured by the Scintillation Counter on Explorer VI—A. Rosen and T. A. Farley. (*J. Geophys. Res.*, vol. 66, pp. 2013–2028; July, 1961.) Results were obtained over a period of four weeks from a counter recording fluxes of electrons above 200 kev and protons above 2 Mev. A geomagnetic storm which occurred about a week after launching the satellite produced an immediate increase in the counting rate; large fluctuations in particle intensity were observed at the edge of the outer Van Allen belt during the storm, which were closely related to simultaneous geomagnetic activity.

523.5 3746
On Meteor Ablation in the Atmosphere—F. Verniani. (*Nuovo Cim.*, vol. 19, pp. 415–442; February, 1961.) Improvements to the usually adopted theory are given and approximate expression suggested for the fundamental equation of ablation of low-velocity meteors.

523.5:621.396.96 3747
Reduction of Meteor Velocities from Continuous-Wave Radio Records—D. W. R. McKinley and E. L. R. Webb. (*Monthly*

Notices Roy. Astron. Soc., vol. 122, no. 3, pp. 255–262; 1961.) An analysis of the reduction technique used at Ottawa shows that in velocity measurements any statistical bias was positive and less than 1 per cent.

550.385.37 3748

Some Studies of Geomagnetic Micropulsations—R. A. Duncan. (*J. Geophys. Res.*, vol. 66, pp. 2087–2094; July, 1961.) Recordings made at four stations in Australia are analyzed. The period of the continuous type of oscillation (*Pc*) increases with latitude, and also varies diurnally. The damped trains of oscillations (*Pt*), occurring mainly near midnight, are followed by magnetic bays with an average delay of about 15 minutes. Effects observed during magnetic storms are discussed.

550.385.4 3749

Some Features of Magnetic Storms in High Latitudes—D. G. Knapp. (*J. Geophys. Res.*, vol. 66, pp. 2053–2085; July, 1961.) Ionospheric currents in high latitudes during magnetic disturbances are deduced from magnetic data. Lists of disturbances, during and prior to the I.G.Y., are given.

551.507.362:523.3/.4 3750

The National Program for Lunar and Planetary Exploration—A. R. Hibbs. (*J. Geophys. Res.*, vol. 66, pp. 2003–2012; July, 1961.) An illustrated description of the "Ranger" and other planned spacecraft.

551.507.362:537.56 3751

Excitation of Plasma Waves by Bodies Moving in Ionized Atmosphere—K. P. Chopra. (*Planet. Space Sci.*, 1961, vol. 5, pp. 288–291; August, 1961.) An ionized cloud, formed in front of a rapidly moving body, excites waves by interaction with the ambient plasma. Extraordinary electromagnetic waves are generated in the presence of a suitable week magnetic field.

551.507.362.1:550.380.8 3752

On the Interplanetary Magnetic Storm: Pioneer V—P. J. Coleman, Jr, C. P. Sonett, and L. Davis, Jr. (*J. Geophys. Res.*, vol. 66, pp. 2043–2046; July, 1961.) A magnetic field of 20 to 50 γ was detected by Pioneer V perpendicular to the sun-earth line during periods of intense solar activity between March 26 and April 6, 1960. Quiet-time fields of 2.7 γ were observed on other occasions.

551.507.362.1:550.385.4:523.14 3753

Magnetic Storms in Interplanetary Space as Observed by Pioneer V—E. W. Greenstadt. (*Nature*, vol. 191, pp. 329–331; July 22, 1961.) A positive correlation is found between the interpanetary field measured at the satellite and the planetary magnetic index a_p during the flight of Pioneer V from launch on March 11, 1960 to the end of April. Magnetic storms at the satellite occur at the same time as earth storms although there is a slight delay towards the end of the period of telemetry.

551.507.362.2 3754

Satellite Flashing-Light System—R. Freed and L. S. Klivans. (*Electronic Ind.*, vol. 20, pp. 94–98; April, 1961.) To provide increased accuracy of the determination of the position of a satellite, a coded flashing-light system could be carried. Design details are given.

551.507.362.2 3755

Effect of an Oblate Rotating Atmosphere on the Orientation of a Satellite Orbit—G. E. Cook. [*Proc. Roy. Soc.* (*London*) *A*, vol. 261, pp. 246–258; April 25, 1961.] For inclinations of 60°–70° in particular, significant rotation of the major axis in the orbital plane occurs due to the atmosphere.

551.507.362.2 3756

Atmospheric Phenomena noted in Simultaneous Observations of 1958 δ2 (Sputnik III)—J. Aarons, H. E. Whitney, R. S. Roger, J. Thomson, J. Bournazel, E. Vassy, H. A. Hess, K. Rawer, N. Carrara, P. Checcacci, B. Landmark, J. Troim, B. Hultqvist and L. Liszka. (*Planet. Space Sci.*, vol. 5, pp. 169–184; July, 1961.) Events occurring in three typical revolutions of Sputnik III are described; measurements were made on the 20 Mc transmissions. Signal drop-outs due to transmitter failure were noted and another type of signal decrease was attributed to localized absorbing regions. Regions of the ionosphere causing scintillation were also identified; they have an extent in the horizontal plane of several hundred km.

551.507.362.2 3757

Methods of Calculating Atmospheric Densities from Satellite Orbit Data—G. V. Groves. (*Planet. Space Sci.*, vol. 5, pp. 314–320; August, 1961. In French.) Formulas relating atmospheric density to the rate of change of period of a satellite as obtained by various workers are reviewed, and are shown to be in sufficient agreement to meet practical needs.

551.507.362.2:523.164:621.391.812 3758

Ray Paths from a Cosmic Radio Source to a Satellite in Orbit—C. B. Haselgrove, J. Haselgrove, and R. C. Jennison. [*Proc. Roy. Soc.* (*London*) *A*, vol. 261, pp. 423–434; May 16, 1961.] A satellite above the F_2 maximum can receive radiation on frequencies that are totally reflected by the ionosphere. Two effects of reflection in the upper part of the ionosphere are discussed: 1) focusing, and 2) interference. Both occur particularly when a satellite enters or leaves a region in which it can receive radiation from a point source in space.

551.507.362.2:523.72 3759

Measurement of Solar X-Radiation—K. A. Pounds. (*J. Brit. IRE*, vol. 22, pp. 171–175; August, 1961.) The X-ray emission measuring equipment to be carried in Skylark rockets and the satellite U.K. 1 is described. Both X-ray flux and spectral shape are to be investigated.

551.507.362.2:551.510.535 3760

Local Electron Densities deduced from the Faraday Fading of Satellite Transmissions using Measurements during Two Consecutive Transits—L. Liszka. (*Planet. Space Sci.*, vol. 5, pp. 213–219; July, 1961.) In the analysis it is assumed that during the period of revolution of the satellite the relative gradients of the local electron density are constant at the same altitudes and the changes in density above the F_2 maximum are the same as those within the F_2 layer. Daytime observations of 1958 δ2 in September, 1959, have been analyzed.

551.507.362.2:621.391.812.63 3761

Scintillations and the Latitude Distribution of Ionospheric Irregularities—D. G. Singleton. (*Nature*, vol. 191, pp. 482–483; July 29, 1961.) Evidence is given in support of Kent's interpretation of the rapid fading of earth-satellite signals (488 of 1960). Mawdsley's alternative explanation of scattering by field-aligned irregularities (4215 of 1960) is not confirmed by experiment.

551.507.362.2:621.396.9 3762

Radio Tracking of Artificial Earth Satellites—Pressey. (See 3784.)

551.507.362.2:621.396.963.3 3763

Tracking and Display of Earth Satellites—Van Golder, Jr. (See 3798.)

551.510.53 3764

Charged Particles in the Upper Atmosphere—A. Dalgarno. (*Ann. Géophys.*, vol. 17, pp. 16–49; January–March, 1961. In English.) A comprehensive review of collision processes involving charged particles in the upper atmosphere. 225 references.

551.510.53 3765

Structure, Variations and Measurements of the Earth's Ionosphere and Exosphere—C. Altman. (*Bull. Res. Counc. Israel*, vol. 90, pp. 39–48; February, 1961.) A survey of present knowledge and work being conducted at the Technion, Israel Institute of Technology, Haifa.

551.510.53 3766

The Distribution of Minor Ions in Electrostatic Equilibrium in the High Atmosphere—P. Mange. (*J. Geophys. Res.*, vol. 65, pp. 3833–3834; November, 1960.) A simple discussion of the factors which govern the distribution of ions in diffusive equilibrium. The scale height of the predominant ion is twice that of the corresponding neutral constituent, and the concentration of a minor light ion can increase with altitude.

551.510.53 3767

Comments on Tidal Winds in the High Atmosphere—B. Haurwitz. (*Planet. Space Sci.*, vol. 5, pp. 196–201; July, 1961.) The accuracy of published data on tidal wind variations are discussed on the basis of computations of the indices of the probable-error circle: variations with seasons and elevation are real although their magnitudes may be unreliable.

551.510.535 3768

Diffusion in the Ionosphere: A Review of some Recent Work—V. C. A. Ferraro. (*Ann. Géophys.*, vol. 17, pp. 82–89; January–March, 1961. In English.) Work by Gliddon and Kendall (2738 of 1960) shows considerable support for the hypothesis that F_1 and F_2 regions are produced by the same source of ionization.

551.510.535 3769

The Lunar Variation of the Virtual Height of the Normal Ionospheric E layer above Fribourg—P. Rougerie. (*Ann. Géophys.*, vol. 17, pp. 145–146; January–March, 1961. In English.) A semidiurnal lunar variation of 0.1 km has been detected with a maximum at 0830 lunar time.

551.510.535 3770

Theory of Overhead Nonblanketing Sporadic E—J. Renau. (*J. Geophys. Res.*, vol. 66, pp. 2121 2128; July, 1961.) Sequences of $h'(f)$ curves are calculated for an E layer in which a horizontal stratum of irregularities 1–2 km thick is slowly descending. The results are very similar to recorded sequences of ionograms showing sporadic E.

551.510.535 3771

Observations on the Ionospheric F Layer at Night: Part 2—The Law of Electron Loss in the F layer—C. S. G. K. Setty. (*J. Inst. Telecommun. Engrs., India*, vol. 7, pp. 65–77; March, 1961.) At night, electrons in the F layer are lost by attachment-like processes. The loss coefficients are of the form $K = K_0 \exp [h_0 - h)/H_k]$ where h_0 is the height at which $K_1 = K_0$ and H_k is the scale height of the loss coefficient. Assuming the loss coefficients are attributable to loss rates in chemical processes, H_k values correspond to those of molecular oxygen and nitrogen. Part 1: 3395 of November.

551.510.535 3772

Equatorial Spread-F in Relation to Post-Sunset Height Changes and Magnetic Activity—M. S. V. G. Rao and B. R. Rao. (*J. Geophys. Res.*, vol. 66, pp. 2113–2120; July, 1961.) The seasonal dependence of the correla-

tions is found, and the data are considered in relation to Martyn's theory of the formation of spread F (see 1555 of 1959).

551.510.535:550.385.4 3773
On the Relation between Magnetic Storm and Ionospheric Disturbances that Occurred on Sept. 13th 1957—Y. Hakura, M. Nagai, and Y. Sano. (*J. Radio Res. Labs., Japan*, vol. 8, pp. 81–95; March, 1961.) The patterns of dense E_s, blackouts and F_2-layer disturbance in the northern hemisphere are compared with the current systems of geomagnetic disturbance at different stages of the storm. With the development of polar-cap blackout, several hours before the sudden commencement of the storm, a current system was produced in the polar cap region. During the main phase, blackouts and E_s coincide with strong currents at auroral latitudes.

551.510.535:551.507.362.1 3774
Upper Atmospheric Turbulence near the 100 km Level—J. E. Blamont and C. de Jager. (*Ann. Géophys.*, vol. 17, pp. 134–144; January–March, 1961. In English.) An examination of observations of a sodium trail produced by a Véronique rocket in the upper atmosphere.

551.510.536 3775
Hydrogen Atoms and Ions in the Thermosphere and Exosphere—D. R. Bates and T. N. L. Patterson. (*Planet. Space Sci.*, vol. 5, pp. 257–273; August, 1961.) The structure of the atmosphere between 100 km and 500 km is discussed in terms of various models. For a further note on the temperature in the exosphere see *ibid.*, p. 328.

551.510.536:551.507.362.2 3776
Variable Conditions of the Terrestrial Exosphere—H. K. Paetzold and H. Zschörner. (*Astronautica Acta*, vol. 6, no. 6, pp. 373–381; 1960.) The well-known features of atmospheric density variations as deduced from satellite observations are discussed. Data for at least ten satellites show evidence of an annual variation in atmospheric density with a minimum in July, the amplitude of the variation increasing with altitude.

551.510.536:551.594.6 3777
Exospheric Electron Density Variations deduced from Whistlers—R. A. Helliwell. (*Ann. Géophys.*, vol. 17, pp. 76–81; January–March, 1961. In English.) New data on electron density are presented. Density is approximately proportional to the strength of the earth's magnetic field. An unexplained annual variation, in which the December value is nearly twice that in June, is reported.

551.593 3778
Altitudes of the Night Airglow Radiations—D. M. Packer. (*Ann. Géophys.*, vol. 17, pp. 67–75; January–March, 1961. In English.) Observational methods for obtaining the layer heights of air-glow emission are briefly reviewed and results derived from ground measurements, rocket flights and kinetic temperatures are discussed.

551.593.551.507.362.1 3779
Attempt to Measure Night Helium Glow—Evidence for Metastable Molecules in the Night Ionosphere—E. T. Byram, T. A. Chubb, and H. Friedman. (*J. Geophys. Res.*, vol. 66, pp. 2095–2100; July, 1961.) A rocket experiment, intended to measure the intensity of night-time He glow (wavelengths 584 Å and 304 Å) gave negative results, but provided some evidence for the existence of metastable molecules above 100 km.

551.594.5 3780
Some Auroral Observations inside the Southern Auroral Zone—J. V. Denholm. (*J. Geophys. Res.*, vol. 66, pp. 2105–2111; July, 1961.)

551.594.6 3781
Guiding of Whistlers by the Magnetic Field—R. Gendrin. (*Planet. Space Sci.*, vol. 5, pp. 274–282; August, 1961. In French.) A mechanism is proposed which explains the wideband noise observed during whistler reception. A particle moving with velocity $c f_H/2f_0$, where f_H is gyrofrequency and f_0 is plasma frequency, causes a wave to be propagated along the earth's magnetic field; all frequency components of the wave travel with the same velocity. See 201 of February (Smith).

551.594.6 3782
The Dispersion of Whistlers Compared with the Geomagnetic Latitudes of their Sources—H. Norinder and E. Knudsen. (*Planet. Space Sci.*, vol. 5, pp. 326–328; August, 1961. In French.) Observational results are presented which indicate that the geomagnetic latitude of lightning discharges is a factor determining the dispersion constant of the related whistlers.

LOCATION AND AIDS TO NAVIGATION

621.396.9 3783
Development Trends of Modern Location Techniques: Correlation Location Methods—F. H. Lange. (*Nachrtech.*, vol. 11, pp. 2–7; January, 1961.) The application of the principles of "correlation electronics" (3630 of 1958) to radiolocation systems is discussed.

621.396.9:551.507.362.2 3784
Radio Tracking of Artificial Earth Satellites—B. G. Pressey. (*J. Brit. IRE*, vol. 22, pp. 97–107; August, 1961.) The three principal methods using 1) radar, 2) Doppler frequency shift, and 3) interferometer are outlined. The construction, operation and performance of the interferometer system used in the U. S. Minitrack network are described.

621.396.933.2 3785
Controlled (h/d) Flight Path System for Use during Climb and Descent—R. D. Ryan. (*J. Inst. Nav.*, vol. 14, pp. 195–201; April, 1961.) Any of a number of accurate straight or curved flight paths may be selected in an attachment for the Australian DME system.

621.396.933.2 3786
Phase Difference Observations at Spaced Aerials and their Application to Direction Finding—W. C. Bain. (*J. Res. NBS*, vol. 65D, pp. 229–232; May/June, 1961.) Measurements on frequencies near 6 Mc are shown to give results indicating that the performance of a wide-aperture direction finder should not fall seriously below theoretical expectation.

621.396.933.2 3787
Research at the National Bureau of Standards applicable to Long-Distance Location and Direclon- Finding Problems—R. Silberstein. (*J. Res. NBS*, vol. 65D, pp. 233–235; May/June, 1961.) A general account of work undertaken since 1941 including references to the development of a technique for determining polarization error, the development of Loran-C, a rapid-scan directional aerial, and the study of non-great-circle bearings.

621.396.933.2 3788
Instrumentation for Propagation and Direction-Finding Measurements—E. C. Hayden. (*J. Res. NBS*, vol. 65D, p. 253; May/June, 1961.) Summary of a conference paper in which the limitations imposed on radio DF systems are discussed and two specific systems for use with wide-aperture arrays are proposed.

621.396.933.2 3789
Brooke Variance Classification System for D.F. Bearings—E. M. L. Beale. (*J. Res. NBS*, vol. 65D, pp. 255–261; May/June, 1961.)

621.396.933.2 3790
Estimation of Variances of Position Lines from Fixes with Unknown Target Positions—E. M. L. Beale. (*J. Res. NBS*, vol. 65D, pp. 263–273; May/June, 1961.) See also 3789 above.

621.396.933.2:621.391.812.63 3791
Influence of Ionospheric Conditions on the Accuracy of High-Frequency Direction Finding—P. J. D. Gething. (*J. Res. NBS*, vol. 65D, pp. 225–228; May/June, 1961.) During ionospheric storms bearing accuracy is reduced when fixes result from signals propagated via the F_2 layer.

621.396.933.2:621.396.663 3792
Design for Spinning-Goniometer Automatic Direction Finding—W. J. Lindsay and D. S. Heim. (*J. Res. NBS*, vol. 65D, pp. 237–243; May/June, 1961.) The construction of an automatic sensing unit and of a bearing read-out computer is considered. The advantages of narrow-band synchronous post-detection filtering are discussed.

621.396.96 3793
Secondary Surveillance Radar—D. H. R. Archer. (*Electronic Engr.*, vol. 33, pp. 414–420 and 490–494; July and August, 1961.) System design problems are discussed, in particular methods of suppressing sidelobe effects. The application of a secondary-radar system for data transmission is considered.

621.396.962.3 3794
Superregenerative Pulse Radar—F. H. Shepard, Jr. (*Proc. Radio Club Amer.*, vol. 37, Winter, 1960/1961.) For pulse reception, where broad bandwidths are used, the SNR is equal to that of other receiving systems. The basic circuit of a superregenerative radar transmitter-receiver is shown and a double-pulse technique for an A-scope display is outlined.

621.396.962.3 3795
A Monopulse Instrumentation System—F. P. Storke, Jr. (PROC. IRE, vol. 49, pp. 1328–1329; August, 1961.) The tracking error relative to the beam width is expressed in terms of the differential phase shifts before and after the comparing hybrid. The importance of the latter is shown and a system is described which is insensitive to phase shifts in the IF amplifier since reference and error signals undergo the same phase shift in it. See 1240 of 1960 (Rhodes).

621.396.962.33 3796
Detection Range Predictions for Pulse Doppler Radar—S. A. Meltzer and S. Thaler. (PROC. IRE, vol. 49, pp. 1299–1307; August, 1961.) A mathematical model is constructed. It is applicable to situations where thermal noise and sidelobe clutter limit detection range, and allows for variation of most of the important radar parameters.

621.396.963.3 3797
C.R.T. Display of Alphanumeric Information Applied to Radar Data Handling—J. S. Johnston. (*J. Brit. IRE*, vol. 22, pp. 139–143; August, 1961.) The problem of extracting and displaying in alpha-numeric form the information presented by long-range radar is discussed. A writing speed of 3×10^5 characters/sec is possible.

621.396.963.3:551.507.362.2 3798
Tracking and Display of Earth Satellites—A. Van Gelder, Jr. (PROC. IRE, vol. 49, pp.

1332–1333; August, 1961.) Comment on 2393 of 1960 (Slack and Sandberg). Several errors are corrected and certain steps in the derivation are questioned.

621.396.969.3:551.507.362.2 3799
Project Echo: Satellite-Tracking Radar—O. E. De Lange. (*Bell. Syst. Tech. J.*, vol. 40, pp. 1157–1182; July, 1961.) A 961-Mc system with 60-ft and 18-ft paraboloids as transmitting and receiving antennas respectively is described. The transmitting system is shared with the "Echo" communications channel, 2.5 kw being then available for radar. The 18-ft paraboloid is conically scanned and feeds a receiver incorporating a parametric amplifier with a sensitivity of −150 dbm in a 100-cps bandwidth. Radar and optical pointing were found usually to agree to within a few tenths of a degree, but computed orbital azimuth data were in error by up to 1.2°.

MATERIALS AND SUBSIDIARY TECHNIQUES

535.215 3800
Temperature-Dependent Bismuth-Cesium Photosurfaces—R. J. Zollweg and C. R. Taylor. (*J. Appl. Phys.*, vol. 32, pp. 1316–1319; July, 1961.) The sensitivity variation with temperature depends on the presence of oxygen and upon the size of the aggregates in the photosurface.

535.215:546.48'221 3801
Photosensitivity and Speed of Response in Cadmium Sulphide—D. Shaw. (*Brit. J. Appl. Phys.*, vol. 12, pp. 337–341; July, 1961.) Photoconductivity and photocurrent decay times have been measured for a large number of crystals of widely varying photosensitivity over an illumination range 0.007–875 ft candles.

535.215:546.48'221 3802
***p*-Type Photoconductivity and Infrared Quenching in Electron-Bombarded CdS**—B. A. Kulp and R. H. Kelley. (*J. Appl. Phys.*, vol. 32, pp. 1290–1292; July, 1961.)

535.215:546.48'221 3803
Analysis of Photojunctions Formed by Diffusing Copper into Insulating Cadmium Sulphide Crystals—R. R. Bockemuehl, J. E. Kauppila, and D. S. Eddy. (*J. Appl. Phys.*, vol. 32, pp. 1324–1330; July, 1961.)

535.37 3804
Lead- and Manganese-Activated Calcium Cadmium Silicate Phosphors—Y. Uehara, Y. Kobuke, I. Masuda, and T. Kushida. (*J. Electrochem. Soc.*, vol. 108, pp. 235–238; March, 1961.)

535.376:546.681'18 3805
Electroluminescence at *p-n* Junctions in Gallium Phosphide—M. Gershenzon and R. M. Mikulyak. (*J. Appl. Phys.*, vol. 32, pp. 1338–1348; July, 1961.)

537.226:538.566.2.029.6 3806
Dispersion of the Permeability and Permittivity of Artificial Dielectrics in the Frequency Range 500–35000 Mc/s I. A. Deryugin and M. A. Sigal. (*Zh. Tekh. Fiz.*, vol. 31, pp. 100–108; January, 1961.) A report of measurements of the frequency dependence of the properties of Cu powders in paraffin.

537.226:546.814–31 3807
Dielectric Properties of SnO_2—L. V. Deshpande and V. G. Bhide. (*Nuovo Cim.*, vol. 19, pp. 816–817; February 16, 1961.) Samples of SnO_2 in ceramic and compressed powder form have a dielectric constant of the order of 10^5 and show ferroelectric properties.

537.227:546.42'824–31 3808
Nonlinearity and Microwave Losses in Cubic Strontium-Titanate—G. Rupprecht, R. O. Bell, and B. D. Silverman. (*Phys. Rev.*, vol. 123, pp. 97–98; July, 1961.) A summary and interpretation of results of measurements made on single crystals, at temperatures from 90°K to 230°K and frequencies from 1 to 36 Gc.

537.227:546.431'824–31 3809
Perfectness of Macrodomains of $BaTiO_3$ Crystals—K. Aizu and O. Nakada. (*J. Phys. Soc. Japan*, vol. 16, pp. 923–927; May, 1961.) A statistical investigation based on thermodynamics shows that a plate thicker than 2×10^{-6} cm contains practically no reversely polarized microdomains.

537.227:546.431'824–31 3810
Surface Layers on Barium Titanate Single Crystals above the Curie Point—H. Schlosser and M. E. Drougard. (*J. Appl. Phys.*, vol. 32, pp. 1227–1231; July, 1961.) Dielectric dispersion measurements have been carried out on $BaTiO_3$ single crystals of different thickness at temperatures above the Curie point up to 180°C.

537.227:546.431'824–31 3811
Investigation of Rare-Earth-Doped Barium Titanate—V. J. Tennery and R. L. Cook. (*J. Amer. Ceram. Soc.*, vol. 44, pp. 187–193; April 1, 1961.) The effect of additions of rare-earth oxides on the dc resistivity of $BaTiO_3$ is investigated.

537.227:546.431'824–31 3812
Effect of WO_3 on Dielectric Properties of $BaTiO_3$ Ceramics—V. Ern and R. E. Newnham. (*J. Amer. Ceram. Soc.*, vol. 44, p. 199; April 1, 1961.)

537.227:546.431'824–31 3813
Dielectric Properties of $BaTiO_3$ Single Crystals in the Paraelectric State from 1 kc/s to 2000 Mc/s—E. Stern and M. Lurio. (*Phys. Rev.*, vol. 123, pp. 117–123; July 1, 1961.)

537.227:621.372.44 3814
Antiferroelectric Ceramics with Field-Enforced Transitions: a New Nonlinear Circuit Element—B. Jaffe. (Proc. IRE, vol. 49, pp. 1264–1267; August, 1961.) Ceramic dielectrics have been prepared which undergo field-enforced antiferroelectric-to-ferroelectric transitions from below −60°C to over 100°C. The transition is indicated by a D/E hysteresis figure with a linear central region and loops showing saturation on either end. Capacitance nonlinearity, energy storage and transducer properties are described.

537.228.1/.2:547.476.3 3815
The Piezoelectricity and Electrostriction of Rochelle Salt—G. Schmidt. (*Z. Phys.*, vol. 161, pp. 579–603; February 14, 1961.) Detailed report of measurements and discussion of results with particular reference to the ferroelectric anomaly of Rochelle salt.

537.228.1:549.514.41 3816
Piezoelectricity of Quartz for Finite Strain—S. Machlup and M. E. Christopher. (*J. Appl. Phys.*, vol. 32, pp. 1387–1391; July, 1961.) Calculation of the principal piezoelectric coefficient using a hard-sphere, rigid-ion model.

537.311.33 3817
Behaviour of Hot Electrons in Microwave Fields—B. V. Paranjape. (*Phys. Rev.*, vol. 122, pp. 1372–1375; June 1, 1961.) A theoretical investigation is made of the currents produced by hot electrons when a weak microwave field is superimposed on a strong steady electric field, and also the effect of a strong microwave field alone. An alternating current at the same frequency as the applied field and leading it in phase is produced.

537.311.33 3818
Electron-Electron Scattering and Transport Phenomena in Nonpolar Semiconductors—J. Appel. (*Phys. Rev.*, vol. 122, pp. 1760–1772; June 15, 1961.) Electron-electron scattering causes electrical conductivity to be reduced less than the electronic heat conductivity. Its influence on electrical conductivity, heat conductivity and the Seebeck coefficient is calculated as a function of temperature, and its effect on transport phenomena is briefly considered.

537.311.33 3819
Alternative Approach to the Solution of Added Carrier Transport Problems in Semiconductors—J. P. McKelvey, R. L. Longini, and T. P. Brody. (*Phys. Rev.*, vol. 123, pp. 51–57; July 1, 1961.) A method is described for computing carrier fluxes by solving the continuity equation in terms of a Green's function.

537.311.33 3820
Mechanism of Impurity Conduction in Semiconductors—J. Mycielski. (*Phys. Rev.*, vol. 123, pp. 99–103; July 1, 1961.) The conductivity of impurities at low temperatures is discussed in terms of jumps over the Coulomb potential barrier between empty and occupied impurity centres. Calculations relating to anomalies of activation energy are made.

537.311.33 3821
Current-Carrier Transport with Space Charge in Semiconductors—W. Van Roosbroeck. (*Phys. Rev.*, vol. 123, pp. 474–490; July 15, 1961.) A theory is developed for one-dimensional drift of carriers, taking into account the space charge which can develop in high-resistance materials. The theory is exact for small-signal field variations.

537.311.33 3822
The Scattering of Phonons by Bound Electrons in a Semiconductor—I. C. Pyle. (*Phil. Mag.*, vol. 6, pp. 609–616; May, 1961.)

537.311.33:534.28 3823
Interaction of Electrons and Holes with Acoustic Waves in Intrinsic Semiconductors—N. Mikoshiba. (*J. Phys. Soc. Japan*, vol. 16, pp. 895–905; May, 1961.) A self-consistent theory is produced which shows that the acoustoelectromotive force is too small to be detected by experiment.

537.311.33:535.215 3824
On the Study of Volume Recombination of Excess Charge Carriers in Semiconductors with the Aid of Photoconductance—B. H. Schultz. (*Philips Res. Rep.*, vol. 16, pp. 175–181; April, 1961.) By measuring amplitude and phase of photoconductance in different ambients, it is possible in some cases to determine the surface effects, and reliable volume-recombination times can be deduced.

537.311.33:535.34–15 3825
Contribution of Lattice Scattering between Nonequivalent Valleys to Free-Carrier Infrared Absorption in Semiconductors—H. Risken and H. J. G. Meyer. (*Phys. Rev.*, vol. 123, pp. 416–419; July 15, 1961.)

537.311.33:538.614 3826
The Faraday Effect in Nondegenerate Semiconductors—B. Donovan and J. Webster. [*Proc. Phys. Soc.* (*London*), vol. 78, pp. 120–132; July 1, 1961.] The theory of the Faraday effect, in relation to microwave and infrared propagation in semiconductors is developed. Frequency and temperature dependence are investigated for *n*-type Ge.

537.311.33:538.63 3827
The Theory of Electrical Conductivity of Semiconductors in a Magnetic Field: Part 1—V. L. Gurevich and Yu. A. Firsov. (*Zh. Eksp. Teor. Fiz.*, vol. 40, pp. 199–213; January, 1961.) A quantum theory of the transverse conductivity of semiconductors in a strong magnetic field is developed, taking account of inelastic scattering of electrons.

537.311.33:538.63 3828
Galvanomagnetic Effects in Semiconductors at High Electric Fields—E. M. Conwell. (*Phys. Rev.*, vol. 123, pp. 454–463; July 15, 1961.) A theory of magnetoconductivity for general energy-band structure is evolved in a form convenient for the calculation of Hall coefficients and other galvanomagnetic effects for either low or high electric field strengths.

537.311.33:538.63 3829
Measurements of the Frequency Dependence of the Gauss Effect in Various Semiconductors up to 2000 Mc/s—M. J. O. Strutt and F. K. von Willisen. (*Arch. elekt. Übertragung*, vol. 15, pp. 25–32; January, 1961.) The Gauss effect in Corbino disks of Ge, InSb and InAs was measured in the frequency range 0–2 Gc as a function of temperature in the range 140°–270°K for flux densities up to 30 Mc. For earlier measurements of this galvanomagnetic effect see 2804 of 1957 (Ramer *et al.*).

537.311.33:539.23 3830
Field-Enhanced Donor Diffusion in Degenerate Semiconductor Layers—W. Shockley. (*J. Appl. Phys.*, vol. 32, pp. 1402–1403; July, 1961.) An expression for the effective diffusion constant is given.

537.311.33:[546.28+546.289]:535.215 3831
Photovoltages in Silicon and Germanium Layers—H. Kallmann, B. Kramer, E. Haidemanakis, W. J. McAleer, H. Barkemeyer, and P. I. Pollak. (*J. Electrochem. Soc.*, vol. 108, pp. 247–251; March, 1961.) Photovoltages of several thousand volts are observed between electrodes 1 cm apart when the layers are maintained at liquid-nitrogen temperatures and strongly illuminated. At room temperature, only a few hundred volts were produced. A possible explanation of this effect is suggested.

537.311.33:[546.28+546.289]:621.317.3(083.7) 3832
IRE Standards on Solid State Devices: Measurement of Minority-Carrier Lifetime in Germanium and Silicon by the Method of Photoconductive Decay—(Proc. IRE, vol. 49, pp. 1292–1299; August, 1961.) Standard 61 IRE 28.S2.

537.311.33:546.28 3833
The Formation of Dislocation-Free Silicon Single Crystals—G. Ziegler. (*Z. Naturforsch.*, vol. 16a, p. 219; February, 1961.) The configuration of dislocations in thin Si rods is investigated to obtain insight into the mechanism of dislocation reduction.

537.311.33:546.28 3834
Low-Frequency Conductivity due to Hopping Processes in Silicon—M. Pollak and T. H. Geballe. (*Phys. Rev.*, vol. 122, pp. 1742–1753; June 15, 1961.) The complex conductivity has been measured in n-type Si with various kinds of impurities at frequencies between 100 cps and 10 kc in the temperature range 1–20° K. In most cases it is several orders of magnitude higher than the measured dc conductivity; this is attributed to polarization caused by hopping processes. A simple theory is derived which is in good agreement with the observed variation of conductivity with frequency and concentration.

537.311.33:546.28 3835
Hot-Electron Emission from Silicon p-n Junctions Parallel to the Surface—J. L. Moll, N. I. Meyer, and D. J. Bartelink. (*Phys. Rev. Lett.*, vol. 7, pp. 87–90; August 1, 1961.) Experimental results are presented and compared with theoretical expressions which take into account the important types of interaction between the hot electrons and the crystal lattice.

537.311.33:546.28 3836
Forward Characteristics of Si p-π-n-Junctions—M. Tokunaga and K. Shono. (*J. Phys. Soc. Japan*, vol. 16, pp. 1029–1030; May, 1961.) A series of junctions were prepared in p-type Si crystals of resistivity 2–5 Ωcm, by diffusing B from one side and P from the other side of the crystal. I/V characteristics of junctions with π-regions of different width are shown and discussed.

537.311.33:546.289 3837
Electronic Effect in the Elastic Constants of Germanium—L. J. Bruner and R. W. Keyes. (*Phys. Rev. Lett.*, vol. 7, pp. 55–56; July 15, 1961.) A measured change in one of the elastic constants (C_{44}) of Ge when heavily doped with As is reported.

537.311.33:546.289 3838
Electric-Field-Induced Modulation of the Absorption due to Interband Transitions of Free Holes in Germanium—M. A. C. S. Brown and E. G. S. Paige. (*Phys. Rev. Lett.*, vol. 7, pp. 84–86; August 1, 1961.) Observations were made of the change in absorption due to a change in the distribution function of the free holes. Experimental data are given and discussed.

537.311.33:546.289 3839
Anodic Oxidation of Germanium—T. Gabor. (*J. Appl. Phys.*, vol. 32, pp. 1361–1363; July, 1961.) "On anodic polarization of etched samples of n-type or near-intrinsic p-type germanium, striations are formed. The periodic depletion of holes is advanced as a tentative explanation of the phenomenon."

537.311.33:546.289 3840
A Study of Growth Processes in Germanium Dendrites using Pulse Electroplating Techniques—R. C. Smith. (*J. Electrochem. Soc.*, vol. 108, pp. 238–241; March, 1961.) Separate mechanisms for axial and lateral growth have been identified. The observed resistivity boundary lines are due to the lateral growth mechanism.

537.311.33:546.289 3841
Influence of Wet and Dry Ambients on Fast Surface States of Germanium—Y. Margoninski and H. E. Farnsworth. (*Phys. Rev.*, vol. 123, pp. 135–140; July 1, 1961.) A specimen of n-type Ge was subjected to different gaseous environments. The effects of N_2, O_2 and water vapor on the surface states can be discussed separately.

537.311.33:546.289 3842
Determination of the Coefficient of Diffusion of Arsenic in Germanium by Measurement of the Thermoelectric Voltage—E. Batifol and G. Duraffourg. (*J. Phys. Radium*, vol. 21, Suppl., *Phys. Appl.*, pp. 207A–216A; November, 1960.) The surface concentration of As is obtained by measurement of 1) thermoelectric power, 2) sheet resistance. The mean value of the diffusion coefficient at 800° C is 1.3×10^{-11} cm²/sec.

537.311.33:546.289 3843
Recombination at Copper and at Nickel Centres in p-Type Germanium—B. H. Schultz. (*Philips Res. Repts.*, vol. 16, pp. 182–186; April, 1961.) An explanation is given for the different temperature dependence of recombination rates at Cu centers for partly compensated and noncompensated crystals. No solution could be found for the discrepancies which occur with Ni.

537.311.33:546.289 3844
Effect of Temperature and Doping on the Reflectivity of Germanium in the Fundamental Absorption Region—M. Cardona and H. S. Sommers, Jr. (*Phys. Rev.*, vol. 122, pp. 1382–1388; June, 1961.)

537.311.33:546.289:538.63 3845
Longitudinal Magnetoresistance in n-Type Germanium: Experimental—W. F. Love and W. F. Wei. (*Phys. Rev.*, vol. 123, pp. 67–73; July 1, 1961.) Curves showing the variation of the magnetoresistance ratio with magnetic field and temperature, in fields up to 300 kg and temperature from 20°K to 300°K, are presented and discussed.

537.311.33:546.289:538.63 3846
Longitudinal Magnetoresistance in n-Type Germanium: Theoretical—S. C. Miller and M. A. Omar. (*Phys. Rev.*, vol. 123, pp. 74–80; July 1, 1961.) Calculations of acoustic scattering give satisfactory agreement with the experimental results at high field strengths (3845 above).

537.311.33:546.289:621.391.822 3847
Slow Decay of Reverse Current and Noise in Field Effect on Ge p†-n Junction—H. Edagawa, Y. Morita, S. Maekawa, and Y. Inuishi. (*J. Phys. Soc. Japan*, vol. 16, pp. 1041–1042; May, 1961.) Current and noise measurements were made simultaneously at the junctions; results are presented in graphical form.

537.311.33:546.289:621.391.822 3848
Recombination Noise of Germanium Single Crystals in the Range of Defect Semiconduction—M. Pilkuhn. (*Z. Naturforsch.*, vol. 16a, pp. 173–182; February, 1961.) The frequency dependence of recombination noise was investigated in the range 100 cps–500 kc for various contact arrangements and specimen surfaces. Also investigated were the temperature characteristics of noise in the range 6–15°K, and the dependence on field strength of the spectral distribution function of noise.

537.311.33:546.289:621.391.822 3849
Fluctuation Phenomena in the Formation of Impact Ionization Avalanches in Ge Single Crystals between 5° and 10° K—M. Pilkuhn. (*Z. Naturforsch.*, vol. 16a, pp. 182–187; February, 1961.) The increase of noise observed during low-temperature breakdown in Ge is shown to be due to recombination effects. See also 3848 above.

537.311.33:546.47'241 3850
The Electrical Properties of Zinc Telluride—H. Tubota, H. Suzuki, and K. Hirakawa. (*J. Phys. Soc. Japan*, vol. 16, pp. 1038–1039; May, 1961.) The electrical resistivities and Hall coefficients of stoichiometric and Sb- or In-doped samples are given in graphical form.

537.311.33:546.681'18 3851
The Preparation and Floating-Zone Processing of Gallium Phosphide—C. J. Frosch and L. Derick. (*J. Electrochem. Soc.*, vol. 108, pp. 251–257; March, 1961.)

537.311.33:[546.682'19+546.682'18 3852
Infrared Cyclotron Resonance in n-Type InAs and InP—E. D. Palik and R. F. Wallis. (*Phys. Rev.*, vol. 123, pp. 131–134; July 1, 1961.)

537.311.33:546.682'86 3853
Anisotropic Segregation in InSb—W. P. Allred and R. T. Bate. (*J. Electrochem. Soc.*, vol. 108, pp. 258–261; March, 1961.)

537.311.33:546.682.86 3854
Pinch Effect in Indium Antimonide—A. G. Chynoweth and A. A. Murray. (*Phys. Rev.*, vol. 123, pp. 515–520; July 15, 1961.) A critical current of 4–5 a for the occurrence of pinch effect in InSb was measured by three different experimental methods.

537.311.33:546.682'86:535.215 3855
Properties and Applications of Indium Antimonide—R. E. J. King and B. E. Bartlett. (*Philips Tech. Rev.*, vol. 22, pp. 217–255; April 5, 1961.) The preparation of InSb crystals and the construction and performance of photocells based on InSb are described.

537.311.33:546.682'86:535.215 3856
Oscillatory Photoconductivity in InSb—W. Engeler, H. Levinstein and C. Stannard, Jr. (*Phys. Rev. Lett.*, vol. 7, pp. 62–63; July 15, 1961.) Cu, Ag, Au and Ni were added to InSb, and an oscillating curve was obtained for the photoconductive response as a function of incident wavelength at liquid-helium temperatures. The oscillations are attributed to the emission of successive longitudinal optical phonons.

537.311.33:546.682'86:538.632 3857
Corbino-Disk Magnetoresistivity Measurements on InSb—M. Green. (*J. Appl. Phys.*, vol. 32, pp. 1286–1289; July, 1961.)

537.311.33:546.811–17:538.63 3858
Magnetoresistance of Oriented Gray Tin Single Crystals—O. N. Tufte and A. W. Ewald. (*Phys. Rev.*, vol. 122, pp. 1431–1436; June 1, 1961.) The low-field magnetoresistance coefficients were evaluated from measurements on *n*- and *p*- type crystals at 77, 195 and 273°K. An explanation is given of the anisotropy observed in *n*-type crystals at 195 and 273°K.

537.311.33:546.824–31 3859
Nonohmic Behaviour in Near-Stoichiometric Rutile (TiO_2)—E. H. Greener and D. H. Whitmore. (*J. Appl. Phys.*, vol. 32, pp. 1320–1324; July, 1961.) Increase in ambient specimen temperature requires a higher field for the transition from ohmic to nonohmic behavior. At 908°C only ohmic currents are exhibited at the highest field-strength used (10 v/cm).

537.311.33:546.824–31:537.323 3860
Thermoelectric Behaviour of Rutile—K. Sakata. (*J. Phys. Soc. Japan*, vol. 16, p. 1026; May, 1961.) Thermo-EMF and conductivity have been measured as functions of temperature for samples sintered in O_2 at different pressures.

537.311.33:621.317.33 3861
Contactless Resistivity Meter for Semiconductors—J. C. Brice and P. Moore. (*J. Sci. Instrum.*, vol. 38, p. 307; July, 1961.) Resistivity is determined as a function of the eddy currents induced in the specimen by a 10-Mc oscillator. Resultant amplitude changes in the oscillator output are measured with a valve voltmeter.

537.311.33:669:061.3 3862
New Techniques for Producing Ultrapure Semiconductors—T. Maguire. (*Electronics*, vol. 34, pp. 41–45; July 7, 1961.) A review is given of the papers presented at the conference on ultrapurification of semiconductor materials, held at Boston, Mass.

537.312.62 3863
Magnetic Properties of Thin Superconducting Tin and Indium Films—B. K. Sevast'yanov. (*Zh. Eksp. Teor. Fiz.*, vol. 40, pp. 52–63; January, 1961.) The conditions for the absence of the normal phase in a superconducting film of finite size arranged at a small angle to a uniform magnetic field are determined. The dependence of the transverse component of the magnetic moment M on the temperature and thickness is determined for tin and indium films of thickness 4×10^{-3}–2×10^{-6} cm.

537.312.62:538.222 3864
Differential Paramagnetic Effect in Superconductors—R. A. Hein and R. L. Falge, Jr. (*Phys. Rev.*, vol. 123, pp. 407–415; July 15, 1961.)

537.312.62:539.23 3865
Size Effects in Thin Superconducting Indium Films—A. M. Toxen. (*Phys. Rev.*, vol. 123, pp. 442–446; July 15, 1961.)

538.221 3866
Distribution of the Magnetization in a Ferromagnet—M. W. Muller. (*Phys. Rev.*, vol. 122, pp. 1485–1489; June 1, 1961.) Analysis provides evidence that a stable nonuniform distribution is produced in a thick ferromagnetic slab in a large applied field, and that domains can appear if the anisotropy field is smaller than the demagnetizing field.

538.221 3867
Change of Thermal and Electrical Conductivity of Ferromagnetic Materials in a Magnetic Field—H. Papadimitraki. (*Z. Naturforsch.*, vol. 16a, p. 217; February, 1961.) Summary of experimental results obtained with Ni; the Lorentz number is plotted as a function of field strength over the range 0–4000 oersteds. Effects in Fe are too small to obtain quantitative results.

538.221 3868
Weak Field Behaviour of the ΔE Effect in Ferromagnetic Cubic-Solid-Solution Alloys—M. Yamamoto and S. Taniguchi. (*J. Phys. Soc. Japan*, vol. 16, pp. 1035–1036; May, 1961.)

538.221 3869
Magnetic Properties of Sintered Iron—H. Dietrich. (*Z. Metallkde*, vol. 52, pp. 232–235; April, 1951.) Magnetic data of unalloyed sintered iron are tabulated and the dependence of the characteristics on the manufacturing process and heat treatment is illustrated.

538.221 3870
On the Influence of the Formation of Subgrain Structures on the Magnetic Properties of Pure Iron—G. Montalenti and C. Sari. (*Nuovo Cim.*, vol. 19, pp. 605–608; February 1, 1961.) The formation of extremely stable subgrain structures which cannot be removed by further heat treatment, reduces considerably the permeability of iron specimens.

538.221 3871
Ferromagnetism in Solid Solutions of Scandium and Indium—B. T. Matthias, A. N. Clogston, H. J. Williams, E. Corenzwit, and R. C. Sherwood. (*Phys. Rev. Lett.*, vol. 7, pp. 7–9; July, 1961.)

538.221 3872
Magnetic Anisotropy and Rotational Hysteresis in Single Crystals of Magnetite Below the Transition Temperature—R. F. Pearson and R. Cooper. [*Proc. Phys. Soc.* (*London*), vol. 78, pp. 17–24; July 1, 1961.] Results of torque measurements, with some theoretical discussion.

538.221 3873
Magnetization of Nickel Single Crystals—L. Tterlikkis and A. W. Jenkins, Jr. (*J. Appl. Phys.*, vol. 32, pp. 1293–1296; July, 1961.) Anisotropy coefficients are calculated from experimental curves. A possible method of measuring internal strain energy is suggested.

538.221 3874
Magnetic Anisotropy of Heusler Single Crystal—K. Aoyagi and M. Sugihara. (*J. Phys. Soc. Japan*, vol. 16, p. 1027; May, 1961.) Experimental details of the growth and ferromagnetic properties of a crystal of Cu_2 Mn-Al.

538.221:537.533.72 3875
An Electron-Optical Method for the Measurement of the State of Magnetization of Ferromagnetic Specimens—C. Schwink. (*Z. Phys.*, vol. 161, pp. 560–578; February 14, 1961.) The feasibility of electron-optical measurements of magnetization is investigated theoretically for a cylinder with gap system [see also 1256 of May (Murrmann and Schwink)].

538.221:539.23 3876
The Preparation of Continuous Single-Crystal Thin Films of Nickel and Nickel-Iron Alloys—O. S. Heavens, F. F. Miller, G. L. Moss, and J. C. Anderson. [*Proc. Phys. Soc.* (*London*), vol. 78, pp. 33–37; July 1, 1961.]

538.221:539.23 3877
Magnetic Anisotropy in Single-Crystal Nickel Films—J. C. Anderson. [*Proc. Phys. Soc.* (*London*), vol. 78, pp. 25–32; July 1, 1961.]

538.221:539.23 3878
Field-Induced and Angle-of-Incidence Anisotropy in Nickel-Iron Films—E. Feldtkeller. (*Z. angew. Phys.*, vol. 13, pp. 74–76; February, 1961.) The magneto-optical Faraday effect is used to determine the contours of anisotropy orientation and field strength and of the wall coercivity.

538.221:539.23:538.61 3879
The Kerr Hysteresis Effect: a Phenomenon of Surface Magnetization—J. Kranz and B. Passon. (*Z. Phys.*, vol. 161, pp. 525–538; February 14, 1961.) Surface-magnetization curves for Fe-Si single crystals are obtained with the aid of the Kerr effect. See also 1281 of 1959 (Kranz and Drechsel).

538.221:539.23:538.614 3880
Observations of Cross-Tie Domain Walls by the Faraday Effect—A. L. Houde. (*J. Appl. Phys.*, vol. 32, pp. 1234–1237; July, 1961.) An apparatus for observation of the microscopic Faraday effect is described. The fine structure of the domain configurations in thin permalloy films has been observed.

538.221:539.23:621.385.833 3881
Transmission-Electron-Microscope Observations of Magnetic Domain Walls—J. T. Michalak and R. C. Glenn. (*J. Appl. Phys.*, vol. 32, pp. 1261–1265; July, 1961.) This technique for domain studies complements other techniques and is especially valuable for investigating magnetic films.

538.221:621.318.134 3882
The Theory of the High-Frequency Magnetic Susceptibility of Ferrodielectrics at Low Temperatures—I. A. Akhiezer, V. G. Bar'yakhtar, and S. V. Peletminsky. (*Zh. Eksp. Teor. Fiz.*, vol. 40, pp. 365–374; January, 1961.) The transverse components of the susceptibility tensor of a ferrite are calculated using methods of quantum field theory and taking both exchange and relativistic interactions between spin waves into account, and the ferromagnetic resonance line width is determined.

538.221:621.318.134 3883
A Note on the Electron Diffusion and the Wall Relaxation in Ferrites—H. Sekizawa. (*J. Phys. Soc. Japan*, vol. 16, pp. 1034–1035; May, 1961.) The distinction between the relaxation times due to the motion of electrons and wall relaxation is established.

538.221:621.318.134:538.652 3884
Theory of Magnetostriction in Cobalt-Manganese Ferrite—J. C. Slonczewski. (*Phys. Rev.*, vol. 122, pp. 1367–1372; June 1, 1961.)

538.221:621.318.4.042.1:534.2–8 3885
Studies of Magnetization Processes of Magnetic Cores by Supersonic Methods—K. Nishiguchi and H. Sawabe. (*Rev. Elec. Commun. Lab., Japan*, vol. 9, pp. 207–213; March/April, 1961.) When an ultrasonic vibration is applied to a magnetic core, the voltage output induced in a winding on the core is proportional to the remanent flux. This principle is applied to nondestructive investigation of the inner structure of magnetic cores.

538.221:621.318.57 3886
Two-Phase Permalloy for High-Speed Switching—E. A. Nesbitt and E. M. Gyorgy. (*J. Appl. Phys.*, vol. 32, pp. 1305–1308; July, 1961.) Gold added to permalloy makes precipitation of a second phase possible; coercive force and the threshold of rotational flux reversal can thus be controlled. Switching cores of such material are four times faster than standard cores.

538.22 3887
Abrupt Magnetic Transition in $MnSn_2$—J. S. Kouvel and C. C. Hartelius. (*Phys. Rev.*, vol. 123, pp. 124–125; July 1, 1961.)

539.2:538.569.4 3888
Spin-Lattice Relaxation in Imperfect Cubic Crystals and in Noncubic Crystals—E. R. Andrew and D. P. Tunstall. [*Proc. Phys. Soc. (London)*, vol. 78, pp. 1–11; July 1, 1961.]

548.5:535.215 3889
Vapour-Phrase Growth of Single Crystals of II–VI Compounds—W. W. Piper and S. J. Polich. (*J. Appl. Phys.*, vol. 32, pp. 1278–1279; July, 1961.)

669.018.5:537.311.33 3890
Capillary Alloying: an Improved Alloying Method—K. Lehovec, K. Busen, J. Casey, C. Pochop, and A. Webb. (*J. Electrochem. Soc.*, vol. 108, pp. 241–247; March, 1961.) Extremely flat, uniformly alloyed metal/semiconductor junctions can be produced with a separation from the wafer surface of less than 0.25 μ. Advantages of the technique over pellet alloying are the high degree of purity of the liquid alloy surface before alloying, and the possibility of comparing alloy compositions conveniently.

MATHEMATICS

512:621.318.57:681.142 3891
Symbolic Logic—B. R. Wilkins. (*Electronic Tech.*, vol. 38, pp. 317–324; September, 1961.) Elements of Boolean algebra and Venn diagrams are explained and their applications to verbal statements and to switching and computer circuits are considered.

517.941 3892
Six 'Natural' Normalizations of the Characteristic Equation of Third Degree—E. Schwartz. (*Arch. elekt. Übertragung*, vol. 15, pp. 94–100; February, 1961.) With the aid of the normalized equations and diagrams derived, the location of the roots in the complex plane can be determined; this leads to the solution of the linear homogeneous differential equation of third order on which the characteristic equation is based.

517.942.82 3893
A Theorem of the Laplace Transformation—G. Fodor. (*Period. Polyt., Bp., Elect. Engrg.*, vol. 5, pp. 41–56; 1961. In German.) The problem of dealing with the Laplace transform of the derivative of a discontinuous function is considered. The method of solution proposed simplifies practical application.

517.942.82 3894
The Solution of Ordinary and Partial Differential Equations by means of the One- and Multi-dimensional Laplace Transformation for Limited Ranges—A. Käch. (*Arch. elekt. Übertragung*, vol. 15, pp. 33–47; January, 1961.)

MEASUREMENTS AND TEST YEAR

529.78:621.317.755 3895
Precise Measurement of a Time Interval of the Order of One Microsecond—J. Bourguignon. (*J. Phys. Radium*, vol. 21, Suppl., *Phys. Appl.*, pp. 217A–218A; November, 1960.) A simple modification of normal oscillographic technique is described, giving a triangular-waveform display with marker traces. Accuracy of the order of 5 nsec is obtained.

621.3.018.41(083.74) 3896
A Magnetic Shield for Beam Frequency Standards—F. S. Barnes, (PROC. IRE, vol. 49, p. 1328; August, 1961.) To reduce the frequency uncertainty of caesium-beam frequency standards, caused by stray electromagnetic fields, a magnetic shield of superconducting material is proposed instead of the more usual mumetal.

621.317(083.74) 3897
Measurement and Standardization—J. Cassassolles. (*Rev. gén. Élect.*, vol. 70, pp. 201–207; April, 1961.) A review of the work done by the Union Technique de l'Électricité (U.T.E.) on standardization of methods of measurement, measuring equipment and different reference standards.

621.317.029.6:[541.135+621.318.134 3898
New Methods of Studying Concentrated Electrolytes and Ferromagnetic Oxides at Very Short Wavelengths—J. C. Lestrade. (*Rev. gén. Élect.*, vol. 70, pp. 99–122; February, 1961.) Techniques of measurement at frequencies up to 4 Gc are described and results of measurements of the permittivity of several concentrated electrolytic solutions and the gyromagnetic resonance of γ-Fe_2O_3 and Fe_3O_4 are presented. An interpretation of observed phenomena is given. 62 references.

621.317.081.6(083.74) 3899
The Origin of International Electrical Units and their Present Situation—R. Hérou. (*Rev. gén. Élect.*, vol. 70, pp. 222L–236L; March, 1961.) A brief history is given of the development of electrical standards and the definitions of the standard ohm, volt, and ampere adopted by international committees from 1881 to 1948 are tabulated.

621.317.332.6.029.6 3900
Measurement of Low Reflection Coefficients at High Frequencies—K. Kohler. (*Frequenz*, vol. 15, pp. 12–17; January, 1961.) The principle of the method which is applicable to coaxial systems and waveguides is described. A commercial-type directional coupler with a quadripole tuned by stubs is used. See also 3567 of 1958 (Linnebach).

621.317.373:621.3.018.783 3901
The Effect of Nonlinear Distortion on Errors in Measuring the Phase Shift between Two Voltages—B. G. Kaduk. (*Izmer. Tekh.*, no. 6, pp. 44–45; June, 1961.) Formulas applicable to the measurement of phase difference are derived.

621.317:4.538.221:539.23 3902
Method for Measuring the Anisotropy Function of Thin Magnetic Films—T. D. Rossing and R. Stolen. (*Rev. Sci. Instr.*, vol. 32, pp. 752–753; June, 1961.) A simple apparatus is described in which the ac field coil and pick-up coil can be rotated together. The method gives a more accurate value for the anisotropy field than the usual hysteresis method.

621.317.725.029.5/.6 3903
Measuring Low-Level R.F. Voltage with Servo Feedback Techniques—T. C. Anderson. (*Electronics*, vol. 34, pp. 63–65; July 14, 1961.) A millivoltmeter is described which has seven voltage ranges, covering 10 mv to 10 v rms, and operates over the frequency range 500 kc–1 Gc.

621.317.733.011.22 3904
A Precision Conductance Bridge of New Design—G. J. Janz and J. D. E. McIntyre. (*J. Electrochem. Soc.*, vol. 108, pp. 272–276; March, 1961.) The bridge is designed for construction from standard commercially available components. The "four-leads" cell technique eliminates lead effects in remote conductance measurements.

621.317.738 3905
Measurements of the Dielectric Properties of Lossy Materials—E. Groubert and P. Caillon. (*J. Phys. Radium*, vol. 21, suppl., *Phys. Appl.*, pp. 155A–160A; November, 1960.) Apparatus for determining the dielectric properties of insulating materials at HF is described. Measurement is based on the variation of the width of the resonance curve of a tuned circuit when an impedance is placed across it.

621.317.77 3906
Construction of a High-Frequency Phase Meter—D. Boussard. (*J. Phys. Radium*, vol. 22, supple., *Phys. Appl.*, pp. 69A–71A; February, 1961.) The meter was designed to measure accurately the phase difference between two points on a conductor system in a linear accelerator. It has a range $+60°$ to $-15°$ and an accuracy within 0.5°.

OTHER APPLICATIONS OF RADIO AND ELECTRONICS

535.376:681.142 3907
The Electroluminescent Matrix for Pattern Display and Recording—D. C. Jeffreys and G. R. Hoffman. (*J. Brit. IRE*, vol. 22, pp. 53–64; July, 1961.) The photographic etching technique and vacuum deposition method of forming the matrix are described and a method of extending the lifetime of electroluminescent layers is noted. Selection problems in this type of matrix system are considered.

621.385.833 3908
The Resolving Power of Spherically Corrected Electrostatic Electron Microscopes—W. E. Meyer. (*Optik, Stuttgart*, vol. 18, no. 2, pp. 69–91; 1961.) The theoretical limit of resolution is calculated and methods of reducing aberration due to misalignments are given.

PROPAGATION OF WAVES

621.391.812.61.029.65 3909
Effect of Polarization on the Attenuation by Rain at Millimetre Wavelength—S. Okamura, K. Funakawa, H. Uda, J. Kato, and T. Oguchi (*J. Radio Res. Labs., Japan*, vol. 8, pp. 73–80; March, 1961.) The attenuation of vertically and horizontally polarized waves is compared using a method for rapidly switching the polarization. It is shown that the attenuation is generally larger for horizontally polarized waves. The measurements are in reasonable agreement with the theoretical calculations of Oguchi (1977 of July).

621.391.812.624.029.64 3910
Antenna Siting Tests at 3480 and 9640 Mc/s on a 173-Mile Tropospheric Scatter Path—N. D. La Frenais and W. J. Lucas. (PROC. IRE, vol. 49, pp. 1325–1326; August, 1961.) Signal recordings made at a favorable and an unfavorable receiving site are compared. Analysis shows how the difference in signal levels measured at the two sites varied as a

function of the system transmission loss. The figures for the dependence on the angular path distances show a dependence of θ^{-3} instead of the normally accepted θ^{-5}. See 683 of March (Geiger *et al.*).

621.391.812.63 3911
Simple Graphical Procedure for Calculating Sky-Wave Field Intensities—K. C. Chadha. (*J. Inst. Telecommun. Engrs. India*, vol. 7, pp. 89–102; March, 1961.) A series of graphical methods of applying the procedures S.P.I.M. [see 199 of 1953 (Rawar)] and RPU-9 (*U. S. Army Signal Corps Report*, No. 9) considerably reduce the labor involved but maintain the accuracy of the systems.

621.391.812.63 3912
Diversity Effects in Long-Distance High-Frequency Radio Pulse Propagation—S. A. Bowhill. (*J. Res. NBS*, vol. 65D, pp. 213–223; May/June, 1961.) Description of spaced-antenna measurements on an 8600-km path between Ceylon and England using pulsed radio signals. Interpretation of results in terms of E- and F-region multiple reflections gives good correlation with observed delay on the echoes received. The results also indicated that most of the diversity arises through phase incoherence between various orders of reflection.

621.391.812.63 3913
Space Analysis of Radio Signals—J. B. Smyth. (*J. Res. NBS*, vol. 65D, pp. 293–297; May/June, 1961.) An antenna is represented as a space-frequency filter. The RF field generated by it is distorted in passing into the ionosphere, generating new space frequencies which are the information contained in the field at the receiving antenna.

621.391.812.63 3914
Transequatorial Back-Scatter Observations of Magnetically Controlled Ionization—J. A. Thomas. (*Nature*, vol. 191, p. 792; August 19, 1961.) Very-long-range transequatorial echoes have been observed at Brisbane with a 16-Mc narrow-beam rotating-antenna back-scatter equipment [3371 of 1960 (Thomas and McNicol)]. They occur on 95 per cent of afternoons and are attributed to the ionospheric-tilt chordal-hop mechanism proposed by Villard *et al.* (244 of 1958).

621.391.812.63:621.396.663. 3915
Propagation Studies Using Direction-Finding Techniques—E. C. Hayden. (*J. Res. Nat. B. S.*, vol. 65D, pp. 197–212; May/June, 1961.) Two methods are described for the study of direction of arrival of individual components of multipath signals, resolution being undertaken by "time of arrival" separation for pulse transmissions or by "direction of arrival" separation using a highly directional antenna system. Some results obtained in studies of reception on 5.155 Mc over a path of 450 km and on 10 Mc over a path of 1000 km are presented.

621.391.812.63.029.4/.5 3916
Comparison between Mode Theory and Ray Theory of V.L.F. Propagation—H. Volland (*J. Res. NBS*, vol. 65D, pp. 357–361; July/August, 1961.) Values of field strength according to mode theory and ray theory in the VLF band are derivable from the same expression of the original vector potential, the result of one theory being the analytic continuation of the other one in another range of convergence. Both theories give the same result between distances of 3000 km and 2000 km. The relation to lightning discharges is considered.

621.391.812.63.029.45 3917
Statistics of a Radio Wave Diffracted by a Random Ionosphere—S. A. Bowhill.) *J. Res. NBS.*, vol. 65D, pp. 275–292; May/June, 1961.) Mathematical methods for evaluating the statistical properties of a random signal diffracted in free space are applied to the random structure of the lower ionosphere at very low frequencies. Allowance is made for sphericity, and anisotropy in the signal variations is permitted.

621.391.812.63.029.45 3918
Excitation of V.L.F. and E.L.F. Radio Waves by a Horizontal Magnetic Dipole—J. Galejs. (*J. Res. NBS*, vol. 65D, pp. 305–311; May/June, 1961.) The VLF and ELF modes excited by a horizontal magnetic dipole in the shell between a finitely conducting earth and an isotropic ionosphere are shown to have an almost transverse magnetic character. Response of the zero-order mode of the magnetic dipole has been calculated.

621.391.812.63.029.53 3919
Characteristics of Ionospherec Waves in the M.F. Band Measured at Night by the Vertical-Incidence Method—S. Hasegawa and T. Kobayashi. (*J. Radio Res. Labs., Japan*, vol. 8, pp. 127–136; March, 1961.) Observations of virtual heights and field intensities on frequencies of 540, 1040 and 1440 kc are described. During summer the one-hop-E mode is predominant over the full frequency range, while in autumn and winter the one-hop-F mode is more important above 1 Mc.

621.391.812.63.029.62 3920
Effect of E_s on V.H.F. Pulse Wave Propagation—K. Aida, T. Koseki, and K. Uchikura. (*J. Radio Res. Labs, Japan*, vol. 8, pp. 117–126; March, 1961.) Observations of VHF propagation over a path of 960 km and vertical soundings near the path midpoint show that during the day, propagation occurs via the E_s layer but during the night, reflection from meteoric dust is more important.

621.391.812.63.029.62 3921
Influence of Types of E_s Layer on E_s-Layer Propagated Waves—A. Sakurazawa. (*J. Radio Res. Labs, Japan*, vol. 8, pp. 97–116; March, 1961.) The factors governing E_s-layer propagation are examined by comparing VHF observations over a 1100-km path with those of E_s at the path midpoint. The analysis shows that the reflecting efficiency of the E_s layer depends on the values of f_0E_s over an area about the midpoint. The attenuation due to the D region is negligible while that due to the E region is most noticeable for propagation via the "h" type E_s.

RECEPTION

621.376.33:621.396.43 3922
Project Echo: F.M. Demodulators with Negative Feedback—C. L. Ruthroff. (*Bell Syst. Tech. J.*, vol. 40, pp. 1149–1156; July, 1961.) The performance of a FM receiver is described in which the beating oscillator is made to follow the instantaneous frequency of the signal. A smaller IF bandwidth can then be used which results in a better SNR than can be obtained with a conventional FM receiver or with SSB techniques.

621.391.82 3923
On the Theory of Amplitude Distribution of Impulsive Random Noise—K. Furutsu and T. Ishida. (*J. Appl. Phys.*, vol. 32, pp. 1206–1221; July, 1961.) Two models are considered and treated mathematically, one for Poisson noise (*e.g.*, electronic noise) and the other for Poisson-Poisson noise (*e.g.*, atmospheric noise). Theoretical distributions are compared with actual atmospheric noise.

621.391.82(545.5) 3924
Measurements of Radio Noise in the Delhi Area: Part I—N. B. Bhatt, M. K. Gupta, and Y. S. N. Murty. (*Def. Sci. J.*, vol. 11, pp. 23–33; January, 1961.) Noise levels measured in and near Delhi in the frequency range 150 kc–21 Mc show little correlation with the CCIR predictions. The diurnal variation was much smaller than expected.

621.391.821:621.396.62 3925
Effect of Receiver Bandwidth on the Amplitude Distribution of V.L.F. Atmospheric Noise—F. F. Fulton, Jr. (*J. Res. NBS*, vol. 65D, pp. 299–304; May/June, 1961.) For an assumed three-term parametric-exponential equation relating cumulative amplitude probability to field-strength threshold, expressions are derived indicating parameter variation as a function of bandwidth.

621.396.62:621.396.43 3926
Project Echo: Receiving System—E. A. Ohm. (*Bell Syst. Tech. J.*, vol. 40, pp. 1065–1094; July, 1961.) An over-all system noise temperature of about 20°K was obtained at 2390 Mc by combining a horn-reflector antenna maser preamplifier and special FM demodulator.

621.396.62:621.396.43 3927
Project Echo: Standby Receiver System—L. U. Kibler. (*Bell Syst. Tech. J.*, vol. 40, pp. 1129–1147; July, 1961.)

621.396.621 3928
Receivers with Zero Intermediate Frequency—M. D. Rubin. (PROC. IRE, vol. 49, pp. 1327–1328; August 1961.) An outline of the advantages and disadvantages of using a zero intermediate frequency. See, *e.g.*, 1677 of 1959 (Greene and Lyons) and 2767 of September (Casey).

621.396.621.072.6:621.391.82 3929
The Effect of Interference on an Automatic Frequency Control System: Part 1—V. I. Kaganov and N. S. Nemirovskii. (*Radiotekh. Elektron.*, vol. 5, pp. 1380–1386; September, 1960.) An analysis of the effect of noise on an AFC system comprising an ideal discriminator, the mean frequency of which is not zero, operating with and without an IF filter.

STATIONS AND COMMUNICATION SYSTEMS

621.391.621.372.54 3930
Prediction of Signals by means of a Simple *RC* Network—A. Schief. (*Arch. elekt. Übertragung*, vol. 15, pp. 91–93; February, 1961.) A linear *RC* filter network for the statistical prediction of signals in noise is designed and experimental results are given.

621.391:621.376.23 3931
Multiple-Burst Detection—F. Corr. (PROC. IRE, vol. 49, p. 1337; August, 1961.) A class of cyclic codes exist which can correct any t bursts of minimum length b in a block of $(2^k-1)b$ bits. A proof is given that this code can alternatively be used to detect any $2t$ bursts of length b in a similar block. bkt check digits will be required.

621.396.2 3932
Spectrum Representation for Vestigial-Sideband Transmission in the Light of Transmission Possibilities between Single- and Double-Sideband Transmission—N. Berger. (*Nachrtech.*, vol. 11, pp. 31–35; January, 1961.)

621.396.43:551.507.362.2 3933
Satellites as Passive Relay Stations for Communications over Long Distances—W. Mansfeld. (*Frequenz*, vol. 15, pp. 1–9; January, 1961.) Conditions for the use of satellites as reflectors are examined. System design features

discussed include the shape and dimensions of the reflectors, transmitter output and antenna diameters.

621.396.43:551.507.362.2 3934
Participation of Bell Telephone Laboratories in Project Echo and Experimental Results—W. C. Jakes, Jr. (*Bell Syst. Tech. J.*, vol. 40, pp. 975–1028; July, 1961.) Two-way voice communication by reflection from a 100-ft diameter spherical balloon satellite orbiting at a height of 1000 miles was demonstrated over a coast-to-coast path in the U.S.A. Modulation tests using carrier frequencies of 960 and 2390 Mc showed FM to be superior to other forms. Measured transmission-path loss agreed closely with theory.

621.396.43:551.507.362.2 3935
Project Echo: System Calculations—C. L. Ruthroff and W. C. Jakes, Jr. (*Bell Syst. Tech. J.*, vol. 40, pp. 1029–1039; July, 1961.)

621.396.934:621.391.822 3936
Overall System Requirements for Low-Noise Performance—C. R. Ditchfield. (*J. Brit. IRE*, vol. 22, pp. 123–127; August, 1961.) The practical limitations of a microwave system for communication with and between satellites are discussed. The limit of performance will probably be determined by ambient noise background rather than receiver noise.

SUBSIDIARY APPARATUS

621–526:621.396.677 3937
Project Echo: Antenna Steering System—R. Klahn, J. A. Norton, and J. A. Githens. (*Bell Syst. Tech. J.*, vol. 40, pp. 1207–1225; July, 1961.) The use of basic orbital information to generate antenna steering instructions for project Echo is discussed. A digital method is described in which predicted pointing data is transmitted by teletype to the antenna site, then stored, and subsequently used when required in real time to control the antenna drive mechanism.

621–526:621.396.677:778.53 3938
Project Echo: Boresight Cameras—L. K. Warthman. (*Bell Syst. Tech. J.*, vol. 40, pp. 1227–1233; July, 1961.) Cameras are attached to the project Echo transmitting and receiving antennas at Holmdel for recording the position of the satellite. An exposure of 1/30 sec at *f*/3.5 was used at 4 frames/sec.

621.3.087.4:621.395.625.3 3939
An Analytical Expression for Describing the Write Process in Magnetic Recording—T. C. Ku. (PROC. IRE, vol. 49, pp. 1337–1338; August, 1961.)

621.3.087.4:621.397 3940
Video-Tape Analyzer—A. A. Goldberg and M. R. Nannah. (*J. Soc. Mot. Pict. Telev. Engrs.*, vol. 70, pp. 85–89; February, 1961.) Tape frequency response, noise contribution, drop-outs and rate of wear are determined and an assessment is made of the decline in picture quality due to repeated playback.

621.311.69:621.383.5 3941
Spectral Response of Solar Cells—B. Dale and F. P. Smith. (*J. Appl. Phys.*, vol. 32, pp. 1377–1381; July, 1961.) Theoretical response curves are derived by an analysis including the effects of carrier diffusion and drift due to the electric field in the surface region.

621.311.69:621.383.5:551.507.362.2 3942
Solar Cells for Communication Satellites in the Van Allen Belt—F. M. Smits, K. D. Smith, and W. L. Brown. (*J. Brit. IRE*, vol. 22, pp. 161–169; August, 1961.) The power output of solar cells on satellites is degraded by radiation damage on passing through the Van Allen belts. Methods of overcoming this are discussed.

621.311.69:629.19 3943
Power Supplies for Space Vehicles—N. W. Snyder. (*Astronautica Acta*, vol. 6, no. 6, pp. 271–310; 1960.) A comprehensive review of types of power systems, energy sources and power converters and an examination of the problems associated with their development as power supplies for space vehicles.

621.314.63 3944
Communication and Destructive Oscillation in Diode Circuits—I. Somos. (*Commun. and Electronics*, no. 54, pp. 162–172; May, 1961. Discussion.) An investigation of these phenomena in Si rectifiers and a study of how commutation may cause destruction of unprotected cells.

621.314.63 3945
A Fatigue-Free Silicon Device Structure—W. B. Green. (*Commun. and Electronics*, no. 54, pp. 186–191; May, 1961. Discussion.) By using hard solder instead of soft solder to make joints in the device, ruptures are no longer produced by cyclic thermal stress.

621.316.72 3946
Passive Voltage and Current Stabilizers using a Bridge Network—A. Caravel. (*J. Phys. Radium*, vol. 21, suppl., *Phys. Appl.*, pp. 187A-190A; November, 1960.) The residual voltage variation, which occurs when a Zener diode is used as a stabilizer, is removed by using a Wheatstone bridge network.

621.316.721.078.3:621.318.3 3947
Transistorized Current Stabilizers for Electromagnets of Medium Power (1 to 10 kW)—M. Sauzade. (*J. Phys. Radium*, vol. 21, Suppl. *Phys. Appl.*, pp. 161A–170A; November, 1960.) Methods of computing the characteristics and determining the stability are given.

621.316.722.1 078 3948
Cathode-Coupled Cascode Stabilizer Circuit—S. G. Jones and R. S. McClean. (*Electronic Engrg.*, vol. 33, pp. 503–505; August, 1961.) In a negative h.v. power supply (-6.8 kv nominal), the peak-to-peak ripple was less than 1.5 v and a ± 10 per cent change in line voltage gave less than 1 v change in output.

TELEVISION AND PHOTOTELEGRAPHY

621.397.12 3949
A High-Speed Facsimile System with Electronic Scanning—K. Kubota, K. Kobayashi, Y. Okajima, and S. Nanbo. (*Rev. Elect. Commun. Lab., Japan*, vol. 9, pp. 214–219; March/April, 1961.)

621.397.331.2 3950
The Problem of Signal/Noise Ratio in Television Camera Tubes—H. Fix and A. Kaufmann. (*Radio Mentor*, vol. 27, pp. 114–116; February, 1961.) Reassessment of the relative merits of various types of camera tube with regard to SNR. This is in closer agreement with subjective assessments and is based on measurements of the spectral composition of statistical fluctuations in camera installations (1326 of June).

621.397.331.22 3951
Image-Orthicon Tubes with Field Mesh—K. Frank. (*Electronische Rundschau*, vol. 15, pp. 66–68; February, 1961.) The picture defects which can be minimized by the use of a field mesh are summarized [see also 2926 of 1957 (Theile and Pilz)]. The disadvantages, such as moiré effects, of this system are discussed and design improvements are suggested.

621.397.331.222 3952
Photoconductive Camera Tubes: the C.F.T.H. Vidicons—M. Blamoutier. (*Onde élect.*, vol. 41, pp. 229-238; March, 1961.)

621.397.331.222 3953
On the Possibility of using Germanium Sulphide Photoresistors as Targets in Television Camera Tubes—V. I. Perevodchikov and E. P. Kuznetsov. (*Radiotekh. Elektron.*, vol. 5, pp. 1478–1483; September, 1960.) A method of preparing high-resistivity GeS photo sensitive layers is described and their main characteristics are given. The basic parameters of a vidicon-type camera tube with a GeS target are discussed.

621.397.331.24 3954
The Reflected-Beam Picture Tube—a Further Step towards a Flat Tube of Large Image Size—P. Neidhardt. (*Nachrtech.*, vol. 11, pp. 27–30; January, 1961.) The principle of operation, design problems and practical possibilities for this type of picture tube are reviewed. See also 4043 of 1960 (Law and Ramberg).

621.397.62:621.396.67 3955
The Permissible Mismatch in Aerial Installations for Television Reception—A. Fiebranz. (*Nachrtech. Z.*, vol. 14, pp. 25–31; January, 1961.) The receiver input voltage is determined for mismatch conditions. Frequency-independent voltage components are found to depend on voltage SWR only, for low-order terms. The effects of mismatch on television picture quality are discussed.

621.397.74 3956
The Technique of the Television Transmissions (Session of the Federal Parliament)—H. Probst. (*Tech. Mitt. PTT.*, vol. 39, pp. 39–44; February, 1961.) Description of studio arrangements camera equipment, mobile and fixed control installations and the transmission system used for relaying interviews from the Parliament Building in Berne.

TRANSMISSION

621.396.61:621.396.43 3957
Project Echo: 960-Mc/s, 10-kW Transmitter—J. P. Schafer and R. H. Brandt. (*Bell Syst. Tech. J.*, vol. 40, pp. 1041–1064; July, 1961.) Driver-modulator units for FM, ph.m, SSB and pulse are described. The main output amplifier consists of a four-stage water-cooled klystron.

TUBES AND THERMIONICS

621.382.2:621.318.7:621.317.3 3958
Measuring Recovery Time of Ultra-Fast Diodes—G. C. Messenger. (*Electronic Ind.*, vol. 20, pp. 99–100; April, 1961.) An indirect method which gives accurate results below 1 nsec is described. Results have been obtained down to 0.05 nsec.

621.382.22:621.376.23.029.64 3959
High-Level Microwave Detector using Avalanche Injection—H. M. Day and A. C. MacPherson. (PROC. IRE, vol. 49, pp. 1333–1334; August, 1961.) An avalanche injection microwave diode has been constructed which has useful properties as a large-signal detector. At 9350 Mc, rectified voltages up to 12v across 200 Ω have been obtained with input power varying from 1 to 3 w.

621.382.23 3960
A Method for Determining the Base Voltage and Contact Resistance of a Conductivity-Modulated Diode—J. M. Swartz and H. C. Gorton. (PROC. IRE, vol. 49, pp. 1326–1327; August, 1961.) The contact resistance is measured from the dynamic change in voltage with current at high levels of carrier injection.

621.382.23:539.12.04 3961
Electron-Bombardment Damage in Silicon Esaki Diodes—R. A. Logan, W. M. Augustyniak, and J. F. Gilbert. (*J. Appl. Phys.*, vol. 32, pp. 1201–1205; July, 1961.) The excess current

in Si Esaki diodes has been shown to be a sensitive indicator of the density and distribution of states introduced into the forbidden gap by electron bombardment. The effects of bombardment and the annealing properties of the radiation damage depend on the specific donor in the *n*-type region.

621.382.23:621.372.44 3962
Large-Signal Circuit Theory for Negative-Resistance Diodes, in particular Tunnel Diodes—M. Schuller and W. W. Gärtner. (PROC. IRE, vol. 49, pp. 1268–1278; August, 1961.) The device and its external circuit are characterized by a system of accurate nonlinear differential equations, and solutions are obtained by an electronic computer. Results agree with measurements.

621.382.23:621.373.431.1 3963
The Tunnel-Diode Pair—Hamilton and Morgan. (See 3677.)

621.382.3:621.317.3 3964
Measurement of Transistor Quadripole Parameters—R. Paul. (*Nachrtech.*, vol. 11, pp. 8–12; January, 1961.) Measuring circuits are given and the accuracy of measurement is estimated. See also *ibid.*, vol. 10, pp. 56–61; February, 1960.)

621.382.3:621.317.7 3965
Transistor Current Gain at U.H.F.—B. N. Harden. (*Electronic Tech.*, vol. 38, pp. 312–316; September, 1961.) "A coaxial-line system and a twin-channel comparator are used to determine amplitude and phase variations of current gain. Results in the frequency range 300–800 Mc are compared with values obtained by a bridge method." See 3426 of 1959 (Smith and Hyde).

621.382.3:621.391.822 3966
Investigation of the Noise of Semiconductors—I. P. Valkó. (*Period. polyt., Bp., Elect. Engrg*, vol. 5, no. 1, pp. 57–73; 1961. In German.) Results of investigations of low-frequency transistor noise are reviewed. Details are given of test equipment for the direct indication of noise amplitude and spectral distribution.

621.382.32 3967
Graphical Analysis of the Operation of the Tecnetron: Parts 1 and 2—A. V. J. Martin and J. Le Mée. (*J. Phys. Radium*, vol. 22, suppl. *Phys. Appl.*, pp. 1A–12A and 83A–90A; February and June, 1961.) The operation of the device in the subcritical field region, where the carrier mobility is considered to be constant, is analyzed graphically and a set of universal curves of the main characteristics is derived. A detailed comparison is made between analytical and graphical approximations. See also 1959 IRE CONVENTION RECORD, vol. 7, pt. 3, pp. 9–17; also, 1341 of 1961 (Martin).

621.382.333 3968
Characteristic Transistor Properties for Communications Applications and their Interrelation—W. Benz. (*Frequenz*, vol. 15, pp. 17–29; January, 1961.) Detailed consideration of the operation of a transistor as an amplifier including a discussion of dc conditions and dependence on temperature, frequency and working point. Transistor noise and nonlinear distortion, and the application of the transistor as a switching device are also mentioned. 52 references.

621.382.333 3969
A Method of Determining the Impurity-Doping Profile of a Transistor from Measurements of Certain of its Electrical Characteristics—J. P. Biet. (*J. Phys. Radium*, vol. 22, suppl., *Phys. Appl.*, pp. 59A–63A; February, 1961.) By measuring the hybrid-π parameters as a function of collector voltage and current, values can be obtained for the resistivity of the base and of the collector region, and the shape of the junction and base width can be ascertained.

621.382.333.33:621.372.632 3970
On Parametric Amplification in Transistors—J. Lindmayer and C. Wrigley; V. W. Vodicka and R. Zuleeg. (PROC. IRE, vol. 49, pp. 1335–1337; August, 1961.) Comment on 4420 of 1960 and 369 of February, and authors' reply.

621.382.333.34 3971
***p-n-p-n* Structures and a Solid-State Silicon Thyratron**—M. Sassier. (*Onde élect.*, vol. 41, pp. 239–246; March, 1961.) The theoretical relations governing the operation of *p-n-p-n* triodes are considered and applied to an analysis of the characteristics of a Si thyratron. Methods of manufacture are outlined.

621.383:535.376 3972
Infrared Detectors based on Phosphors—R. Groth. (*Z. Naturforsch*, vol. 16a, pp. 169–172; February, 1961.) The principle of a detector using infrared-sensitive phosphors is described and experimental results are given which were obtained with a SrS-Ce-Sm phosphor. A sensitivity of 6×10^{-11} was achieved near $\lambda=1\mu$.

621.383.49 3973
Reduction of Optical Reflection by Blooming without Increasing the Surface Recombination in Germanium Photoresistors—F. R. Kessler. (*Z. angew. Phys.*, vol. 13, pp. 72–74; February, 1961.) Comparison of results obtained with vapor-deposited $PbCl_2$ and Se; in the latter case the surface recombination remains unchanged but the sensitivity of the photoresistor is considerably increased.

621.383.51 3974
Germanium Bicrystals and their Application in Grain-Boundary Photocells—H. F. Mataré. (*Elektronische Rundschau*, vol. 15, pp. 57–60 and 207–211; February and May, 1961.) The mechanical and chemical structure of the grain boundary is considered and a model derived. The effect of impurities and the electrical properties of the bicrystal interface are discussed. Practical applications of this type of cell are mentioned. 27 references.

621.383.8 3975
Large-Field Image Intensifier Tubes for Visual, Ultraviolet and Infrared Ranges—L. F. Guyot. (*Onde élect.*, vol. 41, pp. 220–228; March, 1961.) A series of four tubes with 100-mm object field and luminance gain up to 6000 is described.

621.385.032.213.23 3976
Measurement of Oxide-Cathode Evaporation in Thermionic Valves with Radioactive Isotopes—C. Röszler. (*Nachrtech.*, vol. 11, pp. 13–16; January, 1961.) Results of experimental investigations on various types of tube are summarized.

621.385.032.213.23 3977
Suppression of Emission from Portions of Barium-Activated Tungsten Dispenser Cathodes and Adjoining Electrodes—R. Levi and E. S. Rittner. (PROC. IRE, vol. 49, pp. 1323–1324; August, 1961.) A technique for carburizing portions of a Ba-activated cathode to suppress the electron emission from areas where it is undesirable. Reductions in emission of two orders of magnitude are possible.

621.385.032.269.1 3978
The Matching of Pierce Guns to Tunnels—C. J. Milner and K. J. Ausburn. (*Brit. J. Appl. Phys.*, vol. 12, pp. 346–347; July, 1961.) All Pierce guns which shoot the maximum electron current through two identical apertures collinear with the axis of the gun have a unique ratio of cathode to anode radius. The value of this unique ratio is given for four important cases. A simple design procedure and relevant numerical data are given.

621.385.3+621.385.5 3979
A Method of Stabilizing the Gain of Triodes and Pentodes—H. Lorenz. (*Nachrtech.*, vol. 10, pp. 534–536; December, 1960.) The stabilization is effected by using a cathode resistance appropriate to the working point of the tube. The resistance tube is determined by measurement.

621.385.6 3980
Three Interpretations of Space-Charge Waves in Electron Beams—H. Groendijk. (*Tijdschr. ned. Radiogenoot.*, vol. 26, pp. 51–64; July 31, 1961.) The phenomenon is interpreted as 1) a single moving wave with phase velocity equal to the beam velocity and amplitude varying sinusoidally with position, 2) two moving waves of constant amplitude with different phase velocities, and 3) a stream of independent oscillators.

621.385.6:537.533 3981
Propagation in Periodic Electron Beams—W. M. Mueller. (*J. Appl. Phys.*, vol. 32, pp. 1349–1360; July, 1961.) A small-signal analysis of smooth electron beams with periodic variations in their dc parameters reveals the existence of infinite sets of space harmonics of the fast and slow space-charge waves. Various effects and the possible uses of the periodicity in beams are mentioned.

621.385.6:621.372.8 3982
Electromagnetic Radiation from a Beam of Charged Particles Passing near a Waveguide with an Infinite Flange—Yu. N. Dnestrovskiĭ and D. P. Kostomarov. (*Radiotekh. Elektron.*, vol. 5, pp. 1431–1441; September, 1960.) A two-dimensional analysis of the EM radiation from a modulated electron beam passing the flange of a planar waveguide. The problem is reduced to a set of algebraic solutions which are solved analytically for a range of electron velocities.

Translations of Russian Technical Literature

Listed below is information on Russian technical literature in electronics and allied fields which is available in the U. S. in the English language. Further inquiries should be directed to the sources listed. In addition, general information on translation programs in the U. S. may be obtained from the Office of Science Information Service, National Science Foundation, Washington 25, D. C., and from the Office of Technical Services, U. S. Department of Commerce, Washington 25, D. C.

PUBLICATION	FREQUENCY	DESCRIPTION	SPONSOR	ORDER FROM:
Acoustics Journal (Akusticheskii Zhurnal)	Quarterly	Complete journal	National Science Foundation—AIP	American Institute of Physics 335 E. 45 St., New York 17, N. Y.
Automation and Remote Control (Avtomatika i Telemekhanika)	Monthly	Complete journal	National Science Foundation—MIT	Instrument Society of America 313 Sixth Ave., Pittsburgh 22, Pa.
	Monthly	Abstracts only		Office of Technical Services U. S. Dept of Commerce Washington 25, D. C.
Journal of Abstracts, Electrical Engineering (Reserativnyy Zhurnal: Electronika)	Monthly	Abstracts of Russian and non-Russian literature		Office of Technical Services U. S. Dept. of Commerce Washington 25, D. C.
Journal of Experimental and Theoretical Physics (Zhurnal Eksperimentalnoi i Teoreticheskoi Fiziki)	Monthly	Complete journal	National Science Foundation—AIP	American Institute of Physics 335 E. 45 St., New York 17, N. Y.
Journal of Technical Physics (Zhurnal Tekhnicheskoi Fiziki)	Monthly	Complete journal	National Science Foundation—AIP	American Institute of Physics 335 E. 45 St., New York 17, N. Y.
Proceedings of the USSR Academy of Sciences: Applied Physics Section (Doklady Akademii Nauk SSSR: Otdel Prikladnoi Fiziki)	Bimonthly	Complete journal		Consultants Bureau, Inc. 227 W. 17 St., New York 22, N. Y.
Radio Engineering (Radiotekhnika)	Monthly	Complete journal	National Science Foundation—AIEE	Royer & Roger, Inc. 41 E. 28 St., New York 16, N. Y.
	Monthly	Abstracts only		Office of Technical Services U. S. Dept. of Commerce Washington 25, D. C.
Radio Engineering and Electronics (Radiotekhnika i Elektronika)	Monthly	Complete journal	National Science Foundation—AIEE	Royer & Roger, Inc. 41 E. 28 St., New York 16, N. Y.
	Monthly	Abstracts only		Office of Technical Services U. S. Dept. of Commerce Washington 25, D. C.
Solid-State Physics (Fizika Tverdogo Tela)	Monthly	Complete journal	National Science Foundation—AIP	American Institute of Physics 335 E. 45 St., New York 17, N. Y.
Telecommunications (Elektrosviaz')	Monthly	Complete journal	National Science Foundation—AIEE	Royer & Roger, Inc. 41 E. 28 St., New York 16, N. Y.
	Monthly	Abstracts only		Office of Technical Services U. S. Dept. of Commerce Washington 25, D. C.
Automation Express	10/year	A digest: abstracts, summaries, annotations of various journals		International Physical Index, Inc. 1909 Park Ave., New York 35, N. Y.
Electronics Express	10/year	A digest: abstracts, summaries, annotations of various journals		International Physical Index, Inc. 1909 Park Ave., New York, 35, N. Y.
Physics Express	10/year	A digest: abstracts, summaries, annotations of various journals		International Physical Index, Inc. 1909 Park Ave., New York 35, N. Y.
Express Contents of Soviet Journals Currently being Translated into English	Monthly	Advance tables of contents of translated journals		Consultants Bureau, Inc. 227 W. 17 St., New York 22, N. Y.
Technical Translations	Twice a month	Central directory in the U. S. of translations available from all major sources in the U. S.	OTS and Special Libraries Assoc.	Superintendent of Documents U. S. Gov't Printing Office Washington 25, D. C.

Translations of Russian Technical Literature

Listed below is information on Russian technical literature in electronics and allied fields which is available in the U. S. in the English language. Further inquiries should be directed to the sources listed. In addition, general information on translation programs in the U. S. may be obtained from the Office of Science Information Service, National Science Foundation, Washington 25, D. C., and from the Office of Technical Services, U. S. Department of Commerce, Washington 25, D. C.

PUBLICATION	FREQUENCY	DESCRIPTION	SPONSOR	ORDER FROM:
Acoustics Journal (Akusticheskii Zhurnal)	Quarterly	Complete journal	National Science Foundation—AIP	American Institute of Physics 335 E. 45 St., New York 17, N. Y.
Automation and Remote Control (Avtomatika i Telemekhanika)	Monthly	Complete journal	National Science Foundation—MIT	Instrument Society of America 313 Sixth Ave., Pittsburgh 22, Pa.
	Monthly	Abstracts only		Office of Technical Services U. S. Dept of Commerce Washington 25, D. C.
Journal of Abstracts, Electrical Engineering (Reserativnyy Zhurnal: Electronika)	Monthly	Abstracts of Russian and non-Russian literature		Office of Technical Services U. S. Dept. of Commerce Washington 25, D. C.
Journal of Experimental and Theoretical Physics (Zhurnal Eksperimentalnoi i Teoreticheskoi Fiziki)	Monthly	Complete journal	National Science Foundation—AIP	American Institute of Physics 335 E. 45 St., New York 17, N. Y.
Journal of Technical Physics (Zhurnal Tekhnicheskoi Fiziki)	Monthly	Complete journal	National Science Foundation—AIP	American Institute of Physics 335 E. 45 St., New York 17, N. Y.
Proceedings of the USSR Academy of Sciences: Applied Physics Section (Doklady Akademii Nauk SSSR: Otdel Prikladnoi Fiziki)	Bimonthly	Complete journal		Consultants Bureau, Inc. 227 W. 17 St., New York 22, N. Y.
Radio Engineering (Radiotekhnika)	Monthly	Complete journal	National Science Foundation—AIEE	Royer & Roger, Inc. 41 E. 28 St., New York 16, N. Y.
	Monthly	Abstracts only		Office of Technical Services U. S. Dept. of Commerce Washington 25, D. C.
Radio Engineering and Electronics (Radiotekhnika i Elektronika)	Monthly	Complete journal	National Science Foundation—AIEE	Royer & Roger, Inc. 41 E. 28 St., New York 16, N. Y.
	Monthly	Abstracts only		Office of Technical Services U. S. Dept. of Commerce Washington 25, D. C.
Solid-State Physics (Fizika Tverdogo Tela)	Monthly	Complete journal	National Science Foundation—AIP	American Institute of Physics 335 E. 45 St., New York 17, N. Y.
Telecommunications (Elektrosviaz')	Monthly	Complete journal	National Science Foundation—AIEE	Royer & Roger, Inc. 41 E. 28 St., New York 16, N. Y.
	Monthly	Abstracts only		Office of Technical Services U. S. Dept. of Commerce Washington 25, D. C.
Automation Express	10/year	A digest: abstracts, summaries, annotations of various journals		International Physical Index, Inc. 1909 Park Ave., New York 35, N. Y.
Electronics Express	10/year	A digest: abstracts, summaries, annotations of various journals		International Physical Index, Inc. 1909 Park Ave., New York, 35, N. Y.
Physics Express	10/year	A digest: abstracts, summaries, annotations of various journals		International Physical Index, Inc. 1909 Park Ave., New York 35, N. Y.
Express Contents of Soviet Journals Currently being Translated into English	Monthly	Advance tables of contents of translated journals		Consultants Bureau, Inc. 227 W. 17 St., New York 22, N. Y.
Technical Translations	Twice a month	Central directory in the U. S. of translations available from all major sources in the U. S.	OTS and Special Libraries Assoc.	Superintendent of Documents U. S. Gov't Printing Office Washington 25, D. C.

in Si Esaki diodes has been shown to be a sensitive indicator of the density and distribution of states introduced into the forbidden gap by electron bombardment. The effects of bombardment and the annealing properties of the radiation damage depend on the specific donor in the *n*-type region.

621.382.23:621.372.44 3962
Large-Signal Circuit Theory for Negative-Resistance Diodes, in particular Tunnel Diodes—M. Schuller and W. W. Gärtner. (PROC. IRE, vol. 49, pp. 1268–1278; August, 1961.) The device and its external circuit are characterized by a system of accurate nonlinear differential equations, and solutions are obtained by an electronic computer. Results agree with measurements.

621.382.23:621.373.431.1 3963
The Tunnel-Diode Pair—Hamilton and Morgan. (See 3677.)

621.382.3:621.317.3 3964
Measurement of Transistor Quadripole Parameters—R. Paul. (*Nachrtech.*, vol. 11, pp. 8–12; January, 1961.) Measuring circuits are given and the accuracy of measurement is estimated. See also *ibid.*, vol. 10, pp. 56–61; February, 1960.)

621.382.3:621.317.7 3965
Transistor Current Gain at U.H.F.—B. N. Harden. (*Electronic Tech.*, vol. 38, pp. 312–316; September, 1961.) "A coaxial-line system and a twin-channel comparator are used to determine amplitude and phase variations of current gain. Results in the frequency range 300–800 Mc are compared with values obtained by a bridge method." See 3426 of 1959 (Smith and Hyde).

621.382.3:621.391.822 3966
Investigation of the Noise of Semiconductors—I. P. Valkó. (*Period. polyt., Bp., Elect. Engrg*, vol. 5, no. 1, pp. 57–73; 1961. In German.) Results of investigations of low-frequency transistor noise are reviewed. Details are given of test equipment for the direct indication of noise amplitude and spectral distribution.

621.382.32 3967
Graphical Analysis of the Operation of the Tecnetron: Parts 1 and 2—A. V. J. Martin and J. Le Mée. (*J. Phys. Radium*, vol. 22, suppl. *Phys. Appl.*, pp. 1A–12A and 83A–90A; February and June, 1961.) The operation of the device in the subcritical field region, where the carrier mobility is considered to be constant, is analyzed graphically and a set of universal curves of the main characteristics is derived. A detailed comparison is made between analytical and graphical approximations. See also 1959 IRE CONVENTION RECORD, vol. 7, pt. 3, pp. 9–17; also, 1341 of 1961 (Martin).

621.382.333 3968
Characteristic Transistor Properties for Communications Applications and their Interrelation—W. Benz. (*Frequenz*, vol. 15, pp. 17–29; January, 1961.) Detailed consideration of the operation of a transistor as an amplifier including a discussion of dc conditions and dependence on temperature, frequency and working point. Transistor noise and nonlinear distortion, and the application of the transistor as a switching device are also mentioned. 52 references.

621.382.333 3969
A Method of Determining the Impurity-Doping Profile of a Transistor from Measurements of Certain of its Electrical Characteristics—J. P. Biet. (*J. Phys. Radium*, vol. 22, suppl., *Phys. Appl.*, pp. 59A–63A; February, 1961.) By measuring the hybrid-π parameters as a function of collector voltage and current, values can be obtained for the resistivity of the base and of the collector region, and the shape of the junction and base width can be ascertained.

621.382.333.33:621.372.632 3970
On Parametric Amplification in Transistors—J. Lindmayer and C. Wrigley: V. W. Vodicka and R. Zuleeg. (PROC. IRE, vol. 49, pp. 1335–1337; August, 1961.) Comment on 4420 of 1960 and 369 of February, and authors' reply.

621.382.333.34 3971
***p-n-p-n* Structures and a Solid-State Silicon Thyratron**—M. Sassier. (*Onde élect.*, vol. 41, pp. 239–246; March, 1961.) The theoretical relations governing the operation of *p-n-p-n* triodes are considered and applied to an analysis of the characteristics of a Si thyratron. Methods of manufacture are outlined.

621.383:535.376 3972
Infrared Detectors based on Phosphors—R. Groth. (*Z. Naturforsch*, vol. 16a, pp. 169–172; February, 1961.) The principle of a detector using infrared-sensitive phosphors is described and experimental results are given which were obtained with a SrS-Ce-Sm phosphor. A sensitivity of 6×10^{-11} was achieved near $\lambda=1\mu$.

621.383.49 3973
Reduction of Optical Reflection by Blooming without Increasing the Surface Recombination in Germanium Photoresistors—F. R. Kessler. (*Z. angew. Phys.*, vol. 13, pp. 72–74; February, 1961.) Comparison of results obtained with vapor-deposited $PbCl_2$ and Se; in the latter case the surface recombination remains unchanged but the sensitivity of the photoresistor is considerably increased.

621.383.51 3974
Germanium Bicrystals and their Application in Grain-Boundary Photocells—H. F. Mataré. (*Elektronische Rundschau*, vol. 15, pp. 57–60 and 207–211; February and May, 1961.) The mechanical and chemical structure of the grain boundary is considered and a model derived. The effect of impurities and the electrical properties of the bicrystal interface are discussed. Practical applications of this type of cell are mentioned. 27 references.

621.383.8 3975
Large-Field Image Intensifier Tubes for Visual, Ultraviolet and Infrared Ranges—L. F. Guyot. (*Onde élect.*, vol. 41, pp. 220–228; March, 1961.) A series of four tubes with 100-mm object field and luminance gain up to 6000 is described.

621.385.032.213.23 3976
Measurement of Oxide-Cathode Evaporation in Thermionic Valves with Radioactive Isotopes—C. Röszler. (*Nachrtech.*, vol. 11, pp. 13–16; January, 1961.) Results of experimental investigations on various types of tube are summarized.

621.385.032.213.23 3977
Suppression of Emission from Portions of Barium-Activated Tungsten Dispenser Cathodes and Adjoining Electrodes—R. Levi and E. S. Rittner. (PROC. IRE, vol. 49, pp. 1323–1324; August, 1961.) A technique for carburizing portions of a Ba-activated cathode to suppress the electron emission from areas where it is undesirable. Reductions in emission of two orders of magnitude are possible.

621.385.032.269.1 3978
The Matching of Pierce Guns to Tunnels—C. J. Milner and K. J. Ausburn. (*Brit. J. Appl. Phys.*, vol. 12, pp. 346–347; July, 1961.) All Pierce guns which shoot the maximum electron current through two identical apertures collinear with the axis of the gun have a unique ratio of cathode to anode radius. The value of this unique ratio is given for four important cases. A simple design procedure and relevant numerical data are given.

621.385.3+621.385.5 3979
A Method of Stabilizing the Gain of Triodes and Pentodes—H. Lorenz. (*Nachrtech.*, vol. 10, pp. 534–536; December, 1960.) The stabilization is effected by using a cathode resistance appropriate to the working point of the tube. The resistance tube is determined by measurement.

621.385.6 3980
Three Interpretations of Space-Charge Waves in Electron Beams—H. Groendijk. (*Tijdschr. ned. Radiogenoot.*, vol. 26, pp. 51–64; July 31, 1961.) The phenomenon is interpreted as 1) a single moving wave with phase velocity equal to the beam velocity and amplitude varying sinusoidally with position, 2) two moving waves of constant amplitude with different phase velocities, and 3) a stream of independent oscillators.

621.385.6:537.533 3981
Propagation in Periodic Electron Beams—W. M. Mueller. (*J. Appl. Phys.*, vol. 32, pp. 1349–1360; July, 1961.) A small-signal analysis of smooth electron beams with preiodic variations in their dc parameters reveals the existence of infinite sets of space harmonics of the fast and slow space-charge waves. Various effects and the possible uses of the periodicity in beams are mentioned.

621.385.6:621.372.8 3982
Electromagnetic Radiation from a Beam of Charged Particles Passing near a Waveguide with an Infinite Flange—Yu. N. Dnestrovskiĭ and D. P. Kostomarov. (*Radiotekh. Elektron.*, vol. 5, pp. 1431–1441; September, 1960.) A two-dimensional analysis of the EM radiation from a modulated electron beam passing the flange of a planar waveguide. The problem is reduced to a set of algebraic solutions which are solved analytically for a range of electron velocities.